CHARACTERISTICS OF DILUTE GAS-SOLID SUSPENSION FLOWS

BY

VENG-KAI CHAN

A THESIS SUBMITTED FOR THE DEGREE OF

DOCTOR OF PHILOSOPHY

DEPARTMENT OF MECHANICAL ENGINEERING

THE CITY UNIVERSITY

LONDON

NOVEMBER 1976

To
C.C.

ACKNOWLEDGEMENTS

The author would like to express his sincere gratitude to his supervisor, Professor R.A. Duckworth, for his guidance and encouragement throughout this work and to thank the [redacted] for the provision of research grants which have made possible this research. The author is also grateful to the Senate of The City University for providing the research facilities and [redacted] for his technical assistance.

CONTENTS

		PAGE
SUMMARY		7
SYMBOLS		9
LIST OF ILLUSTRATIONS		12
TABLES		14
CHAPTER 1	INTRODUCTION	15
CHAPTER 2	ELECTRODYNAMICS OF A GAS-SOLID SUSPENSION	19
2.1	Charging by Surface Contact	19
2.2	Dynamics of a Cloud of Charged Particles	25
2.3	Turbulent Flow of Charged Gas-Solid Suspension	27
2.4	Static Reduction	29
CHAPTER 3	MOTION OF SOLID PARTICLES SUSPENDED IN A TURBULENT FLUID	31
3.1	Diffusion of Discrete Particles in a Turbulent Fluid	31
3.2	Effects of Electrostatic Force	36
3.3	Effects of Gravity Force	37
3.4	Effects of Magnus Lift Force	37
CHAPTER 4	CONTINUUM MECHANICS OF A GAS-SOLID SUSPENSION FLOW	39
4.1	Behaviour of a Dilute Gaseous Suspension of Particles	41
4.2	Dynamic Equations of a Dilute Suspension	42

		PAGE
4.3	Fully Developed Turbulent Flow of a Gas-Solid Suspension	46
4.4	Characteristic Equations	50
4.5	Simplified Characteristic Equations	54
CHAPTER 5	FRICTION FACTOR OF A GAS-SOLID SUSPENSION FLOW	56
CHAPTER 6	EXPERIMENTAL STUDY	64
6.1	General Description of the Test Rig	64
6.2	Pressure Transducer	67
6.3	Pressure Drop and Friction Factor Measurement	68
6.4	Air Flow Rate Measurement	70
6.5	Solid Flow Rate Measurement	72
6.6	Particle Size Measurement	72
6.7	Electrostatic Charging Measurement	73
6.7.1	Charge Measurement by Deflection Method	82
6.7.2	Electrostatic Ball Probe	85
6.8	Air Ionization	90
6.9	Data Logging and Processing	90
CHAPTER 7	DISCUSSION OF ANALYTICAL RESULTS	95
CHAPTER 8	DISCUSSION OF EXPERIMENTAL RESULTS	164
8.1	Analysis of Pressure Drop Data	164
8.2	Analysis of Charge Current Data	172
CHAPTER 9	CONCLUSIONS	234
APPENDIX 1	TURBULENT DIFFUSION IN FULLY DEVELOPED PIPE FLOW	236

		PAGE
APPENDIX 2	NUMERICAL SOLUTION OF EQUATIONS (4.4.2) - (4.4.5)	240
A.2.1	Numerical Method 1	240
A.2.2	Computational Procedure for Program #XFD7B	244
A.2.3	Computer Program #XFD7B	246
APPENDIX 3	NUMERICAL SOLUTION OF EQUATIONS (4.5.2) - (4.5.4)	260
A.3.1	Numerical Method 2	260
A.3.2	Computational Procedure for Program #XFD3B	261
A.3.3	Computer Program #XFD3B	263
APPENDIX 4	COMPUTER PROGRAM #CYP1	269
APPENDIX 5	COMPUTER PROGRAM #PDP1	272
APPENDIX 6	COMPUTER PROGRAM# PDP2	278
APPENDIX 7	COMPUTER PROGRAM #PJO3	286
APPENDIX 8	COMPUTER PROGRAM# PJO4	292
APPENDIX 9	COMPUTER PROGRAM #PJO5	297
APPENDIX 10	COMPUTER PROGRAM #PJO6	301
LIST OF REFERENCES		305

SUMMARY

A test rig has been constructed for the study of dilute turbulent suspension flow consisting of air and small spherical glass particles in a 3.125 cm copper pipeline. Four particle sizes were used : 35μ, 75μ, 82μ and 380μ mean diameter, and the Reynolds number ranged from 40,000 to 80,000 with mass flow ratios of 0.5 to 3.0. A data logging system has also been developed for rapid data recording and processing.

The experimental data of pressure drop measurement show that within the present ranges of mass flow rates and particle sizes, loading of particles would always result in higher pressure drops and to a good approximation, the suspension friction factor can be expressed as a simple function of the mass flow ratio.

Two methods were used for the measurement of electrostatic charges on the particles : the Deflection Method utilizing high-speed photography techniques and the Electrostatic Ball Probe. The charge to mass ratio was less than 10^{-5} C/kg and charges of both signs were present on the particles. The charge current was found to be the order of 10^{-7} A and was always negative. No correlations were obtained between the pressure drop and charge current data.

The general equations of motion which describe the flow characteristics under the simultaneous influences of gravity, electrostatic, relaxation and diffusion effects are formulated and numerical results of distributions of electric potential, density, velocity, mass flux and diffusivity of the particles have been obtained for various mass flow rates, particle sizes and charge to ratios.

While the effect of electrostatic charging has been shown to be significant on the distribution of particulate density, the distribution of particle velocity is mainly determined by the drag force due to the relative motion between the fluid and the particles. The predicted pipe flow distributions are shown to be in reasonable agreement with experimental results obtained by other workers.

SYMBOLS

Due to the large number of different physical quantities included in various formulations, use of the same letters or symbols for different entries or concepts has been unavoidable. Unless otherwise defined in the text, the following symbols, with their meaning, are understood:

a	Particle radius
A_{12}	Area of impact
B	Magnetic induction
C	Capacitance
C_D	Drag coefficient of a sphere
D	Diffusivity
E	Electric field
E_f	Fermi level
F	Inverse of relaxation time for fluid-particle momentum transfer
F_E	Electric field force
F_G	Gravity force
F_L	Magnus lift force
Fr	Froude number
h_{12}	Charge transfer coefficient
I_b	Ball probe current
J_{12}	Current density
J_D	Mass flux of particles due to diffusion
J_F	Mass flux of particles due to relaxation
k	Elastic property as defined in text
K_m	Effective momentum transfer coefficient
Knp	Knudsen number
ℓ	Characteristic length for charge transfer
L_p	Interaction length between fluid and particles
m	Mass of a particle
M_f	Air flow rate

M_p	Solid flow rate
n_p	Particle concentration number density
P	Pressure
P_{12}	Maximum compression at impact
q	Average charge on a particle
Q_{12}	Charge transfer
(q/m)	Charge to mass ratio
γ^*	Ratio of rebound velocity to incoming velocity
R	Pipe radius
Re	Reynolds number
R_L	Lagrangian correlation coefficient
t	Time
T_L	Integral time scale of turbulence
ΔT_{12}	Duration of impact
u,v,w	Velocity components
$\bar{u}$	Mean fluid velocity
u_o	Fluid velocity at pipe axis
u_τ	Frictional velocity
V	Electric potential
V_c	Contact potential difference
z,r,ϕ	Coordinate system
ϕ	Work function or volume fraction of particles
θ	Angle of impact or inclination
σ	Electrical conductivity
ε	Permittivity
$\bar{\mu}$	Viscosity of the fluid material
μ	Viscosity of the fluid phase
μ_p	Viscosity of the particulate phase
μ_m	Viscosity of the gas-solid suspension
$\bar{\rho}$	Density of the fluid material
ρ	Density of the fluid phase
$\bar{\rho}_p$	Density of the solid particle material
ρ_p	Density of the particulate phase

τ	Shear stress
ν	Poisson's ratio or kinematic viscosity
δ_s	Thickness of the viscous sublayer
α,β	
γ & η	Characteristic parameters

Subscripts

i,j	Tensor
f	Fluid phase
m	Gas-solid suspension
p	Particulate phase
w	Pipe wall
o	Pipe axis

Superscripts

*	Dimensionless quantity
(q)	q th component of a multiphase system

LIST OF ILLUSTRATIONS

FIGURES		PAGE
2.1	Energy diagram of two dissimilar bodies.	20
2.2	Origin of the contact potential difference.	21
2.3	Impact between two elastic spheres.	23
4.1	Effectiveness of momentum transfer from solid particles to the gas.	45
4.2	Co-ordinate system.	47
5.1	Composition of total pressure drop of a gas-solid suspension flow.	58
5.2	Effect of loading of particles on pressure drop.	60
6.1	Schematic layout of the test rig.	65
6.2	Pressure transducer circuit diagram.	69
6.3	Experimental curve relating air friction factor to Reynolds number.	71
6.4	Micrograph of type #1 glass beads.	74
6.5	Micrograph of type #2 glass beads.	75
6.6	Micrograph of type #3 glass beads.	76
6.7	Micrograph of type #4 glass beads.	77
6.8	Type #1 glass beads size distribution.	78
6.9	Type #2 glass beads size distribution.	79
6.10	Type #3 glass beads size distribution.	80
6.11	Type #4 glass beads size distribution.	81
6.12	Deflection of a charged particle under the influence of an electric field.	83
6.13	Transparant viewing section used in the particle deflection measurement.	84
6.14	Electrostatic ball probe.	88
6.15	Electrostatic ball probe circuit diagram.	91

FIGURES		PAGE
6.16	Installation of the 3M Ionizer.	92
6.17	Block diagram of the data logging and processing system.	94
7.1 - 7.60	Analytical curves of various distributions in a fully developed turbulent gas-solid suspension flow.	100
7.61	Mass flux and velocity distributions of 50μ glass beads suspended in air.	163
8.1	Typical traces of mass flow rates and ball probe current signals.	166
8.2 - 8.37	Pressure drop data correlation curves.	176
8.38 - 8.57	Charge current data correlation curves.	213
A.2.	Layout of the lattice of mesh points.	241

TABLES

		PAGE
7.1	Summary of analytical results for the flow characteristic equations (4.4.2 - 4.4.5).	161
7.2	Summary of analytical results for the simplified characteristic equations (4.5.2 - 4.5.4).	162
8.1	Typical standard deviations of data signals.	165
A.1	Eddy diffusion of turbulent flows in pipes.	239

CHAPTER I

INTRODUCTION

The dynamics of gas-solid suspension flows apply to phenomena in the fields of pneumatic conveying, fluidized beds, heterogeneous reactors, metallized propellant rockets and xerography. Apart from the direct application to transfer lines in conveying svstems, cases of fully developed turbulent pipe flow of gas-solid suspension have been studied to clarify the basic hydrodynamic interactions and their boundary conditions.

The majority of past experimental investigations has sought to determine the overall pressure drops for various mass flow rates and particle sizes. Although a few studies have emphasized the measurements of particle velocity and density distributions, each investigation, whatever its purpose, has been very limited in scope and usually results for a few isolated cases were reported.

Among those who have directly measured particle velocity are Hinkle (1) and Doig and Roper (2) who used high speed photographic techniques. Doig and Roper's results show that the particle velocity profiles are quite flat and that the particles have a finite velocity at the wall. Similar results were obtained by McCarthy and Olson (3) who photographically measured the particle velocity in a horizontal pipe. Eichhorn et al (4) inserted two sets of fiber optic rods in the suspension flow and calculated the particle velocities from the time taken for a particle to travel between the two sets of rods. More recently, Kramer and Depew (5) used an optical correlation method to measure particle velocity in vertical pipe flows. Soo et al (6) and Preskin and Dwyer (7) obtained their particle velocity profiles from relative mass flux and concentration measurements.

Attempts also have been made to measure the gas velocity profiles when particles are present in the stream. Trotter (8) tested several stagnation pressure probes in gas-solid suspension flows. His results show that the gas velocity profile approaches to a parabolic shape at low particle concentration and then flattens out in the core region at high particle concentration. Doig and Roper

observed similar trends in vertical pipe flows. Van Zoonen (9) deduced similar gas velocity profiles from particle velocity measurement by assuming that the relative velocity between the particles and the gas was equal to the terminal velocity of the particles. In contrast to the results of Doig and Roper, Trotter and Van Zoonen, Soo et al and Preskin reported that the gas velocity profile was unaffected by the presence of the particles. Preskin made similar measurement but with a fiber optic probe.

Particle density distribution was measured by Doig and Roper who used multi-exposure photography techniques. Van Zoonen used a capacitance probe to measure particle mass flux and calculated particle density distribution from the continuity equation. His results indicate an increase in concentration of particles near the wall. Soo et al also calculated the particle number density from relative mass flux measurement and reported similar results. Both Soo et al and Van Zoonen's results agree well with Doig and Roper's results obtained by absolute measurement at low mass flow ratios. However, at high mass flow ratios Doig and Roper reported that the particle concentration reached a maximum at the pipe centre.

Measurements of friction factors and overall pressure drop of gas-solid suspension flows have been made by many investigators. Based on the assumption that addition of solid particles would always lead to a higher pressure drop, Rose and Barnacle (10), Duckworth and Rose (11) and Duckworth and Kakka (12) have independently derived empirical expressions relating the excess pressure drop due to the presence of the solid particles and the basic pipe flow parameters. While the majority of the workers consistently reported that loading of the solid particles always results in an increase in pressure drop or pressure gradient, quite remarkable effects which may be attributed to reduction of turbulence scale, thickening of the viscous sublayer or electrostatic charging have been observed. These involve both reduction and progressive increase in pressure drop due to the presence of the particles (13 - 19).

In pneumatic conveying systems, particles such as quartz, plastics and foodstuffs become electrostatically charged due to surface contact as they impinge on the pipe walls and other boundaries in feeders and cyclone separators. When two bodies of different fermi levels are brought into contact and then separated, the body with the lower fermi level becomes positively charged and the other negatively charged. The sign of the charge conforms to a tribo-electric series (20, 21) and electrification tends to be intensified by heavy impact, long duration of sliding, large exposed surface area and intense rubbing (22, 23). Electrostatic charging phenomena in gas-solid suspension flow have been studied by Cheng and Soo (24) and Cole et al (25).

Many attempts have been made to predict the pipe flow characteristics of suspension of fine particles, typically those by Baw (26), Soo (27), Wakstein (28), Soo and Tung (29) and Nagarajan and Morgatroyd (30). An extensive discussion of the influence of gravity on the suspension flow characteristics, including considerations of particle size, density and relaxation time, and properties of the fluid was given by Soo (27). Gravity effect was shown to be important in the flow of a suspension of sand in water (31) where electrostatic effect would not be prominent. In the case of a gas-solid suspension flow, the charges on the particles can give rise to a space charge field which interacts with turbulent diffusion and relaxation phenomena but gravity effect is small for small diameter pipes or at large Froude numbers (27, 32). However, for flows of gas-solid suspension in large pipes both effects will be significant.

The main objective of this study is basically two-fold:

(i) The apparent anomalies among the pressure drop data obtained by various workers suggest that experimental works should be carried out to investigate the possibilities of both reduction and increase in

pressure drop of the suspension flow due to the presence of the particles as a result of reduction in turbulence scale, thickening of the viscous sublayer or electrostatic charging. However, we shall concentrate mainly on the effect of electrostatic charging in this work.

(ii) It is also desirable that an analytical model should be developed to predict the effects of electrostatic charging, gravity, relaxation and diffusion on the suspension flow characteristics.

CHAPTER 2

ELECTRODYNAMICS OF A GAS-SOLID SUSPENSION

Although the effect of electrostatic charging can be excluded by definition in theoretical analysis or when dealing truly with a boundless system, electrification of the solid particles always occurs when contact and separation are made between the solid particles and a wall of different materials or similar materials but different surface conditions (20 - 23) and, in some cases may even have an overshadowing effect on transport processes (6, 14, 33, 34).

2.1 Charging by Surface Contact

It is well known that electrification always occurs when two bodies of dissimilar materials or surface conditions are brought into contact and then separated. This charging phenomenon can be best explained with the aid of the energy-level diagram. Consider first two bodies with different Fermi levels completely isolated from one another. The materials of these two bodies are for the moment assumed to be metal; however, similar treatment is also applicable to insulators or for a metal with an insulator. A simplified energy level diagram showing the relative Fermi levels E_{f1} and E_{f2} of the two bodies is given in Fig. (2.1).

Upon contact, electrons flow freely from the higher Fermi level E_{f2} to the lower Fermi level E_{f1}. When the Fermi levels of the two bodies become equal, no further electron flow occurs. Fig. (2.2) shows the new situation after the two bodies have equalized their Fermi levels. The surface of the body (1) is now at a different electrical potential from the surface of the body (2) and the potential difference between the two bodies is known as the contact potential difference V_c. Since the electron flow is never very large, V_c is usually of the order of 1 volt or less. Further, V_c can be expressed in terms of the work functions ϕ_1 and ϕ_2 of the two bodies as

$$V_c = \Phi_1 - \Phi_2 \qquad (2.1.1)$$

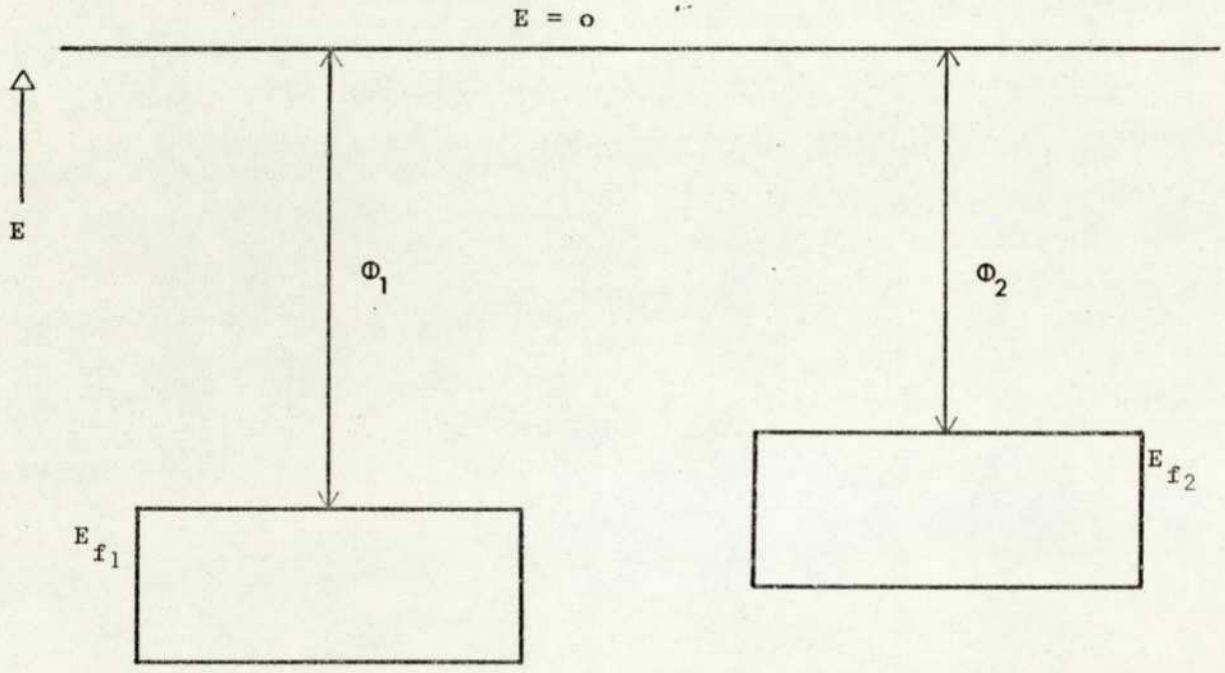

Fig. 2.1. Energy diagram of two dissimilar bodies completely isolated from each other.

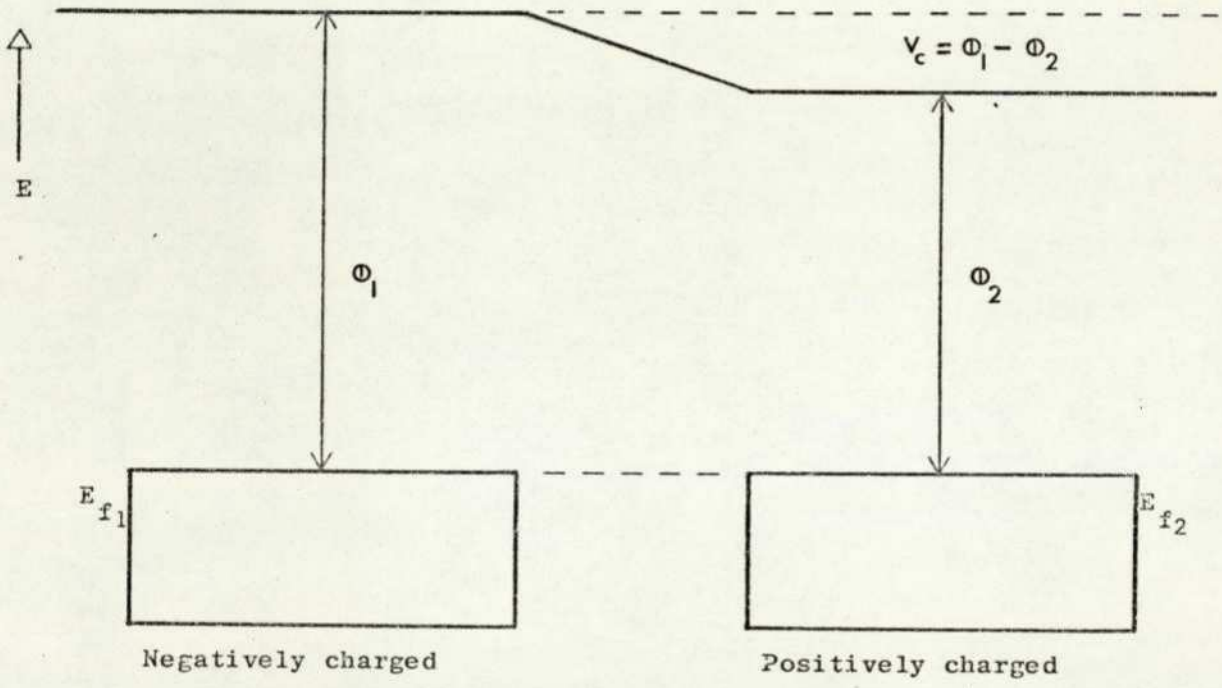

Fig 2.2. Origin of the contact potential difference.

Subsequent separation of the two bodies leaves the one having the lower work function ϕ_2 positively charged and the other negatively charged. The sign of the charge conforms to a triboelectric series (20, 21).

To develop the basic relationship for charge transfer between bodies by impact or collision, consider first the collision of two elastic spheres of radii a_1 and a_2, masses m_1 and m_2, material densities $\bar{\rho}_1$ and $\bar{\rho}_2$, material conductivities σ_1 and σ_2, potentials V_1 and V_2, and velocities u_1 and u_2. The angle of impact θ is defined in Fig. (2.3). The true contact area and the duration of the impact depend on the nature of the contact surface. Even very smooth-appearing surfaces are irregular on a microscopic scale. In fact, on initial contact, one would expect to have at most three contact points. However, under the extremely large pressure of impact, deformation immediately occurs to allow these points to develop into an area of contact. For the idealized system as shown in Fig. (2.3), Rayleigh (35) gave the duration of impact ΔT_{12} as

$$\Delta T_{12} = 5.207 (k_1 + k_2)^{\frac{2}{3}} \left(\frac{a_1 + a_2}{a_1 a_2} \right)^{\frac{1}{3}} \frac{P_{12}^{\frac{2}{3}}}{\Delta u_{12} \cos\theta} \qquad (2.1.2)$$

and the mean area of contact A_{12} as

$$A_{12} = 5.563 (k_1 + k_2)^{\frac{2}{3}} \left(\frac{a_1 a_2}{a_1 + a_2} \right)^{\frac{2}{3}} P_{12}^{\frac{2}{3}} \qquad (2.1.3)$$

where $\Delta u_{12} = |u_1 - u_2|$ is the velocity of approach at the beginning of the impact, k_1 and k_2 are the elastic properties given by

$$k_1 = \frac{(1 - \nu_1^2)}{\pi E_1} \qquad (2.1.4)$$

and

$$k_2 = \frac{(1-\nu_2^2)}{\pi E_2} \qquad (2.1.5)$$

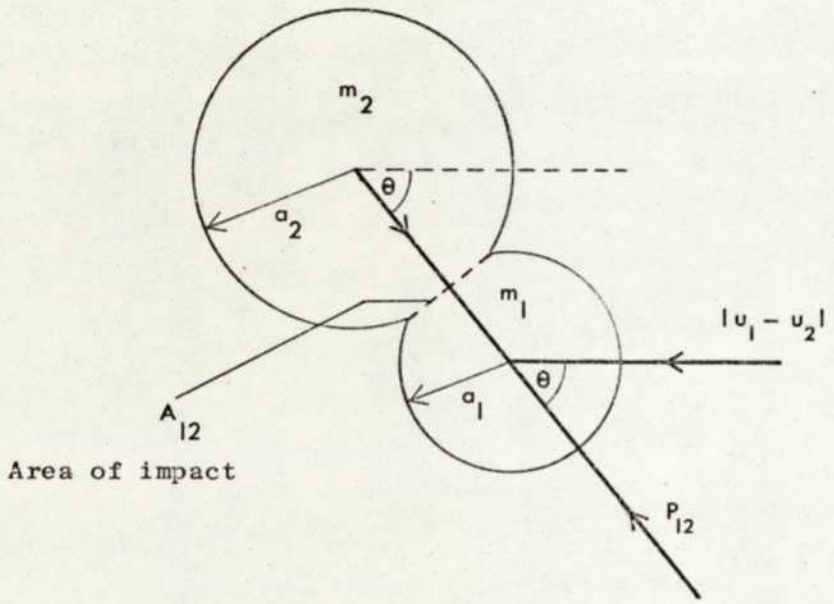

Fig. 2.3. Impact between two elastic spheres.

ν_1 and ν_2 are the Poisson's ratios, and E_1 and E_2 are the moduli of elasticity of the spheres. The maximum compression P_{12} which occurs during the impact is given by

$$P_{12} = 0.535\ (k_1 + k_2)^{-\frac{2}{5}} \left(\frac{m_1 m_2}{m_1 + m_2}\right)^{\frac{3}{5}} \left(\frac{a_1 a_2}{a_1 + a_2}\right)^{\frac{1}{5}} \left\{\Delta u_{12}^2 \left(\frac{1 + \gamma^*}{2}\right) \cos\theta\right\}^{\frac{3}{5}} \qquad (2.1.6)$$

where γ^* is the ratio of the rebound velocity to the incoming velocity.

Over a contact time ΔT_{12}, the current density J_{12} through the mean area of contact Δ_{12} due to charge transfer from sphere (1) to sphere (2) is given by

$$J_{12} = h_{12}\ (V_1 - V_2) = \frac{\sigma_1}{\ell_1}\ (V_1 - V_c) = \frac{\sigma_2}{\ell_2}\ V_c - V_2 \qquad (2.1.7)$$

where h_{12} is the charge transfer coefficient at the contact surface, V_c is the contact potential, and the characteristic charge transfer lengths ℓ_1 and ℓ_2 are expected to be of the same order as a_1 and a_2 respectively (24).

Based on a heat transfer analogy (32), Cheng and Soo (24) gave h_{12} as

$$h_{12} = \left(\frac{\sigma_1 \sigma_2}{\ell_1 \ell_2}\right)^{\frac{1}{2}} \left\{ \left(\frac{\sigma_1 \ell_2}{\sigma_2 \ell_1}\right)^{\frac{1}{2}} + \left(\frac{\sigma_2 \ell_1}{\sigma_1 \ell_2}\right)^{\frac{1}{2}} \right\}^{-1} \qquad (2.1.8)$$

The rate of change of potential of each sphere is given by

$$-C_1 \left(\frac{dV_1}{dt}\right) = C_2 \left(\frac{dV_2}{dt}\right) = J_{12} A_{12} \quad , \qquad (2.1.9)$$

where $C_1 = 4\pi\varepsilon_1 a_1$ and $C_2 = 4\pi\varepsilon_2 a_2$ are the capacitances of the spheres, and ε_1 and ε_2 are the permittivities.

Combining equations (2.1.7) and (2.1.9), we obtain

$$-C_1 \left(\frac{dV_1}{dt}\right) = C_2 \left(\frac{dV_2}{dt}\right) = A_{12} h_{12} (V_1 - V_2) \qquad (2.1.10)$$

For a mean potential difference (V_1-V_2) during the contact, the charge transfer per impact Q_{12} can be obtained from the integration of equation (2.1.10)

$$Q_{12} = h_{12} (V_1 - V_2) A_{12} \Delta T_{12} \tag{2.1.11}$$

where the mean potential difference $(V_1 - V_2)$ is given by

$$V_1 - V_2 = V_c + \frac{q_1}{4\pi\varepsilon_1 a_1} - \frac{q_2}{4\pi\varepsilon_2 a_2} \tag{2.1.12}$$

and q_1 and q_2 are the charges acquired by the spheres.

Finally, combining equations (2.1.2), (2.1.3), (2.1.6) and (2.1.11), we obtain

$$Q_{12} = 12.56 (k_1 + k_2)^{\frac{4}{5}} \left(\frac{a_1 a_2}{a_1 + a_2}\right)^{\frac{3}{5}} \left(\frac{m_1 + m_2}{m_1 m_2}\right)^{\frac{4}{5}} \left(\frac{1 + \gamma^*}{2}\right)^{\frac{4}{5}} \Delta u_{12}^{\frac{3}{5}} \cos\theta^{\frac{-1}{5}} h_{12} (V_1 - V_2) \tag{2.1.13}$$

It is worth noting that in reality, the charge transfer coefficient h_{12} and the contact potential difference $V_c (= \phi_1 - \phi_2)$ are strongly influenced by absorbed surface layers of moisture and surrounding humidity (23).

2.2 Dynamics of a Cloud of Charged Particles

The problem of a cloud of electrically charged particles has been treated analytically by Soo (32, 36) from the point of view of a continuum. In general, the forces and moments acting on a solid particle consist of those due to the net charge, electric dipole in the electric field given rise by the charged particles and external field, and magnetic dipole in the induced magnetic field. Let us consider a large number of uniformly charged particles being kept within a radius R_o in a vacuum. The force F_t acting on a particle due to electric and magnetic fields is given by

$$F_t = q\,(E + U_p \times B) + \nabla(P \cdot E) \qquad (2.2.1)$$

where q is the average charge per particle, E is the electric intensity, U_p is the velocity, P is the dipole moment and B is the magnetic induction which is usually negligible.

If the external constraint is suddenly removed and the particles are allowed to spread into the vacuum, the momentum equation in radial (r) direction is given by (32)

$$m \frac{dv_p}{dt} = qE + \frac{\partial}{\partial r}(PE) \qquad (2.2.2)$$

where
$$E = \frac{1}{4\pi\varepsilon_0 r^2} \int_0^r 4\pi\left(\frac{q}{m}\right) \rho_p r'^2 \, dr' \quad , \qquad (2.2.3)$$

or
$$= \frac{1}{4\pi\varepsilon_0 r^2} \left(\frac{q}{m}\right) M_r \quad , \qquad (2.2.4)$$

for
$$M_r = \int_o^r 4\pi \rho_p r'^2 \, dr' \qquad (2.2.5)$$

and
$$P = \left(\frac{m}{\rho_p}\right)\left\{\frac{3(\varepsilon_r - 1)}{(\varepsilon_r + 2)}\right\} \varepsilon_0 E \qquad (2.2.6)$$

In the above, v_p is the particle velocity in the r-direction, ρ_p is the density concentration of the particles, $\bar{\rho}_p$ is the density of the solid material, m is the mass of a solid particle and ε_r is the dielectric constant.

Substituting equations (2.2.4) and (2.2.6) into (2.2.2), we have

$$\frac{dv_p}{dt} = \frac{1}{\varepsilon_o}\left(\frac{q}{m}\right)^2 \frac{m_r}{4\pi r^2} - \frac{12}{\bar{\rho}_p \varepsilon_o} \frac{(\varepsilon_r - 1)}{(\varepsilon_r + 2)} \left(\frac{q}{m}\right)^2 \left(\frac{m_r^2}{(4\pi)^2 r^5}\right) \quad (2.2.7)$$

It is seen from equation (2.2.7) that the dipole effect due to the gradient of electric intensity produces a deceleration effect against the motion of the particles. The ratio of the force due to dipole F_d to that due to electrostatic repulsion F_r is

$$\frac{F_d}{F_r} = \frac{12(\varepsilon_r - 1)m_r}{\bar{\rho}_p(\varepsilon_r + 2)4\pi r^3} \quad (2.2.8)$$

For a uniform particulate density distribution and $r \to R$, the ratio of F_d/F_r becomes

$$\frac{F_d}{F_r} = \frac{4(\varepsilon_r - 1)\rho_p}{(\varepsilon_r + 2)\bar{\rho}_p} \sim \frac{\rho_p}{\bar{\rho}_p} \quad (2.2.9)$$

Therefore, for a dilute particulate system (i.e. $\bar{\rho}_p >> \rho_p$), the dipole effect due to self-field is negligible.

2.3 Turbulent Flow of Charged Gas-Solid Suspension

We now consider an axi-symmetric system with charged particles moving axially at velocity u_p. The electric field E_r at a radius r is equal to that due to a line source along the axis and is given by

$$E_r = \frac{1}{\pi r \varepsilon_o} \int_o^r 2\pi\rho_p \left(\frac{q}{m}\right) r' dr' \quad (2.3.1)$$

or

$$= \frac{1}{\pi r \varepsilon_o} \left(\frac{q}{m}\right) M'_r \quad (2.3.2)$$

for $$M'_r = \int_0^r 2\pi\rho_p r' dr' \qquad (2.3.3)$$

The equation of motion of the particles in the radial (r) direction due to electric and magnetic field forces is given by

$$\rho_p v_p \frac{\partial v_p}{\partial r} = - JB_\theta + \rho_p \left(\frac{q}{m}\right) E_r \quad , \qquad (2.3.4)$$

where J is the current density due to the mass motion of the particles i.e.

$$J = \rho_p \left(\frac{q}{m}\right) u_p \quad , \qquad (2.3.5)$$

and the magnetic induction B_θ in the circumferential (θ) direction due to the axial motion of the particles

$$B_\theta = \frac{1}{2} \mu J r \qquad (2.3.6)$$

where μ is the permeability of the particle field.

Similarly, it can be seen from equations (2.3.2) to (2.3.6) that the effect of the induced magnetic field on the motion of the particles becomes significant only when

$$u_p^2 \sim \frac{1}{\mu\varepsilon_o} \qquad (2.3.7)$$

Since $1/\mu\varepsilon_o$ is the square of the speed of light in the medium under consideration, we can again neglect the effect due to the induced magnetic field in particulate system. In the case of a turbulent suspension flow of charged solid particles in a pipe made of conducting material, the inside wall of the pipe forms a closed equi-potential surface regardless of its charge and there is no electric field inside of the pipe due to its wall (Gauss law).

This would mean that the particles will be driven towards the wall by electrostatic repulsion among themselves and eventually settle at the pipe wall if there is no fluid turbulence; a sustained gas-solid suspension will therefore have to be due to turbulent diffusion from the wall. The order of magnitude is such that for small glass beads being transported in air at a loading ratio of 1 kg of solids per kg of air, equation (2.3.4) shows that at radius 1 cm from the pipe axis, the acceleration due to the electric field is about 10 times that due to gravity for a charge to mass ratio (q/m) of 0.002 coulomb per kg (36).

2.4 Static Reduction

Very large electric charges are nearly always produced when materials are handled or manipulated but they are not often observed because in most circumstances they immediately leak waay or become neutralized. The build up of these charges can constitute fire and health hazards because of the danger of arcs and high voltage breakdown. A detailed survey of harmful static electrification is given in Reference (37). The methods that are commonly used in static reduction can be summarized as follows:

(a) Relative Humidity: The use of water sprays to raise the humidity (i.e. leaving a water film on the material surface) is an effective method of decreasing the electrical resistance of hydrophilic substances (e.g. glass, glazed porcelain), others such as polythene are less ready to accept water films on their surfaces. Several workers (38, 39, 40) have observed that static electrification in fluidization varies with the relative humidity of the fluidizing gas and at a humidity of about 60% would prevent excessive build-up of charges during fluidization. However, it should be noted that the charges on particles of insulating material will not be dissipated even in damp conditions unless there is a conducting path to earth available (e.g. earthing wires).

(b) Conductivity Agents: Static reduction can also be achieved by treating the surface of insulating materials with electrically conducting films (e.g. metal carbon, conducting rubber). This technique could be useful in pneumatic conveying and fluidizing systems provided the related medium does not hinder the free movement of the particles.

(c) Air Ionization by Electrical Discharge: By ionizing the surrounding air, ions from the air can neutralize the charge resident on the static sources. The efficiency of utilization of ionized air will depend on the effectiveness of the static field in 'pulling' in ions for neutralization of the static charge. Air ionization can be effected by application of a potential of about 8 - 12 kV to a set of fine wires so that a corona discharge is set up at the tips of the wires. However, this method is effective only in the absence of a conducting neighbouring surface because such objects would attract the generated ions by induction effects.

(d) Air Ionization by Radioactive Substances: Static elimination by radioactive sources is an established technique (41) but generally is not very effective when the time available for neutralization is short. Also, a limit may have to be put on the source size for safety reasons. α rays provide the highest concentration of ions but if the source also emits γ rays, the system may be unsafe. β rays sources are capable of generating as many ions as α rays but have a greater penetration and are readily available free from γ rays.

CHAPTER 3

MOTION OF SOLID PARTICLES SUSPENDED IN A TURBULENT FLUID

Preparatory to the analytical treatment of gas-solid suspension flow, it is desirable to give a brief account of the transport phenomena of solid particles suspended in a turbulent fluid. When the stream conditions are such that the flow is inherently turbulent, the interactions between the particles and the fluid are far more complex than in the case of laminar flow. Consequently, this situation is generally less amenable for detailed analysis. The starting point for such an analysis is the motion of a single particle in a turbulent field. It is well known that no established and completely satisfactory procedure is available for treating this subject. The coverage here is intended to demsonstrate the need for a different method of approach.

3.1 Diffusion of Discrete Particles in a Turbulent Fluid

For very dilute particulate systems (i.e. the volume fraction of the particles, ϕ, is less than 1%), we may neglect the interactions between the particles through mutual collisions and through effects on the flow of the fluid in the neighbourhood of the particles, and regard each particle as being alone in the flow field. (This is usually true because under this condition ($\phi < .01$), the particles are at least 5 particle diameters apart).

The character of the particle motion depends on its size relative to the scale of turbulence of the flow as well as its density relative to that of the fluid. Owen (42) suggested if the scale of the mean motion of the fluid is the radius of the pipe R, then the scale of the energetic eddies is of the order of R/10. The condition for imperfect response to the energy containing eddies is

$$F = \frac{10u_\tau}{R} \qquad (3.1.1)$$

where u_τ is the frictional velocity at the pipe wall, $(R/10 \cdot u_\tau)$ is the time scale of the small eddies and the inverse of relaxation time F for momentum transfer between the fluid and the particles is given by

$$F = \frac{3}{4} \frac{C_D|u - u_p|}{a(1 + 2\bar{\rho}_p/\bar{\rho}} \qquad (3.1.2)$$

In equation (3.1.2), a is the radius of a particle, $|u - u_p|$ is the relative velocity between the fluid and particles, $\bar{\rho}$ is the density of the fluid, $\bar{\rho}_p$ is the density of the particles and the drag coefficient C_D is a function of the particle Reynolds number $(Re_p = 2a\bar{\rho}\,|u - u_p|/\bar{\mu})$ i.e.

$$C_D = C_D\,(Re_p) \qquad (3.1.3)$$

For slow relative motion ($Re_p < 1$), Stoke's law of drag of a sphere applies (i.e. $C_D = 24/Re_p$) and equation (3.1.2) reduces to

$$F_s = \frac{9\bar{\mu}}{a^2(2\bar{\rho} + \bar{\rho})} \qquad (3.1.4)$$

Generally, C_D is influenced by the relative turbulent intensity between the fluid and particles. In fact both reduction and increase in C_D as compared with that given by the so-called standard drag curve (43) have been reported (44, 45).

The condition for imperfect response to the large eddies whose scale is comparable with the pipe radius R is

$$F < \frac{u_\tau}{R} \qquad (3.1.5)$$

A simplified situation of the turbulent flow of dilute gas-solid suspension is the case of single particle motion in a turbulent stream. Based on the effects treated by Basset, Boussinesq and Oseen and subsequent modifications by Tchen (46), the equation of motion of

a spherical particle, from a Lagrangian view can be written as

$$\frac{4\pi}{3} a^3 \bar{\rho}_p \frac{dU_p}{dt} = 6\pi\bar{\mu}a(U - U_p) - \frac{4\pi}{3} a^3 \frac{\partial P}{\partial r} + \frac{1}{2} \frac{4\pi}{3} a^3 \frac{d}{dt} (U - U_p) + 6a^2(\pi\bar{\rho}\bar{\mu})^{\frac{1}{2}} \int_{t_o}^{t} \frac{(d/d\tau)(U - U_p)d\tau}{(t - \tau)^{\frac{1}{2}}} + F_e \qquad (3.1.6)$$

where

$$\frac{d}{dt} = \frac{\partial}{\partial t} + (U_p \cdot \nabla) \qquad (3.1.7)$$

The meaning of the various terms in equation (3.1.6) is as follows: The term on the LHS is the force required to accelerate the particle. The first term on the RHS is the viscous drag from Stoke's law. The second term is due to the pressure gradient in the fluid surrounding the particle caused by the acceleration of the fluid. The third term is the force required to accelerate the apparent mass of the particle relative to the ambient fluid. The fourth term is the so-called "Basset" term which takes account of the effect of the deviation in flow pattern from steady state. The last term F_e is the force due to external field. In general, the second, third and fourth terms on the RHS of equation (3.1.6) become important only if the density of the fluid becomes comparable to or higher than that of the particle. The Basset term constitutes an instantaneous flow resistance which becomes substantial (i.e. many times its value at steady state) when the particle is accelerated at high rates (47).

With various assumptions and approximations, Tchen (46) took a Lagrangian spectrum of turbulence and treated a stationary case (i.e. without considering the probability for a particle to be at a certain state at any time but considering what would happen if it is there). Tchen's study was further extended by Hinge (48) in the determination of intensities and diffusivities. He assumed

an exponential form for the Lagrangian correlation coefficient $R_L(t)$ as

$$R_L(t) = \exp(-t/T_L) \tag{3.1.8}$$

and obtained the following relationships:

$$\frac{\overline{\hat{u}^2_p}}{\overline{\hat{u}^2}} = \frac{F_s T_L + G}{F_S T_L + 1} \tag{3.1.9}$$

and

$$\frac{D_p}{D_f} = 1 + \left\{\frac{1 - G^2}{(F_S T_L)^2 - 1}\right\} \left\{\frac{\exp(-F_s t) - \exp(-t/T_L)}{1 - \exp(-t/T_L)}\right\} \tag{3.1.10}$$

where $\overline{\hat{u}^2}$ and $\overline{\hat{u}^2_p}$ are the mean square velocity fluctuations of the fluid and the particles, T_L is the integral time scale of turbulence (Appendix 1) and G is defined as

$$G = \frac{3\bar{\rho}}{(2\bar{\rho}_p + \bar{\rho})} \tag{3.1.11}$$

It can be seen from equation (3.1.9) that if $\bar{\rho}_p = \bar{\rho}$ (i.e. G = 1), the velocity fluctuations and diffusivities of the fluid and particles are the same (i.e. the fluid and particles move together). For solid particles in air, $\bar{\rho}_p >> \bar{\rho}$ (i.e. G = 0), the particle fluctuation velocity is less than that of the fluid unless $F_S T_L >> 1$, which should be true for very small a. For short diffusion times ($T_L >> t$), equation (3.1.10) reduces to

$$\frac{D_p}{D_f} = \frac{F_S T_L}{1 + F_S T_L} = \frac{\overline{\hat{u}^2_p}}{\overline{\hat{u}^2}} \tag{3.1.12}$$

Under these conditions, the particle spread can be much less than that of the fluid if $F_S T_L$ is not much greater than unity. For long diffusion time ($t >> T_L$), equation (3.1.10) reduces to

$$\frac{D_p}{D_f} = 1 \tag{3.1.13}$$

These results of diffusivity ratio (equations (3.1.12) and (3.1.13)) were first given by Tchen.

Several workers have assumed that the very small particles would follow the fluid exactly which gives the immediate results that the ratio of D_p/D_f is unity for all time. In contrast, equation (3.1.10) predicts $(D_p/D_f) = 1$ for long diffusion time only. Using the concept of spectrum of isotropic turbulence and an approximation for $R_L(t)$, Soo (49) obtained

$$\frac{\overline{\hat{u}^2}_p}{\overline{\hat{u}^2}} = 1 - \frac{1}{2}K^2 + \frac{3\cdot1}{2^2}K^4 - \frac{5\cdot3\cdot1}{2^3}K^6 + \ldots. \qquad (3.1.14)$$

for $K << 1$, where

$$K = \frac{2}{F_S T_L} \qquad (3.1.15)$$

is defined as an impulse response parameter.

To account for the effect due to wall interference, Soo and Tien (50) introduced a perturbation parameter $\varepsilon(= a^3G/8)$ and modified equation (3.1.14) into

$$\frac{\overline{\hat{u}^2}_p}{\overline{\hat{u}^2}} = \frac{\pi^{\frac{1}{2}}}{K}\left\{1 - \frac{2\varepsilon}{y^3}\left(\frac{1}{2} + \frac{1}{K^2}\right)\right\}\exp(K^2)\operatorname{erfc}(K^{-1}) - \frac{2\varepsilon}{K^2y^3}$$

where y is the distance from the wall. (3.1.16)

It is seen that the presence of wall effectively reduces the intensity of motion of the particle.

By the introduction of a pseudo-turbulent velocity field, Ahmadi and Goldschmidt (51) were able to solve equation (3.1.6) numerically and obtained solutions for particles of different sizes and densities. Their results indicate that D_p increases with particle size but decreases with particle density. Further, as the particle size approaches zero, the ratio of D_p/D_f becomes unity and is independent of particle density.

Experimental determination of the turbulence characteristics of a suspension of small glass particles (50 - 210μ) was made by Soo et al (33). Within the range of moderate solid loadings (0.2 - 0.4 lb/min), they found that the scale of turbulence and eddy diffusivity were not appreciably affected by the presence of the particles and that the turbulent motion of the particles was anisotropic with $(D_p/D_f) < 1$. Similar results were also obtained by Preskin and Dwyer (7) and Kada and Hanratty (52). More recently, Suneja and Wasan (34) studied the dispersion of both charged and uncharged potassium chloride particles under transverse flow conditions and found that both the diffusion and concentration distribution of the particles were affected by the presence of charges on them.

3.2 Effects of Electrostatic Force

Particles are usually charged in gas-solid flow systems and in the case of a gas-solid suspension flow in a metal pipe, there exists a layer of surface charge at the inner pipe wall being equal in magnitude but opposite in sign to the total charge enclosed by the pipe wall so that there is no electric field inside the pipe due to the wall. The electric potential V at an inner point is given by the Poission's equation

$$\nabla^2 V = -\left(\frac{q}{m}\right)\frac{\rho_p}{\varepsilon_o} \qquad (3.2.1)$$

where ρ_p is the local density of particles, (q/m) is the average charge to mass ratio and ε_o is the permittivity of the fluid (air).

The force F_E acting on a particle due to the local electric field E is given by

$$F_E = qE = -q\nabla V \qquad (3.2.2)$$

If no other external forces exist, the concentration of the particles is higher at the wall than at the centre, and in the case of a non-conducting pipe, effect of non-uniform charge on the wall may show up.

3.3 Effects of Gravity Force

An extensive discussion of the influence of gravity force on suspension flow was given by Soo (27). It was shown that gravity effect was negligible in small pipes or at high Froude numbers but more significant in the flow of water-sand suspension, where electrostatic charge effect would not be prominent.

Gravity effect can be neglected if the material densities of the fluid $\bar{\rho}$ and particles $\bar{\rho}_p$ are the same or if the intensity of the particle motion due to fluid drag or electrostatic force is much greater than that due to gravity. For a pipe making an angle θ with the direction of gravity, the axial and vertical components of gravity force acting on a particle are simply

$$F_A = mg \cos \theta \qquad (3.3.1)$$

and

$$F_V = mg \sin \theta \qquad (3.3.2)$$

3.4 Effects of Magnus Lift Force

The existence of Magnus effect, the lift force acting on particles suspended in a fluid has long been recognized. Poiseuille (53) noticed a corpuscle-free region near the wall of the capillary

during his study of blood flow phenomena. Vejlens (54) observed the trajectories of spherical particles being released from near the wall of a square-cross section tube and found that the particles moved rapidly away from the wall as the particle size increased. One extensive study on this subject was done by Saffman (55) who gave the lift force acting on a sphere of radius a in the radial direction as

$$F_L = 6.46\ (\bar{\rho}\bar{\mu})^{\frac{1}{2}}\ (u_p - u - \Delta u)\ \left|\frac{du}{dr}\right|^{\frac{1}{2}}\ a^2 \qquad (3.4.1)$$

where Δu is the effective velocity of the sphere and $|d\mu/dr|$ is the fluid shear. Saffman further showed that this lift force existed even if the sphere was prevented from rotating.

CHAPTER 4

CONTINUUM MECHANICS OF A GAS-SOLID SUSPENSION FLOW

The continuum mechanics of a multiphase system has been treated by Hinze (48) and extensively by Soo (32), and it has been demonstrated that when dealing with a particulate system or a gaseous mixture of disparate molecular masses, continuum mechanics can be extended to treat the motion of an individual component interacting with other components of the mixture. Treating a mixture as a number of pure components occupying the same volume in space, the density of a mixture ρ_m is given by

$$\rho_m = \sum_{(q)} \rho^{(q)} \tag{4.1}$$

where $\rho^{(q)}$ is the density of component (q) of the mixture occupying the volume of the mixture of n components (q=1,...n).

The i th component of velocity of the mixture U_{mi} is given by

$$\rho_{mi}\, U_{mi} = \sum_{(q)} \rho^{(q)}\, U_i^{(q)} \tag{4.2}$$

and the continuity equation of the mixture is therefore

$$\frac{\partial \rho_m}{\partial t} + \frac{\partial}{\partial x_j} (\rho_m u_{mi}) = 0 \tag{4.3}$$

Illustrating with a Newtonian fluid, the momentum equation of a mixture can be written in the following form,

$$\rho_m \frac{dU_{mi}}{dt_m} = \frac{\partial}{\partial x_j} - P_m \delta_{ji} + \mu_m (\Delta_m)_{ji} + \mu_{m2} \theta_m \delta_{ji} + \rho_m F_{mi} \tag{4.4}$$

where

$$\frac{d}{dt_m} = \frac{\partial}{\partial t} + U_{mj} \frac{\partial}{\partial x_j} \quad , \tag{4.5}$$

the deformation tensor,

$$(\Delta_m)_{ji} = \frac{\partial U_{mi}}{\partial x_j} + \frac{\partial U_{mj}}{\partial x_i} \tag{4.6}$$

the dilatation,

$$\theta_m = \frac{1}{2} (\Delta_m)_{kk} = \frac{\partial U_{mk}}{\partial x_k} \quad , \tag{4.7}$$

and P_m is the overall static pressure of the mixture, μ_m its viscosity, $\mu_{m2} = \zeta_m - \frac{2}{3} \mu_m$, ζ_m is the bulk viscosity and F_{mi} is the i th component of the body force.

For the component (q) of the mixture, the momentum equation can be expressed as

$$\frac{\rho^{(q)} dU_i^{(q)}}{dt^{(q)}} = \frac{\partial}{\partial x_j} -P^{(q)} \delta_{ji} + \mu_m^{(q)} \Delta_{ji}^{(q)} + \mu_{m2}^{(q)} \theta^{(q)} \delta_{ji}$$

$$+ \rho^{(q)} F_i^{(q)} + \rho^{(q)} \sum_{(p)} F^{(qp)} (U_i^{(p)} - U_i^{(q)}) \tag{4.8}$$

where

$$\frac{d}{dt^{(q)}} = \frac{\partial}{\partial t} + U_j^{(q)} \frac{\partial}{\partial x_j} \tag{4.9}$$

$P^{(q)}$ is the static partial pressure of component (q), $F_i^{(q)}$ is the i th component of body force on a unit mass of (q), $F^{(qp)}$ is the time constant of momentum transfer between component (q) and (P), and the deformation tensor and dilatation have similar meaning as defined by equations (4.6) and (4.7) respectively. Further, the interaction of components is such that

$$\sum_{(q)} \sum_{(p)} \rho^{(q)} F^{(qp)} (U_i^{(p)} - U_i^{(q)}) = 0 \tag{4.10}$$

4.1 Behaviour of a Dilute Gaseous Suspension of Particles

Recognizing that in a particulate system, particles of different sizes constitute different phases from the point of view of continuum mechanics, the general formulation of such a system is very complicated. Here we shall consider the idealized case of a dilute suspension ($\phi < .01$) of monodispersed spherical particles such that, in spite of visual discreteness, it may be treated as a quasi-continuum. In addition the following assumptions are made:

(i) The fluid is incompressible and the effect due to its bulk viscosity can be neglected.

(ii) In a dilute suspension with a volume fraction of particles ϕ less than 0.01, the particles are at least 5 particle diameters apart and therefore particle-particle interaction is negligible being compared with particle-fluid interaction. Further, the motion and statistical properties of the fluid are not affected by the presence of the particles (7, 33, 52).

(iii) The drag force acting on the particles is mainly due to the relative motion between the particles and can be found by summation of the drag forces upon individual particles.

(iv) The random velocity of each particle due to its own thermal state is extremely low and Brownian motion can be neglected.

(v) Deceleration of the particles only results in dissipation of energy in wakes and does not contribute to recovery of static pressure; this basic mechanism being confirmed by the kinetic theory of a mixture of disparate molecular masses (32).

(vi) Electrostatic charges on the particles are of the same sign and magnitude, and the presence of these charges can give rise to a space charge field which may interact with turbulent diffusion and relaxation phenomena, though the effects due to electric and magnetic dipoles can be neglected if the electric potential gradient is small (section 2.2).

For the sake of generalization, we shall term the phase constituted by the particles as the particulate phase which has a particulate density distribution ρ_p such that the density of the suspension (mixture) ρ_m is given by

$$\rho_m = \rho_p + \rho \tag{4.1.1}$$

where ρ is the density of the fluid phase. For $\phi < 0.01$, ρ can be approximated by the material density of the fluid $\bar{\rho}$.

4.2 Dynamic Equations of a Dilute Suspension

For a solid particle of finite size, we know that there is a velocity distribution around the particle due to its relative motion and when the relative velocity is high enough, the existence of a wake is expected. Therefore, the concept of continuum mechanics when applied to a particulate suspension must be properly qualified by examining the nature of the fluid motion surrounding the particles.

In the absence of shear motion and body force, the momentum equation of a gaseous suspension of uniformly sized particles can be obtained from equation (4.8) as

$$\rho \frac{dU_i}{dt} + \rho_p \frac{dU_{pi}}{dt_p} = -\frac{\partial P}{\partial x_i} \tag{4.2.1}$$

It is noted that equation (4.2.1) treats the particulate phase as a true continuum i.e. momentum is transferred from the fluid to the particles and vice versa. Soo (32) suggested if the particles are to exert sufficient 'drag' on the fluid, the interparticle spacing ($2a_j$) must be smaller than $2(\delta + a)$ in which δ is the boundary layer thickness at separation and a is the particle radius. According to the experimental results obtained by Froessling (43),

δ is given approximately by

$$\delta \sim (18/Re_p)^{\frac{1}{2}} a \qquad (4.2.2)$$

where Re_p is the particle Reynolds number.

For a uniform particulate density distribution $\rho_p (= \phi \bar{\rho}_p)$, a_i is given by

$$a_i = (\bar{\rho}_p / \rho_p)^{\frac{1}{3}} a = (1/\phi)^{\frac{1}{3}} a \qquad (4.2.3)$$

This leads to the condition for successful transfer of momentum of mass motion with the particle accelerating the fluid

$$\delta + a \geq a_i$$

or

$$\rho_p \geq \bar{\rho}_p (1 + (18/Re_p)^{\frac{1}{2}})^{-3} \qquad (4.2.4)$$

otherwise the fluid simply acts as a free stream with the kinetic energy of the particles dissipated completely in their wakes.
The order of magnitude is such that for a suspension flow of small glass particles ($\bar{\rho}_p \sim 2500$ kg/m^3) in a 3.125 cm diameter pipe with an average air velocity $\bar{u}$ of 20 m/s and $Re_p = 2$, it would require a mean particle concentration of $\rho_p = 39$ kg/m^3 and a mass flow rate ($\sim \pi R^2 \rho_p \bar{u}$) of 0.6 kg/s or a mass flow ratio of 32.
(It should be noted that these figures are used for demonstration purpose only. At high mass flow ratios, particle deposition at the pipe wall and saltation may occur and the flow is no longer fully developed).

To account for all situations, Soo (32) introduced an effective momentum transfer parameter K_m and modified equation (4.2.1) into

$$\rho \frac{dU_i}{dt} + K_m \rho_p \frac{dU_{pi}}{dt_p} = - \frac{\partial P}{\partial x_i} \qquad (4.2.5)$$

for $K_m = 1$ when particles are accelerated by the fluid, and $K_m < 1$ when particles are decelerated by the fluid. In the absence of experimental information, K_m can only be expressed as a discontinuous function of the parameter $\{2a\bar{\rho}(u - u_p)/\bar{\mu}\}(2a)^{-2}n_p^{-2/3}$ as shown in figure (4.1), though a smooth transition is expected. (n_p is the particle number concentration i.e. $\rho_p = 4\frac{\pi}{3}a^3\bar{\rho}_p n_p$)

With this understanding of the qualified continuum approximation, the momentum equation of a suspension of single species of particles now becomes

$$\begin{aligned}\rho dU_i/dt + K_m\rho_p dU_i/dt_p = &-\partial P/\partial x_i + \partial(\bar{\mu}\Delta_{ji})/\partial x_j \\ &+K_m\partial(\mu_p(\Delta_p)_{ji})/\partial x_j + \rho F_i \\ &+K_m\rho_p f_{pi}/m \qquad (4.2.6)\end{aligned}$$

and that for the particulate phase

$$\begin{aligned}\rho_p dU_{pi}/dt_p = &-(\rho_p/\bar{\rho}_p)\partial P/\partial x_i + \rho_p F(U_i - U_{pi}) + \partial(\mu_p(\Delta_p)_{ji})/\partial x_j \\ &+\rho_p f_{pi}/m + \rho_p f'_{pi}/m \qquad (4.2.7)\end{aligned}$$

where f_{pi} is the force acting on each particle by external field forces, f'_{pi} is the fluid force acting on each particle given by equation (3.1.6) and F_i is the body force acting per unit mass of the fluid. For a dilute suspension ($\rho_p/\bar{\rho}_p \ll 1$), the pressure gradient term in equation (4.2.7) can be neglected.

The momentum equation of the fluid phase is obtained by subtracting equation (4.2.7) from equation (4.2.6), i.e.

$$\begin{aligned}\rho dU_i/dt = &-(1-K_m\rho_p/\bar{\rho}_p)\partial P/\partial x_i + \partial(\bar{\mu}\Delta_{ji})/\partial x_j - K_m F\rho_p(U_i - U_{pi}) \\ &+\rho F_i - K_m\rho_p f'_{pi}/m \qquad (4.2.8)\end{aligned}$$

For a dilute gas-solid suspension, viscous forces are mainly contributed by the principal fluid while transfer of momentum of the particles taken place through the action of particle diffusion D_p which is defined as

$$D_p = \mu_p/\rho_p \qquad (4.2.9)$$

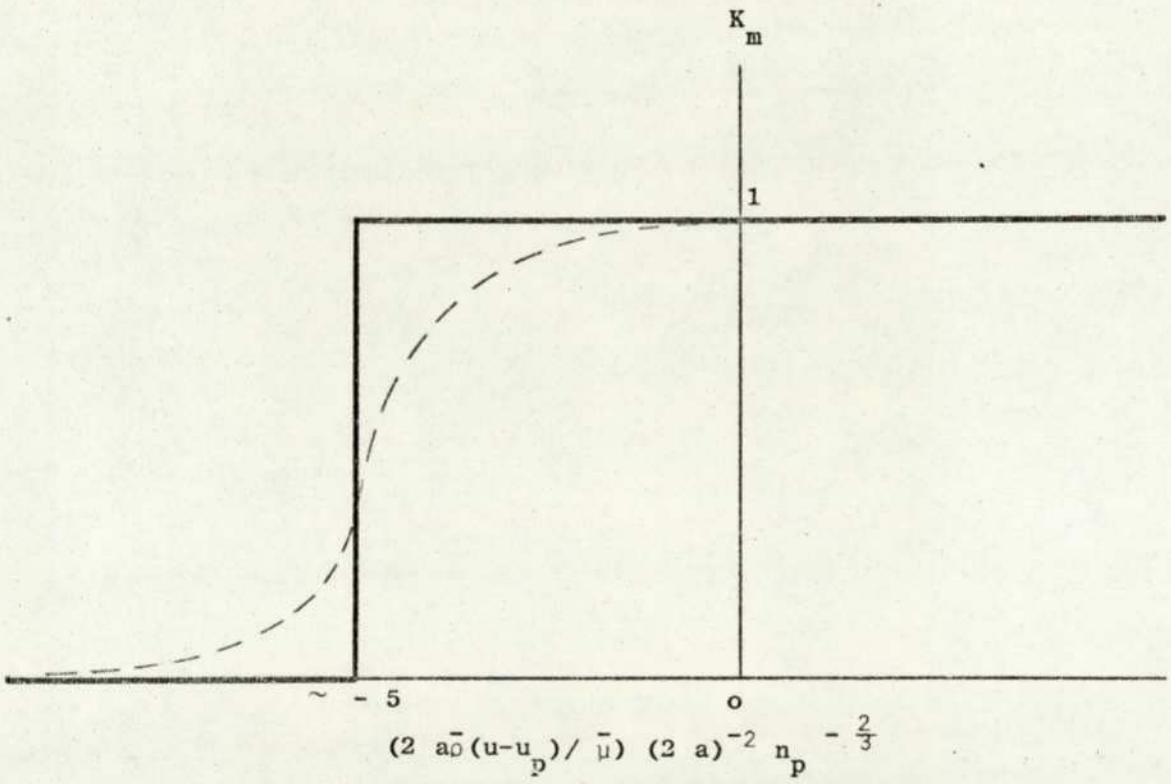

Fig. 4.1. Effectiveness of momentum transfer from solid particles to the gas. (Ref.60).

In place of the continuity equation which is convenient in the absence of relaxation phenomena or external field forces, the equation of diffusion of the particulate phase may be written as

$$\partial\rho_p/\partial t = -\partial(J_{Dj} + J_{Fj})/\partial x_j \qquad (4.2.10)$$

where

$$J_{Dj} = -D_p \partial\rho_p/\partial x_j \qquad (4.2.11)$$

is the mass flux due to diffusion (Fick's law) and

$$J_{Fj} = \rho_p(U_{pj} - U_j) \qquad (4.2.12)$$

is the mass flux due to external fields (i.e. relaxation).

4.3 Fully Developed Turbulent Flow of a Gas-Solid Suspension

The equations of motion of a fully developed turbulent flow of gas-solid suspension based on the foregoing analysis can now be reduced to simple forms, and in terms of the coordinate system (r, z, ϕ) as shown in figure (4.2), fully developed flow exists with $\partial/\partial t = 0$, $v = v_p = 0$, $w = w_p = 0$ and $\partial u/\partial z = \partial u_p/\partial z = 0$. For a pipe making an angle θ with the direction of gravity, the overall momentum equation for the suspension in the z-direction may be obtained from equation (4.2.6)

$$-(\partial P/\partial z)_m - (\rho + K_m\rho_p)g\cos\theta + \{\partial r(\tau_{zr} + K_m\tau_{pzr})/\partial r\}/r$$

$$+ \{\partial(\tau_{z\phi} + K_m\tau_{pz\phi})/\partial\phi\}/r = 0 \qquad (4.3.1)$$

For $\bar{\rho}_p \ll \bar{\rho}$, the pressure gradient term in equation (4.2.7) can be neglected and the equation of motion of the particulate phase becomes

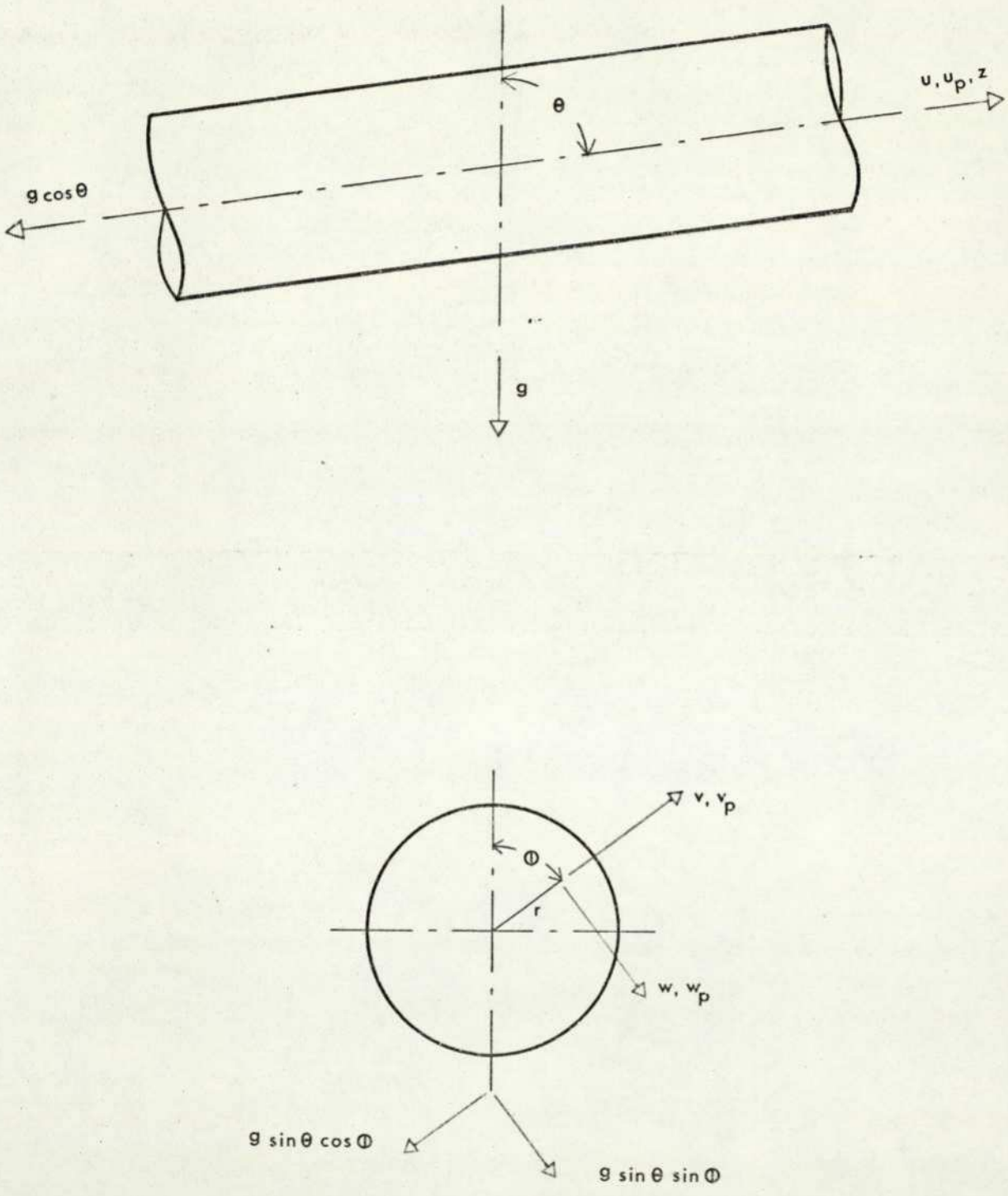

Fig. 4.2. Co-ordinate system.

$$-\rho_p(1 - \bar{\rho}/\rho_p)g\cos\theta + \{\partial(r\tau_{pzr})/\partial r\}/r + \{\partial\tau_{pz\phi}/\partial\phi\}/r + F\rho_p(u - u_p) = 0 \qquad (4.3.2)$$

and similarly for the fluid phase

$$-(\partial P/\partial z)_m - \rho g\cos\theta + \{\partial(r\tau_{zr})/\partial r\}/r + \{\partial\tau_{z\phi}/\partial\phi\}/r - K_m\rho_p\bar{\rho}g\cos\theta/\bar{\rho}_p - K_mF\rho_p(u - u_p) = 0 \qquad (4.3.3)$$

In equations (4.3.1) - (4.3.3), F is the inverse of relaxation time for momentum transfer given by equation (3.1.2) and the 'shear stresses' τ_{pzr} and $\tau_{pz\phi}$ of the particulate phase are defined as

$$\tau_{pzr} = \rho_p D_p \partial u_p/\partial r \qquad (4.3.4)$$

and

$$\tau_{pz\phi} = \rho_p D_p (\partial u_p/\partial\phi)/r \qquad (4.4.5)$$

Next we consider the diffusion of the particles. Under fully developed flow conditions, the sum of the mass fluxes due to diffusion J_D and field force J_F must be zero so that there is no net deposition of particles at the wall. (Equations (4.2.11) and (4.2.12)). Thus,

$$J_D + J_F = -D_p\nabla\rho_p + \rho_p(U_p - U) = 0 \qquad (4.3.6)$$

where $(U_p - U)$ can be determined from the equation of motion of an individual particle under steady state condition,

$$dU_p/dt = F(U - U_p) + F_p/m = 0 \qquad (4.3.7)$$

Combining equations (4.3.6) and (4.3.7), we obtain

$$-D_p \nabla \rho_p + \rho_p F_p / mF = 0 \qquad (4.3.8)$$

where the field force F_p includes the electrostatic force F_E, the Magnus lift force F_L in the radial direction and the gravity force F_G i.e.

$$F_p = F_E + F_L + F_G \qquad (4.3.9)$$

The electrostatic force F_E is given by equation (3.2.2)

$$F_E = -q\nabla V \qquad (4.3.10)$$

and the gravity force F_G can be expressed as

$$F_{Gr} = -(1 - \bar{\rho}/\bar{\rho}_p) mg\sin\theta\cos\phi \qquad (4.3.11)$$

in the r-direction and

$$F_{G\phi} = (1 - \bar{\rho}/\bar{\rho}_p) mg\sin\theta\sin\phi \qquad (4.3.12)$$

in the ϕ-direction.

For the present study we shall consider the case when the particles are not too small compared with the thickness of the viscous sublayer δ_s which is related to the fluid velocity u_o at the core by

$$\delta_s = 60(u_o R\bar{\rho}/\bar{\mu})^{\frac{-7}{8}} R \qquad (4.3.13)$$

and since the shear rate $\partial u/\partial r$ is significant only within δ_s, the lift force F_L can be neglected. (See equation (3.4.1)).

Re-writing equation (4.3.8) in terms of components (r, ϕ), we have

$$-D_p \partial\rho_p/\partial r - (q/m)(\rho_p/F)\partial V/\partial r - \rho_p(1 - \bar{\rho}/\bar{\rho}_p) g\sin\theta\cos\phi/F = 0 \qquad (4.3.14)$$

in the r - direction and

$$-D_p(\partial\rho_p/\partial\phi)/r - (q/m)(\rho_p/Fr)(\partial V/\partial\phi) + \rho_p(1 - \bar{\rho}/\bar{\rho}_p)g\sin\theta\sin\phi/F = 0 \qquad (4.3.15)$$

in the ϕ - direction.

The electric potential V is given by the Poisson's equation, equation (3.2.1) as

$$\{\partial(r\partial V/\partial r)/\partial r\}/r + \{\partial^2 V/\partial\phi^2\}/r^2 = -\rho_p(q/m)/\varepsilon_o \qquad (4.3.16)$$

and we note that for a pipe made of conducting material, V is uniform at the pipe wall, i.e. $\partial V/\partial\phi = 0$ at $r = R$.

4.4 Characteristic Equations

It is seen from the previous section that with well defined boundary conditions, equations (4.3.2), (4.3.14), (4.3.15) and (4.3.16) can be solved simultaneously to give the distributions of u_p, ρ_p, D_p and V of the particulate phase. In order to keep the solutions general, it is convenient to introduce the following dimensionless quantities:

$$r^* = r/R; \quad \rho^* = \rho_p/\rho_{po}; \quad u^* = u/u_o; \quad F^* = F/F_s$$

$$u_p^* = u_p/u_c; \quad V^* = V(q/m)/D_f F_s; \quad D_p^* = D_p/D_f \qquad (4.4.1)$$

where ρ_{po} is the particulate density at the pipe centre, D_f is the turbulent diffusivity of the fluid (Appendix I) and F_s is the inverse of relaxation time when Stoke's law of drag of a sphere applies (Equation (3.1.4)). (The asterisk denotes dimensionless quantities).

Upon normalization of equations (4.3.2), (4.3.14), (4.3.15) and (4.3.16) with the above dimensionless quantities, we obtain the following characteristic equations,

$$-\tfrac{1}{2}\gamma\rho^* + (1/r^*)\partial(r^*\rho^* D_p^* \partial u_p^*/\partial r^*)/\partial r^* + (1/r^{*2})\partial(\rho^* D_p^* \partial u_p^*/\partial\phi)/\partial\phi + \beta F^*\rho^*(u^* - u_p^*) = 0 \tag{4.4.2}$$

$$-D_p^*\partial\rho^*/\partial r^* - (\rho^*/F^*)\partial V^*/\partial r^* - \tfrac{1}{2}\eta(\rho^*/F^*)\cos\phi = 0 \tag{4.4.3}$$

$$-D_p^*(1/r^*)\partial\rho^*/\partial\phi - (\rho^*/F^*)(1/r^*)\partial V^*/\partial\phi + \tfrac{1}{2}\eta(\rho^*/F^*)\sin\phi = 0 \tag{4.4.4}$$

and

$$(1/r^*)\partial(r^*\partial V^*/\partial r^*)/\partial r^* + (1/r^{*2})\partial^2 V^*/\partial\phi^2 = -4\alpha\rho^* \tag{4.4.5}$$

where the characteristic parameters, α, β, γ and η are defined by

$$\alpha = (\rho_{po}/4\varepsilon_o)(q/m)^2(R^2/D_f F_s) \tag{4.4.6}$$

$$\beta = R^2 F_s/D_f \tag{4.4.7}$$

$$\gamma = 2R^2 g\cos\theta(1 - \bar{\rho}/\bar{\rho}_p)/D_f u_o \tag{4.4.8}$$

and

$$\eta = 2Rg\sin\theta(1 - \bar{\rho}/\bar{\rho}_p)/D_f F_s \tag{4.4.9}$$

It is seen that α, β, γ and η are infact correlation parameters characterizing the effects of electrostatic diffusion, relaxation and gravity on the particulate phase. While electrostatic and gravity effects are governed by α, and γ and η respectively, β is the ratio of relaxation time F^{-1} to diffusion time (R^2/D_p) for $F \sim F_s$ and $D_p \sim D_f$.

Further, combining equations (4.4.3) and (4.4.4), we obtain

$$(\partial V^*/\partial r^* + \tfrac{1}{2}\eta\cos\phi)/(\partial V^*/\partial\phi - \tfrac{1}{2}\eta r^*\sin\phi) = (\partial\rho^*/\partial r^*)/(\partial\rho^*/\partial\phi) \qquad (4.4.10)$$

which in turn yields an approximation for ρ^* as

$$\rho^* = \exp(-V^* - \tfrac{1}{2}\eta r^*\cos\phi) \qquad (4.4.11)$$

Equation (4.4.11) implies that under fully developed flow conditions, the distribution of the particulate density is influenced only by the electrostatic and gravity forces.

Using assumption (ii) in section 4.1 that the motion of the fluid phase is not affected by the presence of the particles, the velocity distribution of the fluid can be approximated by a power law of the form

$$u = u_o(1 - r/R)^{\frac{1}{7}} \qquad (4.4.12)$$

or

$$u^* = (1 - r^*)^{\frac{1}{7}} \qquad (4.4.13)$$

Due to the difference in inertia of the particles and fluid, at a solid boundary, particles may have finite velocity even though the fluid attains zero velocity there except at very low pressures.

Soo (27) suggested that the motion of the particles can be treated as in a regime corresponding to a rarefied state of gases with their random motion sustained by fluid turbulence and a slip velocity u_{pw} at the wall

$$u_{pw} = -L_p \left| \partial u_p / \partial r \right|_{r=R-a} \tag{4.4.14}$$

where L_p is an interaction length between the two phases and is given approximately by

$$L_p \sim (\Delta\hat{u}^2)^{\frac{1}{2}}/F \tag{4.4.15}$$

in which $\Delta\hat{u} = \hat{u} - \hat{u}_p$; $(\Delta\hat{u}^2)^{\frac{1}{2}}$ is the R.M.S. relative intensity. (section 3.1)

Re-writing equation (4.4.14) in dimensionless form, we have

$$u^*_{pw} = -Knp \left| \partial u^*_p / \partial r^* \right|_{r^* \sim 1} \tag{4.4.16}$$

where the Knudsen number Knp is defined as

$$Knp = L_p / R \tag{4.4.17}$$

The boundary conditions for the characteristic equations are as follows:

(i) $r^* = 0; \quad \rho^* = 1, \quad V^* = 0.$

(ii) $r^* = 1; \quad (\partial V^*/\partial\phi) = 0, \quad u^*_{pw} = -Knp \left| \partial u^*_p / \partial r^* \right|.$

(iii) $r^* = 0, \quad \phi = \pi/2; \quad \partial/\partial r^* = 0.$

(iv) $\phi = 0, \pi \quad ; \quad \partial/\partial\phi = 0$ for $r^* = 0 \to 1.$

With the above boundary conditions, the characteristic equations (equations (4.4.2) - (4.4.5) and (4.4.11)) can be solved numerically by finite difference approximation, the method of solution being described in Appendix 2.

4.5 Simplified Characteristic Equations

Following a procedure used by Soo and Tung (29) who assumed constant D_p and F, equations (4.3.14) and (4.3.15) can be both integrated to

$$D_p \ln(\rho_p/\rho_{po}) = -(q/m)(V/F) - (r/F)(1 - \bar{\rho}/\bar{\rho}_p)g\sin\theta\cos\phi \tag{4.5.1}$$

and after similar normalization procedure used in the previous section, equations (4.3.2), (4.5.1) and (4.3.16) become

$$-\tfrac{1}{2}\gamma\rho^* + (1/r^*)\partial(r^*\rho^*\partial u_p^*/\partial r^*)/\partial r^* + (1/r^{*2})\partial(\rho^*\partial u_p^*/\partial\phi)/\partial\phi + \beta\rho^*(u^* - u_p^*) = 0 \tag{4.5.2}$$

$$\rho^* = \exp(-V^* - \tfrac{1}{2}\eta r^*\cos\phi) \tag{4.5.3}$$

and

$$(1/r^*)\partial(r^*\partial V^*/\partial r^*)/\partial r^* + (1/r^{*2})\partial^2 V^*/\partial\phi^2 = -4\alpha\rho^* \tag{4.5.4}$$

The characteristic parameters α, β, γ and η and V^* are now re-defined as

$$\alpha = (\rho_{po}/4\varepsilon_o)(q/m)^2(R^2/D_p F) \tag{4.5.5}$$

$$\beta = R\,F/D_p \tag{4.5.6}$$

$$\gamma = 2R^2 g\cos\theta(1 - \bar{\rho}/\bar{\rho}_p)/D_p u_o \tag{4.5.7}$$

$$\eta = 2Rg\sin\theta(1 - \bar{\rho}/\bar{\rho}_p)/D_p F \tag{4.5.8}$$

$$V^* = (q/m)(V/D_p F) \tag{4.5.9}$$

However, no details were given by the authors regarding the approximations of F and D_p used in their analysis. In the case of a non-depositing suspension flow with negligible gravity effect (i.e. $\eta = 0$, $\gamma = 0$, $\partial/\partial\phi = 0$. Soo (27) obtained the following approximations for ρ^* and V^*:

$$\rho^* = (1 - \tfrac{1}{2}\alpha r^{*2})^{-2} \tag{4.5.10}$$

and

$$V^* = 2\ln(1 - \tfrac{1}{2}\alpha r^{*2}) \tag{4.5.11}$$

for $\alpha << 1$.

Thus, at the pipe wall ($r^* = 1$), V^* is a constant

$$V^* = 2\ln(1 - \tfrac{1}{2}\alpha) \tag{4.5.12}$$

For comparison purpose, numerical solutions of equations (4.5.2) - (4.5.4) have also been obtained, the method of solution being described in Appendix 3.

CHAPTER 5

FRICTION FACTOR OF A GAS-SOLID SUSPENSION FLOW

Similar to single phase flows, generalization of pressure drops in gas-solid suspension flows can be made in terms of friction factors. The pressure drop is related to the total shear stress at the pipe wall τ_w by

$$\tau_w = \frac{R}{2} \left(\frac{\partial P}{\partial x} \right)_m \tag{5.1}$$

and the overall friction factor of the suspension C_{fm} can be expressed as

$$C_{fm} = \frac{\tau_w}{\overline{\rho u}^2/8} \tag{5.2}$$

where $\bar{u}$ is the mean velocity of the fluid, R is the pipe radius and $(\partial P/\partial x)_m$ is the pressure gradient along the pipe.

Based on the assumption that addition of solid particles would always lead to higher pressure drop, many workers have obtained empirical relationships between the excess pressure drop due to the solid particles and pertinent pipe flow parameters. Of the earlier study, the method of approach of Rose and Barnacle (10) may be considered typical. They subdivided the overall pressure drop ΔP_m as

$$\Delta P_m = \Delta P + \Delta P_p \tag{5.3}$$

and similarly for C_{fm}

$$C_{fm} = C_f + C_{fp} \tag{5.4}$$

where ΔP is the pressure drop due to the fluid in the absence of the solid particles and ΔP_p is the excess pressure drop due to the particles (Fig. 5.1). Their work was carried further by Duckworth and Rose (11) who derived from experimental data some useful design equations for pressure drop in both hydraulic and pneumatic conveying systems.

Whilst the majority of the workers consistently reported that loading of solid particles always results in an increase in pressure drop, quite remarkable effects which may be attributed to electrification, turbulence reduction or thickening of the viscous sublayer of the fluid have been observed. These involve both reduction and progressive increase in pressure drop due to the presence of the particles.

For particles in the 1 mm diameter range, Clark et al (19) examined the pneumatic flow of sand, granite and carborundum particles and observed that if a particular material is conveyed for a long period, the pressure difference required to maintain the transport progressively increases and can reach a value of some 10 times the initial one. Following their work, Richardson and Mcleman (14) found that not only the pressure drop increased but so did the relative velocity between the particles and the fluid. They suggested that the phenomenon might be explained by the acquisition of electrostatic charge of opposite sign by the main body of the particles and by a dust layer deposited on the pipe wall due to attrition of the particle material. Thus, the particle-wall impact is increased by electrostatic attraction which would account for an increase in both relative velocity and pressure drop.

Referring to the moderately dilute suspensions of small particles within the 10-100 μ diameter range, several workers have observed reduction in pressure drop (i.e. $\Delta P_m < \Delta P$) due to the presence of the particles (14-18). However, the explanation offered by the workers for the cause of this anomalous phenomenon is somewhat diverse.

For small perspex particles, Richardson and Mcleman (14) suggested that due to frictional electrification, the particles and the dust layer deposited on the pipe wall might acquire like charges, thus the particles are driven more towards the pipe axis by electrostatic repulsion resulting in a reduction in pressure drop.

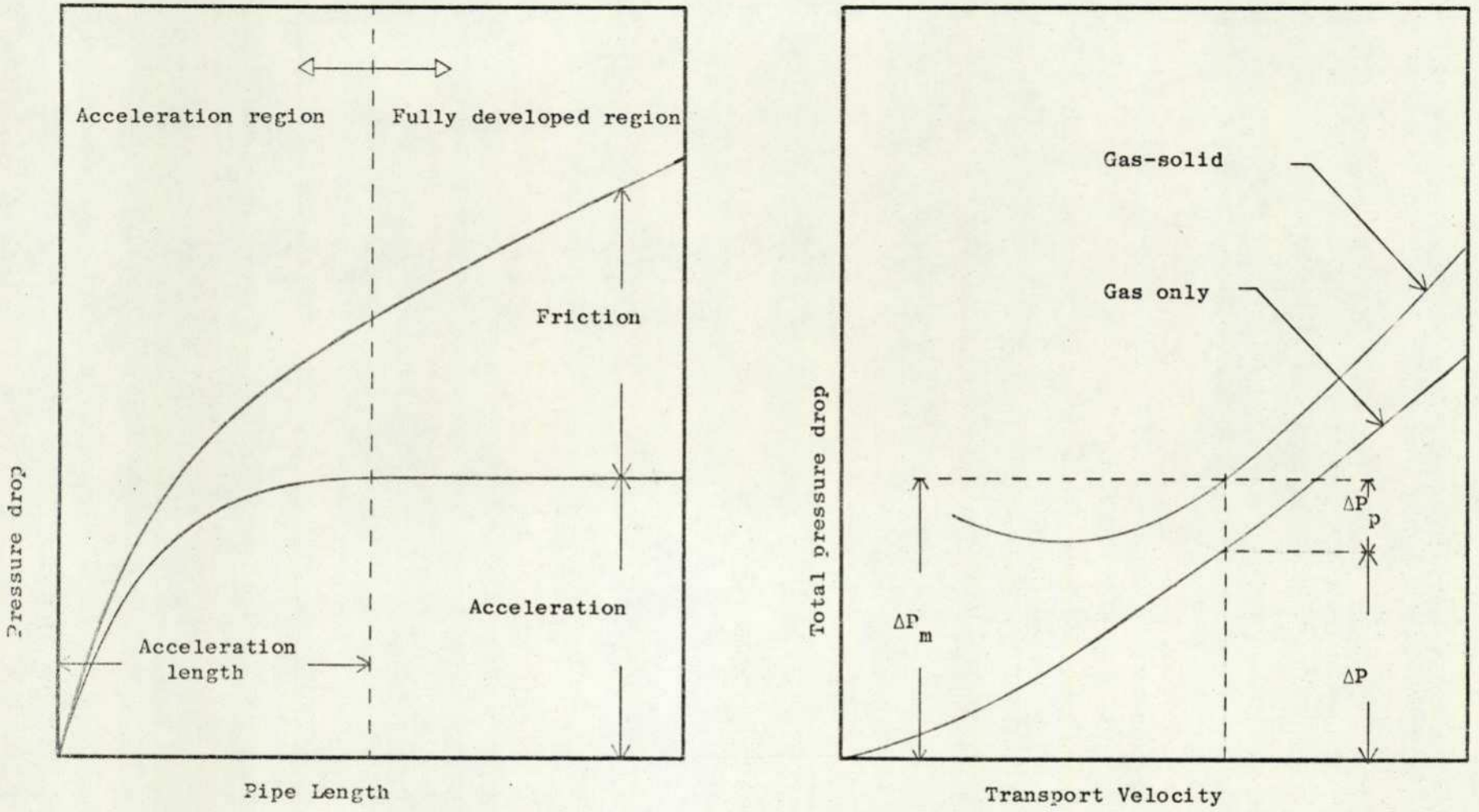

Fig. 5.1. Composition of the total pressure drop of a gas-solid suspension flow.

In an attempt to explain the reduction of pressure drop due to loading of particles, Soo (32) expressed τ_w as the sum of the shear stress τ' due to the fluid with the presence of particles and that due to particle-wall collision τ_p ,

$$\tau_w = \tau' + \tau_p \tag{5.5}$$

It is recognized that within the range of solid loading where such a phenomenon occurs, the velocity profile of the fluid is unaffected by the presence of the particles (6,60) and further that the contribution to τ_w by τ_p is negligible (15,61). Hence, equation (5.5) becomes

$$\tau_w = \tau' \tag{5.6}$$

Following the approach used by Prandtl who expressed the shear stress τ of the fluid in terms of a mixing length ℓ as

$$\tau = \ell^2 \rho \left(\frac{du}{dy} \right)^2 \tag{5.7}$$

Soo (32) gave

$$\tau' = \ell_p^2 \rho \left(\frac{du}{dy} \right)^2 \tag{5.8}$$

where ℓ_p is the mixing length due to the presence of the particles. Thus,

$$\frac{\tau}{\tau'} = \frac{\ell^2}{\ell_p^2} \tag{5.9}$$

Therefore, the decrease in pressure drop may be attributed to a reduction of mixing length due to dissipation of energy by the particles (Fig. 5.2)

Alternatively, Owen (42) suggested that the particles, being driven towards the pipe wall by electrostatic repulsion, tend to congregate at

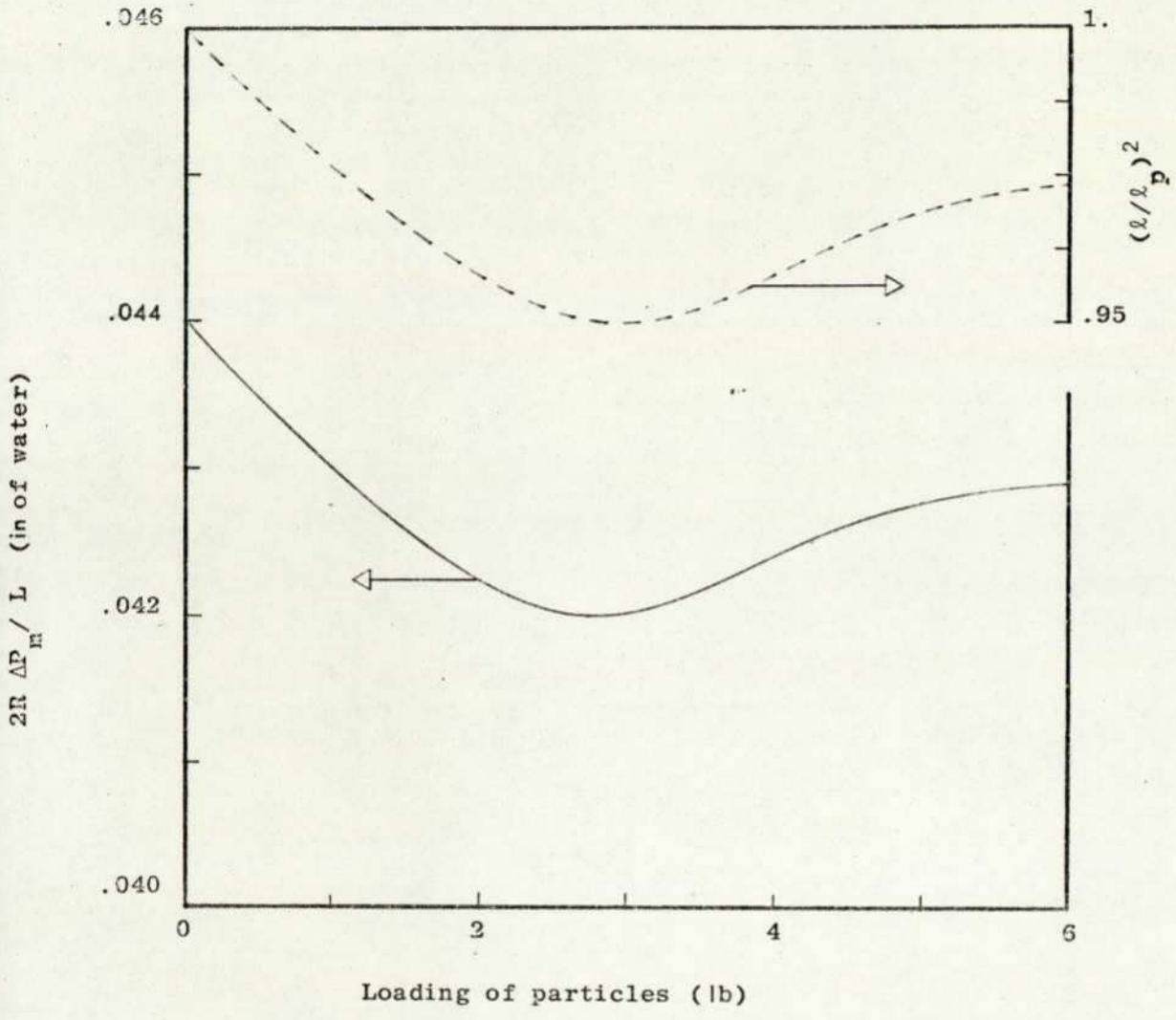

Fig. 5.2. Effect of loading of particles on pressure drop (2R = 5in, L/2R = 47.6, 35μ MgO particles, measurement by Soo (60))

such a distance from the wall that their relaxation time is comparable with the eddy life time there. While the rate of energy transfer from the mean flow to the turbulence near the wall is

$$E_i = \bar{\rho} u_\tau^2 F \quad , \tag{5.10}$$

the rate at which work must be done by the turbulence to maintain zero net rate of particle deposition is

$$E_o = \rho_{pw} v_p^2 F \tag{5.11}$$

where v_p is a drift velocity (Sections 2.2 and 2.3)

Utilizing the experimental results of stratified flows (62), Owen proposed that the turbulence can be affected appreciably when the Richardson number, being defined as the ratio of E_o/E_i, exceeds about 0.1. In the case of Soo's (6) experiment where reduction in pressure drop was observed, Owen showed that E_o/E_i exceeds 0.1 even for a charge to mass ratio of 10^{-6} C/kg.

More recently, Jotaki and Tomita (63) proposed that reduction in ΔP_m or C_{fm} due to presence of the particles may be attributed to thickening of the viscous sublayer of the fluid phase due to additional energy dissipation by the particles. Extending Townsend's (64) theory of attached eddy at the pipe wall, they obtained an approximation for the dimensionless sublayer thickness R_v ,

$$R_v = \frac{\delta_s u_\tau}{\nu} = \left\{ \frac{8 \left(1 + \frac{15}{16} \pi^{\frac{1}{2}} \right)}{1 - \frac{5\pi^{\frac{1}{2}}}{2} \frac{F_s \pi}{u_\tau^2} \frac{\rho_{pw}}{\bar{\rho}}} \right\}^{\frac{1}{2}} \tag{5.12}$$

where δ_s is the thickness of the viscous sublayer (see equation (4.3.13)), F_s is the inverse of relaxation time of the particles when Stoke's law applies (see equation (3.1.4)), ρ_{pw} is the particulate density at the pipe wall and the friction velocity u_τ is defined as

$$u_\tau = \left(\frac{\tau_w}{\bar{\rho}}\right)^{\frac{1}{2}} = \bar{u}\left(\frac{c_{fm}}{8}\right)^{\frac{1}{2}} \qquad (5.13)$$

In order to derive equation (5.12), the following assumptions were made by the authors

(i) There is no relative motion (mean) between the fluid and particles.

(ii) The drag force acting on the particles is mainly due to the fluctuation velocities of the fluid and is governed by Stoke's law.

(iii) The particles do not respond to fluid turbulence and have no fluctuation velocities of their own.

(iv) The density distribution of the particles is uniform (i.e. ρ_{pw} = constant).

It is seen that assumptions (i), (ii) and (iii) are somewhat contradictory. In order to satisfy (i), it would require $a \ll 1$ which makes F_s very large i.e. the relaxation time of the particles may become comparable even with the characteristic time of the small eddies. In that case, the particles will response to fluid turbulence and therefore have their own fluctuation velocities (Section 3.1), thus modifying the drag force accordingly. Further, the assumption of uniform particulate density distribution is also restrictive since it has been shown experimentally that the particulate density varies both radially and circumferentially (6). Nevertheless, for a suspension flow of 35μ glass beads in a 3.12 cm diameter pipe with mean air velocity of 30 m/s and $\rho_{pw}/\rho \sim 3$, equation (5.12) predicts a 12.5% increase in sublayer thickness due to a 20% friction reduction.

In an attempt to test Jotaki and Tomita's theory, Kane et al (18) examined the pneumatic flow of 10-60 μ glass beads and observed friction reductions in both vertical and horizontal flows, being more significant in the former. Because of the finite size of the anemometer probe used in their air velocity profile measurement, velocity traverses were limited to the buffer layer region only and the effect of presence of particles on the sublayer thickness was not determined. However, their method of air flow measurement, by placing an orifice in line with the

suspension flow, is in suspect. Some test works have in fact been carried out with similar orifice arrangement and it was found that for a known air flow rate, the pressure drop across the orifice with presence of particles in the stream was higher than that due to clean air flow alone, thus causing error in air flow calibration e.g. a 5% overestimate of air flow rate will cause an apparent friction reduction of about 10% (Equation (5.2)).

It is seen from the diversity of explanations offered by the workers that the question of friction reduction due to presence of particles is far from being solved and the need for further investigation is evident.

CHAPTER 6

EXPERIMENTAL STUDY

The main objective of the experimental program is to examine the effects of electrostatic charging on the pressure drop of a gas-solid suspension flow. While it is possible to determine whether the electrostatic charges developed on the particles have any significant effects on the flow characteristics by related pressure drop measurement, a thorough investigation would require the determination of the statistical properties of both the particulate and fluid phases which is beyond the scope of this work. Although pressure drop measurement is straightforward, measurements of other parameters and the need for a high degree of accuracy in data recording require the use of both reliable equipments and experimental techniques.

6.1 General Description of the Test Rig

The test rig used for the present study is a modified version of the one used previously by Duckworth and Chan (65), and has been designed for the study of many aspects of gas-solid suspension systems. Details of construction of the test rig can be found in Reference (66) and a brief description is given here.

The general layout of the apparatus is shown in Fig.(6.1) in which the main items of equipment are listed. Ambient air was pumped through the pipeline via the conical entrance section by a centrifugal air blower. The pipeline was made up of three lengths of solid drawn copper pipe of 3.125 cm nominal bore, a 15m test section, a 2m vertical section and a 15m return section. Pressure rings were fitted at convenient intervals along the test section for pressure drop measurement. Air flow rate was controlled by means of a by-pass valve and was metred by an orifice plate located at the entrance section. Solid particles were separated from the air flow by two cyclones. The feed hopper enclosed

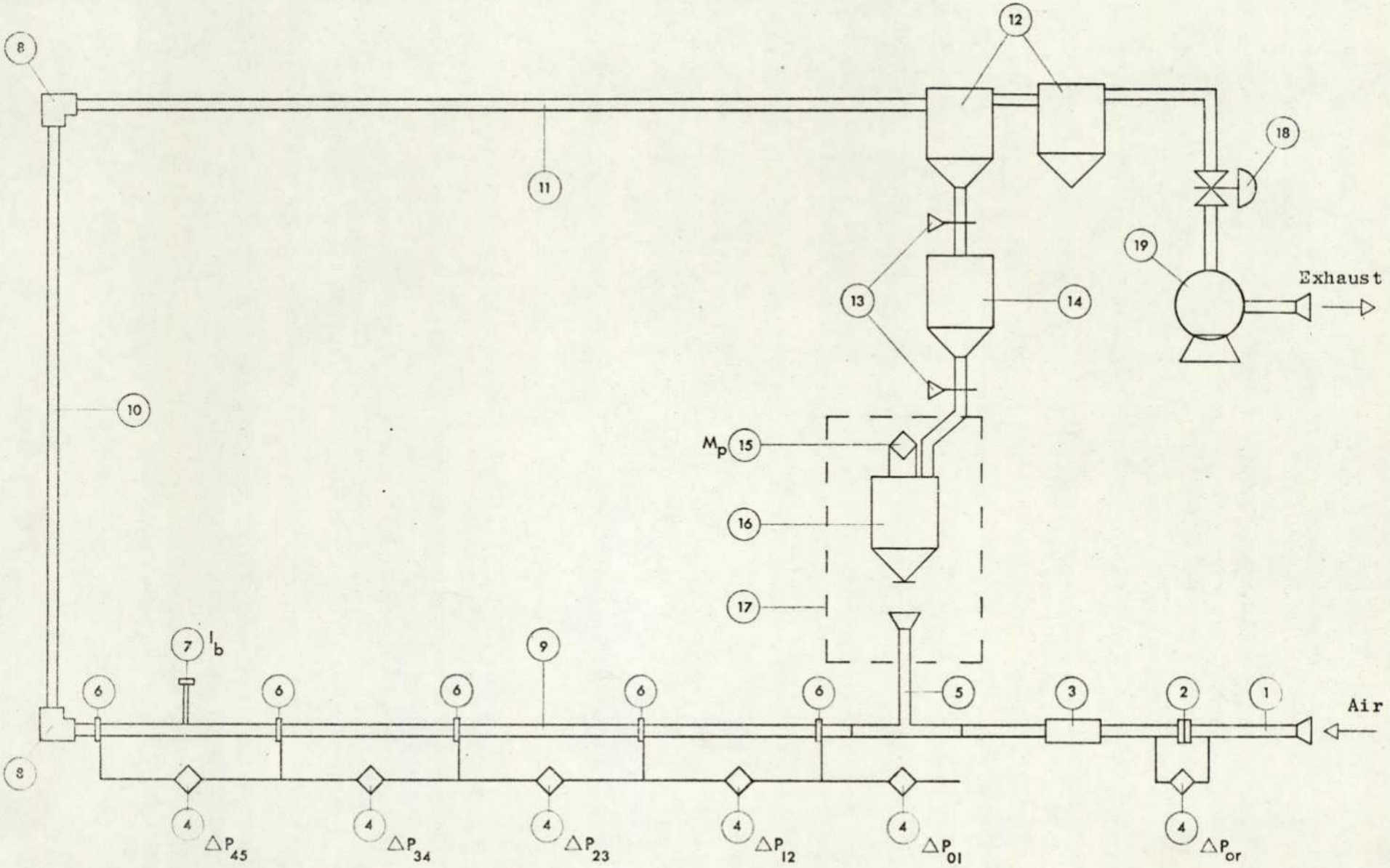

Fig. 6.1. Schematic layout of the test rig. (List of items on next page).

LIST OF ITEMS

1. Conical entrance section.
2. Air flow orifice plate.
3. 3M Ionizer.
4. Pressure transducer.
5. Transparent T-section.
6. Pressure ring.
7. Electrostatic ball probe.
8. Reinforced elbow.
9. Horizontal test section, 15m long and 3.125 cm bore.
10. Vertical section.
11. Return section.
12. Cyclone separator.
13. Flap valve.
14. Intermediate storage hopper.
15. Force transducer for solid flow rate measurement.
16. Solid feeding hopper fitted with an orifice plate.
17. Air box.
18. Air flow by-pass valve.
19. Air blower.

inside the air box was fitted with an orifice plate which can be selected to give required mass flow rates. As soon as the feed hopper was emptied, solid particles were returned to it from the intermediate storage hopper by alternative open-close operation of the two spring-loaded flap valves, thus ensuring continuous operation. A transparent T-section was fitted at the feed point for observation of the flow of particles entering the pipeline.

6.2 Pressure Transducer

When studying the phenomena of gas-solid suspension flow, it is frequently required to measure the magnitude and variation of pressures in the system. These pressures which extend over a wide range of intensities may be static or transient. Pressure measurement utilizing electrical pressure transducers in place of the conventional multiple U-tube monometer system is often preferred, especially when a large amount of data is required. There is a wide range of such equipment available on the market and in fact several manufacturers offer good pressure transducers which are suitable for most purposes but frequently the needs are so unique that a special design is required.

Most transducers are so designed that a pressure differential will cause a variation of capacitance, inductance or resistance which is then tranformed into voltage voltage output by means of bridge circuit network. The outputs from the capacitance or inductance type transducers would require further rectification when used in conjunction with data logging equipment. For this reason, it was decided that a resistance type transducer should be used and further, the need to meet the requirements of high sensitivity, high natural frequency and linear response has led to the conclusion that a diaphragm type transducer would be most appropriate.

Ten diaphragm type transducers were built and the details of construction of the transducers can be found in Reference (67). The pressure sensing element is basically a steel diaphragm, having four strain gauges mounted on its surface (2 on each side). As the diaphragm deflects due to the pressure differential acting across it,

the strain in the diaphragm is sensed by the strain gauges which are connected up to form a Wheatstone bridge circuit, the output being proportional to the pressure differential. The transducers were designed to respond linearly for pressure differential below .5 psi. Each transducer has been calibrated statically and dynamically, and the calibration equation takes the general form

$$\Delta P = C_1 V + C_2 V^2 \qquad (6.2.1)$$

where ΔP is the effective pressure differential in cm of water, V is the voltage output of the transducer, and C_1 and C_2 are the calibration factors. The second term on the RHS of equation (6.2.1) is introduced to account for the slight non-linear behaviour of the transducer at high pressures. Auxiliary amplification circuits with close-loop gain of about 100 were also used to boost the outputs from the transducers (Fig. 6.2).

6.3 Pressure Drop and Friction Factor Measurements

Measurements of static pressure distribution along the 15m test section were made at five longitudinal positions. (At the early stage, eight positions were used). For the present range of mass flow rates, the acceleration length (i.e. the distance required to reach fully developed flow condition) was found to be about 3m downstream of the solids feed point. Within the fully developed flow region, the pressure gradient due only to frictional effect remained sensibly constant and the total pressure drop ΔP_m was regarded as a linear summation of the pressure drop ΔP due to the flow of air alone under the conditions prevailing in the test section and the excess pressure drop ΔP_p attributed to the presence of the solid particles (Chapter 5). It should be noted that this scheme would give useful and logical results as long as $\Delta P_m > \Delta P$.

The air friction factor C_f was pre-determined prior to each session of test runs and updated if necessary. Only a very thin layer of dust was found to be present on the pipe wall and did not appear

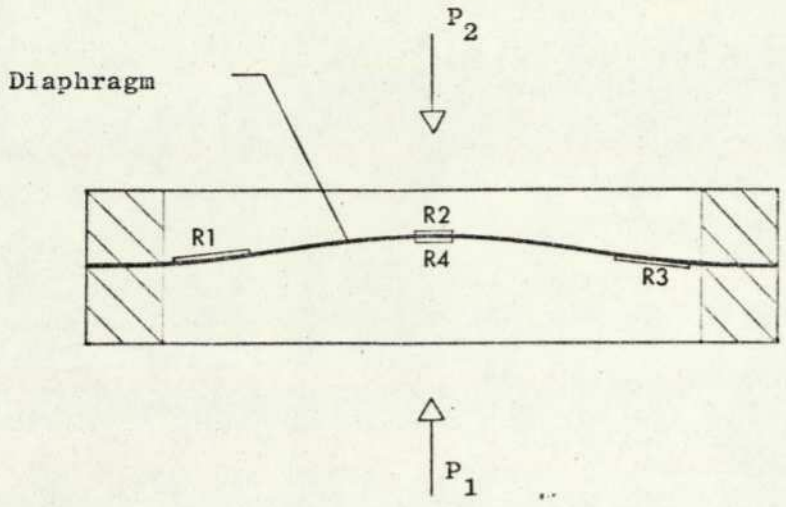

Fig. 6.2. (a) Deflection of a circular diaphragm with built-in edges.
(R1,R2,R3,R4 = 120 ohm strain gauges)

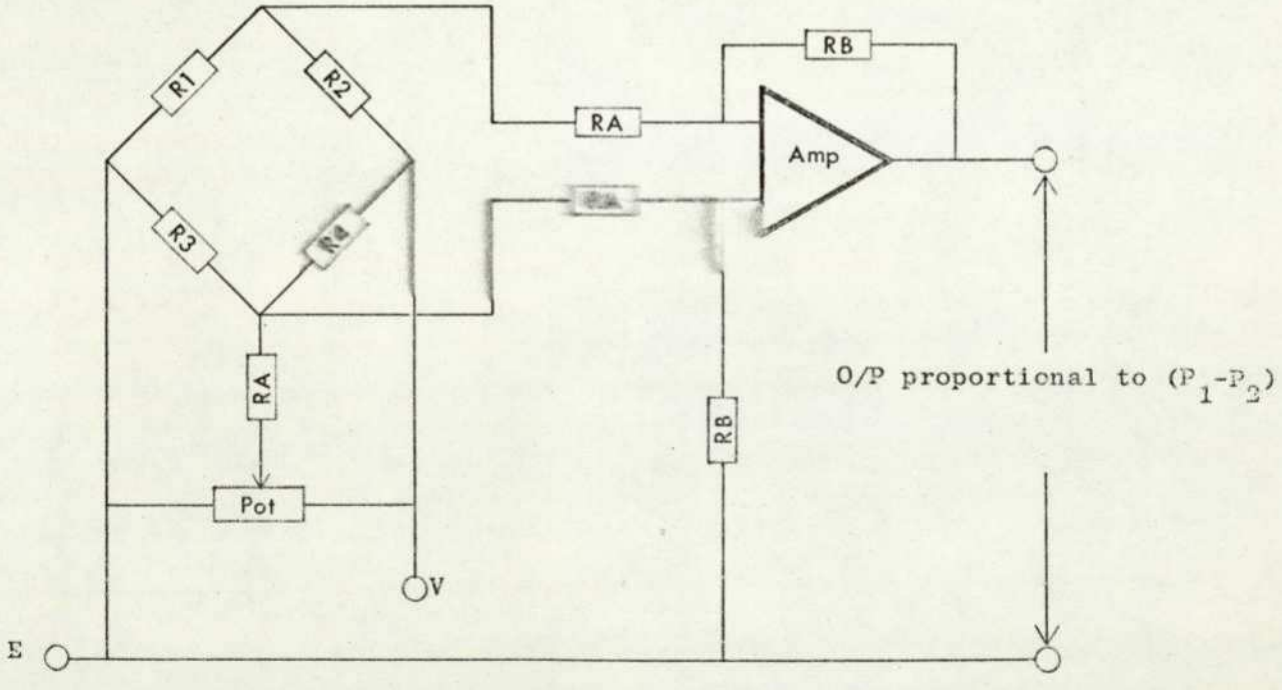

Fig. 6.2. (b) Pressure transducer circuit diagram
(RA = 10k ohm; RB = 1M ohm)

to have any appreciable effect on the air friction (Fig. 6.3).

6.4 Air Flow Rate Measurement

Air flow rate was determined by measuring the pressure drop across the orifice plate which has been calibrated for the present working range. The empirical relationship between the flow rate M_f and the pressure drop ΔP across the orifice is given by

$$M_f = .00785\ (\Delta P \bar{\rho})^{\frac{1}{2}} \quad , \text{kg/sec} \qquad (6.4.1)$$

where $\bar{\ }$ is the density of ambient air and ΔP is in cm of water. Although special care was taken to ensure the air box leak-proof, a small leakage was detected and the calibration equation had to be modified by a leakage factor L_f such that

$$M_f = .00785\ (L_f \Delta P \bar{\rho})^{\frac{1}{2}} \quad , \text{kg/sec} \qquad (6.4.2)$$

where $L_f = 1.1$

Air velocity profile measurements were made by traversing the pipe radius with a Pitot tube and was found that one-seventh power velocity distribution gives excellent agreement with experimental results. Thus

$$u = u_o \left(1 - \frac{r}{R}\right)^{\frac{1}{7}} \quad , \qquad (6.4.3)$$

$$u_o = 1.2\bar{u} \quad , \qquad (6.4.4)$$

and

$$\bar{u} = \frac{M_f}{\pi R^2 \bar{\rho}} \qquad (6.4.5)$$

where u_o is the core velocity, $\bar{u}$ is the mean velocity and R is the pipe radius.

In addition, air humidity was determined by means of a Casella wet and dry hydrometer and checked before and after each test session.

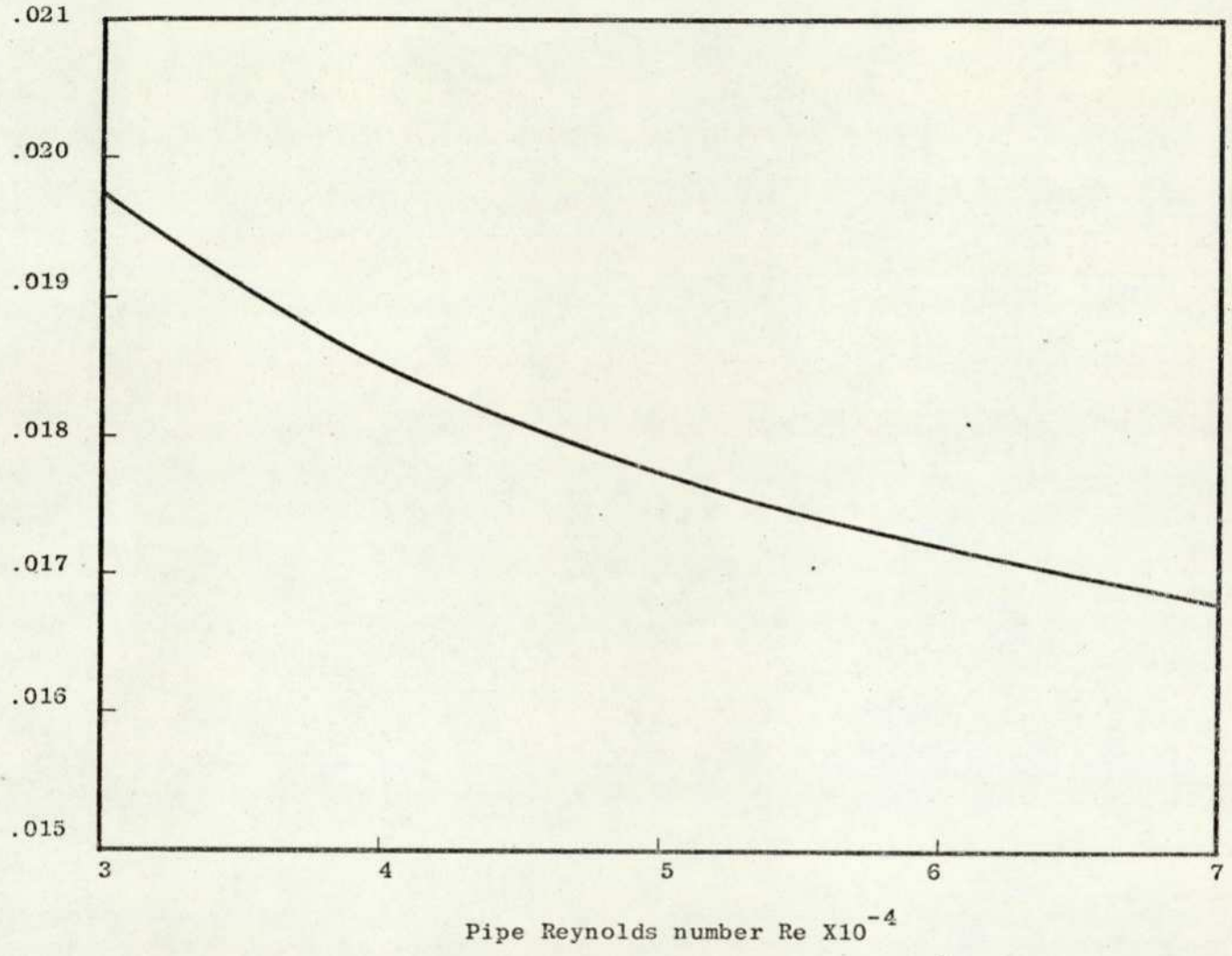

Fig. 6.3. Experimental curve relating air friction factor to Reynolds number. (Pipe diameter = 3.125 cm)

6.5 Solid Flow Rate Measurement

Solid particles were introduced into the air stream from the gravity feed hopper and mass flow rate was controlled by the orifice place. For the larger particles, the feeding system worked very efficiently without the need of pressurization of the hopper. However, slight pulsations occurred at low flow rates of the small particles, probably being caused by bridging or cohesive effects. The weight of solids in the feed hopper was measured by means of a linear force transducer in the form of a cantilever beam which was freely supported at its ends and any change of strain in the beam due to its deflection caused by the weight of solids in the feed hopper was sensed by four strain gauges mounted on it. The strain gauges acted as the four arms of a Wheatstone bridge circuit whose output is directly proportioned to the weight of solids in the hopper. Thus noting the change of voltage signal ΔS from the transducer over a time interval Δt, the mass flow rate of the solids M_p can be evaluated from

$$M_p = C_o \frac{\Delta S}{\Delta t} \qquad (6.5.1)$$

where C_o is a calibration constant. The signal from the force transducer was continuously monitored on a CRO and any deviations from the mean flow condition can be easily detected.

6.6 Particle Size Measurement

Four types of small spherical glass beads, ranging from 15μ to 385μ in diameter were used for the present investigation and microscopy was used as the absolute method of particle size analysis since it is the only method in which individual particles are measured.

The most difficult task in microscopic measurement is perhaps the preparation of the slide which should contain a uniformly dispersed representative sample of the particles. However, if a permanent slide is not required, an effective method is to mix a small sample of the particles with a dispersing fluid (i.e. the mounting medium) and a drop of the mixture is then evenly spread on a microscope slide for photographing.

For the small glass beads, glycerine was found to be a satisfactory mounting medium and for the larger particles, sticky tape was used. It can be seen from the micro-photographs of the four types of glass beads that except for the few shattered fragments, the particles are roughly spherical in shape (Figs. 6.4 - 6.7). The particle size distributions are represented by the cumulative percentage frequency curves as shown in Figs. 6.8 - 6.11 and the mean particle diameter is defined by the 50% cumulative frequency.

6.7 Electrostatic Charging Measurement

The phenomenon of electrostatic charging in particulate systems has already been described in Chapter 2. In practice, dispersoids such as mist, fume, smoke and the very fine particles are charged as a result of the method of their formation and further, the experimental results obtained by Kunkel (68) show that all dust particles are electrostatically charged upon being dispersed into a cloud and that the charging depends more on the surface conditions of the particles and the nature of the surface contact involved than the surrounding conditions such that very small changes in these factors could entail large variations in the observed effects.

Various techniques have been developed to measure charges on the particles in gas-solid suspension flows but they can only provide qualitative results because of the large number of uncontrollable factors involved (6,24,25,69,70). Soo et al (6) used an electrostatic ball probe in conjunction with a fiber-optic probe to measure charges on small glass particles. Electrostatic probes have also been developed for monitoring solid flow rate in particulate systems (69,70). Cole et al (25) derived a relationship between the charges on the particles and the leakage current taken from the pipe wall of a suspension flow. Suneja and Wasan (34) studied the dispersion of charged potassium chloride particles in turbulent air stream and charge measurement was made by means of a Wenix ion spectrometer. A 3M static meter has also been suggested as an alternative but it is believed that these instruments could only provide relative static measurement.

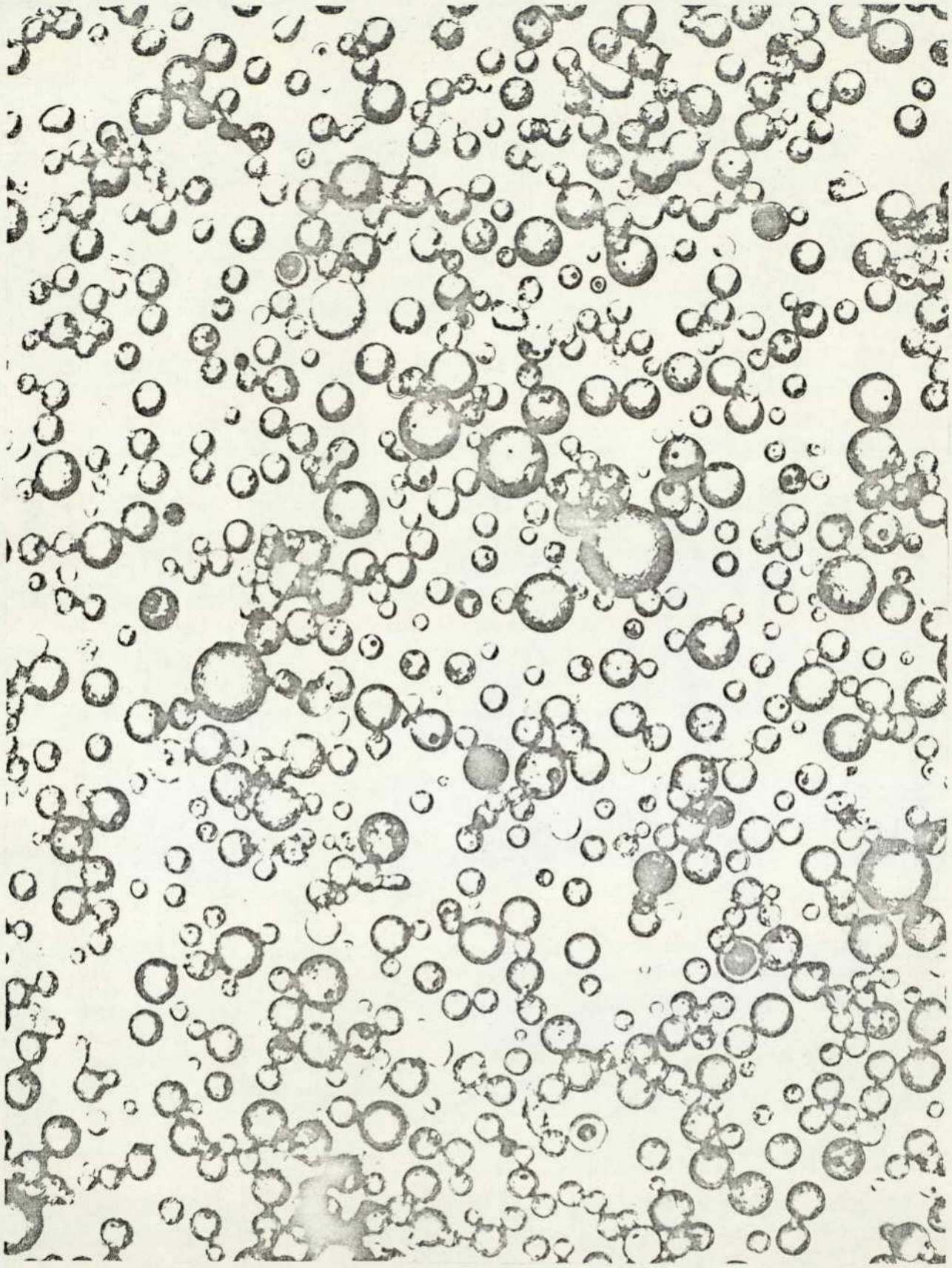

Fig. 6.4. Micrograph of Type 1 glass beads.
(Magnification = 130 : 1; Mean diameter = 35μ)

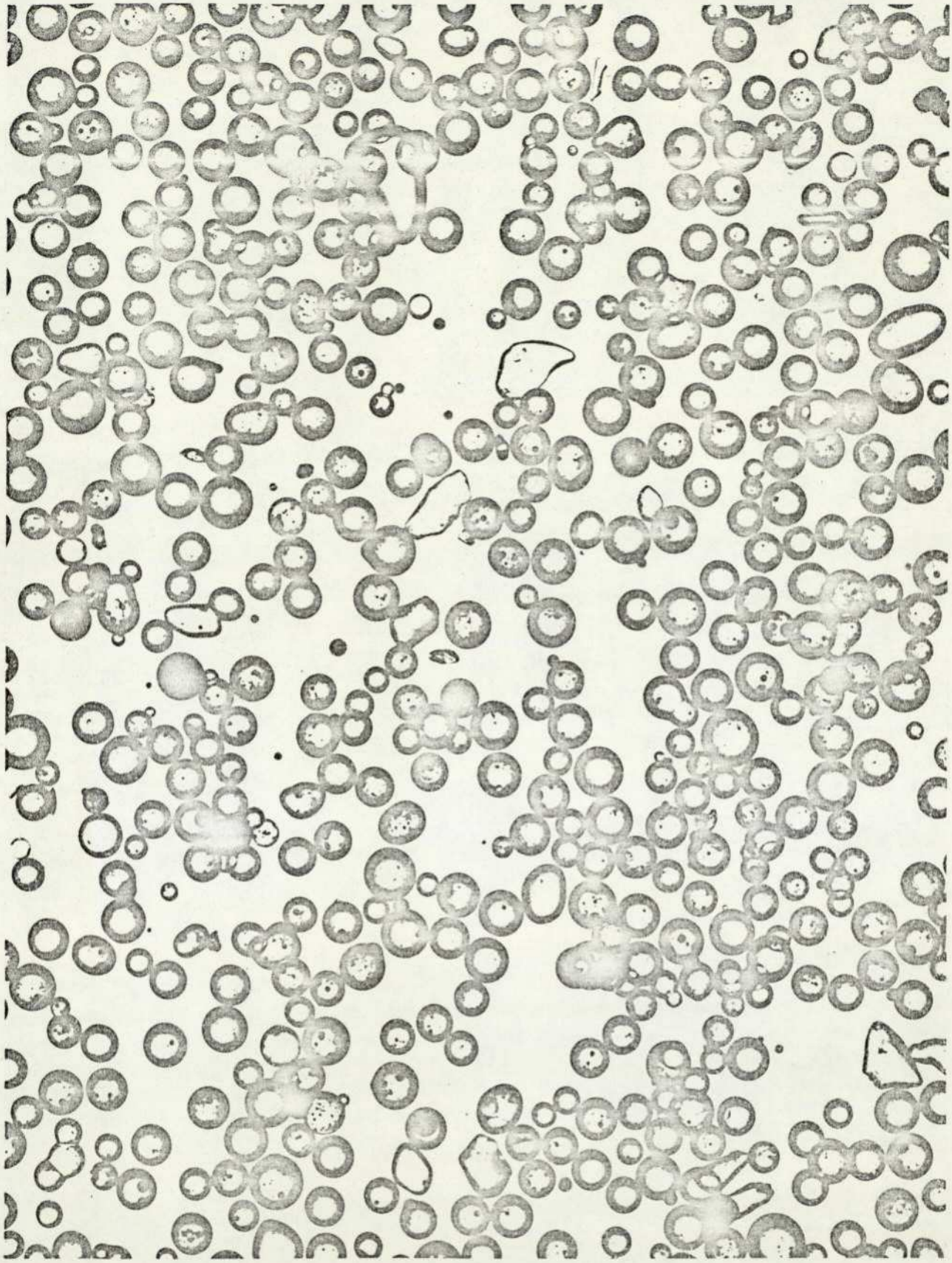

Fig. 6.5. Micrograph of Type 2 glass beads.
(Magnification = 87 : 1; Mean diameter = 75μ)

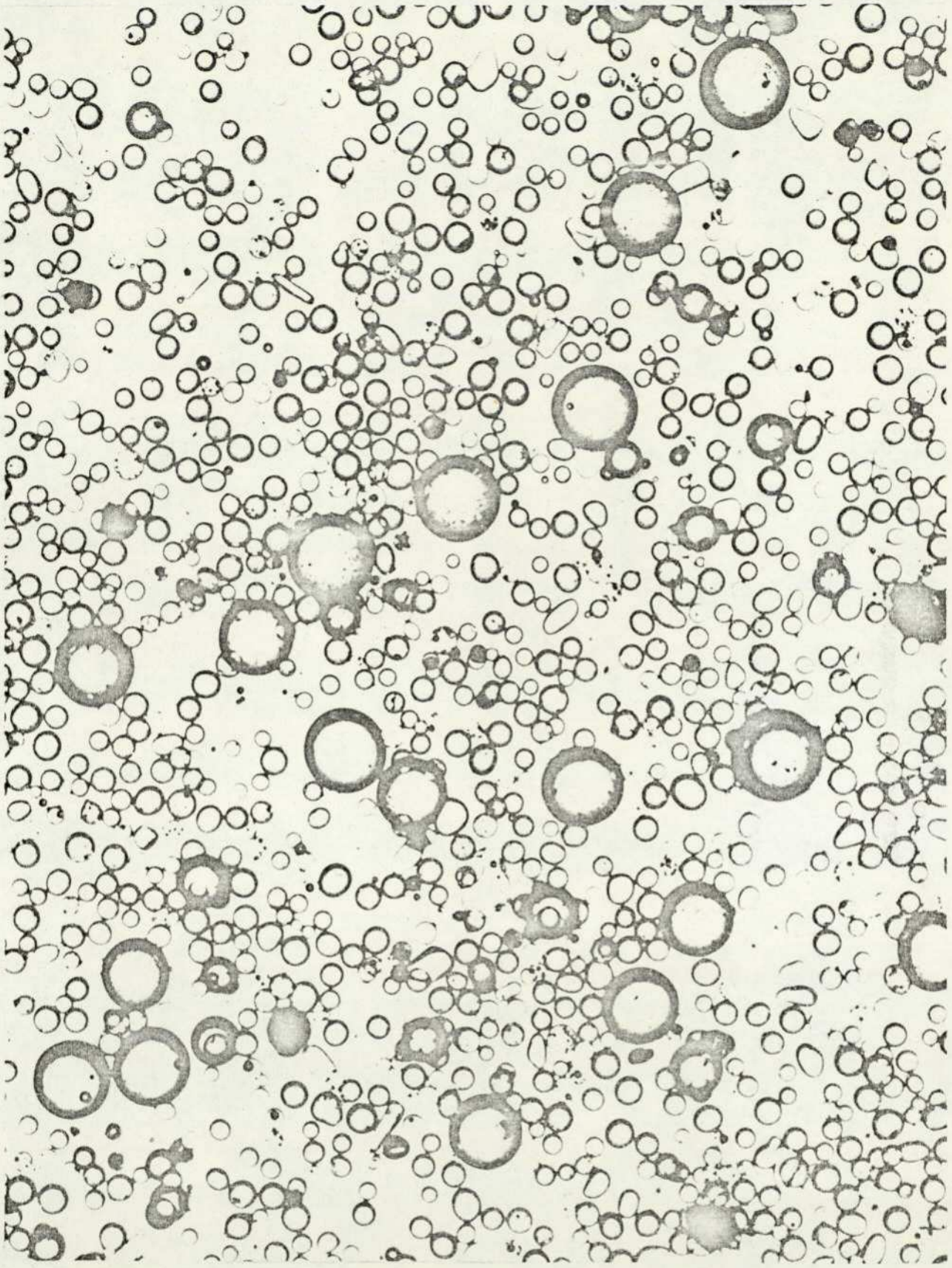

Fig. 6.6. Micrograph of Type 3 glass beads.
(Magnification = 39 : 1; Mean diameter = 82μ)

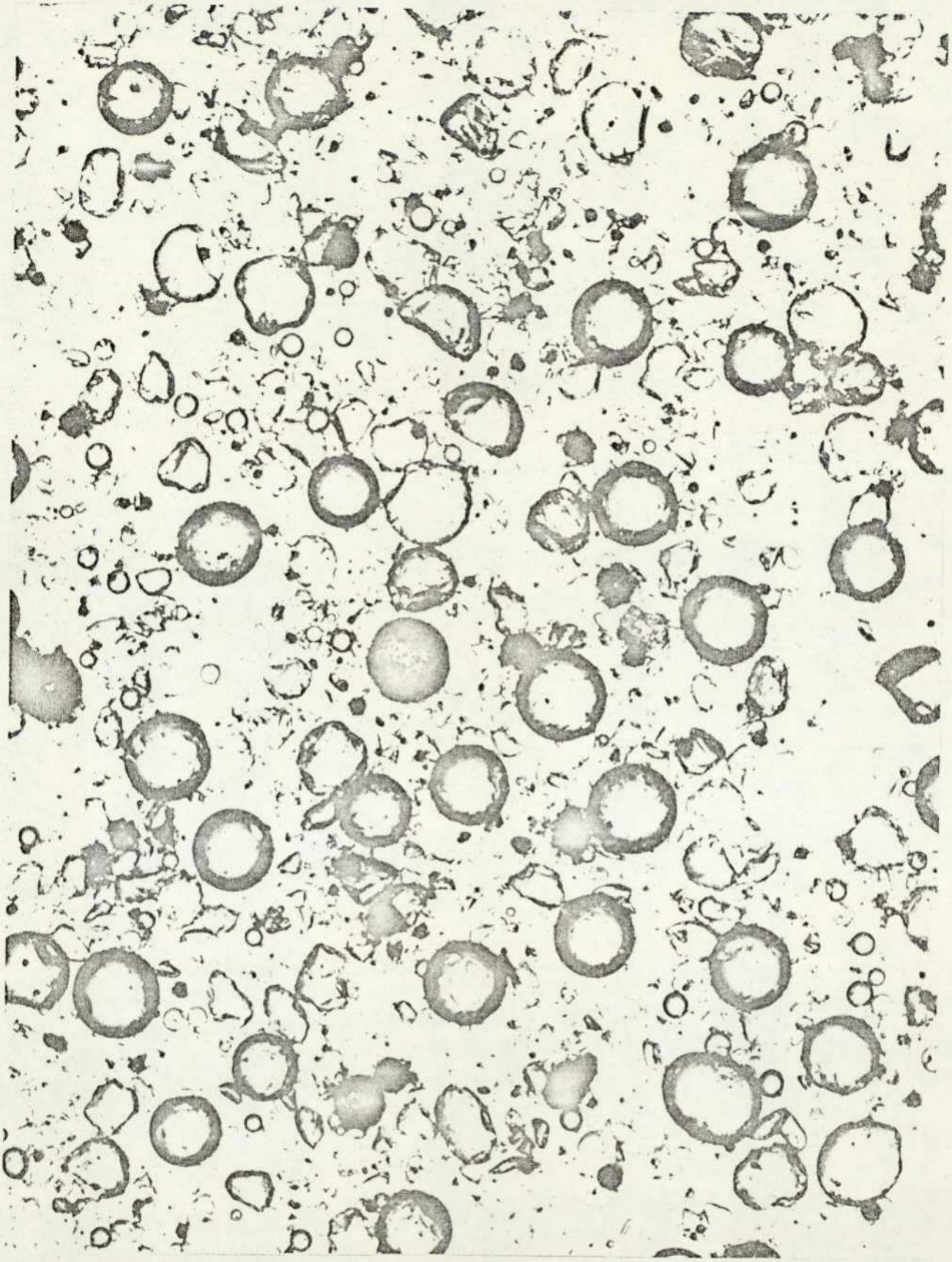

Fig. 6.7. Micrograph of Type 4 glass beads.
(Magnification = 39 : 1; Mean diameter = 380μ)

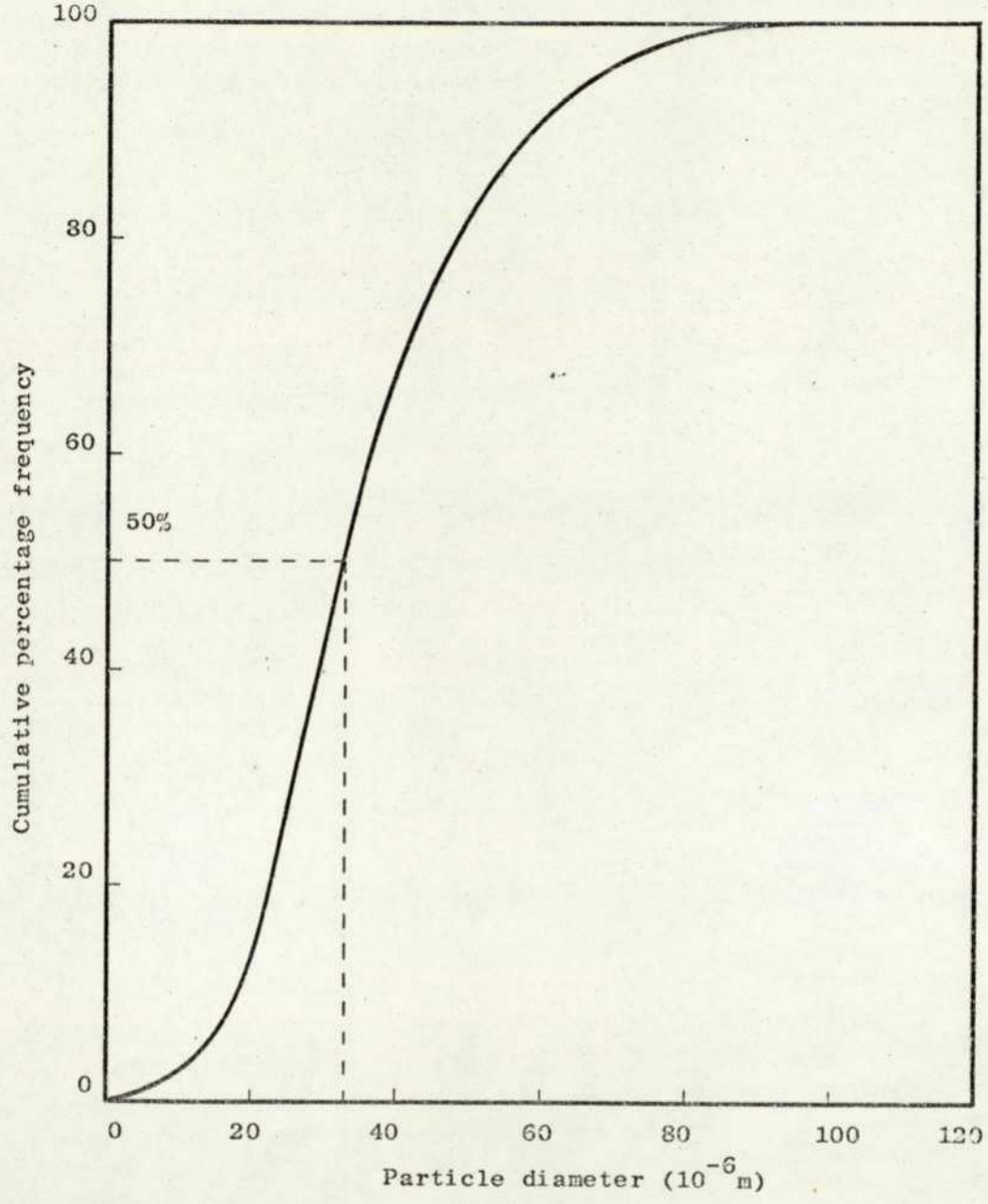

Fig. 6.8. Type # 1 glass beads size distribution
(Mean diameter = 35 x 10^{-6}m)

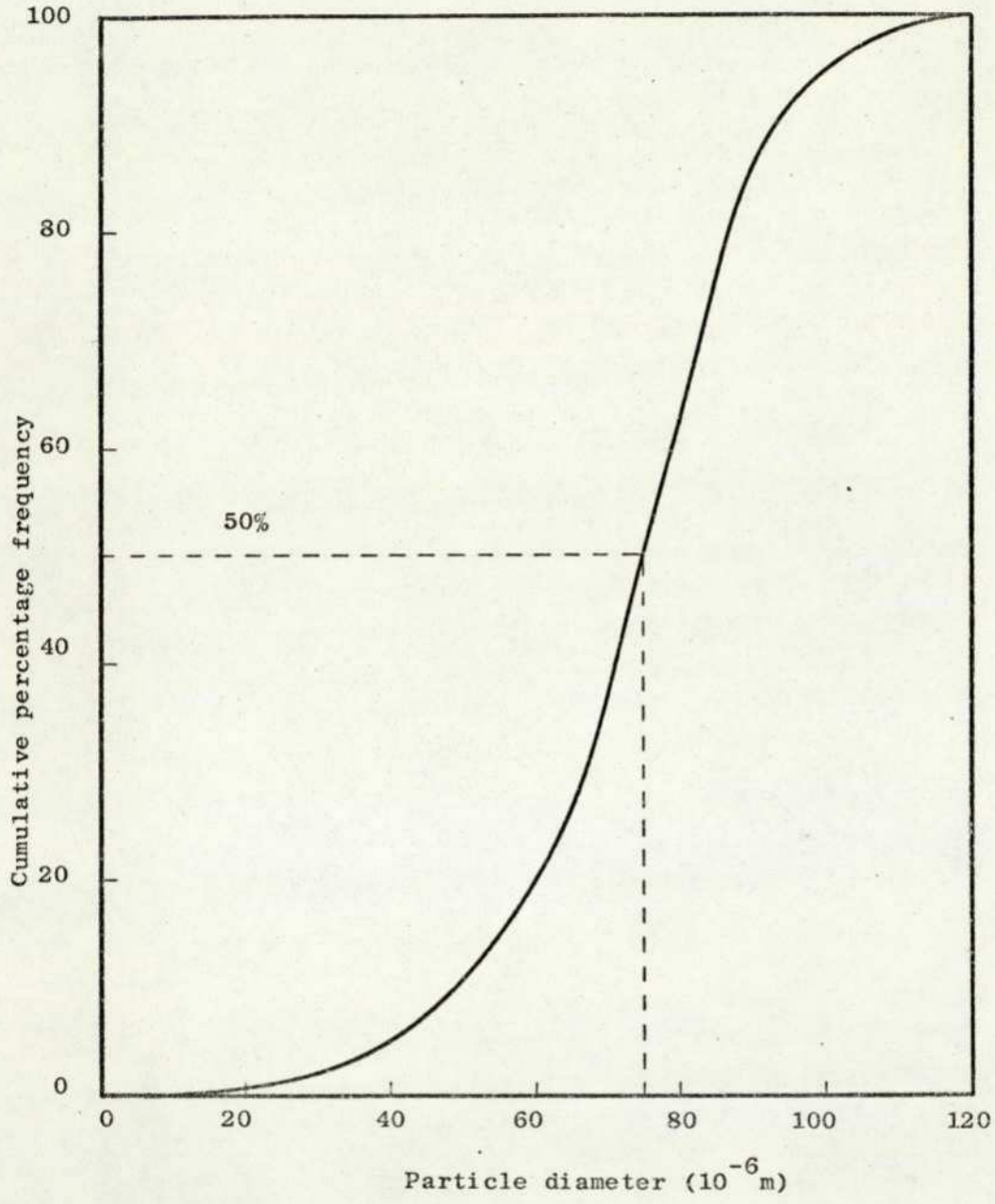

Fig. 6.9. Type # 2 glass beads size distribution
(Mean diameter = 75 x 10^{-6}m)

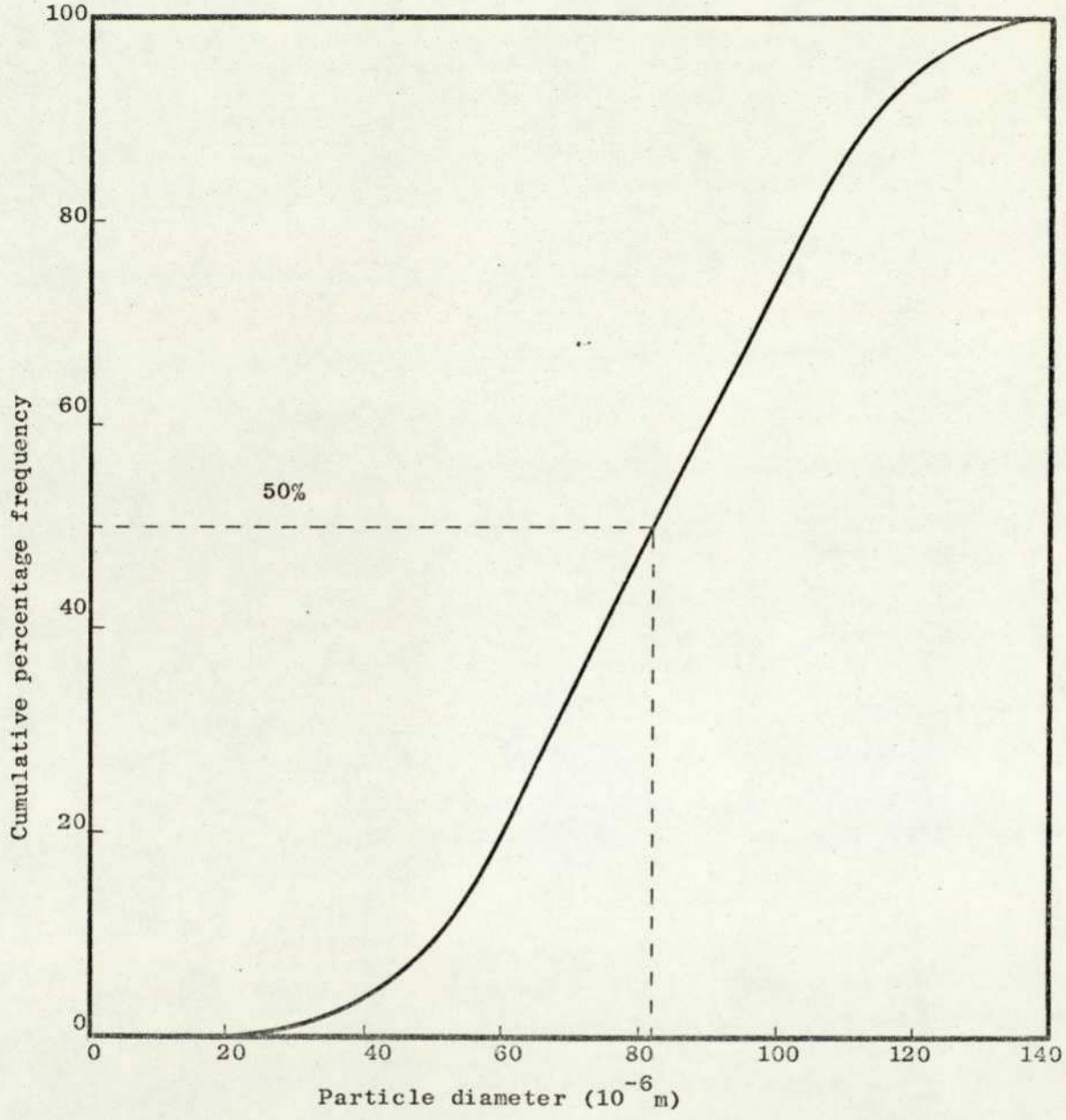

Fig. 6.10. Type # 3 glass beads size distribution (Mean diameter = 82 x 10^{-6}m).

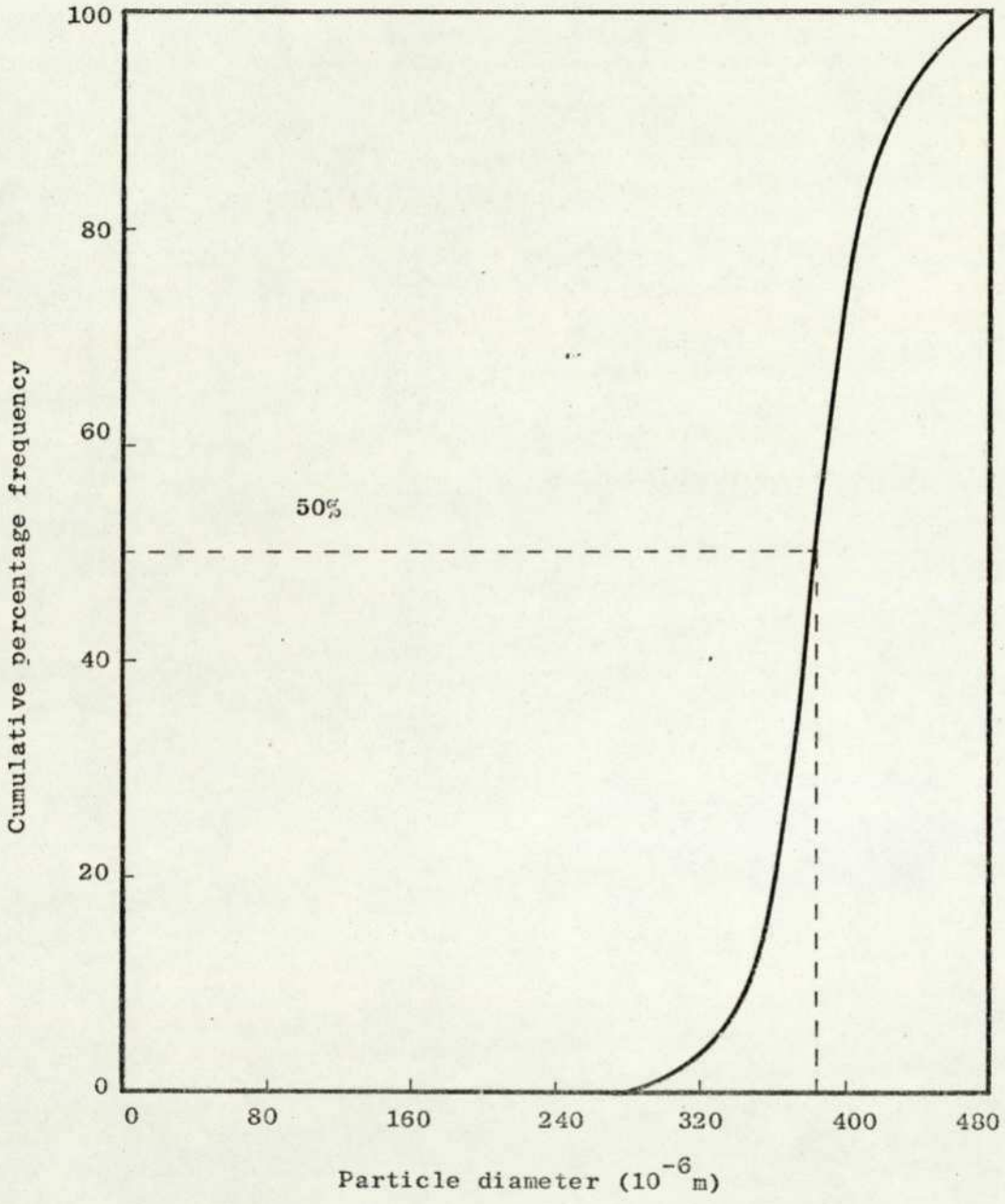

Fig. 6.11. Type # 4 glass beads size distribution.
(Mean diameter = 330 x 10^{-6}m).

For the present work, two methods were used in the measurement of charges on the particles. The electrostatic ball probe was developed when it became apparent that the deflection method, utilizing high speed photographic technique would be too time consuming for the amount of data required.

6.7.1 Charge Measurement by Deflection Method

The deflection method used in the early part of this work is somewhat analogous to the deflection of an electron beam. Consider first a particle of mass m, and charge q, travelling with a steady velocity u_{po} along the axis of a square section duct as shown in Figure 6.12. If an electric potential V is suddenly applied across the duct in the y direction, the subsequent deflection of the particle, assuming slow motion, is given by

$$\frac{d^2y}{dt^2} = E\left(\frac{q}{m}\right) - F_s \frac{dy}{dt} \quad , \qquad (6.7.1.1)$$

where E = V/2R is the electric field acting on the particle and the inverse of relaxation time F_s is given by equation (3.1.4)

Equation (6.7.1.1) has a general solution as

$$y = \left(\frac{q}{m}\right)\left(\frac{E}{F_s}\right)(e^{-F_s t} + F_s t - 1) \quad , \qquad (6.7.1.2)$$

and for short deflection time

$$y = \left(\frac{q}{m}\right)\left(\frac{E}{F_s}\right) t \qquad (6.7.1.3)$$

Thus noting the deflection of the particle and the time of deflection, the charge to mass ratio (q/m) can be evaluated from equation (6.7.1.3).

In order to observe the deflections of the particles, a transparent viewing section (3.125 x 3.125 cm) was fitted at about 8 m downstream of the solid feed point, two 10 cm metal plates being secured on its side walls to form the electrodes (Fig. 6.13).

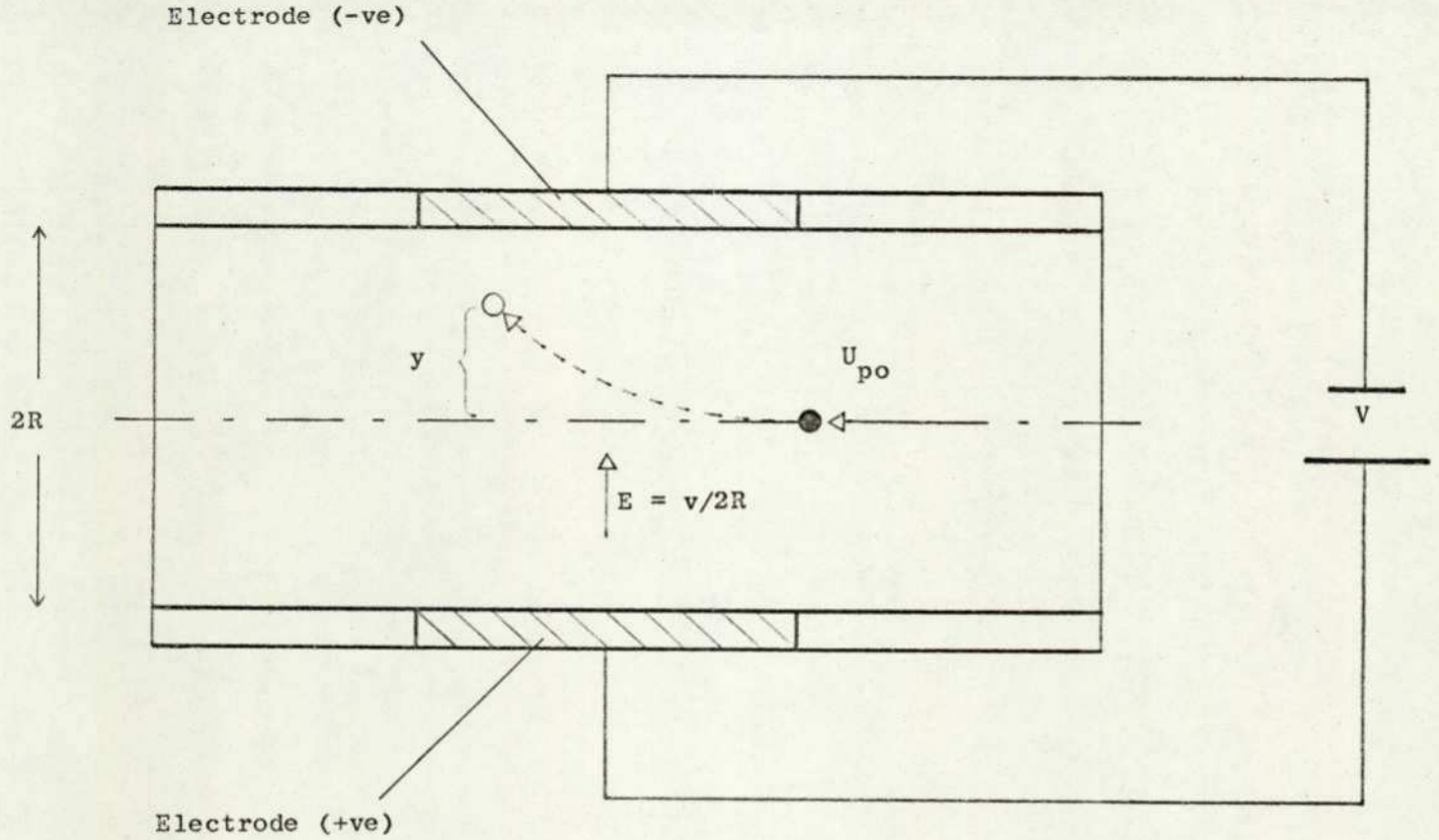

Fig. 6.12. Deflection of a charged particle under the influence of an electric field.

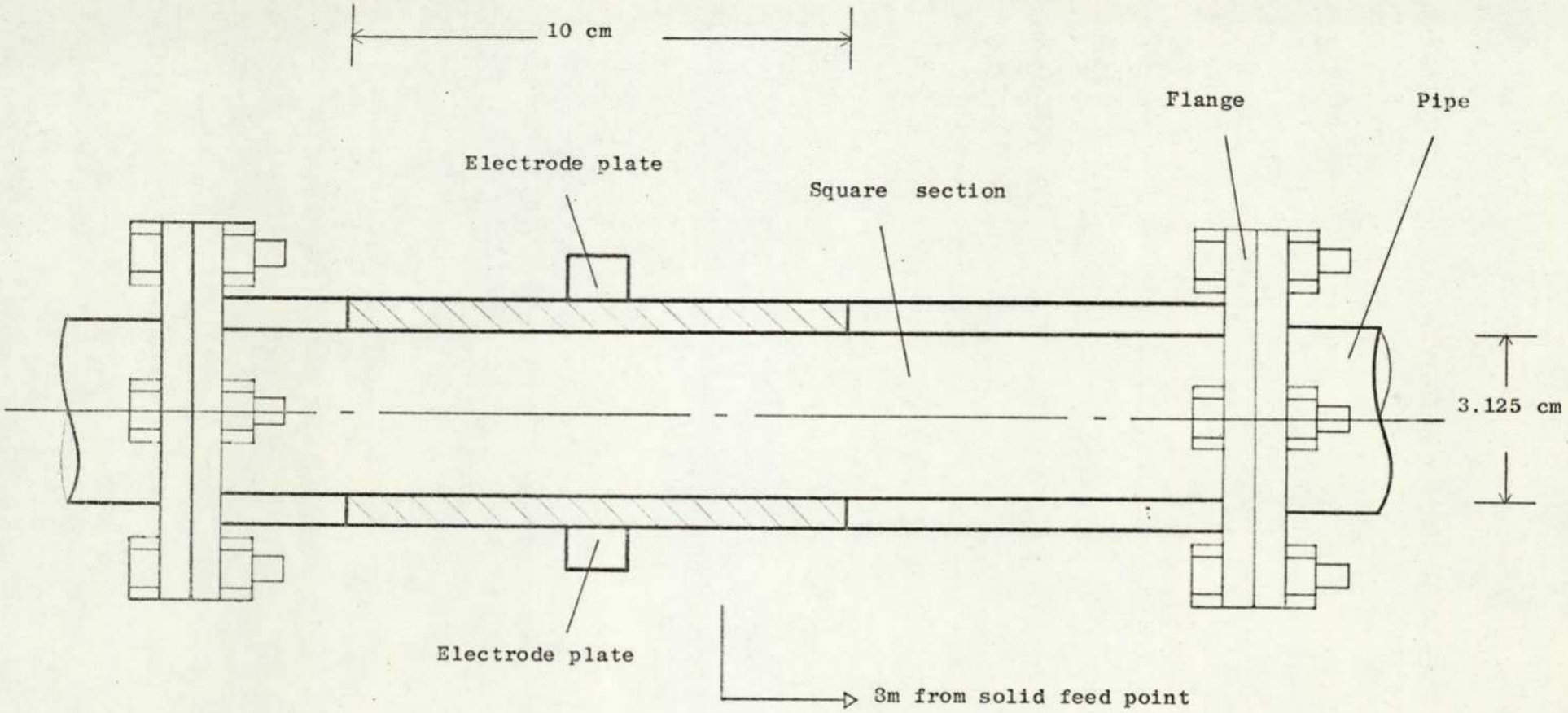

Fig. 6.13. Transparent viewing section used in particle deflection measurement.

High electric potential was supplied by a Brandenburg power pack which has a voltage range of 0 - 30 kV. A Hycam high speed cine camera was directed vertically above the transparent section and with the film running in a direction perpendicular to the flow direction, the paths of individual particles entering the section were therefore traceable. Each run the camera produced a 50 ft length of 16 mm film. The order of magnitude of the deflection is such that for a suspension flow of 80μ glass particles, air velocity of 20 m/sec and a potential of 10 kV being applied across the electrodes, equation (6.7.1.3) predicts a maximum deflection of $.8\times10^{-3}$m for a charge to mass ratio of 10^{-5} c/kg.

To carry out the deflection measurement, the film was projected onto a screen with suitable magnification and knowing the time interval between each frame, time-deflection curves were obtained. Deflections toward both electrodes have been observed and the magnitude of deflection was found to be much smaller than that predicted, thus making accurate measurement very difficult. It was concluded that charges of both signs were present on the particles and that the charge to mass ratio (q/m) was less than 10^{-5} c/kg. Because of these limitations, the analysis procedure was too slow and tedious to yield good statistics, and it became apparent that an alternative method of charge measurement should be used.

6.7.2 Electrostatic Ball Probe

The electrostatic probe theory has been developed by Cheng and Soo (24) and is mainly based on the analysis of charge transfer between two bodies outlined in Section 2.1. In the case of a cloud of particles of mass m, and radius a_1 colliding with a stationary sphere of mass $m_2(>>m_1)$ and radius $a_2(>>a_1)$, the charge transfer Q_{12} produced by each particle per impact can be obtained from equation (2.1.13) as

$$Q_{12} = 12.56\,(k_1 + k_2)^{\frac{4}{5}}\; a_1^{\frac{3}{5}}\; m_1^{\frac{4}{5}} \left(\frac{1+r^*}{2}\right)^{\frac{4}{5}} u_1^{\frac{3}{5}}\; \cos\theta^{-\frac{1}{5}}\; h_{12}(V_1 - V_2) \qquad (6.7.2.1)$$

where u_1 can be treated as the mean velocity of the particles.

For a local concentration of particle ρ_1, the effective charge current I_{12} due to successive charge transfer from the particles to the sphere is therefore

$$I_{12} = 2\pi \int_0^{\pi/2} \eta_{12}\rho_1 u_1 (a_1 + a_2)^2 \left(\frac{Q_{12}}{m}\right) \sin\theta \, d\theta \qquad (6.7.2.2)$$

where the collision coefficient η_{12} is defined as the ratio of the collision cross-section area of the particles to the projected area of the sphere taken normal to the direction of the particle flow.

Substituting Q_{12} from equation (6.7.2.1) into (6.7.2.2), we obtain after integration,

$$I_{12} = 74.13\, a_2^2\, \eta_{12}\rho_1 \left\{ (k_1 + k_2)^4 \left(\frac{1+r^*}{2}\right) \frac{u_1^8}{\bar{\rho}_1} \right\}^{\frac{1}{5}} h_{12}(V_1 - V_2) \qquad (6.7.2.3)$$

or

$$= \pi a_2^2 \rho_1 u_1 \left(\frac{Q}{m}\right) \qquad (6.7.2.4)$$

where $\bar{\rho}_1$ is material density of the particles and (Q/m) is defined as the effective charge transfer per unit mass of particles. In general, the collision coefficient η_{12} is governed by an inertia parameter ψ and a Stokesian parameter ϕ being defined as (32,59)

$$\psi = \frac{2\,\bar{\rho}_1 u_1 a_1^2}{9\mu a_2} \qquad (6.7.2.5)$$

and

$$\phi = \frac{18\,\bar{\rho}\, u_1 a_2}{\bar{\mu}\, \rho_1} \qquad (6.7.2.6)$$

For $\psi > 50$ and $\phi < 100$, which is true for the very small particles, η_{12} is very close to unity (32, 59). Further, for a

metallic sphere and non-conducting particles (i.e. $\sigma_2 >> \sigma_1$), the charge transfer coefficient h_{21} can be obtained from equation (2.1.8)

$$h_{12} \sim \frac{\sigma_1}{\ell_1} \sim \frac{\sigma_1}{a_1} \qquad (6.7.2.7)$$

Based on the foregoing analysis, a ball probe inserted into a suspension flow of particles would pick up current I_b proportional to the local mass flow $\rho_p u_p$ and the effective charge transfer, i.e.

$$I_b = A \rho_p u_p \left(\frac{Q}{m} \right) \qquad (6.7.2.8)$$

where A is the projected area of the ball probe.

Using a dimensional analysis approach, similar relationship was also obtained by Batch et al (69)

$$I_n = \frac{I_b^2}{\varepsilon_p d^2 \bar{\rho} u^2} = f(\varepsilon_p, d, A, \rho_p u_p, \bar{\rho}_p, \sigma_p) \qquad (6.7.2.9)$$

where ε_p is the permittivity, σ_p is the conductivity and d is the particle diameter. Their results indicate that for a given mass flow of particles, the probe current can change with the shape of the probe head.

Although in the absence of absolute measurements of h_{12}, η_{12} and other parameters, it is not possible to evaluate quantitatively the charges on the particles from the charge current, the ball probe can still provide a means of monitoring the dynamic behaviour of electrostatic charging. It essentially consists of a traversing gear and a .625 cm stainless steel ball as shown in Fig. 6.14, the details of construction being given in Reference (46). A small length of pipe in the fully developed flow region, about 8 m downstream of the solid feed point, was cut away to provide for the insertion of the ball probe. Because of the small magnitude of the charge current, amplifying instrument with high input impedance would be required and after a number of trial runs, a Levell D.C.

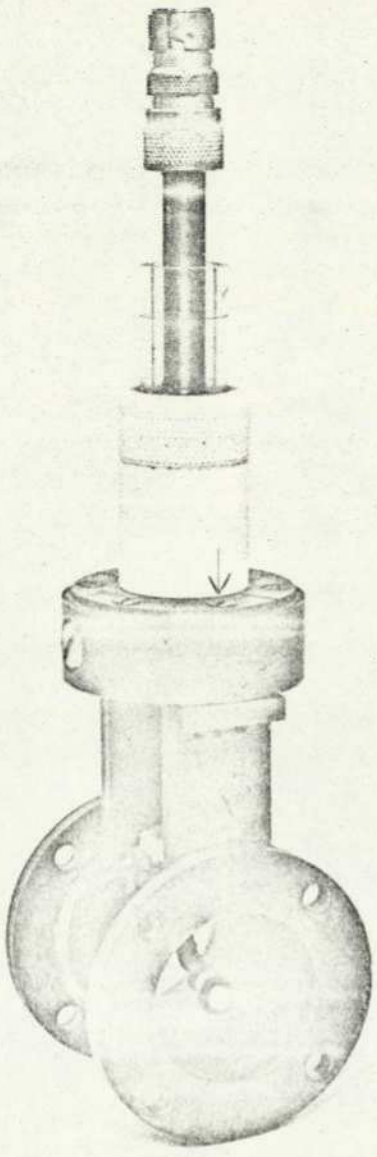

Fig. 6.14 (a). Electrostatic ball probe.

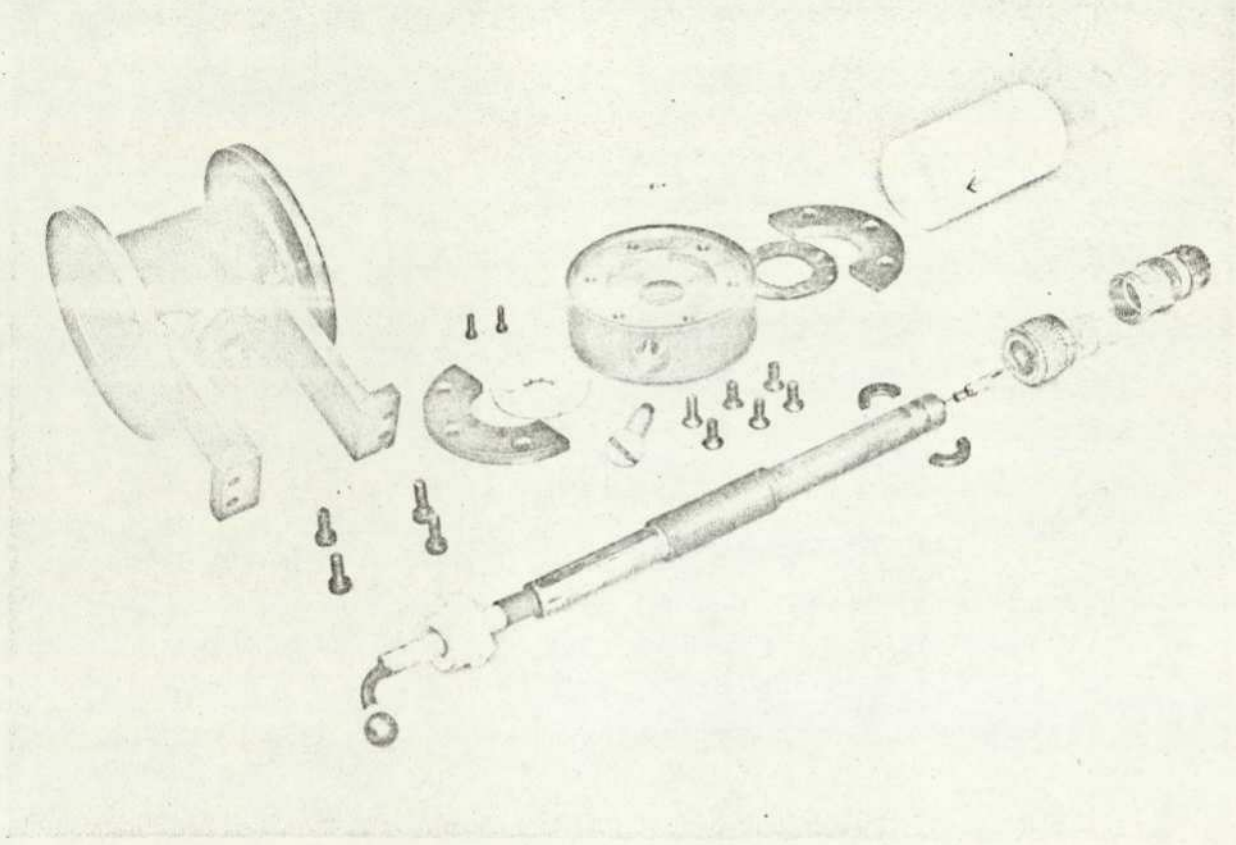

Fig. 6.14 (b). Electrostatic ball probe assembly.

multimeter was found to be acceptable. This instrument not only has high input impedance but also high A.C. cut-out capacity and it produces a voltage output directly proportional to the current input, thus making on-line data logging possible. In addition, a R-C network was also used as a filtering device (Fig. 6.15).

6.8 Air Ionization

In order to determine the effect of electrostatic charging on the pressure drop and friction factor, it is desirable to "vary" the charges on the particles so that comparisons can be made between identical runs. The methods that are commonly used for static reduction have been outlined in Section 2.4 and in this work, radioactive source was chosen because of its simplicity in operation.

Air ionization was provided by a 3M ionized air source unit, Model 907. The ionizer is cylindrical in shape and can be fitted directly in line with the air flow (Fig. 6.16). Doubly positive charged α particles are emitted from the radio isotopes of Polonium 210 which are safely contained in small ceramic beads lined on the inner surface of the unit. The ionization of the air produces effectively a conductive path to drain off any charges on the nearby surfaces.

6.9 Data Logging and Processing

It can be seen from the previous sections that mass flow rates, pressure distribution and current output from the electrostatic ball probe have all been conveniently transformed into D.C. signals which are compatible with most recording instruments. For the present work, the data signals were first pre-amplified by means of integrated circuit operational amplifiers before being fed into the input channels of a Solartron Data Logger which was programmed to scan the addressed input channels continuously at a constant scan speed of 4 CNL/sec. The total scan period was set to allow for at least six scans of each input signal so that time averaging could be made. The signals were then output sequentially in BDC form on paper tape by a Facit tape punch, being driven by a built-in drive unit of the data logger. Manual entries such as date of experiment, ambient temperature and pressure, air humidity and physical properties

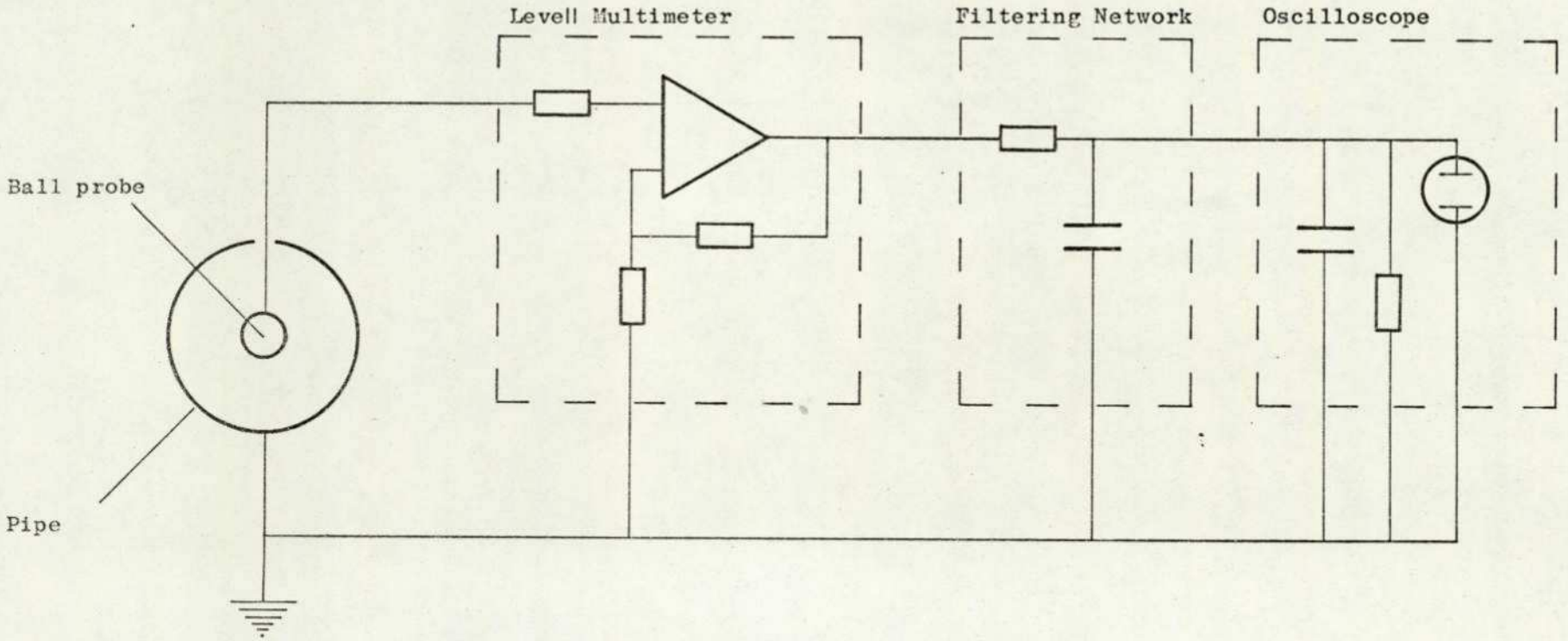

Fig. 6.15. Electrostatic ball probe circuit diagram.

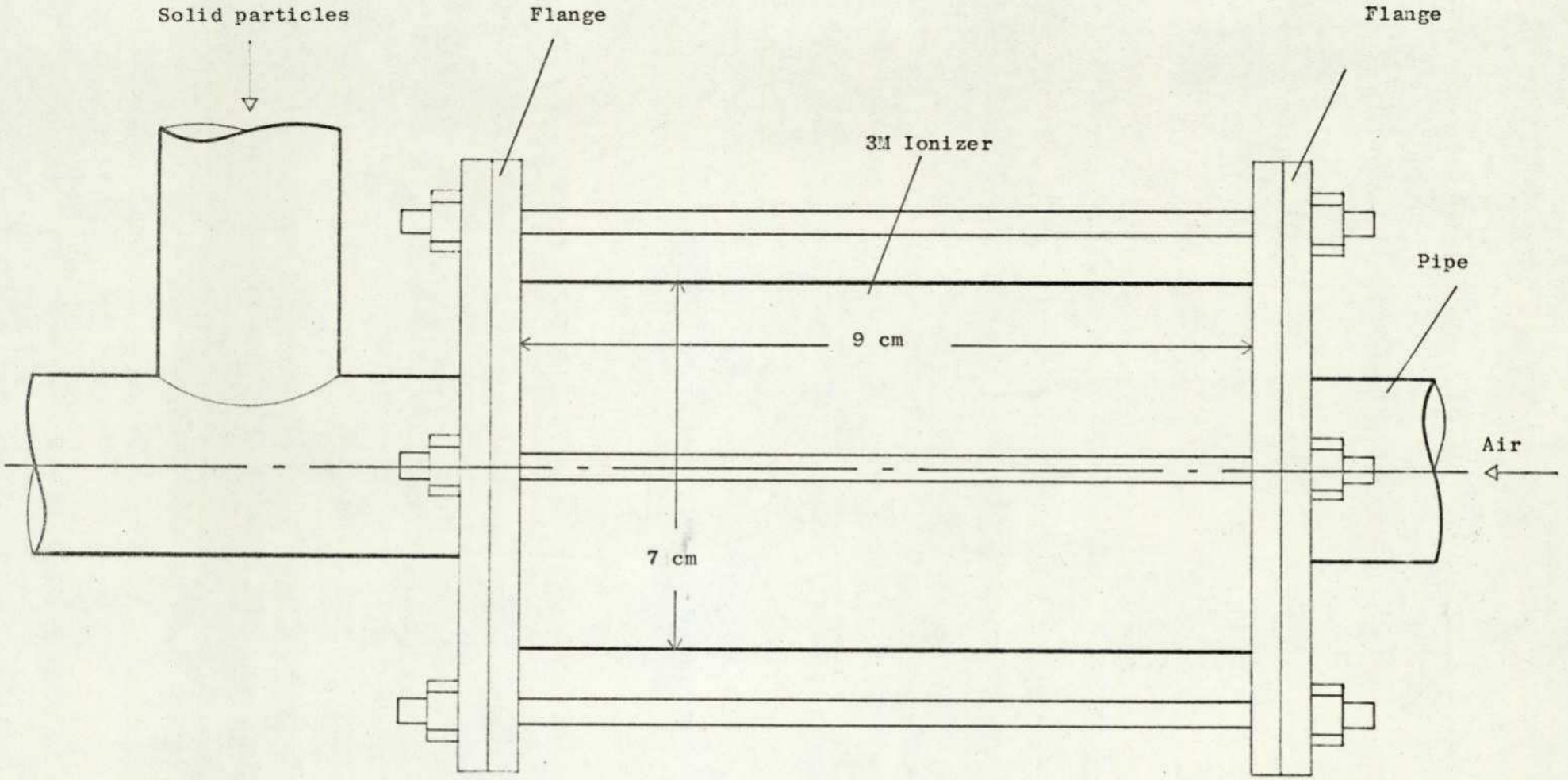

Fig. 6.16. Installation of the 3M Ionizer.

of solid particles were entered on the data tape via a keyboard and further, in order to identify each bit of information on the tape, an index number was entered prior to each manual entry or data scan. The data tapes were then processed by computer programs and stored on disc files for future use. The overall procedure of the data logging and processing system is summarized by the block diagram as shown in Fig. 6.17 and the functions of the computer programs #CPY1, #PDP1, #PDP2, #PJ03 and #PJ04 are assfollows:

#CPY1 : To process data tapes produced by the Solartron/ Facit system and store results on disc files.

#PDP1 : To compute air velocity distribution, air friction factor and other pipe flow parameters.

#PDP2 : To compute mass flow rates, pressure distribution suspension flow friction factors, ball probe current, charge transfer and standard deviations of input signals.

#PJ03 : To sort out data for graphical analysis.

#PJ04 : To perform graph plotting utilizing the Calcomp graph plotting system.

In addition, the mass flow rates and probe current were continuously monitored on a storage type CRO so that fluctuations in the system could be observed and test runs with high fluctuations were deleted.

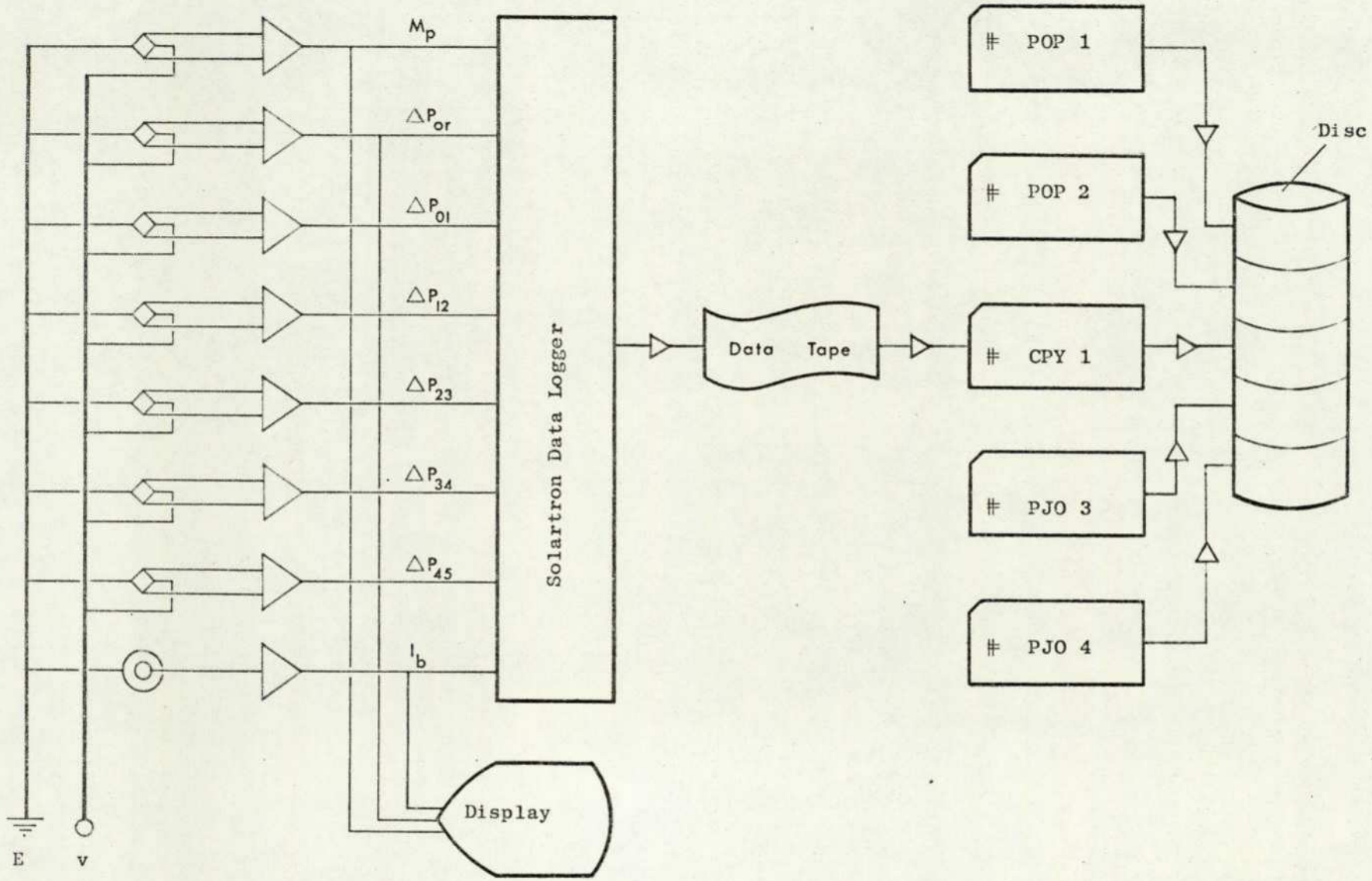

Fig. 6.17. Block diagram of the data logging and processing system.

CHAPTER 7

DISCUSSION OF ANALYTICAL RESULTS

The main objective of the theoretical analysis outlined in Chapter 4 is to describe the electrostatic and gravity effects on the pipe flow characteristics of gas-solid suspensions. The two sets of characteristic equations (Section 4.4 and 4.5) based respectively on the present and Soo and Tung's (29) treatments were solved by the numerical methods given in Appendices 2 and 3. In the present analysis, the particle relaxation time F^{-1} is a function of the local relative velocity $|u-u_p|$ and drag coefficient C_D which itself is determined from a set of equations relating C_D and particle Reynolds number Re_p $(2a\bar{\rho}|u-u_p|\bar{\mu})$, proposed by Morsi and Alexander (59), and the particle diffusivity D_p is governed by the field forces whereas both F and D_p were assumed to be constant by Soo and Tung.

In view of the large number of variables involved in the problem, a series of test cases with mass flow ratios in the range of 0.7 to 2.7, typical charge to mass ratios of 10^{-6} to 10^{-4} c/kg and particle sizes of 35μ (#1) and 75μ (#2) have been studied and the results are present in graphical form as shown in Figs. 7.1 - 7.36 and 7.37 - 7.60, summaries of the results being given in Tables 7.1 and 7.2. Graph plotting was performed by computer programs #PJ05 and #PJ06, utilizing the Calcomp graph plotting system implemented on the ICL 1905 digital computer. (x, o and □ denote distributions in upward vertical, horizontal and downward vertical planes).

We shall first examine the solutions obtained by the present method (i.e. Figs. 7.1 - 7.36) in which α,β,γ, and η are correlation parameters characterizing the electrostatic, diffusion,

relaxation and gravity effects on the suspension flow. The present study indicates that electrostatic effects are usually negligible when α is less than 0.1. β is the ratio of relaxation time F^{-1} to diffusion time (R^2/D_p) for $D_p \sim D_f$, and the analysis shows that large values of β tend to give particle velocity profile close to that of the fluid. The gravity effect on the pipe flow is characterized by γ and η, and at large values of γ, the velocity of the particles may change from concurrent to counter current flow with respect to the fluid. When D_p is small, η becomes large for $\bar{\rho}_p >> \bar{\rho}$ and particle deposition on the pipe wall may occur.

Within the present range of mass flow rates, the electric potential of the particulate phase, being constant at the pipe wall, is symmetrically distributed about the pipe axis and appears to be independent on the size of the particles.

The effect of electrostatic charging on the suspension flow is perhaps most evident from the results of the particulate density distribution ρ_p with respect to different values of q/m. Recalling the definition of α (equation 4.4.6), it is obvious that the extent of electrostatic effect on ρ_p will depend not only on q/m but also on the mass flow rates and the size of the particles. At low mass flow ratios (M_p = .02 kg/sec and u_o = 40. m/sec) or $q/m < 10^{-5}$ c/kg, ρ_p being pre-determined by gravity and diffusion effects is almost unaffected by the presence of charges on the particles. As expected, the particulate density at the bottom of the pipe $\rho_p(R,\pi)$ is higher than that at the top $\rho_p(R,0)$, the ratio of $\rho_p(R,\pi)$ to $\rho_p(R,0)$ being 2 and 4 for the 35μ and 75μ particles, and further ρ_p is uniformly distributed in a horizontal plane through the pipe axis (e.g. Figs. 7.13 and 7.15; Figs. 7.31 and 7.32). As the mass flow ratio increases, the charges on the particles become more significant. For an increase of q/m from 10^{-5} to 10^{-4} c/kg, $\rho_p(R,\pi)$ and $\rho_p(R,0)$ increase by 22% with M_p = .02 kg/sec and u_o = 20. m/sec, and by as much as 40% with M_p = .04 kg/sec, resulting in a lower density of particles at the pipe axis. Under these extreme conditions, ρ_p is no longer

uniformly distributed in the horizontal plane (e.g. Figs. 7.7 and 7.9). Generally, electrostatic effect is less significant at high air velocities even though the effective mass flow ratio may not be low (e.g. Figs. 7.1 and 7.3; Figs. 7.13 and 7.15).

The velocity distribution of the small particles (35μ) is symmetrical about the pipe axis whereas that of the larger particles (75μ) deviates slightly from axial symmetry with their motion lagging relatively more behind the fluid. Because of the lower density of particles at the top of the pipe, a greater particle velocity occurs at the top than at the bottom as a result of momentum balance. The characteristic slip velocity of the particles at the wall u_{pw} is governed only by the Knudsen number Knp. Whilst larger Knp leads to greater u_{pw} at the wall, for the same Knp, u_{pw} decreases as the particle size increases. The predicted velocity distribution of the particles are in good agreement with experimental results obtained by Soo et al (6). As shown in Fig. 7.61, their results indicate that the particles (50μ glass beads) follow almost exactly the motion of the fluid at the pipe centre whereas the present analysis predicts $(u_{po}/u_o) \sim .93$ and $\sim .9$ for the 35μ and 75μ particles respectively. Even at high charge to mass ratios ($q/m \sim 10^{-4}$ c/kg), the particle velocity distribution is affected only to a negligible extent by the presence of charges on the particles. The peak of the mass flux $\rho_p u_p$ appears to be at R/4 below the pipe axis and shifts slightly further to the bottom at high charge to mass ratios.

In contrast to the theoretical analysis described in Section 3.1, the present analysis indicates that D_p is less than that of the fluid D_f and in the case of the smaller particles (35μ), D_p remains sensibly constant in the core region. Generally, the ratio of D_p/D_f is unaffected by M_p but decreases as u_o increases and the distribution of D_p is not influenced by the charges on the particles. However, it is worth noting that the present analysis cannot predict D_p near the wall because of the unknown boundary conditions there. In general, particles are driven to the wall by

gravity and/or electrostatic forces. A completely non-depositing gas-solid suspension flow will have to be due to turbulent diffusion except very close to the wall in the viscous sublayer where turbulent diffusivity vanishes and Magnus lift force becomes significant. Very fine particles ($2a < 1\mu$) are able to traverse the sublayer through the action of Brownian motion but for the larger particles with negligible Brownian diffusivity and relaxation time still being small compared to the characteristic time of the eddies just outside the sublayer, some more powerful mechanism must be called into play to enable the particles to reach the wall.

Although the numerical solutions based on Soo and Tung's method (Figs. 7.37 - 7.60) are similar to those predicted by the present analysis (Figs. 7.1 - 7.24), in contrast to their assumption of constant F (i.e. $|u-u_p|$ = constant), the particle velocity distributions indicate that $|u-u_p|$ varies significantly in the radial direction. However, these results also show similar trends of the effects of electrostatic charging and gravity on the flow characteristics.

We now examine the validity of the continuum approximation and its associate assumption. For fully developed gas-solid suspension flow in horizontal pipe, equation (4.3.3) reduces to

$$-\left(\frac{\partial P}{\partial x}\right)_m + \frac{1}{r}\frac{\partial}{\partial r}(r\tau_{zr}) - K_m F \rho_p (u - u_p) = 0 \qquad (7.1)$$

and that for air alone becomes

$$-\frac{\partial P}{\partial x} + \frac{1}{r}\frac{\partial}{\partial r}(r\tau_{zr}) = 0 \qquad (7.2)$$

where the momentum transfer coefficient $K_m = 1$ for $u > u_p$, as suggested by Soo (32) and $(\partial P/\partial x)_m$ and $(\partial P/\partial x)$ are constant across the pipe section (Section 4.2). Further, the assumption of the motion and statistical properties of the fluid not being affected

by the presence of particles, as guided by the experimental results of various workers (7,33,52), implies that

$$F\rho_p(u - u_p) = -\frac{\partial P}{\partial x}_m + \frac{\partial P}{\partial x} = \text{constant} \qquad (7.3)$$

We see that equation (7.3) can only be satisfied if both ρ_p and $(u - u_p)$ are constant, i.e. uniform particulate density distribution and particle motion constantly lagging behind the fluid. In fact the present results indicate that $F\rho_p(u - u_p)$ is a function of r and ϕ, and u_p can be greater than u near the pipe wall. A plausible explanation is that K_m is not always unity even though particles are accelerated by the fluid but varies according to the local particle density concentration and relative velocity such that $K_m F\rho_p(u - u_p)$ remains constant.

In spite of the inability to predict the overall pressure drop of the suspension, the present analysis indicates that for charge to mass ratio less than 10^{-5} c/kg (i.e. gravity effect being dominant), ρ_p and u_p are not influenced by the charges on the particles and therefore if $F\rho_p(u - u_p)$ can be regarded as the contribution of pressure drop due to the particles, electrostatic effect on the overall pressure drop can also be neglected.

ANALYTICAL CURVES OF VARIOUS DISTRIBUTIONS IN A FULLY DEVELOPED TURBULENT GAS-SOLID SUSPENSION FLOW.

(FIGURES 7.1 - 7.60)

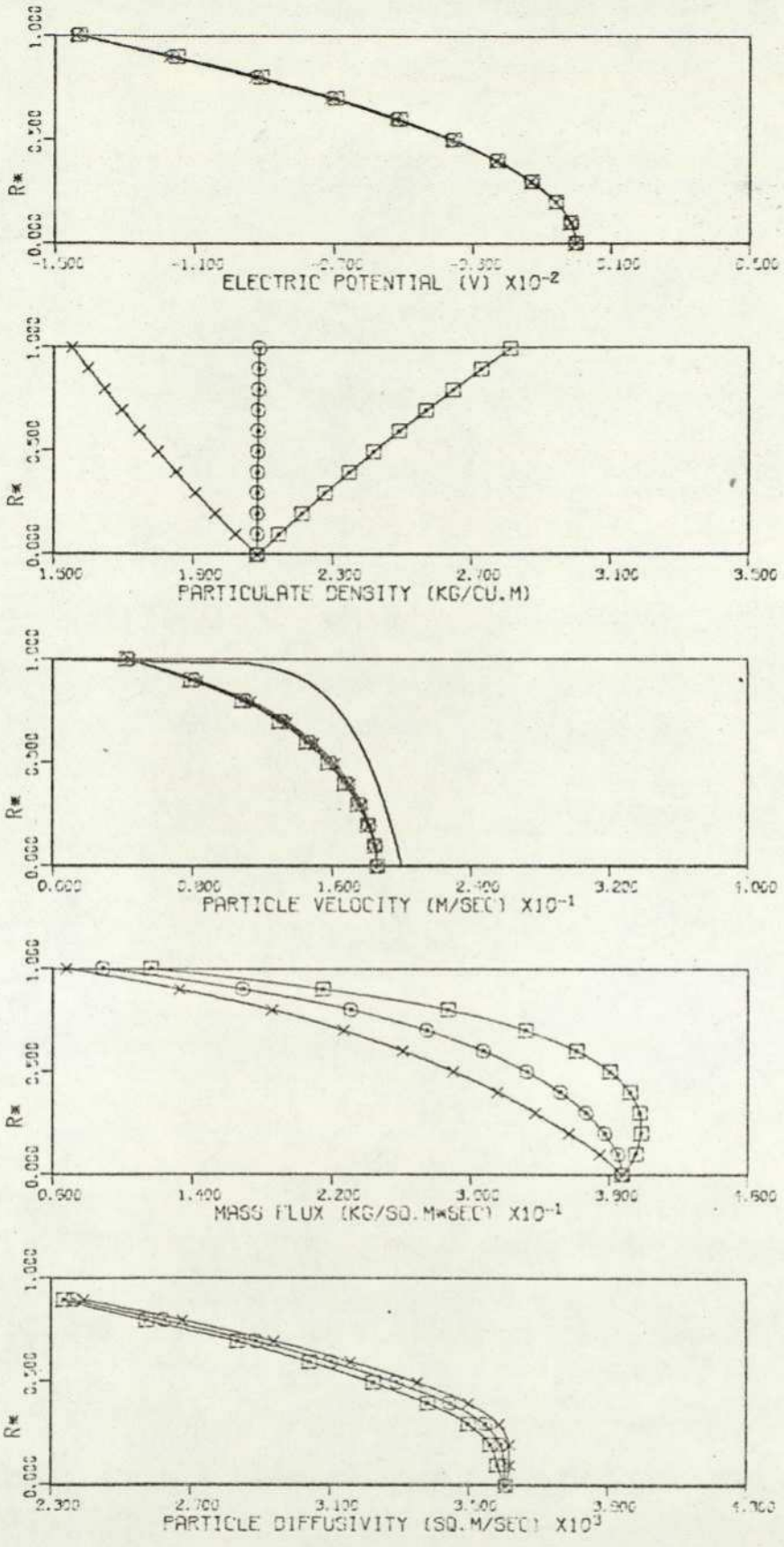

FIGURE :7.1 VARIOUS DISTRIBUTIONS IN A FULLY DEVELOPED TURBULENT GAS-SOLID SUSPENSION FLOW. PARTICLES TYPE #1.

PIPE FLOW PARAMETERS : R=0.156E-01 M, UO=0.200E 02 M/SEC, Q/M=0.100E-04 C/KG, KNP=0.100E 00, DF=0.468E-02 SQ.M/SEC, MP=0.200E-01(EXPT), 0.200E-01 (COMP) KG/SEC. PIPE INCLINATION = 90.0°. ×=0.0°, ⊙=90.0°, ⊡=180.0°, —— AIR.

DATA COMPUTED BY #XFD76, PLOTTED BY #PJDS (TEST 00-01-0-1A).

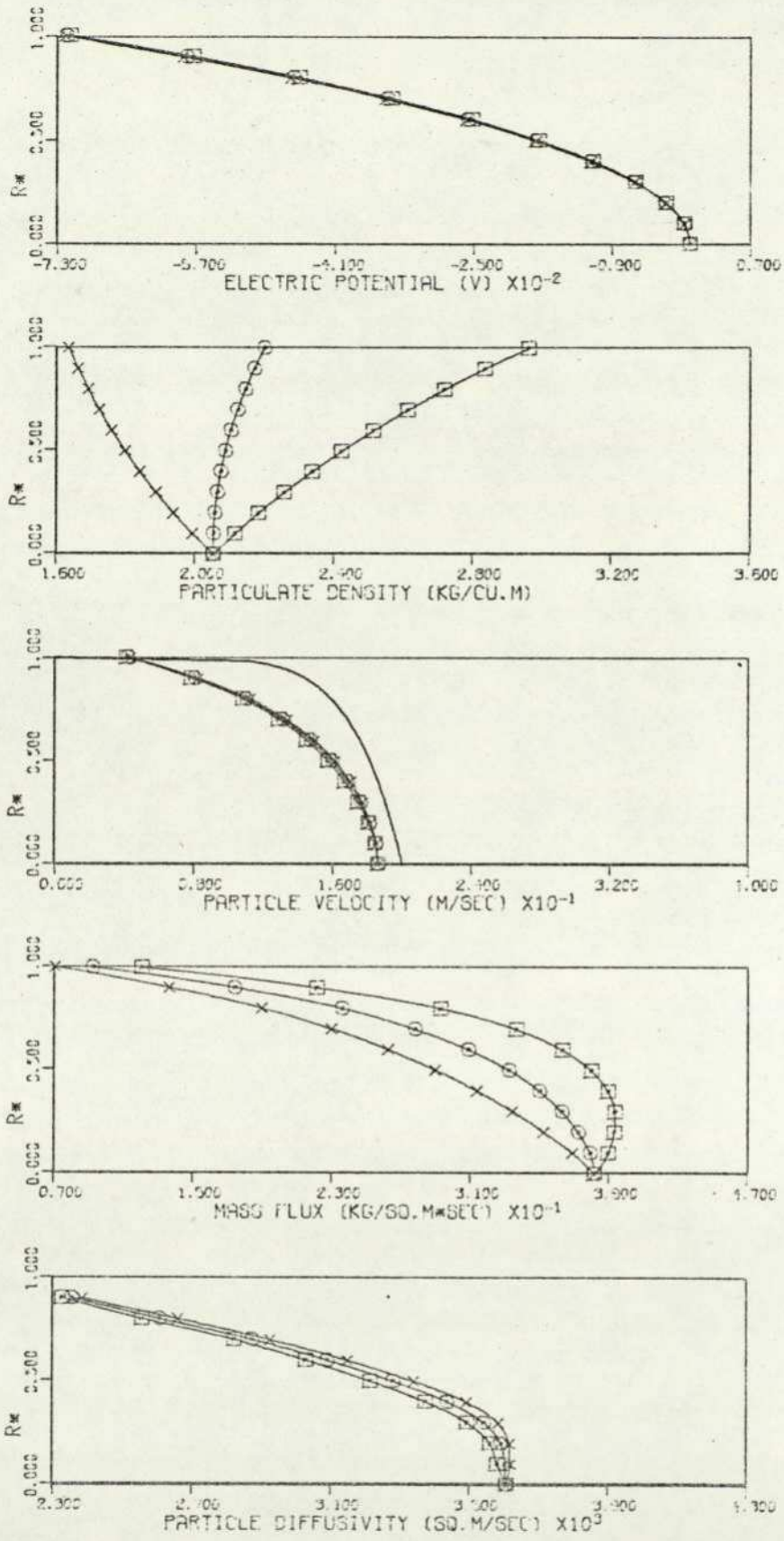

FIGURE : 7.2 VARIOUS DISTRIBUTIONS IN A FULLY DEVELOPED TURBULENT GAS-SOLID SUSPENSION FLOW. PARTICLES TYPE #1.

PIPE FLOW PARAMETERS : R=0.156E-01 M, U0=0.200E 02 M/SEC, Q/M=0.500E-04 C/KG, KNP=0.100E 00, DF=0.469E-02 SQ.M/SEC, MP=0.200E-01(EXPT), 0.202E-01 (COMP) KG/SEC. PIPE INCLINATION = 90.0°. × -0.0°, ⊙ -90.0°, ⊡ -180.0 , —— AIR.

DATA COMPUTED BY #XFD7S, PLOTTED BY #PJ05 (TEST 00-02-0-1A).

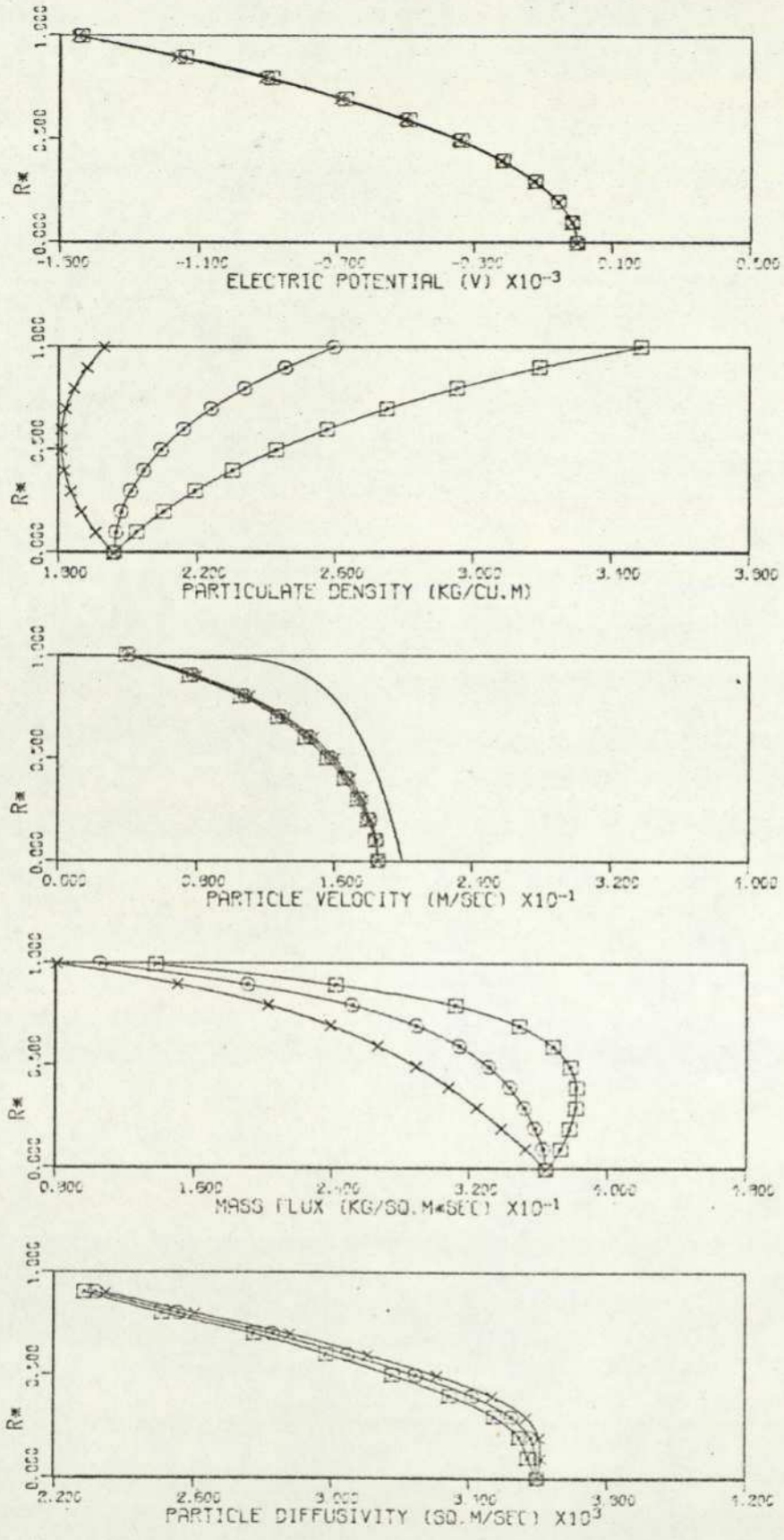

FIGURE : 7.3 VARIOUS DISTRIBUTIONS IN A FULLY DEVELOPED TURBULENT GAS-SOLID SUSPENSION FLOW. PARTICLES TYPE #1.

PIPE FLOW PARAMETERS : R=0.156E-01 M, UO=0.200E 02 M/SEC, O/M=0.100E-03 C/KG, KNP=0.100E 00, DF=0.468E-02 SQ.M/SEC, MP=0.200E-01(EXPT), 0.207E-01 (COMP) KG/SEC. PIPE INCLINATION = 90.0°. ×=0.0°, ⊙=90.0°, ⊡=180.0°, —— AIR.

DATA COMPUTED BY #XFD7B, PLOTTED BY #PL05 (TEST 00-03-0-1A).

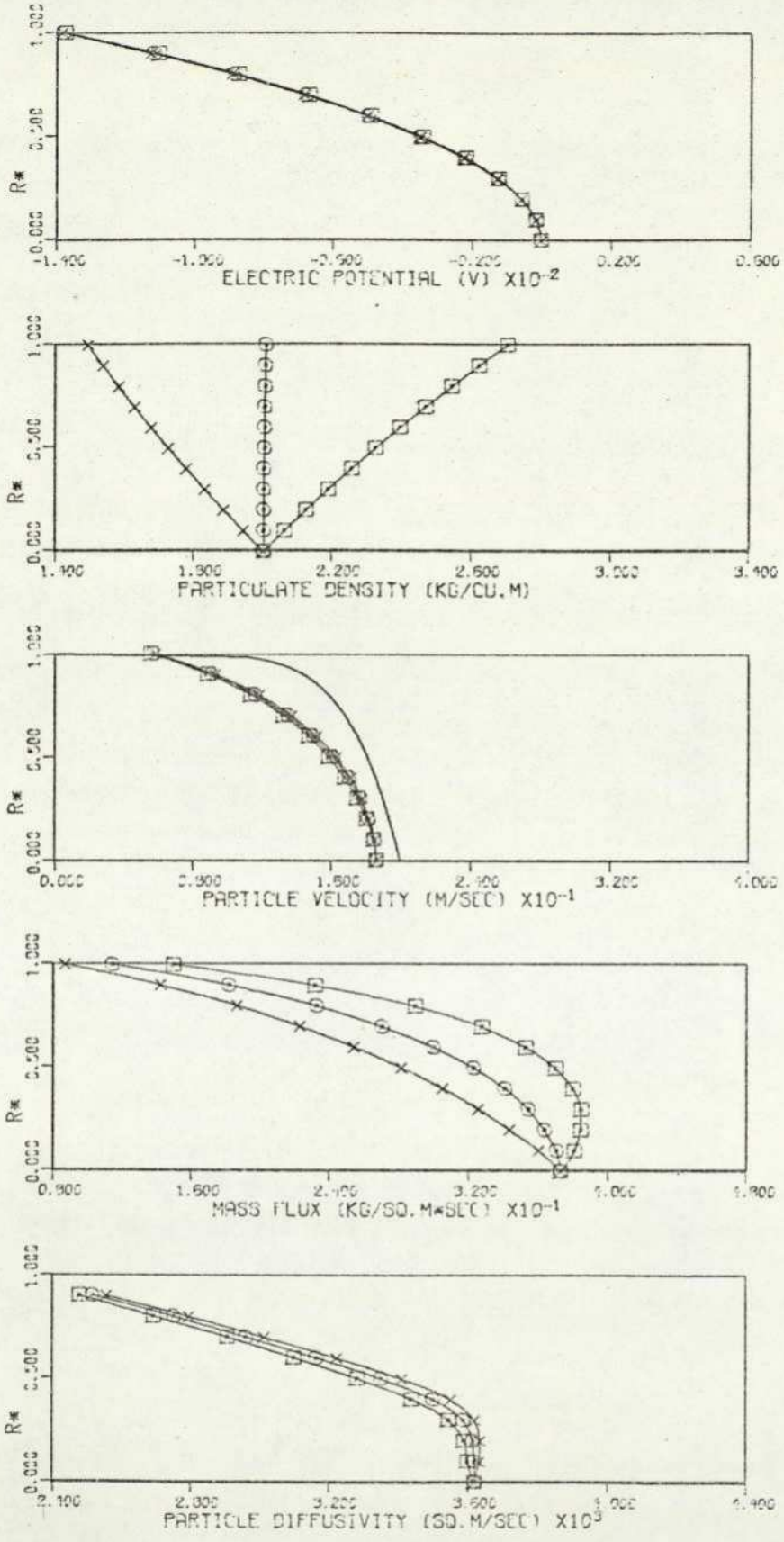

FIGURE : 7.4 VARIOUS DISTRIBUTIONS IN A FULLY DEVELOPED TURBULENT GAS-SOLID SUSPENSION FLOW. PARTICLES TYPE #1.

PIPE FLOW PARAMETERS : R=0.156E-01 M, U0=0.200E 02 M/SEC, Q/M=0.100E-04 C/KG, KNP=0.150E 00, DF=0.468E-02 SQ.M/SEC, MP=0.200E-01(EXPT), 0.200E-01 (COMP) KG/SEC. PIPE INCLINATION = 90.0°. × =0.0°, ⊙ =90.0°, ⊡ =180.0°, —— AIR.

DATA COMPUTED BY #XFD7B. PLOTTED BY #PJ05 (TEST 00-04-0-1A).

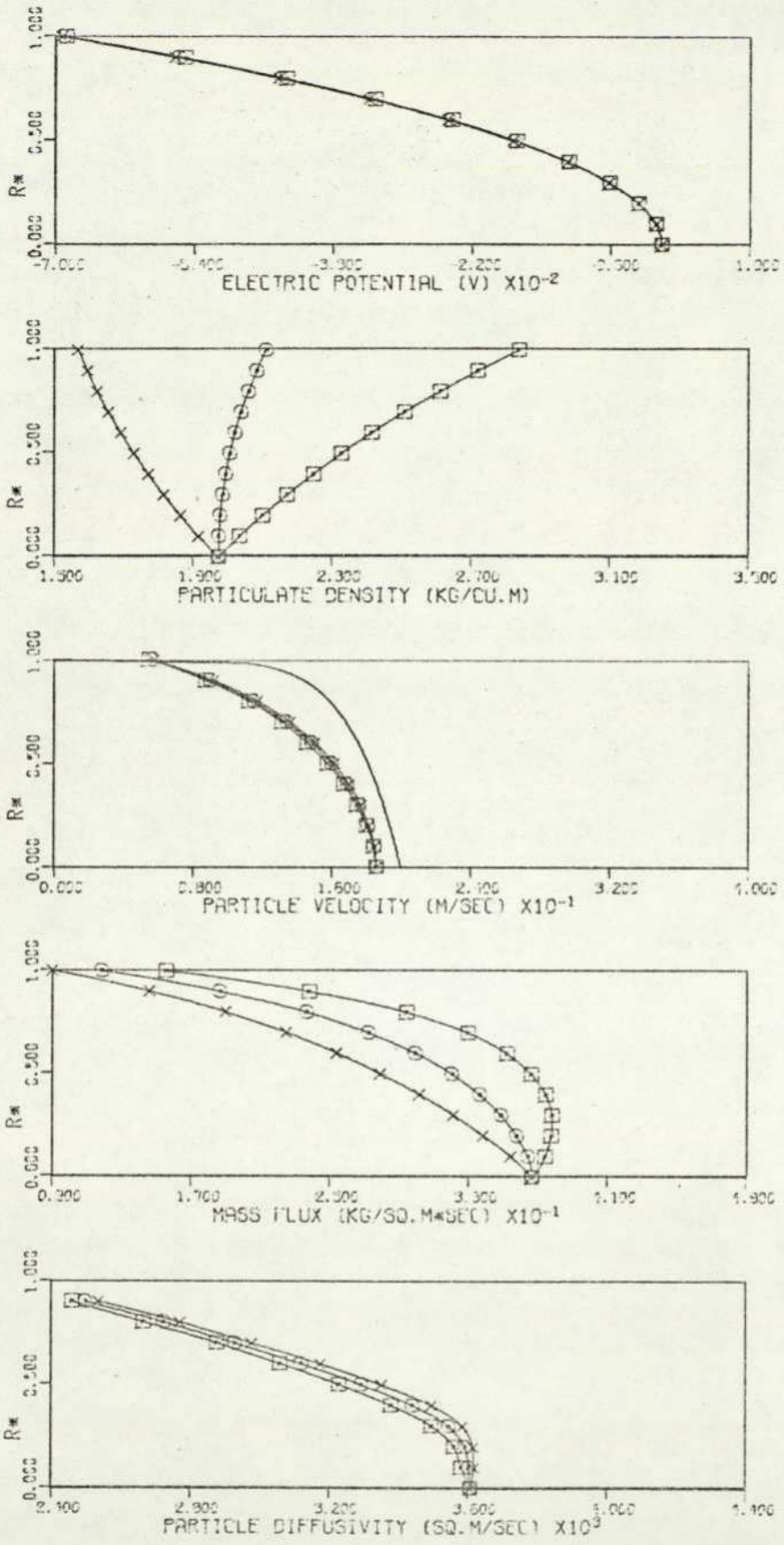

FIGURE : 7.5 VARIOUS DISTRIBUTIONS IN A FULLY DEVELOPED TURBULENT GAS-SOLID SUSPENSION FLOW. PARTICLES TYPE #1.

PIPE FLOW PARAMETERS : R=0.156E-01 M, UO=0.200E 02 M/SEC, Q/M=0.500E-04 C/KG, KNP=0.150E 00, DF=0.468E-02 SQ.M/SEC, MP=0.200E-01(EXPT), 0.201E-01 (COMP) KG/SEC.
PIPE INCLINATION = 90.0°. × =0.0°, ⊙ =90.0°, ⊡ =180.0°, —— AIR.

DATA COMPUTED BY #XFDTB, PLOTTED BY #PL05 (TEST 00-05-0-1A).

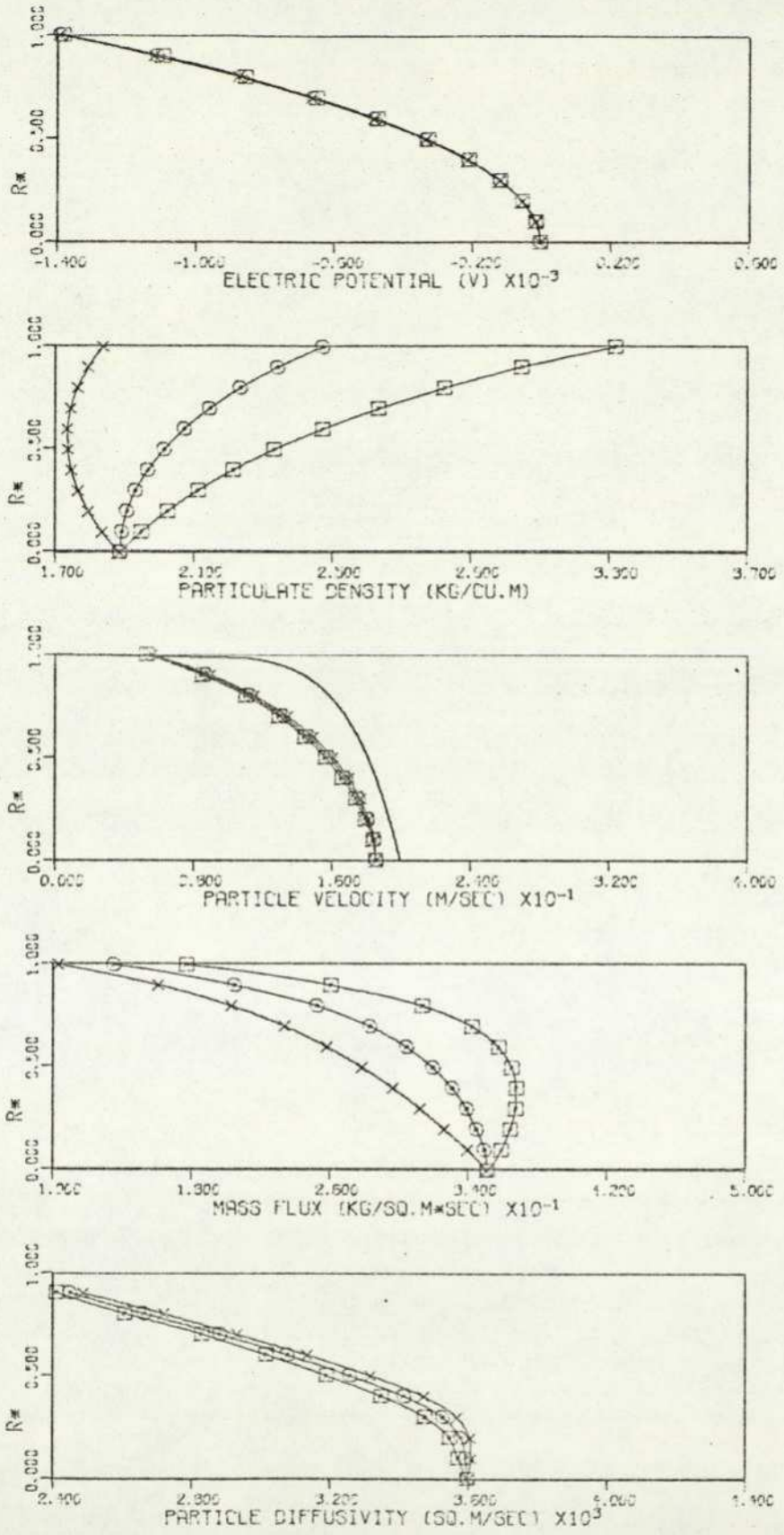

FIGURE : 7.6 VARIOUS DISTRIBUTIONS IN A FULLY DEVELOPED TURBULENT GAS-SOLID SUSPENSION FLOW. PARTICLES TYPE #1.

PIPE FLOW PARAMETERS : R=0.156E-01 M, UO=0.200E 02 M/SEC, Q/M=0.100E-03 C/KG, KNP=0.150E 00, DF=0.469E-02 SQ.M/SEC, MP=0.200E-01(EXPT), 0.206E-01 (COMP) KG/SEC.
PIPE INCLINATION = 90.0°. ×=0.0°, ⊙=90.0°, ⊡=180.0°, —— AIR.

DATA COMPUTED BY #XFD7B, PLOTTED BY #PJ05 (TEST 00-05-0-1A).

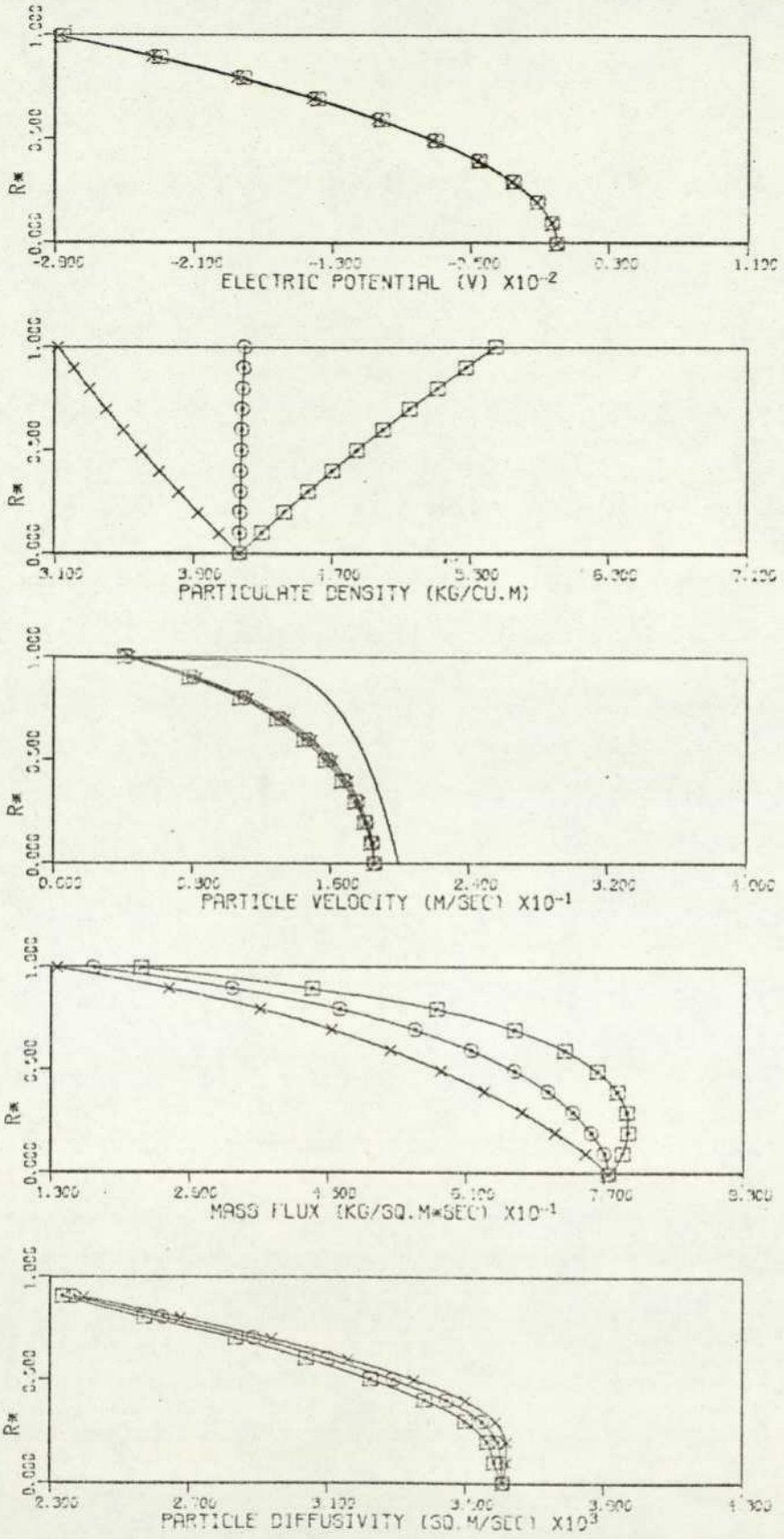

FIGURE : 7.7 VARIOUS DISTRIBUTIONS IN A FULLY DEVELOPED TURBULENT GAS-SOLID SUSPENSION FLOW. PARTICLES TYPE #1.

PIPE FLOW PARAMETERS : R=0.156E-01 M, UO=0.200E 02 M/SEC, Q/M=0.100E-04 C/KG, KNP=0.100E 00, DF=0.469E-02 SQ.M/SEC, MP=0.400E-01(EXPT), 0.400E-01 (COMP) KG/SEC. PIPE INCLINATION = 90.0°. ×=0.0°, ⊙=90.0°, ⊡=180.0°, —— AIR.

DATA COMPUTED BY #XFD76, PLOTTED BY #PJ05 (TEST 00-07-0-19).

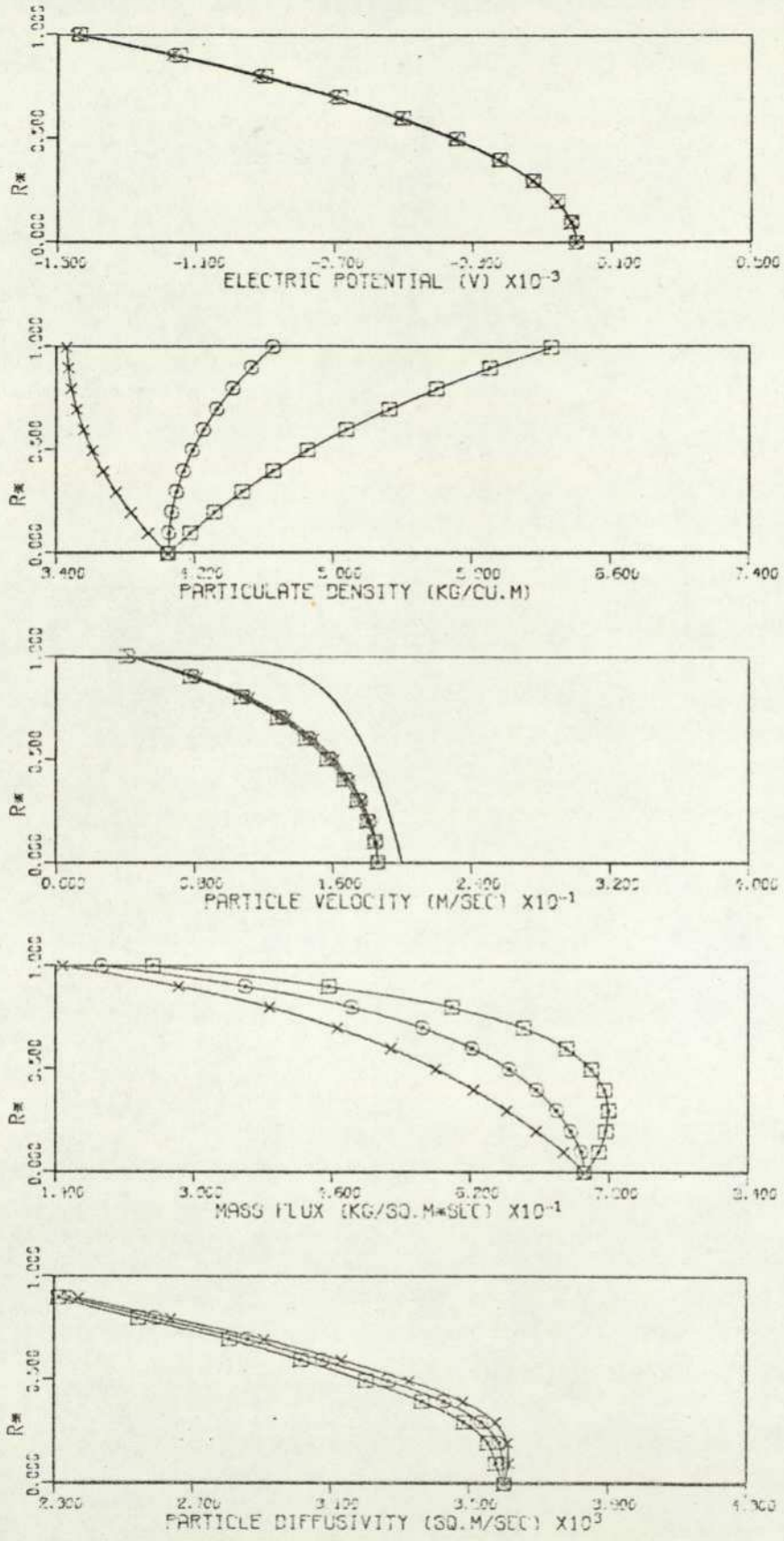

FIGURE : *7.8* VARIOUS DISTRIBUTIONS IN A FULLY DEVELOPED TURBULENT GAS-SOLID SUSPENSION FLOW. PARTICLES TYPE #1.

PIPE FLOW PARAMETERS : R=0.156E-01 M, U0=0.200E 02 M/SEC, Q/M=0.500E-04 C/KG, KNP=0.100E 00, DF=0.463E-02 SQ.M/SEC, MP=0.400E-01(EXPT), 0.407E-01 (COMP) KG/SEC.
PIPE INCLINATION = 90.0°. ×=0.0°, ⊙=90.0°, ⊡=180.0°, —— AIR.

DATA COMPUTED BY #XFD7S, PLOTTED BY #PJDS (TEST 00-08-0-1A).

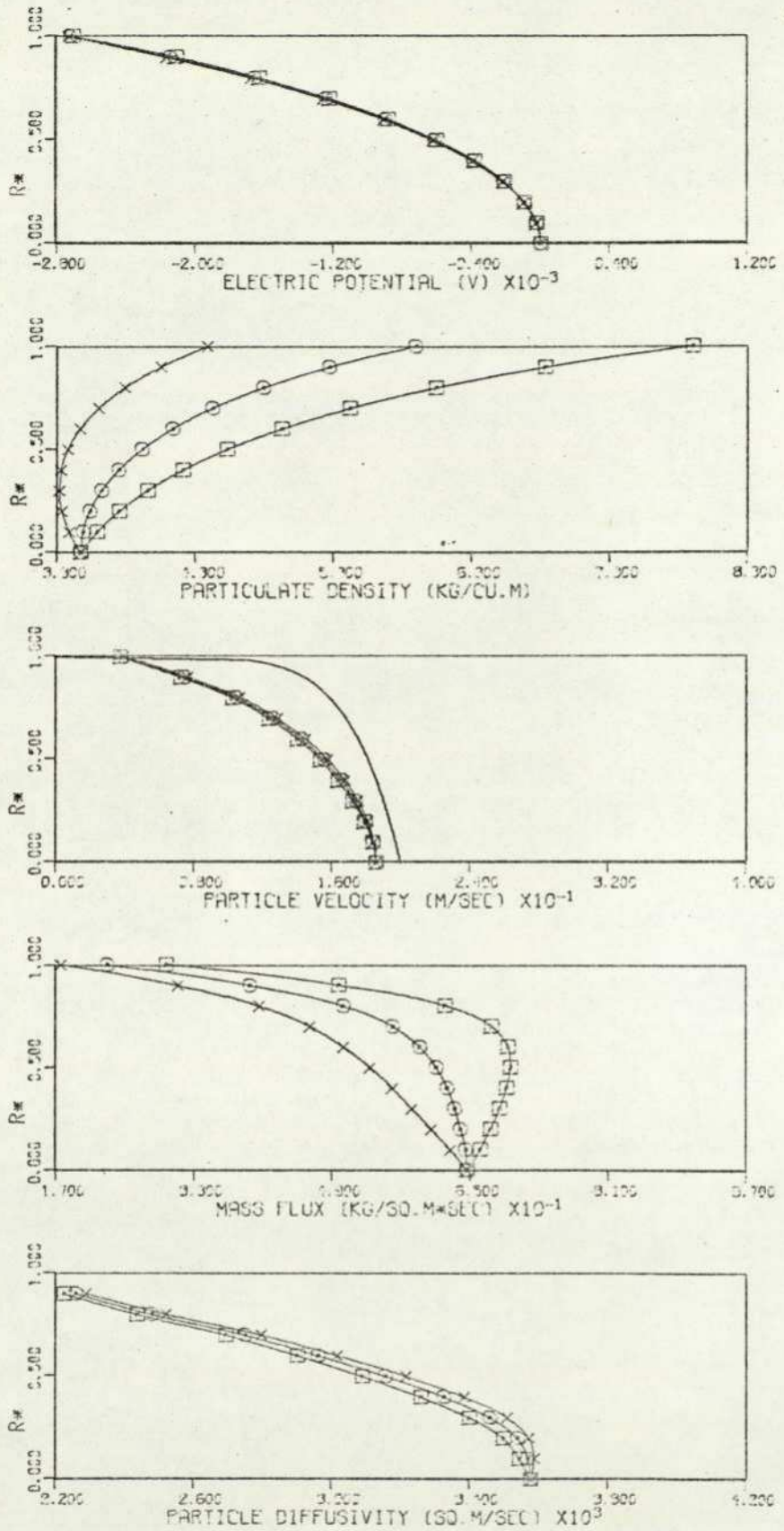

FIGURE : 7.9 VARIOUS DISTRIBUTIONS IN A FULLY DEVELOPED TURBULENT GAS-SOLID SUSPENSION FLOW. PARTICLES TYPE #1.

PIPE FLOW PARAMETERS : R=0.156E-01 M, UO=0.200E 02 M/SEC, Q/M=0.100E-03 C/KG, KNP=0.100E 00, DF=0.469E-02 SQ.M/SEC, MP=0.400E-01(EXPT), 0.395E-01 (COMP) KG/SEC. PIPE INCLINATION = 90.0°. X =0.0°, ⊙ =90.0°, ⊡=180.0°, —— AIR.

DATA COMPUTED BY #XFD7B, PLOTTED BY #PJ05 (TEST 00-03-0-1A).

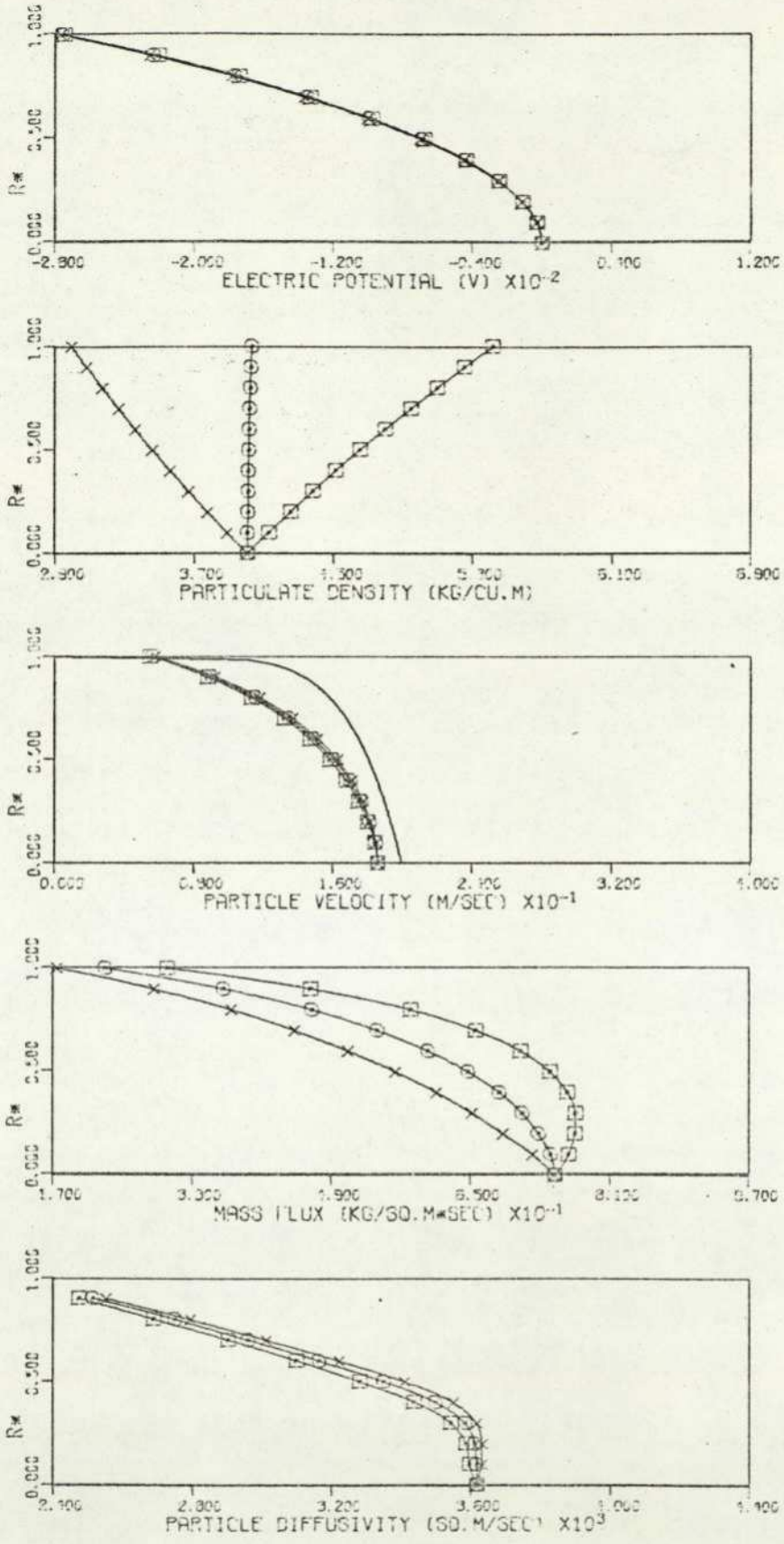

FIGURE : 7.10 VARIOUS DISTRIBUTIONS IN A FULLY DEVELOPED TURBULENT GAS-SOLID SUSPENSION FLOW. PARTICLES TYPE #1.

PIPE FLOW PARAMETERS : R=0.156E-01 M, UO=0.200E 02 M/SEC, Q/M=0.100E-04 C/KG, KNP=0.150E 00, DF=0.469E-02 SQ.M/SEC, MP=0.400E-01(EXPT), 0.400E-01 (COMP) KG/SEC. PIPE INCLINATION = 90.0°. ×+0.0°, ⊙ -90.0°, ⊡+180.0°, —— AIR.

DATA COMPUTED BY #XFD7B, PLOTTED BY #PJ05 (TEST 00-10-0-1A).

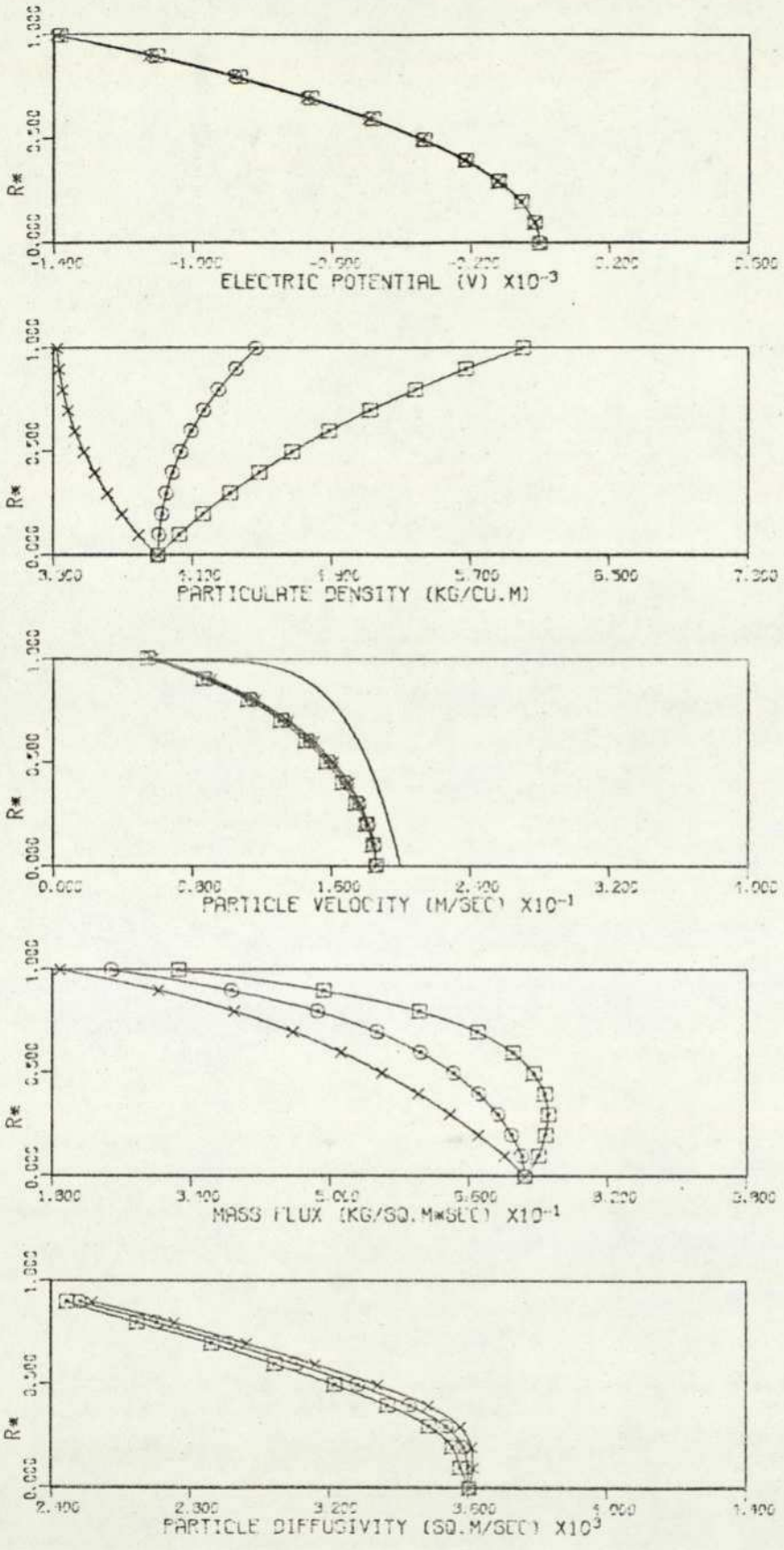

FIGURE : *7.11* VARIOUS DISTRIBUTIONS IN A FULLY DEVELOPED TURBULENT GAS-SOLID SUSPENSION FLOW. PARTICLES TYPE #1.

PIPE FLOW PARAMETERS : R=0.156E-01 M, UO=0.200E 02 M/SEC, O/M=0.500E-04 O/KG, KNP=0.150E 00, DF=0.468E-02 SQ.M/SEC, MP=0.400E-01(EXPT), 0.407E-01 (COMP) KG/SEC.
PIPE INCLINATION = 90.0°. ×=0.0°, ⊙=90.0°, ⊡=180.0°, —— AIR.

DATA COMPUTED BY #XF07S, PLOTTED BY #PJ05 (TEST 00-11-0-1A).

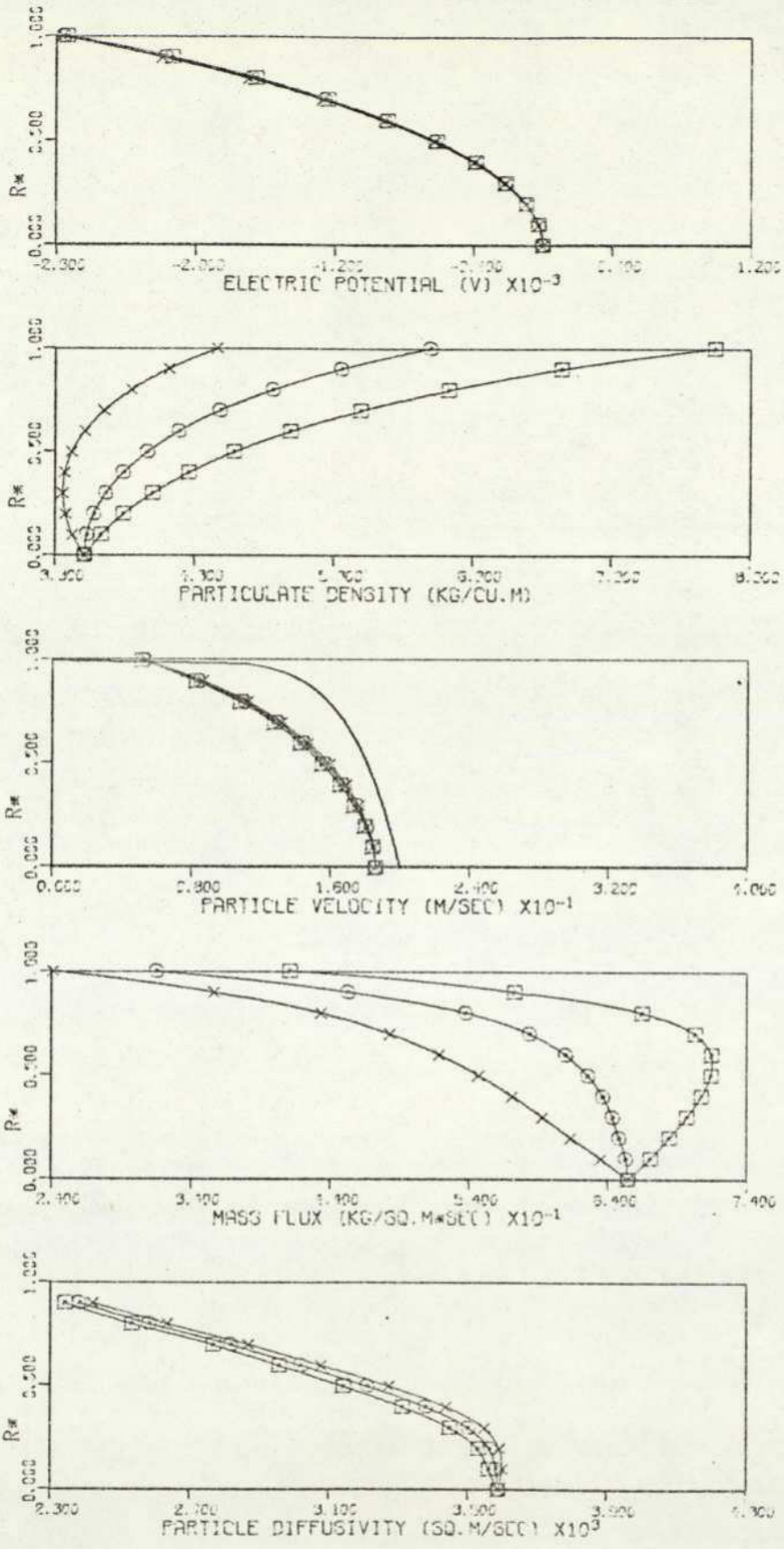

FIGURE : 7.12 VARIOUS DISTRIBUTIONS IN A FULLY DEVELOPED TURBULENT GAS-SOLID SUSPENSION FLOW. PARTICLES TYPE #1.

PIPE FLOW PARAMETERS : R=0.156E-01 M, U0=0.200E 02 M/SEC, Q/M=0.100E-03 C/KG, KNP=0.150E 00, DF=0.469E-02 SQ.M/SEC, MP=0.400E-01(EXPT), 0.421E-01 (COMP) KG/SEC. PIPE INCLINATION = 90.0°. ×=0.0°, ⊙=90.0°, ⊡=180.0°, —— AIR.

DATA COMPUTED BY #XFD78, PLOTTED BY #PJD5 (TEST 00-12-0-1A).

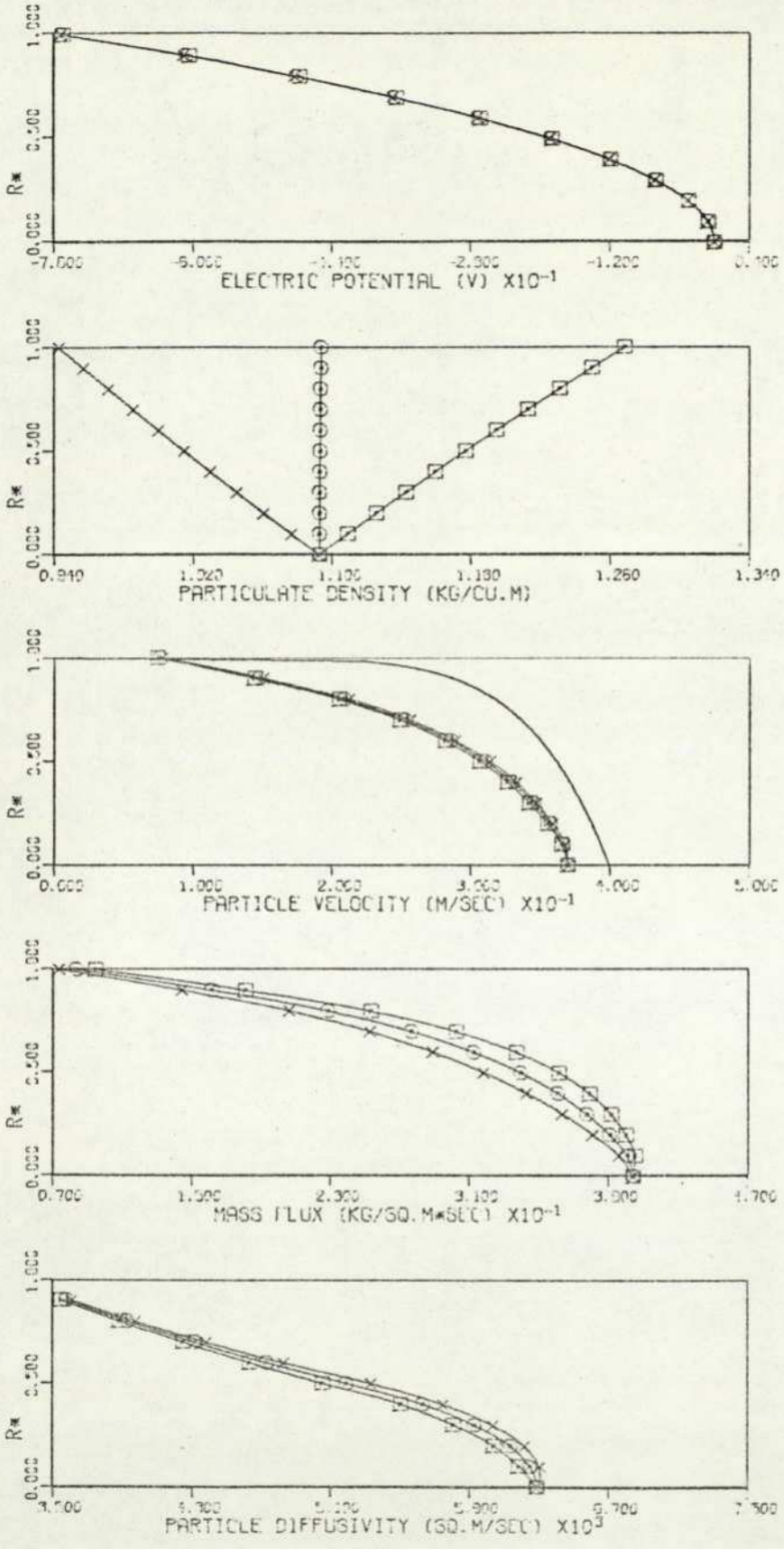

FIGURE :7.13 VARIOUS DISTRIBUTIONS IN A FULLY DEVELOPED TURBULENT GAS-SOLID SUSPENSION FLOW. PARTICLES TYPE #1.

PIPE FLOW PARAMETERS : R=0.156E-01 M, UO=0.400E 02 M/SEC, Q/M=0.100E-04 C/KG, KNP=0.100E 00, DF=0.936E-02 SQ.M/SEC, MP=0.200E-01(EXPT), 0.200E-01 (COMP) KG/SEC.
PIPE INCLINATION = 90.0°. ×=0.0°, ⊙=90.0°, ⊡=180.0°, —— RR.

DATA COMPUTED BY #XFDTB, PLOTTED BY #PJ05 (TEST 00-13-0-1R).

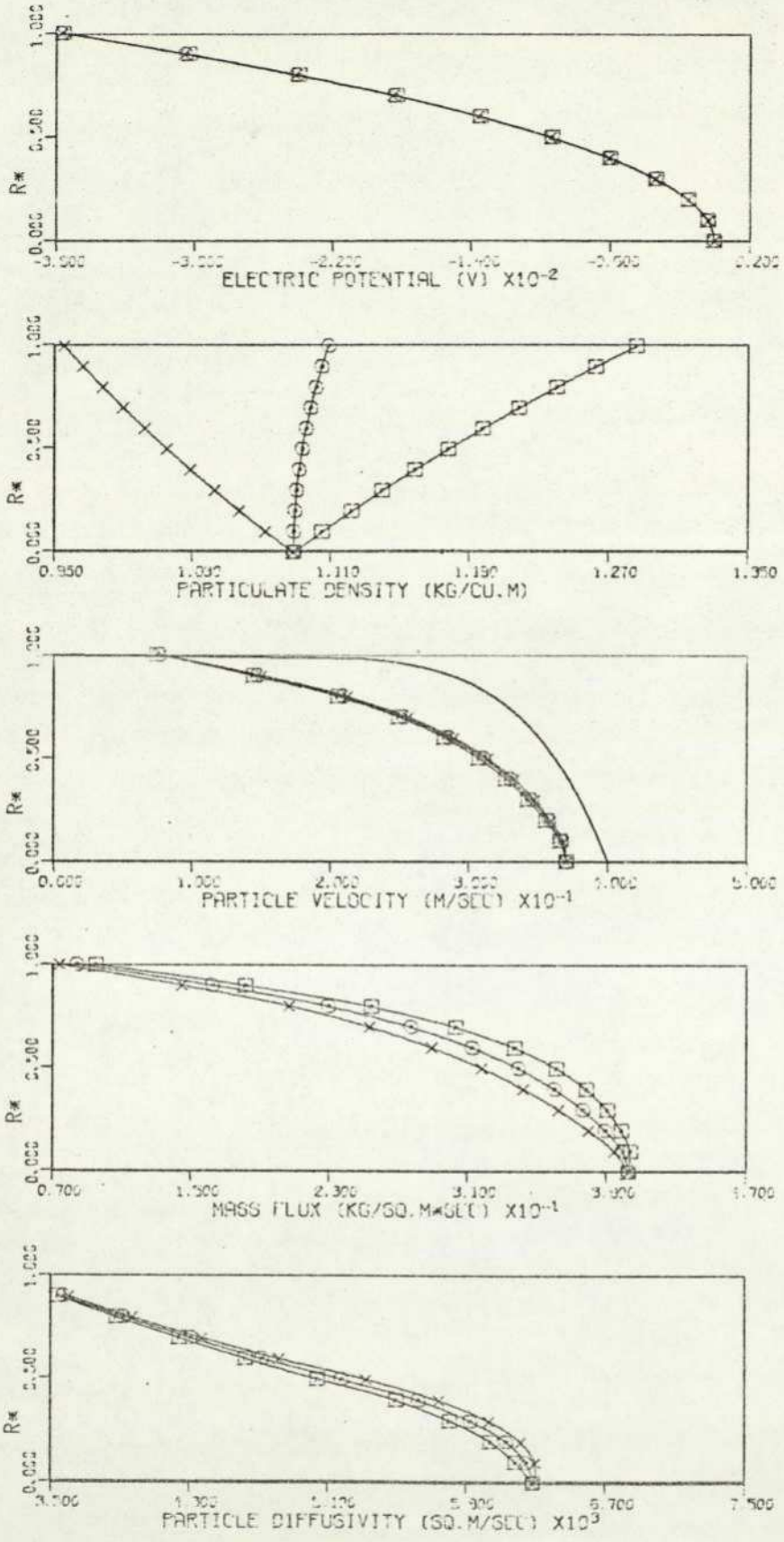

FIGURE :7.14 VARIOUS DISTRIBUTIONS IN A FULLY DEVELOPED TURBULENT GAS-SOLID SUSPENSION FLOW. PARTICLES TYPE #1.

PIPE FLOW PARAMETERS : R=0.156E-01 M, U0=0.400E 02 M/SEC, D/M=0.500E-04 D/KG, KNP=0.100E 00, DF=0.936E-02 SQ.M/SEC, MP=0.200E-01(EXPT), 0.200E-01 (COMP) KG/SEC. PIPE INCLINATION = 90.0°. × =0.0°, ⊙ =90.0°, ⊡ =180.0°, —— AIR.

DATA COMPUTED BY #XFD7B, PLOTTED BY #PJ05 (TEST 00-14-0-1A).

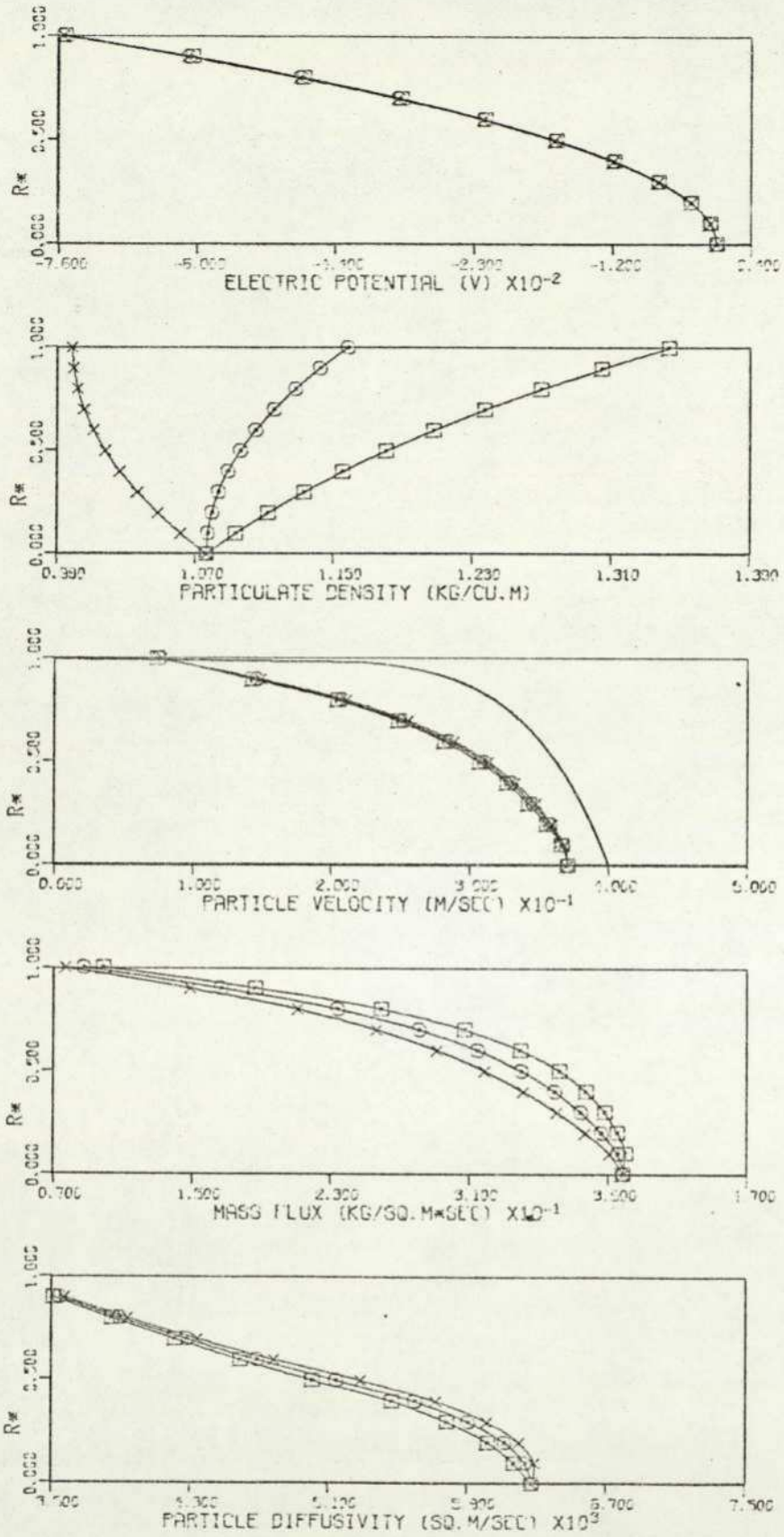

FIGURE :7.15 VARIOUS DISTRIBUTIONS IN A FULLY DEVELOPED TURBULENT GAS-SOLID SUSPENSION FLOW. PARTICLES TYPE #1.

PIPE FLOW PARAMETERS : R=0.156E-01 M, UO=0.400E 02 M/SEC, Q/M=0.100E-03 C/KG, KNP=0.100E 00, DF=0.336E-02 SQ.M/SEC, MP=0.200E-01(EXPT), 0.202E-01 (COMP) KG/SEC. PIPE INCLINATION = 90.0°. × =0.0°, ⊙ =90.0°, ⊡ =180.0°, —— AIR.

DATA COMPUTED BY #XFD78, PLOTTED BY #PJ05 (TEST 00-15-0-19).

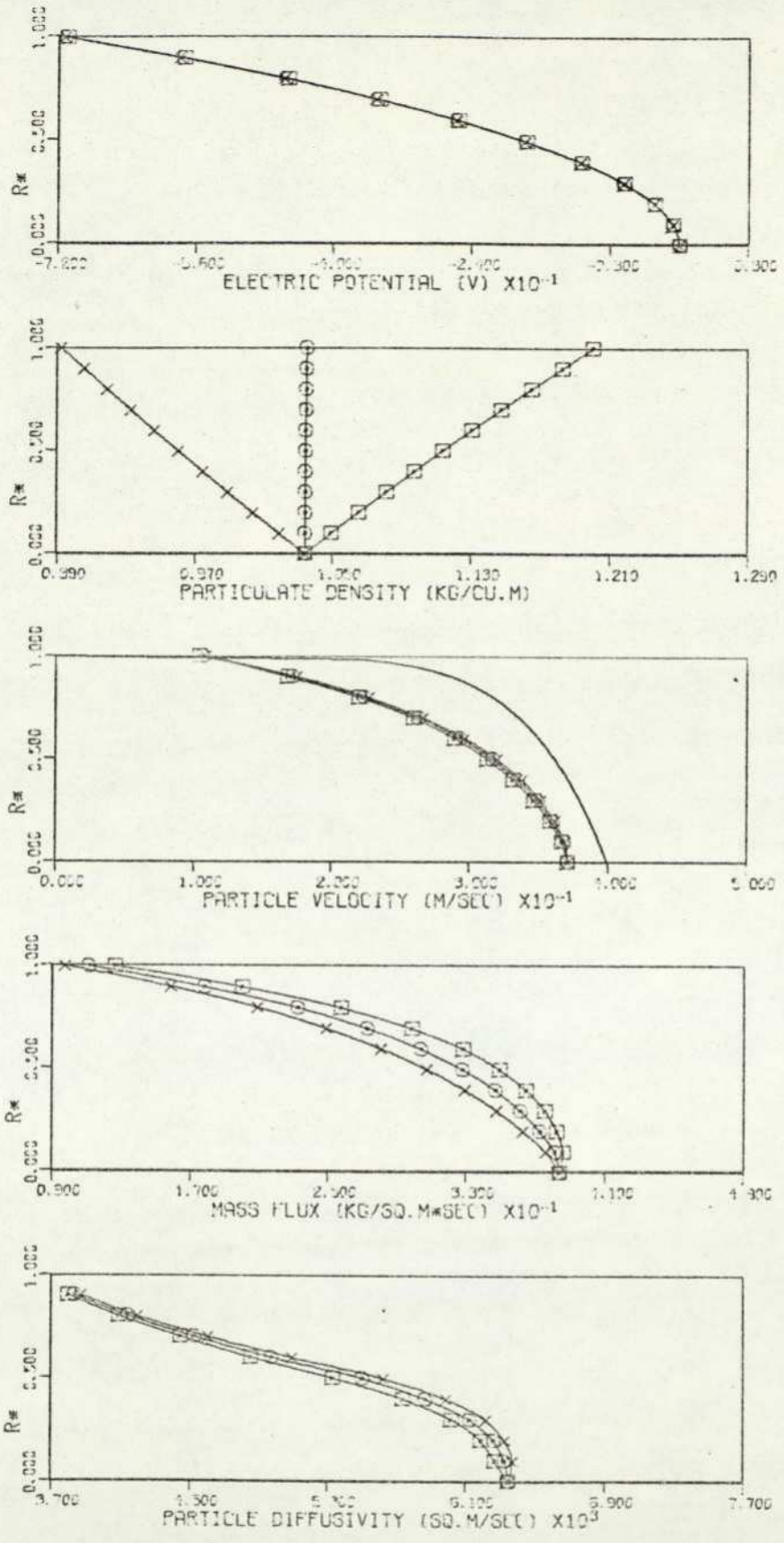

FIGURE :7.16 VARIOUS DISTRIBUTIONS IN A FULLY DEVELOPED TURBULENT GAS-SOLID SUSPENSION FLOW. PARTICLES TYPE #1.

PIPE FLOW PARAMETERS : R=0.156E-01 M, U0=0.400E 02 M/SEC, Q/M=0.100E-04 C/KG, KNP=0.150E 00, DF=0.936E-02 SQ.M/SEC, MP=0.200E-01(EXPT), 0.200E-01 (COMP) KG/SEC
PIPE INCLINATION = 90.0°. ×=0.0°, ⊙=90.0°, ⊡=180.0°, —— AIR.

DATA COMPUTED BY #XFD7B, PLOTTED BY #PJ05 (TEST 00-16-0-1A).

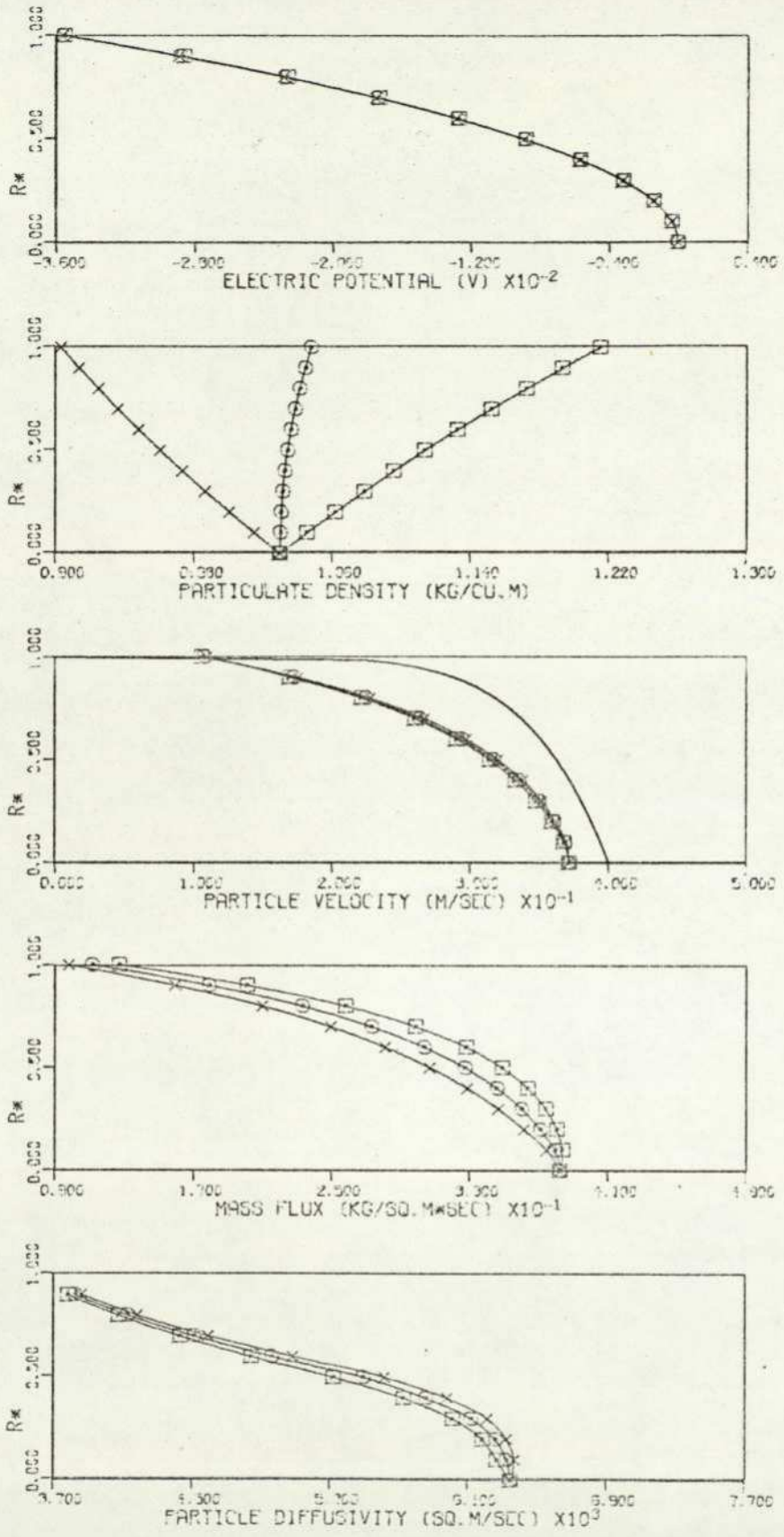

FIGURE : *7.17* VARIOUS DISTRIBUTIONS IN A FULLY DEVELOPED TURBULENT GAS-SOLID SUSPENSION FLOW. PARTICLES TYPE #1.

PIPE FLOW PARAMETERS : R=0.156E-01 M, UO=0.400E 02 M/SEC, Q/M=0.500E-04 C/KG, KNP=0.150E 00, DF=0.336E-02 SQ.M/SEC, MP=0.200E-01(EXPT), 0.200E-01 (COMP) KG/SEC.
PIPE INCLINATION = 90.0°. × +0.0°, ⊙ +90.0°, ⊡ +180.0 , —— AIR.

DATA COMPUTED BY #XF07B, PLOTTED BY #PJ05 (TEST 00-17-0-1A).

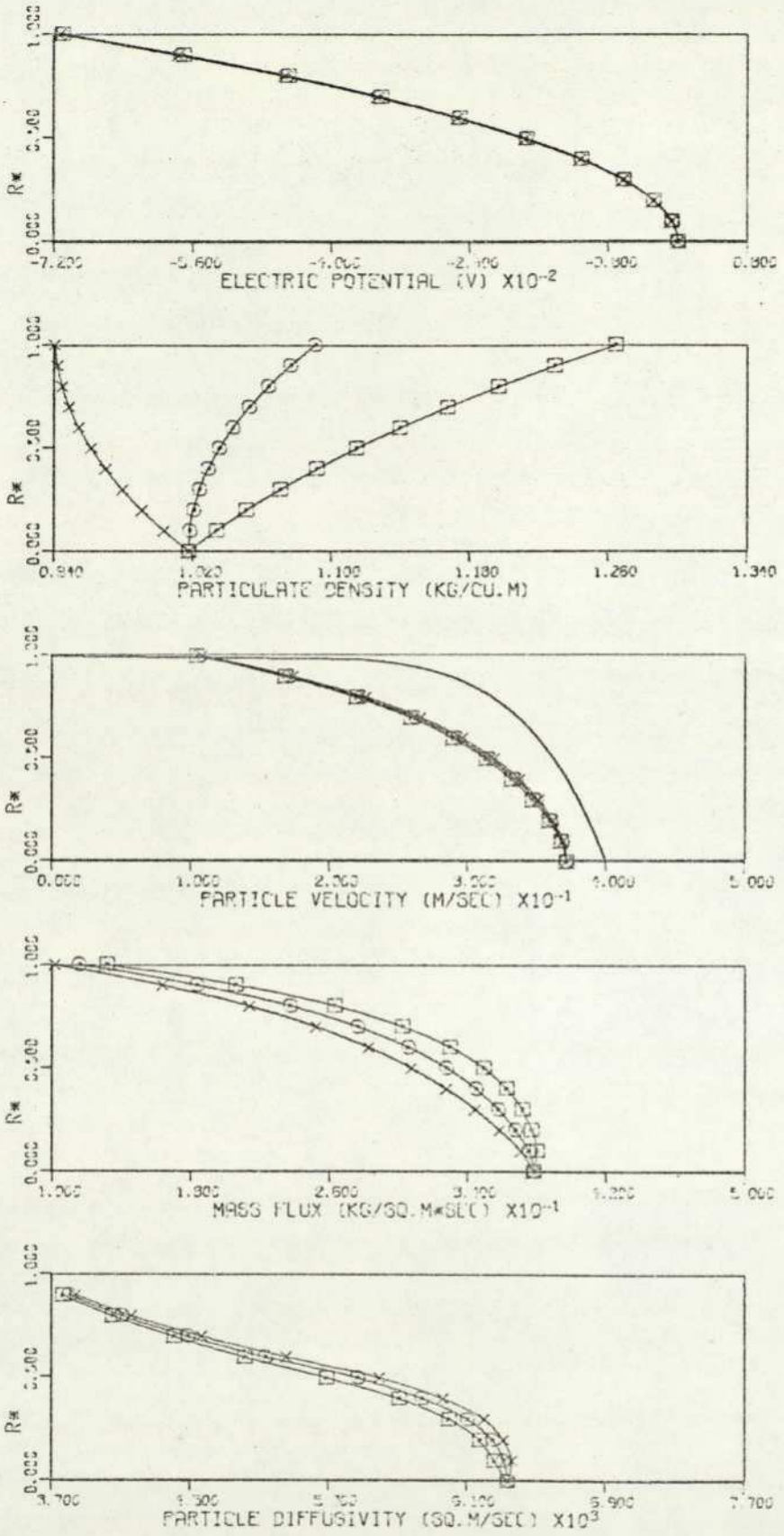

FIGURE : 7.18 VARIOUS DISTRIBUTIONS IN A FULLY DEVELOPED TURBULENT GAS-SOLID SUSPENSION FLOW. PARTICLES TYPE #1.

PIPE FLOW PARAMETERS : R=0.156E-01 M, UO=0.400E 02 M/SEC, Q/M=0.100E-03 C/KG, KNP=0.150E 00, DF=0.336E-02 SQ.M/SEC, MP=0.200E-01(EXPT), 0.202E-01 (COMP) KG/SEC.
PIPE INCLINATION = 90.0°. ×=0.0°, ⊙=90.0°, ⊡=180.0°, —— AIR.

DATA COMPUTED BY #XFD78, PLOTTED BY #PJD5 (TEST 00-18-0-1A).

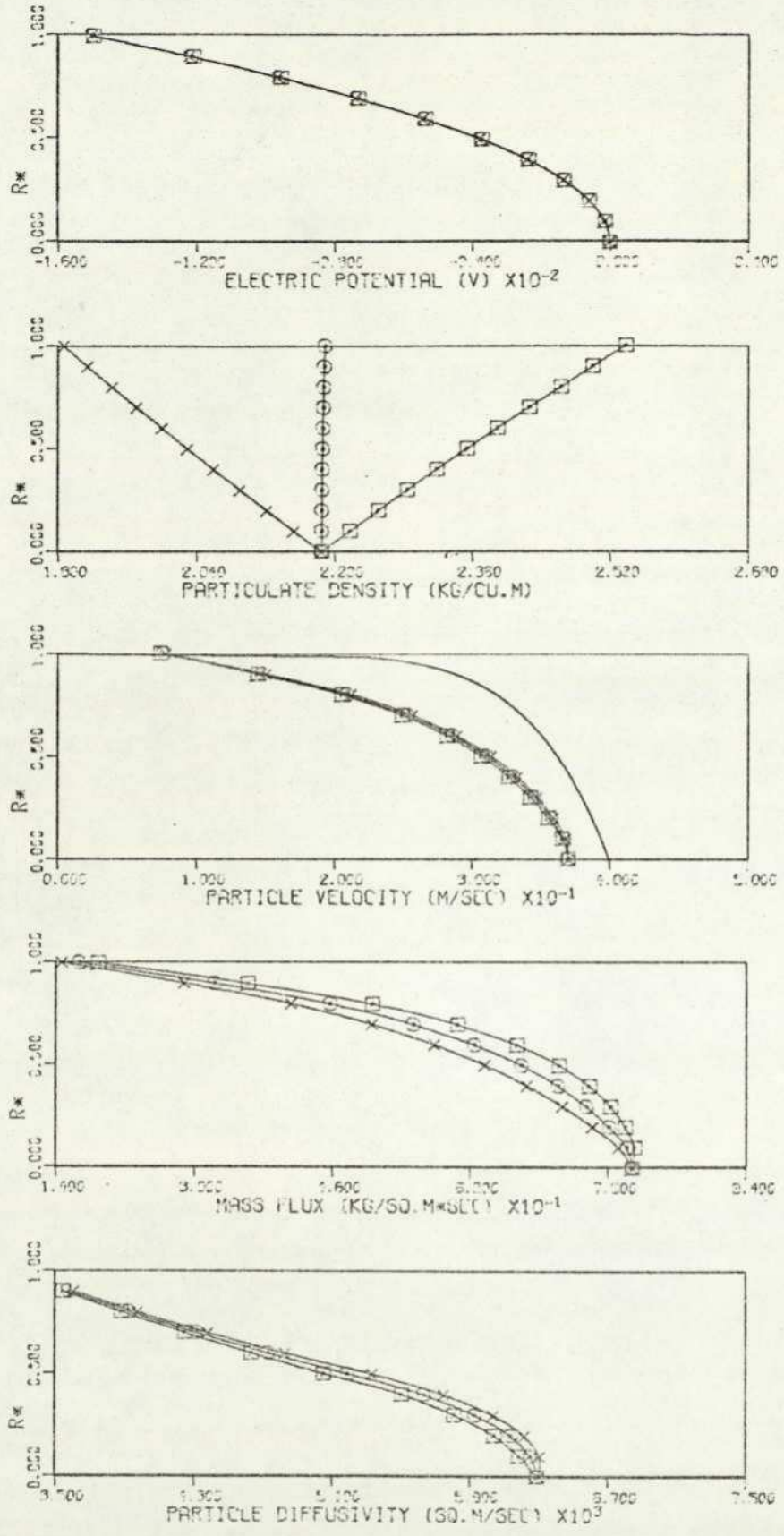

FIGURE : *7.19* VARIOUS DISTRIBUTIONS IN A FULLY DEVELOPED TURBULENT GAS-SOLID SUSPENSION FLOW. PARTICLES TYPE #1.

PIPE FLOW PARAMETERS : R=0.156E-01 M, U0=0.400E 02 M/SEC, Q/M=0.100E-01 C/KG, KNP=0.100E 00, DF=0.936E-02 SQ.M/SEC, MP=0.400E-01(EXPT), 0.400E-01 (COMP) KG/SEC.
PIPE INCLINATION = 90.0°. × =0.0°, ⊙ =90.0°, ⊡ =180.0°, —— AIR.

DATA COMPUTED BY #XFD7B, PLOTTED BY #PJ05 (TEST 00-19-0-1A).

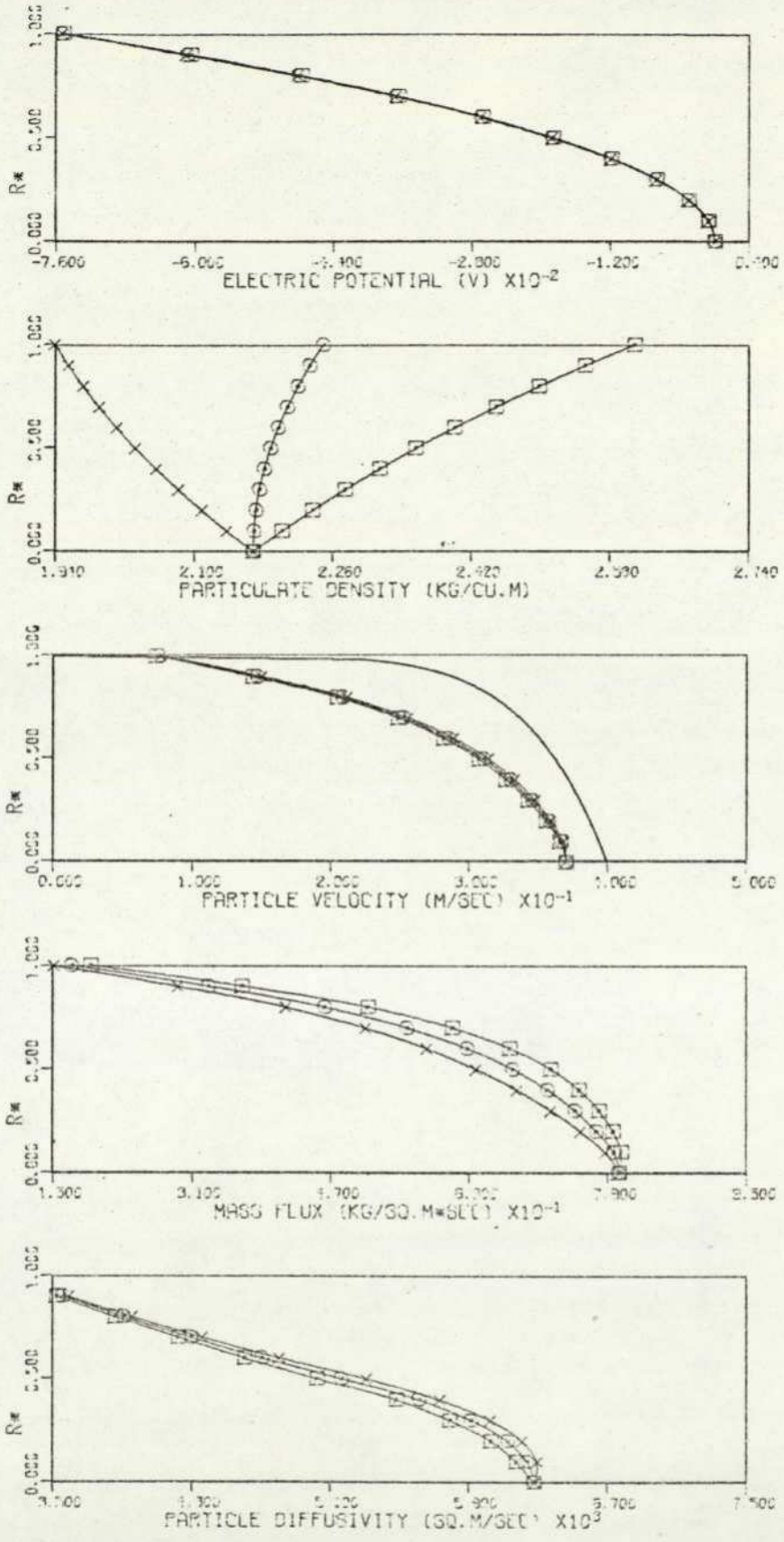

FIGURE :7.20 VARIOUS DISTRIBUTIONS IN A FULLY DEVELOPED TURBULENT GAS-SOLID SUSPENSION FLOW. PARTICLES TYPE #1.

PIPE FLOW PARAMETERS : R=0.156E-01 M, U0=0.400E 02 M/SEC, Q/M=0.500E-04 C/KG, KNP=0.100E 00, DF=0.336E-02 SQ.M/SEC, MP=0.400E-01(EXPT), 0.402E-01 (COMP) KG/SEC
PIPE INCLINATION = 90.0°. ×=0.0°, ⊙=90.0°, ⊡=180.0°, ——— AIR.

DATA COMPUTED BY #XF07B, PLOTTED BY #PJ05 (TEST 00-20-0-1A).

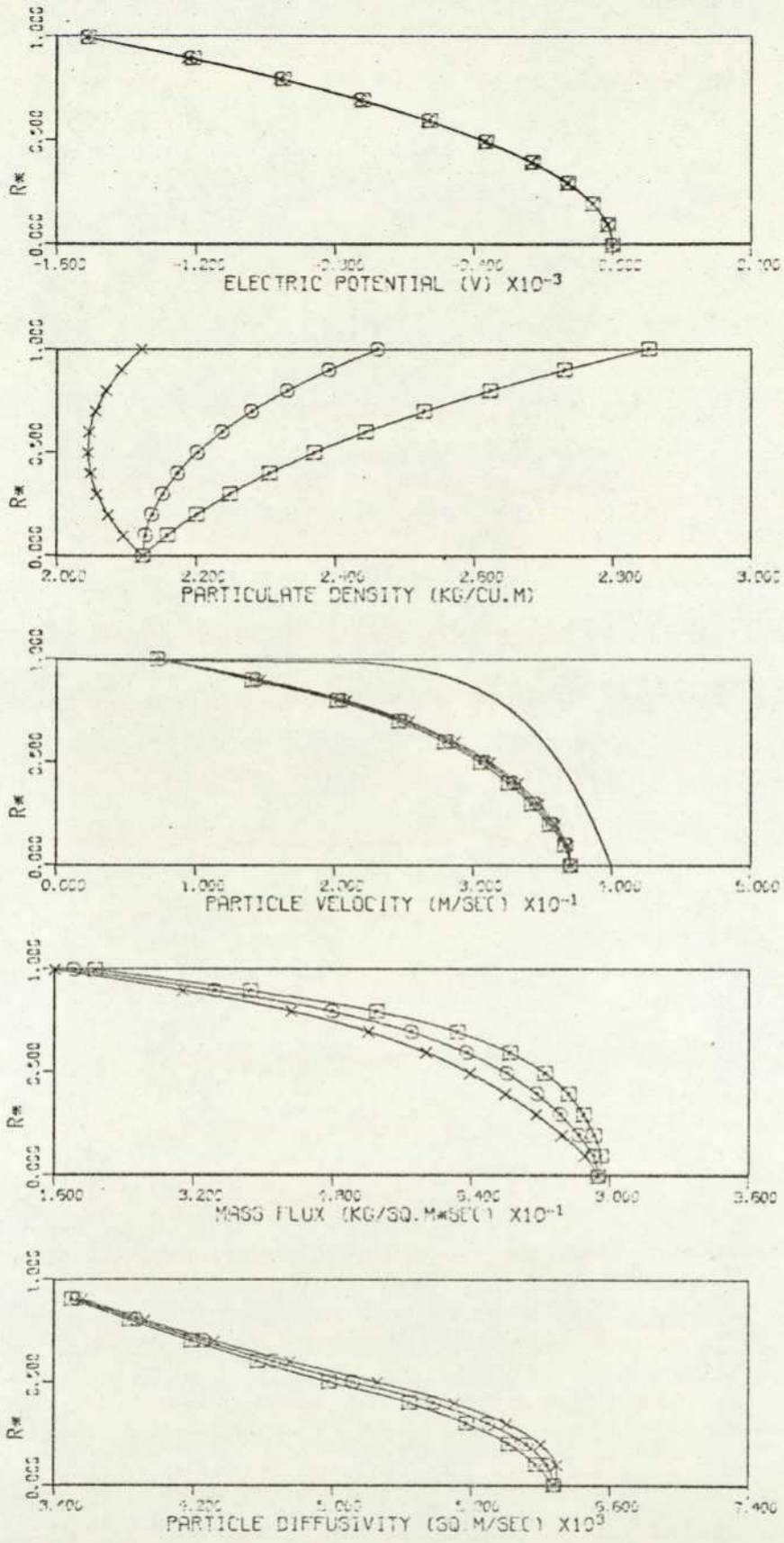

FIGURE : *7.21* VARIOUS DISTRIBUTIONS IN A FULLY DEVELOPED TURBULENT GAS-SOLID SUSPENSION FLOW. PARTICLES TYPE #1.

PIPE FLOW PARAMETERS : R=0.156E-01 M, U0=0.400E 02 M/SEC, Q/M=0.100E-03 C/KG, KNP=0.100E 00, DF=0.939E-02 SQ.M/SEC, MP=0.400E-01(EXPT), 0.407E-01 (COMP) KG/SEC.

PIPE INCLINATION = 90.0°. × =0.0°, ⊙ =90.0°, ⊡ =180.0°, —— AIR.

DATA COMPUTED BY #XFD7S, PLOTTED BY #PJD5 (TEST 00-21-0-1A).

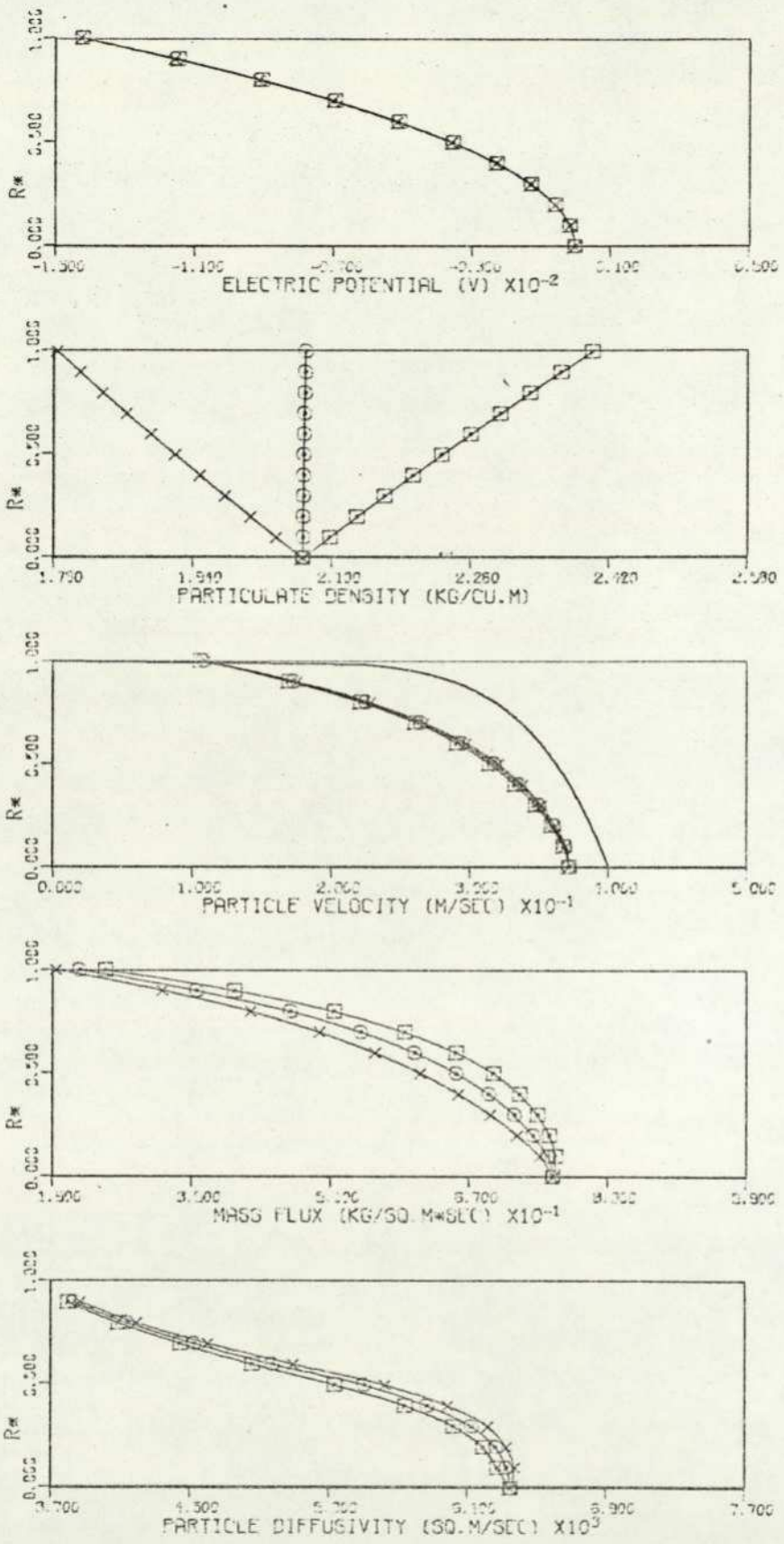

FIGURE : 7.22 VARIOUS DISTRIBUTIONS IN A FULLY DEVELOPED TURBULENT GAS-SOLID SUSPENSION FLOW. PARTICLES TYPE #1.

PIPE FLOW PARAMETERS : R=0.156E-01 M, U0=0.400E 02 M/SEC, Q/M=0.100E-04 C/KG, KNP=0.150E 00, DF=0.339E-02 SQ.M/SEC, MP=0.400E-01(EXPT), 0.400E-01 (COMP) KG/SEC. PIPE INCLINATION = 90.0°. × =0.0°, ⊙ =90.0°, ⊡ =180.0°, —— AIR.

DATA COMPUTED BY #XFD75, PLOTTED BY #PJD5 (TEST 00-22-0-1A).

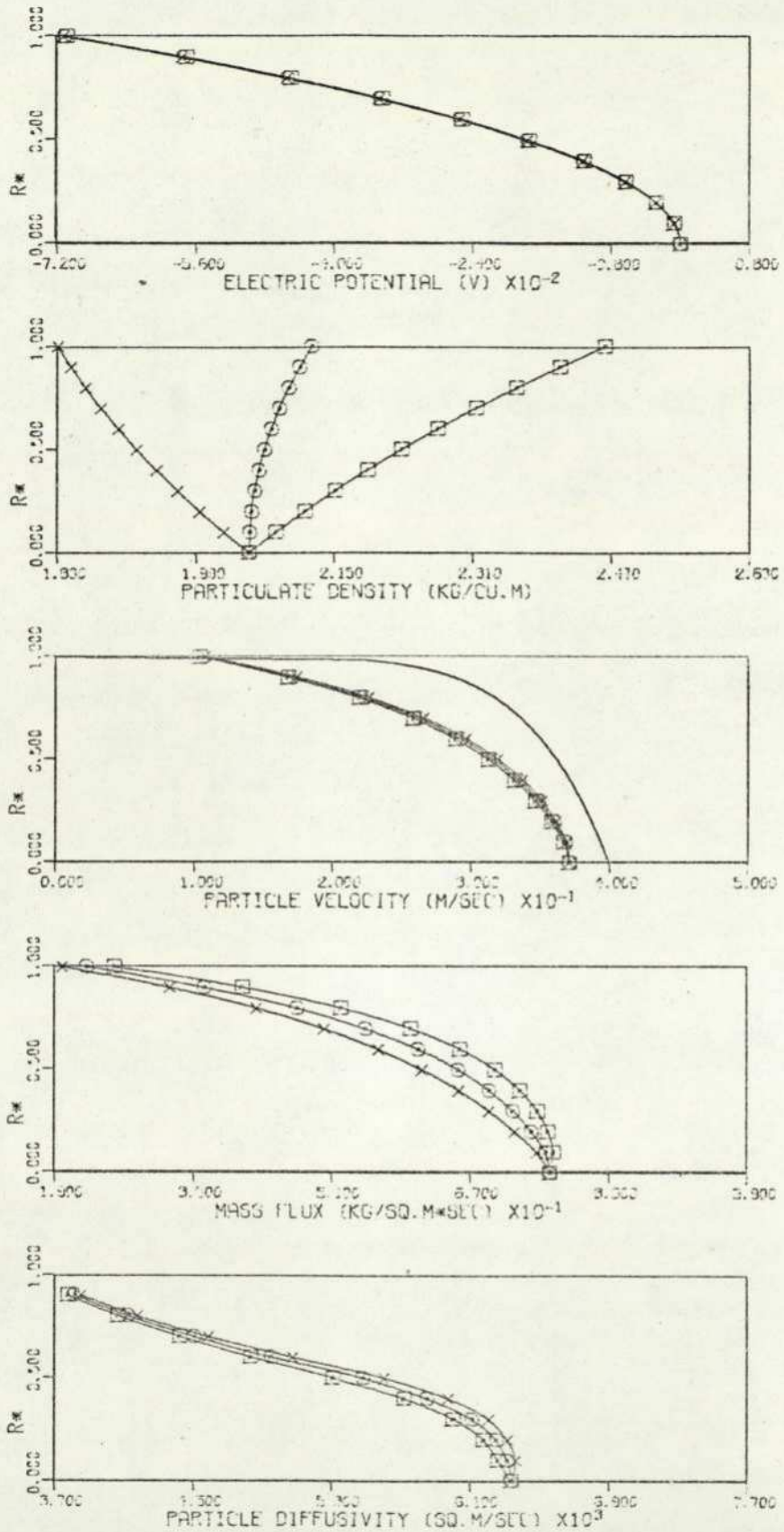

FIGURE : 7.23 VARIOUS DISTRIBUTIONS IN A FULLY DEVELOPED TURBULENT GAS-SOLID SUSPENSION FLOW. PARTICLES TYPE #1.

PIPE FLOW PARAMETERS : R=0.156E-01 M, UO=0.400E 02 M/SEC, Q/M=0.500E-04 C/KG, KNP=0.150E 00, DF=0.336E-02 SQ.M/SEC, MP=0.400E-01(EXPT), 0.402E-01 (COMP) KG/SEC. PIPE INCLINATION = 90.0°. ×=0.0°, ⊙=90.0°, ⊡=180.0°, —— RIP.

DATA COMPUTED BY #XFD76, PLOTTED BY #PJ05 (TEST 00-23-0-1A).

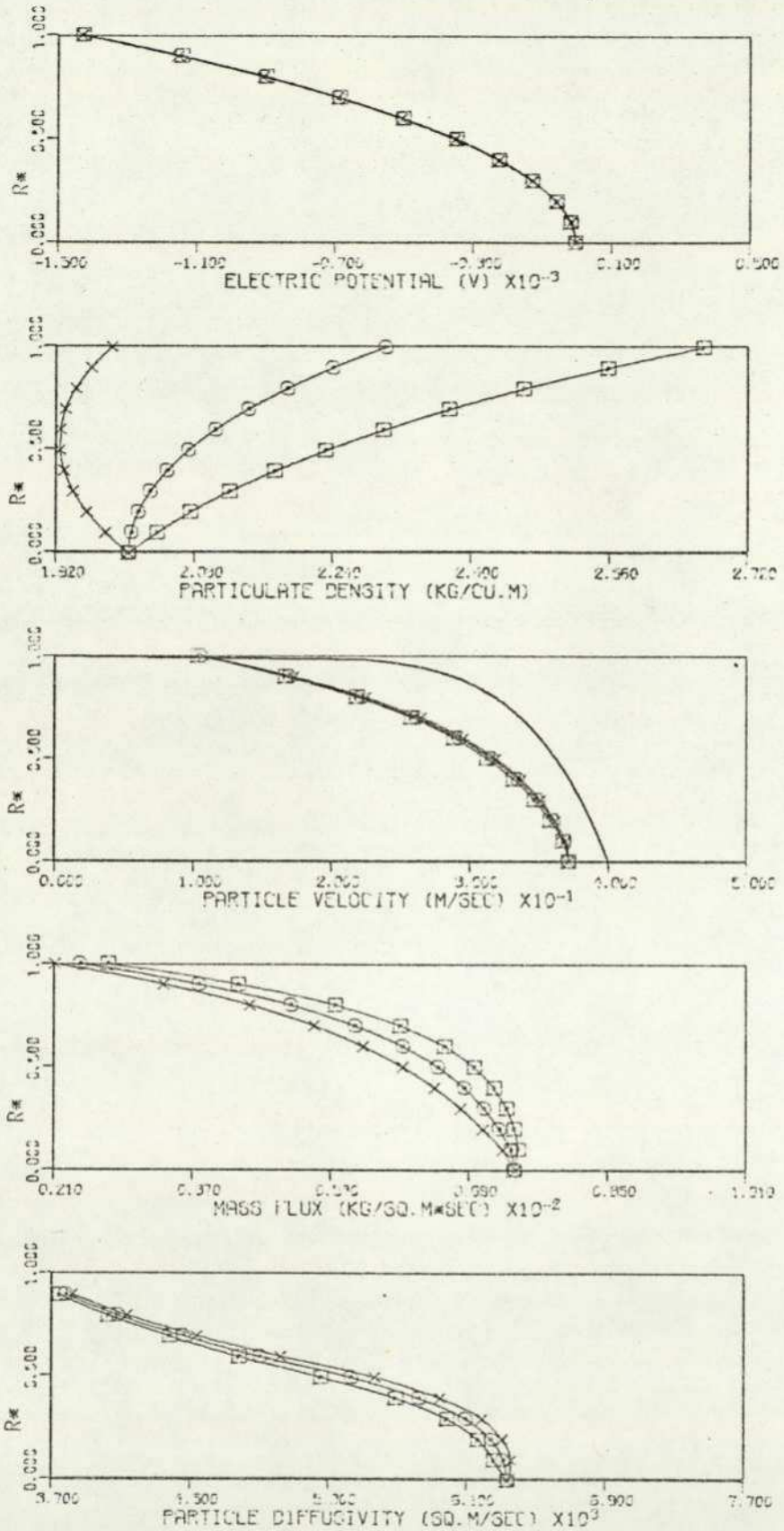

FIGURE : 7.24 VARIOUS DISTRIBUTIONS IN A FULLY DEVELOPED TURBULENT GAS-SOLID SUSPENSION FLOW. PARTICLES TYPE #1.

PIPE FLOW PARAMETERS : R=0.156E-01 M, UO=0.400E 02 M/SEC, Q/M=0.100E-03 C/KG, KNP=0.150E 00, DF=0.336E-02 SQ.M/SEC, MP=0.400E-01(EXPT), 0.407E-01 (COMP) KG/SEC. PIPE INCLINATION = 90.0°. × =0.0°, ⊙ =90.0°, ⊡ =180.0°, —— RIR.

DATA COMPUTED BY #XF07B, PLOTTED BY #PJ05 (TEST 00-21-0-1A).

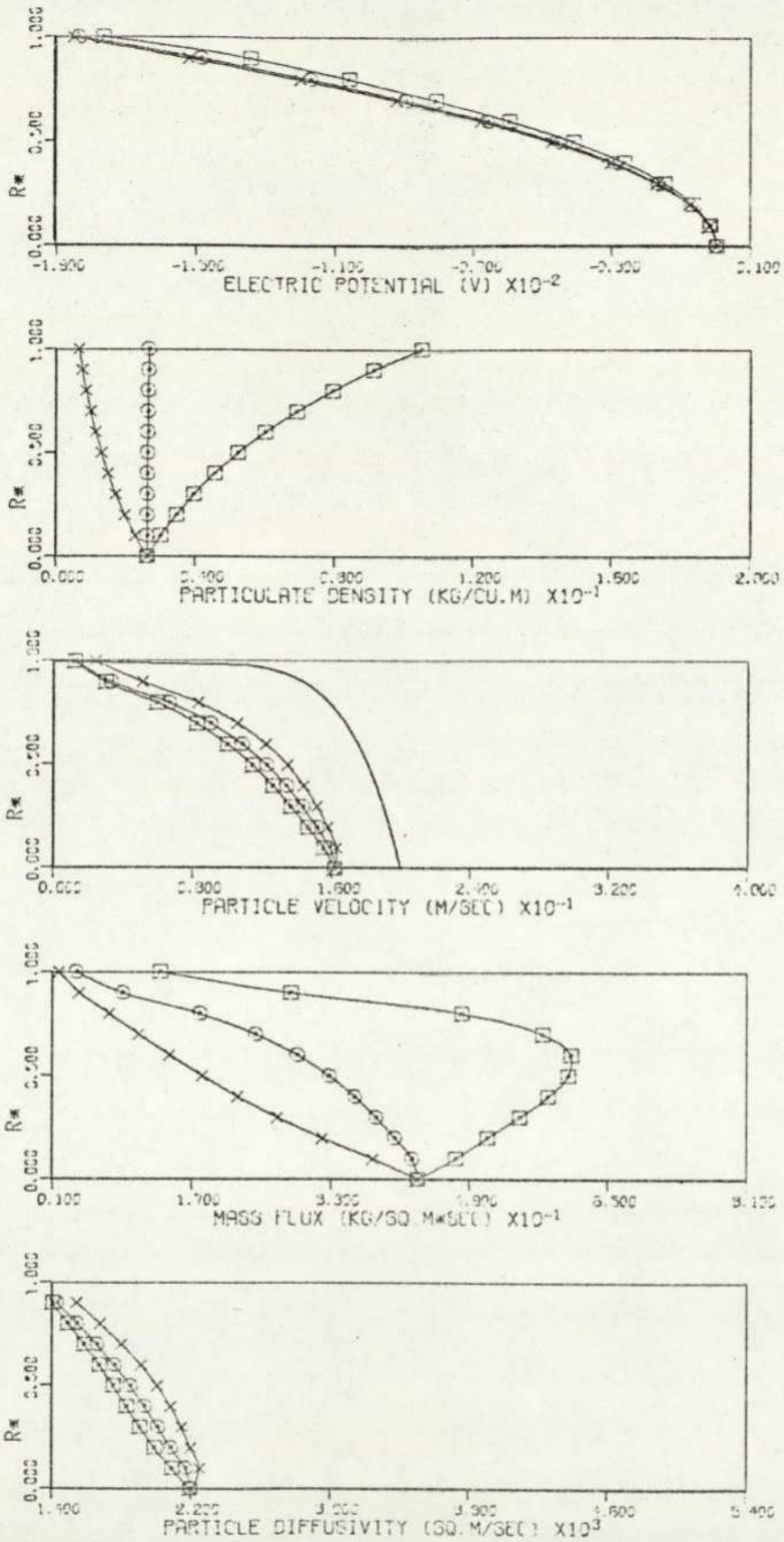

FIGURE : 7.25 VARIOUS DISTRIBUTIONS IN A FULLY DEVELOPED TURBULENT GAS-SOLID SUSPENSION FLOW. PARTICLES TYPE #2.

PIPE FLOW PARAMETERS : R=0.156E-01 M, UO=0.200E 02 M/SEC, Q/M=0.100E-04 C/KG, KNP=0.100E 00, DF=0.469E-02 SQ.M/SEC, MP=0.200E-01(EXPT), 0.200E-01 (COMP) KG/SEC.
PIPE INCLINATION = 90.0°. × =0.0°, ⊙ =90.0°, ⊡ =180.0°, —— RIR.

DATA COMPUTED BY #XFD78, PLOTTED BY #PJ05 (TEST 01-01-0-2R).

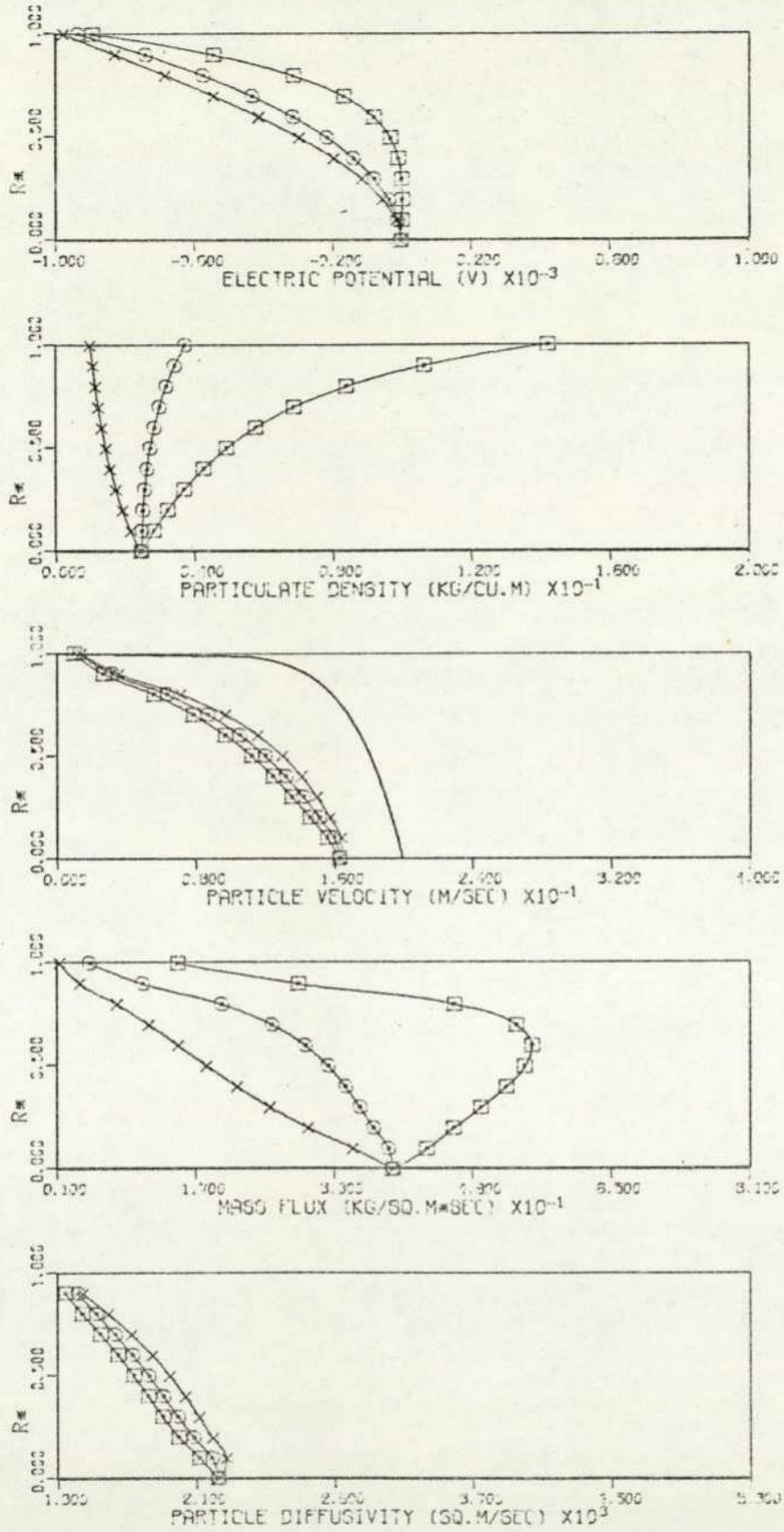

FIGURE : 7.26 VARIOUS DISTRIBUTIONS IN A FULLY DEVELOPED TURBULENT GAS-SOLID SUSPENSION FLOW. PARTICLES TYPE #2.

PIPE FLOW PARAMETERS : R=0.156E-01 M, UO=0.200E 02 M/SEC, O/M=0.500E-04 C/KG, KNP=0.100E 00, DF=0.463E-02 SQ.M/SEC, MP=0.200E-01(EXPT), 0.199E-01 (COMP) KG/SEC. PIPE INCLINATION = 90.0°. ×-0.0°, ⊙ +90.0°, ⊡+180.0°, —— AIR.

DATA COMPUTED BY #XFD7B. PLOTTED BY #PJ05 (TEST 01-02-0-2A).

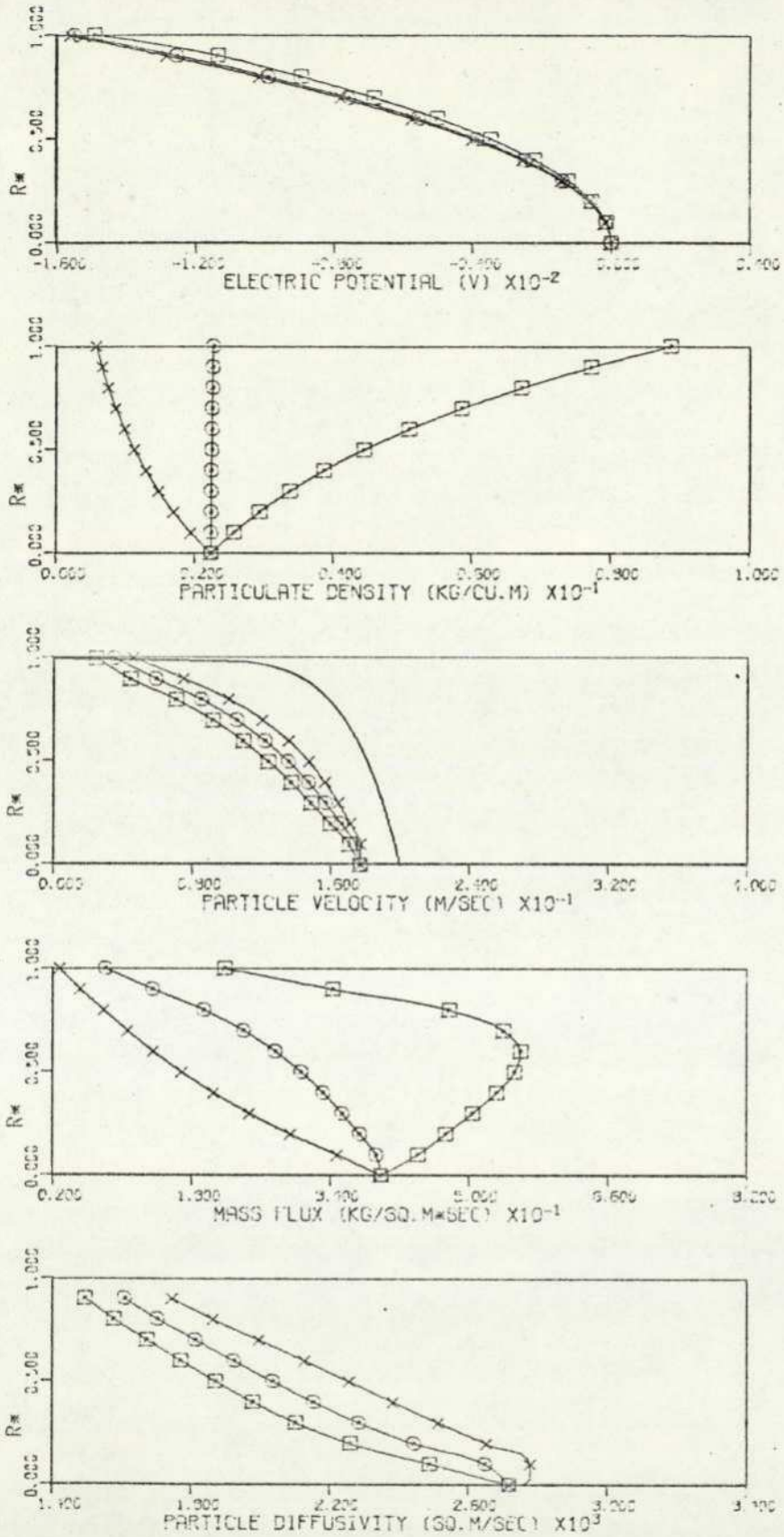

FIGURE : 7.27 VARIOUS DISTRIBUTIONS IN A FULLY DEVELOPED TURBULENT GAS-SOLID SUSPENSION FLOW. PARTICLES TYPE #2.

PIPE FLOW PARAMETERS : R=0.156E-01 M, U0=0.200E 02 M/SEC, Q/M=0.100E-04 C/KG, KNP=0.150E 00, DF=0.163E-02 SQ.M/SEC, MP=0.200E-01(EXPT), 0.200E-01 (COMP) KG/SEC. PIPE INCLINATION = 90.0°. ×=0.0°, ⊙=90.0°, ⊡=180.0°, —— AIR.

DATA COMPUTED BY #XFD70, PLOTTED BY #PJ05 (TEST 01-04-0-2A).

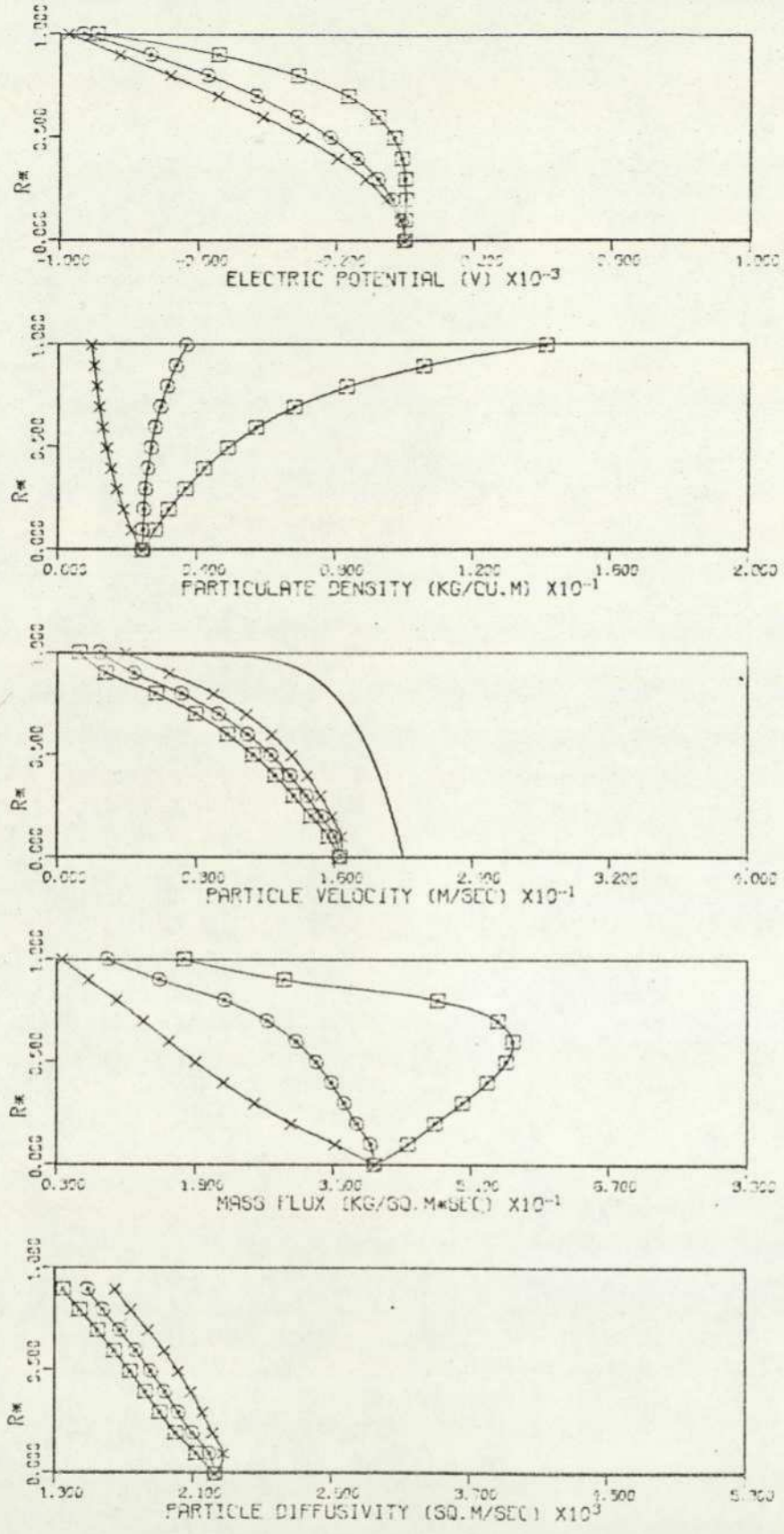

FIGURE : 7.28 VARIOUS DISTRIBUTIONS IN A FULLY DEVELOPED TURBULENT GAS-SOLID SUSPENSION FLOW. PARTICLES TYPE #2.

PIPE FLOW PARAMETERS : R=0.156E-01 M, UO=0.200E 02 M/SEC, Q/M=0.500E-04 C/KG, KNP=0.150E 00, DF=0.468E-02 SQ.M/SEC, MP=0.200E-01(EXPT), 0.209E-01 (COMP) KG/SEC. PIPE INCLINATION = 90.0°. ×=0.0°, ⊙=30.0°, ⊡=+80.0°, —— AIR.

DATA COMPUTED BY #XFD7B, PLOTTED BY #PJDS (TEST 01-05-0-29).

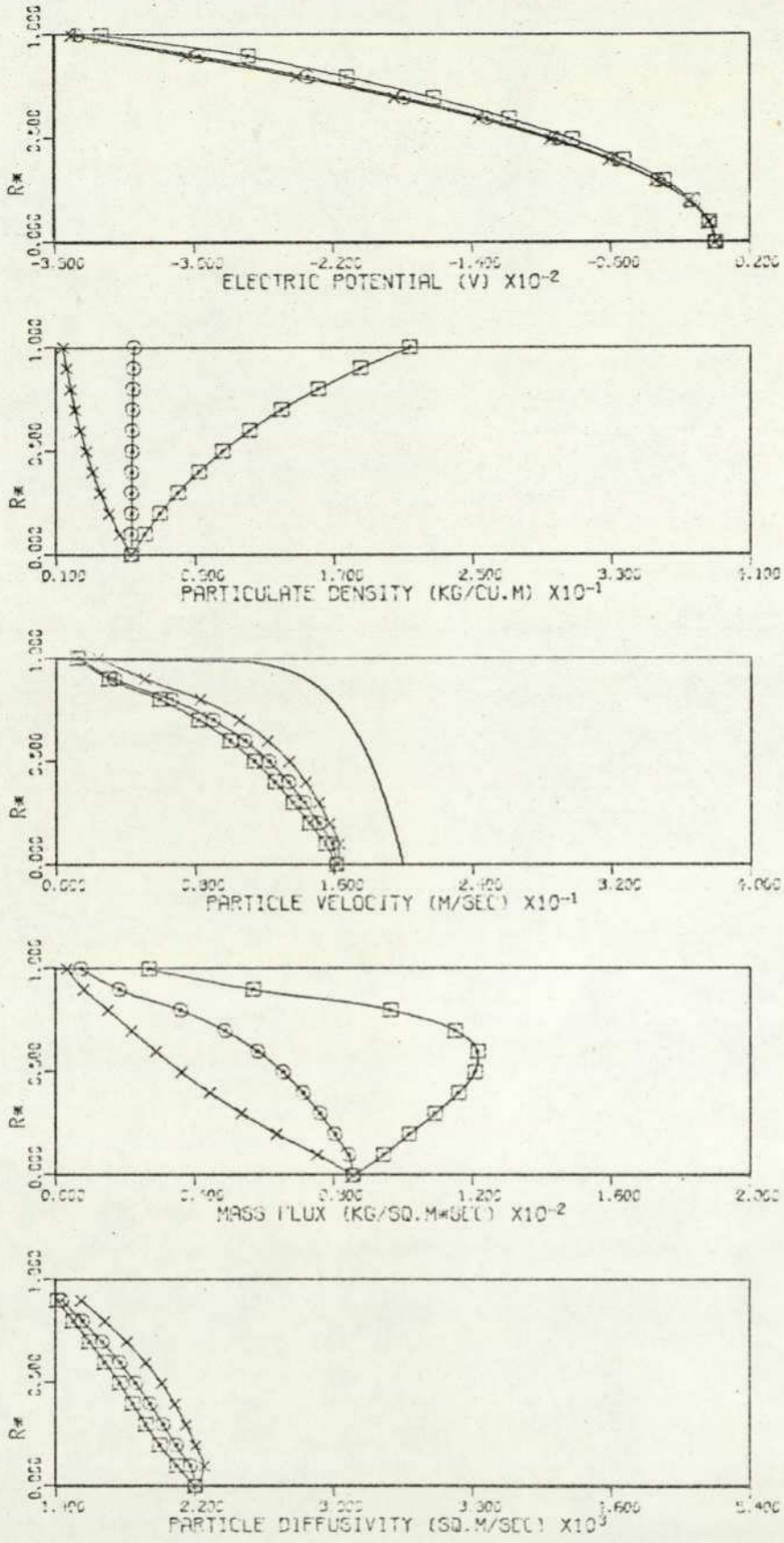

FIGURE : 7.29 VARIOUS DISTRIBUTIONS IN A FULLY DEVELOPED TURBULENT GAS-SOLID SUSPENSION FLOW. PARTICLES TYPE #2.

PIPE FLOW PARAMETERS : R=0.156E-01 M, UO=0.200E 02 M/SEC, Q/M=0.100E-04 C/KG, KNP=0.100E 00, DF=0.469E-02 SQ.M/SEC, MP=0.400E-01(EXPT), 0.402E-01 (COMP) KG/SEC
PIPE INCLINATION = 90.0°. × =0.0°, ⊙ =90.0°, ⊡ =180.0°, —— AIR.

DATA COMPUTED BY #XFD7B, PLOTTED BY #PJ05 (TEST 01-07-0-2A).

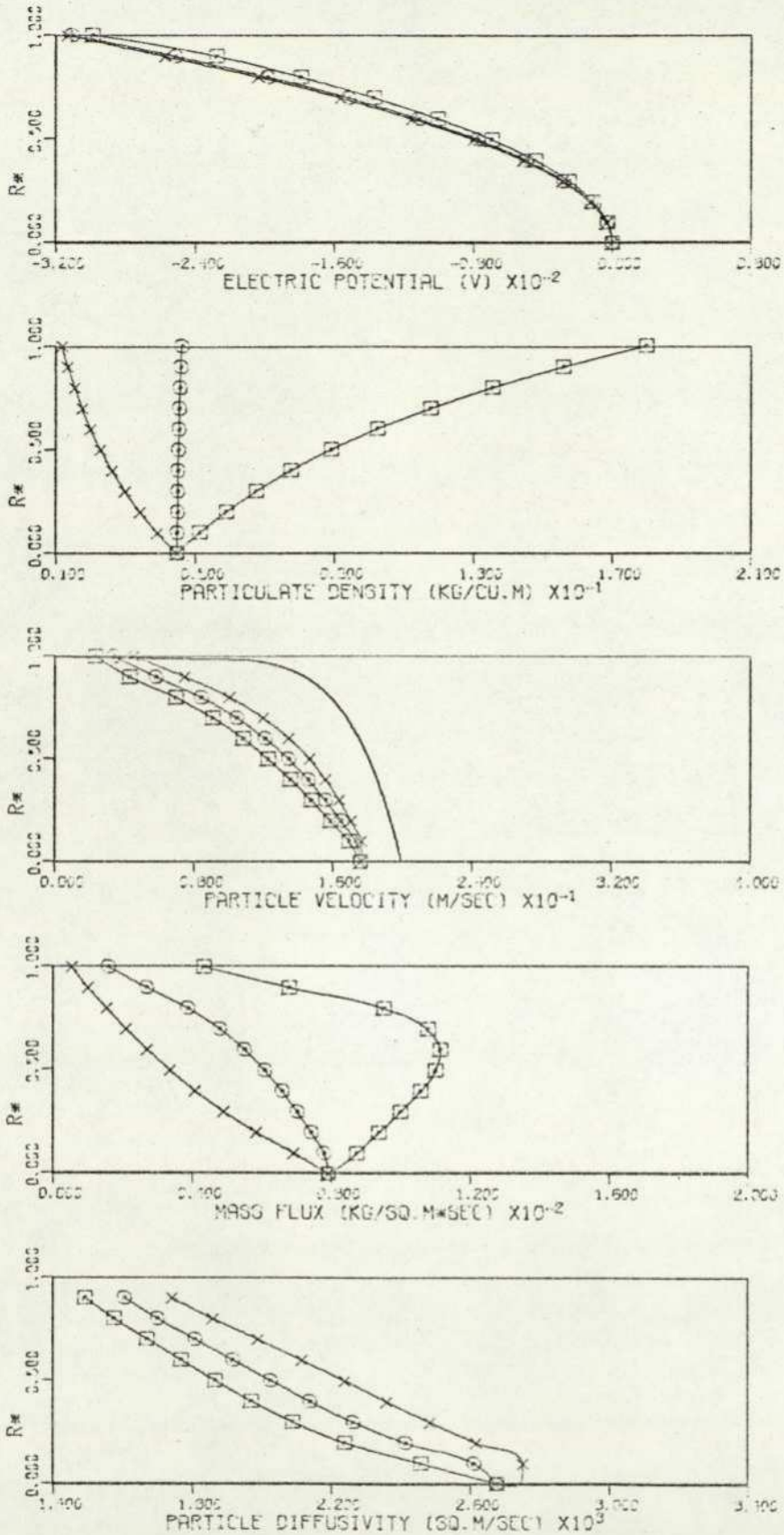

FIGURE : 7.30 VARIOUS DISTRIBUTIONS IN A FULLY DEVELOPED TURBULENT GAS-SOLID SUSPENSION FLOW. PARTICLES TYPE #2.

PIPE FLOW PARAMETERS . R=0.156E-01 M, UO=0.200E 02 M/SEC Q/M=0.100E-04 C/KG.
KNP=0.150E 00, DF=0.469E-02 SQ.M/SEC, MP=0.400E-01(EXPT), 0.393E-01 (COMP) KG/SEC.
PIPE INCLINATION = 90.0°. ×=0.0°, ⊙=30.0°, ⊡=180.0°, —— RIR.

DATA COMPUTED BY #XFD7B, PLOTTED BY #PJD5 (TEST 01-10-0-2A).

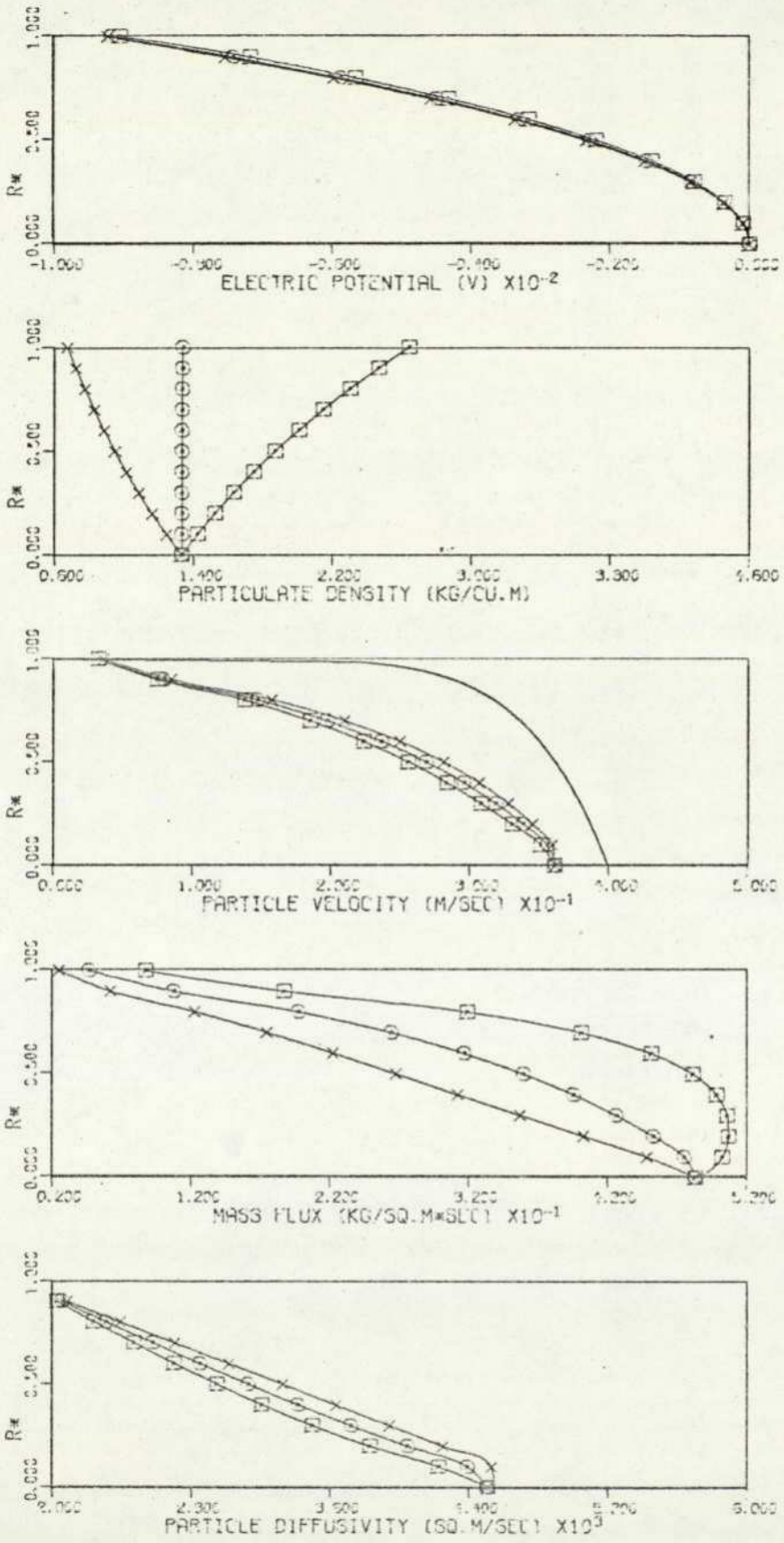

FIGURE : 7.31 VARIOUS DISTRIBUTIONS IN A FULLY DEVELOPED TURBULENT GAS-SOLID SUSPENSION FLOW. PARTICLES TYPE #2.

PIPE FLOW PARAMETERS : R=0.156E-01 M, UO=0.400E 02 M/SEC, Q/M=0.100E-04 C/KG, KNP=0.100E 00, DF=0.336E-02 SQ.M/SEC, MP=0.200E-01(EXPT), 0.200E-01 (COMP) KG/SEC. PIPE INCLINATION = 90.0°. × =0.0°, ⊙ =90.0°, ⊡ =180.0°, —— AIR.

DATA COMPUTED BY #XFD26, PLOTTED BY #PL05 (TEST 01-13-0-2A).

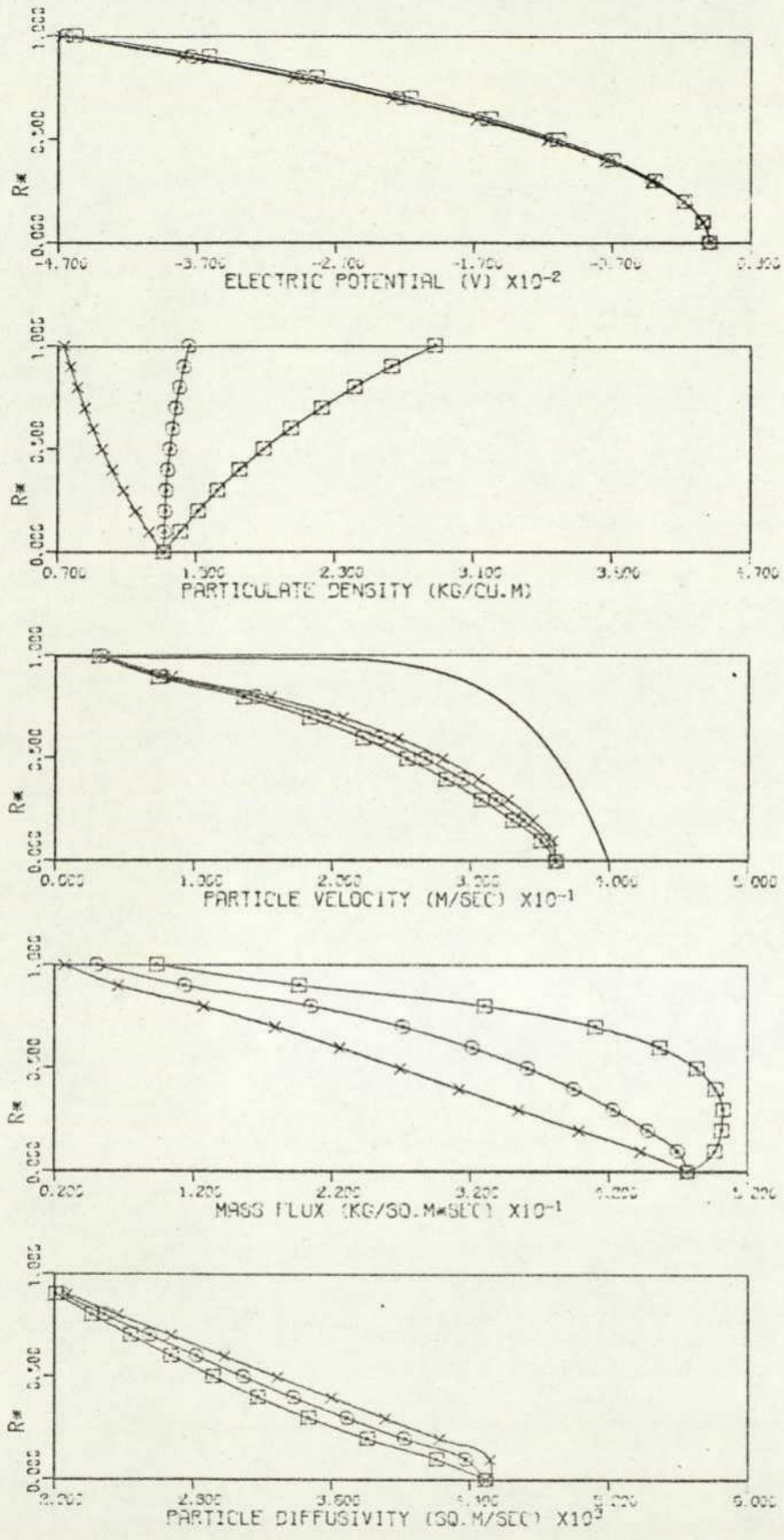

FIGURE : 7.32 VARIOUS DISTRIBUTIONS IN A FULLY DEVELOPED TURBULENT GAS-SOLID SUSPENSION FLOW. PARTICLES TYPE #2.

PIPE FLOW PARAMETERS : R=0.156E-01 M, U0=0.400E 02 M/SEC, Q/M=0.500E-04 C/KG, KNP=0.100E 00, DF=0.336E-02 SQ.M/SEC, MP=0.200E-01(EXPT), 0.203E-01 (COMP) KG/SEC. PIPE INCLINATION = 90.0°. × -0.0°, ⊙ -30.0°, ⊡ -180.0°, —— 91P.

DATA COMPUTED BY #XFD78, PLOTTED BY #PJ05 (TEST 01-14-0-2A).

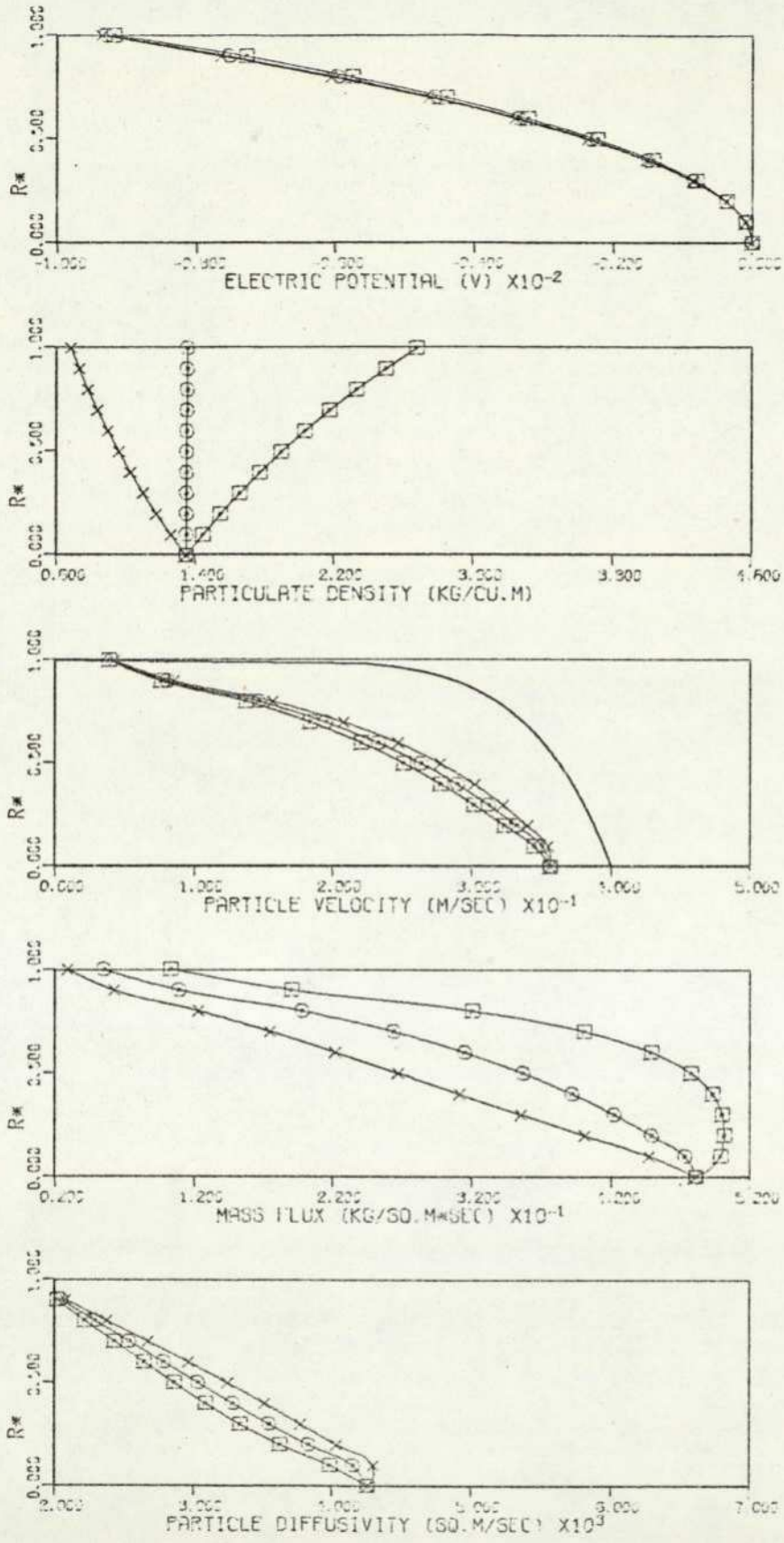

FIGURE : 7.33 VARIOUS DISTRIBUTIONS IN A FULLY DEVELOPED TURBULENT GAS-SOLID SUSPENSION FLOW. PARTICLES TYPE #2.

PIPE FLOW PARAMETERS : P=0.156E-01 M, UO=0.400E 02 M/SEC, Q/M=0.100E-04 C/KG, KNP=0.150E 00, DF=0.336E-02 SQ.M/SEC, MP=0.200E-01(EXPT), 0.200E-01 (COMP) KG/SEC. PIPE INCLINATION = 90.0°. × 0.0°, ⊙ 90.0°, ⊡ 180.0° , —— RIR.

DATA COMPUTED BY #XFD70, PLOTTED BY #PJ05 (TEST 01-16-0-2A).

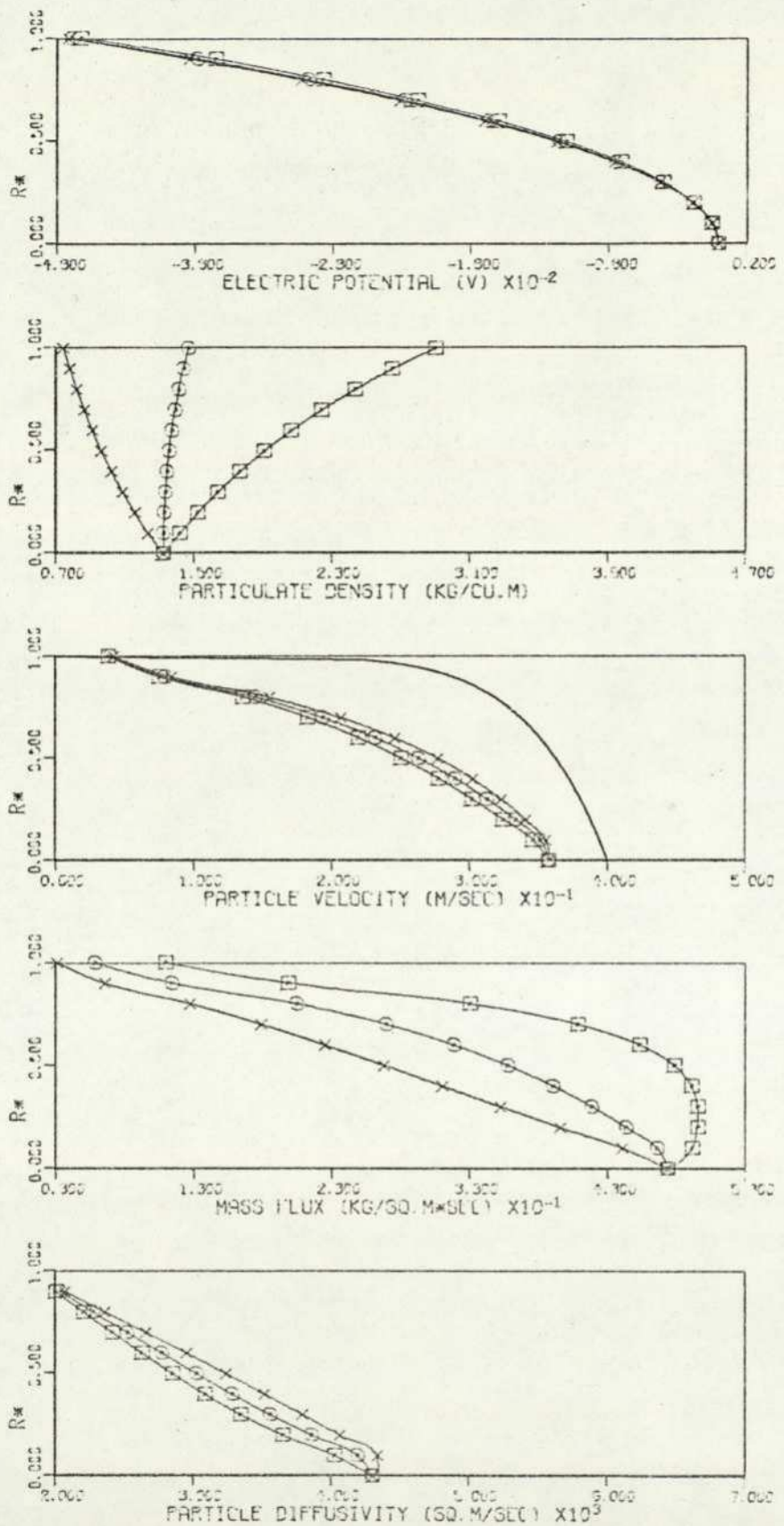

FIGURE : 7.34 VARIOUS DISTRIBUTIONS IN A FULLY DEVELOPED TURBULENT GAS-SOLID SUSPENSION FLOW. PARTICLES TYPE #2.

PIPE FLOW PARAMETERS : R=0.156E-01 M, UO=0.400E 02 M/SEC, O/M=0.500E-04 O/KG, KNP=0.150E 00, DF=0.936E-02 SQ.M/SEC, MP=0.205E-01(EXPT), 0.203E-01 (COMP) KG/SEC. PIPE INCLINATION = 90.0°. × =0.0°, ⊙ =30.0°, ⊞ =180.0°, —— RIR.

DATA COMPUTED BY #XF078, PLOTTED BY #PJ05 (TEST 01-17-0-2A).

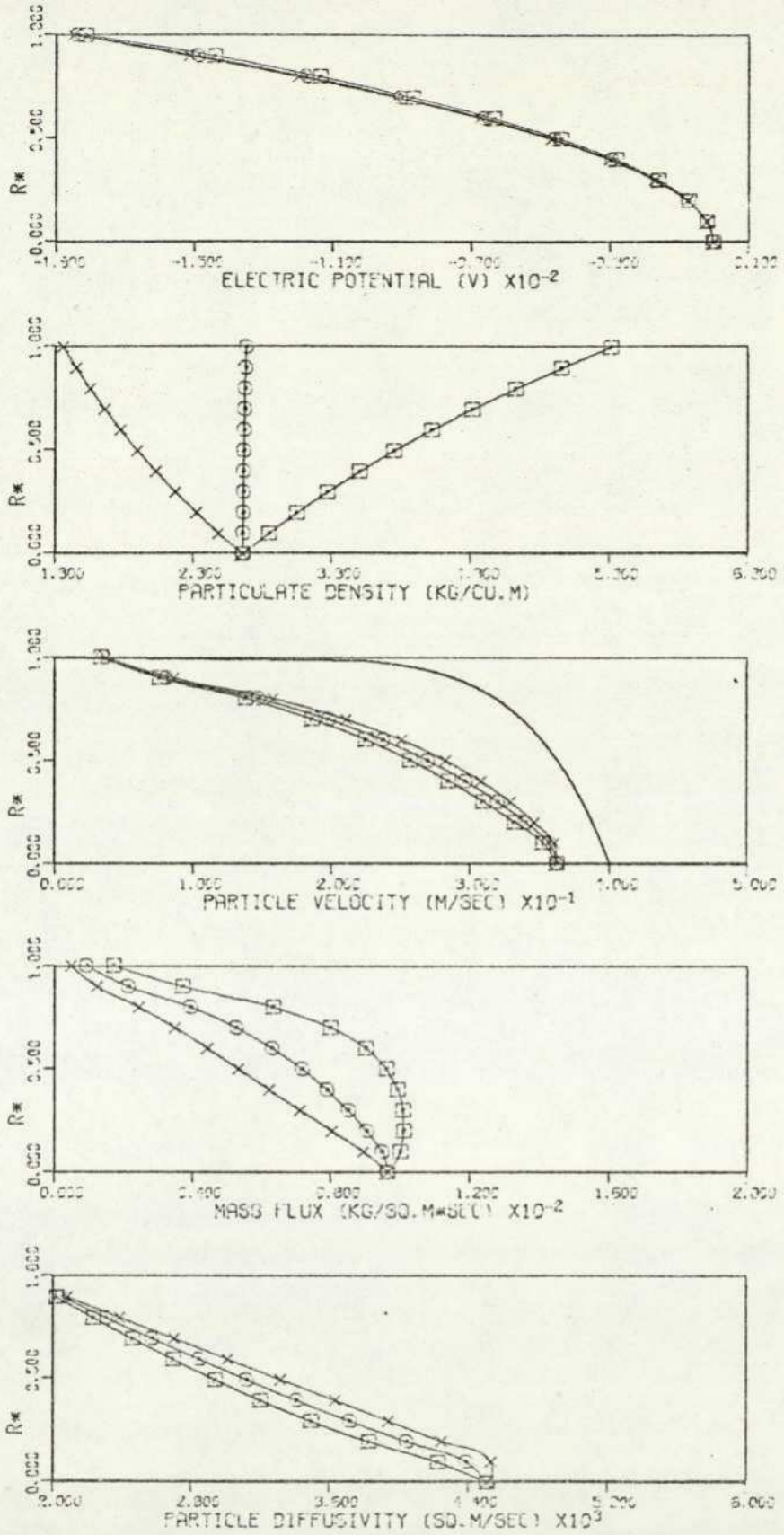

FIGURE : 7.35 VARIOUS DISTRIBUTIONS IN A FULLY DEVELOPED TURBULENT GAS-SOLID SUSPENSION FLOW. PARTICLES TYPE #2.

PIPE FLOW PARAMETERS : R=0.156E-01 M, UO=0.400E 02 M/SEC, D/M=0.100E-04 C/KG, KNP=0.100E 00, DF=0.336E-02 SQ.M/SEC, MP=0.400E-01(EXPT), 0.400E-01 (COMP) KG/SEC. PIPE INCLINATION = 90.0°. ×=0.0°, ⊙=30.0°, ⊡=180.0°, —— AIR.

DATA COMPUTED BY #XFDTB, PLOTTED BY #PLT05 (TEST 01-19-0-2A).

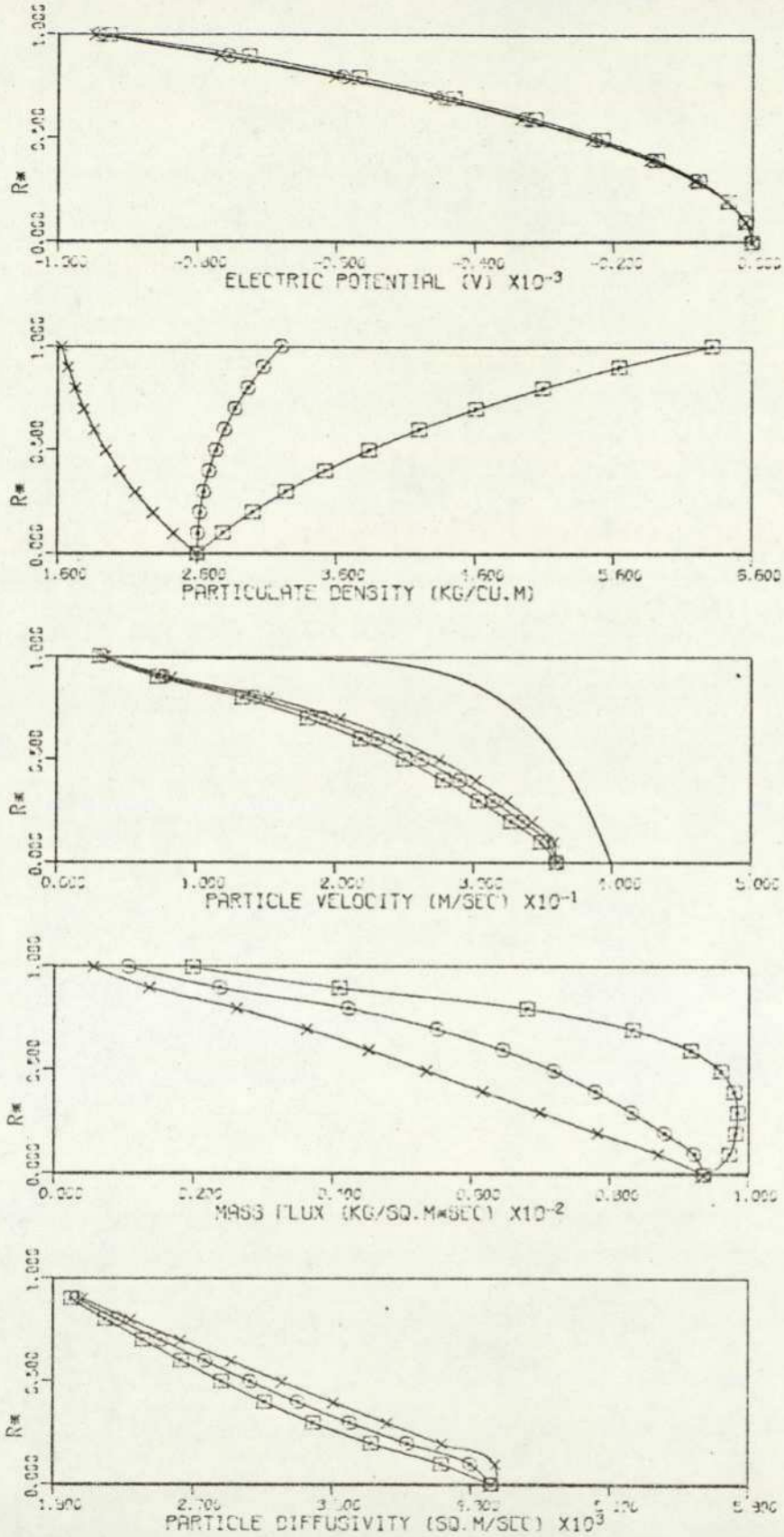

FIGURE : 7.36 VARIOUS DISTRIBUTIONS IN A FULLY DEVELOPED TURBULENT GAS-SOLID SUSPENSION FLOW. PARTICLES TYPE #2.

PIPE FLOW PARAMETERS : R=0.156E-01 M, UO=0.400E 02 M/SEC, Q/M=0.500E-04 C/KG, KNP=0.100E 00, DF=0.936E-02 SQ.M/SEC, MP=0.400E-01(EXPT), 0.409E-01 (COMP) KG/SEC. PIPE INCLINATION = 90.0°. × +0.0°, ⊙ -90.0°, ⊡ -180.0°, —— AIR.

DATA COMPUTED BY #XFD7B, PLOTTED BY #PJ05 (TEST 01-20-0-2A).

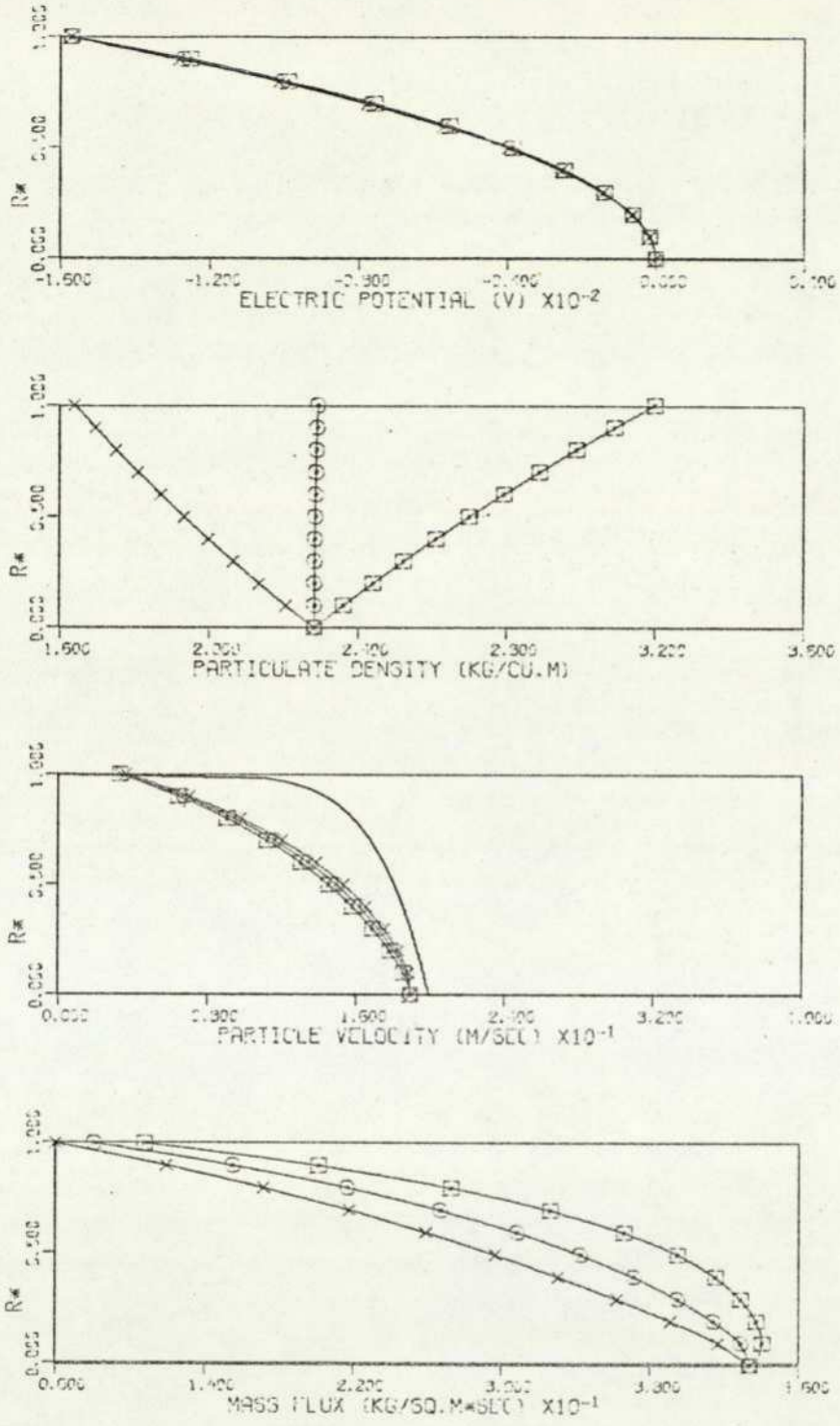

FIGURE : 7.37 VARIOUS DISTRIBUTIONS IN A FULLY DEVELOPED TURBULENT GAS-SOLID SUSPENSION FLOW. PARTICLES TYPE #1.

PIPE FLOW PARAMETERS : R=0.156E-01 M, UO=0.200E 02 M/SEC, Q/M=0.100E-04 C/KG, KNP=0.100E 00, DF=0.312E-02 SQ.M/SEC, MP=0.200E-01(EXPT), 0.200E-01 (COMP) KG/SEC
PIPE INCLINATION = 90.0°. × =0.0°, ⊙ =90.0°, ⊡ =180.0°, —— AIR.

DATA COMPUTED BY #XFD3S, PLOTTED BY #PJDS (TEST 00-01-0-15).

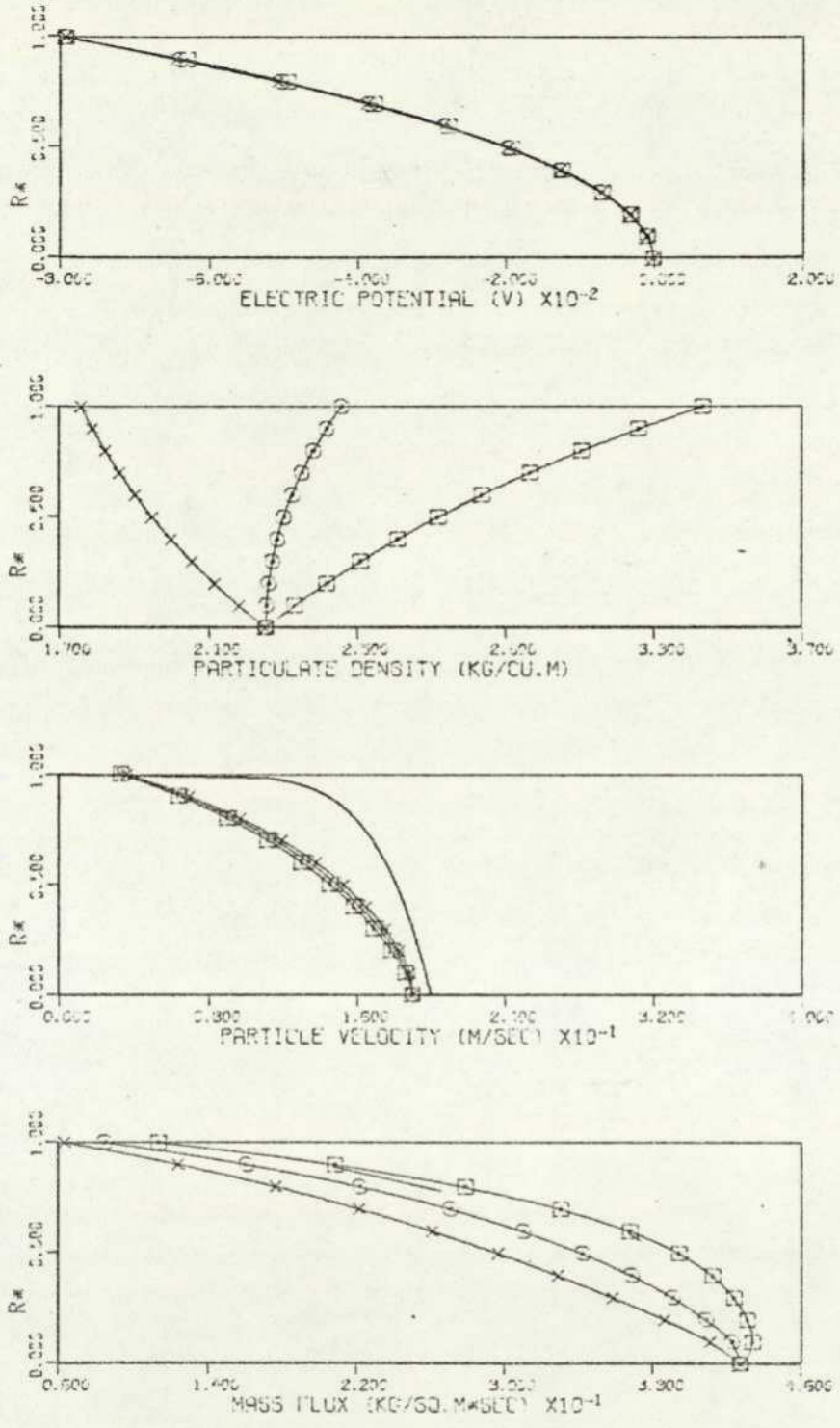

FIGURE 7.38 VARIOUS DISTRIBUTIONS IN A FULLY DEVELOPED TURBULENT GAS-SOLID SUSPENSION FLOW. PARTICLES TYPE #1.

PIPE FLOW PARAMETERS : R=0.156E-01 M, UO=0.200E 02 M/SEC, Q/M=0.500E-04 C/KG, KNP=0.100E 00, DF=0.312E-02 SQ.M/SEC, MP=0.200E-01(EXPT), 0.202E-01 (COMP) KG/SEC. PIPE INCLINATION = 90.0°. × 0.0°, ⊙ 90.0°, ⊡ 180.0°, —— AIR.

DATA COMPUTED BY #XF030, PLOTTED BY #PJ06 (TEST 00-02-0-1B).

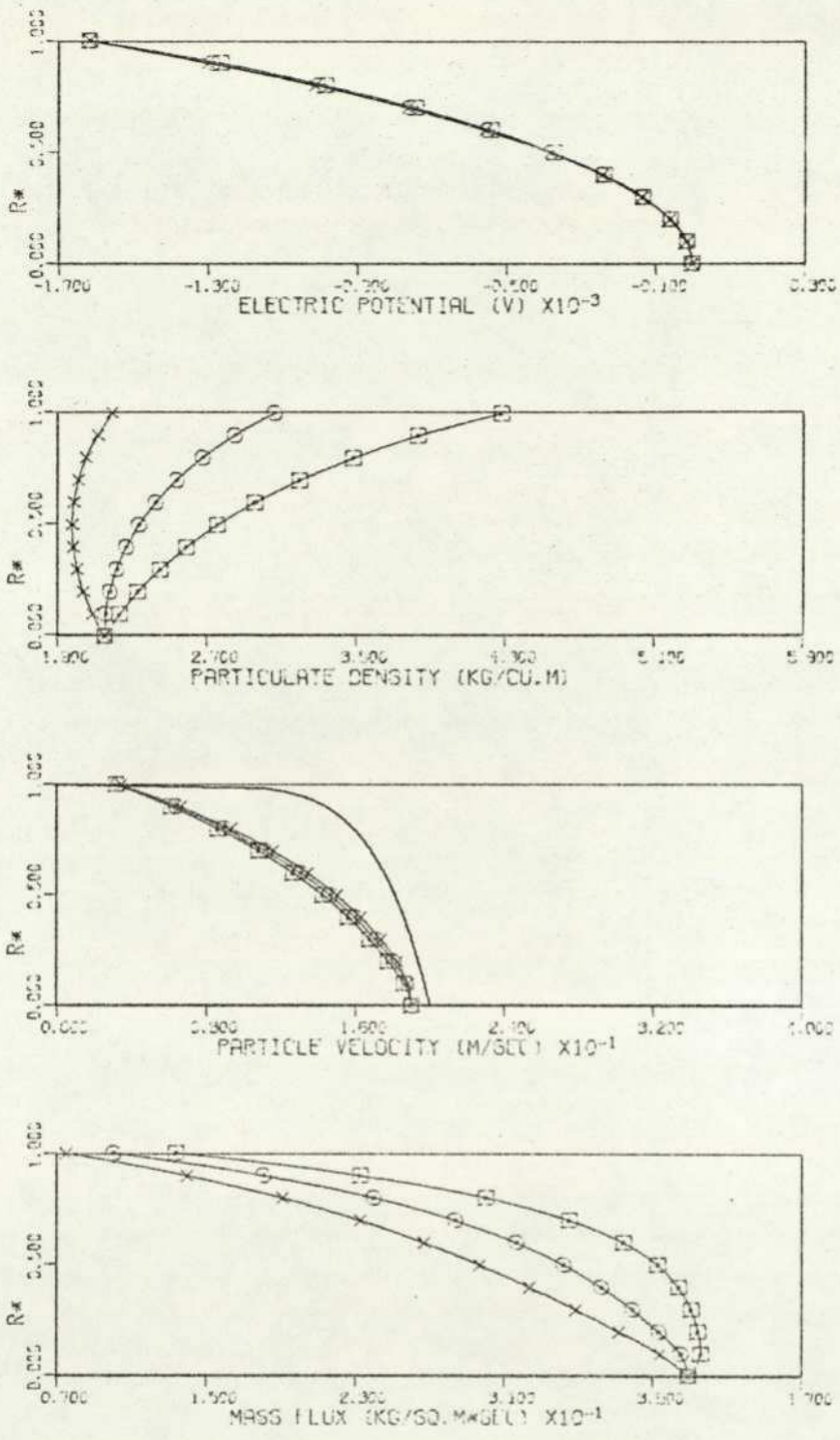

FIGURE : 7.39 VARIOUS DISTRIBUTIONS IN A FULLY DEVELOPED TURBULENT GAS-SOLID SUSPENSION FLOW. PARTICLES TYPE #1.

PIPE FLOW PARAMETERS : R=0.156E-01 M, U0=0.200E 02 M/SEC, Q/M=0.100E-03 C/KG,
KNP=0.100E 00, DF=0.312E-02 SQ.M/SEC, MP=0.200E-01(EXPT), 0.208E-01 (COMP) KG/SEC.
PIPE INCLINATION = 90.0°. × =0.0°, ⊙ =90.0°, ⊡ =180.0°, —— AIR.

DATA COMPUTED BY #XF035, PLOTTED BY #PJDS (TEST 00-03-0-15).

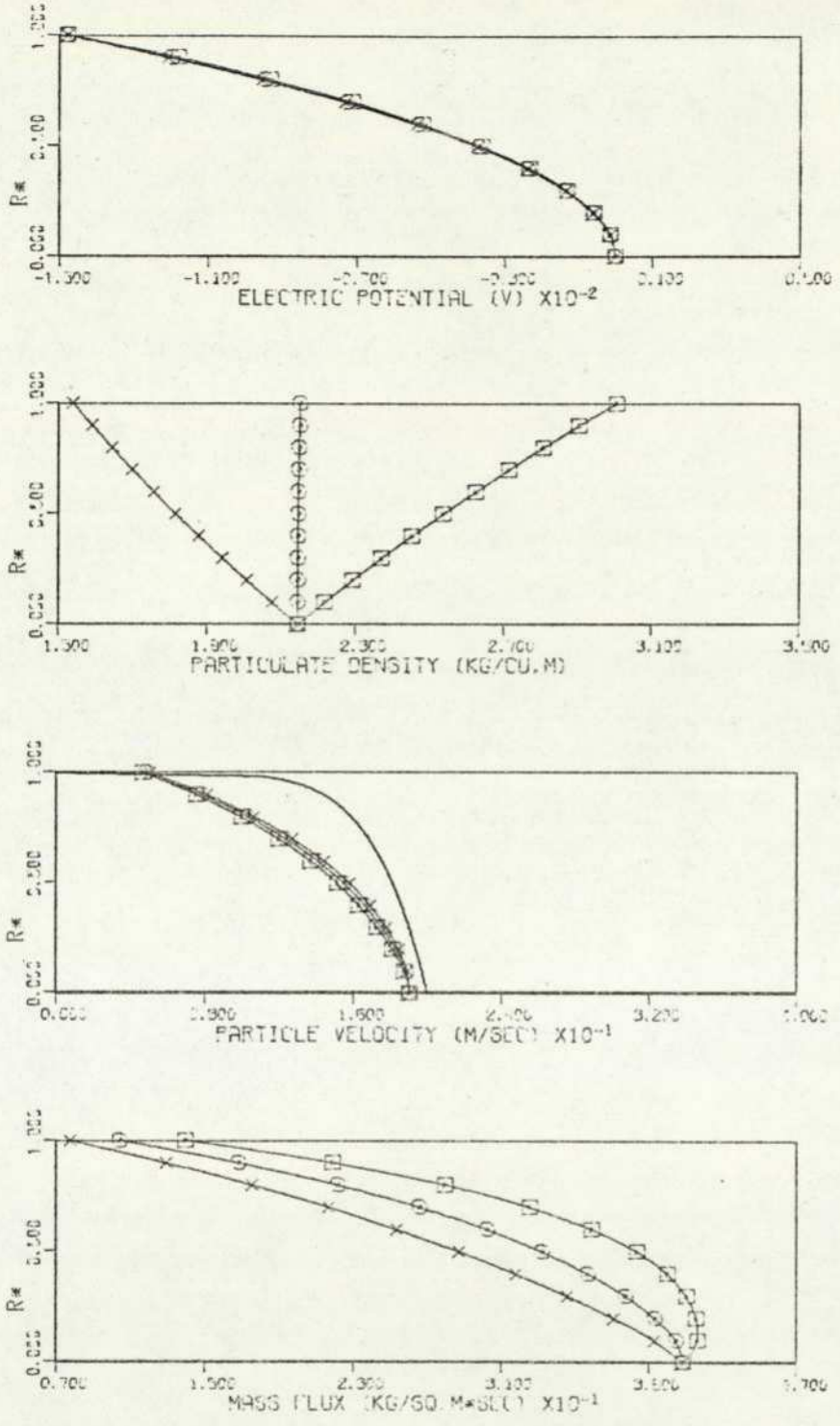

FIGURE : *7.40* VARIOUS DISTRIBUTIONS IN A FULLY DEVELOPED TURBULENT GAS-SOLID SUSPENSION FLOW. PARTICLES TYPE #1.

PIPE FLOW PARAMETERS : R=0.156E-01 M, U0=0.200E 02 M/SEC, Q/M=0.100E-04 C/KG, KNP=0.150E 00, DF=0.312E-02 SQ.M/SEC, MP=0.200E-01(EXPT), 0.200E-01 (COMP) KG/SEC. PIPE INCLINATION = 90.0°. × =0.0°, ⊙ =90.0°, ⊡ =180.0°, —— RIR.

DATA COMPUTED BY #XFD35, PLOTTED BY #PL06 (TEST 00-01-0-15).

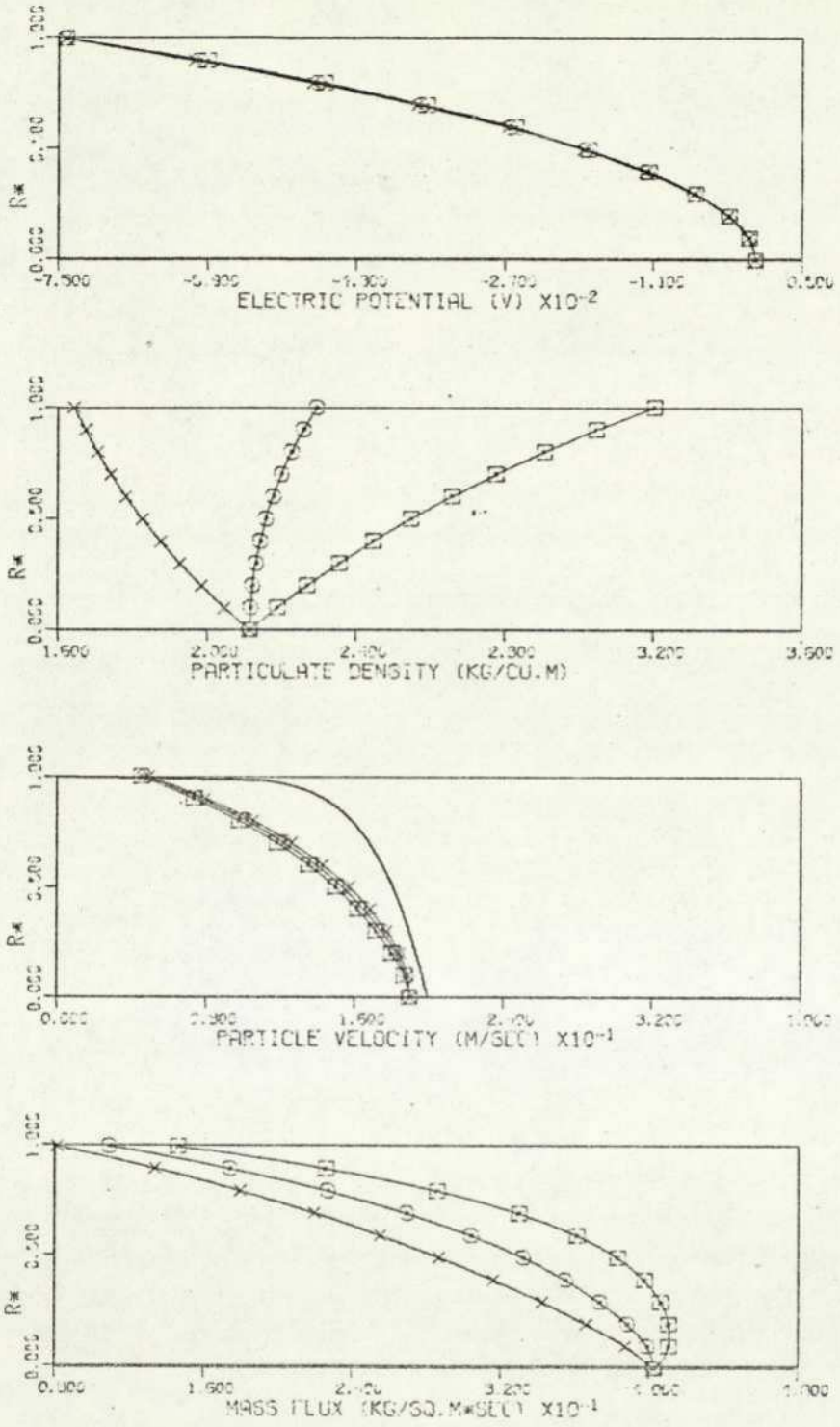

FIGURE : 7.41 VARIOUS DISTRIBUTIONS IN A FULLY DEVELOPED TURBULENT GAS-SOLID SUSPENSION FLOW. PARTICLES TYPE #1.

PIPE FLOW PARAMETERS : R=0.156E-01 M, UO=0.203E 02 M/SEC, O/M=0.500E-04 C/KG, KNP=0.150E 00, DF=0.312E-02 SQ.M/SEC, MP=0.203E-01(EXPT), 0.202E-01 (COMP) KG/SEC. PIPE INCLINATION = 90.0°. × -0.0°, ⊙ -90.0°, ⊡ -180.0°, —— AIR.

DATA COMPUTED BY #XF03G, PLOTTED BY #PJ06 (TEST 00-05-0-15).

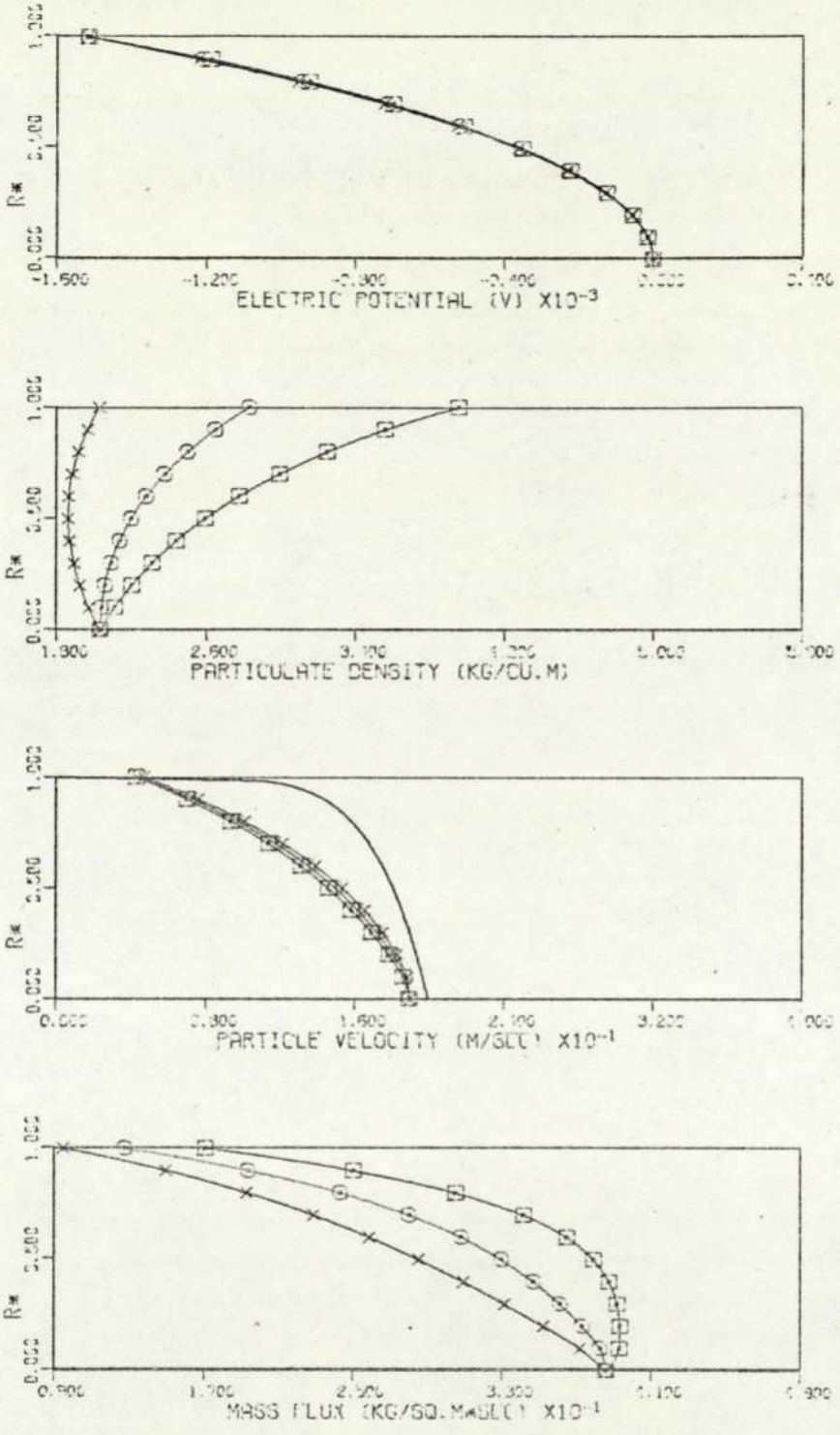

FIGURE : 7.42 VARIOUS DISTRIBUTIONS IN A FULLY DEVELOPED TURBULENT GAS-SOLID SUSPENSION FLOW. PARTICLES TYPE #1.

PIPE FLOW PARAMETERS : R=0.156E-01 M, UO=0.200E 02 M/SEC, O/M=0.100E-03 O/KG, KNP=0.150E 00, DF=0.312E-02 SQ.M/SEC, MP=0.200E-01(EXPT), 0.207E-01 (COMP) KG/SEC. PIPE INCLINATION = 90.0°. ×=0.0°, ⊙=90.0°, ⊡=180.0 , —— AIR.

DATA COMPUTED BY #XFD30, PLOTTED BY #PJ05 (TEST 00-06-0-1B).

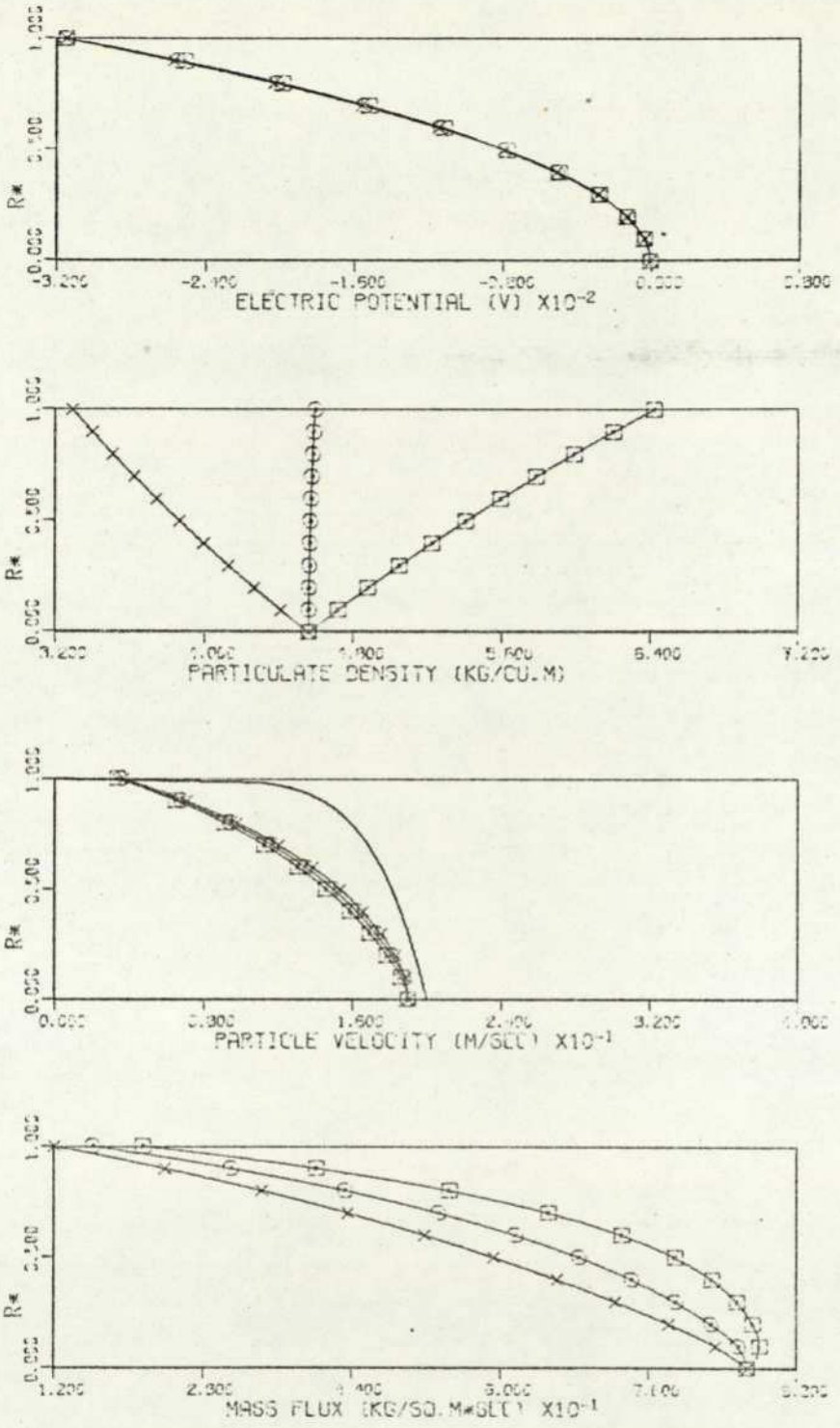

FIGURE 7.43 VARIOUS DISTRIBUTIONS IN A FULLY DEVELOPED TURBULENT GAS-SOLID SUSPENSION FLOW. PARTICLES TYPE #1.

PIPE FLOW PARAMETERS , R=0.156E-01 M, UO=0.200E 02 M/SEC, Q/M=0.100E-01 C/KG, KNP=0.100E 00, DF=0.312E-02 SQ.M/SEC, MP=0.400E-01(EXPT), 0.400E-01 (COMP) KG/SEC. PIPE INCLINATION = 90.0°. × =0.0°, ⊙ =90.0°, ⊡ =180.0°, —— AIR.

DATA COMPUTED BY #XFD3B, PLOTTED BY #PJ05 (TEST 00-07-0-1B).

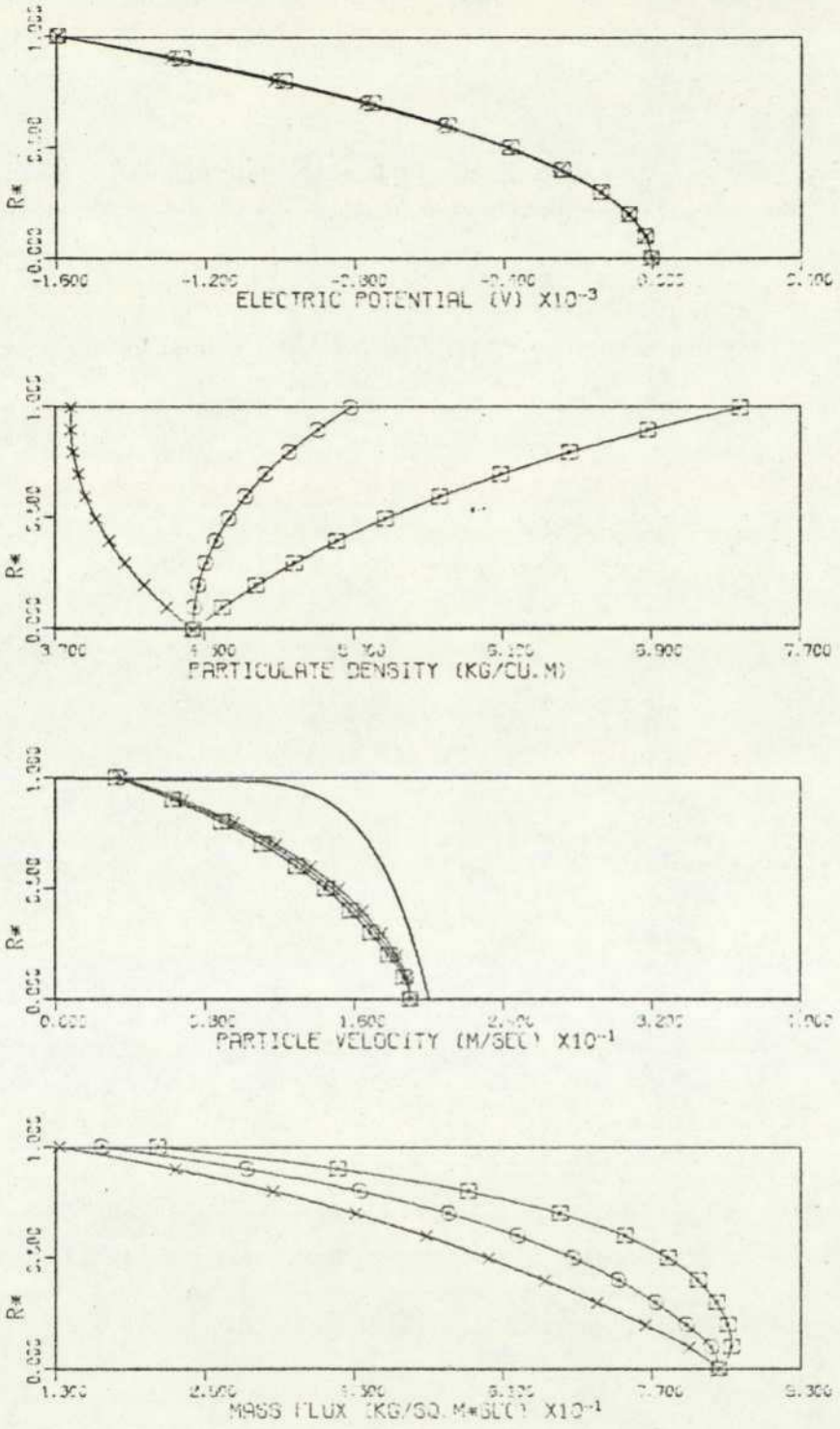

FIGURE :7.44 VARIOUS DISTRIBUTIONS IN A FULLY DEVELOPED TURBULENT GAS-SOLID SUSPENSION FLOW. PARTICLES TYPE #1.

PIPE FLOW PARAMETERS : R=0.156E-01 M, UO=0.200E 02 M/SEC, Q/M=0.500E-04 C/KG,
KNP=0.100E 00, DF=0.312E-02 SQ.M/SEC, MP=0.400E-01(EXPT), 0.405E-01 (COMP) KG/SEC.
PIPE INCLINATION = 30.0°. × 0.0°, ⊙ 90.0°, ⊡ 180.0°, —— AIR.

DATA COMPUTED BY #XFD3S, PLOTTED BY #PJD5 (TEST 00-09-0-16).

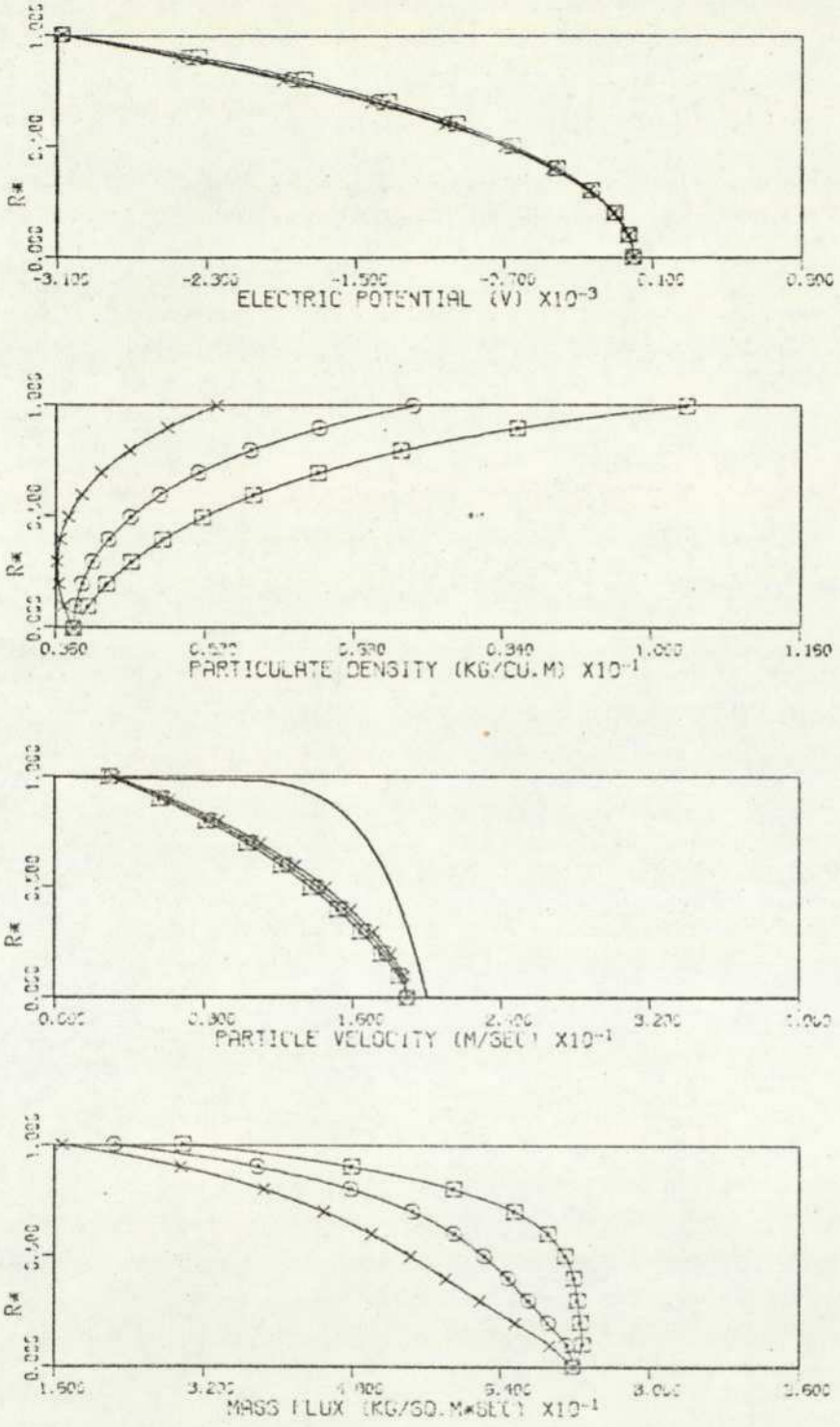

FIGURE 7.45 VARIOUS DISTRIBUTIONS IN A FULLY DEVELOPED TURBULENT GAS-SOLID SUSPENSION FLOW. PARTICLES TYPE #1.

PIPE FLOW PARAMETERS : R=0.156E-01 M. U0=0.200E 02 M/SEC. Q/M=0.100E-03 C/KG.
KNP=0.100E 00. DF=0.312E-02 SQ.M/SEC. MP=0.400E-01(EXPT). 0.300E-01 (COMP) KG/SEC.
PIPE INCLINATION = 90.0°. × =0.0°, ⊙ =90.0°, ⊡ =180.0°, —— RIR.

DATA COMPUTED BY #MFD3S. PLOTTED BY #PJOS (TEST 00-00-0-15).

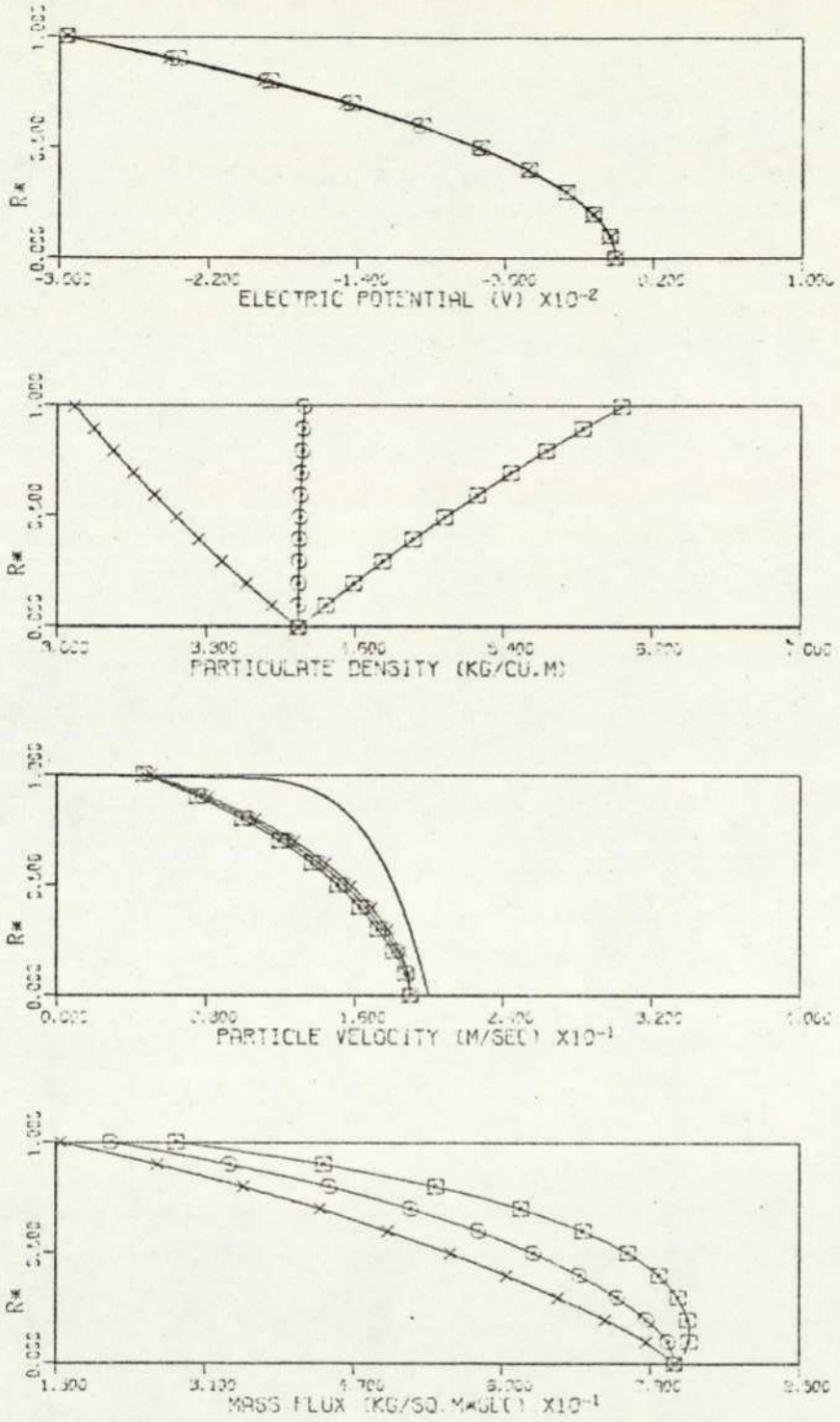

FIGURE 7.46 VARIOUS DISTRIBUTIONS IN A FULLY DEVELOPED TURBULENT GAS-SOLID SUSPENSION FLOW. PARTICLES TYPE #1.

PIPE FLOW PARAMETERS : R=0.156E-01 M, UO=0.200E 02 M/SEC, Q/M=0.100E-04 C/KG, KNP=0.150E 00, DF=0.312E-02 SQ.M/SEC, MP=0.400E-01(EXPT), 0.400E-01 (COMP) KG/SEC. PIPE INCLINATION = 90.0°. × =0.0°, ⊙ =90.0°, ⊡ =180.0°, —— AIR.

DATA COMPUTED BY #XFD3S, PLOTTED BY #PJ06 (TEST 00-10-0-1B).

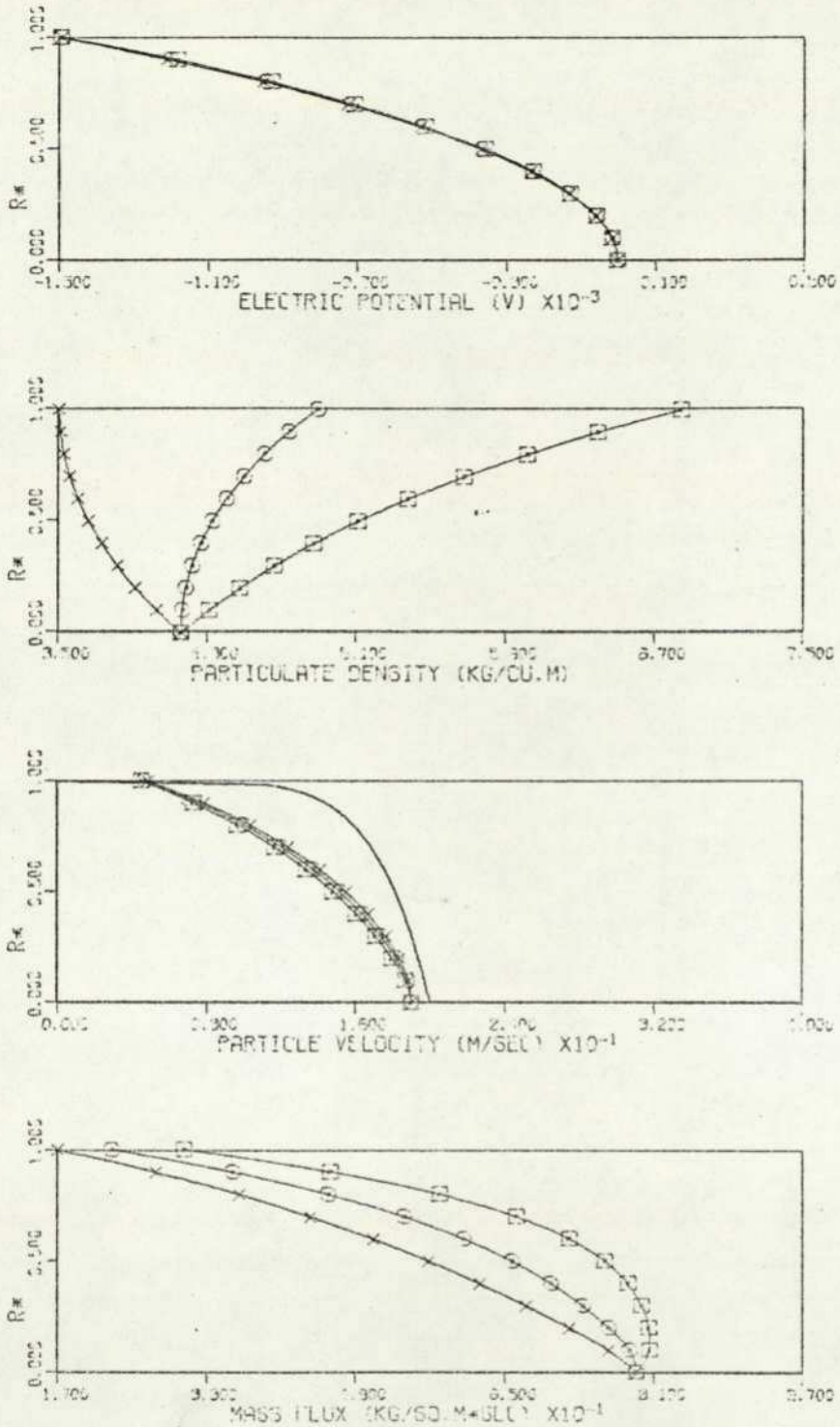

FIGURE 7.47 VARIOUS DISTRIBUTIONS IN A FULLY DEVELOPED TURBULENT GAS-SOLID SUSPENSION FLOW. PARTICLES TYPE #1.

PIPE FLOW PARAMETERS : P=0.156E-01 M, UO=0.200E 02 M/SEC, Q/M=0.500E-04 C/KG,
KNP=0.100E 00, DF=0.312E-02 SQ.M/SEC MP=0.400E-01(EXPT), 0.405E-01 (COMP) KG/SEC
PIPE INCLINATION = 90.0°. × =0.0°, ⊙ =30.0°, ⊡ =90.0°, ——— AIR.

DATA COMPUTED BY #XF03B, PLOTTED BY #PL05 (TEST 00-11-0-15).

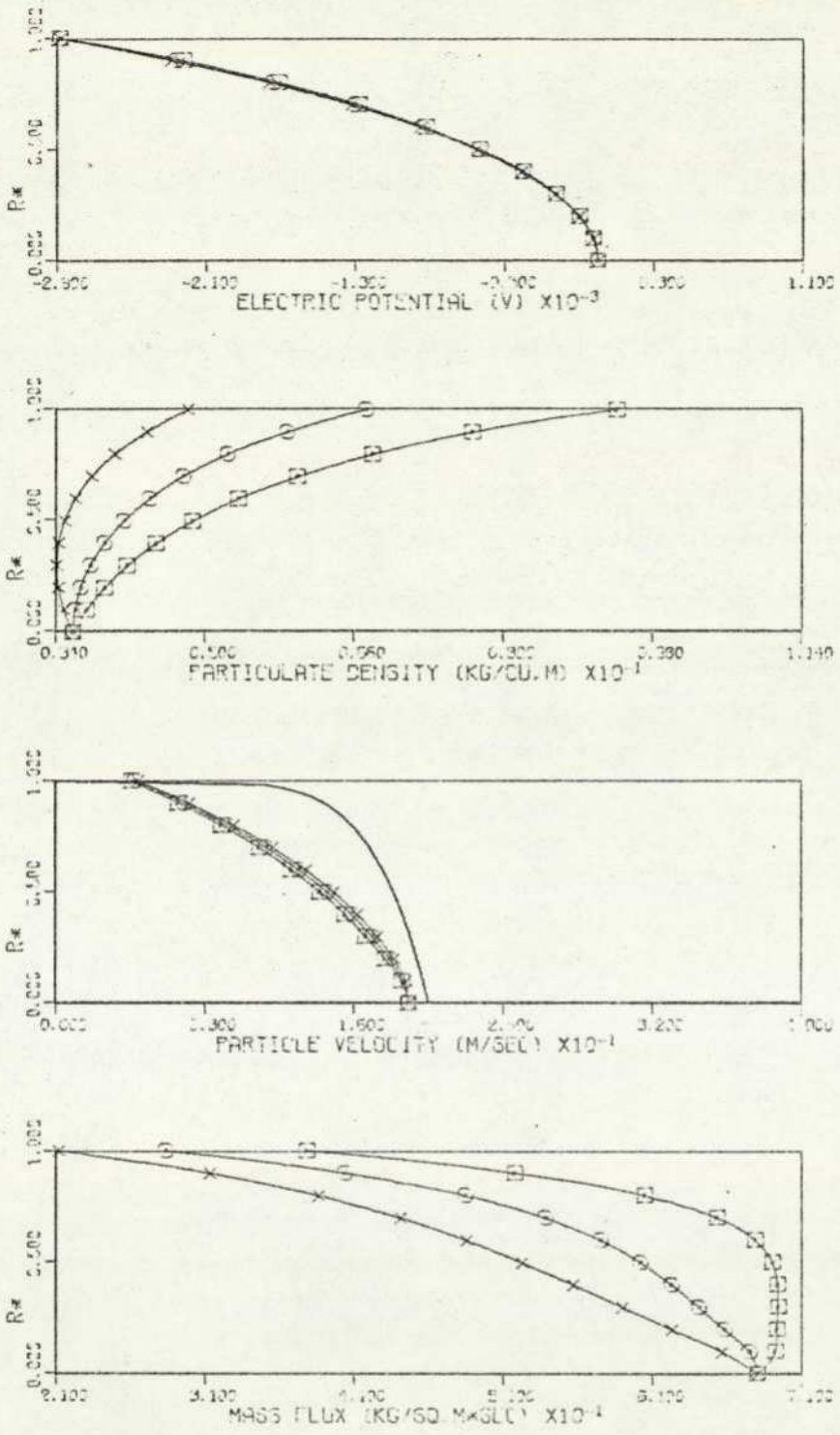

FIGURE .7.48 VARIOUS DISTRIBUTIONS IN A FULLY DEVELOPED TURBULENT GAS-SOLID SUSPENSION FLOW. PARTICLES TYPE #1.

PIPE FLOW PARAMETERS : R=0.156E-01 M. UO=0.200E 02 M/SEC. Q/M=0.100E-03 C/KG.
KNP=0.150E 00. DF=0.312E-02 SQ.M/SEC. MP=0.400E-01(EXPT), 0.396E-01 (COMP) KG/SEC
PIPE INCLINATION = 90.0°. × =0.0°, ⊙ =30.0°, ⊡ =180.0°, —— AIR.

DATA COMPUTED BY #XFD3B. PLOTTED BY #PL06 (TEST 00-12-0-18).

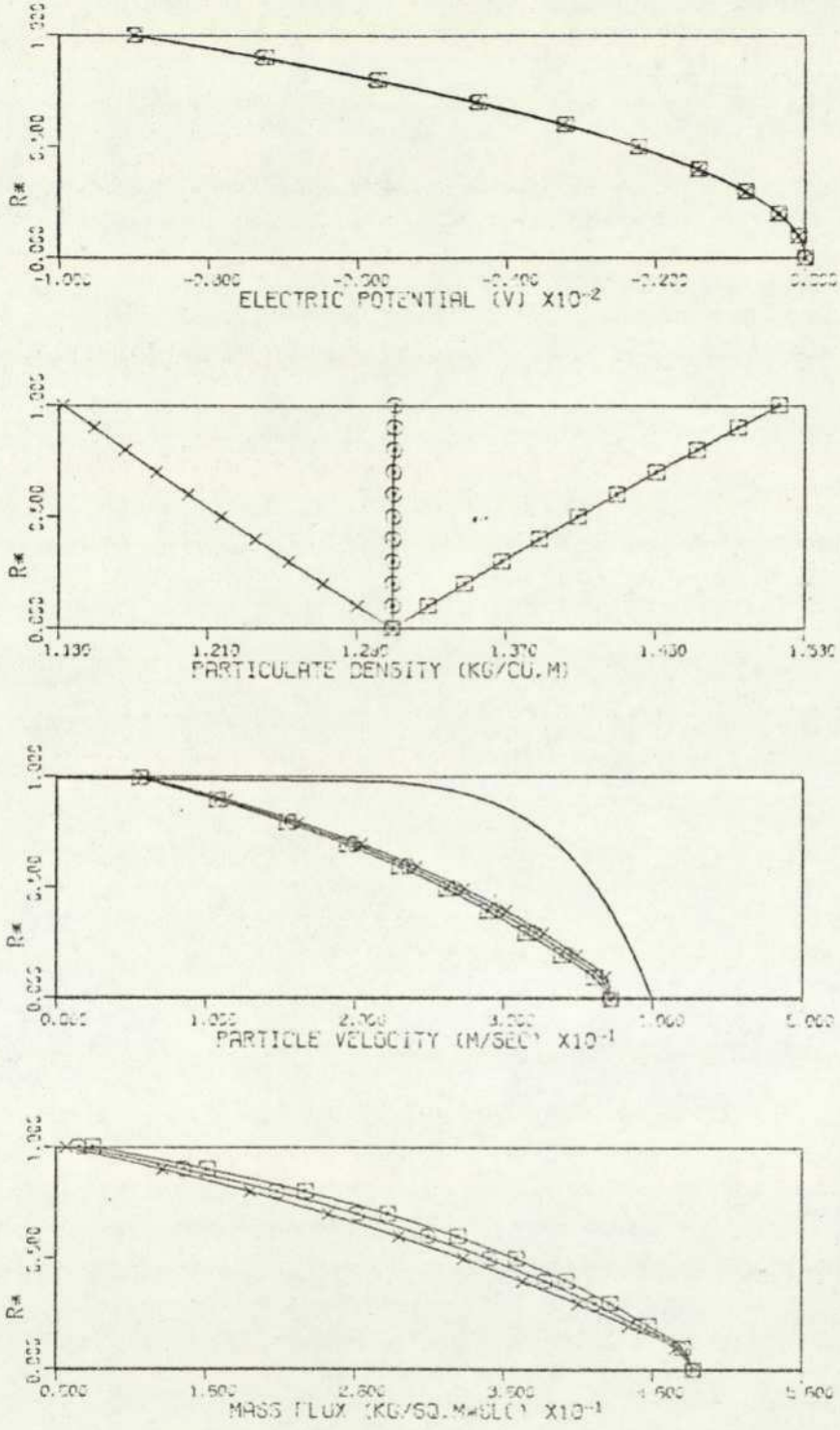

FIGURE 7.49 VARIOUS DISTRIBUTIONS IN A FULLY DEVELOPED TURBULENT GAS-SOLID SUSPENSION FLOW. PARTICLES TYPE #1.

PIPE FLOW PARAMETERS : R=0.156E-01 M, U0=0.400E 02 M/SEC, Q/M=0.100E-04 C/KG, KNP=0.100E 00, DF=0.621E-02 SQ.M/SEC, MP=0.200E-01(EXPT), 0.200E-01 (COMP) KG/SEC
PIPE INCLINATION = 90.0°. × 0.0°, ⊙ 90.0°, ⊡ 180.0°, —— AIR.

DATA COMPUTED BY #XFD3S, PLOTTED BY #PJ05 (TEST 00-13-0-15).

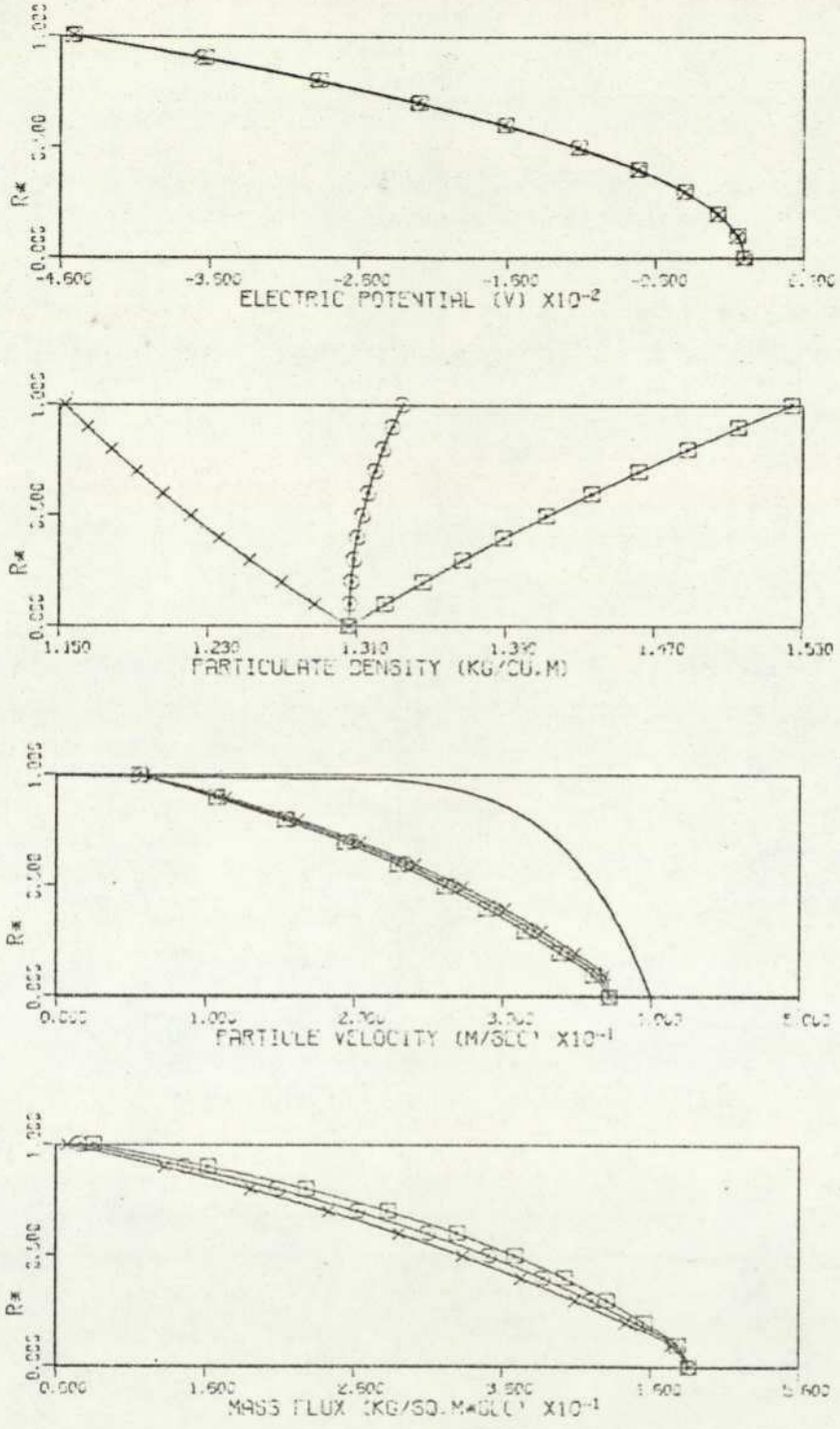

FIGURE 7.50 VARIOUS DISTRIBUTIONS IN A FULLY DEVELOPED TURBULENT GAS-SOLID SUSPENSION FLOW. PARTICLES TYPE #1.

PIPE FLOW PARAMETERS : R=0.156E-01 M, UO=0.400E 02 M/SEC, Q/M=0.500E-04 C/KG,
KNP=0.100E 00, DF=0.624E-02 SQ.M/SEC, MP=0.200E-01(EXPT), 0.201E-01 (COMP) KG/SEC
PIPE INCLINATION = 90.0°. ×=0.0°, ⊙=90.0°, ⊡=180.0°, —— AIR.

DATA COMPUTED BY #XFD3S, PLOTTED BY #PL05 (TEST 00-14-0-16).

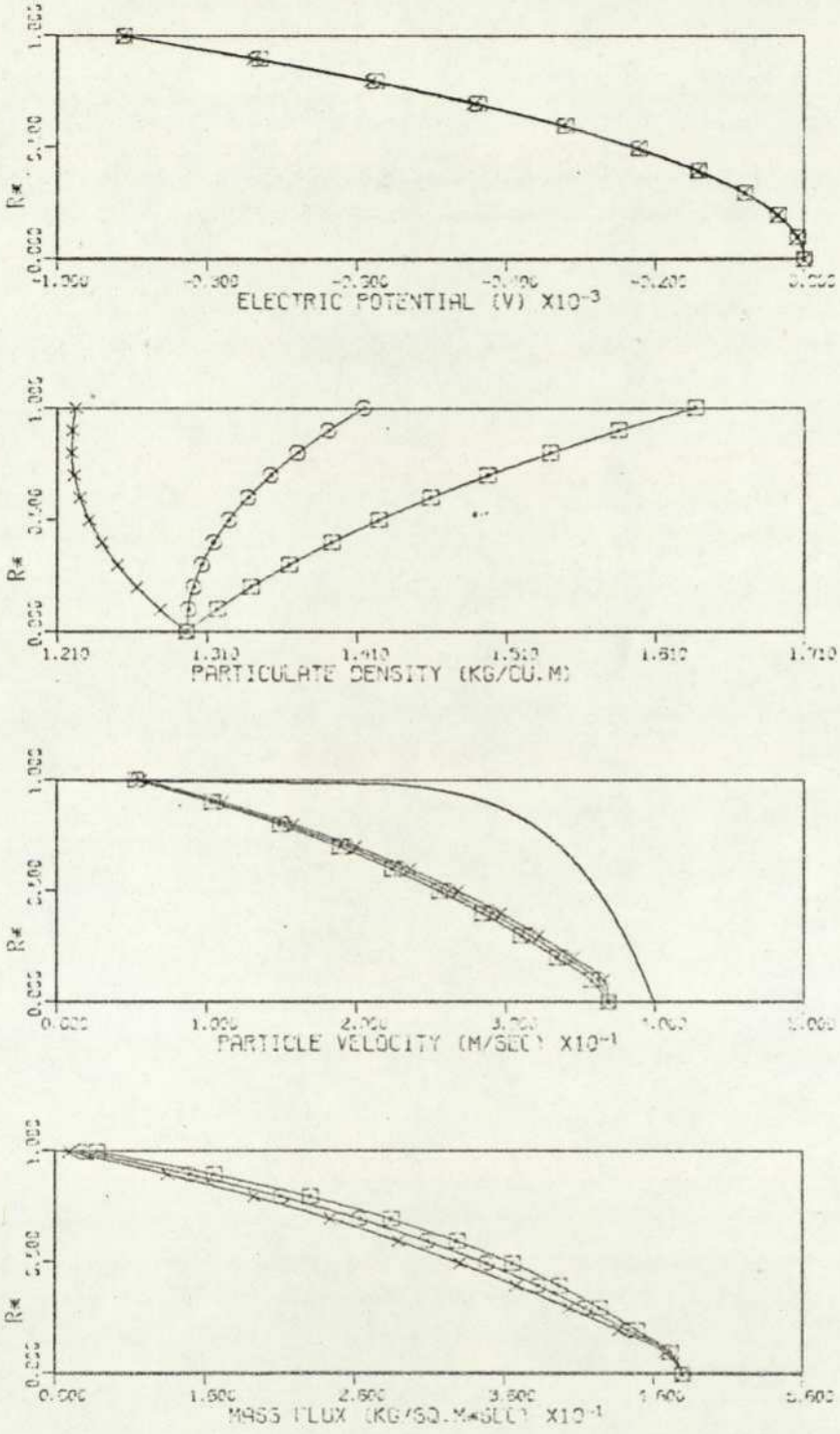

FIGURE 7.51 VARIOUS DISTRIBUTIONS IN A FULLY DEVELOPED TURBULENT GAS-SOLID SUSPENSION FLOW. PARTICLES TYPE #1.

PIPE FLOW PARAMETERS : P=0.156E-01 M. UO=0.300E 02 M/SEC. O/M=0.100E-03 O/KG.
KNP=0.100E 00, DF=0.621E-02 SQ.M/SEC. MP=0.200E-01(EXPT), 0.200E-01 (COMP) KG/SEC.
PIPE INCLINATION = 90.0°. ×=0.0°, ⊙=90.0°, ⊡=180.0°, +—— AIR.

DATA COMPUTED BY #XF03S, PLOTTED BY #PL05 (TEST 00-15-0-1S).

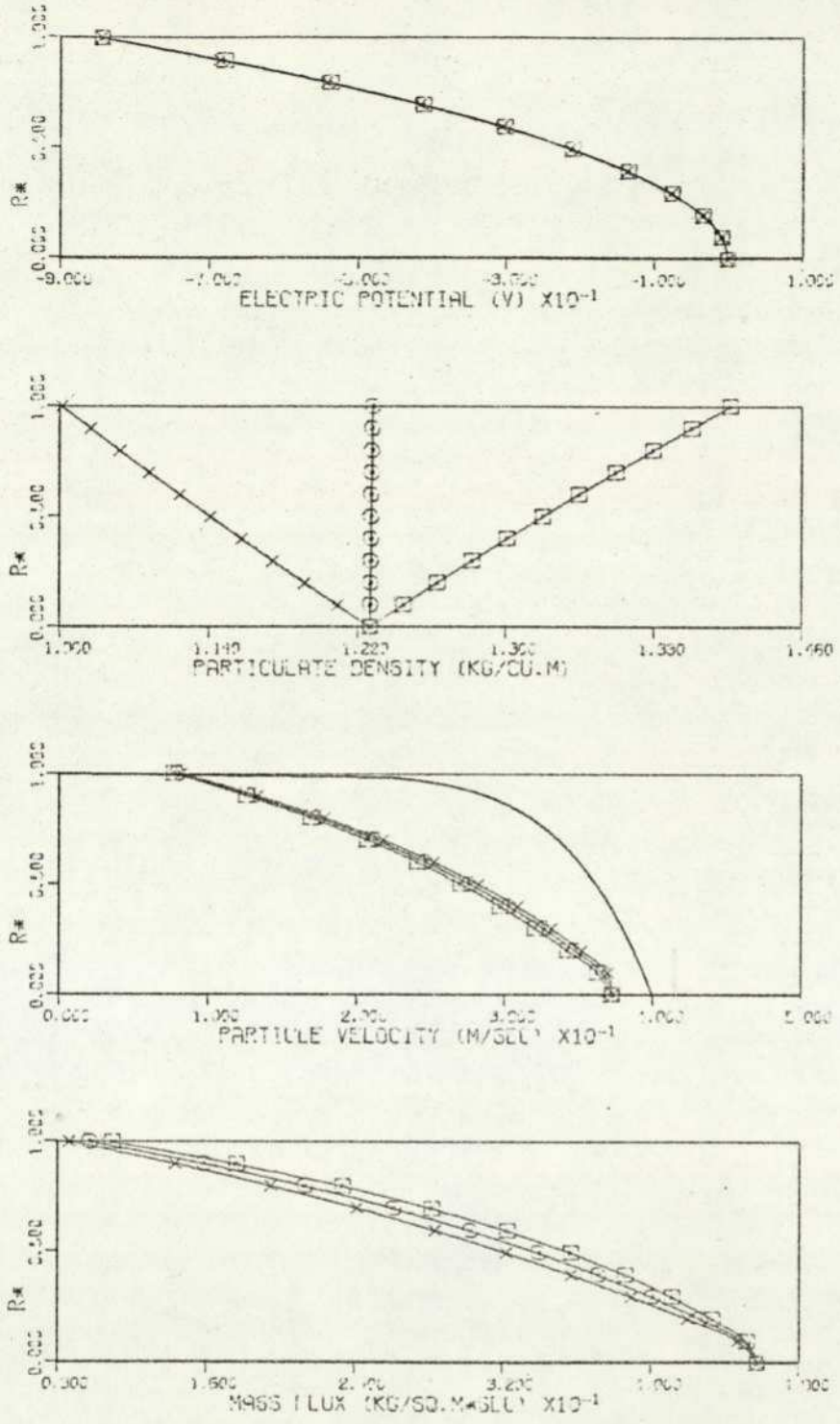

FIGURE : *7.52* VARIOUS DISTRIBUTIONS IN A FULLY DEVELOPED TURBULENT GAS-SOLID SUSPENSION FLOW. PARTICLES TYPE #1.

PIPE FLOW PARAMETERS : R=0.156E-01 M, UO=0.400E 02 M/SEC, Q/M=0.100E-04 C/KG, KNP=0.150E 00, DF=0.624E-02 SQ.M/SEC, MP=0.200E-01(EXPT), 0.200E-01 (COMP) KG/SEC

PIPE INCLINATION = 90.0°. ×=0.0°, ⊙=90.0°, ⊡=180.0°, ——— AIR.

DATA COMPUTED BY #XF03B, PLOTTED BY #PJ05 (TEST 00-16-0-1B).

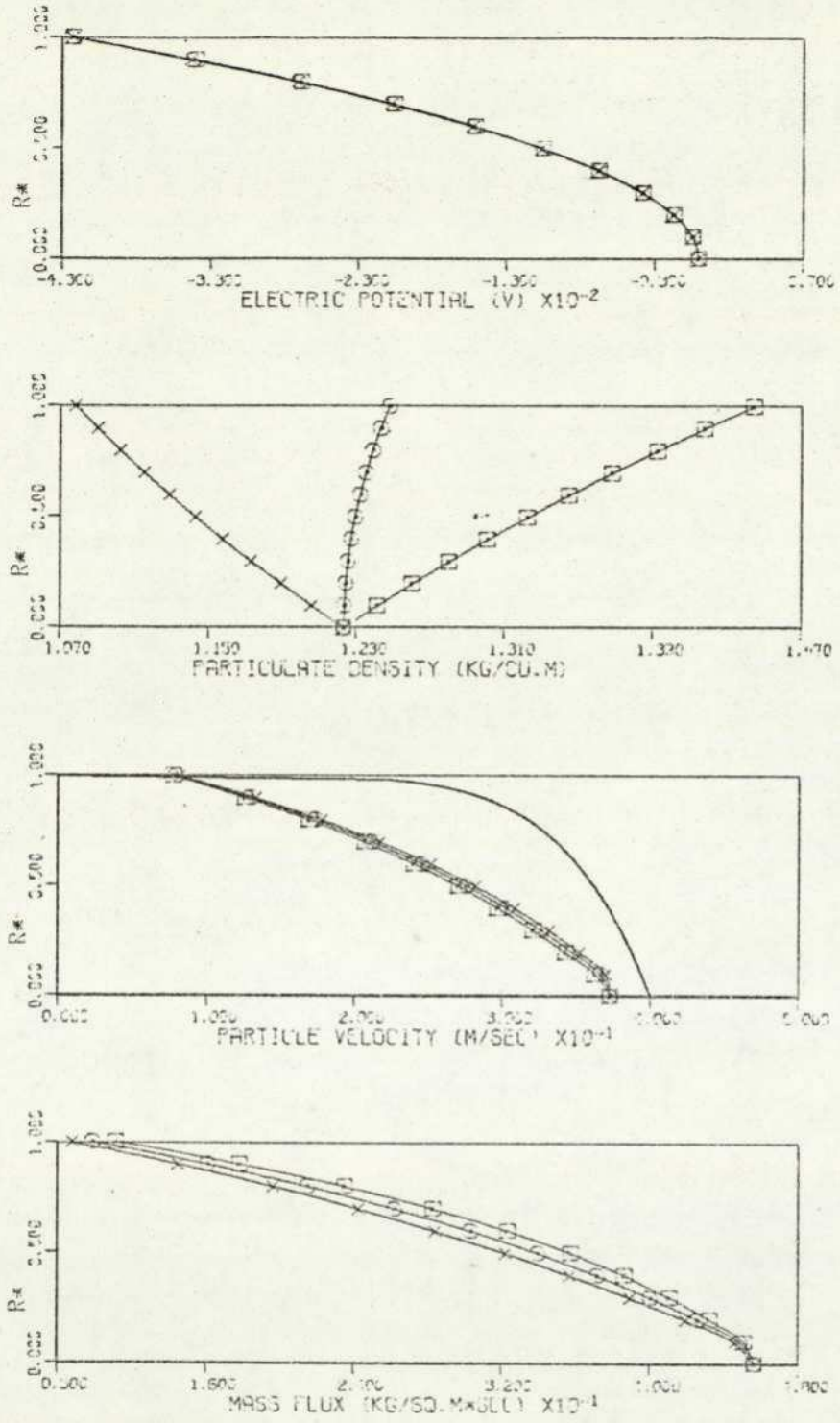

FIGURE : 7.53 VARIOUS DISTRIBUTIONS IN A FULLY DEVELOPED TURBULENT GAS-SOLID SUSPENSION FLOW. PARTICLES TYPE #1.

PIPE FLOW PARAMETERS : R=0.156E-01 M. UO=0.100E 02 M/SEC. Q/M=0.500E-04 C/KG.
KNP=0.150E 00. DF=0.601E-02 SQ.M/SEC. MP=0.200E-01(EXPT), 0.200E-01 (COMP) KG/SEC.
PIPE INCLINATION = 90.0° X -0.0°, ⊙ -90.0°, ⊡ -180.0°, —— AIR.

DATA COMPUTED BY #XF036, PLOTTED BY #PL05 (TEST 00-17-0-15).

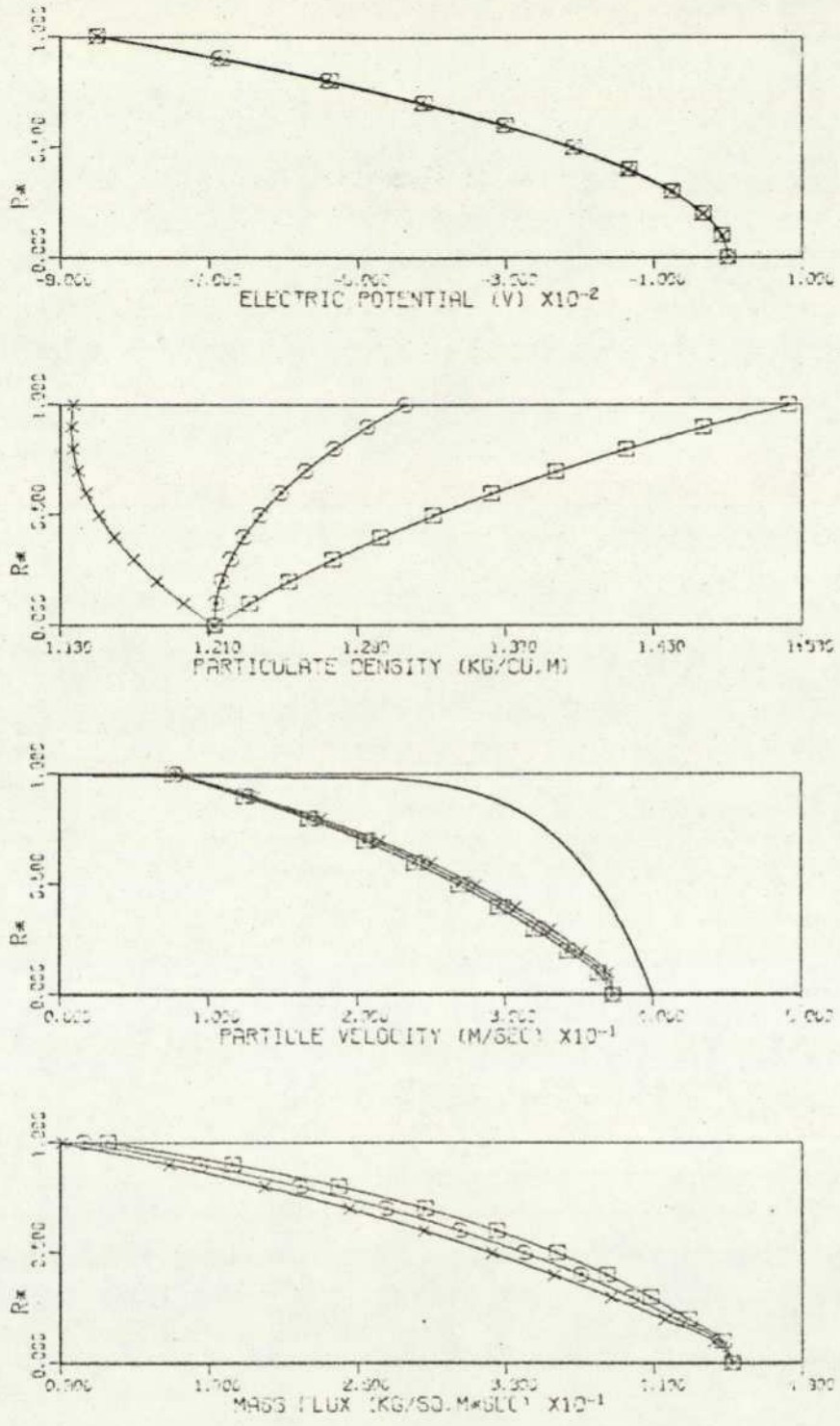

FIGURE 7.54 VARIOUS DISTRIBUTIONS IN A FULLY DEVELOPED TURBULENT GAS-SOLID SUSPENSION FLOW. PARTICLES TYPE #1.

PIPE FLOW PARAMETERS : R=0.156E-01 M, UO=0.400E 02 M/SEC, O/M=0.100E-03 O/KG, KNP=0.150E 00, DF=0.524E-02 SQ.M/SEC, MP=0.200E-01(EXPT), 0.202E-01 (COMP) KG/SEC. PIPE INCLINATION = 90.0°. × 0.0°, ⊙ 90.0°, ⊡ 180.0°, —— AIR.

DATA COMPUTED BY #XF035, PLOTTED BY #PL05 (TEST 00-18-0-15).

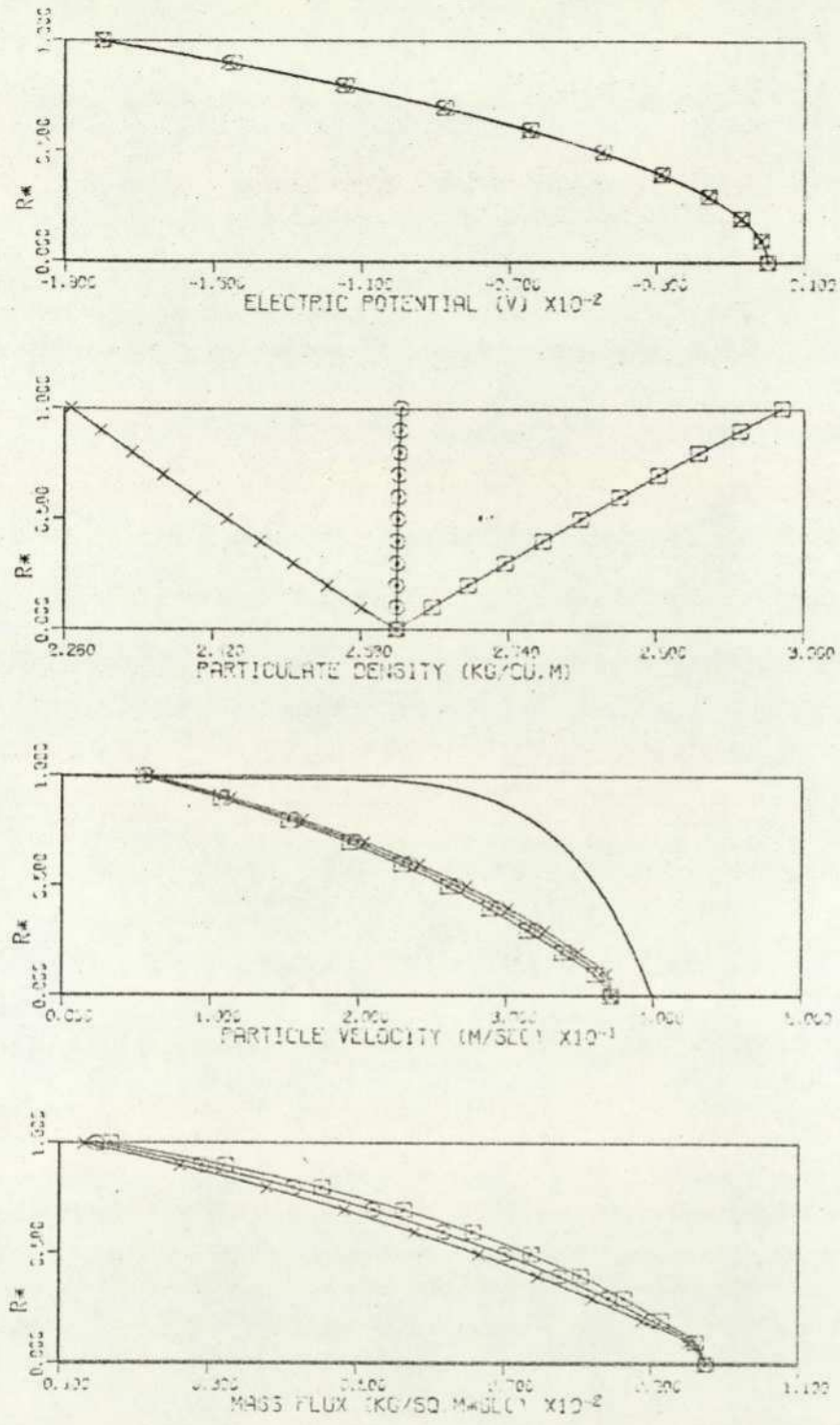

FIGURE 7.55 VARIOUS DISTRIBUTIONS IN A FULLY DEVELOPED TURBULENT GAS-SOLID SUSPENSION FLOW. PARTICLES TYPE #1.

PIPE FLOW PARAMETERS : R=0.156E-01 M, UO=0.400E 02 M/SEC, O/M=0.100E-04 O/KG,
KNP=0.100E 00, DF=0.621E-02 SQ.M/SEC, MP=0.400E-01(EXPT), 0.400E-01 (COMP) KG/SEC
PIPE INCLINATION = 90.0° × 40.0°, ⊙ 60.0°, ⊡ 80.0°, —— RIR.

DATA COMPUTED BY #XF036, PLOTTED BY #PJ00 (TEST 00-10-0-15).

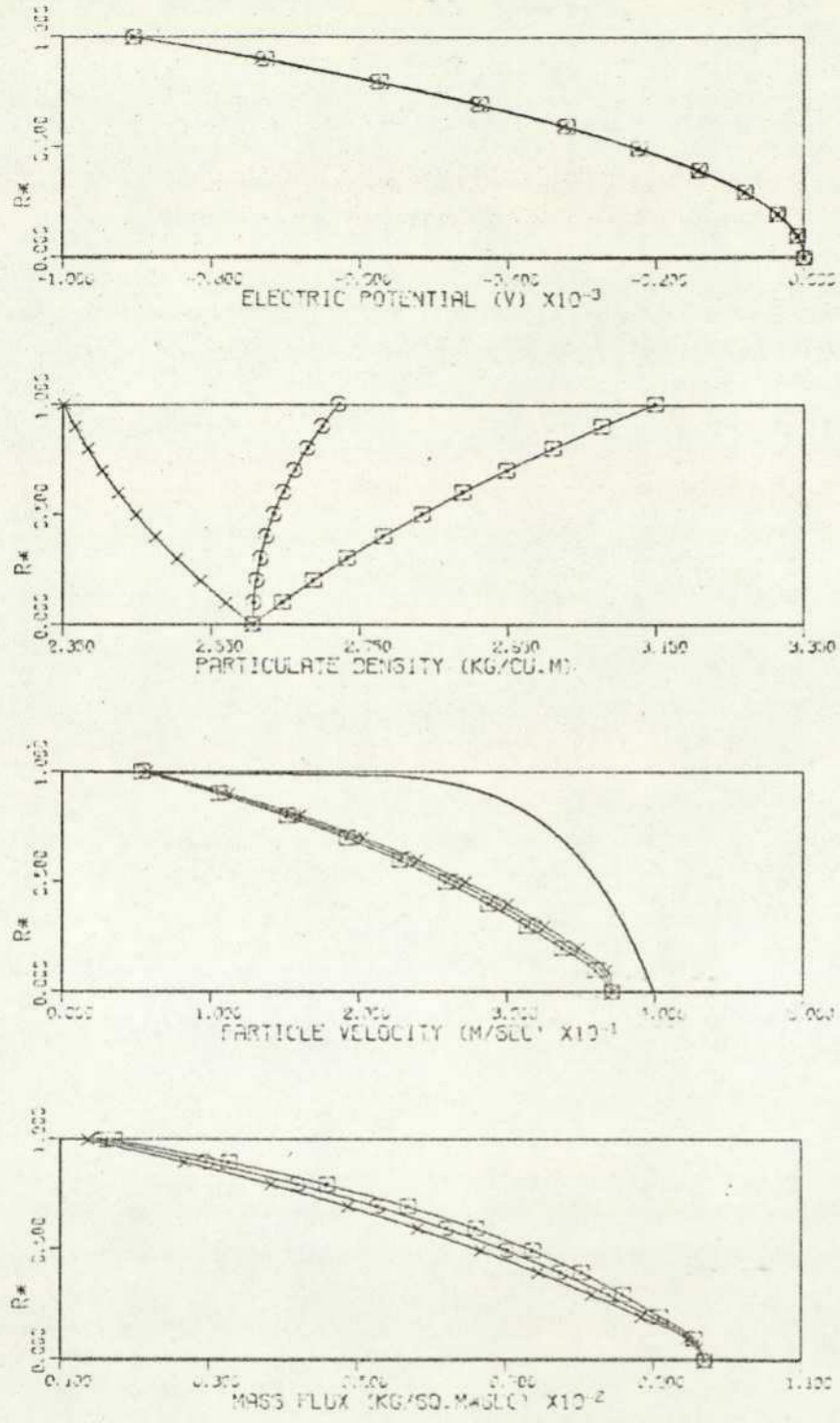

FIGURE : 7.56 VARIOUS DISTRIBUTIONS IN A FULLY DEVELOPED TURBULENT GAS-SOLID SUSPENSION FLOW. PARTICLES TYPE #1.

PIPE FLOW PARAMETERS : R=0.156E-01 M, UO=0.400E 02 M/SEC, Q/M=0.500E-03 C/KG, KNP=0.100E 00, DF=0.924E-02 SQ.M/SEC, MP=0.400E-01(EXPT), 0.402E-01 (COMP) KG/SEC. PIPE INCLINATION = 90.0°. × -0.0°, ⊙ +30.0°, ⊡ +60.0°, —— AIR.

DATA COMPUTED BY #XF035, PLOTTED BY #PL05 (TEST 00-20-0-15).

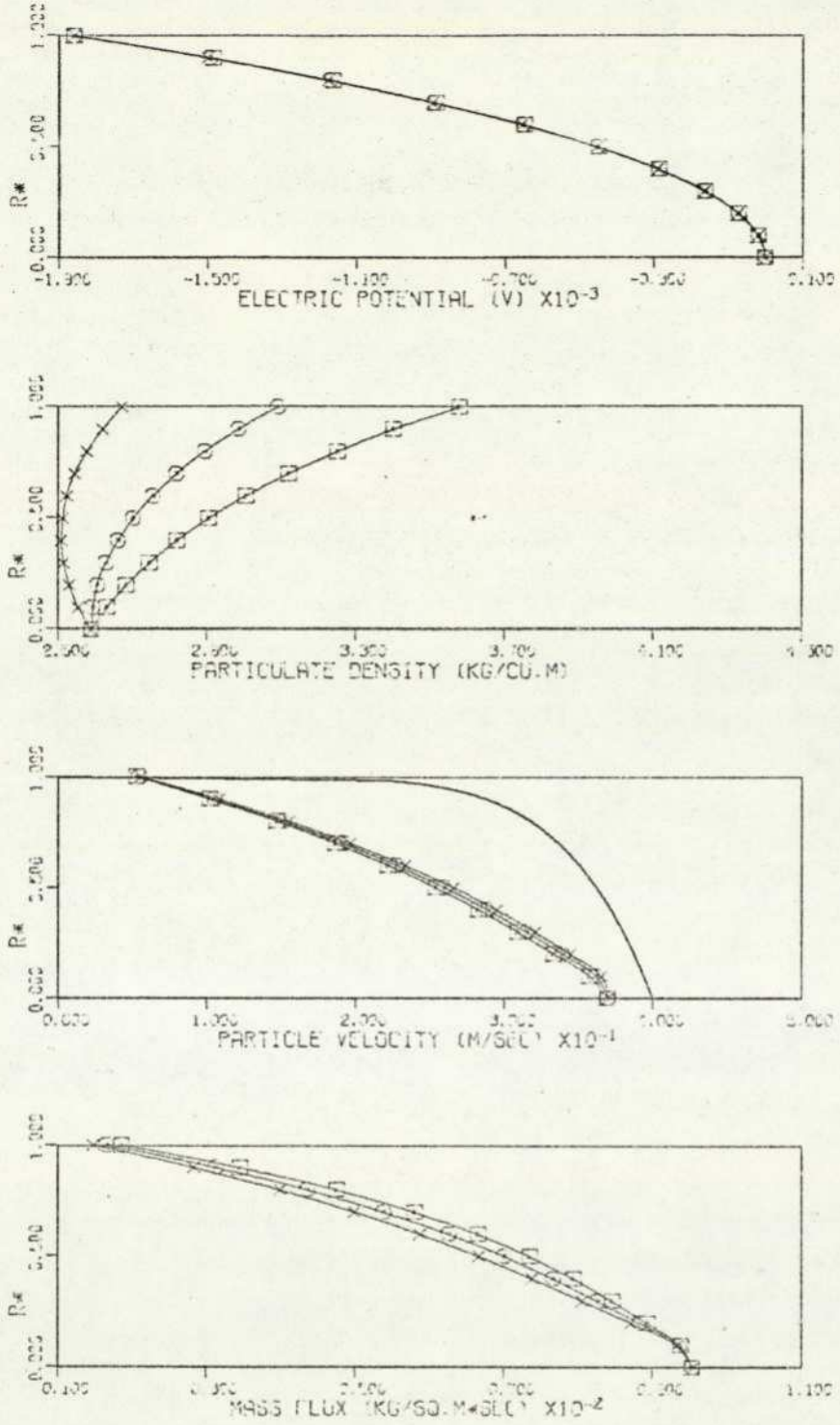

FIGURE 7.57 VARIOUS DISTRIBUTIONS IN A FULLY DEVELOPED TURBULENT GAS-SOLID SUSPENSION FLOW. PARTICLES TYPE #1.

PIPE FLOW PARAMETERS : R=0.156E-01 M, U0=0.400E 02 M/SEC, Q/M=0.100E-03 C/KG,
KNP=0.100E 00, DF=0.804E-02 SQ.M/SEC, MP=0.400E-01(EXPT), 0.400E-01 (COMP) KG/SEC
PIPE INCLINATION = 90.0°. ×=0.0°, ⊕=90.0°, ⊡=180.0°, —— AIR.

DATA COMPUTED BY #XFD3G, PLOTTED BY #PJ05 (TEST 09-21-0-15).

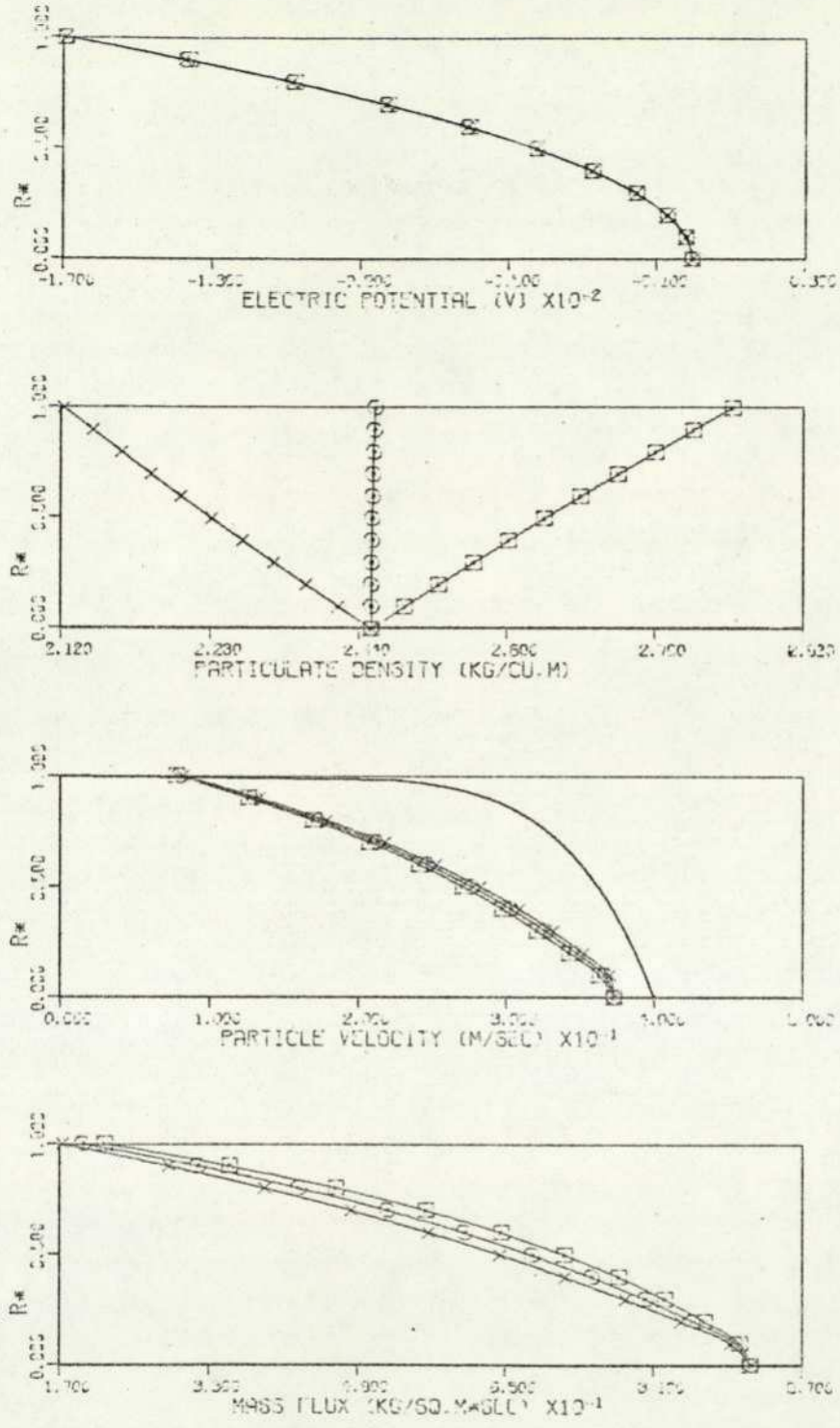

FIGURE 7.58 VARIOUS DISTRIBUTIONS IN A FULLY DEVELOPED TURBULENT GAS-SOLID SUSPENSION FLOW. PARTICLES TYPE #1.

PIPE FLOW PARAMETERS : R=0.106E-01 M, UO=0.400E 02 M/SEC, Q/M=0.100E-01 C/KG, KNP=0.150E 00, DF=0.624E-02 SQ.M/SEC, MP=0.400E-01(EXPT), 0.400E-01 (COMP) KG/SEC
PIPE INCLINATION = 90.0°. ×=0.0°, ⊙=90.0°, ⊡=180.0°, —— AIR.

DATA COMPUTED BY #XF03B, PLOTTED BY #PL05 (TEST 00-22-0-15).

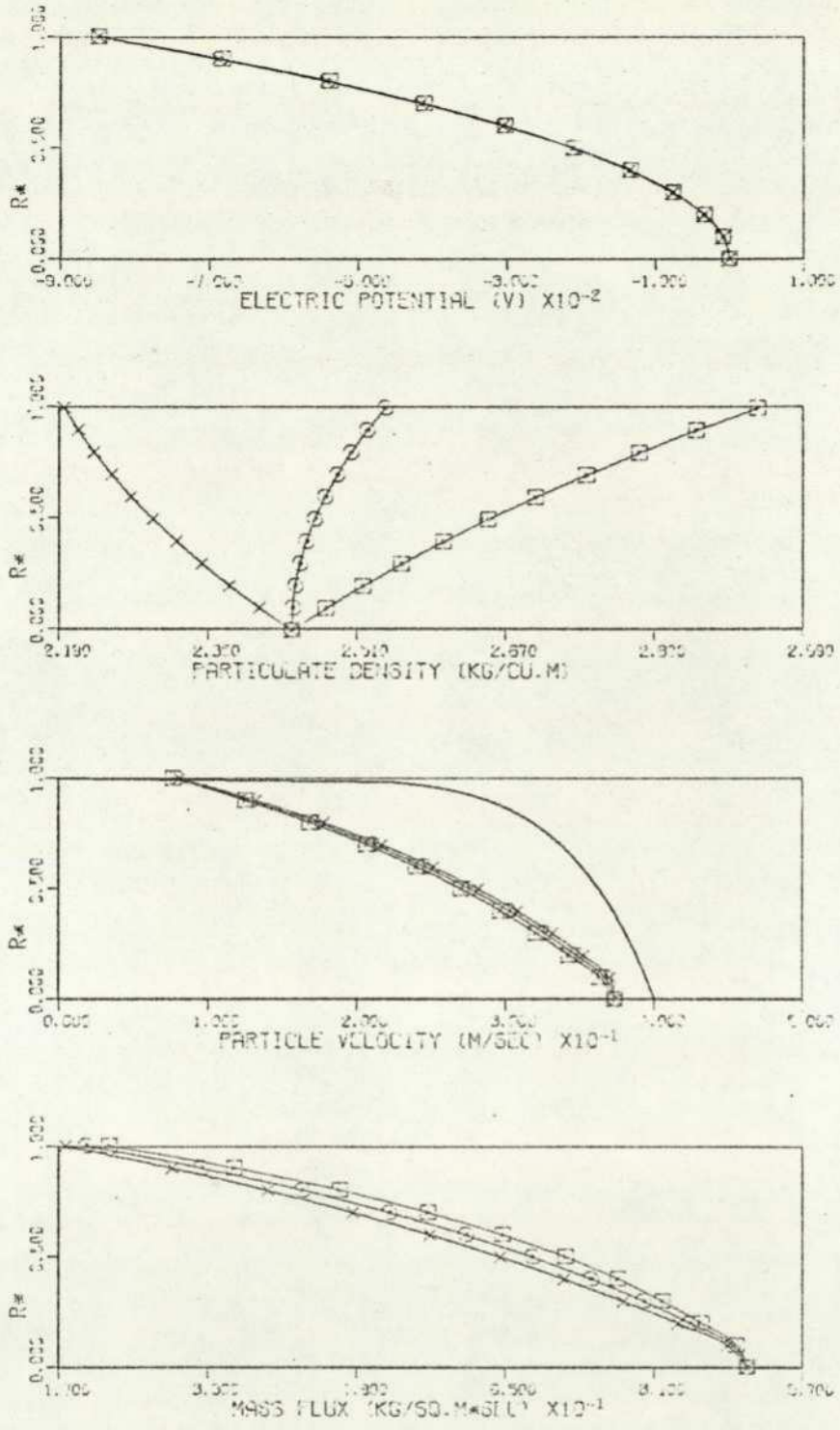

FIGURE . *7.59* VARIOUS DISTRIBUTIONS IN A FULLY DEVELOPED TURBULENT GAS-SOLID SUSPENSION FLOW. PARTICLES TYPE #1.

PIPE FLOW PARAMETERS . R=0.156E-01 M, UO=0.400E 02 M/SEC. Q/M=0.500E-01 Q/KG.
KNP=0.150E 00, DF=0.621E-02 SQ.M/SEC, MP=0.400E-01(EXPT), 0.402E-01 (COMP) KG/SEC
PIPE INCLINATION = 90.0°. ×=0.0°, ⊙=90.0°, ⊡=180.0 , ——— AIR.

DATA COMPUTED BY #XF038, PLOTTED BY #PJ05 (TEST 00-23-0-18).

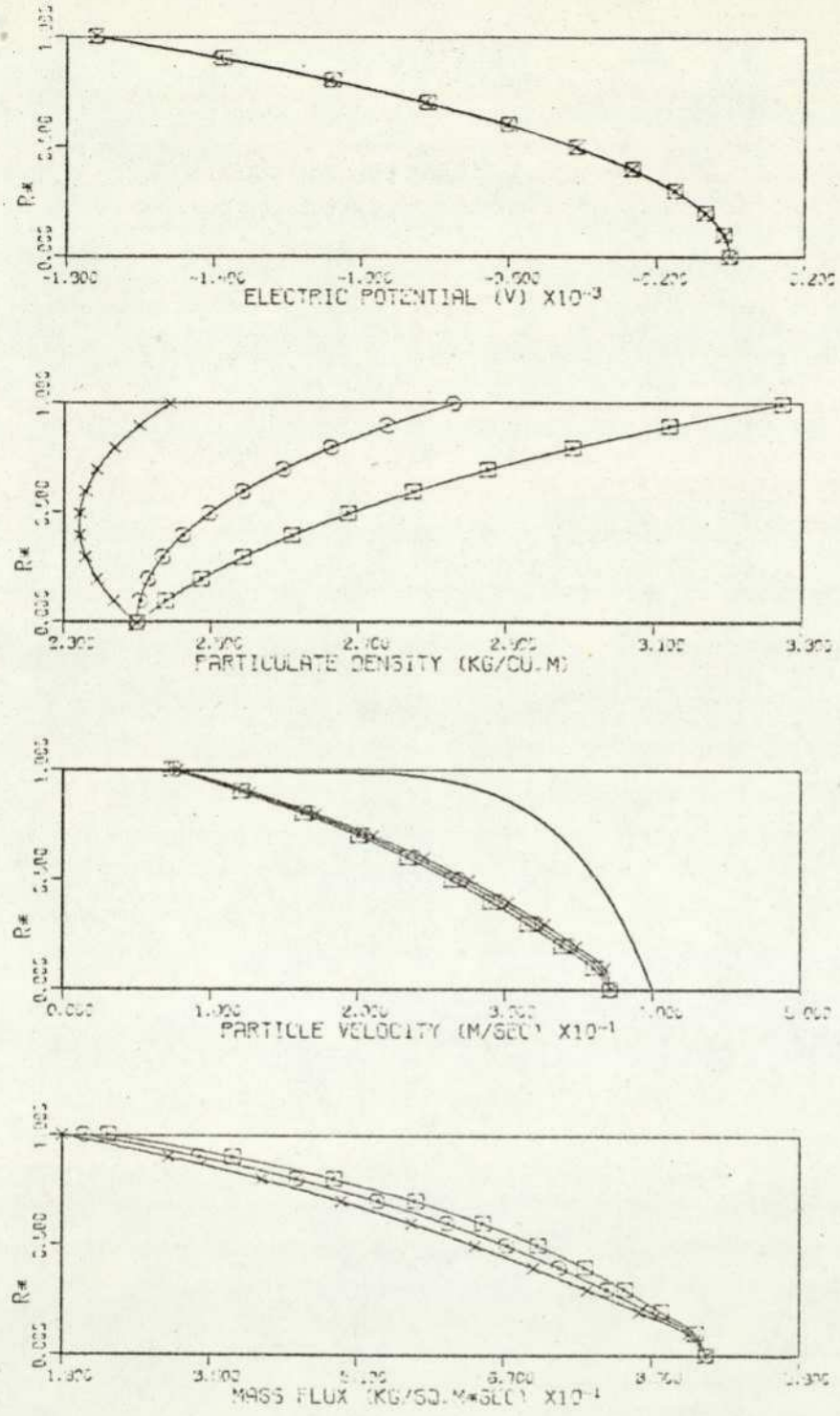

FIGURE . *7.60* VARIOUS DISTRIBUTIONS IN A FULLY DEVELOPED TURBULENT GAS-SOLID SUSPENSION FLOW. PARTICLES TYPE #1.

PIPE FLOW PARAMETERS : R=0.156E-01 M. UO=0.400E 02 M/SEC. Q/M=0.100E-03 C/KG.
KNP=0.150E 00. DF=0.624E-02 SQ.M/SEC. MP=0.400E-01(EXPT). 0.404E-01 (COMP) KG/SEC
PIPE INCLINATION = 90.0°. × =0.0°, ⊙ =90.0°, ⊡ =180.0°, —— RIP.

DATA COMPUTED BY #XF038, PLOTTED BY #PJ06 (TEST 00-21-0-18).

SUMMARY OF TEST CASES :

	DS	QM	KNP	MPX	U0	RP0	MP	RMP	G(M,N)	UP(1,N)			CA	CB	CC	CE	C1	Figure
									G(1,N)	UP(1,1)	UP(M,N)							
00-01-0-1A	0.35E-04	0.10E-04	.10	.02	20.	2.09	1.97	.020	0.75	1.35	.930	.220	.207	0.28E-02	5.7	0.0	0.59	1.59	7.1
00-02-0-1A	0.35E-04	0.50E-04	.10	.02	20.	2.06	2.02	.020	0.80	1.44	.930	.218	.205	0.69E-01	5.7	0.0	0.59	1.57	7.2
00-03-0-1A	0.35E-04	0.10E-03	.10	.02	20.	1.96	2.17	.021	0.98	1.78	.930	.210	.198	0.26E 00	5.7	0.0	0.59	1.50	7.3
00-04-0-1A	0.35E-04	0.10E-04	.15	.02	20.	2.00	2.05	.020	0.75	1.35	.931	.292	.278	0.27E-02	5.7	0.0	0.59	1.53	7.4
00-05-0-1A	0.35E-04	0.50E-04	.15	.02	20.	1.97	2.09	.020	0.79	1.44	.930	.289	.275	0.66E-01	5.7	0.0	0.59	1.51	7.5
00-06-0-1A	0.35E-04	0.10E-03	.15	.02	20.	1.89	2.24	.021	0.97	1.76	.930	.281	.267	0.25E 00	5.7	0.0	0.59	1.44	7.6
00-07-0-1A	0.35E-04	0.10E-04	.10	.04	20.	4.17	1.97	.040	0.75	1.35	.930	.220	.207	0.56E-02	5.7	0.0	0.59	1.59	7.7
00-08-0-1A	0.35E-04	0.50E-04	.10	.04	20.	4.05	2.07	.041	0.86	1.55	.930	.215	.203	0.13E 00	5.7	0.0	0.59	1.55	7.8
00-09-0-1A	0.35E-04	0.10E-03	.10	.04	20.	3.48	2.33	.040	1.26	2.27	.929	.200	.188	0.46E 00	5.7	0.0	0.59	1.33	7.9
00-10-0-1A	0.35E-04	0.10E-04	.15	.04	20.	4.01	2.05	.040	0.75	1.35	.931	.292	.278	0.53E-02	5.7	0.0	0.59	1.53	7.10
00-11-0-1A	0.35E-04	0.50E-04	.15	.04	20.	3.90	2.14	.041	0.85	1.54	.930	.286	.272	0.13E 00	5.7	0.0	0.59	1.49	7.11
00-12-0-1A	0.35E-04	0.10E-03	.15	.04	20.	3.52	2.46	.042	1.27	2.29	.930	.270	.255	0.47E 00	5.7	0.0	0.59	1.34	7.12
00-13-0-1A	0.35E-04	0.10E-04	.10	.02	40.	1.09	1.88	.020	0.86	1.16	.926	.196	.187	0.73E-03	2.9	0.0	0.30	1.67	7.13
00-14-0-1A	0.35E-04	0.50E-04	.10	.02	40.	1.09	1.89	.020	0.88	1.18	.926	.195	.186	0.18E-01	2.9	0.0	0.30	1.66	7.14
00-15-0-1A	0.35E-04	0.10E-03	.10	.02	40.	1.08	1.93	.020	0.93	1.25	.926	.192	.184	0.72E-01	2.9	0.0	0.30	1.65	7.15
00-16-0-1A	0.35E-04	0.10E-04	.15	.02	40.	1.03	1.99	.020	0.86	1.16	.929	.273	.263	0.69E-03	2.9	0.0	0.30	1.58	7.16
00-17-0-1A	0.35E-04	0.50E-04	.15	.02	40.	1.03	2.00	.020	0.88	1.18	.929	.272	.262	0.17E-01	2.9	0.0	0.30	1.58	7.17
00-18-0-1A	0.35E-04	0.10E-03	.15	.02	40.	1.02	2.04	.020	0.92	1.24	.929	.270	.260	0.68E-01	2.9	0.0	0.30	1.56	7.18
00-19-0-1A	0.35E-04	0.10E-04	.10	.04	40.	2.18	1.88	.040	0.86	1.16	.926	.196	.187	0.15E-02	2.9	0.0	0.30	1.67	7.19
00-20-0-1A	0.35E-04	0.50E-04	.10	.04	40.	2.17	1.90	.040	0.89	1.20	.926	.194	.185	0.36E-01	2.9	0.0	0.30	1.66	7.20
00-21-0-1A	0.35E-04	0.10E-03	.10	.04	40.	2.12	1.97	.041	1.00	1.34	.926	.190	.181	0.14E 00	2.9	0.0	0.30	1.62	7.21
00-22-0-1A	0.35E-04	0.10E-04	.15	.04	40.	2.07	1.99	.040	0.86	1.16	.929	.273	.263	0.14E-02	2.9	0.0	0.30	1.58	7.22
00-23-0-1A	0.35E-04	0.50E-04	.15	.04	40.	2.05	2.01	.040	0.89	1.20	.929	.271	.261	0.34E-01	2.9	0.0	0.30	1.57	7.23
00-24-0-1A	0.35E-04	0.10E-03	.15	.04	40.	2.00	2.08	.041	0.99	1.33	.929	.267	.257	0.13E 00	2.9	0.0	0.30	1.53	7.24
01-01-0-2A	0.75E-04	0.10E-04	.10	.02	20.	2.66	1.55	.020	0.26	3.97	.809	.123	.063	0.16E-01	1.2	0.0	2.72	2.03	7.25
01-02-0-2A	0.75E-04	0.50E-04	.10	.02	20.	2.45	1.67	.020	0.40	5.81	.815	.071	.053	0.37E 00	1.2	0.0	2.72	1.87	7.26
01-04-0-2A	0.75E-04	0.10E-04	.15	.02	20.	2.25	1.83	.020	0.26	3.96	.887	.231	.122	0.14E-01	1.2	0.0	2.72	1.72	7.27
01-05-0-2A	0.75E-04	0.50E-04	.15	.02	20.	2.44	1.75	.021	0.40	5.80	.816	.194	.063	0.37E 00	1.2	0.0	2.72	1.87	7.28
01-07-0-2A	0.75E-04	0.10E-04	.10	.04	20.	5.30	1.56	.040	0.26	4.03	.809	.122	.063	0.32E-01	1.2	0.0	2.72	2.03	7.29
01-10-0-2A	0.75E-04	0.10E-04	.15	.04	20.	4.49	1.83	.040	0.26	4.01	.883	.229	.120	0.27E-01	1.2	0.0	2.72	1.72	7.30
01-13-0-2A	0.75E-04	0.10E-04	.10	.02	40.	1.33	1.54	.020	0.51	1.98	.905	.092	.082	0.41E-02	0.6	0.0	1.36	2.04	7.31
01-14-0-2A	0.75E-04	0.50E-04	.10	.02	40.	1.32	1.58	.020	0.56	2.19	.905	.090	.080	0.10E 00	0.6	0.0	1.36	2.01	7.32
01-16-0-2A	0.75E-04	0.10E-04	.15	.02	40.	1.35	1.52	.020	0.51	1.98	.890	.106	.096	0.41E-02	0.6	0.0	1.36	2.07	7.33
01-17-0-2A	0.75E-04	0.50E-04	.15	.02	40.	1.33	1.57	.020	0.56	2.19	.893	.105	.095	0.10E 00	0.6	0.0	1.36	2.03	7.34
01-19-0-2A	0.75E-04	0.10E-04	.10	.04	40.	2.67	1.54	.040	0.51	1.99	.905	.092	.082	0.82E-02	0.6	0.0	1.36	2.04	7.35
01-20-0-2A	0.75E-04	0.50E-04	.10	.04	40.	2.60	1.62	.041	0.62	2.43	.900	.088	.079	0.20E 00	0.6	0.0	1.36	1.99	7.36
01-22-0-2A	0.75E-04	0.10E-04	.15	.04	40.	2.70	1.52	.040	0.51	1.99	.890	.106	.096	0.83E-02	0.6	0.0	1.36	2.07	
01-23-0-2A	0.75E-04	0.50E-04	.15	.04	40.	2.62	1.62	.041	0.63	2.43	.897	.103	.093	0.20E 00	0.6	0.0	1.36	2.00	
02-01-0-2A	0.75E-04	0.10E-04	.10	.02	20.	2.92	1.41	.020	1.02	1.02	.871	.068	.068	0.18E-01	1.2	0.1	0.00	2.23	
02-02-0-2A	0.75E-04	0.50E-04	.10	.02	20.	2.55	1.60	.020	1.54	1.54	.894	.065	.065	0.39E 00	1.2	0.1	0.00	1.95	

Table 7.1. Summary of analytical results for the flow characteristic equations (4.4.2) - (4.4.5)

	DS	QM	KNP	MPX	U0	RP0	MP	RMP	G(M,N) G(1,N)	UP(1,N) UP(1,1)	UP(M,N)		CA	CB	CC	CE	C1	Figure
00-01-0-18	0.35E-04	0.10E-04	.10	.02	20.	2.28	1.80	.020	0.72	1.40	.950	.184	.169	0.34E-02	11.4	0.0	0.67	1.75	7.37
00-02-0-18	0.35E-04	0.50E-04	.10	.02	20.	2.25	1.84	.020	0.78	1.52	.950	.181	.166	0.85E-01	11.4	0.0	0.67	1.72	7.38
00-03-0-18	0.35E-04	0.10E-03	.10	.02	20.	2.15	1.98	.021	1.02	1.99	.949	.171	.156	0.32E 00	11.4	0.0	0.67	1.65	7.39
00-04-0-18	0.35E-04	0.10E-04	.15	.02	20.	2.15	1.91	.020	0.72	1.40	.952	.252	.232	0.32E-02	11.4	0.0	0.67	1.64	7.40
00-05-0-18	0.35E-04	0.50E-04	.15	.02	20.	2.12	1.96	.020	0.78	1.51	.952	.248	.229	0.79E-01	11.4	0.0	0.67	1.62	7.41
00-06-0-18	0.35E-04	0.10E-03	.15	.02	20.	2.03	2.10	.021	1.00	1.94	.950	.235	.216	0.31E 00	11.4	0.0	0.67	1.55	7.42
00-07-0-18	0.35E-04	0.10E-04	.10	.04	20.	4.56	1.80	.040	0.72	1.41	.950	.184	.169	0.69E-02	11.4	0.0	0.67	1.74	7.43
00-08-0-18	0.35E-04	0.50E-04	.10	.04	20.	4.44	1.89	.041	0.85	1.66	.950	.178	.163	0.17E 00	11.4	0.0	0.67	1.70	7.44
00-09-0-18	0.35E-04	0.10E-03	.10	.04	20.	3.80	2.14	.039	1.40	2.73	.946	.159	.143	0.57E 00	11.4	0.0	0.67	1.45	7.45
00-10-0-18	0.35E-04	0.10E-04	.15	.04	20.	4.29	1.92	.040	0.72	1.41	.952	.252	.232	0.64E-02	11.4	0.0	0.67	1.64	7.46
00-11-0-18	0.35E-04	0.50E-04	.15	.04	20.	4.17	2.00	.040	0.84	1.64	.950	.243	.224	0.16E 00	11.4	0.0	0.67	1.59	7.47
00-12-0-18	0.35E-04	0.10E-03	.15	.04	20.	3.59	2.26	.040	1.34	2.62	.947	.220	.201	0.54E 00	11.4	0.0	0.67	1.37	7.48
00-13-0-18	0.35E-04	0.10E-04	.10	.02	40.	1.31	1.57	.020	0.86	1.16	.930	.147	.138	0.86E-03	6.5	0.0	0.29	2.00	7.49
00-14-0-18	0.35E-04	0.50E-04	.10	.02	40.	1.31	1.58	.020	0.88	1.18	.930	.146	.137	0.21E-01	6.5	0.0	0.29	2.00	7.50
00-15-0-18	0.35E-04	0.10E-03	.10	.02	40.	1.30	1.59	.020	0.94	1.26	.924	.143	.134	0.85E-01	6.5	0.0	0.29	1.98	7.51
00-16-0-18	0.35E-04	0.10E-04	.15	.02	40.	1.25	1.67	.020	0.86	1.16	.933	.205	.193	0.81E-03	6.5	0.0	0.29	1.88	7.52
00-17-0-18	0.35E-04	0.50E-04	.15	.02	40.	1.22	1.68	.020	0.88	1.18	.933	.204	.192	0.20E-01	6.5	0.0	0.29	1.87	7.53
00-18-0-18	0.35E-04	0.10E-03	.15	.02	40.	1.21	1.71	.020	0.94	1.26	.932	.201	.189	0.80E-01	6.5	0.0	0.29	1.86	7.54
00-19-0-18	0.35E-04	0.10E-04	.10	.04	40.	2.62	1.57	.040	0.87	1.16	.930	.147	.138	0.17E-02	6.5	0.0	0.29	2.00	7.55
00-20-0-18	0.35E-04	0.50E-04	.10	.04	40.	2.61	1.58	.040	0.90	1.21	.930	.145	.137	0.43E-01	6.5	0.0	0.29	1.99	7.56
00-21-0-18	0.35E-04	0.10E-03	.10	.04	40.	2.59	1.62	.041	1.03	1.38	.923	.139	.131	0.17E 00	6.5	0.0	0.29	1.98	7.57
00-22-0-18	0.35E-04	0.10E-04	.15	.04	40.	2.45	1.68	.040	0.87	1.16	.933	.205	.193	0.16E-02	6.5	0.0	0.29	1.88	7.58
00-23-0-18	0.35E-04	0.50E-04	.15	.04	40.	2.44	1.69	.040	0.90	1.21	.933	.203	.191	0.40E-01	6.5	0.0	0.29	1.87	7.59
00-24-0-18	0.35E-04	0.10E-03	.15	.04	40.	2.40	1.73	.040	1.02	1.36	.927	.195	.184	0.16E 00	6.5	0.0	0.29	1.83	7.60
02-01-0-28	0.75E-04	0.10E-04	.10	.02	20.	1.43	2.87	.020	1.00	1.00	.950	.569	.568	0.42E-02	1.4	0.0	0.00	1.09	
02-02-0-28	0.75E-04	0.50E-04	.10	.02	20.	1.31	3.01	.019	1.10	1.10	.950	.569	.568	0.97E-01	1.4	0.0	0.00	1.00	
01-01-0-28	0.75E-04	0.10E-04	.10	.02	20.	1.31	3.03	.019	0.52	1.94	.950	.569	.568	0.39E-02	1.4	0.0	1.32	1.00	
01-02-0-28	0.75E-04	0.50E-04	.10	.02	20.	1.31	3.17	.020	0.57	2.14	.950	.569	.568	0.97E-01	1.4	0.0	1.32	1.00	
01-04-0-28	0.75E-04	0.10E-04	.15	.02	20.	1.31	3.06	.019	0.52	1.94	.950	.656	.656	0.39E-02	1.4	0.0	1.32	1.00	
01-05-0-28	0.75E-04	0.50E-04	.15	.02	20.	1.31	3.20	.020	0.57	2.14	.950	.656	.656	0.97E-01	1.4	0.0	1.32	1.00	
01-07-0-28	0.75E-04	0.10E-04	.10	.04	20.	2.62	3.03	.039	0.52	1.95	.950	.569	.568	0.78E-02	1.4	0.0	1.32	1.00	
01-08-0-28	0.75E-04	0.50E-04	.10	.04	20.	2.46	3.31	.040	0.63	2.34	.950	.569	.568	0.18E 00	1.4	0.0	1.32	0.94	
01-10-0-28	0.75E-04	0.10E-04	.15	.04	20.	2.62	3.06	.039	0.52	1.95	.950	.656	.656	0.78E-02	1.4	0.0	1.32	1.00	
01-11-0-28	0.75E-04	0.50E-04	.15	.04	20.	2.44	3.35	.040	0.62	2.34	.950	.656	.656	0.18E 00	1.4	0.0	1.32	0.93	
01-13-0-28	0.75E-04	0.10E-04	.10	.02	40.	0.71	2.89	.020	0.77	1.30	.950	.569	.569	0.84E-03	0.9	0.0	0.52	1.09	
01-14-0-28	0.75E-04	0.50E-04	.10	.02	40.	0.70	2.92	.020	0.79	1.33	.950	.569	.569	0.21E-01	0.9	0.0	0.52	1.08	
01-16-0-28	0.75E-04	0.10E-04	.15	.02	40.	0.70	2.92	.020	0.77	1.30	.950	.657	.657	0.83E-03	0.9	0.0	0.52	1.08	
01-17-0-28	0.75E-04	0.50E-04	.15	.02	40.	0.70	2.95	.020	0.79	1.33	.950	.657	.657	0.21E-01	0.9	0.0	0.52	1.07	
01-19-0-28	0.75E-04	0.10E-04	.10	.04	40.	1.42	2.90	.040	0.77	1.30	.950	.569	.569	0.17E-02	0.9	0.0	0.52	1.09	
01-20-0-28	0.75E-04	0.50E-04	.10	.04	40.	1.39	2.95	.040	0.80	1.35	.950	.569	.569	0.41E-01	0.9	0.0	0.52	1.07	
01-22-0-28	0.75E-04	0.10E-04	.15	.04	40.	1.41	2.92	.040	0.77	1.30	.950	.657	.657	0.17E-02	0.9	0.0	0.52	1.08	
01-23-0-28	0.75E-04	0.50E-04	.15	.04	40.	1.38	2.98	.040	0.80	1.35	.950	.657	.657	0.41E-01	0.9	0.0	0.52	1.06	

Table 7.2. Summary of analytical results for the simplified characteristic equations (4.5.2) - (4.5.4).

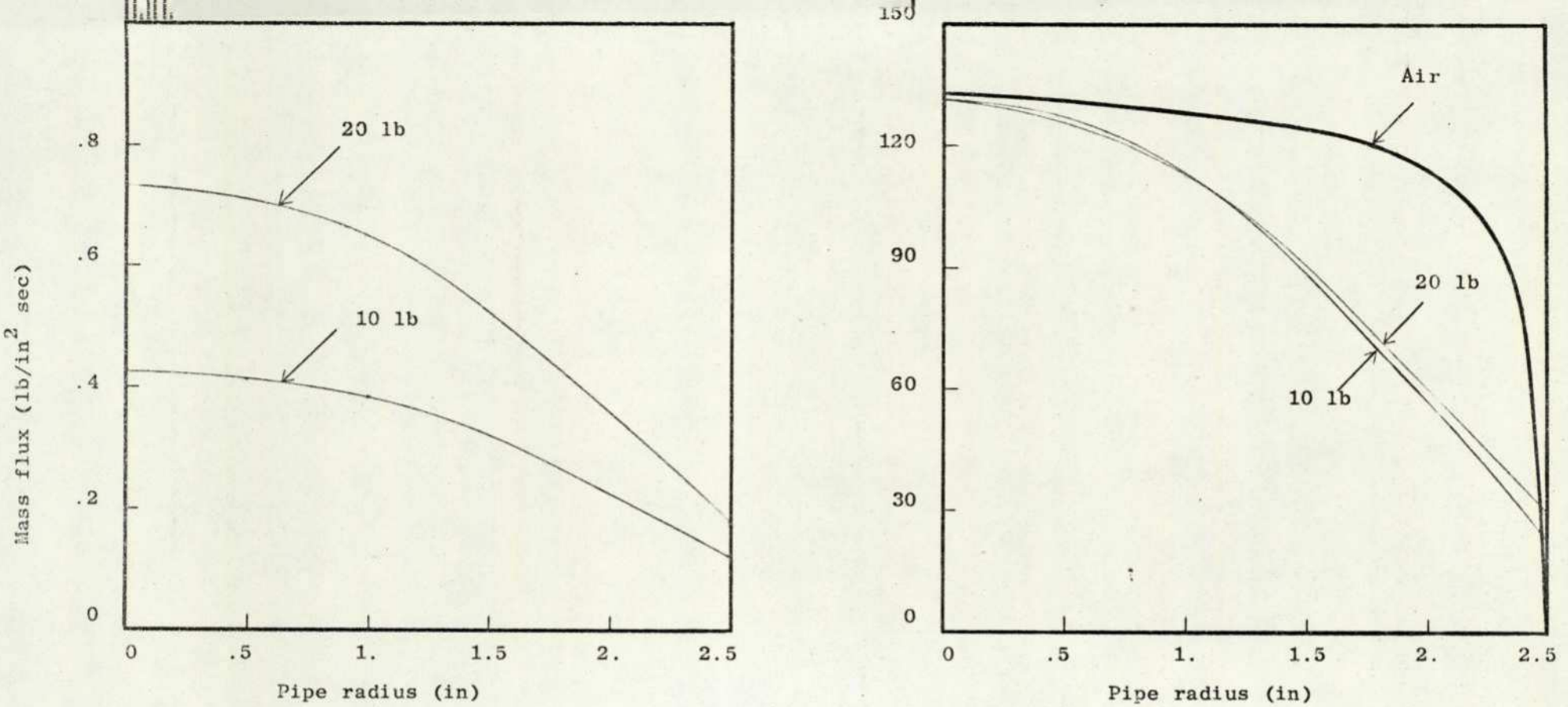

Fig. 7.61. Mass flux and velocity distributions of 50 μ glass beads suspended in air. (Measurement by Soo et al (6)).

CHAPTER 8

DISCUSSION OF EXPERIMENTAL RESULTS

A series of test runs with air and solid flow rates in the range of .016 - .045 kg/sec has been carried out in both air and ionized air. For each test run, at least 6 sampling signals of mass flow rates, pressure drops and charge current were recorded and mean values were computed by means of time averaging, standard deviations of the signals being given in Table 8.1. The large deviations of the solid flow rate signals were mainly due to pulsations occurred at low feeding rates and did not appear to correlate with the deviations of other signals. Typical traces of mass flow rates and charge current signals are shown in Fig. 8.1.

8.1 Analysis of Pressure Drop Data

Following the procedure of dimensional analysis used by Duckworth and Rose (11), it would seem appropriate to correlate the pressure drop data in terms of the pertinent variables and since we are only concerned with the fully developed flow region, the pressure gradient $(\partial P/\partial x)_m$ and friction factors C_{fm} and C_{fp} are therefore related by equations (5.1 - 5.4). Further, it has been shown by Duckworth and Rose that for a given size of particles, the following functional relationships exist

$$C_{fm} = f_1 (Re, Fr, M_p/M_f) \qquad (8.1.1)$$

and

$$C_{fp} = f_2 (Re, Fr, M_p/M_f) \qquad (8.1.2)$$

where Re ($= 2R\rho\bar{u}/\bar{\mu}$) is the pipe flow Reynolds number, Fr ($= \bar{u}^2/2Rg$) is the Fronde number and (M_p/M_f) is the mass flow ratio.

In order to demonstrate the above relationships, parametric curves relating $(\partial P/\partial x)_m$, C_{fm} and C_{fp} to Re, Fr and M_p/M_f were plotted

Particle / Standard Deviation	Type #1	Type #2	Type # 3	Type # 4
Ball probe current	.004-.012	.004-.012	.005-.016	.025-.050
Solid flow rate	.070-.330	.040-.160	.020-.016	.020-.120
Air flow rate	.001-.004	.001-.004	.001-.004	.001-.004
Pressure drop	.002-.006	.002-.006	.002-.006	.002-.006

Table 8.1. Typical standard deviations of data signals.

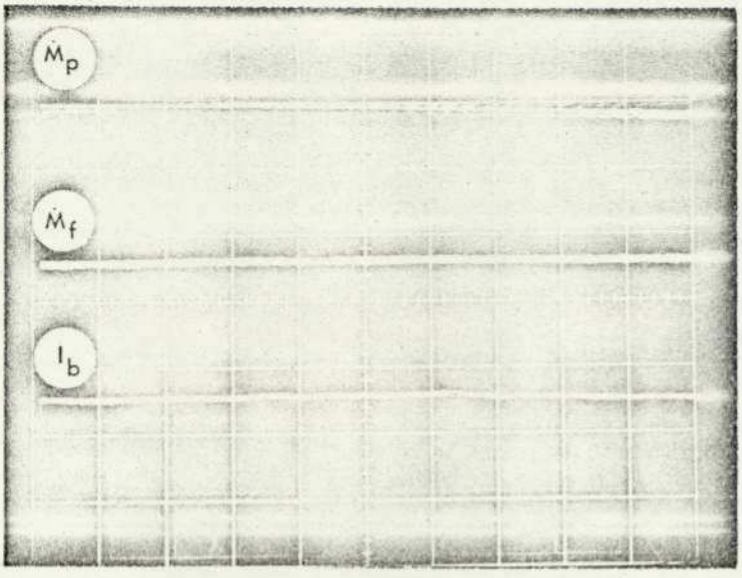

Fig. 8.1 (a).

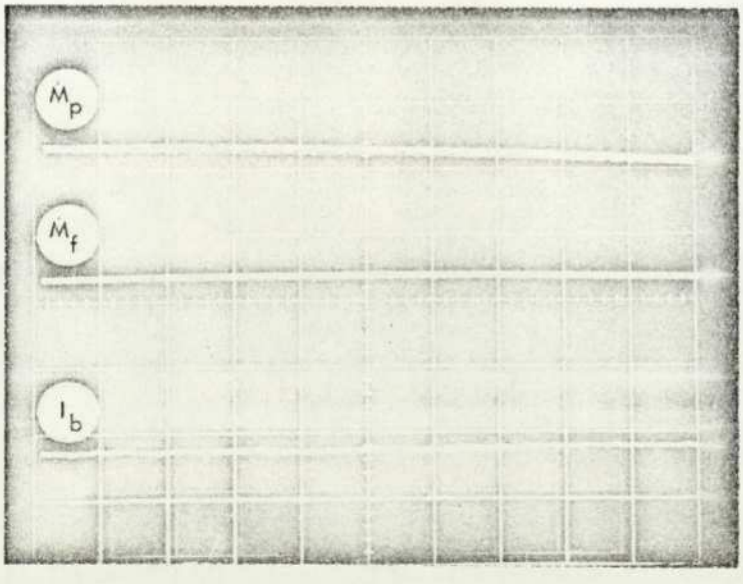

Fig. 8.1 (b).

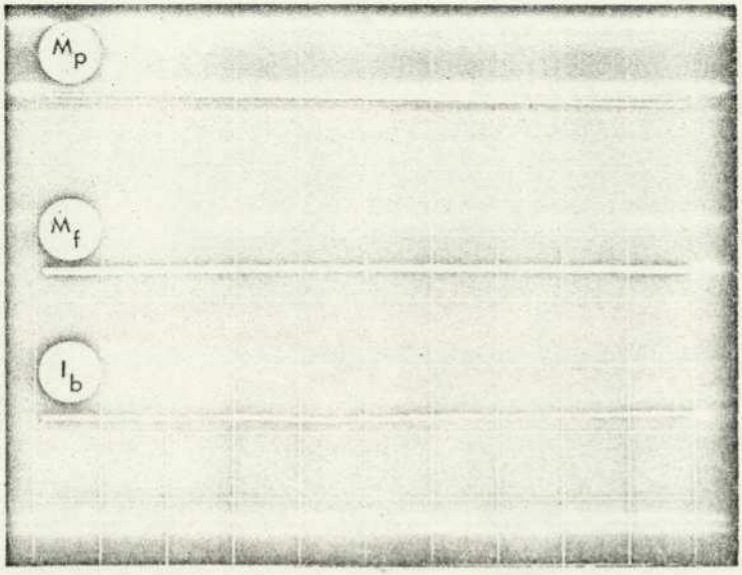

Fig. 8.1 (c).

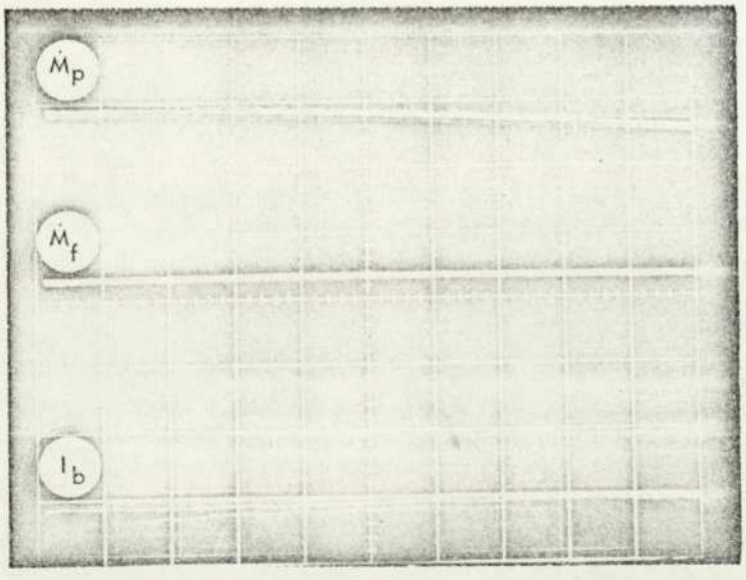

Fig. 8.1 (d).

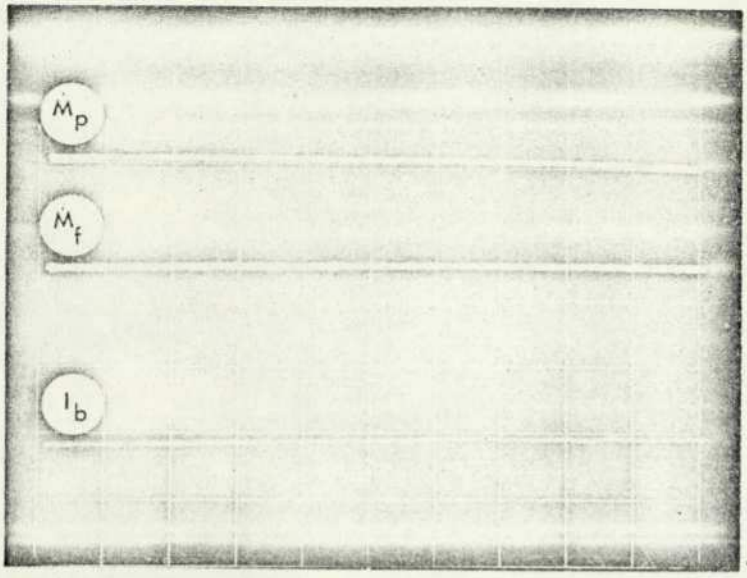

Fig. 8.1 (e).

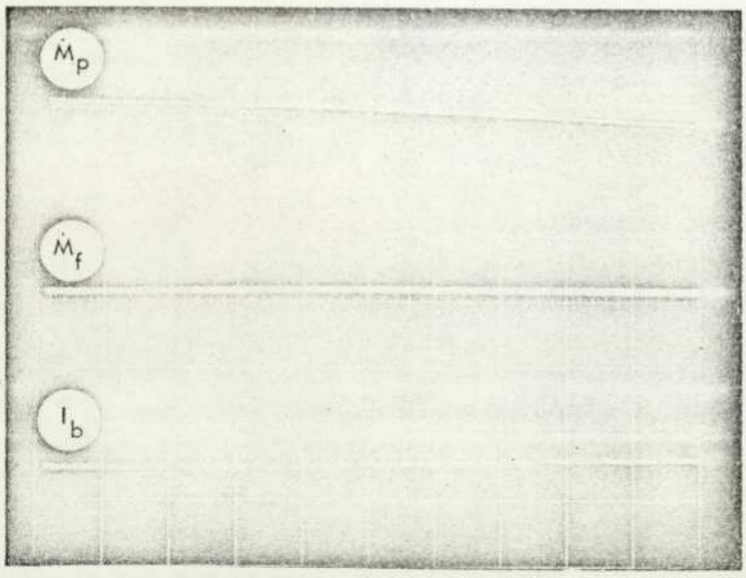

Fig. 8.1 (f).

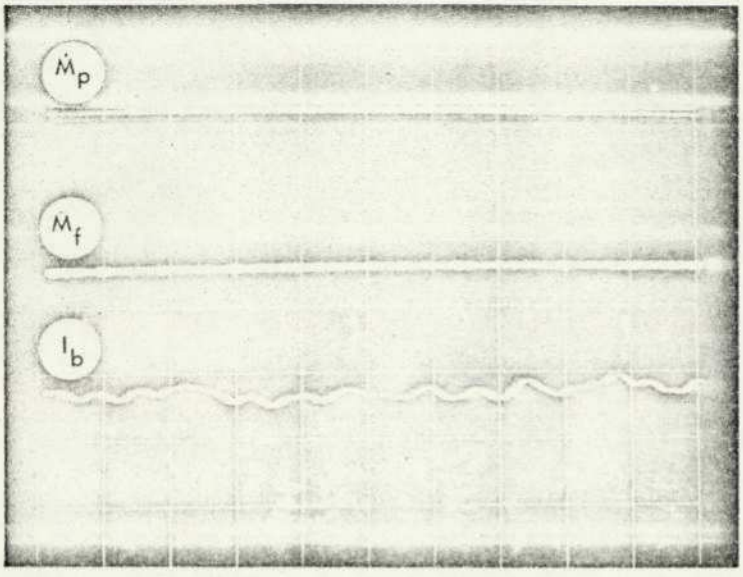

Fig. 8.1 (g).

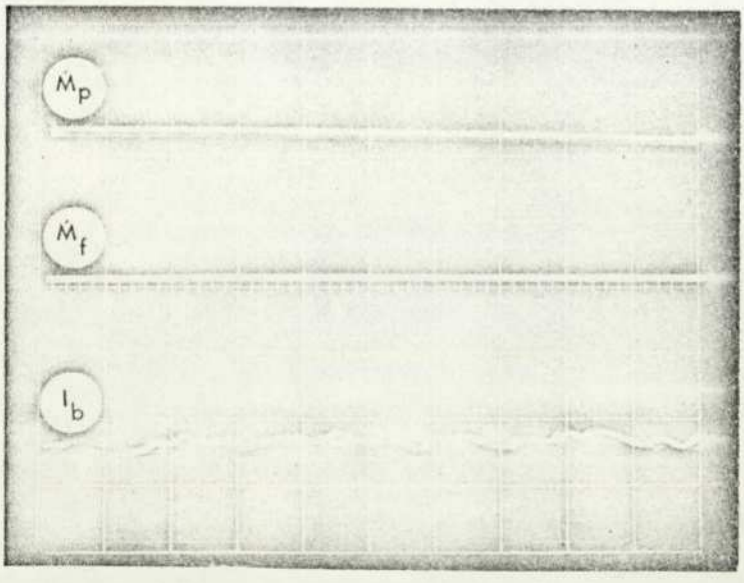

Fig. 8.1 (h).

Fig. No.	Particles	M_f (kg/sec)	M_p (kg/sec)	$-I_b$ (μA)
8.1 (a)	Type #1	.0344	.0175	.0390
" (b)	"	.0181	.0324	.0190
" (c)	Type #2	.0300	.0191	.0240
" (d)	"	.0179	.0346	.0110
" (e)	Type # 3	.0326	.0186	.0200
" (f)	"	.0182	.0462	.0150
" (g)	Type # 4	.0352	.0155	.0028
" (h)	"	.0180	.0157	.0023

Fig. 8.1. Typical traces of mass flow rates and ball probe current. (Time scale = .5 sec/cm)

for each type of particles. As shown in Figs. 8.2 - 8.5, $(\partial P/\partial x)_m$ increases almost linearly with Re along each of the constant M_p curves and the spacings between the curves appear to be dependent on the relative difference in M_p. The curves numbered with an asterisk denote test runs in ionized air. Although the results of the type #1 particles show considerable scatter, the trend is still evident. Under dynamically similar conditions, the pressure drops measured in 'ionized air' were generally higher than those measured in 'unionized air', which corresponds to higher charge current being measured in the latter case.

The curves showing the functional relationships between C_{fm} vs. Re and C_{fp} vs. Re for various M_p have the same trend as that of a single phase Newtonian fluid. (Figs. 8.6 - 8.9 and 8.10 - 8.13) Both C_{fm} and C_{fp} approach to some sensibly constant values at high Re and again, the spacings between the curves seem to be dependent on the relative difference in M_p.

The effects of Fr on $(\partial P/\partial x)_m$, C_{fm} and C_{fp} are shown in Figs. 8.14 - 8.25, and upon comparison with the Re parametric curves (Figs. 8.2-8.13), the seemingly similar behaviour of the Fr parametric curves suggests that equations (8.1.1) and (8.1.2) can be reduced to

$$C_{fm} = f_3 (Re, M_p/M_f) = f_4 (Fr, M_p/M_f) \qquad (8.1.3)$$

and

$$C_{fp} = f_5 (Re, M_p/M_f) = f_6 (Fr, M_p/M_f) \qquad (8.1.4)$$

Further, plotting $(\partial P/\partial x)_m$, C_{fm} and C_{fp} vs. (M_p/M_f) for various Re as shown in Figs. 8.26 - 8.37, we see that C_{fm} and C_{fp} increase linearly with (M_p/M_f) and are almost independent of Re. Thus, if the effect of electrostatic charging can be completely neglected and the presence of particles would always lead to higher pressure drop, C_{fm} and C_{fp} can be expressed as a single function of (M_p/M_f),

$$C_{fm} = C_f + f (M_p/M_f) \qquad (8.1.5)$$

and

$$C_{fp} = f (M_p/M_f) \qquad (8.1.6)$$

To a good approximation, the present results show that

$$f\ (M_p/M_f) = k\left(\frac{M_p}{M_f}\right) \qquad (8.1.7)$$

where k = .016 for type #1 particles
= .035 for types #2 and #3 particles
= .038 for type# 4 particles;

within the ranges of $.7 \leqslant (M_p/M_f) \leqslant 2.7$ and $.4 \times 10^5 \leqslant Re \leqslant .6 \times 10^5$.

In general, the present pressure drop results are in good agreement with those obtained by Duckworth and Kakka (12) and for similar ranges of mass flow rates, they gave

$$C_{fm} = C_f + C_1\left(\frac{a}{R}\right)^{C_2}\left(\frac{M_p}{M_f}\right) \qquad (8.1.8)$$

where C_1 and C_2 are correlation constant.

Similarly, McCarthy and Olson (3) obtained for high speed gas-solid suspension flow ($.2 \times 10^6 \leqslant Re \leqslant .5 \times 10^6$)

$$\frac{C_{fm}}{C_f} = 1 + .8\left(\frac{M_p}{M_f}\right) + .5\left(\frac{M_p}{M_f}\right)^2 \qquad (8.1.9)$$

8.2 Analysis of Charge Current Data

Earlier results of charge measurement using the deflection method as described in Section 6.7.1 are not presented here and only the charge current results obtained with the electrostatic ball probe will be analysed. Charge current was measured with the ball probe fixed at the pipe axis and in all readings taken, the charge current was negative. Background current was checked in both air and ionized air and such current if existed was not measurable. Both air humidity (36 - 46%) and air ionization were found to have only negligible effect on the ball probe current.

As shown in Figs. 8.38 - 8.41, the charge current I_b increases with both M_p and Re but does so more rapidly with the latter, and this

is further seen by plotting the dimensionless current I_n vs. (M_p/M_f) (Figs. 8.42 - 8.45). Upon comparison of the magnitudes of I_b for the 4 types of particle, it is seen that over the same ranges of M_p and Re, I_b is much greater for the small particles (e.g. I_b for the type# 1 particles is about 8 times that for the type# 4 particles). However, I_b appears to be dependent on the initial state of the physical conditions of the particles, being much higher in the first runs than those measured during the subsequent runs for the same M_p and Re. Similar phenomenon was also observed by Cole et al (25) during their investigation of electrostatic charging effects in high speed gas-solid suspension flow. There are two apparent reasons.

Recalling the charge current equation (6.7.2.3), the potential difference $(V_1 - V_2)$ which accounts for the charge transfer produced for collision with the ball probe is independent of M_p and Re (Subscripts 1 and 2 denote the particles and the ball probe respectively). By definition, $(V_1 - V_2)$ is made up of two parts, $V_c (= \phi_1 - \phi_2)$ and $(q_1/4\pi\varepsilon a_1)$ for an earthed probe (Section 2.1). Although V_c cannot be determined from the present data, usually being of the order of 1V, it is expected to be negative because the work function of steel ϕ_2 is greater than that for glass ϕ_1. According to the charge measurement carried out by Soo et al (6) q_1 is positive for glass particles being transported in metal pipe. For -ve charge current, the magnitude of V_c(-ve) must be always greater than $(q_1/4\pi\varepsilon a_1)$, and if the particles are initially uncharged (i.e. $q_1 \sim o$), the effective potential difference $(V_1 - V_2)$ at the impact is therefore entirely due to V_c. Upon collision with the pipe wall and other boundaries, the particles become positively charged (i.e. $q > 0$) and the potential difference at the impact is reduced from V_c to $(V_c + q_1/4\pi\varepsilon a_1)$, resulting in lower charge transfer and hence lower current. Alternatively, both the contact potential difference V_c and conductivity σ, are highly influenced by absorbed surface layers of moisture and even a slight change in surface conditions of the particles can cause large variations in V_c and σ_1, thus altering the rate of charge transfer.

If the characteristic charge transfer length ℓ_1 is comparable with a_1, as suggested by Cheng and Soo (24), the charge transfer coefficient h_{12} is therefore given by equation (6.7.2.2) as (σ_1/a_1) for $\sigma_2\ell_1 >> \sigma_1\ell_2$. For 35μ glass particles ($\bar{\rho}_1$ = 2400 kg/m^3; $E_1 = .6 \times 10^{11}$ N/m^2; $\nu_1 = .25$; $\varepsilon_1 = .6 \times 10^{-10}$ farads; $\sigma_1 = .2 \times 10^{-6}$ mho/m; u_1 = 25 m/s; ρ_1 = 1.5 kg/m^3; $q_1/m_1 = 10^{-6}$ c/kg), a 6250μ steel ball probe ($E_2 = 2 \times 10^{12}$ N/m^2; $\nu_2 = .3$), V_c = -1V and $\eta_{12} = 1$, equation (6.7.2.3) predicts a charge current of about $.4 \times 10^{-12}$A which is much smaller than the average experimental value ($.2 \times 10^{-7}$A). This suggests that modification of h_{12} or ℓ_1 is required.

Defining ℓ_1 as a critical distance of separation beyond which no charge transfer can take place, Cole et al (25) suggested that ℓ_1/a_1 is of the order of 10^{-5} and that the contact area at the impact is given by $2\pi a_1\ell_1.Z_c$, where Z_c is a modification factor, taking into account the surface roughness of the particles (23). Based on the modified ℓ_1 which effectively increases the rate of charge transfer by 10^5 times, the charge current becomes $.4 \times 10^{-7}$A and is in good agreement with experimental results.

Correlation between pressure drop and charge current data was made by plotting $(\partial P/\partial x)_m$, C_{fm} and C_{fp} vs. (Q/m) as shown in Figs. 8.46 - 8.57. It can be seen that for constant M_p and Re, the pressure drop and friction factors are generally higher at low (Q/m). Although earlier charge measurement using the deflection method (Section 6.7.1) has suggested that (q/m) is less than 10^{-5} c/kg, in the absence of simultaneous measurements of V_c and q, any explanation for such phenomenon must be largely speculative. For small glass particles of 50 - 250μ diameter range, being transported in a brass duct, maximum (q/m) of about 3×10^{-6} c/kg was measured by Soo et al (6). If their results can be used as a general guide to the order of magnitude of electrostatic charges acquired by the particles in the present work, it is readily seen from the analytical results (Chapter 7) that for (q/m) < 10^{-5} c/kg, the flow characteristics and the overall pressure drop are not affected by the charges on the particles. The difference in (Q/m) measured under dynamically similar conditions might have been caused by changes in surface conditions of the particles which

would not only affect V_c and σ_1, but also the physical friction between the particles and the pipe wall, thus showing up a difference in pressure drops.

PRESSURE DROP DATA CORRELATION CURVES

(FIGURES 8.2 - 8.37)

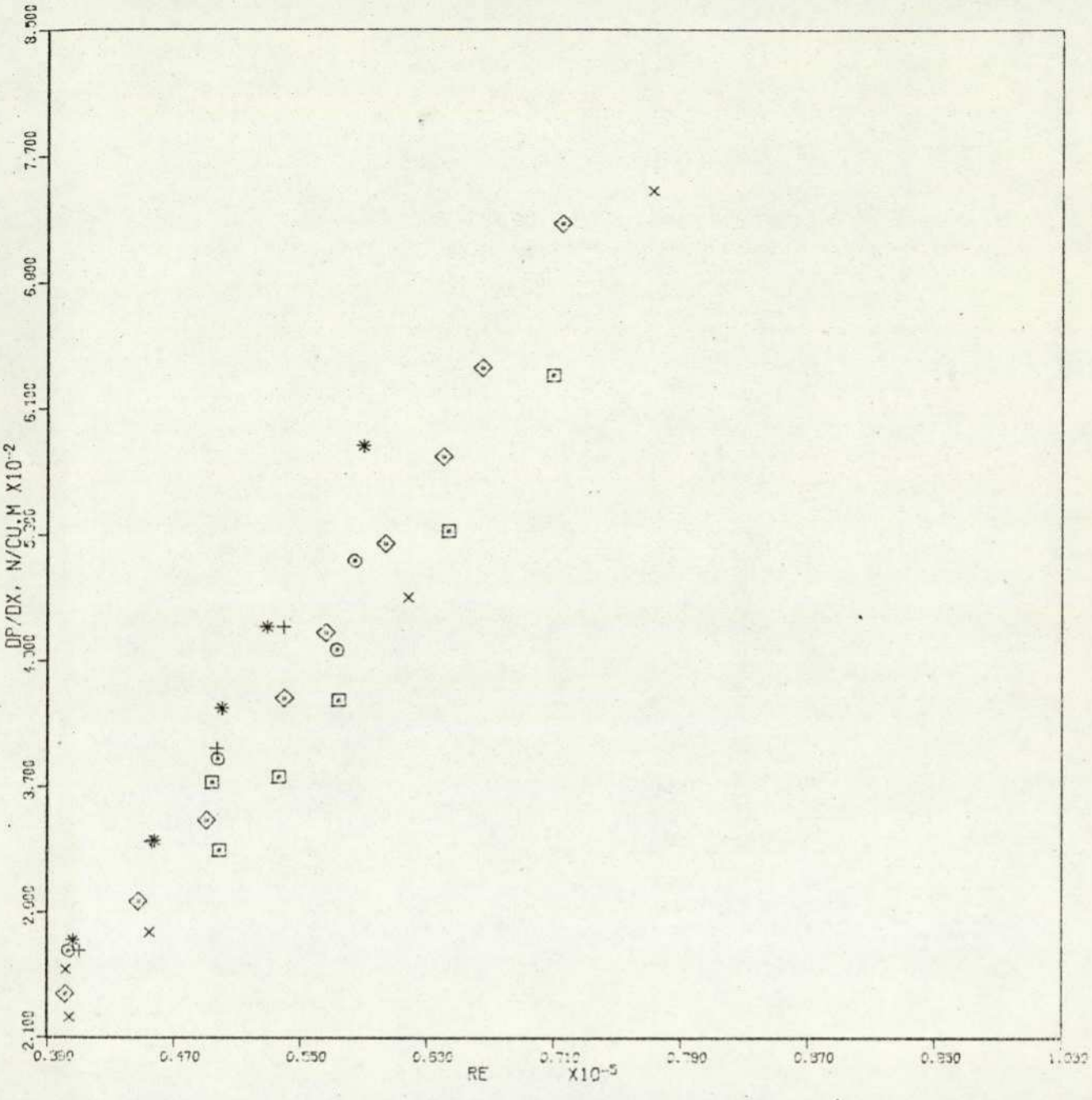

FIGURE : 8.2 PRESSURE GRADIENT, (DP/DX) VS. REYNOLDS NUMBER, RE.
GLASS BEADS TYPE #1.

CONSTANT PARAMETER(S) : MP, KG/SEC

CURVE 01	× .	0.172E-01
CURVE 02*	⊙	0.172E-01
CURVE 03	⊡	0.181E-01
CURVE 04	◇	0.229E-01
CURVE 05	+	0.292E-01
CURVE 06	*	0.332E-01

DATA COMPUTED BY #PDP2, O/P BY #PJ03, PLOTTED BY #PJ04 (01-07-09-14-02-00) .

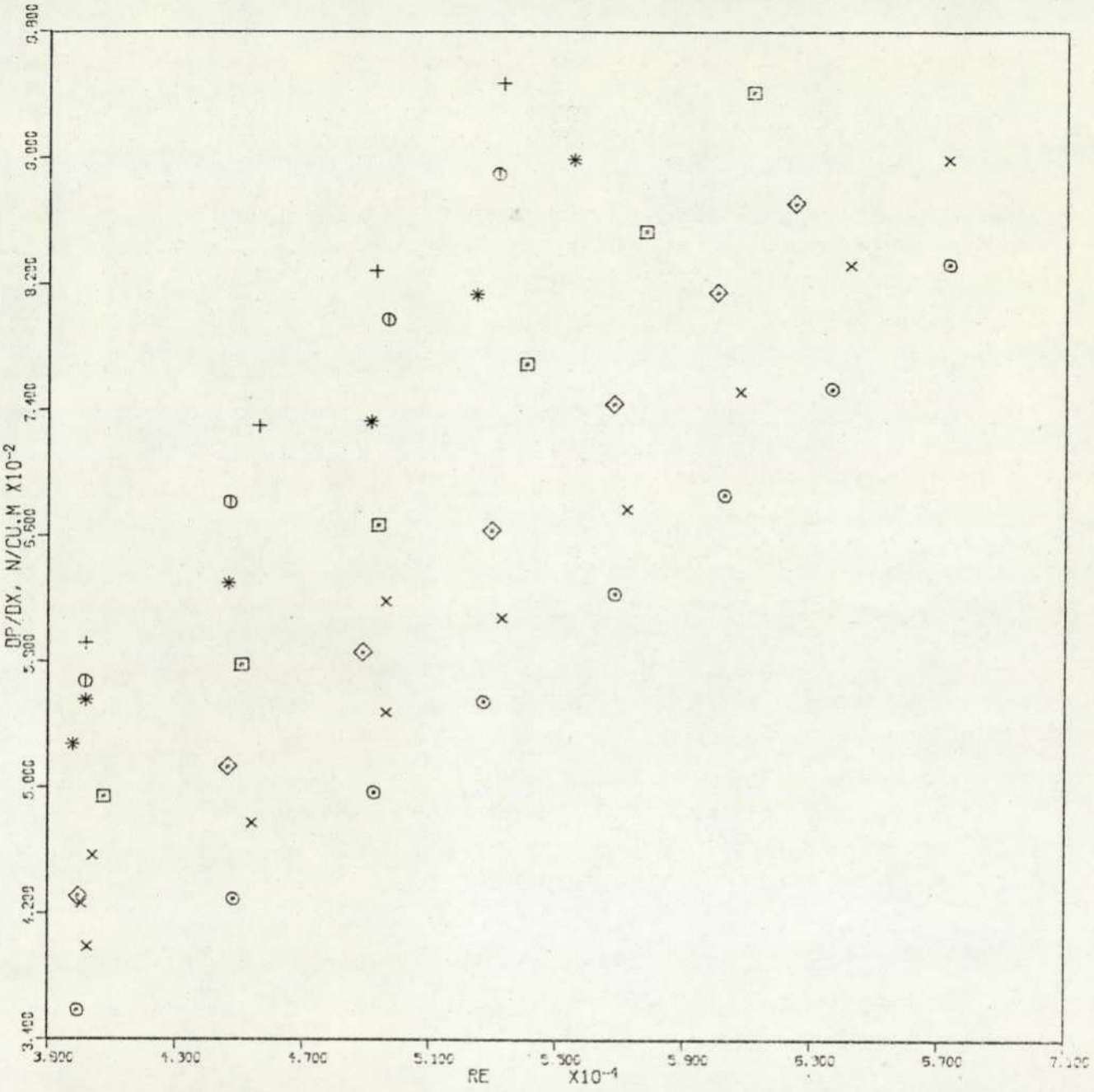

FIGURE : 8.3 PRESSURE GRADIENT, (DP/DX) VS. REYNOLDS NUMBER, RE.
GLASS BEADS TYPE #2.

CONSTANT PARAMETER(S) : MP, KG/SEC

CURVE 01	×	0.190E-01
CURVE 02*	⊙	0.190E-01
CURVE 03	⊡	0.246E-01
CURVE 04*	◇	0.245E-01
CURVE 05	+	0.343E-01
CURVE 06*	✳	0.344E-01
CURVE 07*	⊕	0.365E-01

DATA COMPUTED BY #PDP2, O/P BY #PJ03. PLOTTED BY #PJ04 (02-07-09-14-02-00) .

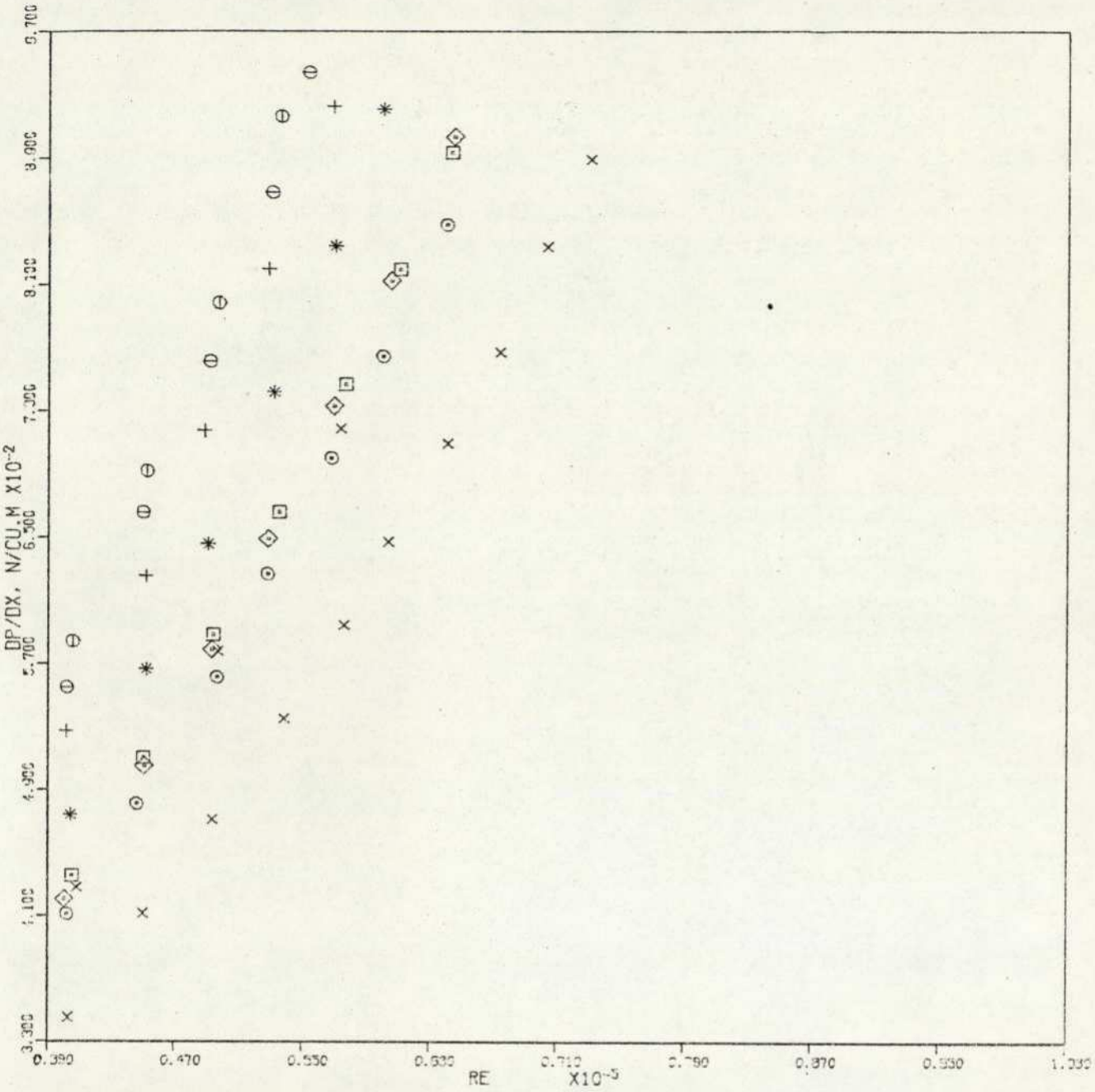

FIGURE :8.4 PRESSURE GRADIENT, (DP/DX) VS. REYNOLDS NUMBER, RE.
GLASS BEADS TYPE #3.

CONSTANT PARAMETER(S) : MP, KG/SEC

CURVE 01	×	0.188E-01
CURVE 02*	⊙	0.187E-01
CURVE 03	⊡	0.243E-01
CURVE 04*	◇	0.245E-01
CURVE 05	+	0.343E-01
CURVE 06*	*	0.344E-01
CURVE 07	⊖	0.364E-01
CURVE 08*	⊖	0.365E-01

DATA COMPUTED BY #PDP2, O/P BY #PJ03, PLOTTED BY #PJ04 (03-07-09-14-02-00) .

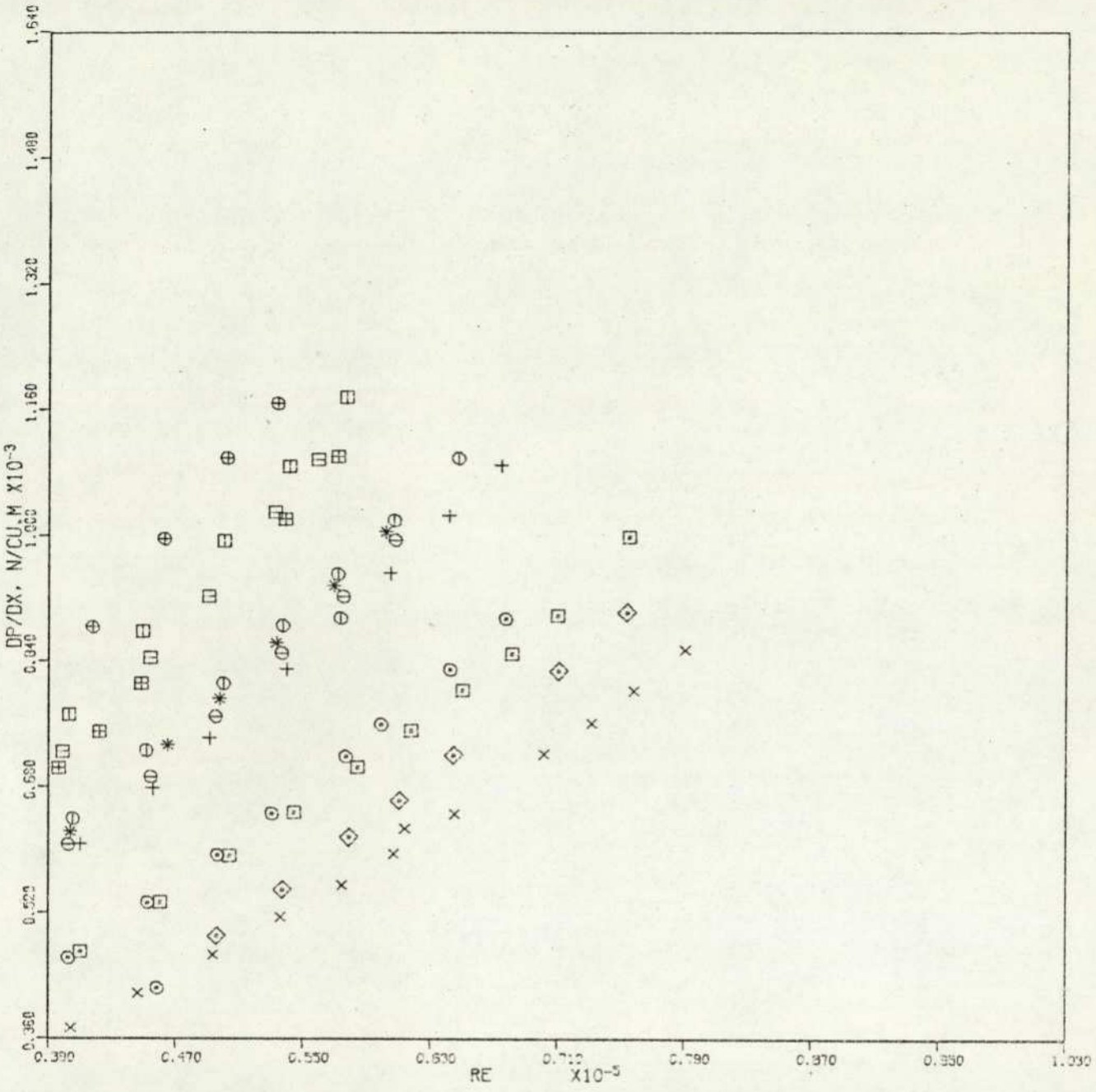

FIGURE :8.5 PRESSURE GRADIENT, (DP/DX) VS. REYNOLDS NUMBER, RE.
GLASS BEADS TYPE #4.

CONSTANT PARAMETER(S) : MP, KG/SEC

CURVE 01	×	0.156E-01
CURVE 02*	⊙	0.196E-01
CURVE 03	⊡	0.204E-01
CURVE 04*	◇	0.204E-01
CURVE 05	+	0.294E-01
CURVE 06*	*	0.290E-01
CURVE 07	⊕	0.312E-01
CURVE 08*	⊖	0.324E-01
CURVE 09	⊞	0.405E-01
CURVE 10*	⊟	0.401E-01
CURVE 11	⊖	0.454E-01
CURVE 12*	⊞	0.453E-01

DATA COMPUTED BY #PDP2. O/P BY #PJ03. PLOTTED BY #PJ04 (04-07-09-14-02-00) .

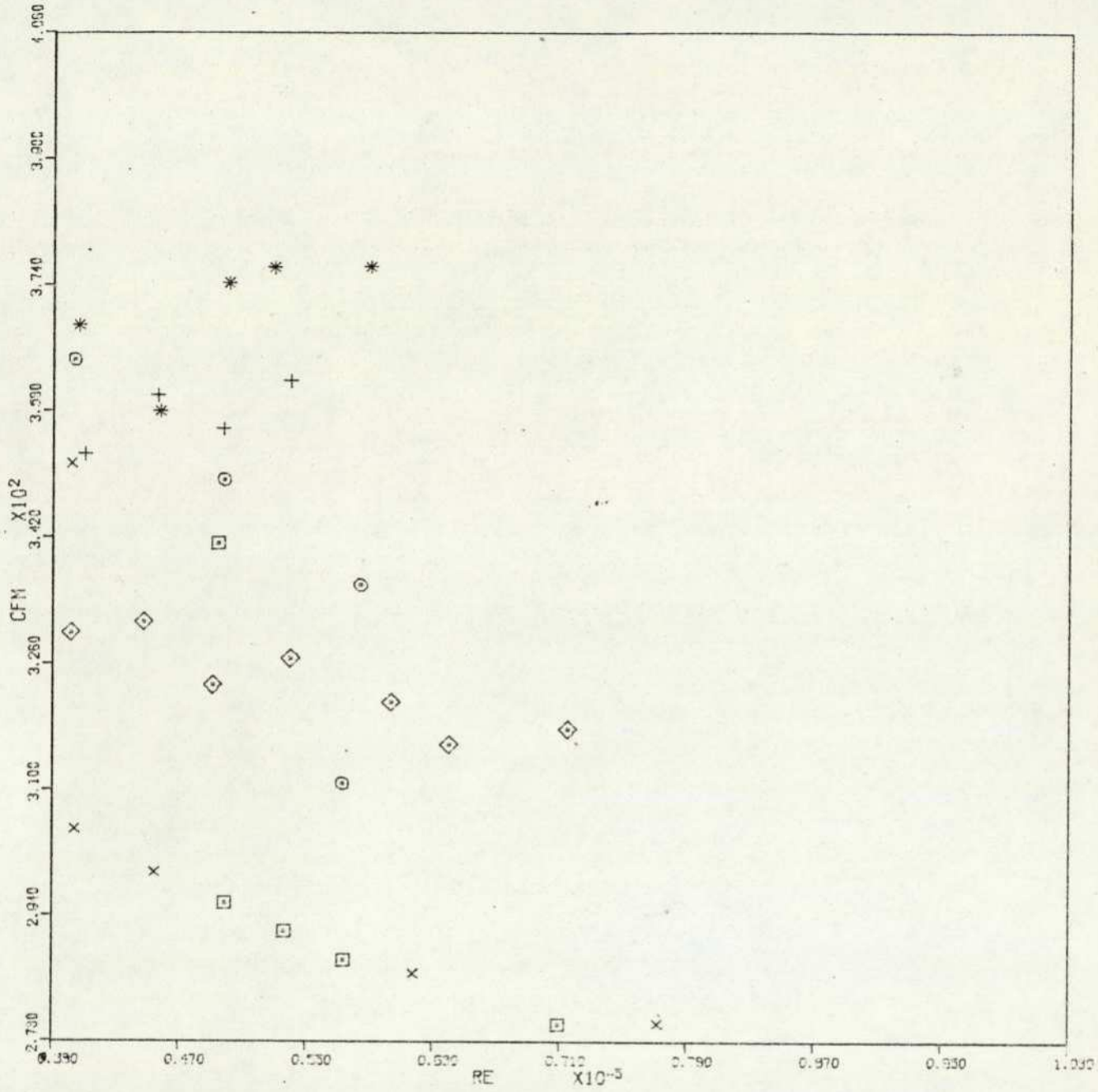

FIGURE : *8.6* SUSPENSION FRICTION FACTOR, CFM VS. REYNOLDS NUMBER, RE. GLASS BEADS TYPE #1.

CONSTANT PARAMETER(S) : MP, KG/SEC

CURVE 01	×	0.172E-01
CURVE 02*	⊙	0.172E-01
CURVE 03	⊡	0.182E-01
CURVE 04	◇	0.228E-01
CURVE 05	+	0.292E-01
CURVE 06	✳	0.332E-01

DATA COMPUTED BY #PDP2, O/P BY #PJ03. PLOTTED BY #PJ04 (01-07-10-14-02-00) .

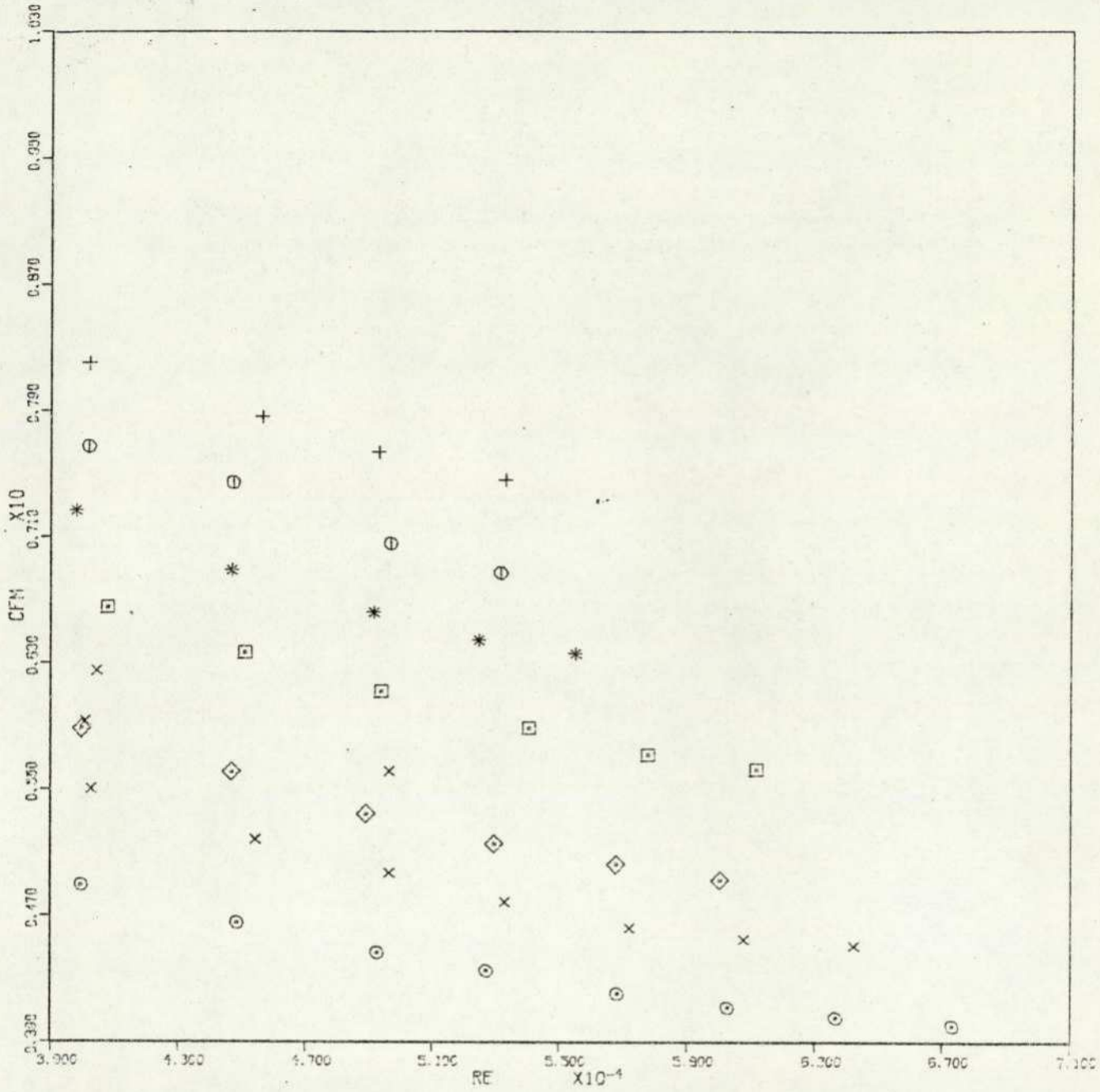

FIGURE : 8.7 SUSPENSION FRICTION FACTOR, CFM VS. REYNOLDS NUMBER, RE. GLASS BEADS TYPE #2.

CONSTANT PARAMETER(S) : MP, KG/SEC

CURVE 01	×	0.189E-01
CURVE 02*	⊙	0.190E-01
CURVE 03	⊡	0.246E-01
CURVE 04*	◈	0.245E-01
CURVE 05	+	0.343E-01
CURVE 06*	✳	0.344E-01
CURVE 07*	⊕	0.365E-01

DATA COMPUTED BY #PDP2. O/P BY #PJ03. PLOTTED BY #PJ04 (02-07-10-14-02-00) .

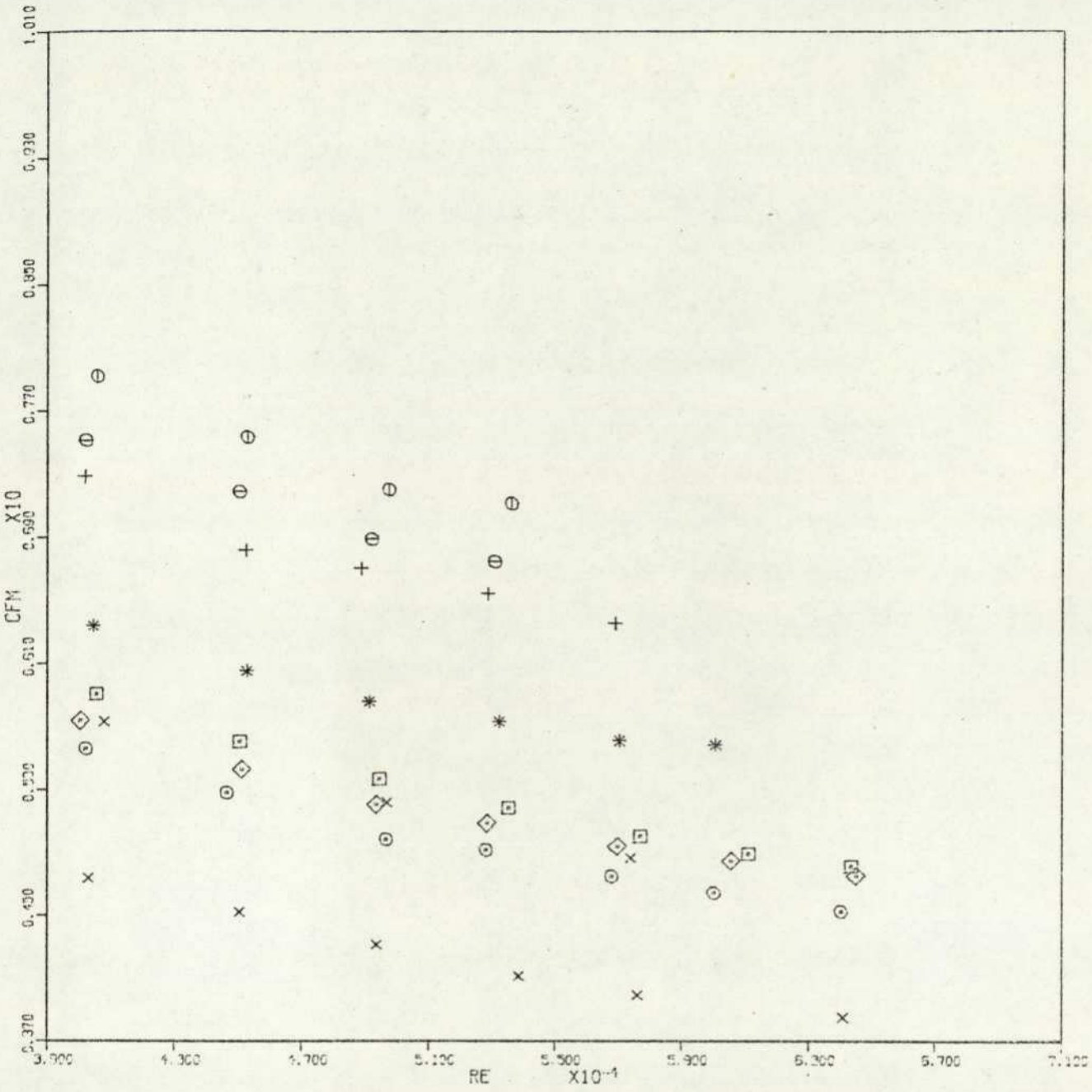

FIGURE : 8.8 SUSPENSION FRICTION FACTOR, CFM VS. REYNOLDS NUMBER, RE. GLASS BEADS TYPE #3.

CONSTANT PARAMETER(S) : MP, KG/SEC

CURVE 01	×	0.187E-01
CURVE 02*	⊙	0.187E-01
CURVE 03	⊡	0.243E-01
CURVE 04*	◇	0.245E-01
CURVE 05	+	0.343E-01
CURVE 06*	✳	0.344E-01
CURVE 07	⊕	0.364E-01
CURVE 08*	⊖	0.367E-01

DATA COMPUTED BY #PDP2. O/P BY #PJ03. PLOTTED BY #PJ04 (03-07-10-14-02-00) .

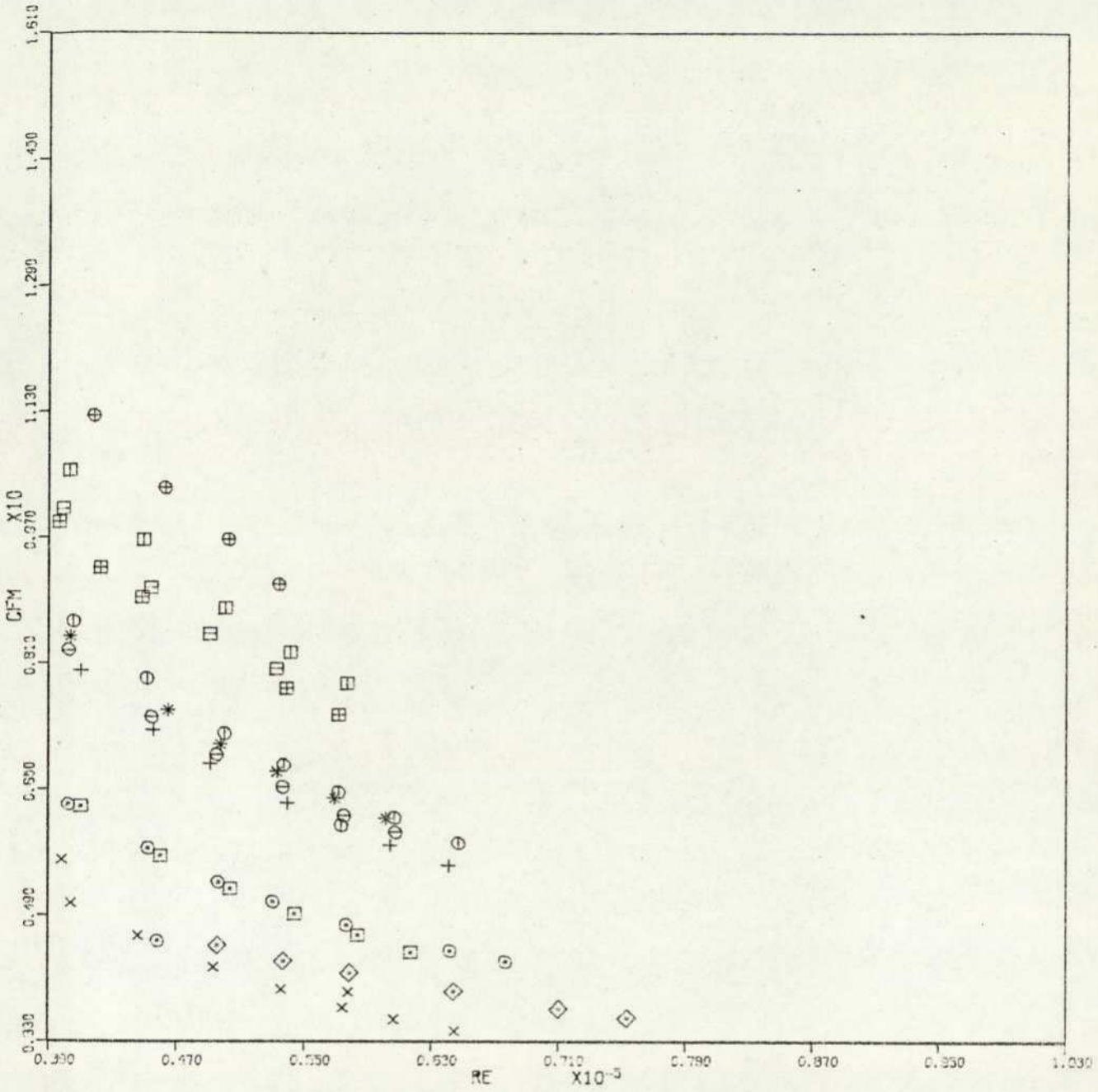

FIGURE : 8.9 SUSPENSION FRICTION FACTOR, CFM VS. REYNOLDS NUMBER, RE. GLASS BEADS TYPE #4.

CONSTANT PARAMETER(S) : MP, KG/SEC

CURVE 01	×	0.156E-01
CURVE 02*	⊙	0.195E-01
CURVE 03	⊡	0.204E-01
CURVE 04*	◇	0.204E-01
CURVE 05	+	0.294E-01
CURVE 06*	✳	0.290E-01
CURVE 07	⊕	0.312E-01
CURVE 08*	⊖	0.324E-01
CURVE 09	⊞	0.405E-01
CURVE 10*	⊟	0.401E-01
CURVE 11	⊕	0.454E-01
CURVE 12*	⊞	0.453E-01

DATA COMPUTED BY #PDP2. O/P BY #PJ03. PLOTTED BY #PJ04 (04-07-10-14-02-00) .

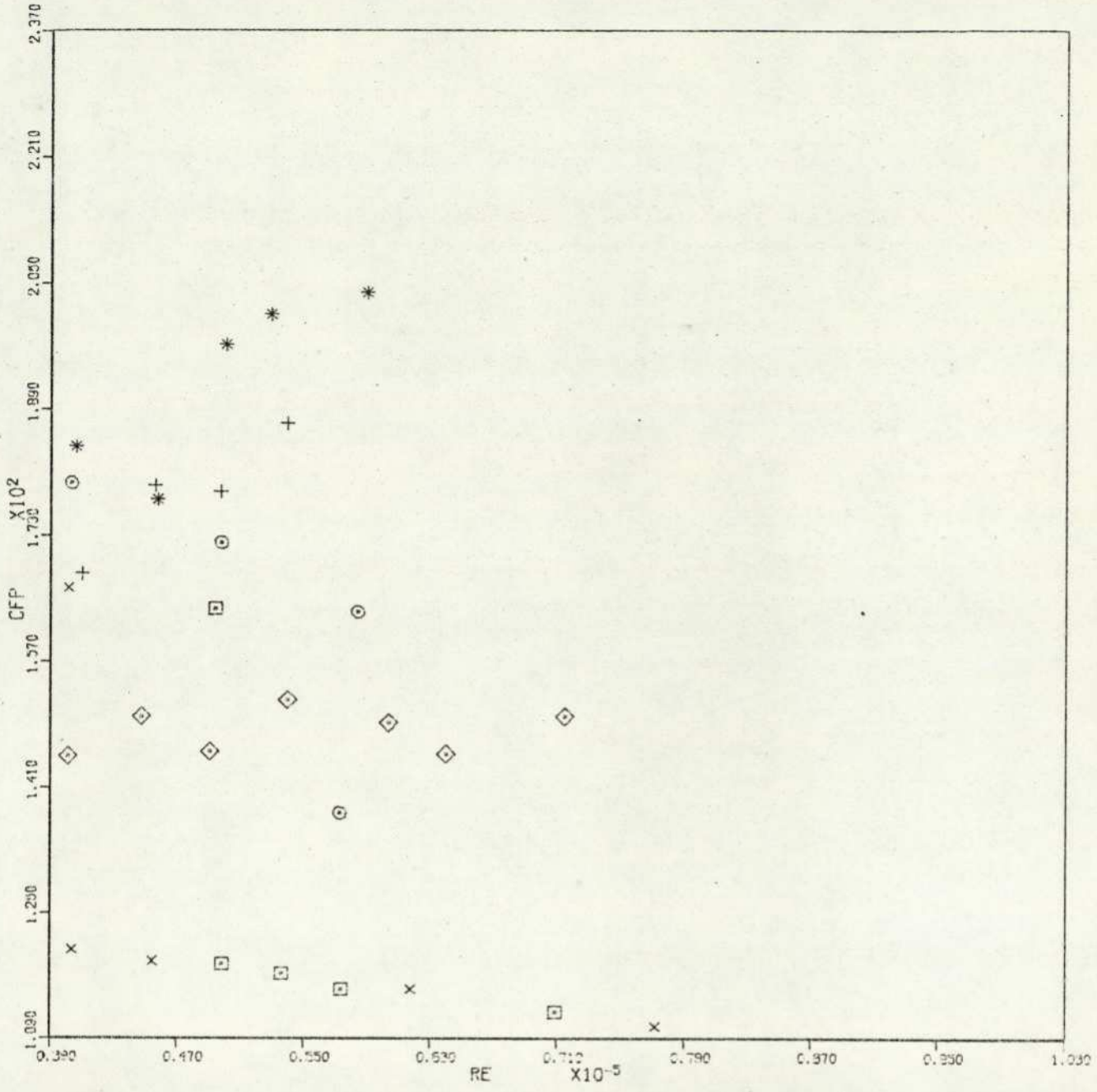

FIGURE :8.10 PARTICLES FRICTION FACTOR, CFP VS. REYNOLDS NUMBER, RE.
GLASS BEADS TYPE #1.

CONSTANT PARAMETER(S) : MP, KG/SEC

CURVE 01	×	0.172E-01
CURVE 02*	⊙	0.172E-01
CURVE 03	⊡	0.182E-01
CURVE 04	◇	0.228E-01
CURVE 05	+	0.292E-01
CURVE 06	*	0.332E-01

DATA COMPUTED BY #PDP2. O/P BY #PJ03. PLOTTED BY #PJ04 (01-07-11-14-02-00) .

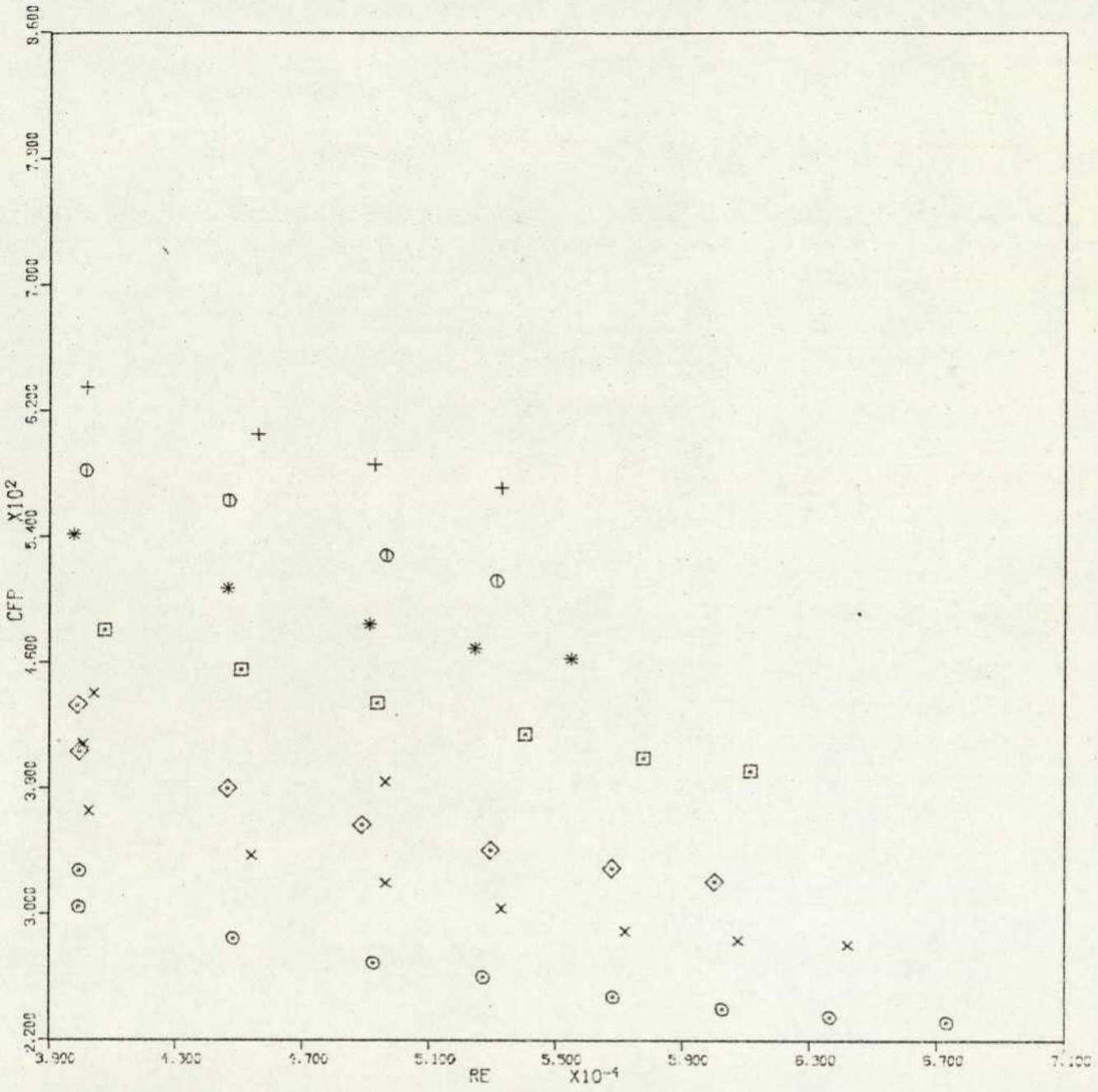

FIGURE : 8.11 PARTICLES FRICTION FACTOR, CFP VS. REYNOLDS NUMBER, RE.
GLASS BEADS TYPE #2.

CONSTANT PARAMETER(S) : MP, KG/SEC

CURVE 01	×	0.189E-01
CURVE 02*	⊙	0.190E-01
CURVE 03	⊡	0.246E-01
CURVE 04*	◈	0.245E-01
CURVE 05	+	0.343E-01
CURVE 06*	✳	0.344E-01
CURVE 07*	⊕	0.365E-01

DATA COMPUTED BY #PDP2. O/P BY #PJ03. PLOTTED BY #PJ04 (02-07-11-14-02-00) .

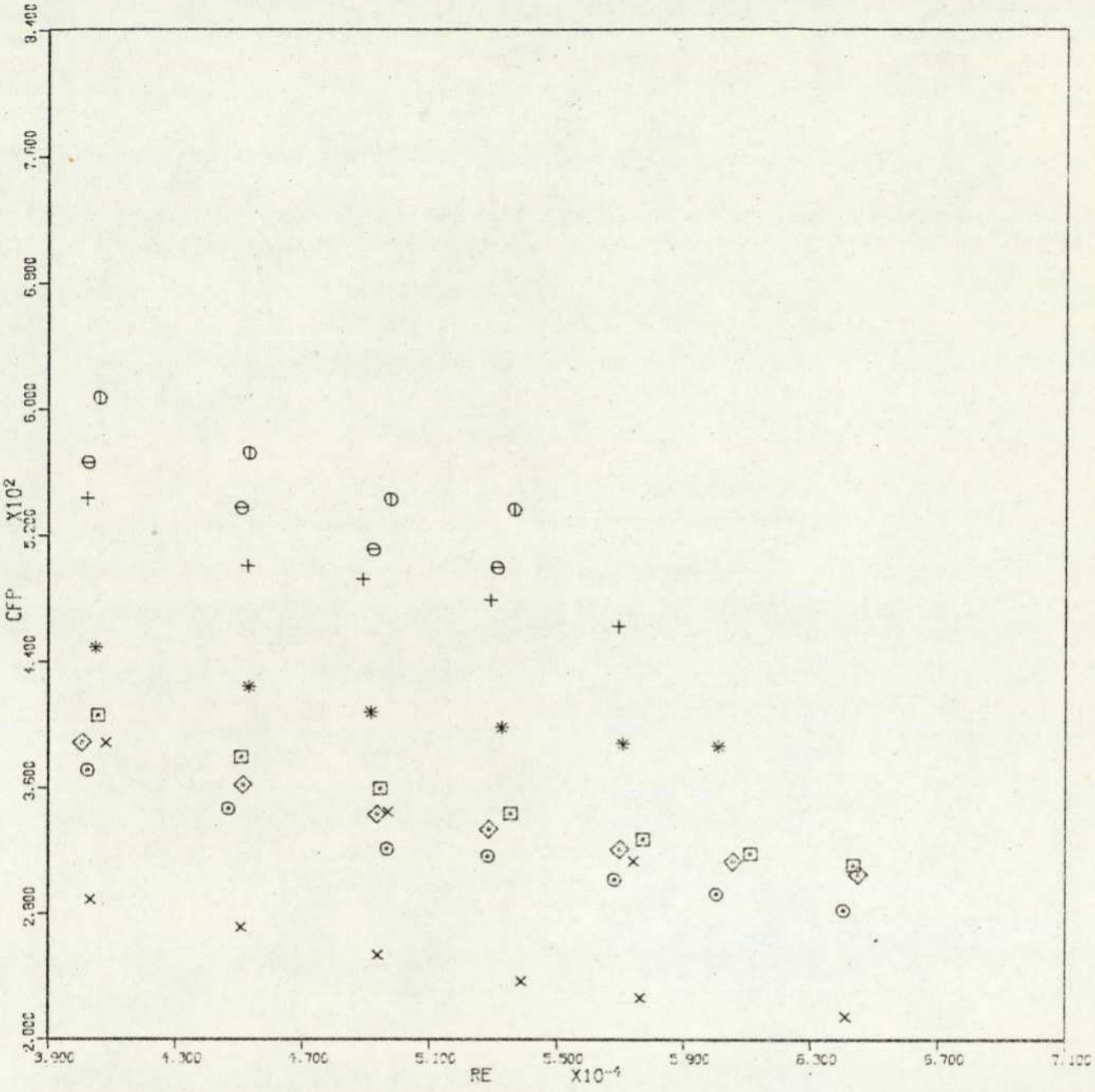

FIGURE : 8.12 PARTICLES FRICTION FACTOR, CFP VS. REYNOLDS NUMBER, RE.
GLASS BEADS TYPE #3.

CONSTANT PARAMETER(S) : MP, KG/SEC

CURVE 01	×	0.187E-01
CURVE 02*	⊙	0.187E-01
CURVE 03	⊡	0.243E-01
CURVE 04*	◇	0.245E-01
CURVE 05	+	0.343E-01
CURVE 06*	✳	0.344E-01
CURVE 07	⊕	0.364E-01
CURVE 08*	⊖	0.367E-01

DATA COMPUTED BY #PDP2. O/P BY #PJ03. PLOTTED BY #PJ04 (03-07-11-14-02-00) .

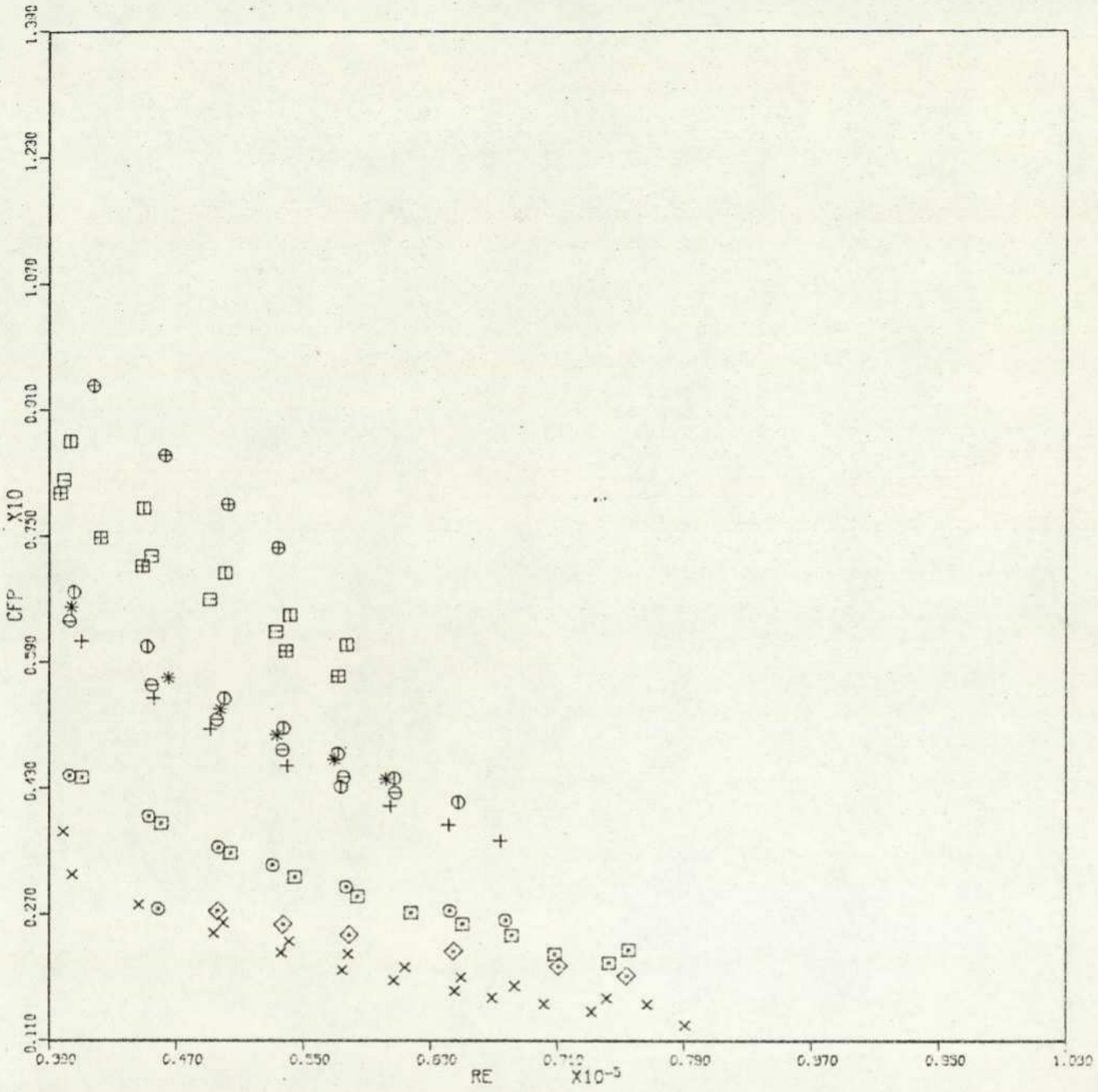

FIGURE 8.13 PARTICLES FRICTION FACTOR, CFP VS. REYNOLDS NUMBER, RE. GLASS BEADS TYPE #4.

CONSTANT PARAMETER(S) : MP, KG/SEC

CURVE 01	×	0.156E-01
CURVE 02*	⊙	0.195E-01
CURVE 03	⊡	0.204E-01
CURVE 04*	◇	0.204E-01
CURVE 05	+	0.294E-01
CURVE 06*	*	0.290E-01
CURVE 07	⊕	0.312E-01
CURVE 08*	⊖	0.324E-01
CURVE 09	⊞	0.405E-01
CURVE 10*	⊟	0.401E-01
CURVE 11	⊕	0.454E-01
CURVE 12*	⊞	0.453E-01

DATA COMPUTED BY #PDP2. O/P BY #PJ03. PLOTTED BY #PJ04 (04-07-11-14-02-00) .

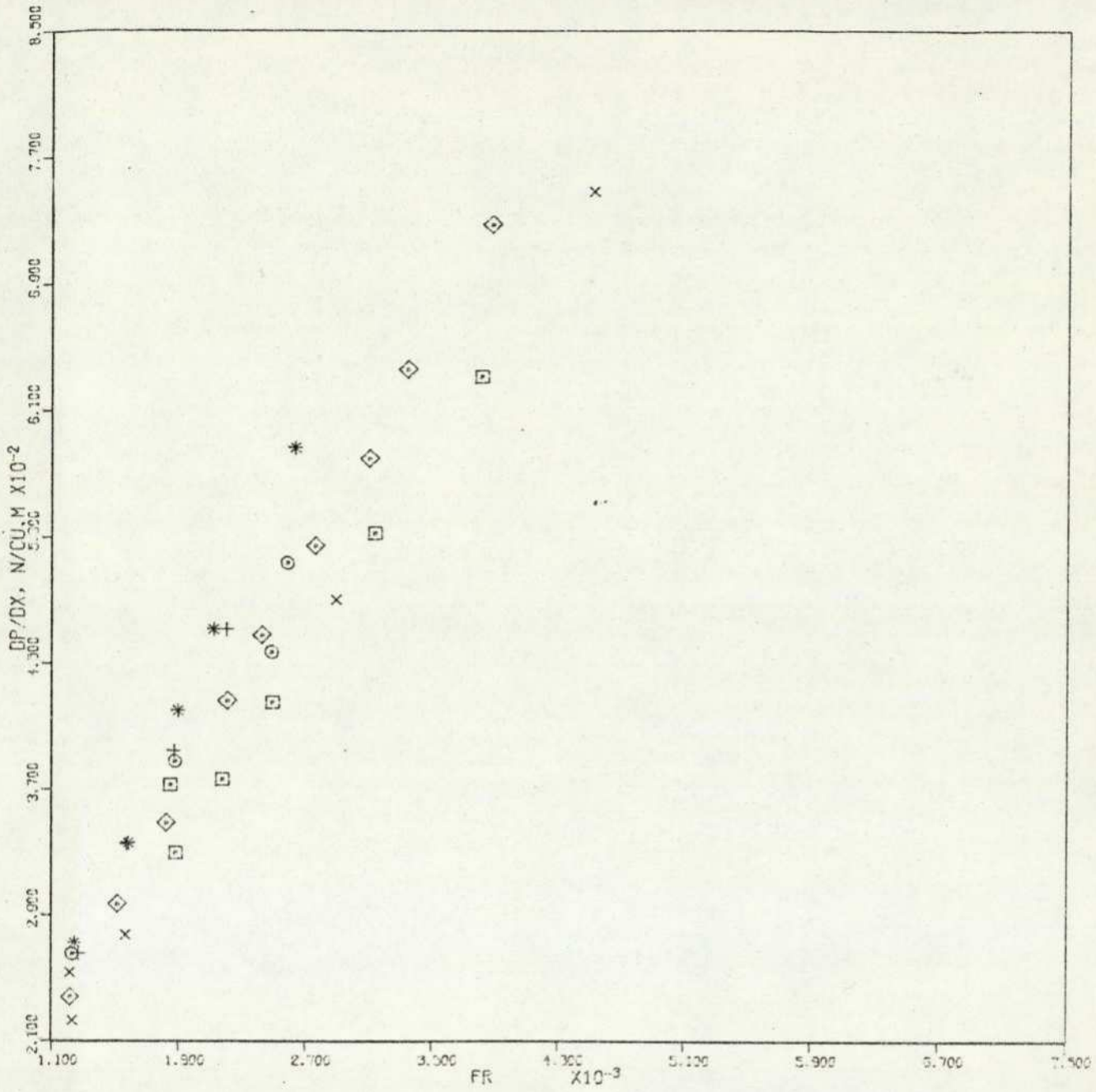

FIGURE : 8.14 PRESSURE GRADIENT, (DP/DX) VS. FROUDE NUMBER, FR.
GLASS BEADS TYPE #1.

CONSTANT PARAMETER(S) : MP, KG/SEC

CURVE 01	×	0.172E-01
CURVE 02*	⊙	0.172E-01
CURVE 03	⊡	0.181E-01
CURVE 04	◇	0.223E-01
CURVE 05	+	0.292E-01
CURVE 06	*	0.332E-01

DATA COMPUTED BY #PDP2. O/P BY #PJ03. PLOTTED BY #PJ04 (01-08-09-14-02-00) .

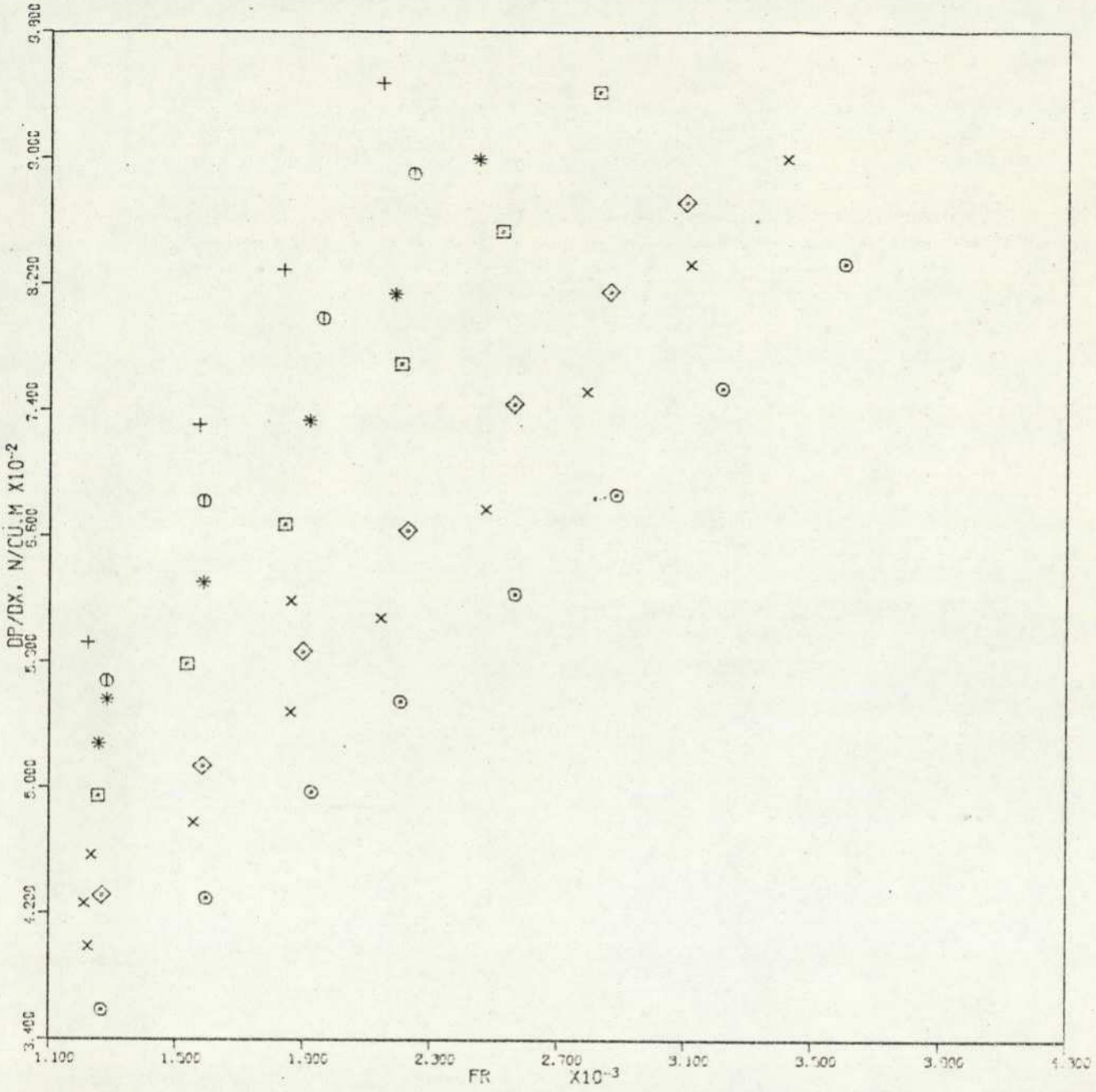

FIGURE : 8.15 PRESSURE GRADIENT, (DP/DX) VS. FROUDE NUMBER, FR.
GLASS BEADS TYPE #2.

CONSTANT PARAMETER(S) : MP. KG/SEC

CURVE 01	×	0.190E-01
CURVE 02*	⊙	0.190E-01
CURVE 03	⊡	0.246E-01
CURVE 04*	◇	0.245E-01
CURVE 05	+	0.343E-01
CURVE 06*	✳	0.344E-01
CURVE 07*	⊕	0.365E-01

DATA COMPUTED BY #PDP2. O/P BY #PJ03. PLOTTED BY #PJ04 (02-09-09-14-02-00) .

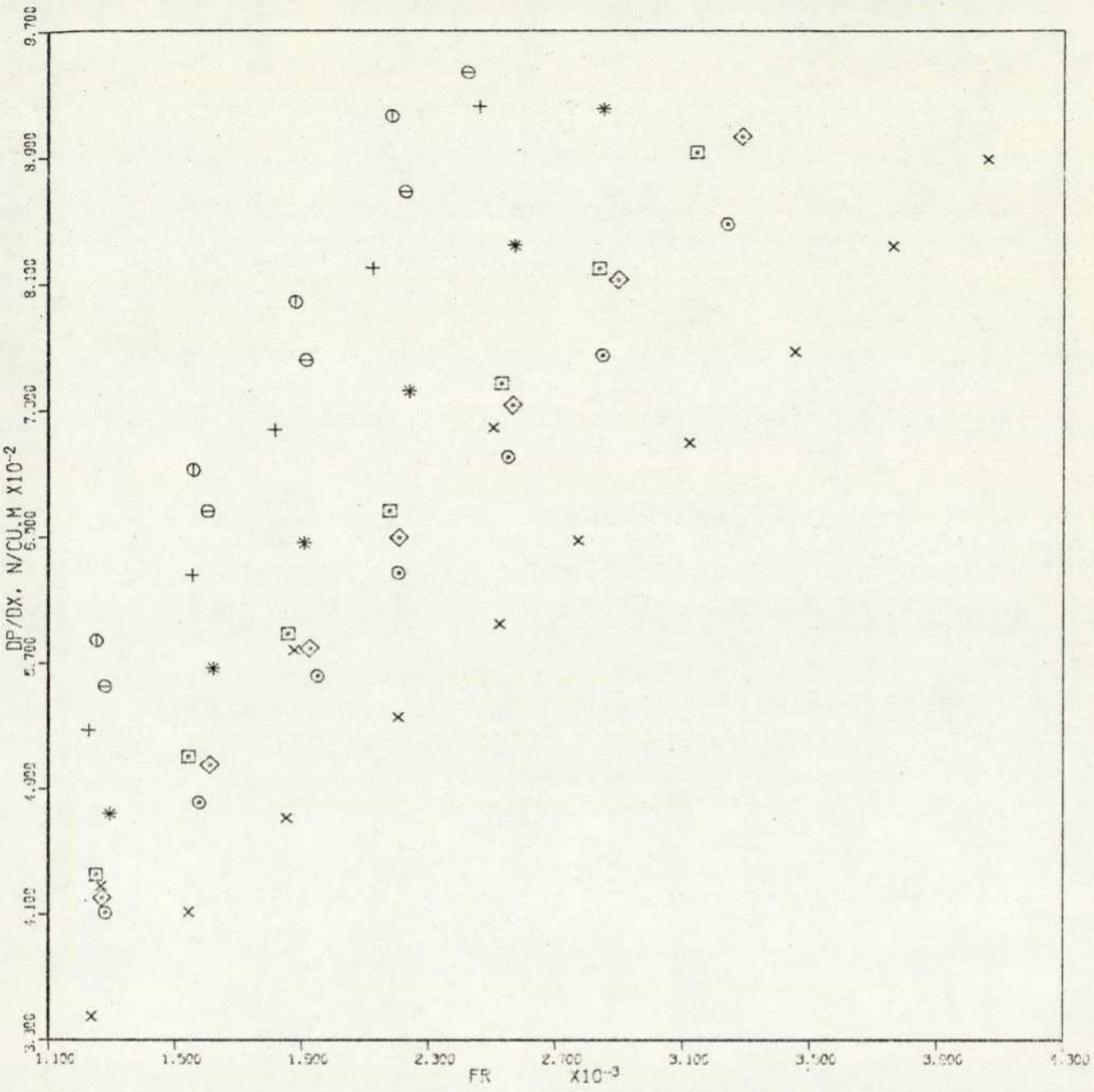

FIGURE :8.16 PRESSURE GRADIENT, (DP/DX) VS. FROUDE NUMBER, FR.
GLASS BEADS TYPE #3.

CONSTANT PARAMETER(S) : MP, KG/SEC

CURVE 01	×	0.189E-01
CURVE 02 *	⊙	0.187E-01
CURVE 03	⊡	0.243E-01
CURVE 04 *	◇	0.245E-01
CURVE 05	+	0.343E-01
CURVE 06 *	*	0.344E-01
CURVE 07	⊕	0.364E-01
CURVE 08 *	⊖	0.365E-01

DATA COMPUTED BY #PDP2, O/P BY #PJ03, PLOTTED BY #PJ04 (03-08-08-14-02-00) .

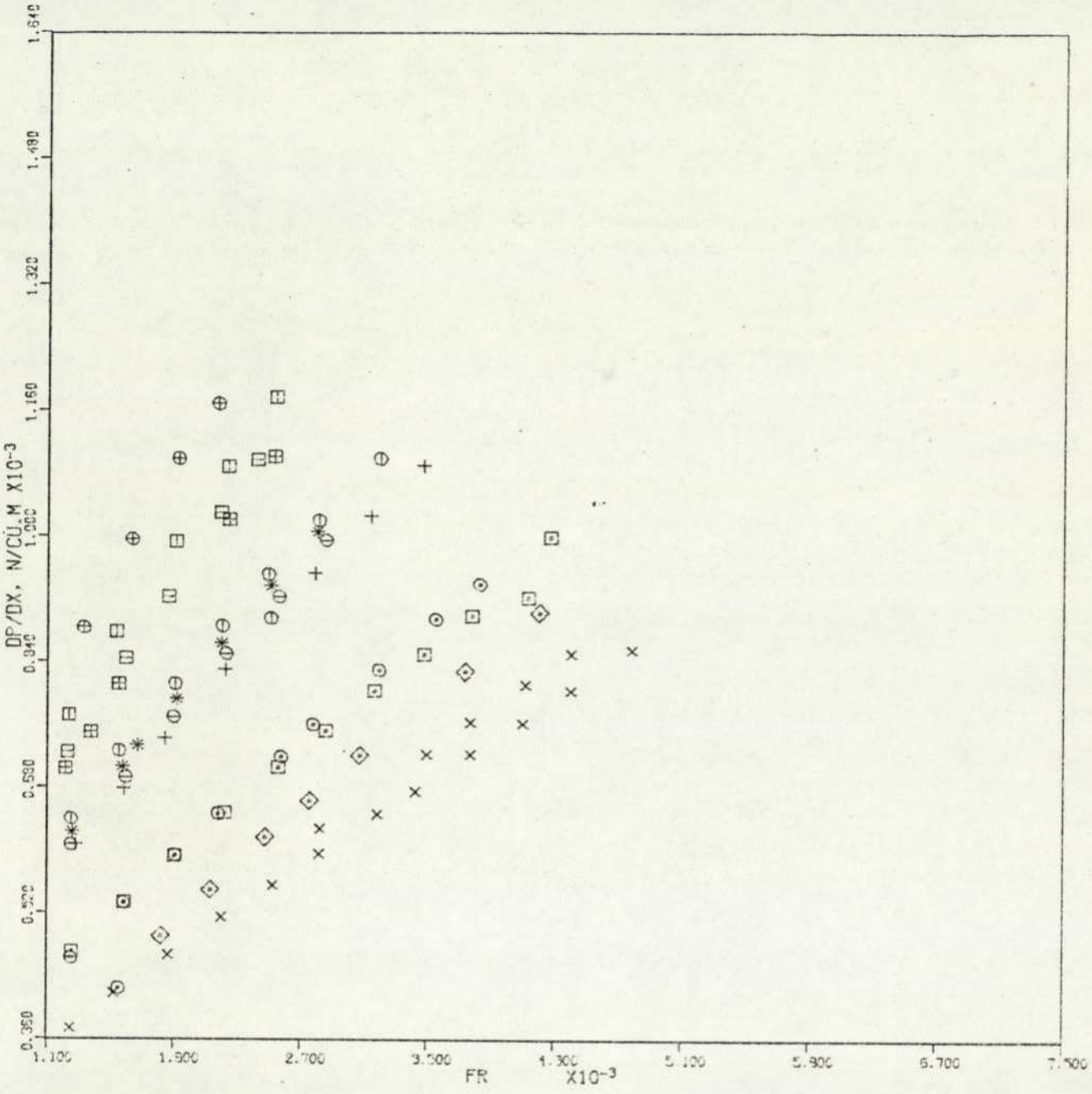

FIGURE :8.17 PRESSURE GRADIENT, (DP/DX) VS. FROUDE NUMBER, FR.
GLASS BEADS TYPE #4.

CONSTANT PARAMETER(S) : MP, KG/SEC

CURVE 01	×	0.157E-01
CURVE 02*	⊙	0.195E-01
CURVE 03	⊡	0.204E-01
CURVE 04*	◈	0.204E-01
CURVE 05	+	0.294E-01
CURVE 06*	✳	0.290E-01
CURVE 07	⊕	0.312E-01
CURVE 08*	⊖	0.324E-01
CURVE 09	⊞	0.405E-01
CURVE 10*	⊟	0.401E-01
CURVE 11	⊕	0.454E-01
CURVE 12*	⊞	0.453E-01

DATA COMPUTED BY #PDP2, O/P BY #PJ03, PLOTTED BY #PJ04 (04-09-09-14-02-00) .

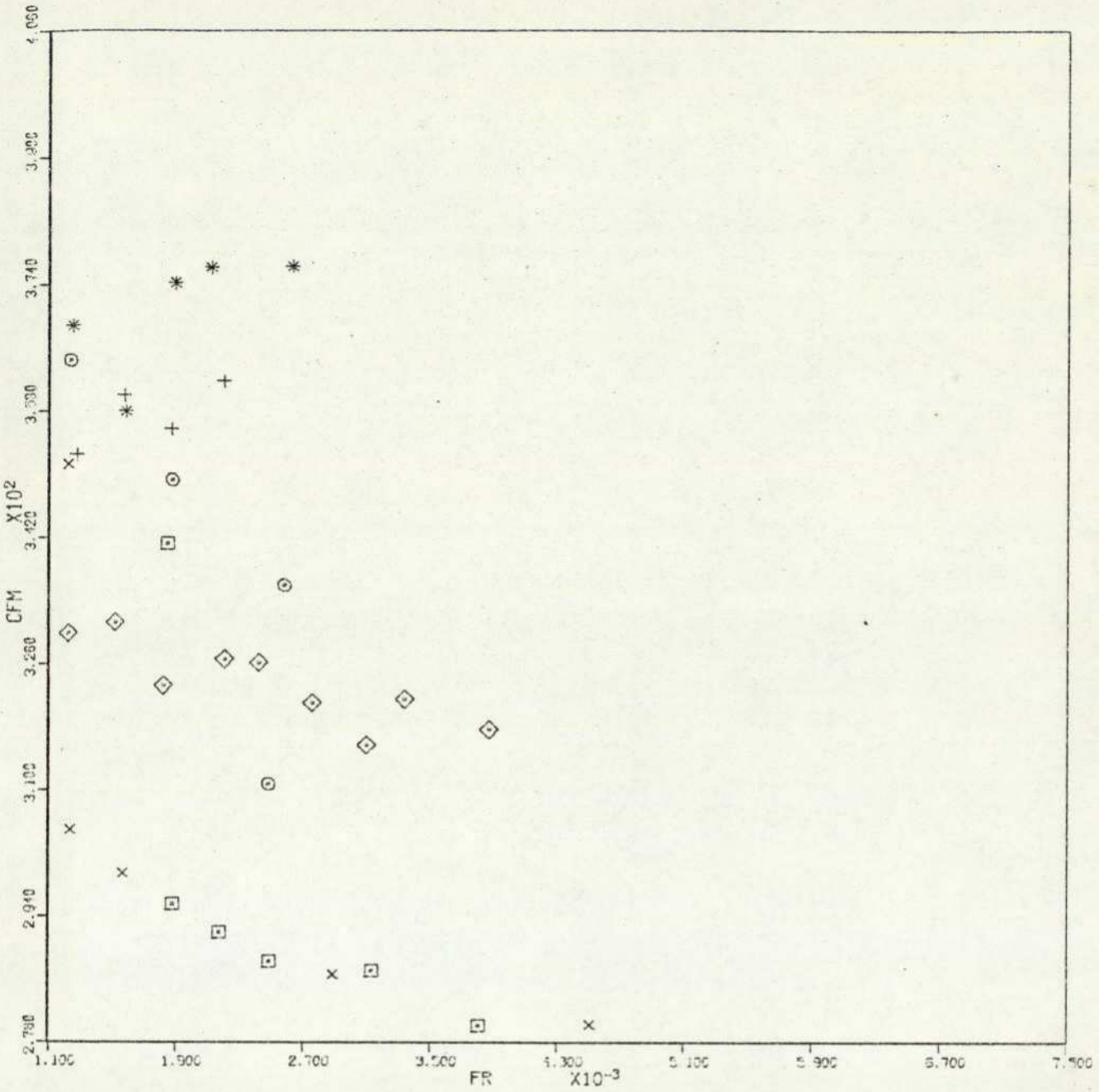

FIGURE :8.18 SUSPENSION FRICTION FACTOR, CFM VS. FROUDE NUMBER, FR. GLASS BEADS TYPE #1.

CONSTANT PARAMETER(S) : MP, KG/SEC

CURVE 01	×	0.172E-01
CURVE 02*	⊙	0.172E-01
CURVE 03	⊡	0.181E-01
CURVE 04	◇	0.229E-01
CURVE 05	+	0.292E-01
CURVE 06	*	0.332E-01

DATA COMPUTED BY #PDP2, O/P BY #PJ03, PLOTTED BY #PJ04 (01-09-10-14-02-00) .

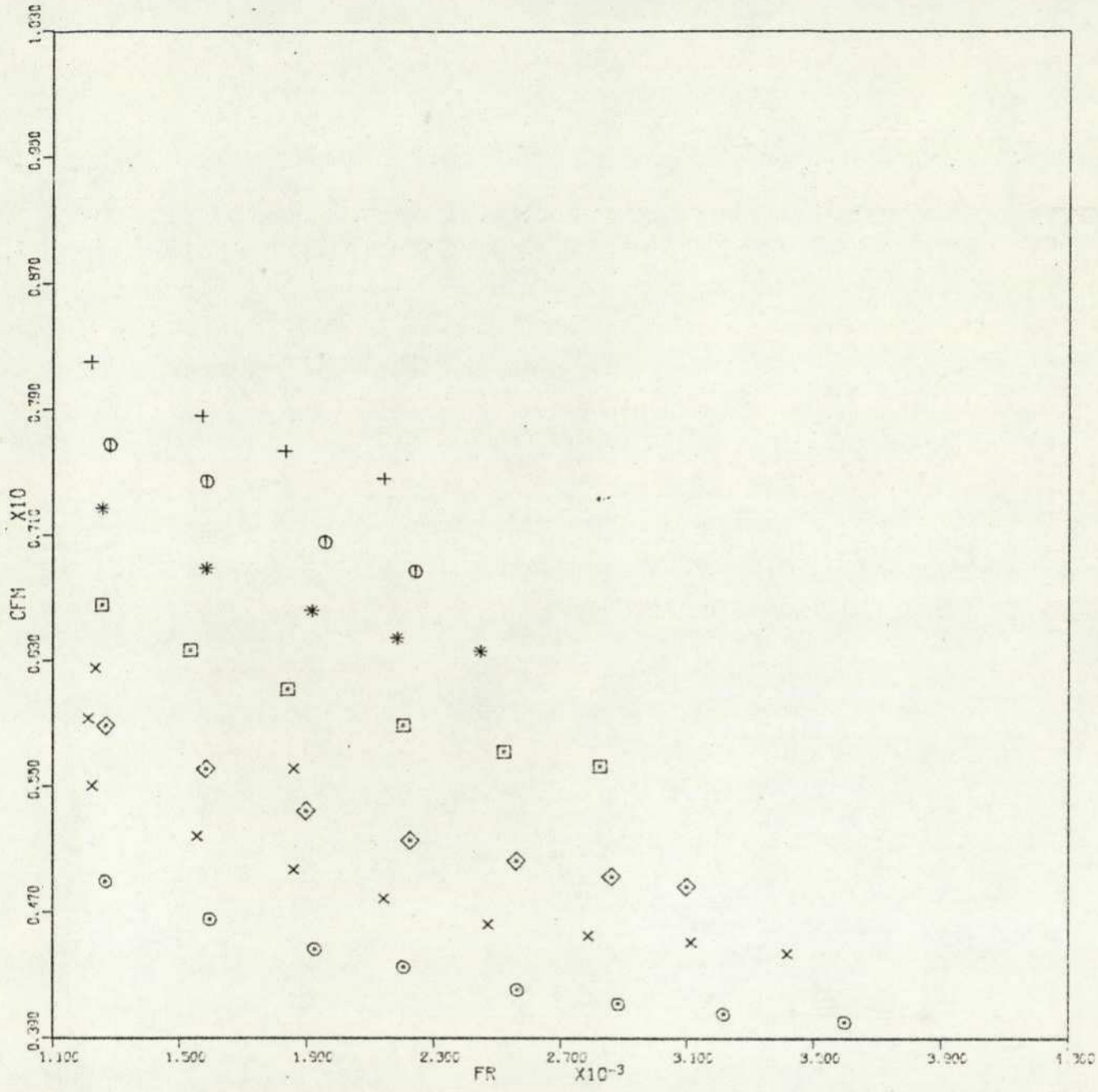

FIGURE 8.19 SUSPENSION FRICTION FACTOR, CFM VS. FROUDE NUMBER, FR. GLASS BEADS TYPE #2.

CONSTANT PARAMETER(S) : MP, KG/SEC

CURVE 01	×	0.190E-01
CURVE 02*	⊙	0.190E-01
CURVE 03	⊡	0.246E-01
CURVE 04*	◇	0.245E-01
CURVE 05	+	0.343E-01
CURVE 06*	✳	0.344E-01
CURVE 07*	⊕	0.365E-01

DATA COMPUTED BY #PDP2. O/P BY #PJ03. PLOTTED BY #PJ04 (02-08-10-14-02-00) .

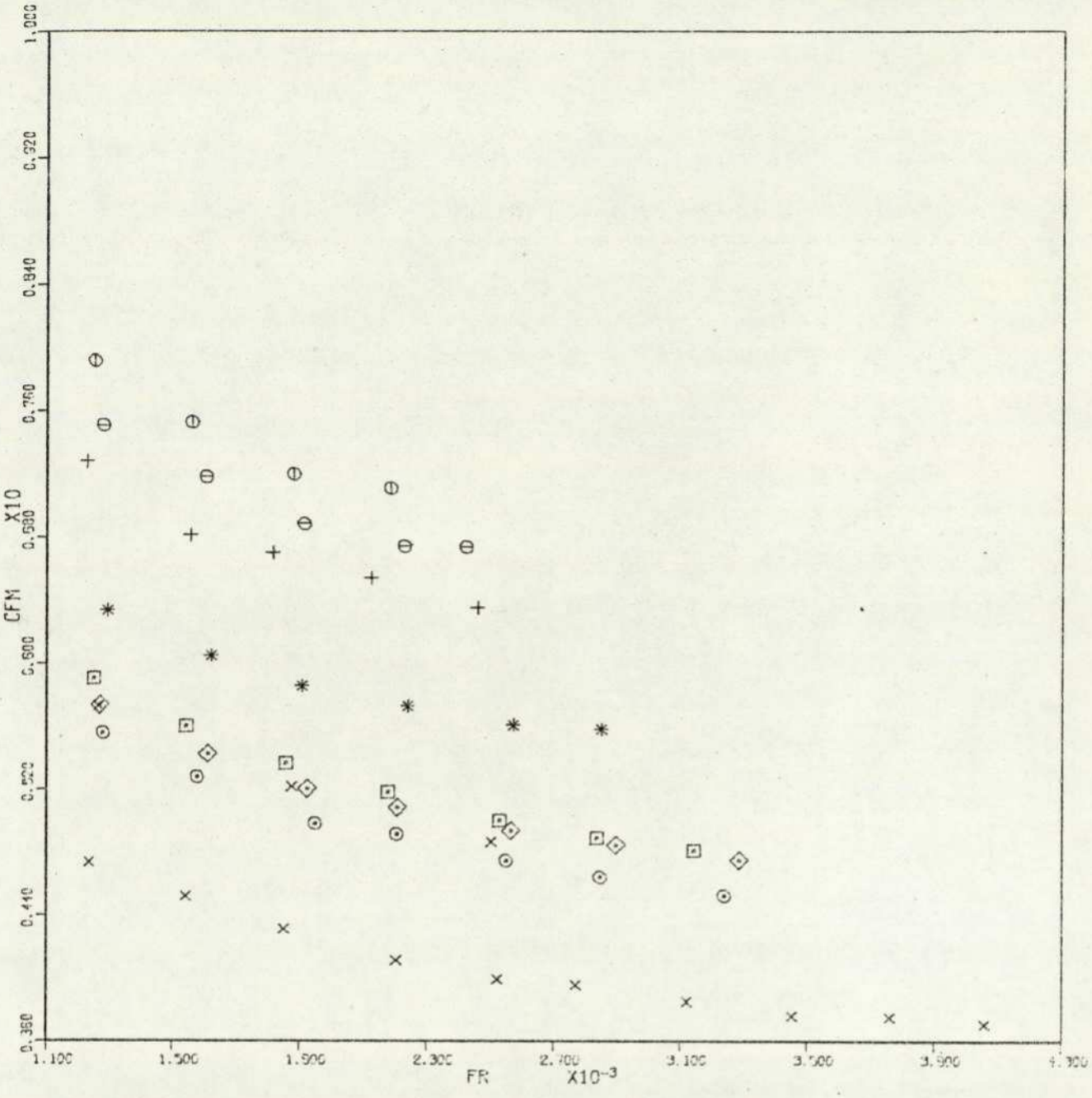

FIGURE : 8.20 SUSPENSION FRICTION FACTOR, CFM VS. FROUDE NUMBER, FR. GLASS BEADS TYPE #3.

CONSTANT PARAMETER(S) : MP, KG/SEC

CURVE 01	×	0.188E-01
CURVE 02*	⊙	0.187E-01
CURVE 03	⊡	0.243E-01
CURVE 04*	◈	0.245E-01
CURVE 05	+	0.343E-01
CURVE 06*	✳	0.344E-01
CURVE 07	⊕	0.364E-01
CURVE 08*	⊖	0.365E-01

DATA COMPUTED BY #PDP2, O/P BY #PJ03, PLOTTED BY #PJ04 (03-09-10-14-02-00) .

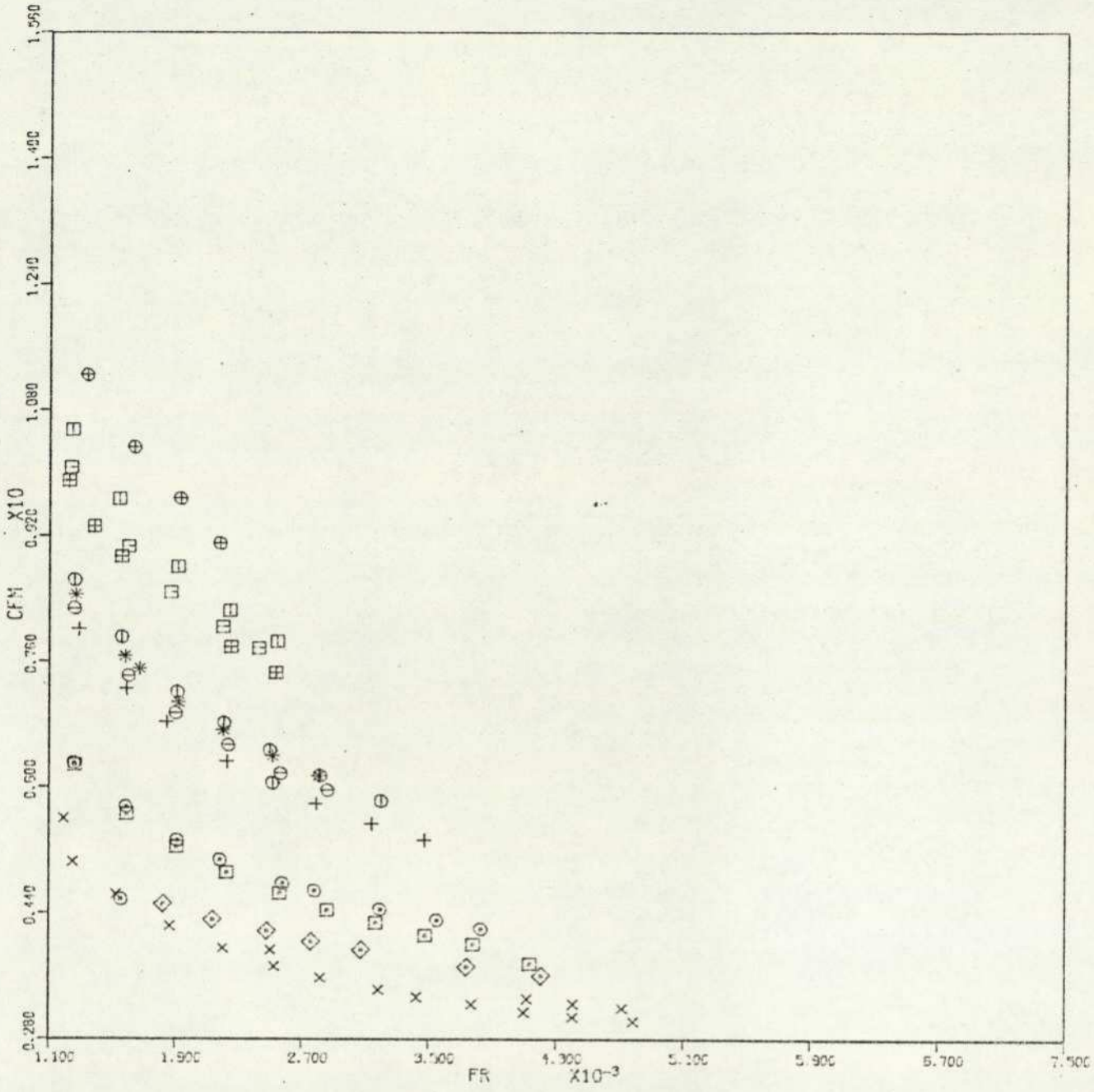

FIGURE : 8.21 SUSPENSION FRICTION FACTOR, CFM VS. FROUDE NUMBER, FR. GLASS BEADS TYPE #4.

CONSTANT PARAMETER(S) : MP, KG/SEC

CURVE 01	×	0.156E-01
CURVE 02 *	⊙	0.195E-01
CURVE 03	⊡	0.204E-01
CURVE 04 *	◇	0.204E-01
CURVE 05	+	0.294E-01
CURVE 06 *	✳	0.290E-01
CURVE 07	⊕	0.312E-01
CURVE 08 *	⊖	0.324E-01
CURVE 09	⊞	0.405E-01
CURVE 10 *	⊟	0.401E-01
CURVE 11	⊕	0.454E-01
CURVE 12 *	⊞	0.453E-01

DATA COMPUTED BY #PDP2, O/P BY #PJ03, PLOTTED BY #PJ04 (04-09-10-14-02-00) .

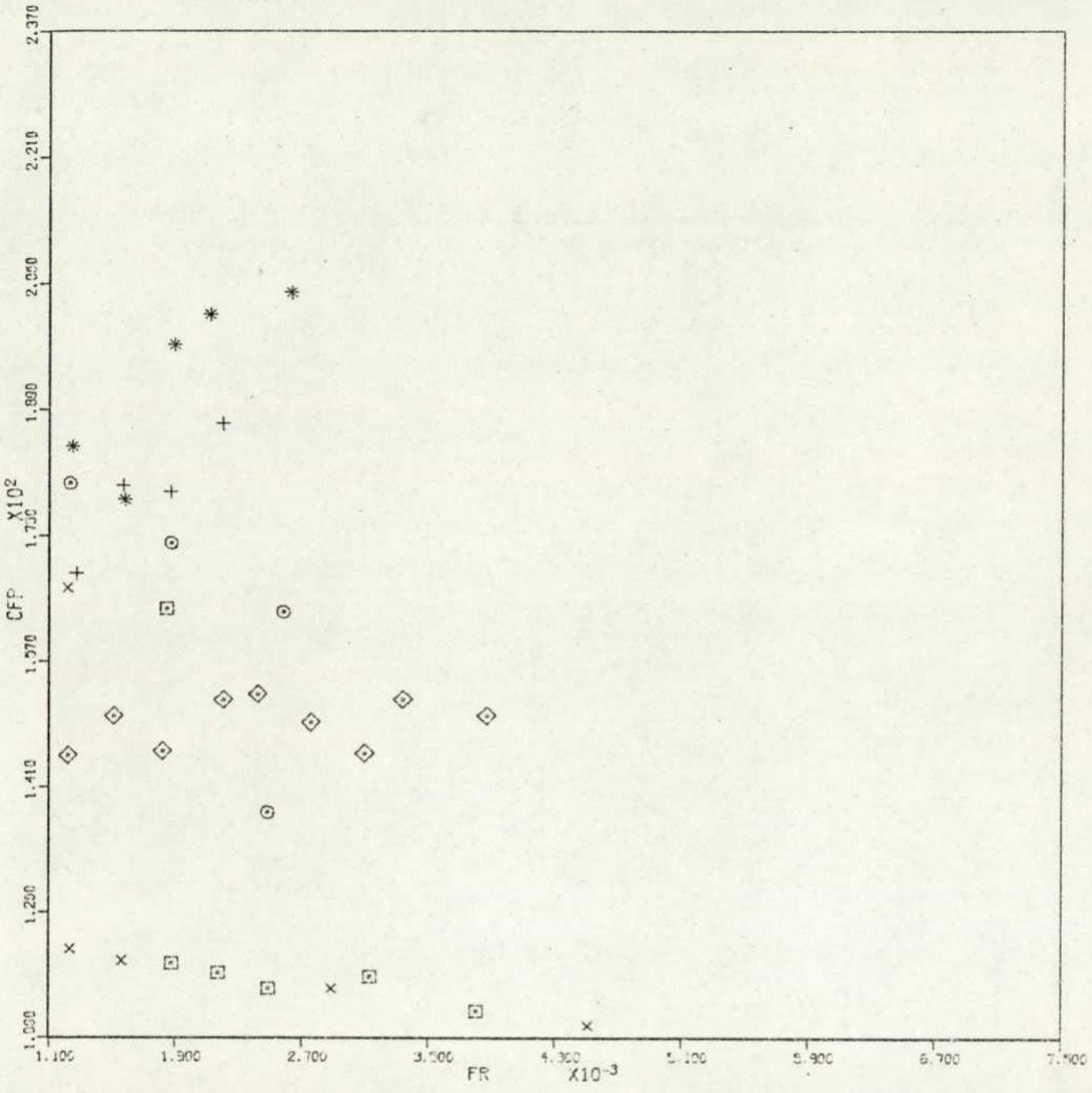

FIGURE : 8.22 PARTICLES FRICTION FACTOR, CFP VS. FROUDE NUMBER, FR.
GLASS BEADS TYPE #1.

CONSTANT PARAMETER(S) : MP, KG/SEC

CURVE 01	×	0.172E-01
CURVE 02*	⊙	0.172E-01
CURVE 03	⊡	0.181E-01
CURVE 04	◇	0.229E-01
CURVE 05	+	0.282E-01
CURVE 06	*	0.332E-01

DATA COMPUTED BY #PDP2. O/P BY #PJ03. PLOTTED BY #PJ04 (01-08-11-14-02-00) .

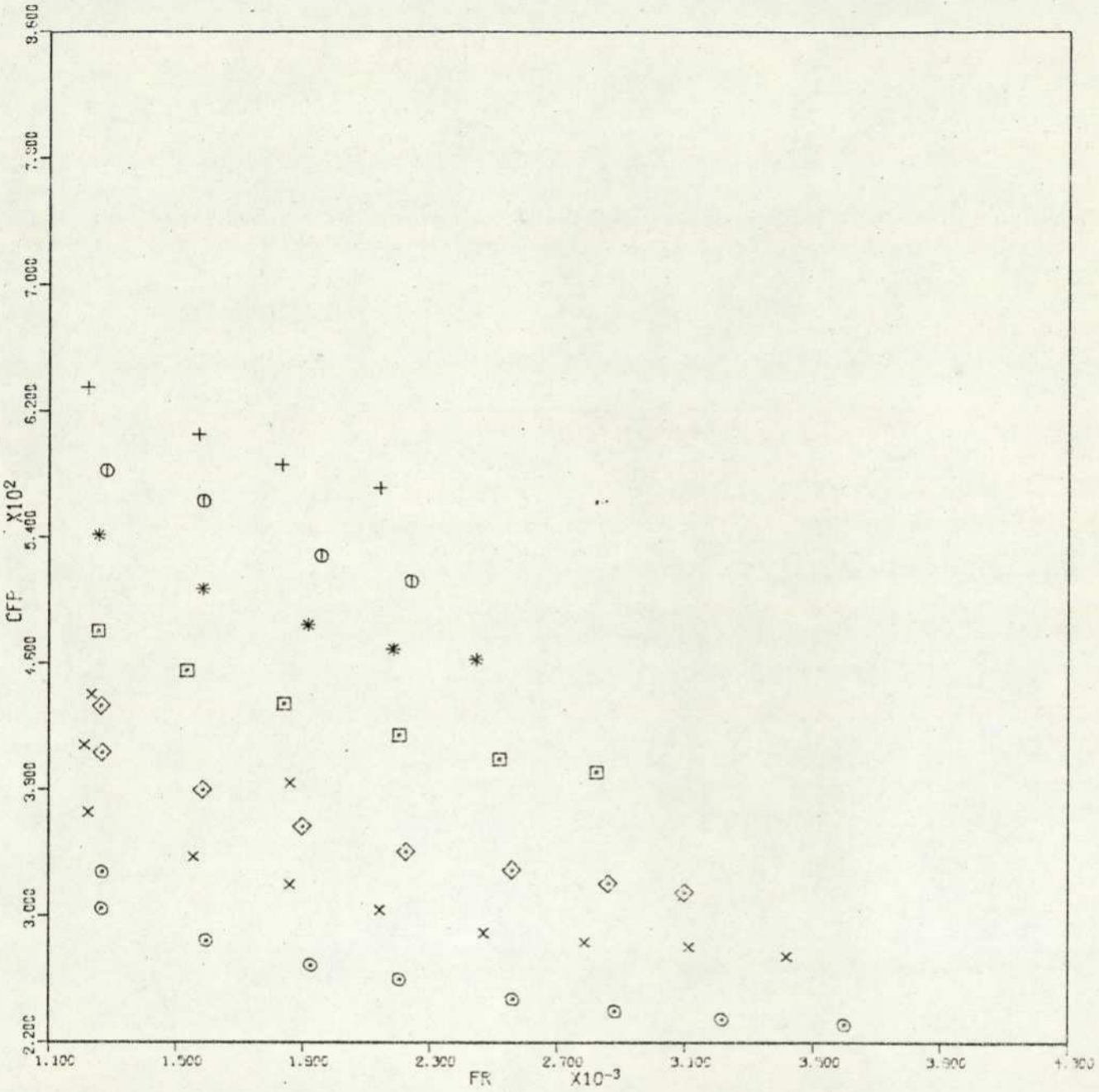

FIGURE : 8.23 PARTICLES FRICTION FACTOR, CFP VS. FROUDE NUMBER, FR.
GLASS BEADS TYPE #2.

CONSTANT PARAMETER(S) : MP, KG/SEC

CURVE 01	×	0.190E-01
CURVE 02*	⊙	0.190E-01
CURVE 03	⊡	0.246E-01
CURVE 04*	◇	0.245E-01
CURVE 05	+	0.343E-01
CURVE 06*	*	0.344E-01
CURVE 07*	⊕	0.365E-01

DATA COMPUTED BY #PDP2. O/P BY #PJ03. PLOTTED BY #PJ04 (02-08-11-14-02-00)

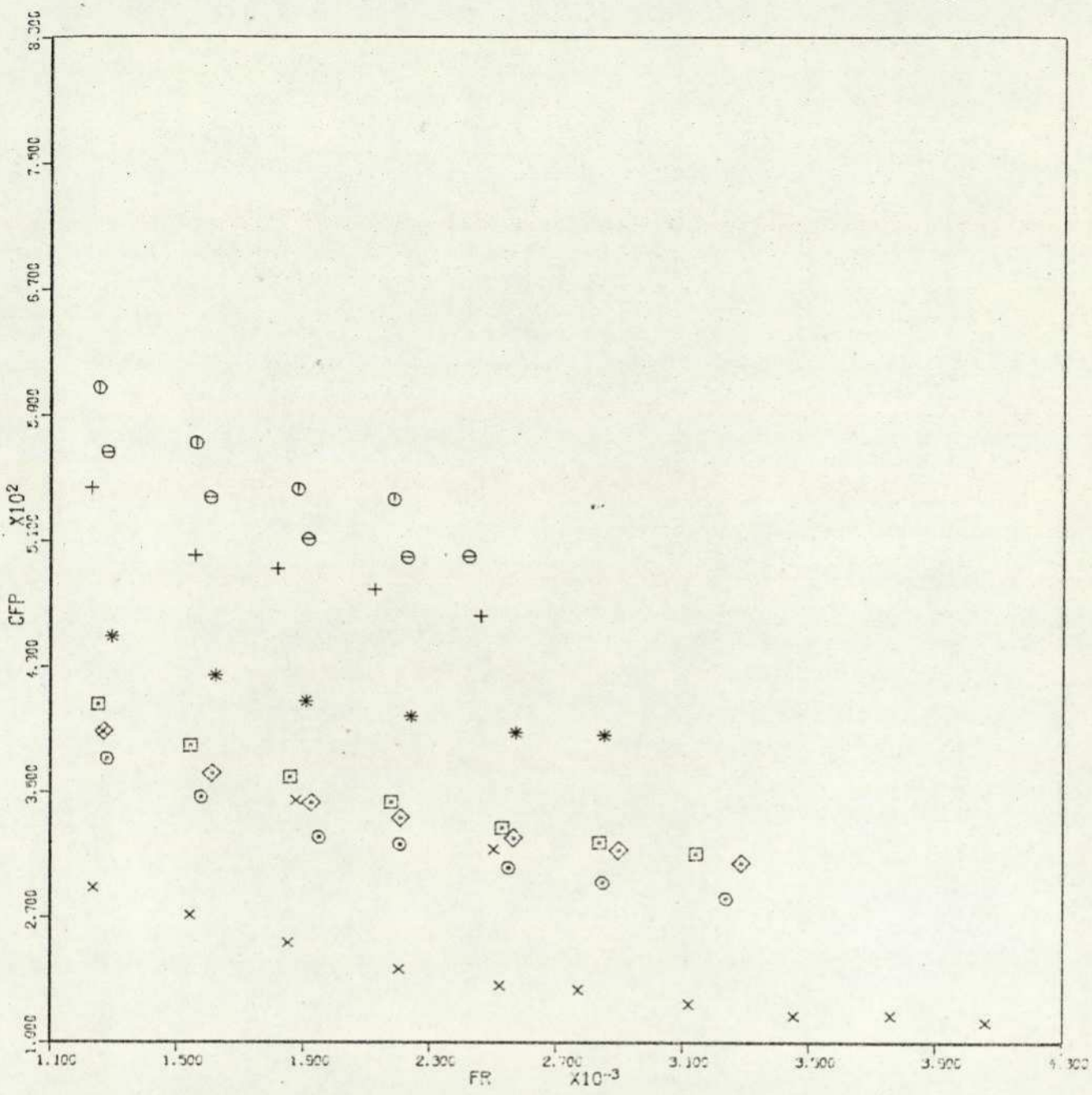

FIGURE : *8.24* PARTICLES FRICTION FACTOR, CFP VS. FROUDE NUMBER, FR.
GLASS BEADS TYPE #3.

CONSTANT PARAMETER(S) : MP, KG/SEC

CURVE 01	×	0.189E-01
CURVE 02*	⊙	0.187E-01
CURVE 03	⊡	0.243E-01
CURVE 04*	◇	0.245E-01
CURVE 05	+	0.343E-01
CURVE 06*	*	0.344E-01
CURVE 07	⊕	0.364E-01
CURVE 08*	⊖	0.365E-01

DATA COMPUTED BY #PDP2. O/P BY #PJ03. PLOTTED BY #PJ04 (03-08-11-14-02-00) .

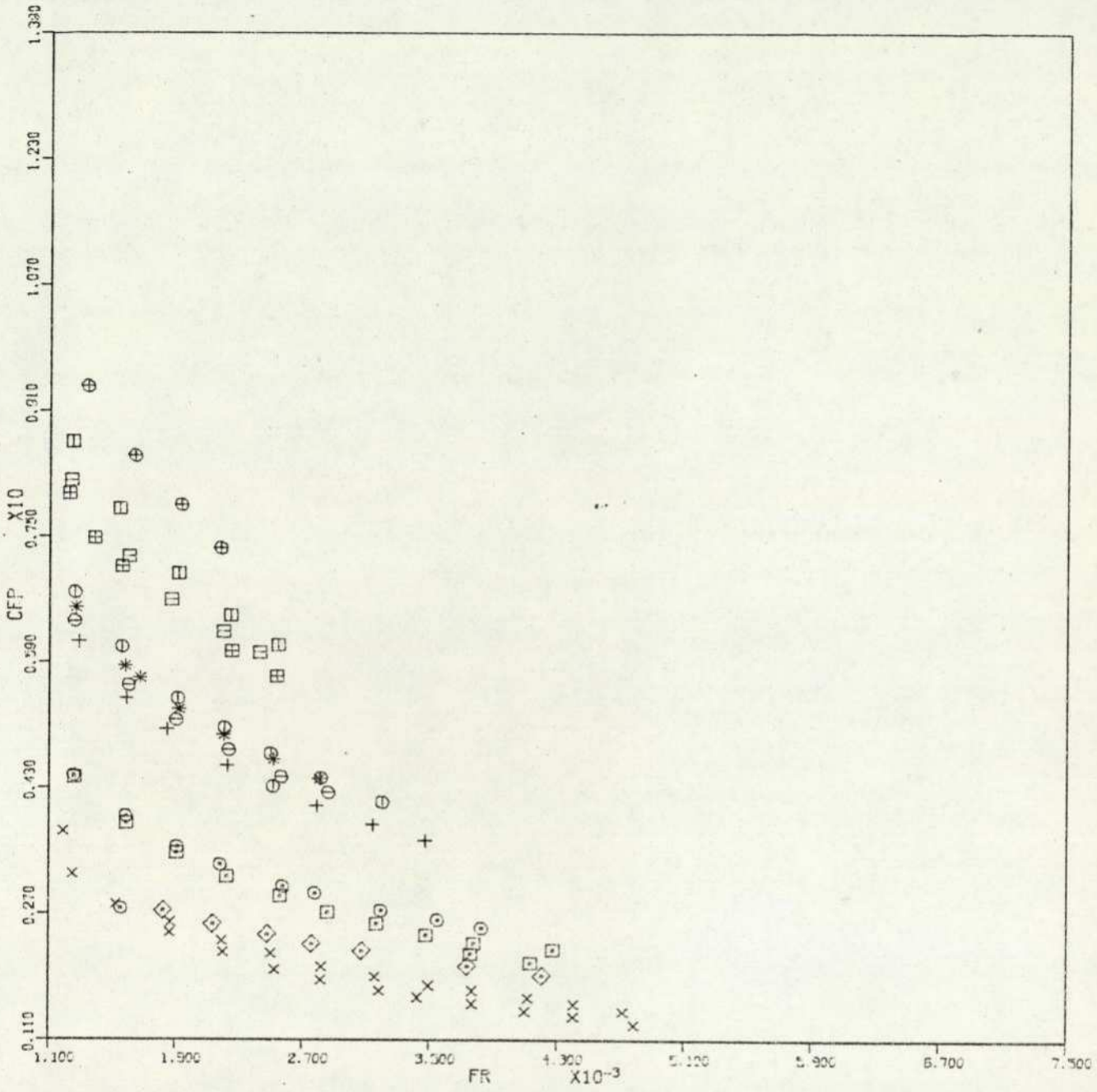

FIGURE : 8.25 PARTICLES FRICTION FACTOR, CFP VS. FROUDE NUMBER, FR.
GLASS BEADS TYPE #4.

CONSTANT PARAMETER(S) : MP, KG/SEC

CURVE 01	×	0.156E-01
CURVE 02*	⊙	0.195E-01
CURVE 03	⊡	0.204E-01
CURVE 04*	◇	0.204E-01
CURVE 05	+	0.294E-01
CURVE 06*	✳	0.290E-01
CURVE 07	⊕	0.312E-01
CURVE 08*	⊖	0.324E-01
CURVE 09	⊞	0.405E-01
CURVE 10*	⊟	0.401E-01
CURVE 11	⊕	0.454E-01
CURVE 12*	⊞	0.453E-01

DATA COMPUTED BY #PDP2. O/P BY #PJ03. PLOTTED BY #PJ04 (04-08-11-14-02-00) .

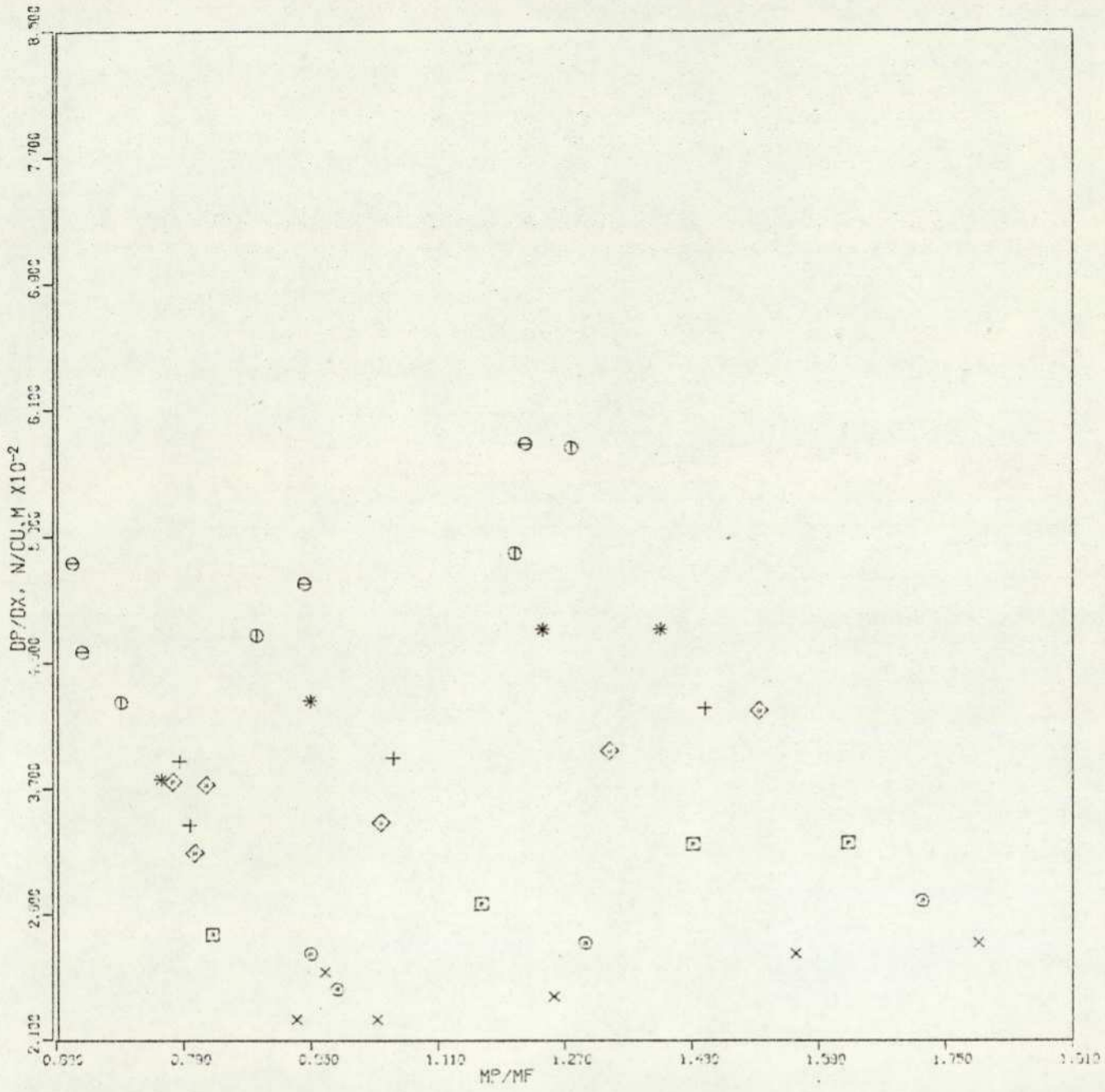

FIGURE : 8.26 PRESSURE GRADIENT, (DP/DX) VS. MASS FLOW RATIO, (MP/MF). GLASS BEADS TYPE #1.

CONSTANT PARAMETER(S) : RE

CURVE 01	×	0.405E 05
CURVE 02*	⊙	0.409E 05
CURVE 03	⊡	0.454E 05
CURVE 04	◇	0.496E 05
CURVE 05*	+	0.494E 05
CURVE 06	✳	0.536E 05
CURVE 07	⊕	0.574E 05
CURVE 08*	⊖	0.576E 05

DATA COMPUTED BY #PDP2, O/P BY #PJ03, PLOTTED BY #PJ04 (01-04-03-14-07-00) .

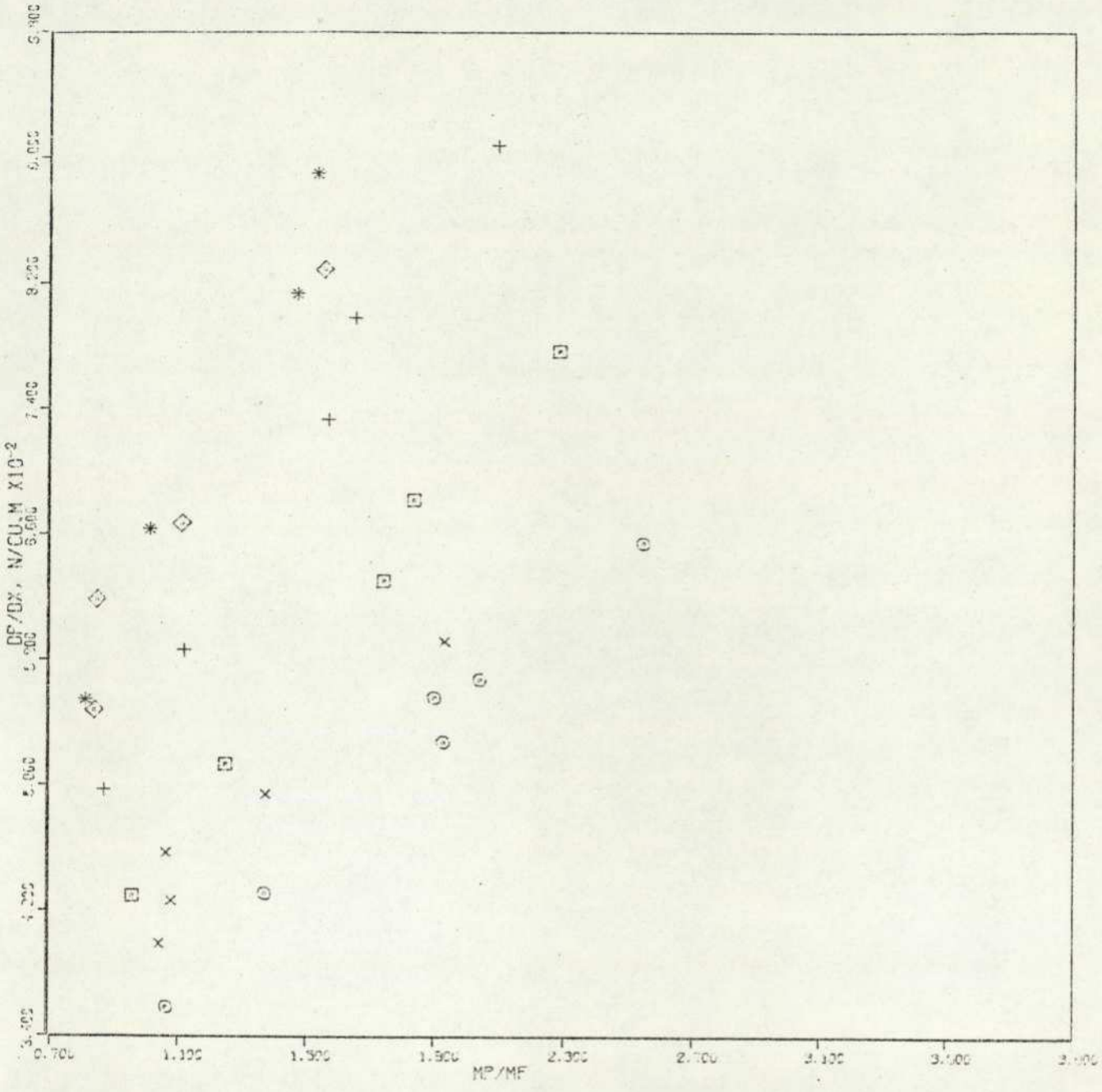

FIGURE : 8.27 PRESSURE GRADIENT, (DP/DX) VS. MASS FLOW RATIO, (MP/MF). GLASS BEADS TYPE #2.

CONSTANT PARAMETER(S) : RE

CURVE 01	×	0.403E 05
CURVE 02*	⊙	0.400E 05
CURVE 03*	⊡	0.447E 05
CURVE 04	◇	0.495E 05
CURVE 05*	+	0.492E 05
CURVE 06*	*	0.528E 05

DATA COMPUTED BY #PDP2, O/P BY #PJ03, PLOTTED BY #PJ04 (02-04-03-14-07-00) .

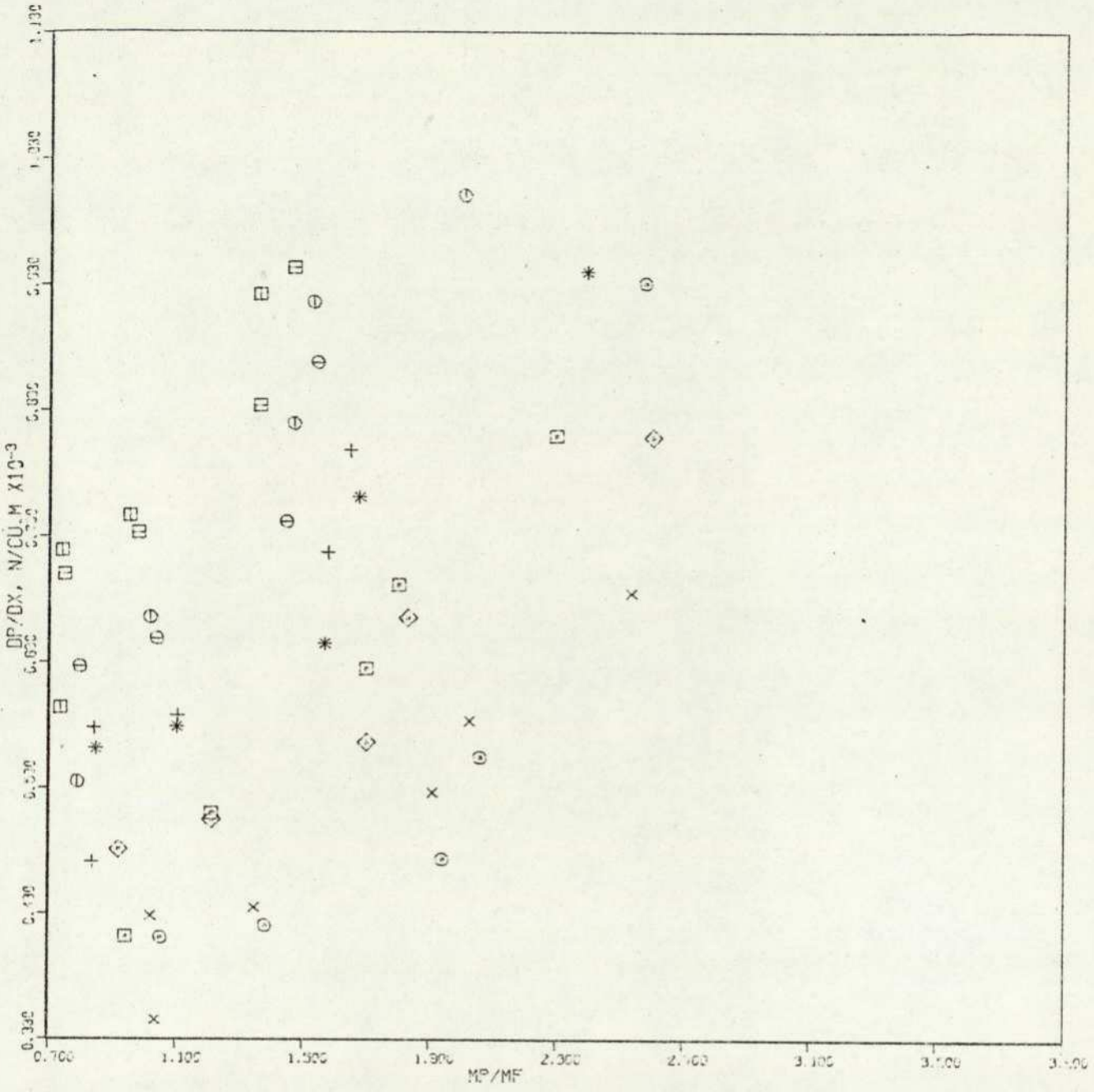

FIGURE :8.28 PRESSURE GRADIENT, (DP/DX) VS. MASS FLOW RATIO, (MP/MF), GLASS BEADS TYPE #3.

CONSTANT PARAMETER(S) : RE

CURVE 01	×	0.408E 05
CURVE 02*	⊙	0.403E 05
CURVE 03	⊡	0.452E 05
CURVE 04*	◈	0.450E 05
CURVE 05	+	0.494E 05
CURVE 06*	*	0.493E 05
CURVE 07	⊕	0.532E 05
CURVE 08*	⊖	0.530E 05
CURVE 09	⊞	0.574E 05
CURVE 10*	⊟	0.566E 05

DATA: COMPUTED BY #PDP2, O/P BY #PJ03, PLOTTED BY #PJ04 (03-04-03-14-07-00) .

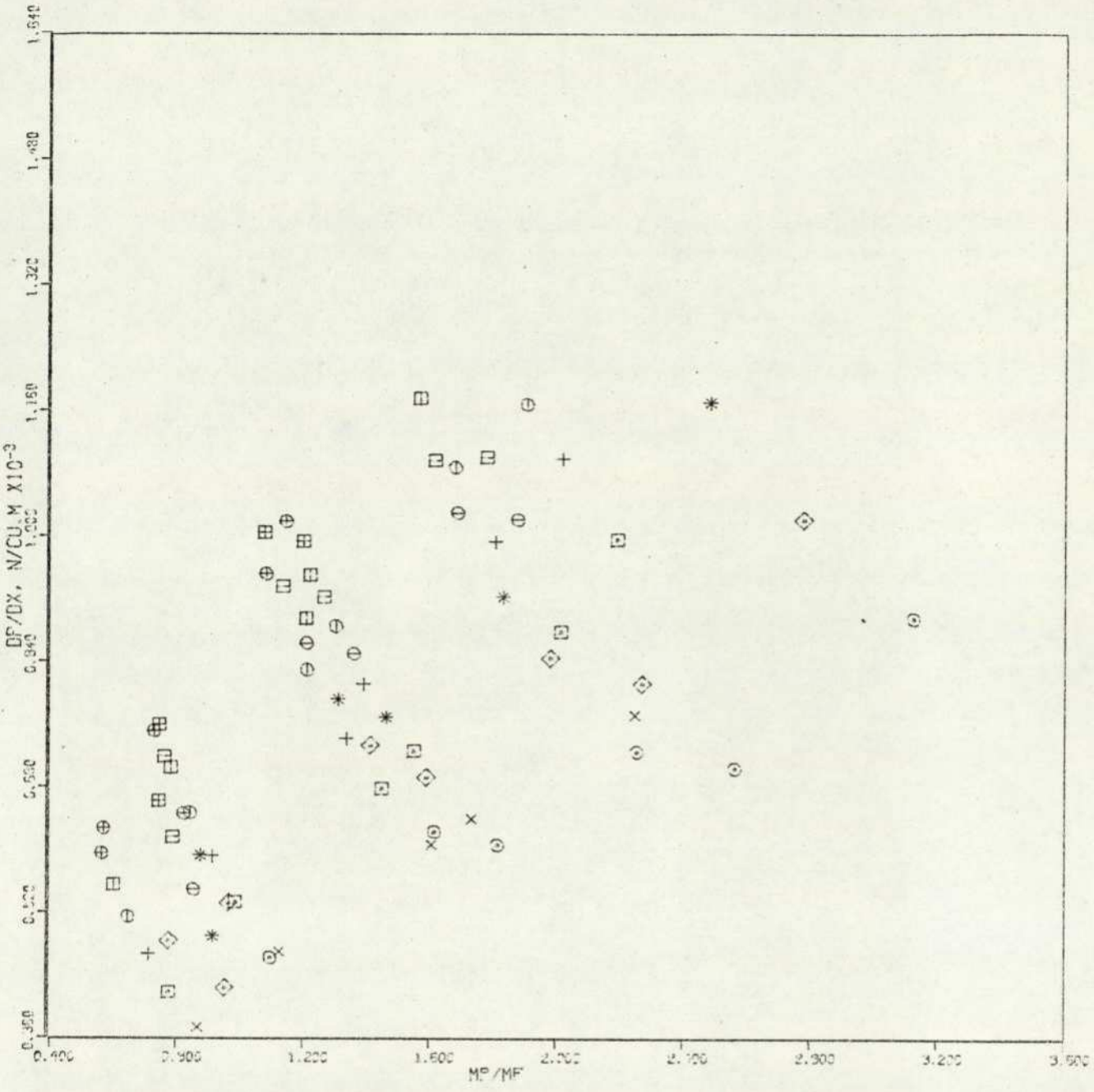

FIGURE : 8.29 PRESSURE GRADIENT, (DP/DX) VS. MASS FLOW RATIO, (MP/MF). GLASS BEADS TYPE #4.

CONSTANT PARAMETER(S) : RE

CURVE 01	×	0.407E 05
CURVE 02*	⊙	0.401E 05
CURVE 03	⊡	0.455E 05
CURVE 04*	◈	0.454E 05
CURVE 05	+	0.498E 05
CURVE 06*	✳	0.498E 05
CURVE 07	⊕	0.533E 05
CURVE 09*	⊖	0.535E 05
CURVE 09	⊞	0.578E 05
CURVE 10*	⊟	0.572E 05
CURVE 11	⊕	0.610E 05
CURVE 12*	⊞	0.605E 05

DATA COMPUTED BY #PDP2, O/P BY #PJ03, PLOTTED BY #PJ04 (01-04-03-14-07-00) .

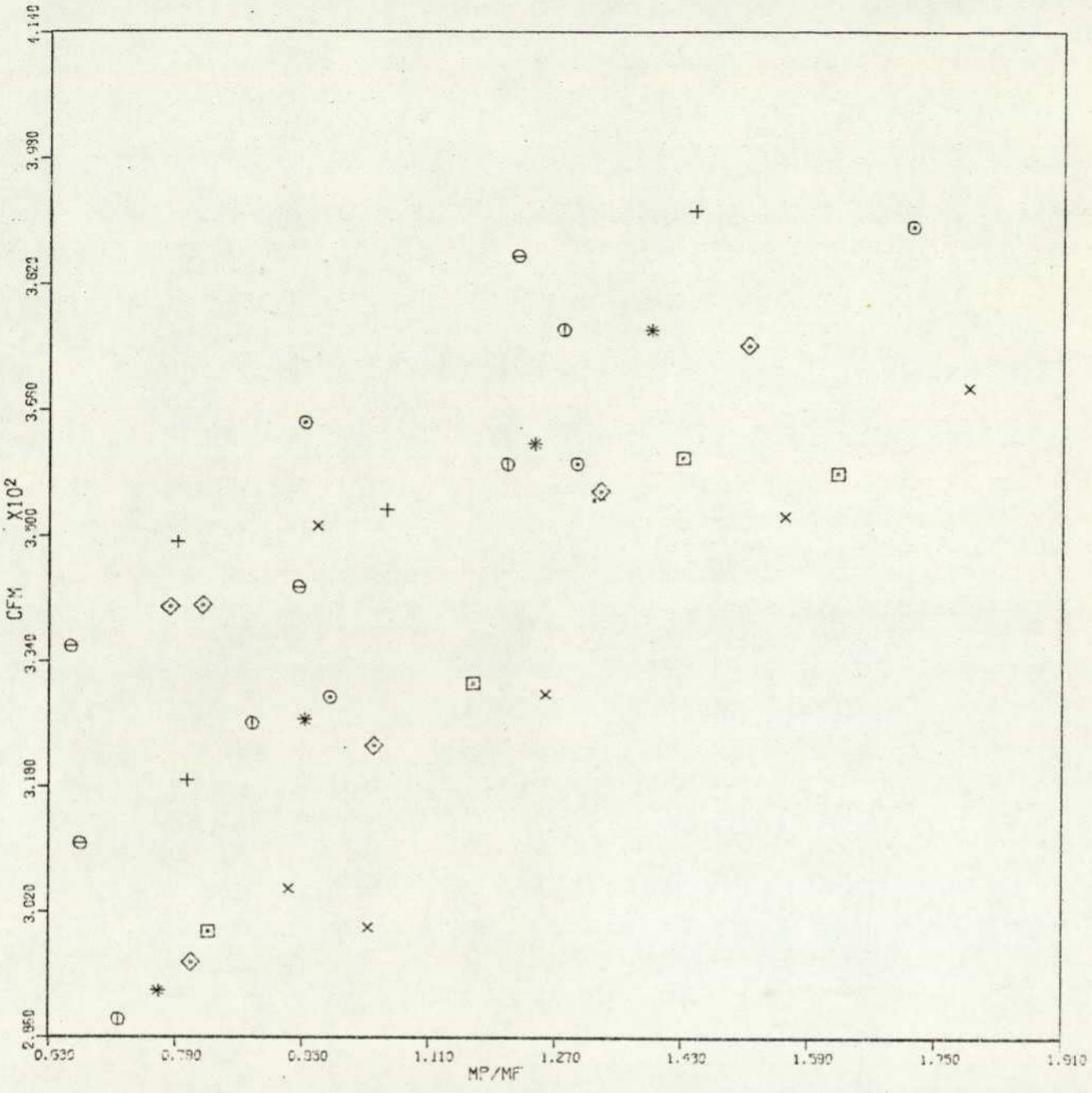

FIGURE : 8.30 SUSPENSION FRICTION FACTOR, CFM VS. MASS FLOW RATIO, (MP/MF). GLASS BEADS TYPE #1.

CONSTANT PARAMETER(S) : RE

CURVE 01	×	0.405E 05
CURVE 02*	⊙	0.408E 05
CURVE 03	⊡	0.454E 05
CURVE 04	◈	0.496E 05
CURVE 05*	+	0.494E 05
CURVE 06	*	0.536E 05
CURVE 07	⊕	0.574E 05
CURVE 08*	⊖	0.578E 05

DATA COMPUTED BY #PDP2. O/P BY #PJ03. PLOTTED BY #PJ04 (01-04-10-14-07-00) .

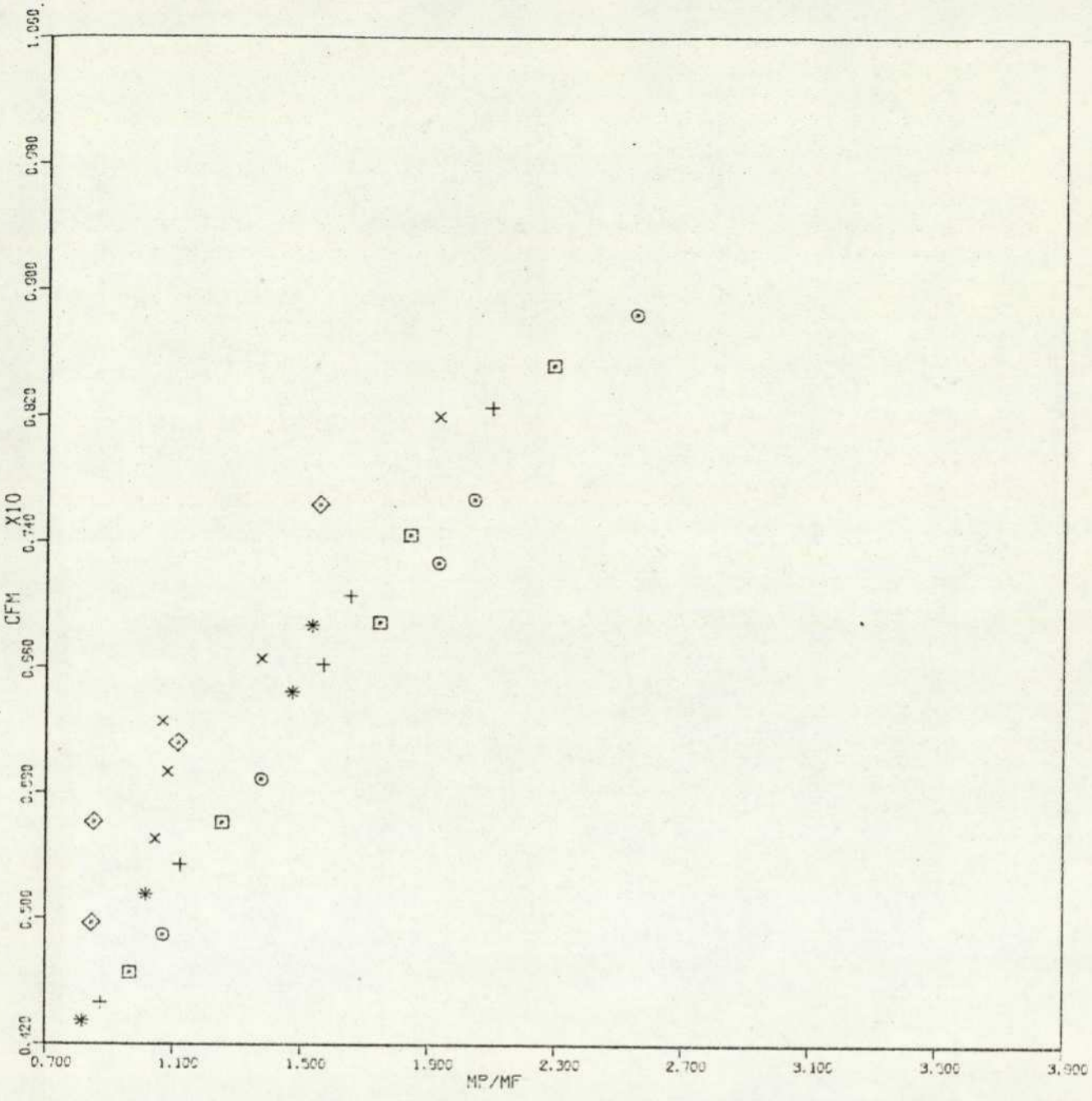

FIGURE : 8.31 SUSPENSION FRICTION FACTOR, CFM VS. MASS FLOW RATIO, (MP/MF). GLASS BEADS TYPE #2.

CONSTANT PARAMETER(S) : RE

CURVE 01	×	0.403E 05
CURVE 02*	⊙	0.400E 05
CURVE 03*	⊡	0.447E 05
CURVE 04	◇	0.495E 05
CURVE 05*	+	0.492E 05
CURVE 06*	*	0.528E 05

DATA COMPUTED BY #PDP2. O/P BY #PJ03. PLOTTED BY #PJ04 (02-04-10-14-07-00) .

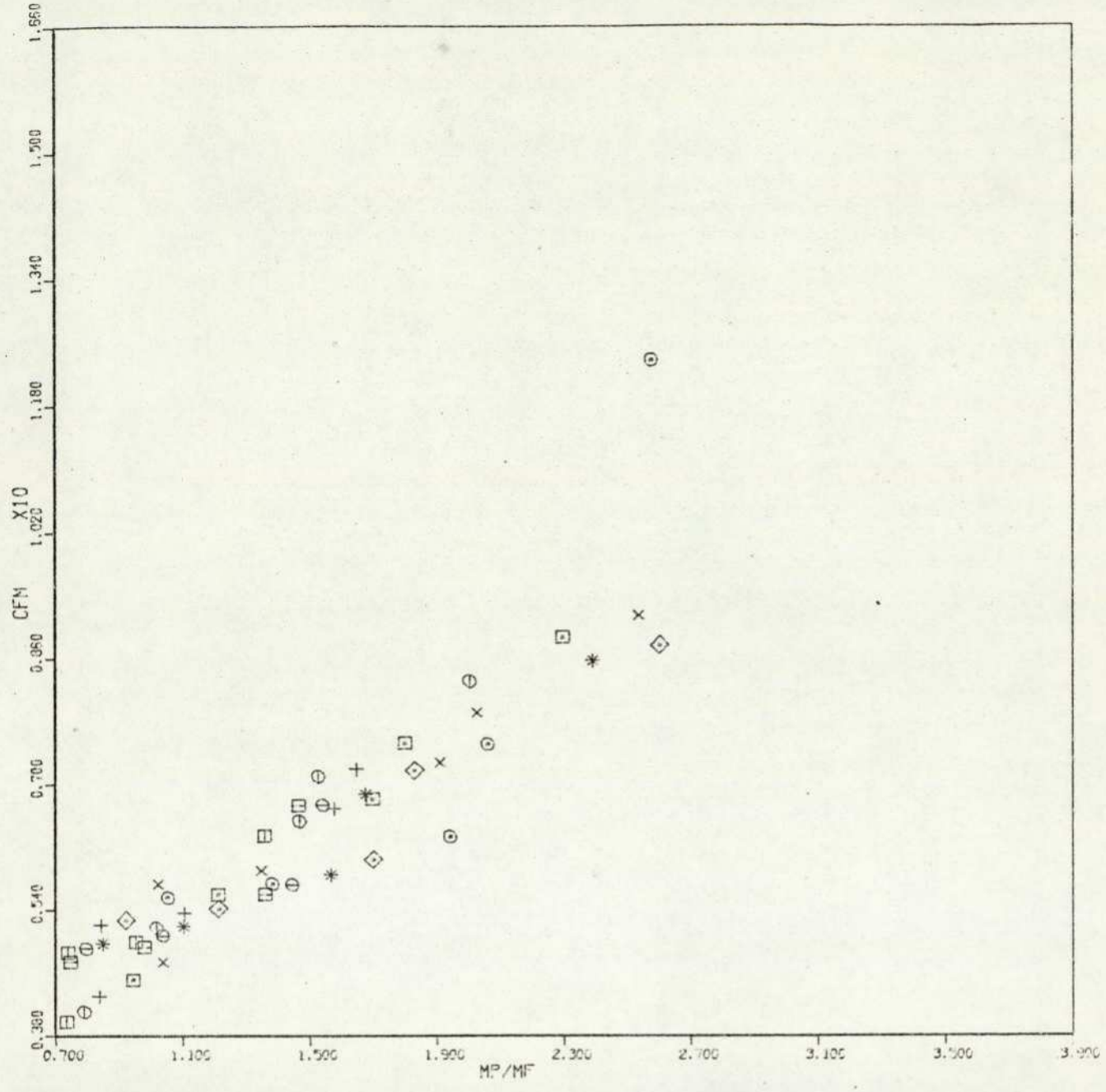

FIGURE : *8.32* SUSPENSION FRICTION FACTOR, CFM VS. MASS FLOW RATIO, (MP/MF). GLASS BEADS TYPE #3.

CONSTANT PARAMETER(S) : RE

CURVE 01	×	0.406E 05
CURVE 02*	⊙	0.403E 05
CURVE 03	⊡	0.452E 05
CURVE 04*	◇	0.450E 05
CURVE 05	+	0.494E 05
CURVE 06*	✳	0.493E 05
CURVE 07	⊕	0.532E 05
CURVE 08*	⊖	0.530E 05
CURVE 09	⊞	0.574E 05
CURVE 10*	⊟	0.566E 05

DATA COMPUTED BY #PDP2. O/P BY #PJ03. PLOTTED BY #PJ04 (03-04-10-14-07-00) .

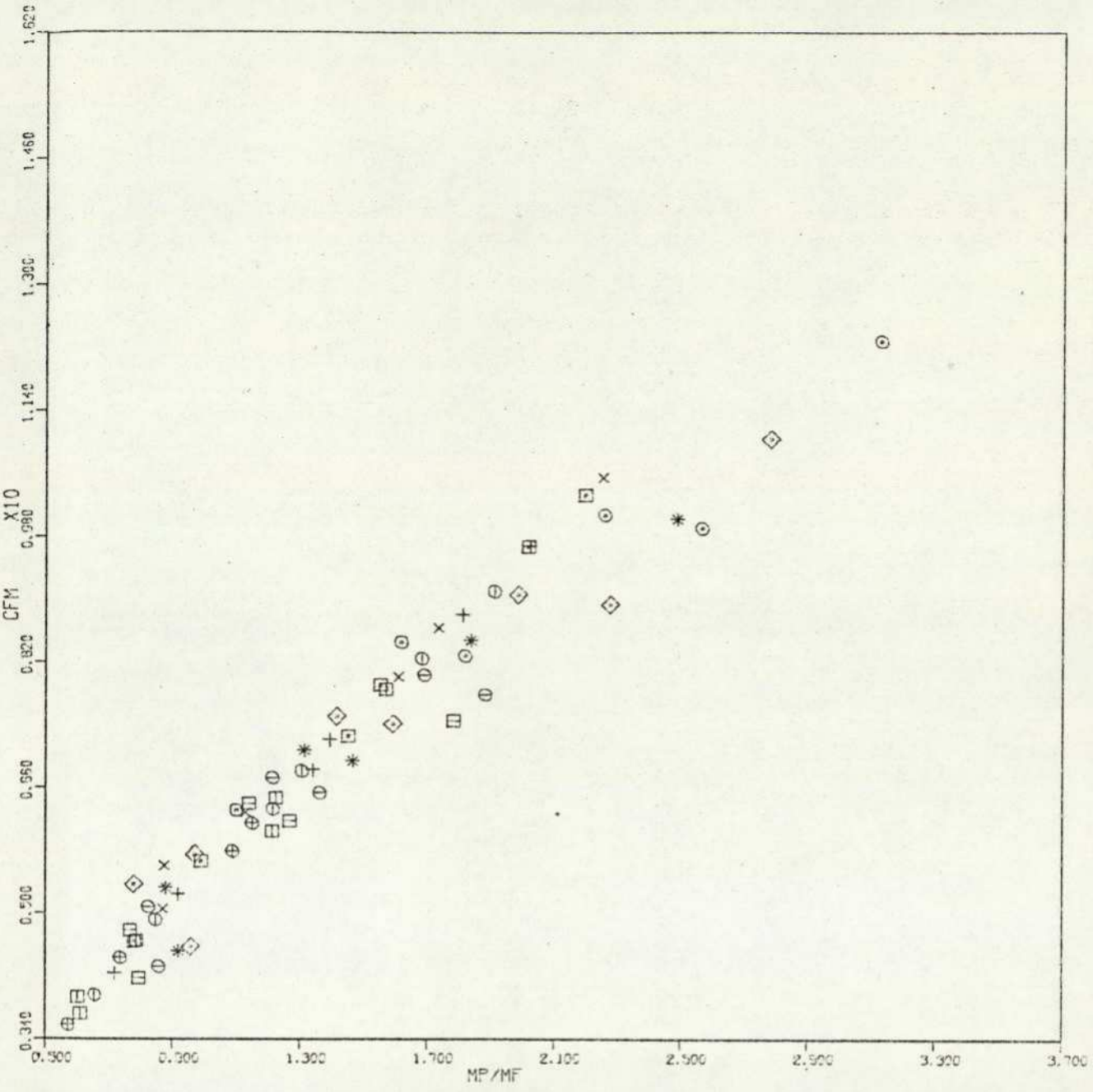

FIGURE :8.33 SUSPENSION FRICTION FACTOR, CFM VS. MASS FLOW RATIO, (MP/MF). GLASS BEADS TYPE #4.

CONSTANT PARAMETER(S) : RE

CURVE 01	×	0.406E 05
CURVE 02*	⊙	0.401E 05
CURVE 03	⊡	0.455E 05
CURVE 04*	◇	0.454E 05
CURVE 05	+	0.499E 05
CURVE 06*	*	0.498E 05
CURVE 07	⊕	0.539E 05
CURVE 08*	⊖	0.535E 05
CURVE 09	⊞	0.577E 05
CURVE 10*	⊟	0.575E 05
CURVE 11	⊕	0.609E 05

DATA COMPUTED BY #PDP2, O/P BY #PJ03, PLOTTED BY #PJ04 (04-04-10-14-07-00) .

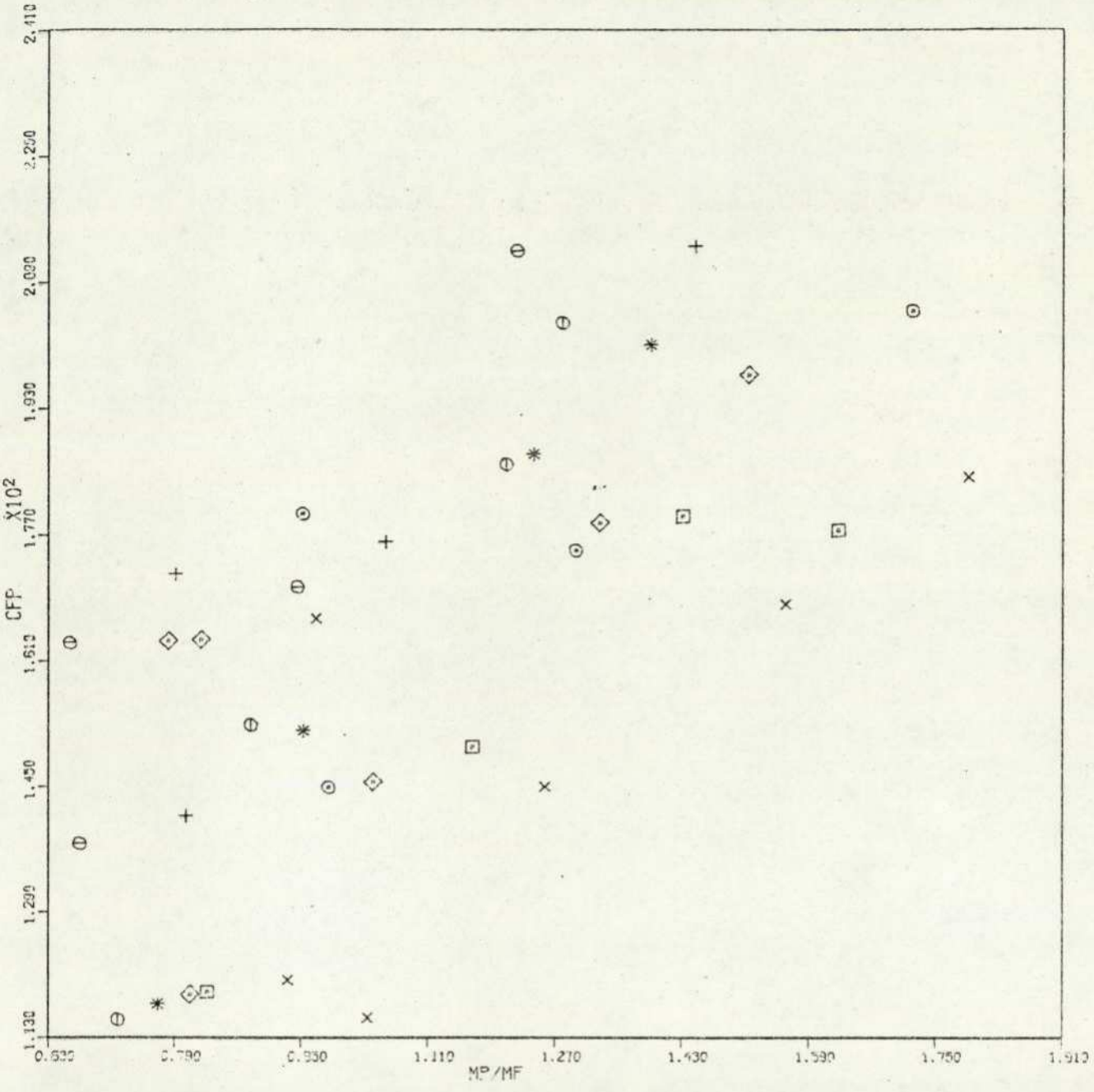

FIGURE : 8.34 PARTICLES FRICTION FACTOR, CFP VS. MASS FLOW RATIO, (MP/MF). GLASS BEADS TYPE #1.

CONSTANT PARAMETER(S) : RE

CURVE 01	×	0.405E 05
CURVE 02*	⊙	0.408E 05
CURVE 03	⊡	0.454E 05
CURVE 04	◇	0.496E 05
CURVE 05*	+	0.494E 05
CURVE 06	*	0.536E 05
CURVE 07	⊕	0.574E 05
CURVE 08*	⊖	0.578E 05

DATA COMPUTED BY #PDP2. O/P BY #PJ03. PLOTTED BY #PJ04 (01-04-11-14-07-00) .

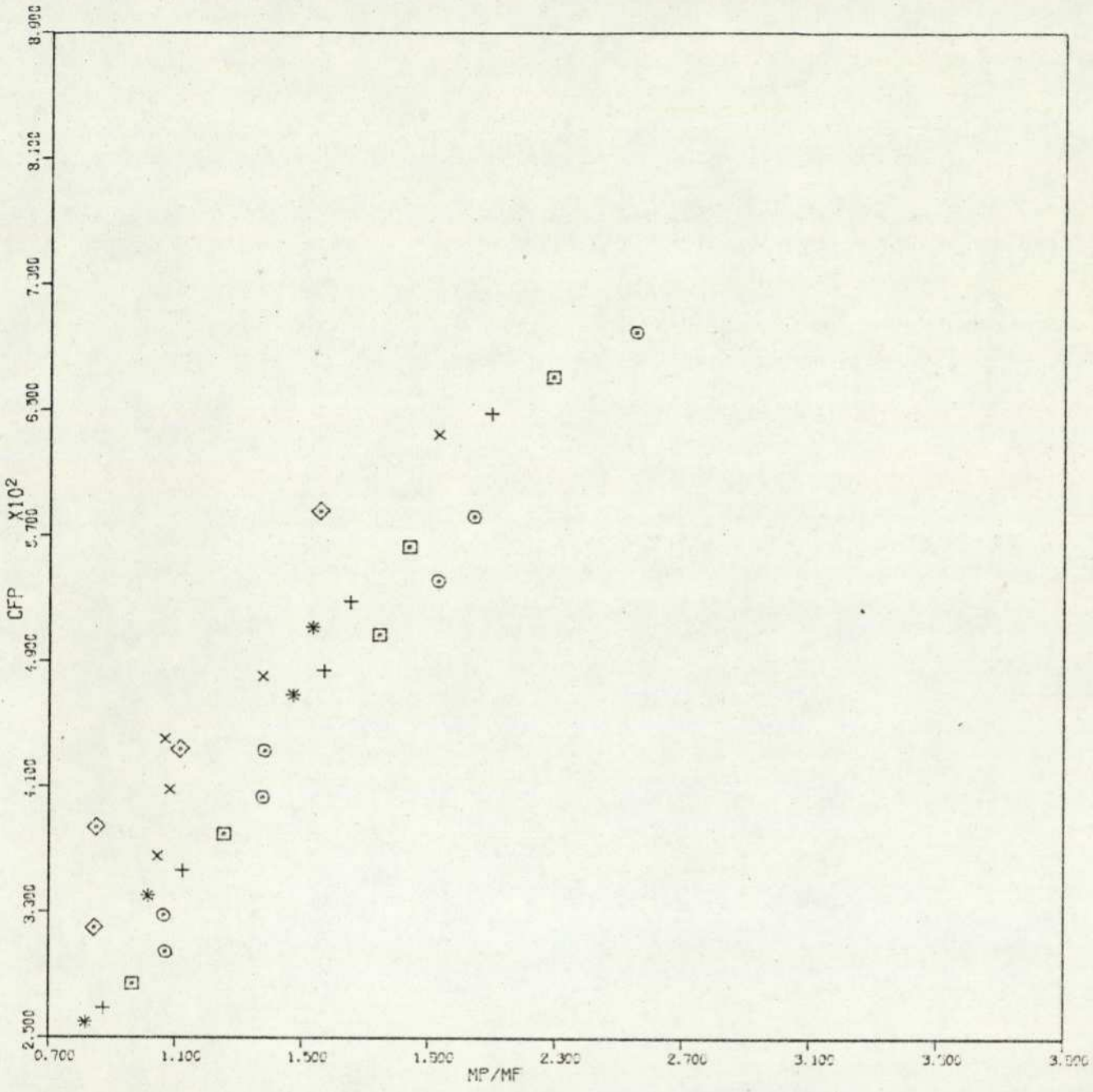

FIGURE :8.35 PARTICLES FRICTION FACTOR, CFP VS. MASS FLOW RATIO, (MP/MF). GLASS BEADS TYPE #2.

CONSTANT PARAMETER(S) : RE

CURVE 01	×	0.403E 05
CURVE 02*	⊙	0.400E 05
CURVE 03*	⊡	0.447E 05
CURVE 04	◇	0.495E 05
CURVE 05*	+	0.492E 05
CURVE 06*	*	0.528E 05

DATA COMPUTED BY #PDP2. O/P BY #PJ03. PLOTTED BY #PJ04 (02-04-11-14-07-00) .

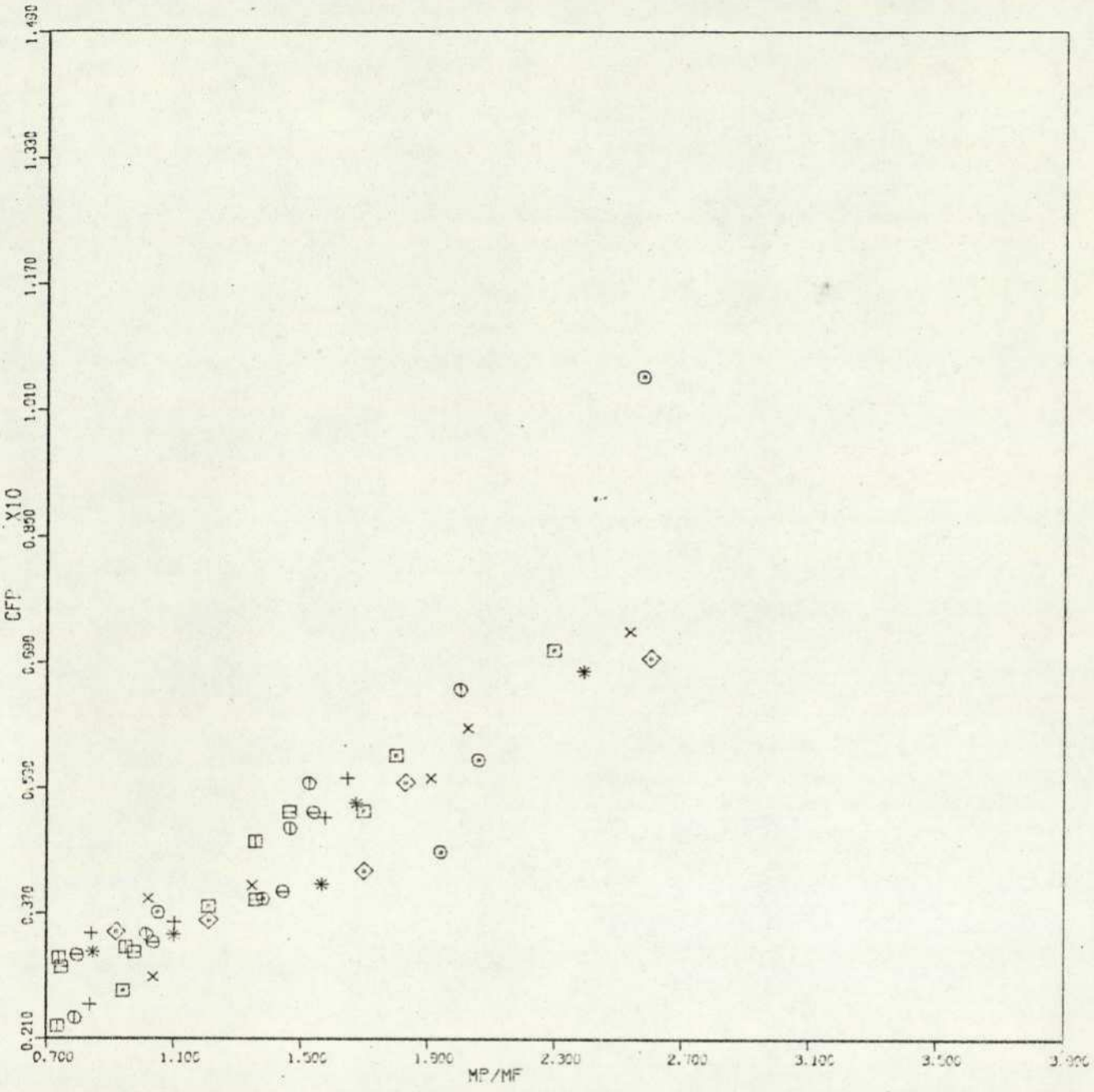

FIGURE : 8.36 PARTICLES FRICTION FACTOR, CFP VS. MASS FLOW RATIO, (MP/MF). GLASS BEADS TYPE #3.

CONSTANT PARAMETER(S) : RE

CURVE 01	×	0.406E 05
CURVE 02*	⊙	0.403E 05
CURVE 03	⊡	0.452E 05
CURVE 04*	◇	0.450E 05
CURVE 05	+	0.494E 05
CURVE 06*	*	0.493E 05
CURVE 07	⊕	0.532E 05
CURVE 08*	⊖	0.530E 05
CURVE 09	⊞	0.574E 05
CURVE 10*	⊟	0.566E 05

DATA COMPUTED BY #PDP2. O/P BY #PJ03. PLOTTED BY #PJ04 (03-04-11-14-07-00) .

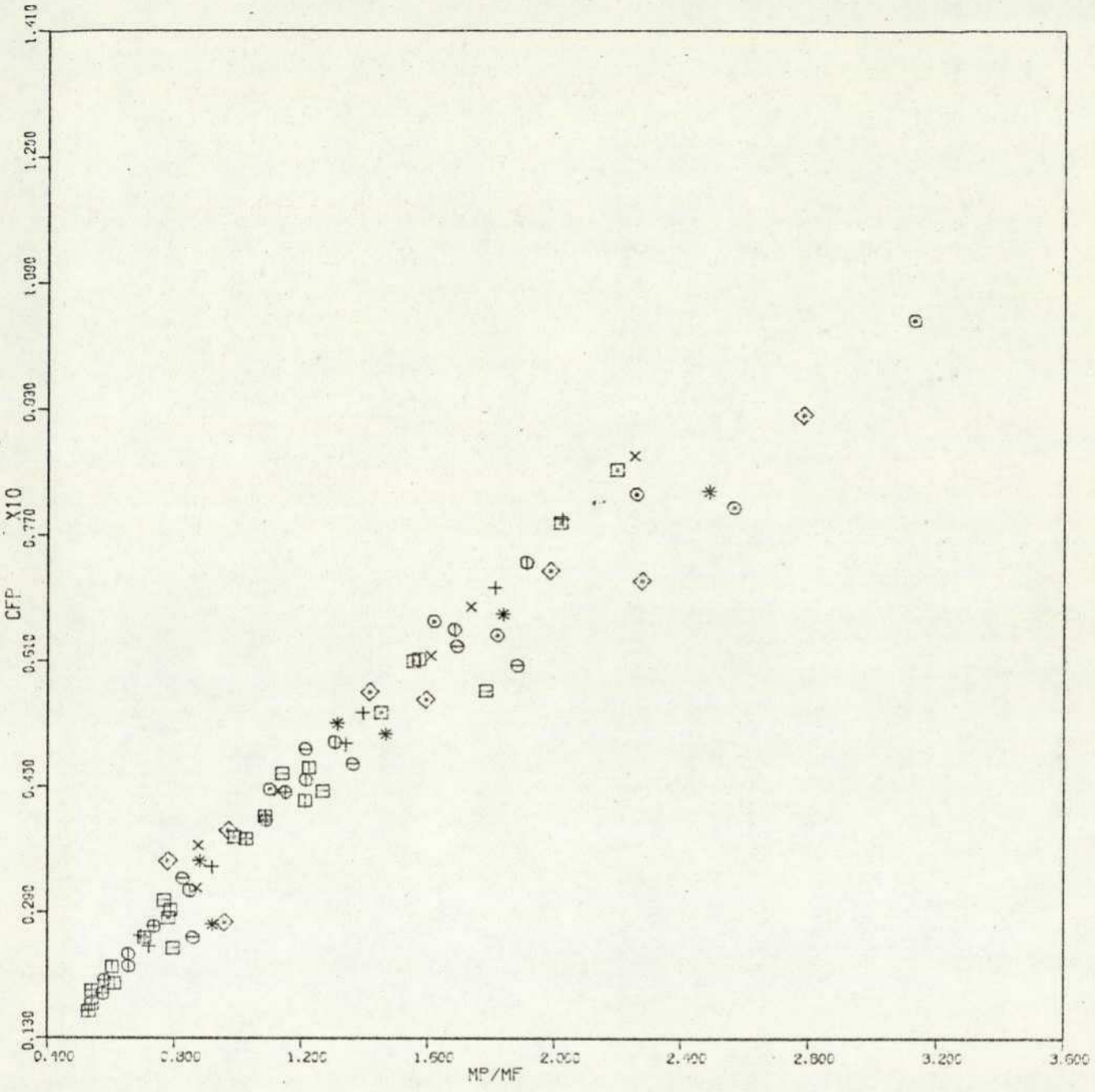

FIGURE : 8.37 PARTICLES FRICTION FACTOR, CFP VS. MASS FLOW RATIO, (MP/MF). GLASS BEADS TYPE #4.

CONSTANT PARAMETER(S) : RE

CURVE 01	×	0.406E 05
CURVE 02*	⊙	0.401E 05
CURVE 03	⊡	0.455E 05
CURVE 04*	◇	0.454E 05
CURVE 05	+	0.499E 05
CURVE 06*	✳	0.498E 05
CURVE 07	⊕	0.539E 05
CURVE 08*	⊖	0.535E 05
CURVE 09	⊞	0.577E 05
CURVE 10*	⊟	0.575E 05
CURVE 11	⊕	0.610E 05
CURVE 12	⊞	0.651E 05

DATA COMPUTED BY #PDP2, O/P BY #PJ03, PLOTTED BY #PJ04 (04-04-11-14-07-00) .

CHARGE CURRENT DATA CORRELATION CURVES

(FIGURES 8.38 - 8.57)

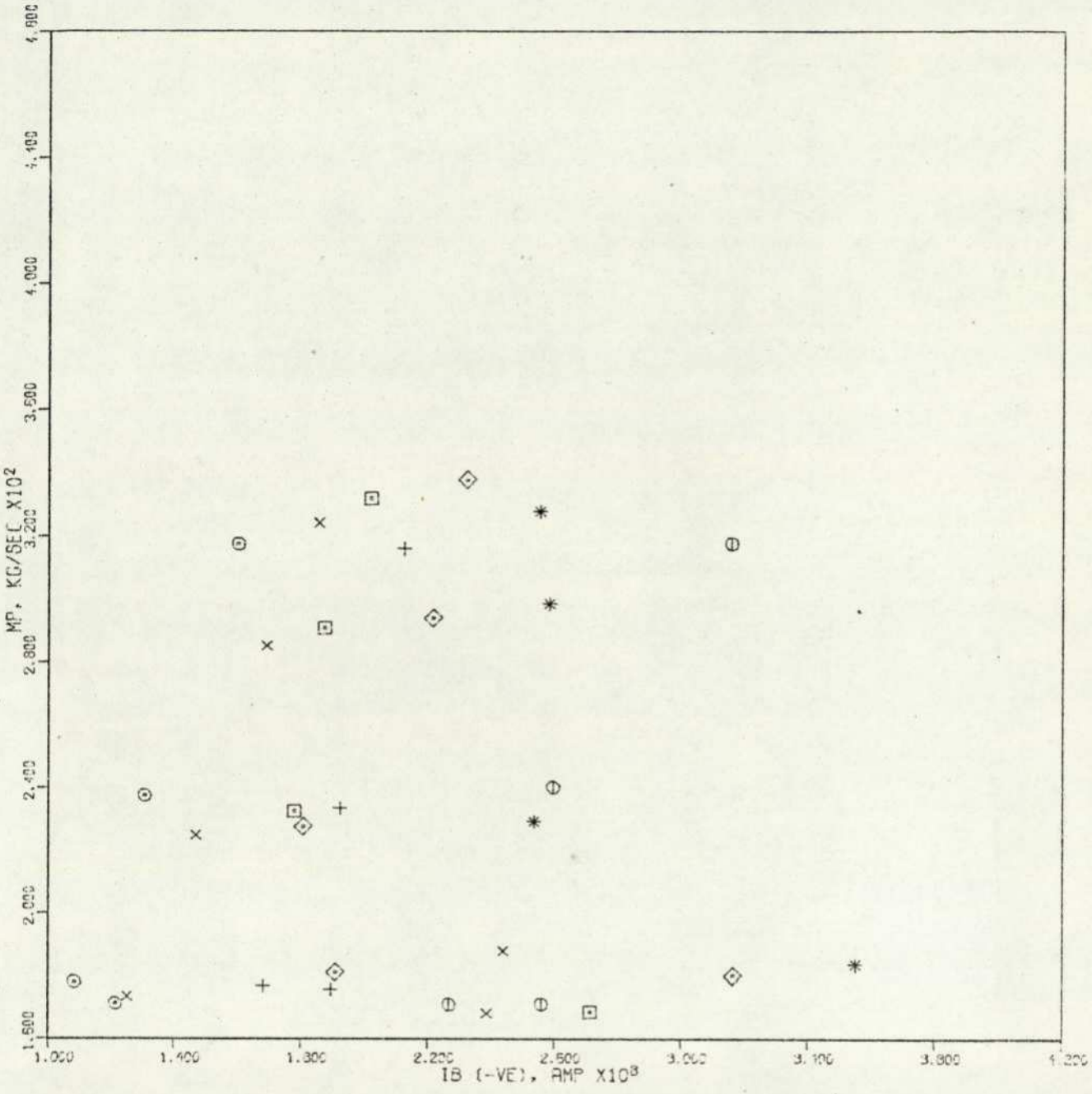

FIGURE : 8.38 MASS FLOW RATE OF PARTICLES, MP VS. BALL PROBE CURRENT, IB. GLASS BEADS TYPE #1.

CONSTANT PARAMETER(S) : RE

CURVE 01	×	0.405E 05
CURVE 02*	⊙	0.408E 05
CURVE 03	⊡	0.454E 05
CURVE 04*	◇	0.496E 05
CURVE 05*	+	0.494E 05
CURVE 06	*	0.536E 05
CURVE 07*	⊕	0.578E 05

DATA COMPUTED BY #PDP2. O/P BY #PJ03. PLOTTED BY #PJ04 (01-12-02-14-07-00) .

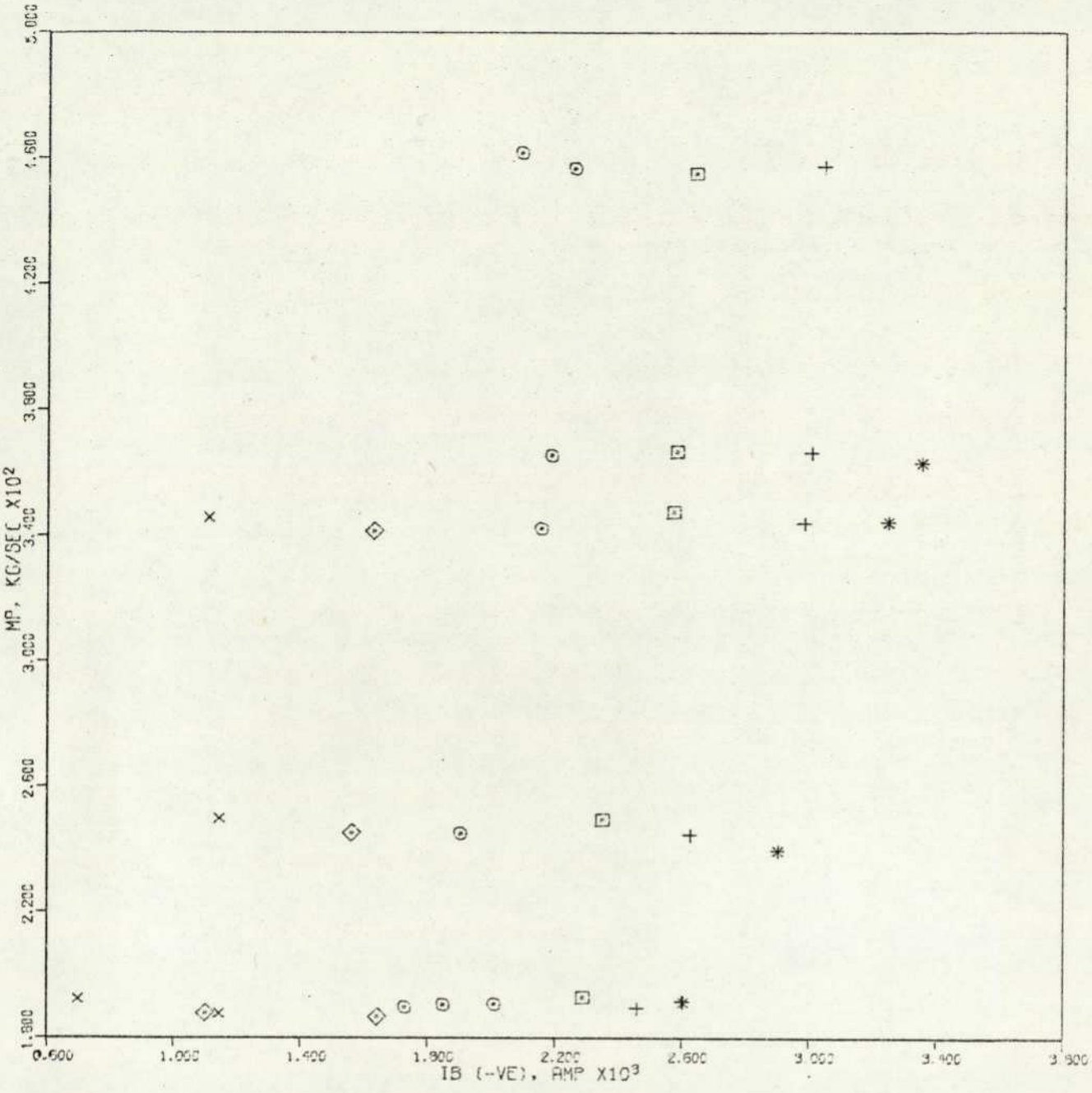

FIGURE : 8.39 MASS FLOW RATE OF PARTICLES, MP VS. BALL PROBE CURRENT, IB. GLASS BEADS TYPE #2.

CONSTANT PARAMETER(S) : RE

CURVE 01	×	0.404E 05
CURVE 02*	⊙	0.400E 05
CURVE 03*	⊡	0.447E 05
CURVE 04	◇	0.495E 05
CURVE 05*	+	0.492E 05
CURVE 06*	*	0.528E 05

DATA COMPUTED BY #PDP2. O/P BY #PJ03. PLOTTED BY #PJ04 (02-12-02-14-07-00) .

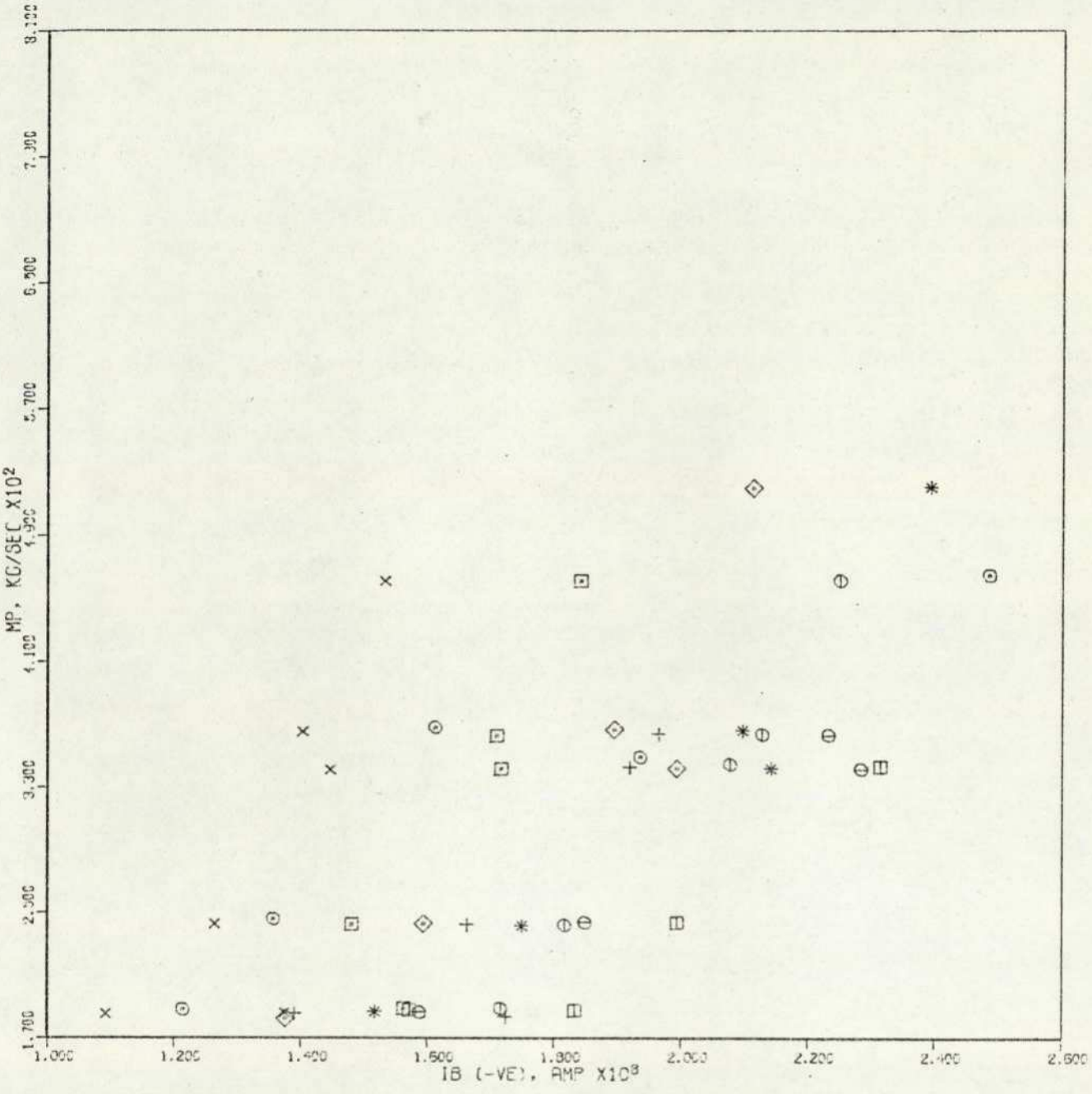

FIGURE : 8.40 MASS FLOW RATE OF PARTICLES, MP VS. BALL PROBE CURRENT, IB. GLASS BEADS TYPE #3.

CONSTANT PARAMETER(S) : RE

CURVE 01	×	0.406E 05
CURVE 02*	⊙	0.403E 05
CURVE 03	⊡	0.452E 05
CURVE 04*	◇	0.450E 05
CURVE 05	+	0.494E 05
CURVE 06*	✳	0.493E 05
CURVE 07	⊕	0.532E 05
CURVE 08*	⊖	0.530E 05
CURVE 09	⊞	0.574E 05

DATA COMPUTED BY #PDP2. O/P BY #PJ03. PLOTTED BY #PJ04 (03-12-02-14-07-00) .

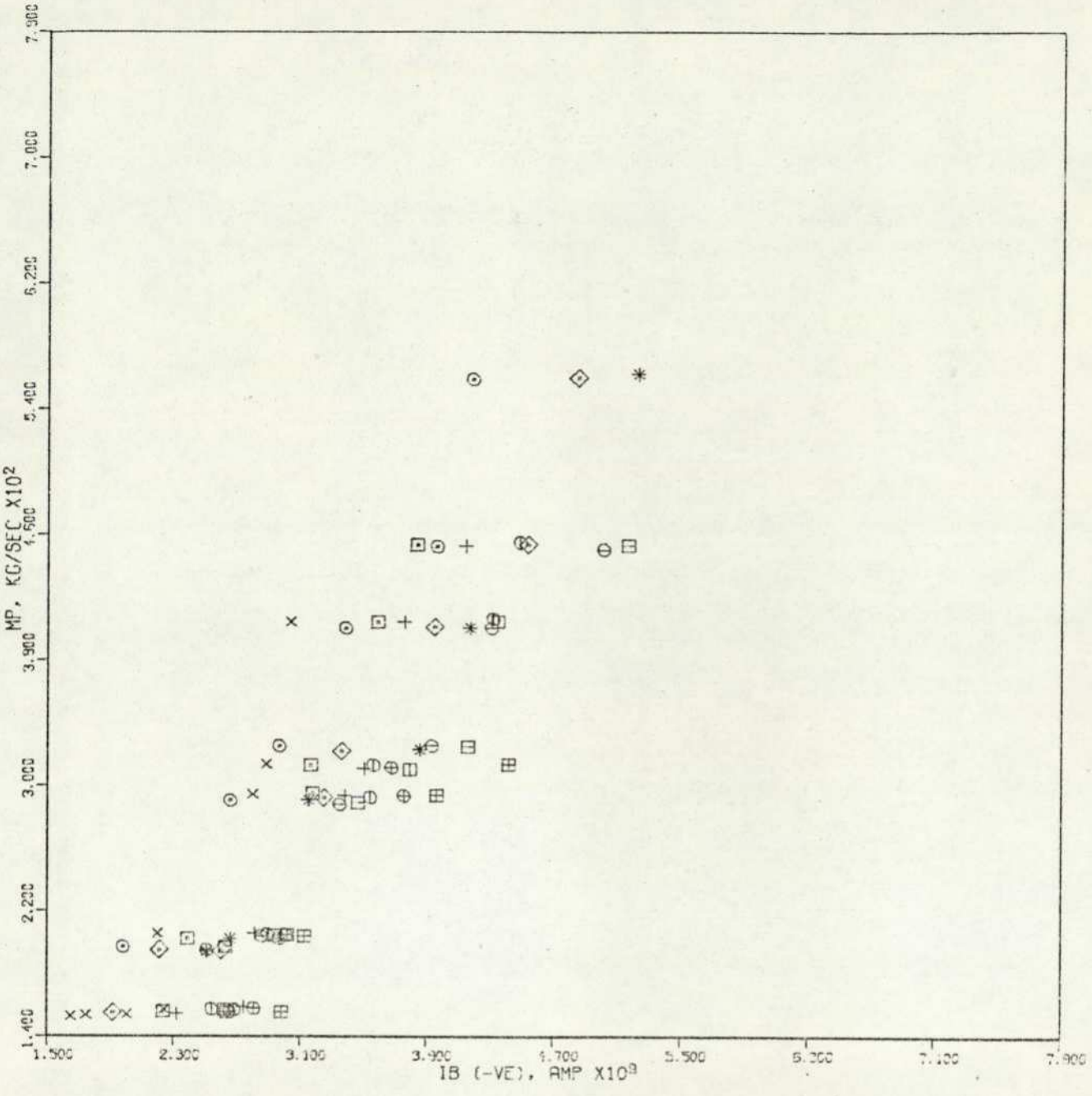

FIGURE : 8.41 MASS FLOW RATE OF PARTICLES, MP VS. BALL PROBE CURRENT, IB. GLASS BEADS TYPE #4.

CONSTANT PARAMETER(S) : RE

CURVE 01	×	0.405E 05
CURVE 02*	⊙	0.401E 05
CURVE 03	⊡	0.455E 05
CURVE 04*	◇	0.454E 05
CURVE 05	+	0.499E 05
CURVE 06*	✳	0.498E 05
CURVE 07	⊕	0.539E 05
CURVE 08*	⊖	0.535E 05
CURVE 09	⊞	0.578E 05
CURVE 10*	⊟	0.575E 05
CURVE 11	⊕	0.610E 05
CURVE 12	⊞	0.647E 05

DATA COMPUTED BY #PDP2. O/P BY #PJ03. PLOTTED BY #PJ04 (04-12-02-14-07-00) .

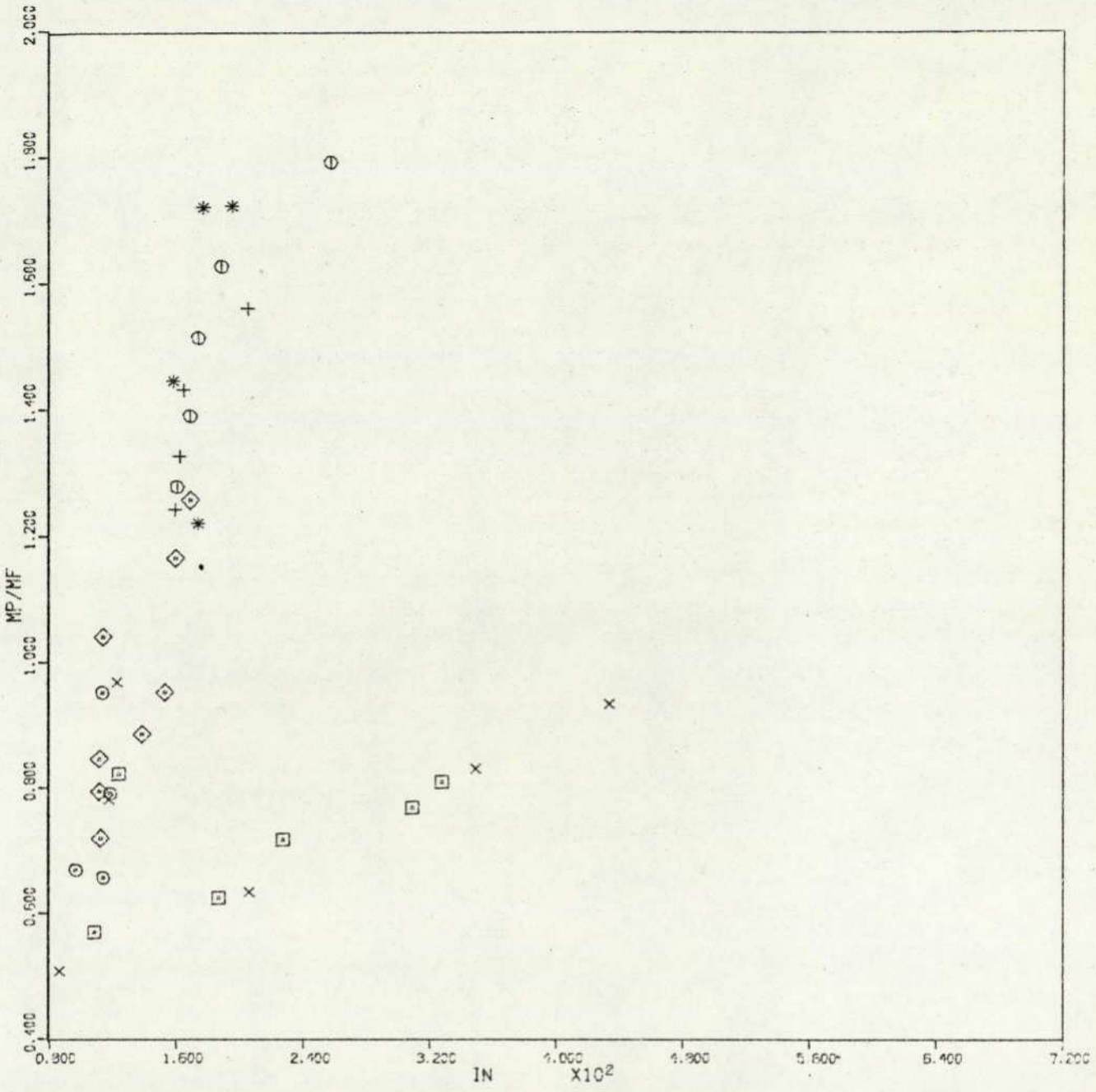

FIGURE : 8.42 MASS FLOW RATIO, (MP/MF) VS. DIMENSIONLESS CURRENT NUMBER, IN. GLASS BEADS TYPE #1.

CONSTANT PARAMETER(S) : MP, KG/SEC

CURVE 01	×	0.172E-01
CURVE 02*	⊙	0.172E-01
CURVE 03	⊡	0.181E-01
CURVE 04	◈	0.228E-01
CURVE 05	+	0.292E-01
CURVE 06*	✳	0.317E-01
CURVE 07	⊕	0.332E-01

DATA COMPUTED BY #PDP2, O/P BY #PJ03, PLOTTED BY #PJ04 (01-13-04-00-02-00) .

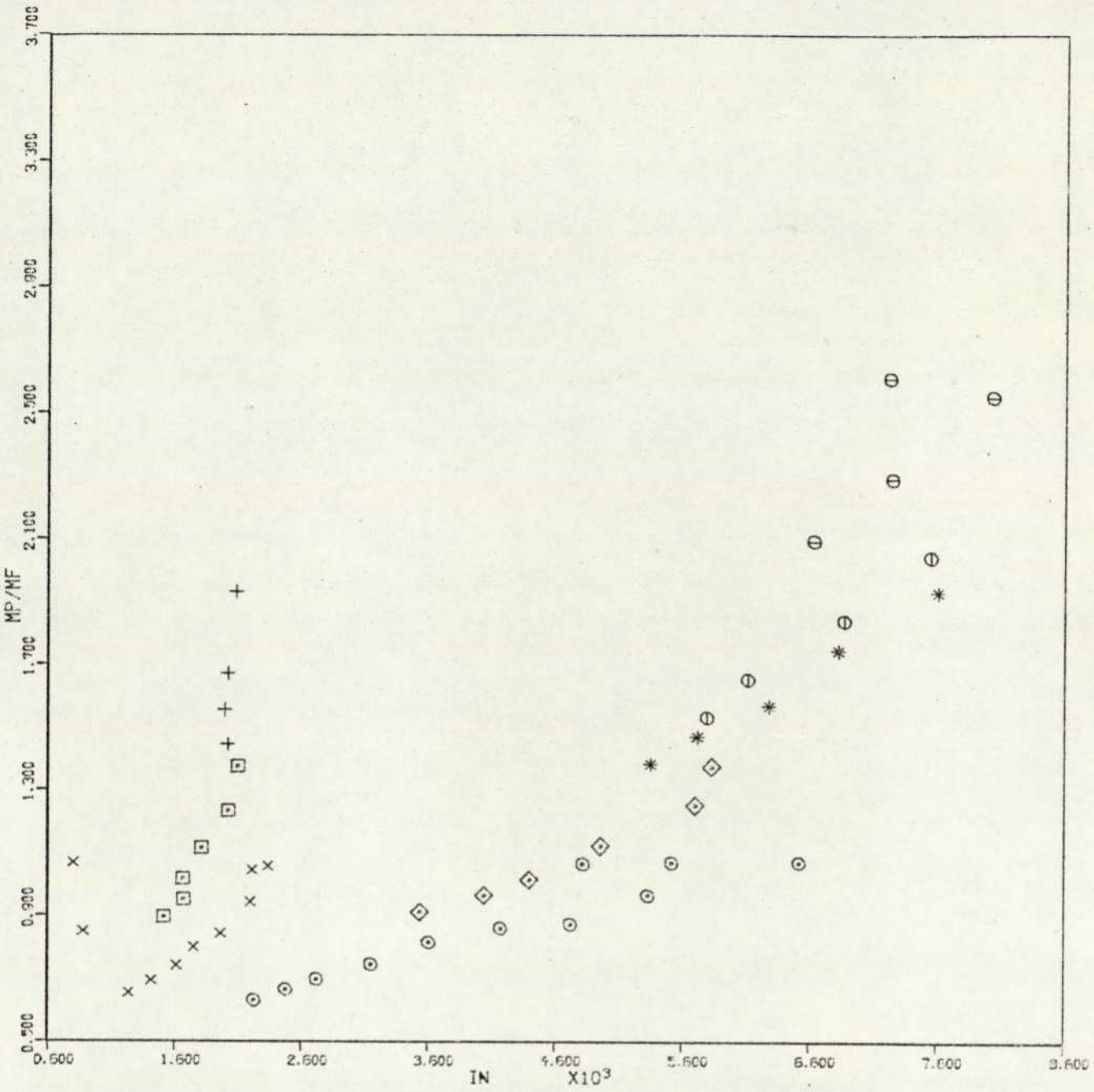

FIGURE : 8.43 MASS FLOW RATIO, (MP/MF) VS. DIMENSIONLESS CURRENT NUMBER, IN. GLASS BEADS TYPE #2.

CONSTANT PARAMETER(S) : MP, KG/SEC

CURVE 01	×	0.189E-01
CURVE 02*	⊙	0.190E-01
CURVE 03	⊡	0.246E-01
CURVE 04*	◇	0.245E-01
CURVE 05	+	0.343E-01
CURVE 06*	✳	0.344E-01
CURVE 07*	⊖	0.365E-01
CURVE 08*	⊖	0.458E-01

DATA COMPUTED BY #PDP2. O/P BY #PJ03. PLOTTED BY #PJ04 (02-13-04-00-02-00) .

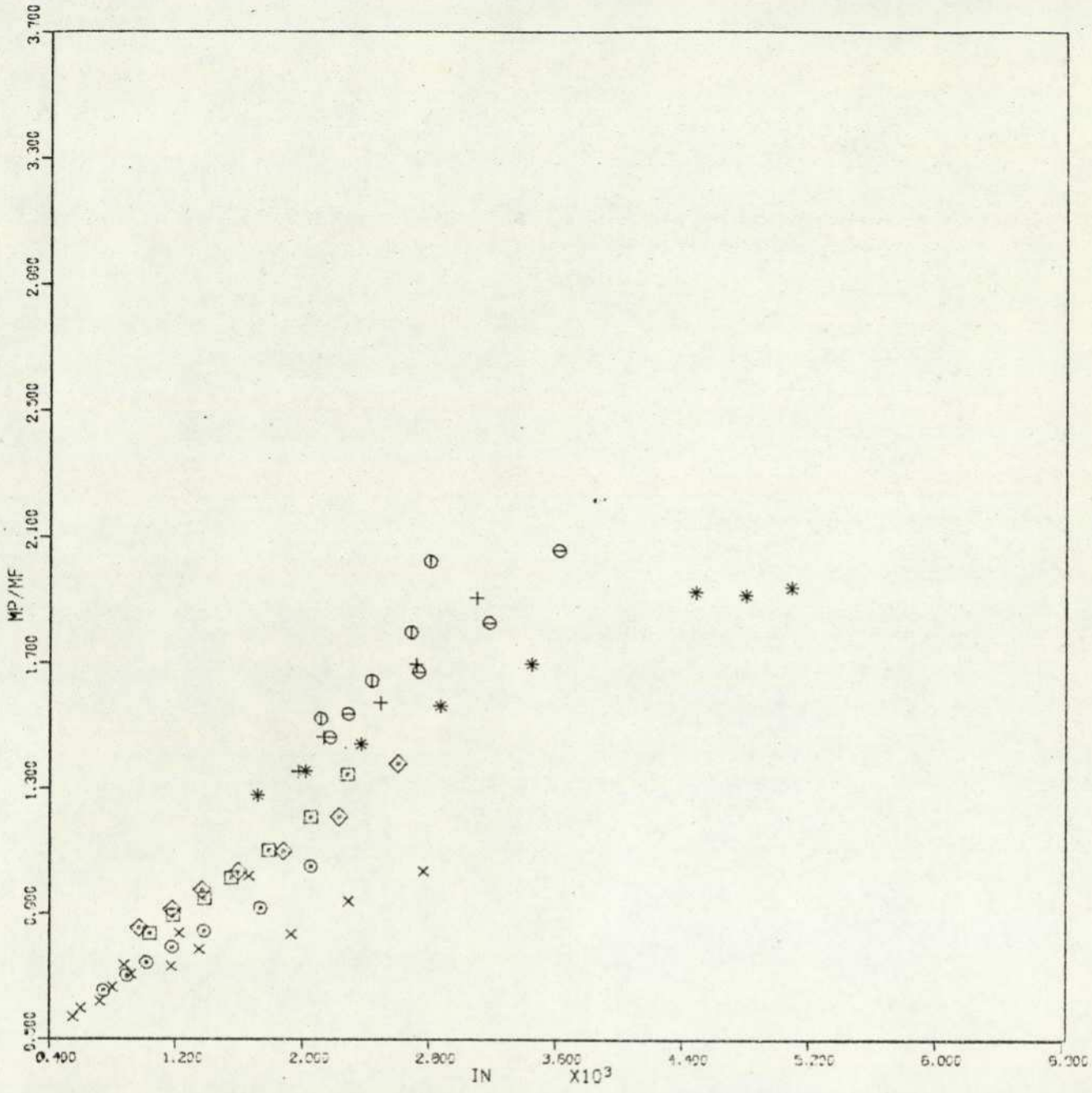

FIGURE 8.44 MASS FLOW RATIO, (MP/MF) VS. DIMENSIONLESS CURRENT NUMBER, IN. GLASS BEADS TYPE #3.

CONSTANT PARAMETER(S) : MP, KG/SEC

CURVE 01	×	0.188E-01
CURVE 02*	⊙	0.187E-01
CURVE 03	⊡	0.243E-01
CURVE 04*	◈	0.245E-01
CURVE 05	+	0.343E-01
CURVE 06*	✳	0.344E-01
CURVE 07	⊕	0.364E-01
CURVE 08*	⊖	0.365E-01

DATA COMPUTED BY #PDP2, O/P BY #PJ03, PLOTTED BY #PJ04 (03-13-04-00-02-00) .

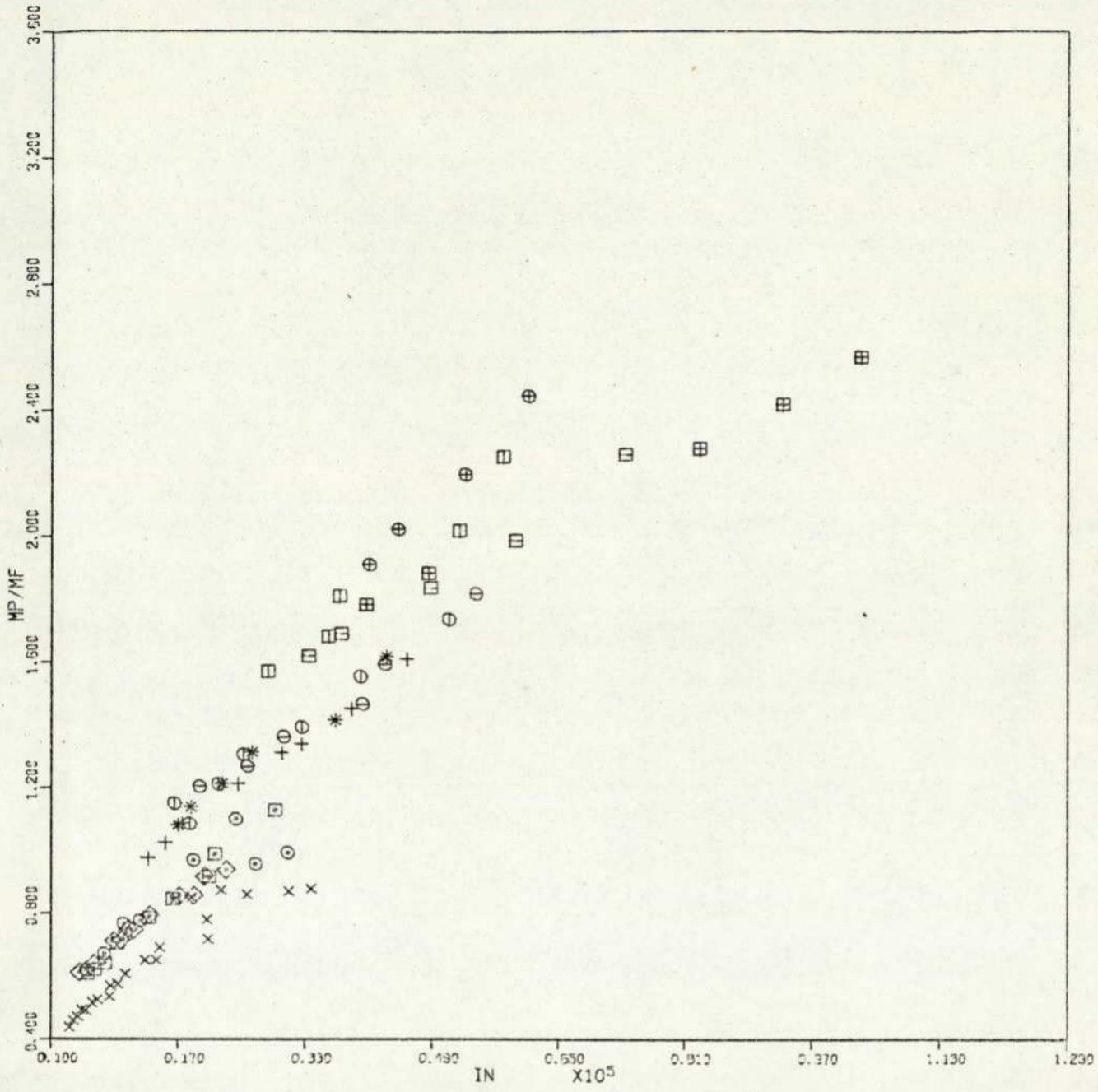

FIGURE :8.45 MASS FLOW RATIO, (MP/MF) VS. DIMENSIONLESS CURRENT NUMBER, IN. GLASS BEADS TYPE #4.

CONSTANT PARAMETER(S) : MP, KG/SEC

CURVE 01	×	0.156E-01
CURVE 02*	⊙	0.196E-01
CURVE 03	⊡	0.204E-01
CURVE 04*	◈	0.204E-01
CURVE 05	+	0.294E-01
CURVE 06*	✳	0.290E-01
CURVE 07	⊕	0.312E-01
CURVE 08*	⊖	0.324E-01
CURVE 09	⊞	0.405E-01
CURVE 10*	⊟	0.401E-01
CURVE 11	⊕	0.454E-01
CURVE 12*	⊞	0.453E-01

DATA COMPUTED BY #PDP2, O/P BY #PJ03, PLOTTED BY #PJ04 (04-13-04-00-02-00) .

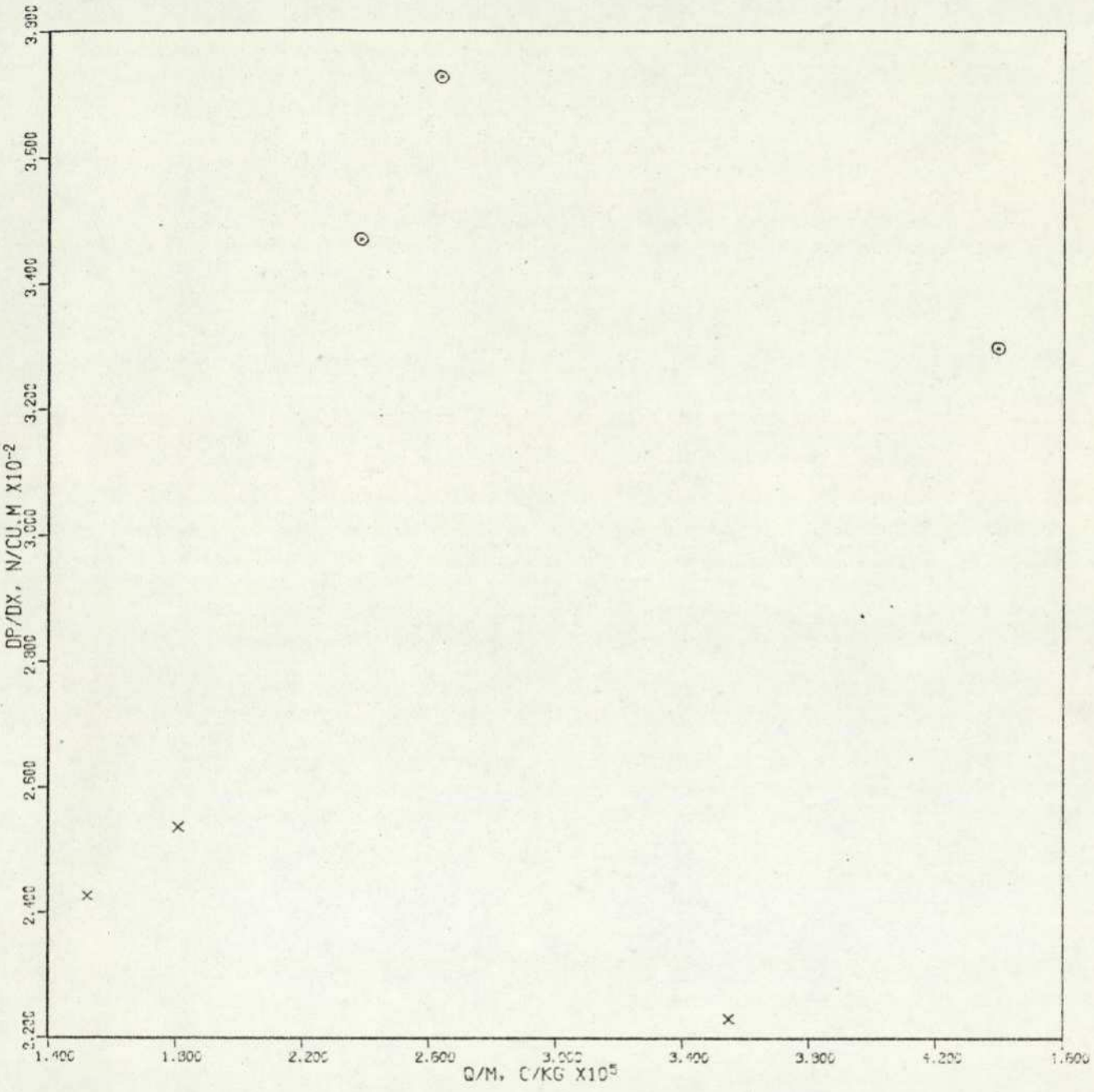

FIGURE 8.46 EFFECT OF ELECTROSTATIC CHARGE ON PRESSURE GRADIENT. GLASS BEADS TYPE #1.

CONSTANT PARAMETER(S) :		RE	MP, KG/SEC
CURVE 01	×	0.404E 05	0.173E-01
CURVE 02	⊙	0.495E 05	0.179E-01

DATA COMPUTED BY #PDP2. O/P BY #PJ03. PLOTTED BY #PJ04 (01-14-09-00-07-02) .

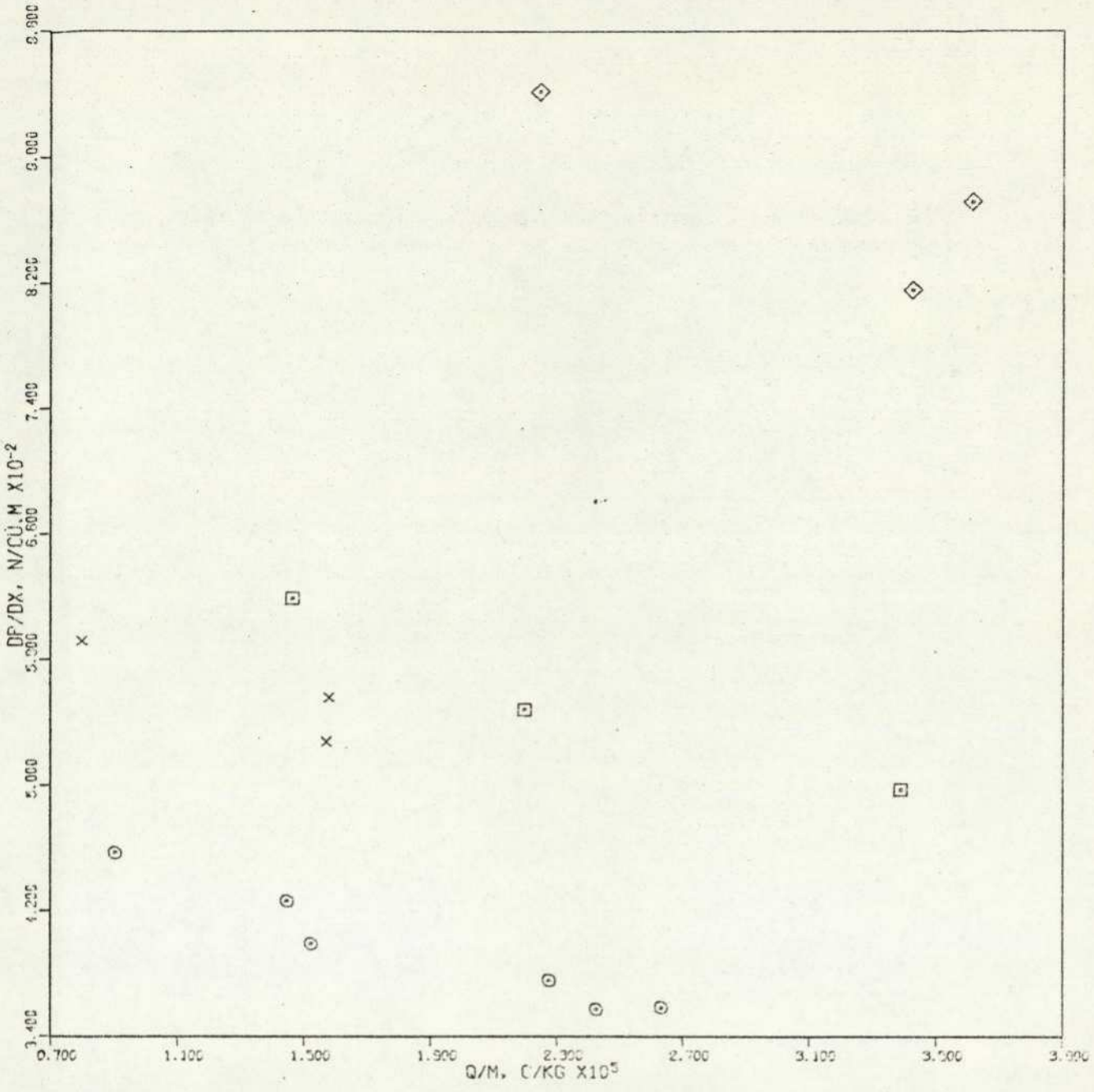

FIGURE :8.47 EFFECT OF ELECTROSTATIC CHARGE ON PRESSURE GRADIENT. GLASS BEADS TYPE #2.

CONSTANT PARAMETER(S) :		RE	MP, KG/SEC
CURVE 01	×	0.401E 05	0.343E-01
CURVE 02	⊙	0.401E 05	0.191E-01
CURVE 03	⊡	0.495E 05	0.189E-01
CURVE 04	◈	0.612E 05	0.245E-01

DATA COMPUTED BY #PDP2, O/P BY #PJ03, PLOTTED BY #PJ04 (02-14-09-00-07-02) .

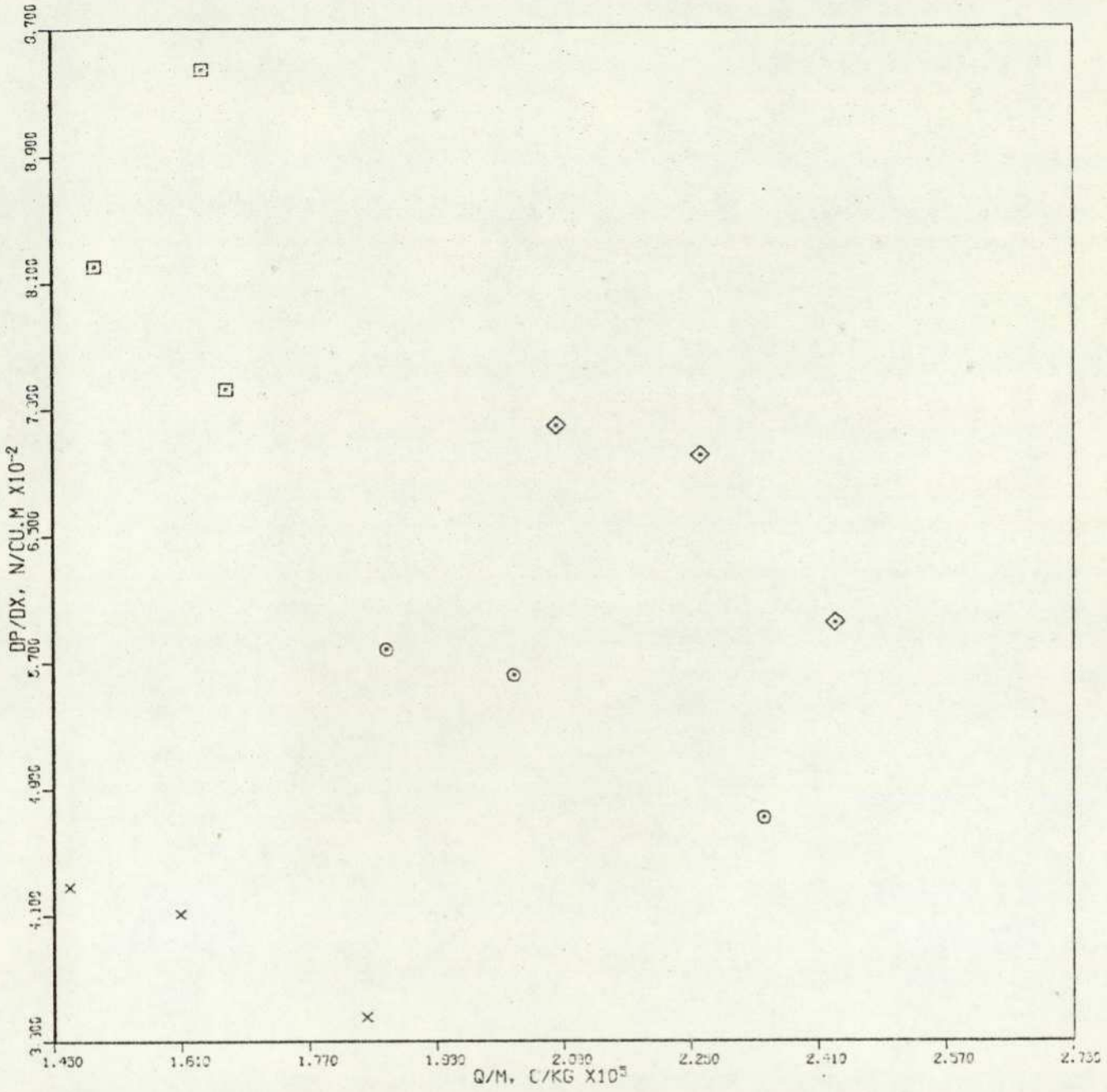

FIGURE : 8.48 EFFECT OF ELECTROSTATIC CHARGE ON PRESSURE GRADIENT.
GLASS BEADS TYPE #3.

CONSTANT PARAMETER(S) :		RE	MP, KG/SEC
CURVE 01	×	0.405E 05	0.187E-01
CURVE 02	⊙	0.496E 05	0.186E-01
CURVE 03	⊡	0.538E 05	0.349E-01
CURVE 04	◇	0.573E 05	0.189E-01

DATA COMPUTED BY #FDP2. O/P BY #PJ03. PLOTTED BY #PJ04 (03-14-09-00-07-02) .

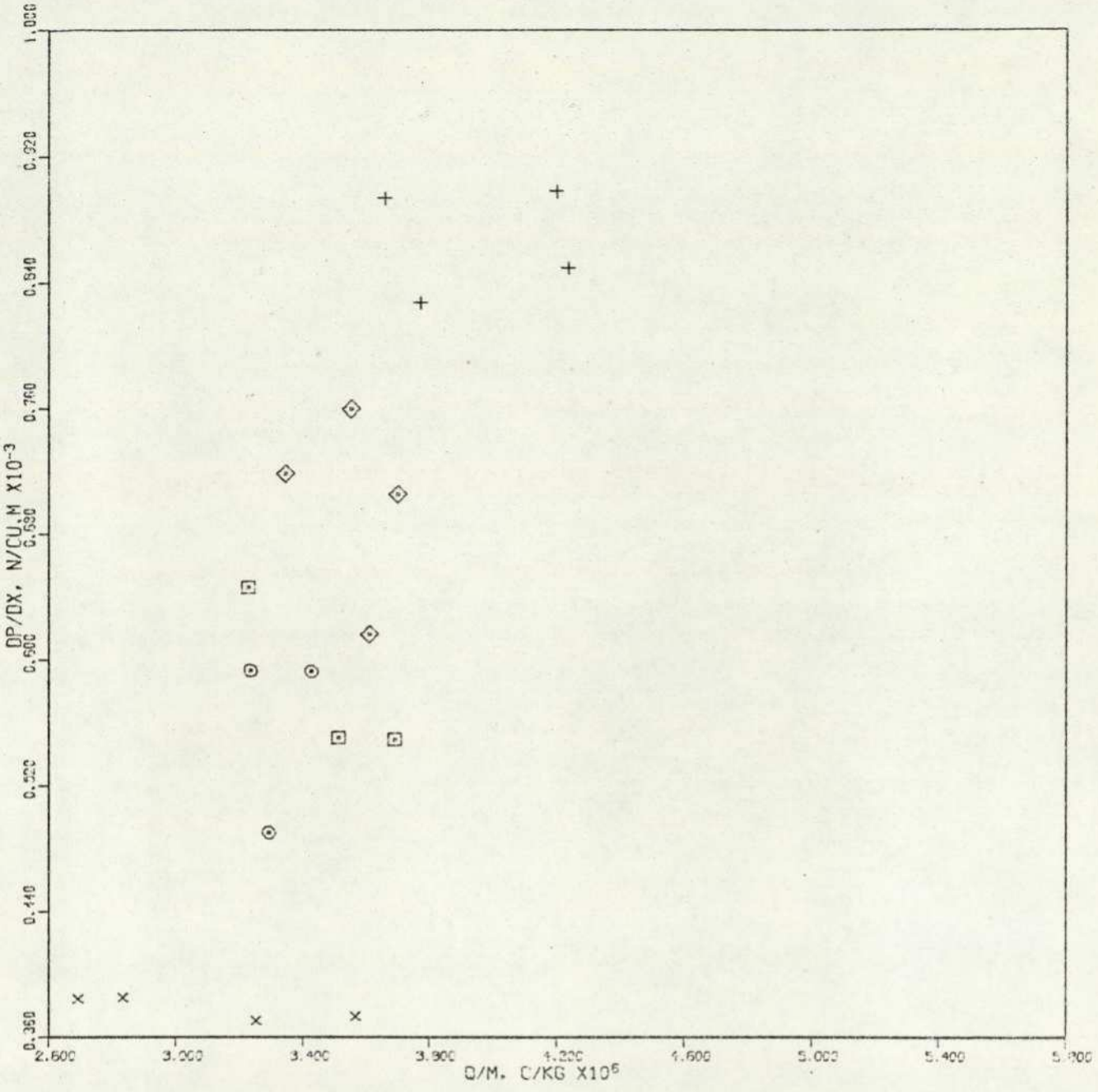

FIGURE : 3.49 EFFECT OF ELECTROSTATIC CHARGE ON PRESSURE GRADIENT.
GLASS BEADS TYPE #4.

CONSTANT PARAMETER(S) :		RE	MP, KG/SEC
CURVE 01	×	0.403E 05	0.155E-01
CURVE 02	⊙	0.499E 05	0.201E-01
CURVE 03	⊡	0.535E 05	0.201E-01
CURVE 04	◈	0.585E 05	0.201E-01
CURVE 05	+	0.695E 05	0.201E-01

DATA COMPUTED BY #PDP2. O/P BY #PJ03. PLOTTED BY #PJ04 (04-14-09-00-07-02) .

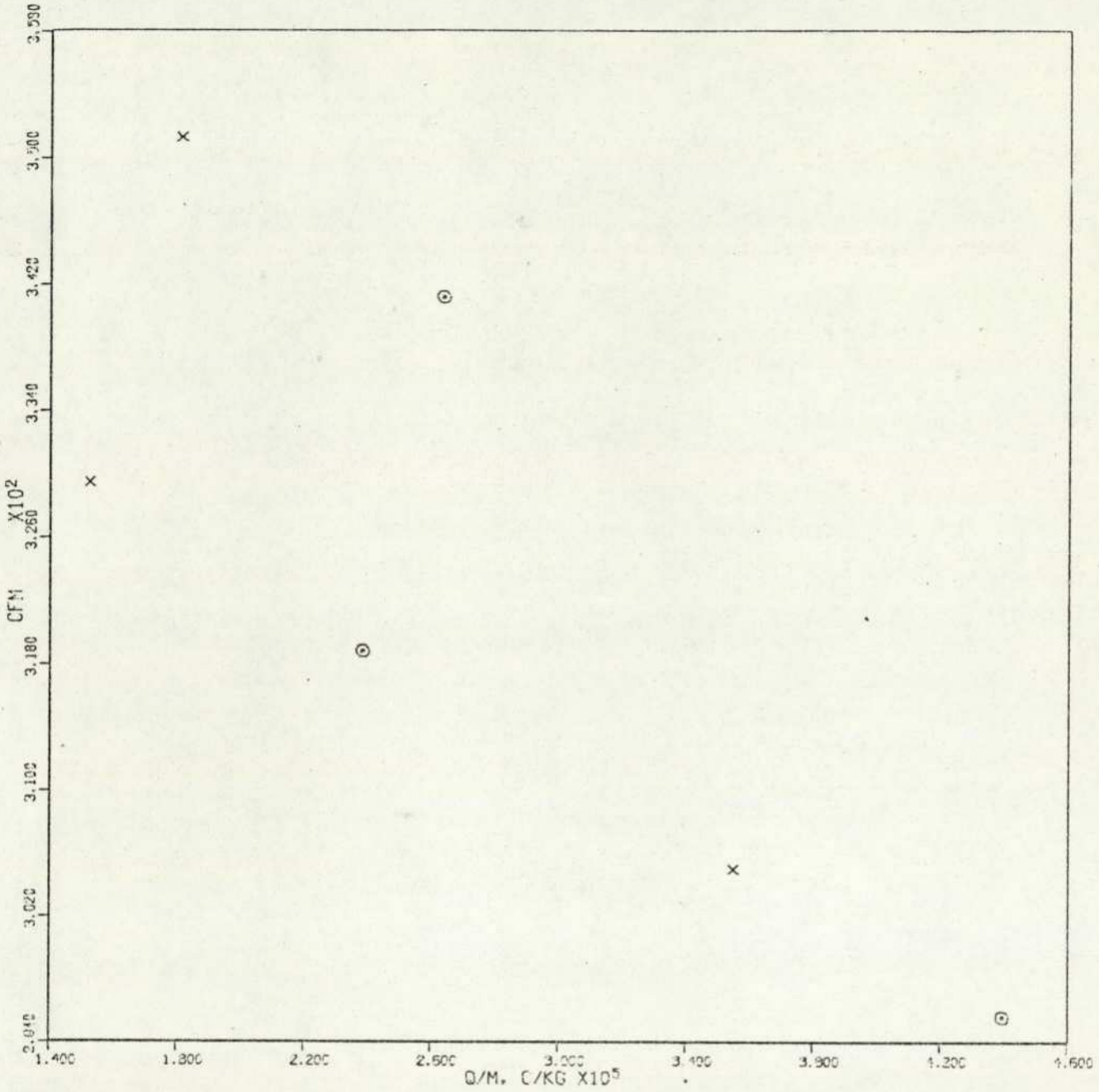

FIGURE : 8.50 EFFECT OF ELECTROSTATIC CHARGE ON SUSPENSION FRICTION FACTOR. GLASS BEADS TYPE #1.

CONSTANT PARAMETER(S) :		RE	MP, KG/SEC
CURVE 01	×	0.404E 05	0.173E-01
CURVE 02	⊙	0.495E 05	0.179E-01

DATA COMPUTED BY #PDP2, O/P BY #PJ03, PLOTTED BY #PJ04 (01-14-10-00-07-02) .

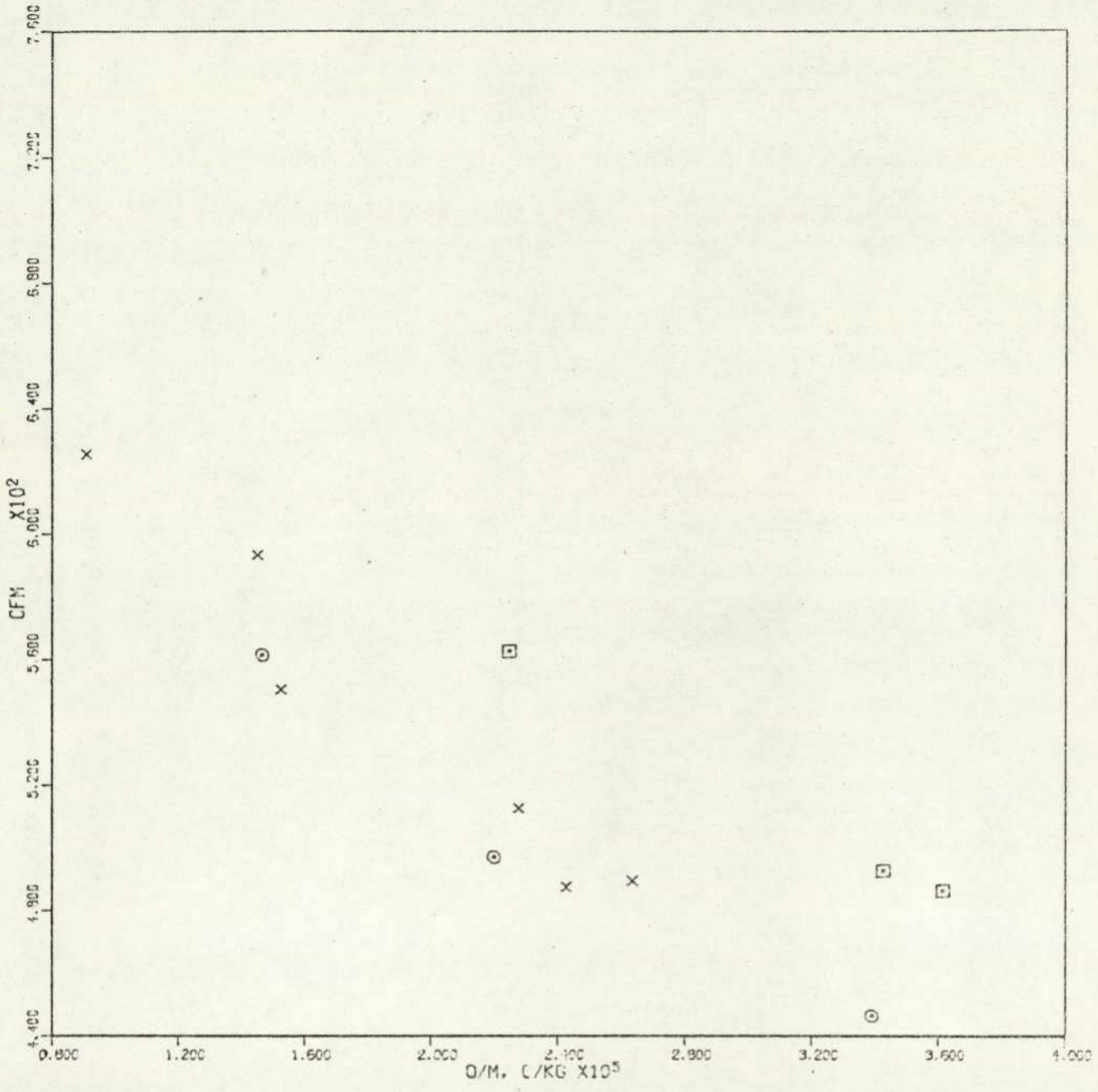

FIGURE : 8.51 EFFECT OF ELECTROSTATIC CHARGE ON SUSPENSION FRICTION FACTOR. GLASS BEADS TYPE #2.

CONSTANT PARAMETER(S) :		RE	MP, KG/SEC
CURVE 01	×	0.401E 05	0.191E-01
CURVE 02	⊙	0.495E 05	0.189E-01
CURVE 03	⊡	0.612E 05	0.245E-01

DATA COMPUTED BY #PDP2, O/P BY #PJ03, PLOTTED BY #PJ04 (02-14-10-00-07-02) .

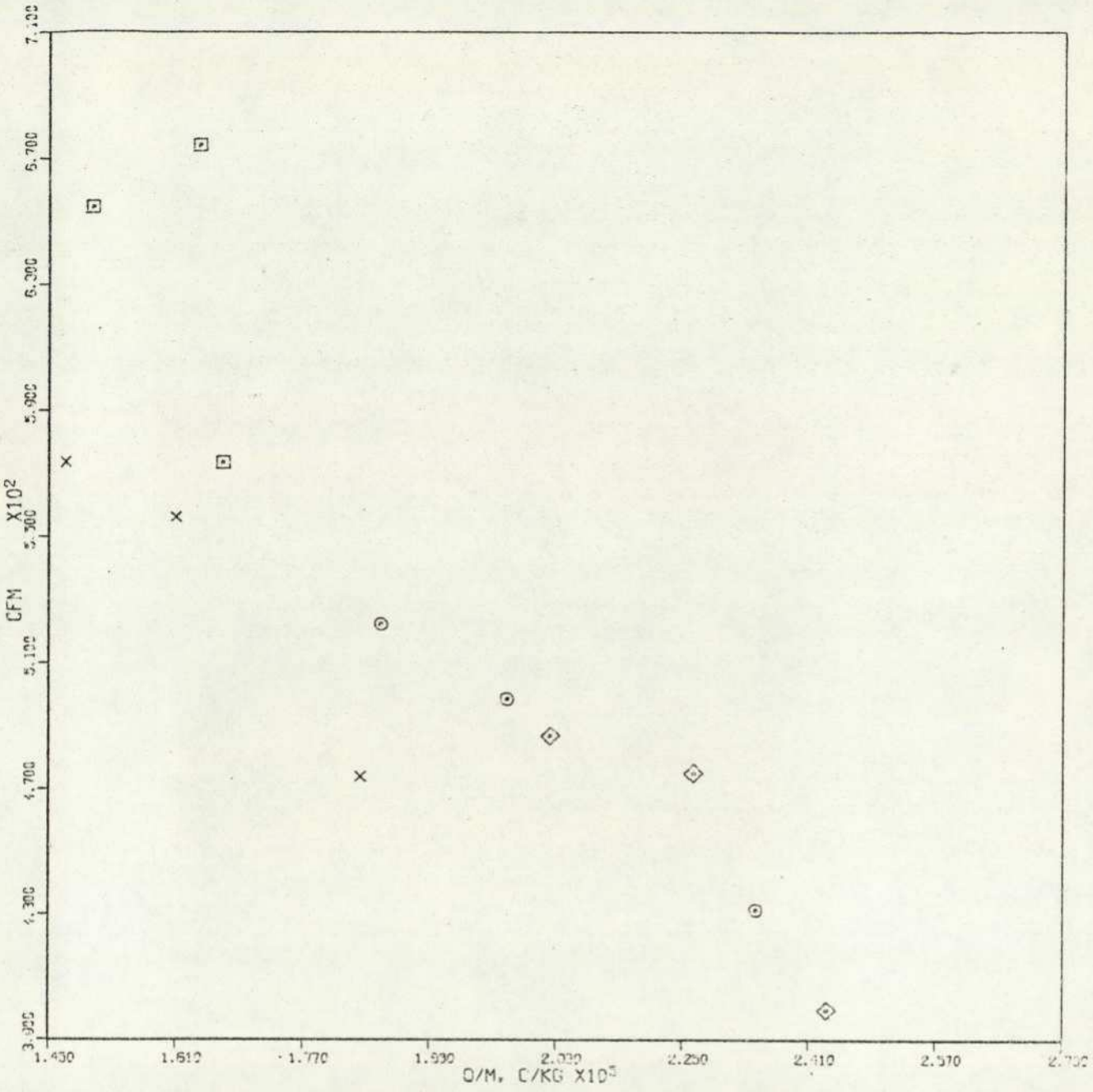

FIGURE : 8.52 EFFECT OF ELECTROSTATIC CHARGE ON SUSPENSION FRICTION FACTOR. GLASS BEADS TYPE #3.

CONSTANT PARAMETER(S) :		RE	MP, KG/SEC
CURVE 01	×	0.405E 05	0.187E-01
CURVE 02	⊙	0.496E 05	0.186E-01
CURVE 03	⊡	0.538E 05	0.349E-01
CURVE 04	◈	0.573E 05	0.189E-01

DATA COMPUTED BY #PDP2, O/P BY #PJ03, PLOTTED BY #PJ04 (03-14-10-00-07-02) .

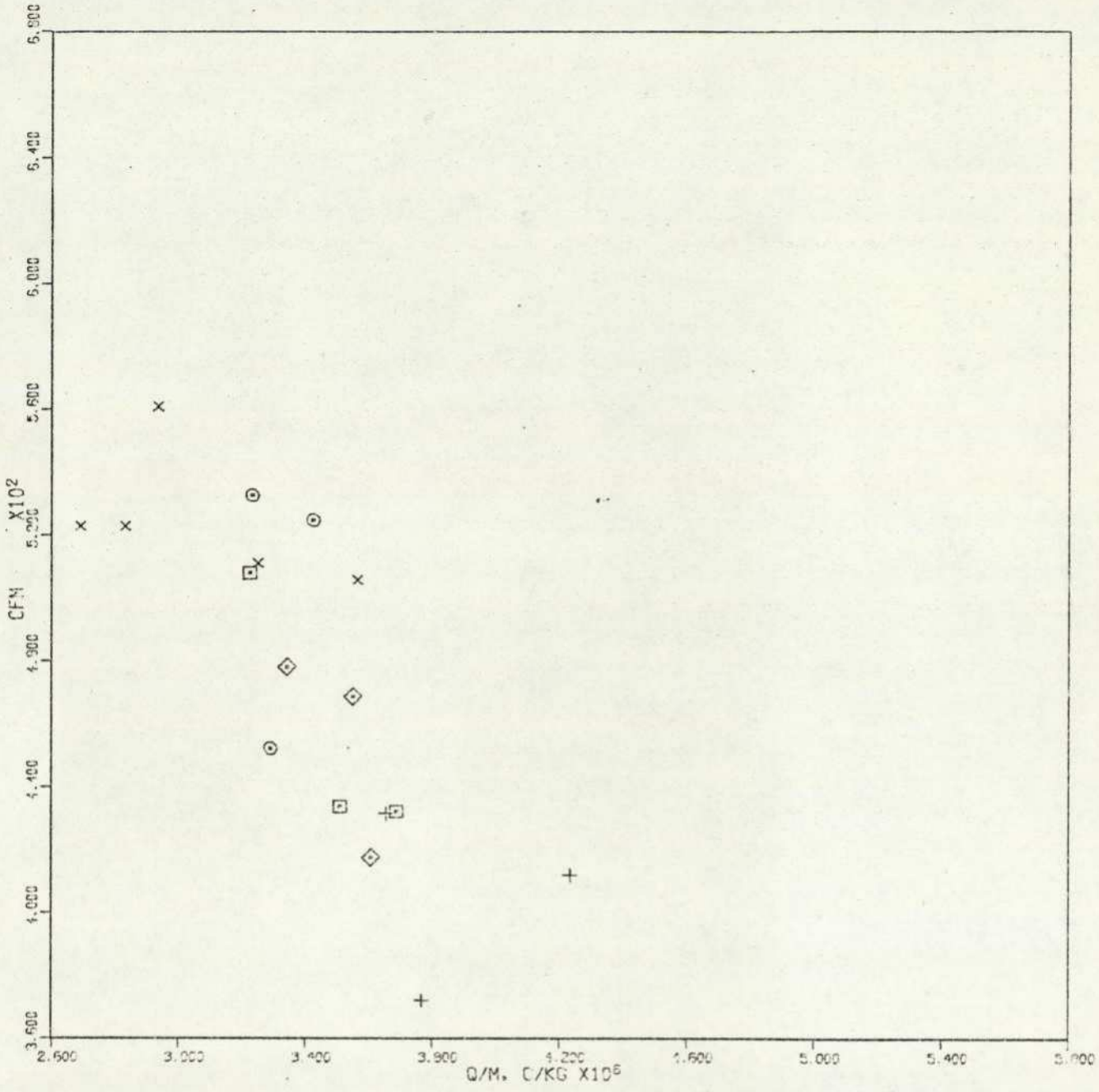

FIGURE : 8.53 EFFECT OF ELECTROSTATIC CHARGE ON SUSPENSION FRICTION FACTOR. GLASS BEADS TYPE #4.

CONSTANT PARAMETER(S) :		RE	MP, KG/SEC
CURVE 01	×	0.402E 05	0.155E-01
CURVE 02	⊙	0.499E 05	0.201E-01
CURVE 03	⊡	0.535E 05	0.201E-01
CURVE 04	◈	0.585E 05	0.200E-01
CURVE 05	+	0.690E 05	0.200E-01

DATA COMPUTED BY #PDP2, O/P BY #PJ03. PLOTTED BY #PJ04 (04-14-10-00-07-02) .

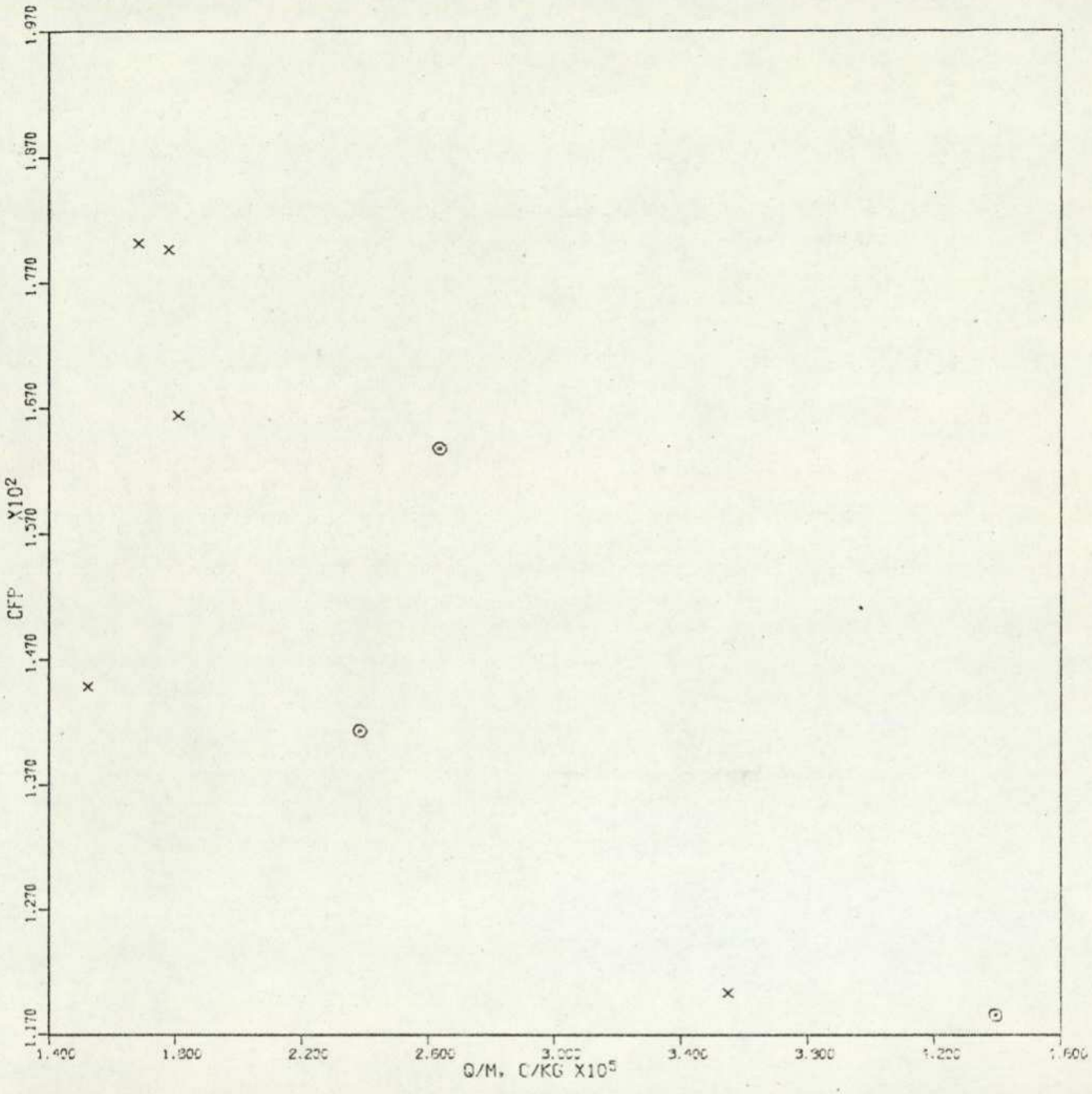

FIGURE : 8.54 EFFECT OF ELECTROSTATIC CHARGE ON PARTICLES FRICTION FACTOR.
GLASS BEADS TYPE #1.

CONSTANT PARAMETER(S) :		RE	MP, KG/SEC
CURVE 01	×	0.403E 05	0.174E-01
CURVE 02	⊙	0.495E 05	0.179E-01

DATA COMPUTED BY #PDP2, O/P BY #PJ03, PLOTTED BY #PJ04 (01-14-11-00-07-02) .

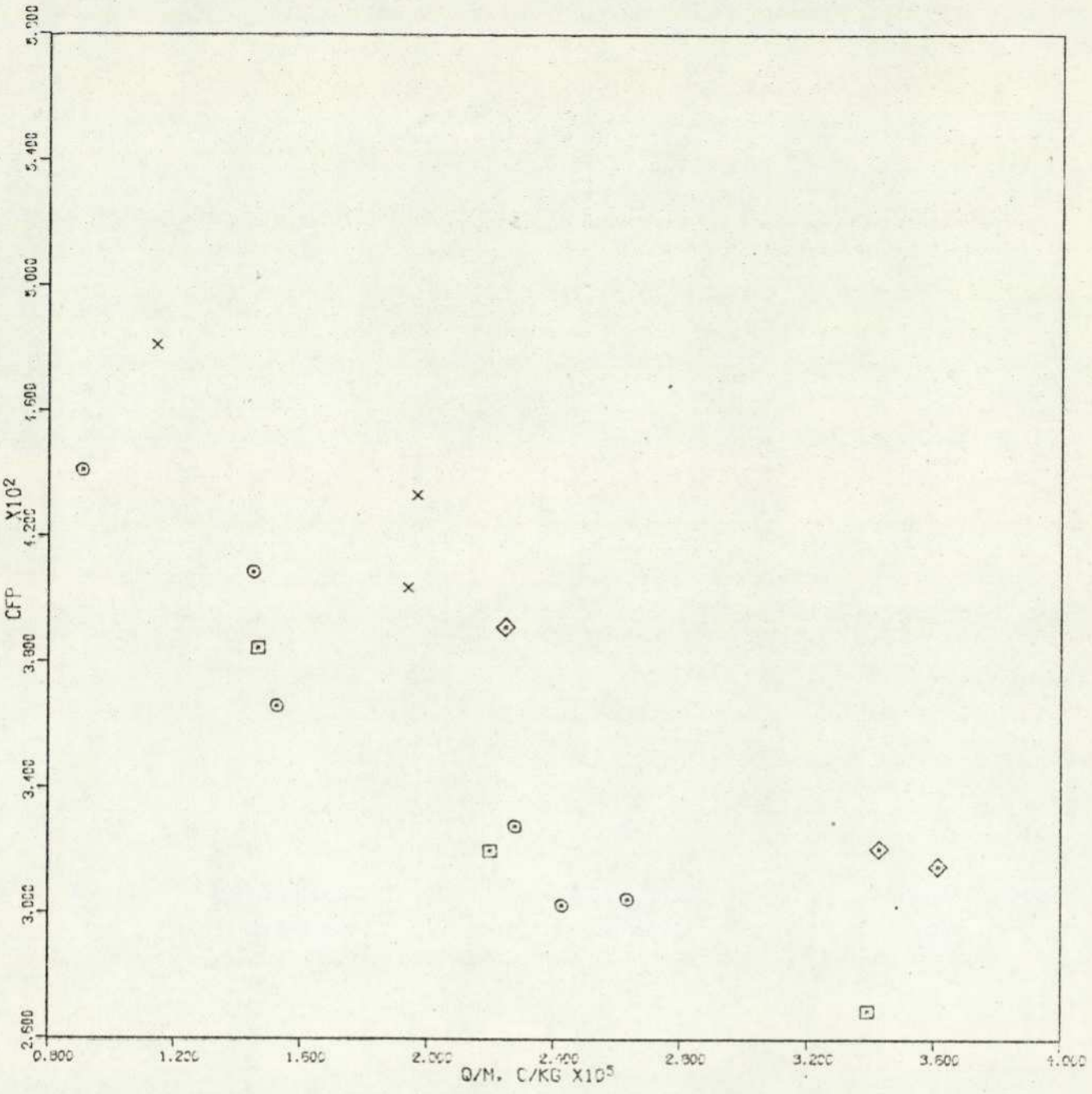

FIGURE : 8.55 EFFECT OF ELECTROSTATIC CHARGE ON PARTICLES FRICTION FACTOR.
GLASS BEADS TYPE #2.

CONSTANT PARAMETER(S) :		RE	MP, KG/SEC
CURVE 01	×	0.402E 05	0.247E-01
CURVE 02	⊙	0.401E 05	0.191E-01
CURVE 03	⊡	0.495E 05	0.189E-01
CURVE 04	◈	0.612E 05	0.245E-01

DATA COMPUTED BY #PDP2. O/P BY #PJ03. PLOTTED BY #PJ04 (02-14-11-00-07-02) .

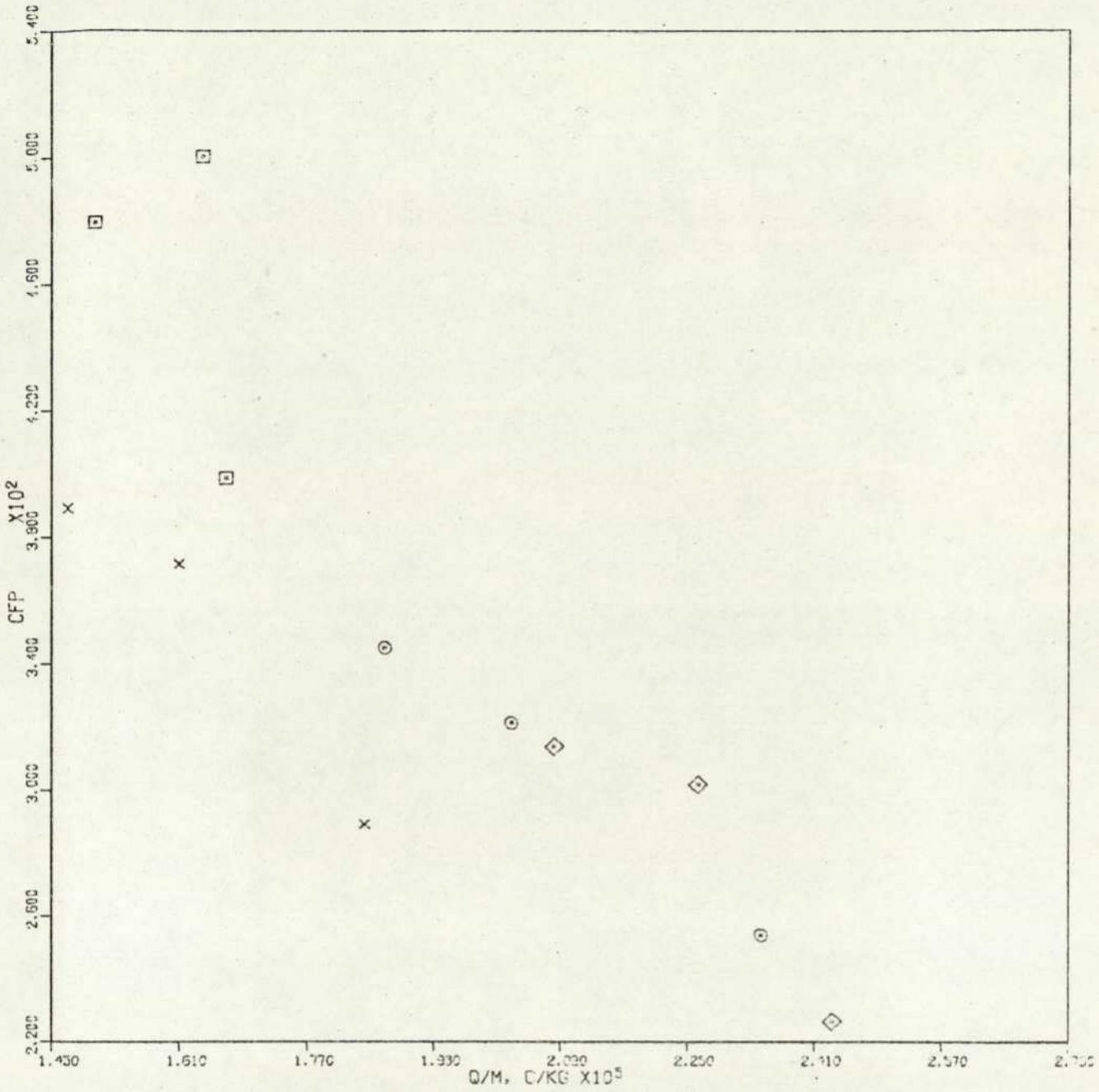

FIGURE : 8.56 EFFECT OF ELECTROSTATIC CHARGE ON PARTICLES FRICTION FACTOR. GLASS BEADS TYPE #3.

CONSTANT PARAMETER(S) :		RE	MP, KG/SEC
CURVE 01	×	0.405E 05	0.187E-01
CURVE 02	⊙	0.496E 05	0.186E-01
CURVE 03	⊡	0.539E 05	0.349E-01
CURVE 04	◈	0.573E 05	0.189E-01

DATA COMPUTED BY #PDP2, O/P BY #PJ03, PLOTTED BY #PJ04 (03-14-11-00-07-02) .

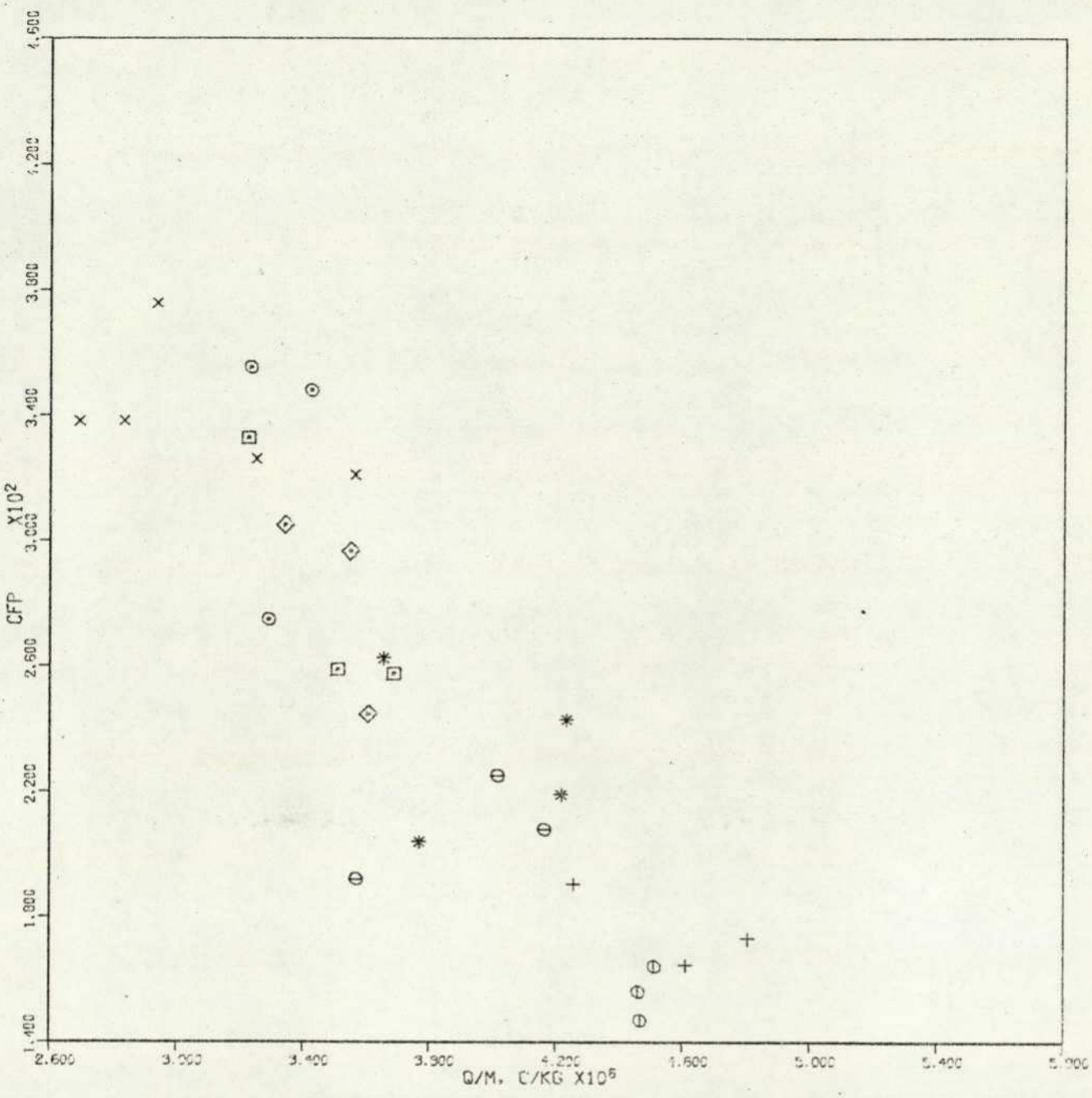

FIGURE : 8.57 EFFECT OF ELECTROSTATIC CHARGE ON PARTICLES FRICTION FACTOR. GLASS BEADS TYPE #4.

CONSTANT PARAMETER(S) :		RE	MP, KG/SEC
CURVE 01	×	0.402E 05	0.155E-01
CURVE 02	⊙	0.499E 05	0.201E-01
CURVE 03	⊡	0.535E 05	0.201E-01
CURVE 04	◈	0.585E 05	0.200E-01
CURVE 05	+	0.655E 05	0.156E-01
CURVE 06	✳	0.695E 05	0.201E-01
CURVE 07	⊕	0.747E 05	0.156E-01
CURVE 08	⊖	0.751E 05	0.205E-01

DATA COMPUTED BY #PDP2, O/P BY #PJ03, PLOTTED BY #PJ04 (04-14-11-00-07-02) .

CHAPTER 9

CONCLUSIONS

The present study indicates that any measurement or analysis of gas-solid suspension flow should always include consideration of the effect of electrostatic charging, and within the present range of variables, the following conclusions are reached ;

(1) The pipe flow of gas-solid suspension is basically a phenomenon of interactions among electrostatic, gravity, relaxation and diffusion effects which are governed by the characteristic parameters α, β, γ and η. For given fluid velocity profile, the distributions of electric potential, density, mass flux and diffusivity of the particulate phase can be completely determined from these parameters.

(2) The mathematical modelling of dilute gas-solid suspension flow is a valid approach. Although results of computations of horizontal flow are illustrated here, the present model is also applicable to inclined flows, buoyant particles and mono-dispersed suspensions with particle size distribution.

(3) The effect of electrification has been shown to be significant on the distribution of particulate density whereas the particle velocity distribution is mainly determined by the drag force due to relative motion between the two phases. The extent of electrostatic effect on the flow characteristics, however, depends very much on the charge to mass ratio as well as the mass flow rates, being more prominent at high mass flow and charge to mass ratios but less significant at high air flow rates.

(4) Inclusion of Magnus lift force in the analysis is feasible but it is believed that its effect is limited only within the thickness of boundary layer. However, depending on whether the flow is upward or downward, the Magnus lift force might drive the particles towards or away from the pipe axis.

(5) When dealing with a concentrated suspension, the basic equations should be modified to take into account any deviations of fluid flow characteristics due to presence of particles.

(6) The experimental results show that loading of particles would always result in higher pressure drops and to a good approximation, the suspension friction factor can be expressed as a simple function of mass flow ratio.

(7) The charge transfer current was found to be to the order of 10^{-7} Amp and was not affected by air humidity. Although the degree of air ionization was not determined, it is believed that the effect of ionization provided by the radio-active source was very small. With suitable modification, the electrostatic ball probe can provide a means of monitoring solid flow rate in particulate systems.

(8) Charges of both signs were present and the degree of asymmetry varied with the proportion of particles colliding with the pipe walls and other boundaries of the system. The net effective charge to mass ratio was less than 10^{5} c/kg.

Further work is currently being carried out at the City University, using Laser Doppler techniques to measure the velocities and turbulence intensities of both phases, and it is hoped that these results can be used to refine the present analysis.

APPENDIX 1

TURBULENT DIFFUSION IN FULLY DEVELOPED PIPE FLOW

Taylor's theory of diffusion by continuous movement has been extensively treated in the literature (48, 56, 57) and for illustration purposes, we shall consider a fluid particle initially at rest is released at the origin of a cartesian coordinate system. After some diffusion time t, the particle moves to a point (x, y, z) such that

$$x = \int_0^t u(\tau)\,d\tau \qquad \text{(A.1.1)}$$

$$y = \int_0^t v(\tau)\,d\tau \qquad \text{(A.1.2)}$$

and

$$z = \int_0^t w(\tau)\,d\tau \qquad \text{(A.1.3)}$$

where $u(\tau)$, $v(\tau)$ and $w(\tau)$ are the Lagrangian turbulent velocity components of the fluid particle.

Since the fluid is 'at rest' except for the turbulence, the time mean displacements over all particles have the same properties as the mean turbulent velocities i.e. $\bar{x} = \bar{y} = \bar{z} = 0$. However, the displacement variances will depend on the diffusion time, e.g. in the y-direction

$$\frac{1}{2}\,\overline{\frac{dy^2}{dt}} = \overline{\frac{dy}{dt}\,y} = \overline{v(t)\int_0^t v(\tau)\,d\tau} \qquad \text{(A.1.4)}$$

and when the average motion of a great many fluid particles is considered, equation (A.1.4) may be written in terms of the Lagrangian correlation coefficient $R(\tau)$ as

$$\frac{1}{2}\,\frac{dy^2}{dt} = \bar{v}^2 \int_0^t R(\tau)\,d\tau \qquad \text{(A.1.5)}$$

where $$R(\tau) = \frac{\overline{v(t)v(t+\tau)}}{\bar{v}^2} \qquad \text{(A.1.6)}$$

and $\bar{v}^2$ is the Lagrangian time average velocity.

If the turbulence is homogeneous and isotropic, $\bar{u}^2 = \bar{v}^2 = \bar{w}^2$ and $\bar{x}^2 = \bar{y}^2 = \bar{z}^2$ e.g. the mean square displacement in the y-direction becomes

$$\bar{y}^2 = 2\,\bar{v}^2 \int_0^t \left(\int_0^t R(\tau)\,d\tau \right) dt \qquad \text{(A.1.7}$$

In In general $R(\tau)$ decreases from 1 to 0 in a time t_1 which is defined by

$$T_L = \int_0^{t_1} R(\tau)\,d\tau = \int_0^{\infty} R(\tau)\,d\tau = \text{constant} \qquad \text{(A.1.8)}$$

and $$\Lambda_L = (\bar{v}^2)^{\frac{1}{2}} \int_0^{t_1} R(\tau)\,d\tau = \text{constant} \qquad \text{(A.1.9)}$$

where T_L is the Lagrangian integral time scale and Λ_L is the integral length scale of the turbulence. Thus, for $t > t_1$, equation (A.1.7) reduces to

$$\frac{1}{2}\,\frac{d\bar{y}^2}{dt} = (\bar{v}^2)^{\frac{1}{2}} \Lambda_L \ , \qquad \text{(A.1.10)}$$

which is similar to Einstein's equation for diffusion by Brownian movement, i.e.

$$D_m = \frac{1}{2}\,\frac{d\bar{y}^2}{dt} \qquad \text{(A.1.11)}$$

By analogy, Taylor defined a turbulent diffusivity D_f for $t > t_1$ as

$$D_f = \frac{1}{2} \frac{d\bar{y}^2}{dt} \qquad (A.1.12)$$

Measurements of turbulent diffusivity in pipe flow have been made by many workers (33, 52, 56-58) and using the correlation of $(D_f/2Ru_o)$ vs. Re_o ($= 2R\bar{\rho}u_o/\mu$) as suggested by Kada and Hanratty (52), u_o being the fluid velocity at the pipe centre, a summary of experimental results is given in Table (A.1). Comparison of these data shows that greater extent of mixing exists in small pipes and that $(D_f/2Ru_o)$ is almost independent on Re_o. For the present study we shall assume

$$D_f = .015 \times R \times u_o \qquad (A.1.13)$$

for $R \leqslant .0156$m.

Authors	2R, in.	Re x 10^{-5}	$D_f/2Ru_o$ x 10^2
Kada and Hanratty (52)	1.5	.20	.110
(Water)	"	.50	.080
Baldwin and Walsh (56)	8.0	2.9	.110
(Air)	"	4.2	.100
	"	5.3	.098
	"	6.3	.110
Towle and Sherwood (58)	6.0	.12	.270
(Air)	"	.25	.190
	"	.56	.150
	"	1.2	.130
	12.0	.44	.200
	"	.91	.180
Soo et al (33)	3.0	.38	.400
(Air)	"	.84	.440
	"	.13	.570
Groenhof (57)	$D_f/2Ru_\tau$ = .04;		
(Air)	for 2R = 2.0 in. and $Re_o \geq .2 \times 10^5$		

Table A.1. Eddy diffusion of turbulent flows in pipes.

APPENDIX 2

NUMERICAL SOLUTION OF EQUATIONS (4.4.2) - (4.4.5)

Since the flow under fully developed conditions is symmetric with respect to a vertical plane through the pipe axis, only half of the pipe cross-section is required for the complete solution. The layout of the lattice of mesh prints used for the finite difference approximation is shown in Fig. (A.2).

A2.1 Numerical Method

Re-writing the characteristic equations in difference forms (dropping the asterisks for simplicity but all quantities are dimensionless), we now have,

$$-\tfrac{1}{2}\gamma\rho(i,j) + \{1/r(j)\}\partial\{r(j)\rho(i,j)D_p(i,j)\partial u_p(i,j)/\partial r\}/\partial r + \{1/r(i,j)^2\}\partial\{\rho(i,j)D_p(i,j)\partial u_p(i,j)/\partial\phi\}/\partial\phi + \beta F(i,j)\rho(i,j)\{u(j) - u_p(i,j)\} = 0 \qquad (A.2.1.1)$$

$$-D_p(i,j)\partial\rho(i,j)/\partial r - \{\rho(i,j)/F(i,j)\}\partial V(i,j)/\partial r - \tfrac{1}{2}\eta\{\rho(i,j)/F(i,j)\}\cos\phi(i) = 0 \qquad (A.2.1.2)$$

$$-D_p(i,j)\{1/r(j)\}\partial\rho(i,j)/\partial\phi - \{\rho(i,j)/F(i,j)\}\{1/r(j)\}\partial V(i,j)/\partial\phi + \tfrac{1}{2}\eta\{\rho(i,j)/F(i,j)\}\sin\phi(i) = 0 \qquad (A.2.1.3)$$

$$\{1/r(j)\}\partial\{r(j)\partial V(i,j)/\partial r\}/\partial r + \{1/r(j)^2\}\partial^2 V(i,j)/\partial\phi^2 = -4\alpha\rho(i,j) \qquad (A.2.1.4)$$

and

$$\rho(i,j) = \exp\{-V(i,j) - \tfrac{1}{2}\eta r(j)\cos\phi(i)\} \qquad (A.2.1.5)$$

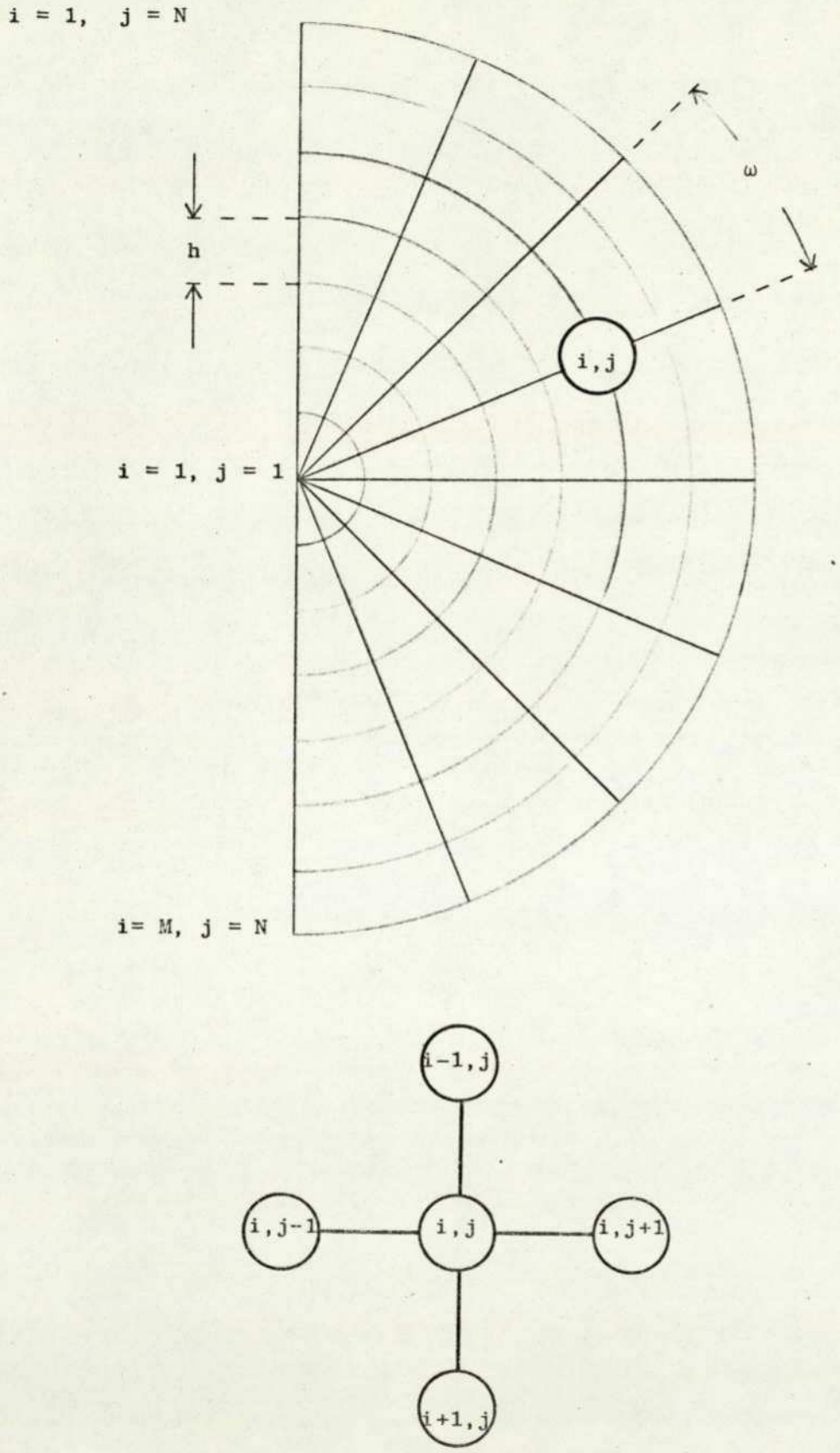

Fig. A.2. Layout of the lattice of mesh points.

where

$$r(j) = \{j - 1\}h \tag{A.2.1.6}$$

$$\phi(i) = \{i - 1\}w \tag{A.2.1.7}$$

$$u(j) = \{1 - r(j)\}^{\frac{1}{7}} \tag{A.2.1.8}$$

for i = 1, m and j = 1, n; and the step sizes are

$$h = 1/(n - 1) \tag{A.2.1.9}$$

and

$$w = \pi/(m - 1) \tag{A.2.1.10}$$

At each mesh point (designated by the indeces i in the ϕ-direction and j in the r-direction), the finite difference approximations for the partial derivatives of a continuous function $f(r,\phi)$ are given by

$$\partial f(i,j)/\partial r = \{f(i,j+1) - f(i,j-1)\}/2h, \quad \text{for } j = 2, n-1 \tag{A.2.1.11}$$

$$= \{f(i,j-2) - 4f(i,j-1) + 3f(i,j)\}/2h, \quad \text{for } j = n \tag{A.2.1.12}$$

$$= \{-f(i,j+2) + 4f(i,j+1) - 3f(i,j)\}/2h, \quad \text{for } j = 1. \tag{A.2.1.13}$$

$$\partial f(i,j)/\partial \phi = \{f(i+1,j) - f(i-1,j)\}/2w, \text{ for } i = 1, m \tag{A.2.1.14}$$

$$\partial^2 f(i,j)/\partial r^2 = \{f(i,j+1) - 2f(i,j) + f(i,j-1)\}/h^2 \quad \text{for } j = 2, n-1 \tag{A.2.1.15}$$

$$= \{-f(i,j-3) + 4f(i,j-2) - 5f(i,j-1) + 2f(i,j)\}/h^2 \quad \text{for } j = n \tag{A.2.1.16}$$

$$= \{2f(i,j) - 5f(i,j+1) + 4f(i,j+2) - f(i,j+3)\}/h^2$$
$$\text{for } j = 1 \qquad \text{(A.2.1.17)}$$

$$\partial^2 f(i,j)/\partial\phi^2 = \{f(i+1,j) - 2f(i,j) + f(i-1,j)\}/w^2$$
$$\text{for } i = 1, m \qquad \text{(A.2.1.18)}$$

and by symmetry

$$f(i-1,j) = f(i+1,j), \text{ for } j = 2, n \text{ and } i = 1 \text{ or } m. \qquad \text{(A.2.1.19)}$$

Substituting the difference approximations into equations (A.2.1.1) - (A.2.1.4) it can be shown in general that

$$u_p(i,j) = b(i,j) + b(i,j+1)u_p(i,j+1) + b(i+1,j)u_p(i+1,j) + b(i,j-1)u_p(i,j-1) + b(i-1,j)u_p(i-1,j) \qquad \text{(A.2.1.20)}$$

and

$$V(i,j) = c(i,j) + c(i,j+1)V(i,j+1) + c(i+1,j)V(i+1,j) + c(i,j-1)V(i,j-1) + c(i-1,j)V(i-1,j) \qquad \text{(A.2.1.21)}$$

where b's and c's are the difference coefficients to be determined at each mesh point (i,j).

The boundary conditions for $u_p(i,j)$ are now given by

$$u_p(i,j) = \{4u_p(i,j-1) - u_p(i,j-2)\}/\{2h/Knp + 3\}$$
$$\text{for } j = n \qquad \text{(A.2.1.22)}$$

and

$$u_p(i,j) = \{4u_p(i,j+1) - u_p(i,j+2)\}/3$$
$$\text{for } j = 1 \text{ and } \phi(i) = \pi/2 \text{ (m must be an odd number)} \qquad \text{(A.2.1.23)}$$

A.2.2 Computational Procedure

The finite difference equations (A.2.1.1) - (A.2.1.5) can be solved systematically by means of a Gauss-Seidel type iterative process in which a first approximation is used to calculate a second approximation which in turn is used to calculate a third and so on. The process is said to be convergent when the difference between successive approximations approach to some reference value. The rate of convergence can be improved considerably by using the most recent iterates as soon as they are available. Computer programs (#XFD7A and #XFD7B) have been written to perform the iteration and the computational procedure is summarized as follows :

1. Set master iteration counter q to 1.

2. Assume initial ρ_{po} from

$$\rho_{po} = c_1(M_p/\pi R^2 u_o)$$

where c_1(=1.2 to 1.6) may be treated as a calibration constant (Reference 6).

3. Compute the characteristic parameters α, β, γ and η; step sizes h and w; (r(j),j=1,n),(ϕ(i),i=1,m) and (u(j),j=1,n).

4. Assume initial ((V(i,j), ρ_p(i,j),j=1,n),i=1,m) from equations (4.5.11) and (4.4.11) respectively.

5. Set iterative counter k to 1.

6. Compute current V(i,j)'s and ρ_p(i,j)'s from equations (A.2.1.4) and (A.2.1.5).

7. Check for convergence

$$|1- \{\rho_p(i,j)\}_k/\{\rho_p(i,j)\}_{k-1}| \leq \delta \quad \text{for } i = 1, m;\ j = 2, n$$

where δ is the limit of convergence.

(a) If the above is true, go to step 8.

(b) If false, set k to k+1. If k .LE. 100, go back to step 6, otherwise terminate execution.

8. Assume initial $((u_p(i,j),j=1,n),i=1,m)$.

9. Set new iteration counter p to 1.

10. Compute $((F(i,j),j=2,n-1),i=1,m)$ from equation (3.1.2) in which the drag coefficient C_D is calculated from a set of ' C_D vs. Re ' equations proposed by Morsi and Alexander (59).

11. Compute $((D_p(i,j),j=2,n-1),i=1,m)$ from equations (A.2.1.2) and (A.2.1.3).

12. Compute $((u_p(i,j),j=1,n),i=1,m)$ from equation (A.2.1.1).

13. Check for convergence :

$$|1 - \{u_p(i,j)\}_p/\{u_p(i,j)\}_{p-1}| \leq \delta \quad \text{for } i = 1, m;\ j = 2, n$$

(a) If the above is true, go to step 14.

(b) If false, set p to p+1. If p .LE. 100 go back to step 10, otherwise terminate execution.

14. Compute new mass flow rate M'_p by integrating $\rho_p u_p$ across the pipe section i.e.

$$M'_p = 2 \int_0^{\pi} \int_0^{R} \rho_p u_p r dr d\phi.$$

15. Check for convergence :

$$|1 - M'_p/M_p| \leq \delta$$

(a) If the above is true, case solved.

(b) If false, set q to q+1. If q .LE. 100, compute $\{\rho_{po}\}_{new} = \{\rho_{po}\}_{old}(M_p/M'_p)$ and go back to step 3, otherwise terminate execution.

In conclusion, it worth noting that the equations being solved are of course the finite difference equations. Stability and convergence are therefore not directly associated with the original characteristic equations and hence the system equations will not always converge for a given set of α, β, γ, η and Knp.

A.2.3 Computer Program #XFD7B

The function of #XFD7B is to perform the iteration process outlined in the previous section.

Program Symbols

C1	c_1 as defined in A.2.2.
CA, CB, CC, CE	characteristic parameters α, β, γ and η.
CFA	air friction factor C_f.
DF	turbulent diffusivity D_f, (m^2/sec).
DP	particle diffusivity D_p, (m^2/sec).
DS	particle diameter 2a or d, (m).
EO	permittivity ε_o, (farad/m).
F	dimensionless inverse of relaxation time F*.
FS	Stokesian inverse of relaxation time F_s, (sec^{-1}).
G	dimensionless particulate density ρ^*_p.
H	step size h, (m).
KNP	Knudsen number Knp.
M, N	number of mesh points (Fig. A.2).
MP	dimensionless solid flow rate $(M_p/R^2\rho_{po}u_o)$.
MPX	solid flow rate M_p, (kg/sec).
MX	dimensionless mass flux $(\rho_p u_p/\rho_{po}u_o)$
PG	$F\rho_p(u - u_p)$, (kg/m^2sec^2).

QM	charge to mass ratio (q/m), (c/kg).
RE	pipe Reynolds number Re.
RHOF	fluid density $\bar{\rho}$, (kg/m^3).
RHOP	particle density $\bar{\rho}_p$, (kg/m^3).
RMP	computed solid flow rate, (kg/sec).
RPO	particulate density at pipe axis ρ_{po}, (kg/m^3).
RR	pipe radius R, (m).
SC	Schmidt number (D_f/D_p).
THA	pipe inclination θ, (radian).
UO	fluid velocity at pipe axis u_o, (m/sec).
UF	dimensionless fluid velocity u*.
UN	mean fluid velocity $\bar{u}$, (m/sec).
UP, UQ	dimensionless particle velocity u_p^*.
UY	fluid velocity at (R-a) from pipe axis, (m/sec).
V	dimensionless electric potential V*.
VF	volume fraction of particles.
VISC	dynamic viscosity $\bar{\mu}$, ($kgsec/m^2$).
VR	electric potential V, (V).
W	step size w, (radian).

Input Data Sequence

1. (REF(I),I=1,4), M, N, RLT

where (REF(I),I=1,4) is a 32-character general heading of each series of test cases, RLT is the limit of convergence and the data format is (4A8, 2I3, F5.3).

2. (REF(I),I=5,6), DS, MPX, QM, RPO, UO, KNP, SC;

3. EO, RHOF, RHOP, RR, THA, VISC

where (REF(I),I=5,6) is a 10-character case title and the data formats are (A8, A2, 7E10.3) and (8E10.3) respectively.

Results and Estimation of Computing Time

DP, G, MX, PG, UP, V and VR at each mesh point are listed on line-printer. For M=11 and N=11, the mill time is about 38 sec per case on the ICL 1905E.

```
WORK(ED)
SEND TO(GEOMSEMICOMP)
LIST (LP)
PROGRAM (XFD7B)
COMPACT
INPUT 5 = CRD
OUTPUT 6 = LPD
USE    7 = ED1/UNFORMATTED(HYB66000CHN3)/512
TRACE 0
END
```

```
C
C     V K CHAN
C
C     PROGRAM #XFD7B
C
C     NUMERICAL SOLUTIONS OF EQUATIONS (4.4.2) - (4.4.5)
C
C     METHOD OUTLINED IN APPENDIX 2
C
C
C     ERROR CONDITIONS
C
C     IFLAG = 1    NO ERROR
C     IFLAG = 2    RE OUT OF RANGE    (#XPST)
C     IFLAG = 3    CA GREATER THAN 1.9
C     IFLAG = 4    ARG IN EXP(ARG) GREATER THAN 2.5    (#XPST)
C     IFLAG = 5    #XCPV FAILS TO CONVERGE
C     IFLAG = 6    ARG IN EXP(ARG) GREATER THAN 2.5    (#XCPV)
C     IFLAG = 7    ZERO 1ST DERIVATIVE OF G(I,J) DETECTED    (#XFD7B)
C     IFLAG = 8    RE OUT OF RANGE    (#XDPF)
C     IFLAG = 9    #XCDP FAILS TO CONVERGE
C     IFLAG =10    RMP DOES FAILS TO CONVERGE WITH MPX
C
      MASTER XFD7B
      REAL KNP,MP,NX,MPX
      DIMENSION REF(6)
      COMMON /BLK1/ A(21),B(5),C(21,5),DP(21,21),F(21,21),G(21,21)
      COMMON /BLK1/ HX(21,21),PG(21,21),R(21),UF(21),UP(21,21)
      COMMON /BLK1/ UQ(21,21),V(21,21),VR(21,21),Z(21,21)
      COMMON /BLK2/ KNP,QM,RPD,M,M1,MC,N,N1,RLT,H,W
      COMMON /BLK3/ CA,CB,CC,CE,DF,DS,FS,E0,RHOF,RHOP,RM,THA,U0,UY,VISC
```

```
   50 FORMAT(4A8,2I3,F5.3)
   51 FORMAT(8E10.3)
   52 FORMAT(A8,A2,/E10.3)
   60 FORMAT(1H2, 6A8,3X,4H( M=,I2,4H  N=,I2,6H  RLT=,F5.3,2H )//)
   61 FORMAT(7H     DS=,E10.3,7H     E0=,E10.3,7H  RHOF=,E10.3,
     1       7H  RHOP=,E10.3,7H     RR=,E10.3,7H   THA=,E10.3,
     2       7H     U0=,E10.3///7H  VISC=,E10.3,7H   KNP=,E10.3,
     3       7H     QM=,E10.3,7H     C1=,E10.3,7H    CA=,E10.3,
     4       7H     CB=,E10.3,7H     CC=,E10.3///7H    CE=,E10.3,
     5       7H     MP=,E10.3,7H   RMP=,E10.3,7H    VF=,E10.3,
     6       7H     UY=,E10.3,7H     DF=,E10.3,7H   MPX=,E10.3)
   62 FORMAT(//8H IFLAG =,I2)
   64 FORMAT(/25H ((G(I,J),J=1,N),I=1,M) :,//(E10.3,10E11.3))
   65 FORMAT(/25H ((V(I,J),J=1,N),I=1,M) :,//(E10.3,10E11.3))
   66 FORMAT(/26H ((VR(I,J),J=1,N),I=1,M) :,//(E10.3,10E11.3))
   67 FORMAT(/26H ((UP(I,J),J=1,N),I=1,M) :,//(E10.3,10E11.3))
   68 FORMAT(/26H ((MX(I,J),J=1,N),I=1,M) :,//(E10.3,10E11.3))
   69 FORMAT(/26H ((DP(I,J),J=1,N),I=1,M) :,//(E10.3,10E11.3))
   70 FORMAT(/26H ((PG(I,J),J=1,N),I=1,M) :,//(E10.3,10E11.3))
   71 FORMAT(1H2,3A8,A2,5X,4H( M=,I2,4H  N=,I2,6H  RLT=,F5.3,2H )///
     1       24H SUMMARY OF TEST CASES :///15X,2HDS,8X,2HQM,5X,3HKNP,
     2       4H MPX,3H U0,5H  RP0,4H  MP,4X,3HRMP,5H  G1N,5H  GMN,
     3       5H UP11,5H UP1N,5H UPMN,4X,2HCA,7X,2HCB,4X,2HCC,5H   CE,
     4       4H  C1//)
   72 FORMAT(1X,A8,A2,2E10.2,2(1X,F3.2),F4.0,2F5.2,1X,F4.3,2F5.2,
     1       3(1X,F4.3),E10.2,2F6.1,2F5.2)
      REWIND 7
      KASE=0
      PI=3.1415927
C
C     DATA INPUT
C
      READ(5,50) (REF(I),I=1,4),M,N,RLT
  100 READ(5,52) (REF(I),I=5,6),DS,MPX,QM,RP0,U0,KNP,SC
C
C     TSET FOR END OF INPUT
C
      IF( U0 .LT. 1. ) GO TO 400
      READ(5,51) E0,RHOF,RHOP,RR,THA,VISC
      MIT=0
      C1=0.0
C
  101 ITN=0
      MP=0.0
      RMP=0.0
      VF=0.0
C
C     CALL #XPST TO PRESET INITIAL CONDITIONS AND COMPUTE BASIC PARAMETERS
C
      CALL XPST(IFLAG)
      IF( IFLAG .NE. 1 ) GO TO 360
C
C     CALL #XCPV TO COMPUTE DIMENSIONLESS PARTICULATE DENSITY G(I,J)
C     AND ELECTRIC POTENTIAL V(I,J)
C
  114 CALL XCPV(IFLAG)
      IF( IFLAG .NE. 1 ) GO TO 360
  124 ITN=0
C
C     TEST FOR 1ST DERIVATIVES OF G(I,J) WITH RESPECT TO R
C
      DO 126 I=1,M
      DO 126 J=2,N
      IF( FDR(G,I,J) .EQ. 0.0 ) GO TO 350
  126 CONTINUE
C
```

```
C     CALL #XDPF TO COMPUTE PARTICLE DIFFUSIVITY DP(I,J) AND TIME
C     CONSTANT F(I,J)
C
  128 CALL XDPF(IFLAG)
      IF( IFLAG .NE. 1 ) GO TO 360
C     CALL #XCUP TO COMPUTE PARTICLES VELOCITY UP(I,J)
C
  130 CALL XCUP
C
C     CALL #RSCT TO TEST CONVERGENCE AND RESET UQ(I,J) = UP(I,J)
C
  131 CALL RSCT(UP,UQ,DIFF,M,N)
  133 ITN=ITN+1
      IF( DIFF .LE. RLT ) GO TO 134
      IF( ITN .LT. 100 ) GO TO 128
      IFLAG=9
      GO TO 360
C
C     COMPUTE MASS FLUX MX(I,J), SOLIDS FLOW RATE RMP & VOLUME FRACTION VF
C
  134 DO 137 I=1,M
      DO 137 J=1,N
      PG(I,J)=F(I,J)*G(I,J)*ABS(UF(J)-UP(I,J))*FS*UQ*RP0
      IF( QM .LT. ,1E-20 ) GO TO 136
      VR(I,J)=DF*FS*V(I,J)/QM
  136 DP(I,J)=DP(I,J)*DF
  137 MX(I,J)=G(I,J)*UP(I,J)
      DO 142 J=2,M1
      AR=0.5*PI*(R(J+1)*R(J+1)-R(J)*R(J))/FLOAT(M1)
      DO 142 I=1,M1
      VF=VF+.25*AR*( G(I,J)+ G(I,J+1)+ G(I+1,J+1)+ G(I+1,J))
  142 MP=MP+.25*AR*(MX(I,J)+MX(I,J+1)+MX(I+1,J+1)+MX(I+1,J))
      AR=0.5*PI*R(2)*R(2)/FLOAT(M1)
      DO 146 I=1,M1
      VF=VF+AR*( G(1,1)+ G(I,2)+ G(I+1,2))/3.
  146 MP=MP+AR*(MX(1,1)+MX(I,2)+MX(I+1,2))/3.
      MP=2.*MP
      RMP=RR*RR*RP0     *UQ*MP
      VF=2.*RP0     *VF/(RHOP*PI)
C
C     COMPARE MPX WITH RMP
C
      IF( ABS(1.-MPX/RMP) .LE. .05 ) GO TO 300
      RP0=RP0*MPX/RMP
      MIT=MIT+1
      IF( MIT .LE. 10 ) GO TO 101
      IFLAG = 10
      GO TO 360
  300 C1=RP0*PI*RR*RR*UQ/MPX
      KASE=KASE+1
      WRITE(6,60) (REF(I),I=1,6),M,N,RLT
      WRITE(6,61) DS,E0,RHOF,RHOP,RR,THA,UQ,VISC,RNP,QM,C1,
     1            CA,CB,CC,CE,MP,RMP,VF,UY,DF,MPX
      WRITE(6,69) ((DP(I,J),J=1,N),I=1,M)
      WRITE(6,64) ((G(I,J),J=1,N),I=1,M)
      WRITE(6,68) ((MX(I,J),J=1,N),I=1,M)
      WRITE(6,70) ((PG(I,J),J=1,N),I=1,M)
      WRITE(6,60) (REF(I),I=1,6),M,N,RLT
      WRITE(6,67) ((UP(I,J),J=1,N),I=1,M)
      WRITE(6,65) ((V(I,J),J=1,N),I=1,M)
      WRITE(6,66) ((VR(I,J),J=1,N),I=1,M)
C
C     STORE RESULTS ON DISC FILE FOR GRAPH PLOTTING PROGRAM #PJ05
C
      WRITE(7) (REF(I),I=1,6),M,N,DS,THA,UQ,RNP,QM,RP0,CA,CB,CC,
     1         CE,MP,RMP,VF,UY,DF,((DP(I,J),G(I,J),MX(I,J),PG(I,J),
```

```
     2          UP(I,J),V(I,J),VR(I,J),J=1,N),I=1,M),RR,MPX,C1
      GO TO 100
  350 IFLAG=7
  360 WRITE(6,60) (REF(I),I=1,6),M,N,RLT
      WRITE(6,61) DS,EO,RHOF,RHOP,RR,THA,UO,VISC,KNP,QM,C1,
     1            CA,CB,CC,CE,MP,RMP,VF,UY,DF,MPX
      WRITE(6,62) IFLAG
      GO TO 100
  400 REWIND 7
      WRITE(6,71) (REF(I),I=1,4),M,N,RLT
      DO 410 K=1,KASE
      READ(7)  (REF(I),I=1,6),M,N,DS,THA,UO,KNP,QM,RPO,CA,CB,CC,
     1         CE,MP,RMP,VF,UY,DF,((DP(I,J),G(I,J),MX(I,J),PG(I,J),
     2         UP(I,J),V(I,J),VR(I,J),J=1,N),I=1,M),RR,MPX,C1
  410 WRITE(6,72) (REF(I),I=5,6),DS,QM,KNP,MPX,UO,RPO,MP,RMP,G(1,N),
     1            G(M,N),UP(1,1),UP(1,N),UP(M,N),CA,CB,CC,CE,C1
      REWIND 7
      STOP
      END

, LENGTH  1388, NAME  XFD7B
```

```
      FUNCTION FDR(F,I,J)
C
CC    COMPUTE 1ST DERIVATIVE OF F(I,J) WITH RESPECT TO R
C
      DIMENSION F(21,21)
      COMMON /BLK2/ KNP,QM,RPO,M,M1,MC,N,N1,RLT,H,W
      IF( J .EQ. 1 ) GO TO 104
      IF( J .EQ. N ) GO TO 106
      FDR=0.5*(F(I,J+1)-F(I,J-1))/H
      RETURN
  104 FDR=0.5*(-F(I,J+2)+4.*F(I,J+1)-3.*F(I,J))/H
      RETURN
  106 FDR=0.5*(F(I,J-2)-4.*F(I,J-1)+3.*F(I,J))/H
      RETURN
      END

, LENGTH   141, NAME  FDR
```

```
      FUNCTION FDW(F,I,J)
C
C     COMPUTE 1ST DERIVATIVE OF F(I,J) WITH RESPECT TO W
C
      DIMENSION F(21,21)
      COMMON /BLK2/ KNP,QM,RPQ,M,M1,MC,N,N1,RLT,H,W
      IF( I .EQ. 1  .OR.  I .EQ. M ) GO TO 103
      FDW=0.5*(F(I+1,J)-F(I-1,J))/W
      RETURN
  103 FDW=0.0
      RETURN
      END
```

```
, LENGTH    70, NAME  FDW
```

```
      SUBROUTINE FNEW(Y,M,XBEG,DX,N,XINT,YINT,IC)
C
C     #FNEW IS A NEWTON'S FORWARD INTERPOLATION SUBROUTINE
C
C     COMPUTE YINT FOR GIVEN XINT FROM Y(M)
C
      DIMENSION Y(10),D(10)
      IC=1
      MQ=INT((XINT-XBEG+DX)/DX)
      IF( M-N-1 ) 121,121,101
  101 IF( MQ ) 120,120,102
  102 IF( MQ-M ) 103,103,120
  103 IF( M-MQ-N ) 104,105,105
  104 MQ=M-N
  105 FMQ=FLOAT(MQ-1)
      XQ=XBEG+FMQ*DX
      U=(XINT-XQ)/DX
      A=U
      YINT=Y(MQ)
  106 DO 107 I=1,N
      J=MQ+I-1
  107 D(I)=Y(J+1)-Y(J)
      IF( N-1 ) 121,110,108
  108 DO 109 K=2,N
      DO 109 I=K,N
      L=N+K-I
  109 D(L)=D(L)-D(L-1)
  110 DO 111 K=1,N
      YINT=YINT+A*D(K)
      FK=FLOAT(K)
  111 A=A*(U-FK)/(FK+1.)
```

```
      RETURN
  120 IC=0
      RETURN
  121 IC=2
      RETURN
      END

, LENGTH   214, NAME  FNEW
```

```
      SUBROUTINE RSCT(A,B,DIFF,M,N)
C
C     COMPARE A(I,J) WITH B(I,J)
C     SET B(I,J)=A(I,J)
C     THE MAXIMUM DIFFERENCE BETWEEN A(I,J) AND B(I,J) IS RETURNED AS DIFF
C
      DIMENSION A(21,21),B(21,21)
      DIFF=0.0
      DO 106 I=1,M
      DO 106 J=1,N
      IF( J .EQ. 1 ) GO TO 106
      RMX=ABS(1.-B(I,J)/A(I,J))
      IF( RMX .GT. DIFF ) DIFF=RMX
  106 B(I,J)=A(I,J)
      RETURN
      END

, LENGTH    97, NAME  RSCT
```

```
      SUBROUTINE XCPV(IFLAG)
C
C     COMPUTE G(I,J) AND V(I,J) FROM EQUATIONS (A.2.1.4) & (A.2.1.5)
C
      REAL KNP,MP,MX
      COMMON /BLK1/ A(21),B(5),C(21,5),UP(21,21),F(21,21),G(21,21)
      COMMON /BLK1/ MX(21,21),PG(21,21),R(21),UF(21),UP(21,21)
      COMMON /BLK1/ UO(21,21),V(21,21),VR(21,21),Z(21,21)
      COMMON /BLK2/ KNP,QM,RPO,M,M1,MC,N,N1,RLT,H,W
      COMMON /BLK3/ CA,CB,CC,CE,DF,DS,FS,EO,RHOF,RHOP,RR,THA,UO,UY,VISC
      ITN=0
      IFLAG=1
      CALL RSCT(G,Z,DIFF,M,N)
  102 DIFF =0.0
      DO 112 I=1,M
      I11=I+1
      IF( I .EQ. M ) I11=M-1
      I01=I-1
      IF( I .EQ. 1 ) I01=2
      DO 112 J=2,N
      IF( J .EQ. N ) GO TO 110
      V(I,J)=C(J,1)*V(I,J+1)+C(J,2)*V(I11,J)+C(J,3)*V(I,J-1)+
     1    C(J,4)*V(I01,J)+C(J,5)*G(I,J)
      GO TO 111
  110 V(I,J)=((4.*H+10.)*V(I,J-1)-(H+8.)*V(I,J-2)+2.*V(I,J-3)
     1       -8.*H*H*CA*G(I,J)-2.*((H/W)**2)*(V(I11,J)+V(I01,J)))/
     2       (3.*H+4.-4.*((H/W)**2))
  111 ARG    =    (-V(I,J)-.5*CE*A(I)*R(J))
      IF( ARG .GT. 2.5 ) GO TO 200
  112 G(I,J)=EXP(ARG)
      ITN=ITN+1
C
C     TEST FOR CONVERGENCE
C
      CALL RSCT(G,Z,DIFF,M,N)
      IF( DIFF .LE. RLT ) RETURN
      IF( ITN .LT. 200 ) GO TO 102
      IFLAG = 5
      RETURN
  200 IFLAG = 6
      RETURN
      END

, LENGTH   327, NAME  XCPV
```

```
      SUBROUTINE XCUP
C
C     COMPUTE UP(I,J) FROM EQUATION  (A.2.1.1)
C
      REAL KNP,MP,MX
      COMMON /BLK1/ A(21),B(5),C(21,5),DP(21,21),F(21,21),G(21,21)
      COMMON /BLK1/ HX(21,21),PG(21,21),R(21),UF(21),UP(21,21)
      COMMON /BLK1/ UQ(21,21),V(21,21),VR(21,21),Z(21,21)
      COMMON /BLK2/ KNP,QM,RP0,M,M1,MC,N,N1,RLT,H,W
      COMMON /BLK3/ CA,CB,CC,CE,DF,DS,FS,E0,RHOF,RHOP,RR,THA,U0,UY,VISC
      DO 116 I=1,M
      I11=I+1
      IF( I .EQ. M ) I11=M-1
      I01=I-1
      IF( I .EQ. 1 ) I01=2
      DO 116 J=2,N1
      SUM1=G(I,J)*(-.5*CC+F(I,J)*UF(J)*CB+DP(I,J)*((UP(I,J+1)+UP(I,J-1))
     1    /(H*H)+(UP(I11,J)+UP(I01,J))/(R(J)*W)**2))
      SUM2=FDR(UP,I,J)*((G(I,J)*DP(I,J)/R(J))+DP(I,J)*FDR(G,I,J)+
     1     G(I,J)*FDR(DP,I,J))
      SUM3=FDW(UP,I,J)*((DP(I,J)*FDW(G,I,J))+G(I,J)*FDW(DP,I,J))/
     1     (R(J)*R(J))
      SUM4=G(I,J)*(F(I,J)*CB+2.*DP(I,J)*((1./(H*H))+1./(R(J)*W)**2))
  116 UP(I,J)=(SUM1+SUM2+SUM3)/SUM4
      DO 123 I=1,M
  123 UP(I,N)=(4.*UP(I,N-1)-UP(I,N-2))/(3.+2.*H/KNP)
      UP0=(4.*UP(MC,2)-UP(MC,3))/3.
      DO 126 I=1,M
  126 UP(I,1)=UP0
      RETURN
      END

, LENGTH   357, NAME  XCUP
```

```
      SUBROUTINE XDPF(IFLAG)
C
C     COMPUTE F(I,J) AND DP(I,J) FROM EQUATIONS (A.2.1-2) , (A.2.1-3) &
C
      REAL KNP,MX,MP
      COMMON /BLK1/ A(21),B(5),C(21,5),DP(21,21),F(21,21),G(21,21)
      COMMON /BLK1/ MX(21,21),PG(21,21),R(21),UF(21),UP(21,21)
      COMMON /BLK1/ UQ(21,21),V(21,21),VR(21,21),Z(21,21)
      COMMON /BLK2/ KNP,QM,RP0,M,M1,MC,N,N1,RLT,H,W
      COMMON /BLK3/ CA,CB,CC,CE,DF,DS,FS,E0,RHOF,RHOP,RK,THA,U0,UY,VISC
      IFLAG=1
      DO 104 I=1,M
      DO 104 J=1,N
      DU=ABS(U0*(UQ(I,J)-UF(J)))
      RE=RHOF*DS*DU/VISC
C
C     COMPUTE CDINT FROM MORSI'S DRAG COEFFICIENT EQUATIONS
C
      IF( RE .GT. 1000. ) GO TO 110
      IF( RE .LE. .1 ) CDINT=24./RE
      IF( RE .GT. .1  .AND.  RE .LE. 1.0 )
     1     CDINT=(22.73/RE)+(.0903/(RE*RE))+3.69
      IF( RE .GT. 1.  .AND.  RE .LE. 10. )
     1     CDINT=(29.1667/RE)-(3.8889/(RE*RE))+1.222
      IF( RE .GT. 10.  .AND.  RE .LE. 100. )
     1     CDINT=(46.5/RE)-(116.667/(RE*RE))+.61667
      IF( RE .GT. 100. )
     1     CDINT=(98.33/RE)-(2778./(RE*RE))+.3644
  104 F(I,J)=.75*CDINT*RHOF*DU/(DS*FS*(RHOP+.5*RHOF))
      DO 105 I=1,M
      DO 105 J=2,N
  105 DP(I,J)=(-G(I,J)/F(I,J))*(FDR(V,I,J)+.5*CE*A(I))/FDR(G,I,J)
      DP0=(4.*DP(MC,2)-DP(MC,3))/3.
      DO 106 I=1,M
  106 DP(I,1)=DP0
      RETURN
  110 IFLAG = 8
      RETURN
      END

, LENGTH   278, NAME  XDPF
```

```
      SUBROUTINE XPST(IFLAG)
C
C     PRESET INITIAL CONDITIONS
C
      REAL KNP,MX,MP
      COMMON /BLK1/ A(21),B(5),C(21,5),DP(21,21),F(21,21),G(21,21)
      COMMON /BLK1/ MX(21,21),PG(21,21),R(21),UF(21),UP(21,21)
      COMMON /BLK1/ UQ(21,21),V(21,21),VR(21,21),Z(21,21)
      COMMON /BLK2/ KNP,QM,RP0,M,M1,MC,N,N1,RLT,H,W
      COMMON /BLK3/ CA,CB,CC,CE,DF,DS,FS,E0,RHOF,RHOP,RR,THA,U0,UY,VISC
      COMMON /BLK4/ CFA(10)
C
C     COMPUTE INTEGRATION STEP SIZES AND BASIC PARAMETERS
C     M MUST BE AN ODD NUMBER
C
      PI=3.1415926
      M1=M-1
      N1=N-1
      MC=(M/2)+1
      H=1./FLOAT(N1)
      W=PI/FLOAT(M1)
      DF=.015*RR*U0
      FS=18.*VISC/(DS*DS*(RHOP+.5*RHOF))
      CA=RP0*((QM*RR)**2)/(4.*E0*DF*FS)
      IF( CA .GT. 1.9 ) GO TO 140
      CB=RR*RR*FS/DF
      CC=19.62*RR*RR*COS(PI*THA/180.)*(1.-(RHOF/RHOP))/(DF*U0)
      IF( CC .LE. .1E-05 ) CC=0.0
      CE=19.62*RR*SIN(PI*THA/180.)*(1.-(RHOF/RHOP))/(DF*FS)
      UN=.81*U0
      RE=2.*RR*RHOF*UN/VISC
C
C     CALL #FNEW TO COMPUTE FINT FOR GIVEN RE FROM CFA
C
      CALL FNEW(CFA,10,.3E+5,.5E+4,5,RE,FINT,IFLAG)
      IF( IFLAG .NE. 1 ) GO TO 130
C
C     COMPUTE FLUID VELOCITY UY NEAR PIPE WALL
C
      UY=.0625*DS*RHOF*UN*UN*FINT/VISC
C
C     ASSUME INITIAL G(I,J) AND V(I,J)
C
      DO 110 I=1,M
      A(I)=FLOAT(I-1)*W
  110 A(I)=COS(A(I))
      DO 117 J=1,N
      R(J)=FLOAT(J-1)*H
      UF(J)=(1.-R(J))**.142857
      IF( J .EQ. N ) UF(J)=UY/U0
      DUM=.95*UF(J)
      DO 117 I=1,M
      V(I,J)=2.*(ALOG(1.-CA*R(J)*R(J)/2.))
      ARG    =    (-V(I,J)-.5*CE*A(I)*R(J))
      IF( ARG .GT. 2.5 ) GO TO 150
      G(I,J)=EXP(ARG)
      DP(I,J)=0.0
      F(I,J)=0.0
      MX(I,J)=0.0
      VR(I,J)=0.0
      PG(I,J)=0.0
      Z(I,J)=0.0
      UP(I,J)=DUM
  117 UQ(I,J)=DUM
```

```
C
C       COMPUTE COEFFICIENT C(I,J) FOR EQUATION (A.2.1.21)
C
        DO 120 J=2,N
        DUM=2.*((1./(W*W))+(R(J)/H)**2)
        C(J,1)=((R(J)/(2.*H))+(R(J)/H)**2)/DUM
        C(J,2)=1./(W*W*DUM)
        C(J,3)=(((R(J)/H)**2)-R(J)/(2.*H))/DUM
        C(J,4)=C(J,2)
  120   C(J,5)=4.*CA*R(J)*R(J)/DUM
        RETURN
  130   IFLAG=2
        RETURN
  140   IFLAG = 3
        RETURN
  150   IFLAG = 4
        RETURN
        END

, LENGTH   538, NAME  XPST
```

```
        BLOCK DATA
C
C       AIR FRICTION CFA TABLE
C
        COMMON /BLK4/ CFA(10)
        DATA CFA/  .0197,.0191,.0185,.0181,.0177,.0174,.0172,.0170,
     1           .0168,.0168/
        END
```

APPENDIX 3

NUMERICAL SOLUTION OF EQUATIONS (4.5.2) - (4.5.4)

Because of the assumption of constant F and D_p, solution of the simplified characteristic equations becomes relatively simple. The lattice of mesh points, step sizes and finite difference approximations are similarly defined as those given in Appendix 2.

A.3.1 Numerical Method

Re-writing the characteristic equations in difference forms (dropping the asterisks for simplicity), we obtain

$$-\tfrac{1}{2}\gamma\rho(i,j) + \{1/r(j)\}\partial\{r(j)\rho(i,j)\partial u_p(i,j)/\partial r\}/\partial r + \{1/r(j)^2\}\partial\{\rho(i,j)\partial u_p(i,j)/\partial\phi\}/\partial\phi + \beta\rho(i,j)\{u(j) - u_p(i,j)\} = 0 \qquad (A.3.1.1)$$

$$\rho(i,j) = \exp\{-V(i,j) - \tfrac{1}{2}\eta r(j)\cos\phi(i)\} \qquad (A.3.1.2)$$

$$\{1/r(j)\}\partial\{r(j)\partial V(i,j)/\partial r\}/\partial r + \{1/r(j)^2\}\partial^2 V(i,j)/\partial\phi^2 = -4\alpha\rho(i,j) \qquad (A.3.1.3)$$

for i = 1, m and j = 1, n.

Similarly, it can be shown that

$$u_p(i,j) = b'(i,j) + b'(i,j+1)u_p(i,j+1) + b'(i+1,j)u_p(i+1,j) + b'(i,j-1)u_p(i,j-1) + b'(i-1,j)u_p(i-1,j) \qquad (A.3.1.4)$$

and

$$V(i,j) = c'(i,j) + c'(i,j+1)V(i,j+1) + c'(i+1,j)V(i+1,j) + c'(i,j-1)V(i,j-1) + c'(i-1,j)V(i-1,j) \qquad (A.3.1.5)$$

where b's and c's are the difference coefficients to be determined at each mesh point (i,j).

Following the assumption made by Soo and Tung (29) that at the pipe wall the net effect of gravity on V is zero, additional boundary conditions can be obtained from equations (4.5.12) and (4.5.3),

$$V(i,j) = 2\ln(1 - \tfrac{1}{2}\alpha) \qquad \text{(A.3.1.6)}$$

and

$$\rho(i,j) = \exp\{-V(i,j) - \tfrac{1}{2}\eta\cos\phi(i)\} \qquad \text{(A.3.1.7)}$$

for j = n and i = 1, m.

With the knowledge of the distributions of D_p and u_p obtained from equations (A.2.1.1) - (A.2.1.5), it is possible to estimate some average values for F and D_p i.e.

$$F = \tfrac{3}{4}C_d\Delta u/a(1 + 2\bar{\rho}_p/\bar{\rho}) \qquad \text{(A.3.1.8)}$$

and

$$D_p = \{\text{constant}\}Ru_o \qquad \text{(A.3.1.9)}$$

where Δu may be treated as the slip velocity between the two phases.

A.3.2 Computational Procedure

Similary, equations (A.3.1.1) - (A.3.1.3) can be solved by an iterative process, the computational procedure being outlined as follows :

1. Set master iteration counter q to 1.

2. Assume initial ρ_{po} from

$$\rho_{po} = c_1(M_p/\pi R^2 u_o)$$

3. Compute the characteristic parameters α, β, γ and η; step sizes h and w; (r(j),j=1,n), (ϕ(i),i=1,m) and (u(j),j=1,n).

4. Assume initial ((V(i,j), ρ_p(i,j),j=2,n-1),i=1,m) from equations (4.5.11) and (4.4.11) respectively.

5. Set iteration counter k to 1.

6. Compute current V(i,j)'s and ρ_p(i,j)'s from equations (A.3.1.2) and (A.3.1.3).

7. Check for convergence :

$$|1 - \{\rho_p(i,j)\}_k/\{\rho_p(i,j)\}_{k-1}| \leq \delta \quad \text{for i=1, m and j=2, n-1}$$

(a) If the above is true, go to step 8.

(b) If false, set k to k+1. If k .LE. 100, go back to step 6, otherwise terminate execution.

8. Assume initial ((u_p(i,j), j=1,n), i=1,m).

9. Set iteration counter p to 1.

10. Compute current u_p(i,j)'s from equation (A.3.1.1).

11. Check for convergence :

$$|1 - \{u_p(i,j)\}_p/\{u_p(i,j)\}_{p-1}| \leq \delta \quad \text{for i=1,m and j=1,n}$$

(a) If the above is true, go to step 12.

(b) If false, set p to p+1. If p .LE. 100 go back to step 10, otherwise terminate execution.

12. Compute new mass flow rate $M'_p = 2 \int_0^{\pi} \int_0^{R} \rho_p u_p r dr d\phi$.

13. Check for convergence :

$$|1 - M'_p/M_p| \leq \delta$$

(a) If the above is true, case solved.

(b) If false, set q to q + 1. If q .LE. 100 compute $\{\rho_{po}\}_{new} = \{\rho_{po}\}_{old}(M_p/M'_p)$ and go back to step 3, otherwise terminate execution.

A.3.3 Computer Program# XFD3B

The function of# XFD3B is to perform the iteration process outlined in the previous section.

Program Symbol

Program symbols are similary defined as those in# XFD7B.

Estimation of Computing Time

For M=11 and N=11, the mill time is about 9 sec per case on the ICL 1905E.

```
TION BY #XFAT MK 5A     DATE  04/05/76  TIME  21.09.42


      WORK(ED)
      SEND TO(GEOSSEMICOMP)
      LIST (LP)
      PROGRAM (XFD3B)
      COMPACT
      INPUT 5 = CR0
      OUTPUT 6 = LP0
      USE    7 = ED1/UNFORMATTED(HYB66000CHN4)/512
      TRACE 0
      END
```

```
C
C     V K CHAN
C
C     PROGRAM #XFD3B
C
C     NUMERICAL SOLUTIONS OF EQUATIONS  (4.5.2) - (4.5.4)
C
C     METHOD OUTLINED IN APPENDIX  3
C
      MASTER XFD3B
      REAL KNP,MP,MX,MPX
      DIMENSION REF(6)
      COMMON /BLK1/ A(15),C(15,5),G(15,15),V(15,15),R(15),UF(15)
      COMMON /BLK2/ B(15,15,5),UP(15,15),PG(15,15),VR(15,15),MX(15,15)
   50 FORMAT(4A8,2I3,F5.3)
   51 FORMAT(8E10.3)
   52 FORMAT(A8,A2,7E10.3)
   60 FORMAT(1H2, 6A8,3X,4H( N=,I2,4H  N=,I2,6H  RLT=,F5.3,2H )/)
   61 FORMAT(7H     DS=,E10.3,7H     E0=,E10.3,7H  RHOF=,E10.3,
     1       7H  RHOP=,E10.3,7H     RR=,E10.3,7H   THA=,E10.3,
     2       7H     U0=,E10.3//7H  VISC=,E10.3,7H   KNP=,E10.3,
     3       7H     QM=,E10.3,7H     C1=,E10.3,7H    SC=,E10.3,
     4       7H     DP=,E10.3,7H     CA=,E10.3//7H    CB=,E10.3,
     5       7H     CC=,E10.3,7H     CE=,E10.3,7H    MP=,E10.3,
     6       7H    RMP=,E10.3,7H     VF=,E10.3,7H   MPX=,E10.3)
   62 FORMAT(/15H CA TOO LARGE :,E10.3/)
   63 FORMAT(//34H G(I,J) AND V(I,J) DO NOT CONVERGE///)
   64 FORMAT(/25H ((G(I,J),J=1,N),I=1,M) :,//(F10.3,10E11.3))
   65 FORMAT(/25H ((V(I,J),J=1,N),I=1,M) :,//(F10.3,10E11.3))
```

```
   66 FORMAT(/26H ((VR(I,J),J=1,N),I=1,M) :,//(F10.3,10E11.3))
   67 FORMAT(/26H ((UP(I,J),J=1,N),I=1,M) :,//(F10.3,10E11.3))
   68 FORMAT(/26H ((MX(I,J),J=1,N),I=1,M) :,//(F10.3,10E11.3))
   69 FORMAT(//24H UP(I,J) DO NOT CONVERGE//)
   70 FORMAT(/26H ((PG(I,J),J=1,N),I=1,M) :,//(F10.3,10E11.3))
   71 FORMAT(1H2,3A8,A2,5X,4H( M=,I2,4H  N=,I2,6H  RLT=,F5.3,2H )///
     1       24H SUMMARY OF TEST CASES :///15X,2HDS,8X,2HQM,5X,3HKNP,
     2       4H MPX,3H U0,5H  RP0,4H  MP,4X,3HRMP,5H  G1N,5H  GMN,
     3       5H UP11,5H UP1N,5H UPMN,4X,2HCA,7X,2HCB,4X,2HCC,5H  CE,
     4       4H  C1//)
   72 FORMAT(1X,A8,A2,2E10.2,2(1X,F3.2),F4.0,2F5.2,1X,F4.3,2F5.2,
     1       3(1X,F4.3),E10.2,2F6.1,2F5.2)
   73 FORMAT(1H2,29HRMP DID NOT CONVERGE WITH MPX)
      REWIND 7
      KASE = 0
      PI=3.1415926
C
C     DATA INPUT
C
      READ(5,50) (REF(I),I=1,4),M,N,RLT
  100 READ(5,52) (REF(I),I=5,6),DS,MPX,QM,RP0,U0,KNP,SC
C
C     TEST FOR END OF INPUT
C
      IF( U0 .LT. 1. ) GO TO 400
      READ(5,51) E0,RHOF,RHOP,RR,THA,VISC
      IF( DS .GT. .36E-04 ) SC=.50
      MIT=0
  101 RMP=0.0

      MP=0.0
      VF=0.0
C
C     COMPUTE BASIC PARAMETERS
C     ASSUME AVERAGE SLIP VELOCITY DU
C
      DU=.07*U0
      RE=RHOF*DS*DU/VISC
C
C     COMPUTE CDINT FROM MORSI'S DRAG COEFFICIENT EQUATIONS
C
      IF( RE .GT. 1000. ) GO TO 100
      IF( RE .LE. .1 ) CDINT=24./RE
      IF( RE .GT. .1  .AND.  RE .LE. 1.0 )
     1    CDINT=(22.73/RE)+(.0903/(RE*RE))+3.69
      IF( RE .GT. 1.  .AND.  RE .LE. 10. )
     1    CDINT=(29.1667/RE)-(3.8889/(RE*RE))+1.222
      IF( RE .GT. 10.  .AND.  RE .LE. 100. )
     1    CDINT=(46.5/RE)-(116.667/(RE*RE))+.61667
      IF( RE .GT. 100. )
     1    CDINT=(98.33/RE)-(2778./(RE*RE))+.3644
      F=.75*CDINT*RHOF*DU/(DS*(RHOP+.5*RHOF))
      DP=.010*RR*U0/SC
      CA=RP0*((QM*RR)**2)/(4.*E0*DP*F)
      CB=RR*RR*F/DP
      CC=19.62*RR*RR*COS(PI*THA/180.)*(1.-(RHOF/RHOP))/(DP*U0)
      IF( CC .LE. .1E-05 ) CC=0.0
      CE=19.62*RR*SIN(PI*THA/180.)*(1.-(RHOF/RHOP))/(DP*F)
C
C     CHECK LIMIT OF CA
C
      IF( CA .LT. 1.99 ) GO TO 102
```

```
      WRITE(6,60) (REF(I),I=1,6),M,N,RLT
      WRITE(6,62) CA
      GO TO 100
  102 MC=(M/2)+1
      M1=M-1
      N1=N-1
      FM1=FLOAT(M1)
      FN1=FLOAT(N1)
C
C     COMPUTE STEP SIZES
C
      H=1.0/FN1
      W=PI/FM1
      DO 103 I=1,M
      A(I)=FLOAT(I-1)*W
  103 A(I)=COS(A(I))
C
C     COMPUTE FLUID VELOCITY PROFILE UF(J)
C
      DO 104 J=1,N
      R(J)=FLOAT(J-1)*H
  104 UF(J)=(1.-R(J))**.143
C
C     COMPUTE COEFF C(I,J) FOR EQUATION (A.3.15)
C
      DO 105 J=2,N1
      DUM=2.*((1./(W*U))*(R(J)/H)**2)
      C(J,1)=((R(J)/(2.*H))+(R(J)/H)**2)/DUM
      C(J,2)=1./(W*W*DUM)
      C(J,3)=(((R(J)/H)**2)-R(J)/(2.*H))/DUM
      C(J,4)=C(J,2)
  105 C(J,5)= 4.*CA*R(J)*R(J)/DUM
C
C     ASSUME INITIAL V(I,J) AND G(I,J)
C
      DO 106 I=1,M
      DO 106 J=1,N
      V(I,J)=2.*(ALOG(1.-CA*R(J)*R(J)/2.))
  106 G(I,J)=EXP(-V(I,J)-.5*CE*A(I)*R(J))
C
C     START ITERATION FOR G(I,J) AND V(I,J)
C
      ITN=1
  108 GDIF=0.0
      DO 109 I=1,M
      I11=I+1
      I01=I-1
      IF( I .EQ. 1 ) I01=2
      IF( I .EQ. M ) I11=M-1
      DO 109 J=2,N1
      J01=J-1
      J11=J+1
      V(I,J)=C(J,1)*V(I,J+1)+C(J,2)*V(I11,J)+C(J,3)*V(I,J-1)+
     1       C(J,4)*V(I01,J)+C(J,5)*G(I,J)
      DUM    =EXP(-V(I,J)-.5*CE*A(I)*R(J))
      RMX=ABS(1.-G(I,J)/DUM)
      IF( RMX .GT. GDIF ) GDIF=RMX
  109 G(I,J)=DUM
C
C     TEST FOR CONVERGENCE
C
      IF( GDIF .LE. RLT ) GO TO 110
```

```
      ITN=ITN+1
      IF( ITN .LE. 200 ) GO TO 108
      WRITE(6,63)
      GO TO 100
C
C     COMPUTE COEFF B(I,J,K) FOR EQUATION (A.3.1.4).
C
  110 DO 210 I=1,M
      I11=I+1
      I01=I-1
      IF( I .EQ. 1 ) I01=2
      IF( I .EQ. M ) I11=M-1
      DO 210 J=2,N1
      J01=J-1
      J11=J+1
      SUM1=G(I,J)/(H*H)
      SUM2=((G(I,J)/R(J))+(G(I,J11)-G(I,J01))/(2.*H))/(2.*H)
      SUM3=G(I,J)/(R(J)*R(J)*W*W)
      SUM4=(G(I11,J)-G(I01,J))/(4.*R(J)*R(J)*W*W)
      SUM5=G(I,J)*(CB*UF(J)-.5*CC)
      SUM6=G(I,J)*((2./(H*H))+(2./(R(J)*R(J)*W*W))+CB)
      B(I,J,1)=(SUM1+SUM2)/SUM6
      B(I,J,2)=(SUM3+SUM4)/SUM6
      B(I,J,3)=(SUM1-SUM2)/SUM6
      B(I,J,4)=(SUM3-SUM4)/SUM6
  210 B(I,J,5)=SUM5/SUM6
C
C     START ITERATION FOR UP(I,J)
C
      DO 211 I=1,M
      DO 211 J=1,N
  211 UP(I,J)=.95
      ITN=1
  212 UDIF=0.0
      DO 213 I=1,M
      I01=I-1
      I11=I+1
      IF( I .EQ. 1 ) I01=2
      IF( I .EQ. M ) I11=M-1
      DO 213 J=2,N1
      J01=J-1
      J11=J+1
      DUM=B(I,J,1)*UP(I,J11)+B(I,J,2)*UP(I11,J)+B(I,J,3)*UP(I,J01)
     1    +B(I,J,4)*UP(I01,J)+B(I,J,5)
      RMX=ABS(1.-UP(I,J)/DUM)
      IF( RMX .GT. UDIF ) UDIF=RMX
  213 UP(I,J)=DUM
C
C     UPDATE BOUNDARY VALUES
C
      DO 214 I=1,M
  214 UP(I,N)=(4.*UP(I,N-1)-UP(I,N-2))/(3.+2.*H/KND)
      UP0=(4.*UP(MC,2)-UP(MC,3))/3.
      DO 215 I=1,M
  215 UP(I,1)=UP0
C
C     TEST FOR CONVERGENCE
C
      IF( UDIF .LE. RLT ) GO TO 234
  217 ITN=ITN+1
      IF( ITN .LE. 200 ) GO TO 212
      WRITE(6,69)
```

```
      GO TO 100
C
C     COMPUTE MASS FLUX MX(I,J), SOLIDS FLOW RATE RMP AND VOLUME
C     FRACTION VF
C
  234 DO 237 I=1,M
      DO 237 J=1,N
      PG(I,J)=RP0     *U0*G(I,J)*F*ABS(UF(J)-UP(I,J))
      VR(I,J)=0.0
      IF( QM .LT. .1E-20 ) GO TO 236
      VR(I,J)=DP*F*V(I,J)/QM
  236 MX(I,J)=G(I,J)*UP(I,J)
  237 CONTINUE
      DO 242 J=2,M1
      AR=0.5*PI*(R(J+1)*R(J+1)-R(J)*R(J))/FM1
      DO 242 I=1,M1
      VF=VF+.25*AR*( G(I,J)+ G(I,J+1)+ G(I+1,J+1)+ G(I+1,J))
  242 MP=MP+.25*AR*(MX(I,J)+MX(I,J+1)+MX(I+1,J+1)+MX(I+1,J))
      AR=0.5*PI*R(2)*R(2)/FM1
      DO 246 I=1,M1
      VF=VF+AR*( G(1,1)+ G(I,2)+ G(I+1,2))/3.
  246 MP=MP+AR*(MX(1,1)+MX(I,2)+MX(I+1,2))/3.
      MP=2.*MP
      RMP=RR*RR*RP0     *U0*MP
      VF=2.*RP0     *VF/(RHOP*PI)
      IF( ABS(1.-MPX/RMP) .LE. .05 ) GO TO 300
      RP0=RP0*MPX/RMP
      MIT=MIT+1
      IF( MIT .LE. 10 ) GO TO 101
      WRITE(6,73)
      GO TO 100
  300 C1=RP0*PI*RR*RR*U0/MPX
      KASE=KASE+1
      WRITE(6,60) (REF(I),I=1,6),M,N,RLT
      WRITE(6,61) DS,E0,RHOF,RHOP,RR,THA,U0,VISC,KNP,QM,C1,SC,DP,
     1            CA,CB,CC,CE,MP,RMP,VF,MPX
      WRITE(6,64) ((G(I,J),J=1,N),I=1,M)
      WRITE(6,68) ((MX(I,J),J=1,N),I=1,M)
      WRITE(6,70) ((PG(I,J),J=1,N),I=1,M)
      WRITE(6,60) (REF(I),I=1,6),M,N,RLT
      WRITE(6,67) ((UP(I,J),J=1,N),I=1,M)
      WRITE(6,65) ((V(I,J),J=1,N),I=1,M)
      WRITE(6,66) ((VR(I,J),J=1,N),I=1,M)
C
C     STORE RESULTS ON DISC FILE FOR GRAPH PLOTTING PROGRAM #PJ06
C
      WRITE(7) (REF(I),I=1,6),M,N,DS,THA,U0,KNP,QM,RP0,SC,DP,RR,MPX,
     1         CA,CB,CC,CE,MP,RMP,VF,((G(I,J),MX(I,J),PG(I,J),UP(I,J),
     2         V(I,J),VR(I,J),J=1,N),I=1,M),C1
      GO TO 100
  400 REWIND 7
      WRITE(6,71) (REF(I),I=1,4),M,N,RLT
      DO 410 K=1,KASE
      READ(7)  (REF(I),I=1,6),M,N,DS,THA,U0,KNP,QM,RP0,SC,DP,RR,MPX,
     1         CA,CB,CC,CE,MP,RMP,VF,((G(I,J),MX(I,J),PG(I,J),UP(I,J),
     2         V(I,J),VR(I,J),J=1,N),I=1,M),C1
  410 WRITE(6,72) (REF(I),I=5,6),DS,QM,KNP,MPX,U0,RP0,MP,RMP,G(1,N),
                  G(M,N),UP(1,1),UP(1,N),UP(M,N),CA,CB,CC,CE,C1
      REWIND 7
      STOP
      END
```

APPENDIX 4

COMPUTER PROGRAM #CYP1

The function of #CYP1 is to copy and sort out experimental data on paper tape produced by the Solartron-Facit system and store required data on disc files.

Program Symbols

DATE	date of experiment
INDEX	entry identifier
KB	data signals
KDS	particle diameter
KNL	number of channels per scan
KRH	relative hummidity
KROS	particl density
KSCALE	ball probe current scale factor
PRESS	ambient pressure
TEMP	ambient temperature
TN	data tape number
TYPE	type od particles

* All quantities are in BCD integer form.

```
C
C       V K CHAN
C
C       PROGRAM #CPY1 : COPY DATA FROM P/T ON TO DISC
C
        INTEGER TN, DATE,TEMP,PRESS,TYPE
        DIMENSION KA(48),KB(48),KC(48)
C
C       TELETYPE MESSAGE
C
  100   WRITE(7,70)
   70   FORMAT(30H TYPE 20 TO GO!)
        READ(8,80) JJ
   80   FORMAT(I2)
        IF( JJ .NE. 20 ) STOP
C
C       READ DATA TAPE
C
        READ(5,50) TN,DATE,TEMP,PRESS,KRH,KNL
   50   FORMAT(I4)
        WRITE(6,60) TN,DATE,TEMP,PRESS,KRH,KNL
   60   FORMAT(1H1,8I6)
        WRITE(9,90) TN,DATE,TEMP,PRESS,KRH,KNL
   90   FORMAT(8I5)
C
C       CHECK INDEX (DATA MARKER)
C
  106   READ(5,50) INDEX
        IF( INDEX .EQ. 0 ) GO TO 106
        GO TO (109,116,123,123,123,130,123,123,200),INDEX
  109   READ(5,50) TYPE,KROS
        READ(5,50) IX
        IF( IX .EQ. 0 ) GO TO 106
        WRITE(6,61) INDEX
   61   FORMAT(8I6)
        WRITE(9,90) INDEX
        WRITE(6,61) TYPE,KROS
        WRITE(9,90) TYPE,KROS
        GO TO 137
  116   READ(5,50) KDS
        READ(5,50) IX
        IF( IX .EQ. 0 ) GO TO 106
        WRITE(6,61) INDEX
        WRITE(9,90) INDEX
        WRITE(6,61) KDS
        WRITE(9,90) KDS
        GO TO 137
  123   READ(5,51) (KA(I),KB(I),KC(I),I=1,48)
   51   FORMAT(I3,I5,2I3,I5,2I3,I5,2I3,I5,11)
        READ(5,50) IX
        IF( IX .EQ. 0 ) GO TO 106
        WRITE(6,61) INDEX
        WRITE(9,90) INDEX
        WRITE(6,61) (KC(I),I=1,48)
        WRITE(9,90) (KB(I),I=1,48)
        GO TO 137
```

```
  130 READ(5,50) KSCALE
      READ(5,50) IX
      IF( IX .EQ. 0 ) GO TO 106
      WRITE(6,61) INDEX
      WRITE(9,90) INDEX
      WRITE(6,61) KSCALE
      WRITE(9,90) KSCALE
  137 INDEX=IX
      GO TO (109,116,123,123,123,130,123,123,200),INDEX
  200 WRITE(6,61) INDEX
      WRITE(9,90) INDEX
      WRITE(7,71) TN
   71 FORMAT(12H LOADED TAPE,I3)
      GO TO 100
      END

1372 ENTRY   00222
```

CT

APPENDIX 5

COMPUTER PROGRAM #PDP1

The function of #PDP1 is to perform numerical calculations for air velocity distribution, air friction factor and other pipe flow parameters.

Program Symbols

CF	calibration constants for pressure transducers
DF	eddy diffusivity, (m^2/sec)
DUN	computed velocity gradient at pipe wall, (sec^{-1})
DUW	experimental velocity gradient at pipe wall, (sec^{-1})
FA	air friction factor
MF	air flow rate, (kg/sec)
P	data signals
PG	pressure gradient, (kg/m^2sec^2)
PR	ambient pressure,(cm of Hg)
SW	wall shear stress, (N/m^2)
TR	ambient temperature, (Deg. C)
VS	frictional velocity, (m/sec)

```
TION BY #XFAT MK 5A     DATE  04/05/76  TIME  21.14.43


      WORK(ED)
      SEND TO(GEOSSEMICOMP)
      LIST(LP)
      PROGRAM (PDP1)
      COMPACT
      INPUT 5 = CR0
      OUTPUT 6 = LP0
      USE 7 = ED1/FORMATTED(RYB66000CHN2)/512
      TRACE 0
      END
```

```
      MASTER PDP1
      REAL MF
      INTEGER TN,DATE,TEMP,PRESS
      DIMENSION REF(4),P(8),Z(8),IS(6,8),Y(10),C(10),DF(15)
      COMMON /BLK1/ AR,RR,KSCAN,RKF,X(10),CF(7,2),DU1(15),R(15),UF(15)
      READ(5,50) (REF(I),I=1,4)
   50 FORMAT(4A8)
      CALL DVEI
  103 READ(7,70) TN,DATE,TEMP,PRESS,KNL
   70 FORMAT(8I5)
      LINE=14
      TR=(FLOAT(TEMP)/100.)+273.
      PR=FLOAT(PRESS)/100.
      RHOF=4.6444*PR/TR
      VISC=(.00672/(TR+120.))*((TR/273.)**1.5)
  108 READ(7,70) INDEX
      IF( INDEX .EQ. 9 ) GO TO 200
      READ(7,70) ((IS(I,J),J=1,KNL),I=1,KSCAN)
      DO 115 J=1,7
      P(J)=0.0
      DO 114 I=1,KSCAN
  114 P(J)=P(J)+FLOAT(IS(I,J))
  115 P(J)=P(J)/FLOAT(KSCAN)
      IF( INDEX .NE. 3 ) GO TO 119
      DO 118 J=1,KNL
  118 Z(J)=P(J)
      GO TO 108
  119 DO 121 J=1,7
      P(J)=P(J)-Z(J)
```

```
  121 P(J)=(CF(J,1)+CF(J,2)*P(J))*P(J)
      MF=0.00785*SQRT(RKF*RHOF*P(2))
      UN=MF/(AP*RHOF)
      U0=1.224*UN
      RE=2.*RR*RHOF*UN/VISC
      Y(1)=0.0
      DO 128 I=2,5
      P(I+2)=P(I+2)+P(I+1)
  128 Y(I)=P(I+2)-P(3)
C     CALL #LTSQ TO SMOOTH DATA
      CALL LTSQ(0,2,5,X,Y,C,IFLAG)
      IF( IFLAG .NE. 1 ) GO TO 108
      PG=-98.1*(C(1)+11.*C(2))
      SW=-0.5*RR*PG
      VS=SQRT(SW/RHOF)
      FA=8.*SU/(RHOF*UN*UN)
      DUW=-SW/VISC
      DUN=U0*DU1(11)/RR
      DO 138 I=2,10
  138 DF(I)=((CR*RR*R(I)*PG/(2.*U0*DU1(I)))-VISC)/RHOF
      LINE=LINE+1
      IF( LINE .LE. 14 ) GO TO 144
      LINE=1
      WRITE(6,60) (REF(I),I=1,4),TN,DATE
   60 FORMAT(1H2,4A8,5X,4HTAPE,I3,1H-,I4//)
      WRITE(6,61)
   61 FORMAT(9X,3HMF ,8X,3HUN ,8X,3HRE ,8X,3HPG ,8X,3HSW ,8X,3HVS ,
     1       8X,3HFA ,8X,3HDUW,8X,3HDUN/)
  144 WRITE(6,62) MF,UN,RE,PG,SW,VS,FA,DUW,DUN
   62 FORMAT(5X,9E11.3)
      WRITE(6,63) (DF(I),I=2,10)
   63 FORMAT(5H DF :,9E11.3)
      DO 146 I=2,10
  146 DF(I)=DF(I)/(2.*RR*UN)
      WRITE(6,65) (DF(I),I=2,10)
   65 FORMAT(5H DF1 ,9E11.3/)
      GO TO 108
  200 IF( TN .NE. 49 ) GO TO 103
      REWIND 7
      STOP
      END

LENGTH    490, NAME  PDP1
```

```
      SUBROUTINE DVEL
      COMMON /BLK1/ AR,RR,KSCAN,RKF,X(10),CF(7,2),DU1(15),R(15),UF(15)
      DO 102 I=1,11
      R(I)=.1*FLOAT(I-1)
  102 UF(I)=(1.-R(I))**.142857
      DO 104 I=2,10
  104 DU1(I)=(UF(I+1)-UF(I-1))*5.
      DU1(11)=(UF(9)-4.*UF(10))*5.
      RETURN
      END
```

```
LENGTH     75, NAME  DVEL
```

```
      SUBROUTINE GAUSID(A,M,N,B,C,X,Y,IC)
C     THIS PROGRAM WILL SOLVE AN N BY N SYSTEM OF LINEAR EQUATIONS
C     USING THE GAUSS-SEIDEL METHOD
      DIMENSION A(10,10),B(10),C(10),R(10,11),X(10),Y(10)
      IC=1
  100 ERR=.0001
  113 K=0
      MM=M+1
      DO 111 I=1,M
      IF( A(I,I) ) 112,114,112
  112 C(I)=1.
      R(I,MM)=B(I)/A(I,I)
      DO 111 J=1,M
  111 R(I,J)=A(I,J)/A(I,I)
  101 E=0.0
      DO 103 I=1,M
      P=R(I,MM)
      DO 102 J=1,M
  102 P=P-R(I,J)*C(J)
      C(I)=C(I)+P
  103 E=E+ABS(P)
      IF( E-ERR ) 104,104,105
  105 K=K+1
      IF( 1000-K ) 106,101,101
  106 ERR=ERR*10.0
      IF( ERR .LE. 0.0011) GO TO 113
  114 IC=0
  104 RETURN
      END
```

LENGTH 185, NAME GAUSID

```
      SUBROUTINE LTSQ(KT,M,N,X,Y,C,IC)
      DIMENSION X(10),Y(10),C(10),F(10,10),A(10,10),B(10)
C     M UNKNOWN COEFFS AND N PAIRS OF (X,Y)
      IF( KT .EQ. 1 ) GO TO 100
      DO 101 J=1,N
      DO 101 I=1,M
  101 F(I,J)=X(J)**I
      GO TO 400
  100 DO 200 J=1,N
  200 F(1,J)=1.0
      DO 300 J=1,N
      DO 300 I=2,M
  300 F(I,J)=X(J)**(I-1)
  400 DO 103 I=1,M
      DO 103 K=1,I
      A(K,I)=0.0
      DO 102 J=1,N
  102 A(K,I)=A(K,I)+F(I,J)*F(K,J)
  103 A(I,K)=A(K,I)
      DO 104 K=1,M
      B(K)=0.0
      DO 104 J=1,N
  104 B(K)=B(K)+Y(J)*F(K,J)
      CALL GAUSID(A,M,N,B,C,X,Y,IC)
      RETURN
      END
```

LENGTH 232, NAME LTSQ

```
BLOCK DATA
COMMON /BLK1/ AR,RR,KSCAN,RKF,X(10),CF(7,2),DU1(15),R(15),UF(15)
DATA AR,RR,KSCAN,RKF/ .000767,.015625,6.1.11 /
DATA X / 0.0,2.93,5.1,7.54,9.98,0.0,0.0,0.0,0.0,0.0,0.0 /
DATA CF / .65E-03,.015,.0193,.01964,.01737,.01577,.0165,0.0,
     .169E-05,.176E-05,.2378E-05,.172E-05,.1018E-05,.1906E-05 /
END
```

APPENDIX 6

COMPUTER PROGRAM #PDP2

The function of #PDP2 is to perform numerical calculations for mass flow rates, pressure distribution, suspension friction factors, ball probe current, charge transfer and standard deviations of data input signals, and store results on disc files.

Program Symbols

CFA	air friction factor C_f
CFM	suspension friction factor C_{fm}
CFP	particle friction factor C_{fp}
FR	Froude number
IB	ball probe current I_b, (amp)
IN	dimensionless current number I_n
MF	air flow rate M_f, (kg/sec)
MP	solid flow rate M_p, (kg/sec)
MR	mass flow ratio (M_p/M_f)
PGM	pressure gradient of suspension flow $(\partial P/\partial x)_m$, (kg/m^2sec^2)
PR	ambient pressure (cm of Hg)
QM	charge transfer per unit mass (Q/M), (c/kg)
RE	Reynolds number Re
RPO	estimated particulate density at pipe axis, (kg/m^3)
TR	ambient temperature, (Deg. C)
UN	mean fluid velocity $\bar{u}$, (m/sec)

* Others are defined in #XFD7B and #CYP1.

```
[04/05/76 AT 21.18

TION BY #XEAT HK 5A    DATE  04/05/76  TIME  21.18.15


      WORK(ED)
      SEND TO(GEOSSEMICOMP)
      LIST (LP)
      PROGRAM (PDP2)
      COMPACT
      INPUT 5 = CR0
      OUTPUT 6 = LP0
      USE 7 = ED1/FORMATTED(HYB66000CHN1)/512
      OUTPUT 8 = MT0/UNFORMATTED(MAG TAPE 001)/512
      TRACE 0
      END
```

```
C
C     V K CHAN
C
C     DATA PROCESSING PROGRAM #PDP2
C     I/P DATA PRE-SORTED BY #CPY1
C
      MASTER PDP2
      REAL MF,MP,MR,IB,IN
      INTEGER TYPE,TN,DATE,TEMP,PRESS
      DIMENSION AA(90,14),C(10),IA(90,4),IS(6,8),P(8),REF(2),Y(10),Z(8)
      COMMON /BLK1/ AR,CF(7,2),DD(5),CFA(10),KSCAN,RKF,RR,TIME(10),X(10)
   50 FORMAT(2A8)
   60 FORMAT(1H2,2A8,3X,4HTAPE,I3,1H-,I4,3X,1HC,F5.1,3H K,,F5.1,
     1       4H HG,,I3,4H%RH),3X,4HPAGE,I2,3H OF,I2//)
   61 FORMAT(14X,2HMF,9X,2HMP,8X,3HMP/(A*U),4X,5HMP/MF,6X,2HUN,
     1       9X,2HU0,9X,2HRE/)
   62 FORMAT(13,1H-,I2,1H-,I1,1H-,I1,7E11.3/)
   63 FORMAT(14X,2HFR,9X,5HDP/DX,6X,3HCFM,8X,3HCFP,8X,2HIB,9X,
     1       2HIN,9X,3HR/M/)
   71 FORMAT(8I5)
      REWIND 8
C
C     READ DATA REFERENCE
C
      READ(5,50) (REF(I),I=1,2)
C
C     READ EXPERIMENTAL DATA (SIGNALS) ON DISC FILE PRODUCED BY #CPY1
C
  101 READ(7,71) TN,DATE,TEMP,PRESS,KRH,KNI
```

```
C
C     COMPUTE AMBIENT TEMPERATURE TR, PRESSURE PR, AIR DENSITY RHOF
C     AND DYNAMIC VISCOSITY VISC
C
      TR=(FLOAT(TEMP)/100.)+273.
      PR=FLOAT(PRESS)/100.
      RHOF=4.6444*(PR/TR)
      NUM=0
      VISC=(.00672/(TR+120.))*((TR/273.)**1.5)
  108 READ(7,71) INDEX
      GO TO (110,112,115,115,115,113,115,115,200), INDEX
  110 READ(7,71) TYPE,KS
      RHOP=FLOAT(KS)
      DS=DD(TYPE)
      GO TO 108
  112 READ(7,71) KDUM
      GO TO 108
  113 READ(7,71) KSCALE
      SCALE=FLOAT(KSCALE)*.1E-12
      GO TO 108
  115 READ(7,71) ((IS(I,J),J=1,KNL),I=1,KSCAN)
C
C     COMPUTE TIME AVERAGING OF EACH SIGNAL P(J)
C
      DO 120 J=2,KNL
      P(J)=0.0
      DO 119 I=1,KSCAN
  119 P(J)=P(J)+FLOAT(IS(I,J))
  120 P(J)=P(J)/FLOAT(KSCAN)
      IF( INDEX .NE. 3 ) GO TO 124
      DO 123 J=2,KNL
  123 Z(J)=P(J)
      GO TO 108
  124 DO 125 I=1,KSCAN
  125 Y(I)=FLOAT(IS(I,1))
C
C      CALL #LTSQ TO FIT BEST STRAIGHT LINE THROUGH MASS/ TIME POINTS
C
      CALL LTSQ(1,2,KSCAN,TIME,Y,C,IFLAG)
      IF( IFLAG .NE. 1 ) GO TO 108
      MP=-CF(1,1)*C(2)
C
C     CONVERT P(J) INTO PHYSICAL QUANTITIES
C
      DO 131 J=2,KNL
      P(J)=P(J)-Z(J)
      IF( J .EQ. KNL ) GO TO 132
  131 P(J)=(CF(J,1)+CF(J,2)*P(J))*P(J)
  132 Y(1)=0.0
      DO 135 I=2,5
      P(I+2)=P(I+2)+P(I+1)
  135 Y(I)=P(I+2)-P(3)
C
C     CALL #LTSQ TO FIT PRESSURE DISTRIBUTION CURVE
C
      CALL LTSQ(0,2,5,X,Y,C,IFLAG)
      IF( IFLAG .NE. 1 ) GO TO 108
C
C     COMPUTE AIR FLOW RATE MF, MEAN AIR VELOCITY UN AND REYNOLDS
C     NUMBER RE
C
      MF=.00785*SQRT(RKF*RHOF*P(2))
```

```
      UN=MF/(AR*RHOF)
      RE=2.*RHOF*UN*RR/VISC

C     CALL #FNEW TO INTERPOLATE AIR FRICTION FACTOR FINT FROM CFA

      CALL FNEW(CFA,10,.3E+5,.5E+4,5,RE,FINT,IFLAG)
      IF( IFLAG .NE. 1 ) GO TO 108
C
C     COMPUTE AIR VELOCITY AT PIPE CENTRE U0, MASS FLOW RATIO MR,
C     FROUDE NUMBER FR, PRESSURE GRADIENT PGM, SUSPENSION FRICTION
C     FACTOR CFM, PARTICLES FRICTION FACTOR CFP, CHARGE CURRENT IB,
C     DIMENSIONLESS CHARGE CURRENT NUMBER IN AND CHARGE TRANSFER PER UNIT
C     MASS QM
C
      U0=1.224*UN
      RP0=MP/(AR*UN)
      MR=MP/MF
      FR=UN*UN/(19.62*RR)
      PGM=98.1*(C(1)+11.*C(2))
      CFM=4.*RP*PGM/(RHOF*UN*UN)
      CFP=CFM-FINT
      IB=P(8)*SCALE
      IN=(IB*IB)/(DS*DS*RHOF*(0.62E-10)*(UN**4))
      QM=-IB/(RP0*UN*0.3068E-4)
      NUM=NUM+1
      IA(NUM,1)=TN
      IA(NUM,2)=NUM
      IA(NUM,3)=INDEX
      IA(NUM,4)=TYPE
      AA(NUM,1)=MF
      AA(NUM,2)=MP
      AA(NUM,3)=RP0
      AA(NUM,4)=MR
      AA(NUM,5)=UN
      AA(NUM,6)=U0
      AA(NUM,7)=RE
      AA(NUM,8)=FR
      AA(NUM,9)=PGM
      AA(NUM,10)=CFM
      AA(NUM,11)=CFP
      AA(NUM,12)=IB
      AA(NUM,13)=IN
      AA(NUM,14)=QM
      GO TO 108

      STORE RESULTS ON M/T

  200 WRITE(8) TN,DATE,TR,PR,KRH,NUM,((IA(I,J),J=1,4),I=1,NUM),
     1         ((AA(I,J),J=1,14),I=1,NUM)
      LP=(NUM/30)
      IF( (30*LP) .LT. NUM ) LP=LP+1
      LP=2*LP
      KP=0
      DO 213 I=1,NUM
      IF( (((I-1)/30)*30) .NE. (I-1) ) GO TO 213
      KP=KP+1
      WRITE(6,60) (REF(K),K=1,2),TN,DATE,TR,PR,KRH,KP,LP
      WRITE(6,61)
  213 WRITE(6,62) (IA(I,J),J=1,4),(AA(I,J),J=1,7)
      DO 222 I=1,NUM
      IF( (((I-1)/30)*30) .NE. (I-1) ) GO TO 222
      KP=KP+1
```

```
      WRITE(6,60) (REF(K),K=1,2),TN,DATE,TR,PR,KRH,KP,LP
      WRITE(6,63)
  222 WRITE(6,62) (IA(I,J),J=1,4),(AA(I,J),J=8,14)
C
C     CHECK FOR END OF TAPE
C
      IF( TN .NE. 43 ) GO TO 101
      REWIND 7
      STOP
      END


LENGTH   836, NAME  PDP2
```

```
      SUBROUTINE LTSQ(KT,M,N,X,Y,C,IC)
C
C     LEAST SQUARES CURVE FITTING PROGRAM
C     M UNKNOWN COEFFS AND N PAIRS OF (X,Y)
C
      DIMENSION X(10),Y(10),C(10),F(10,10),A(10,10),B(10)
      IF( KT .EQ. 1 ) GO TO 100
      DO 101 J=1,N
      DO 101 I=1,M
  101 F(I,J)=X(J)**I
      GO TO 400
  100 DO 200 J=1,N
  200 F(1,J)=1.0
      DO 300 J=1,N
      DO 300 I=2,M
  300 F(I,J)=X(J)**(I-1)
  400 DO 103 I=1,M
      DO 103 K=1,I
      A(K,I)=0.0
      DO 102 J=1,N
  102 A(K,I)=A(K,I)+F(I,J)*F(K,J)
  103 A(I,K)=A(K,I)
      DO 104 K=1,M
      B(K)=0.0
      DO 104 J=1,N
  104 B(K)=B(K)+Y(J)*F(K,J)
      CALL GAUSID(A,M,N,B,C,X,Y,IC)
      RETURN
      END
```

LENGTH 232, NAME LTSQ

```
      SUBROUTINE GAUSID(A,M,N,B,C,X,Y,IC)
C
C     THIS PROGRAM WILL SOLVE AN N BY N SYSTEM OF LINEAR EQUATIONS
C     USING THE GAUSS-SEIDEL METHOD
C
      DIMENSION A(10,10),B(10),C(10),R(10,11),X(10),Y(10)
      IC=1
  100 ERR=.0001
  113 K=0
      MM=M+1
      DO 111 I=1,M
      IF( A(I,I) ) 112,114,112
  112 C(I)=1.
      R(I,MM)=B(I)/A(I,I)
      DO 111 J=1,M
  111 R(I,J)=A(I,J)/A(I,I)
  101 E=0.0
      DO 103 I=1,M
      P=R(I,MM)
      DO 102 J=1,M
  102 P=P-R(I,J)*C(J)
      C(I)=C(I)+P
  103 E=E+ABS(P)
      IF( E-ERR ) 104,104,105
  105 K=K+1
      IF( 1000-K ) 106,101,101
  106 ERR=ERR*10.0
      IF( ERR  LE. 0.0011) GO TO 113
  114 IC=0
```

```
104 RETURN
    END

LENGTH   185, NAME  GAUSYD
```

```
    SUBROUTINE FNEW(Y,M,XBEG,DX,N,XINT,YINT,IC)

    #FNEW IS A NEWTON'S FORWARD INTERPOLATION SUBROUTINE
    COMPUTE YINT FOR GIVEN XINT FROM Y(M)

    DIMENSION Y(10),D(10)
    IC=1
    MO=INT((XINT-XBEG+DX)/DX)
    IF( M-N-1) 121,121,101
101 IF( MO ) 120,120,102
102 IF( MO-M ) 103,103,120
103 IF( M-MO-N ) 104,105,105
104 MO=M-N
105 FMO=FLOAT(MO-1)
    XO=XBEG+FMO*DX
    U=(XINT-XO)/DX
    A=U
    YINT=Y(MO)
106 DO 107 I=1,N
    J=MO+I-1
107 D(I)=Y(J+1)-Y(J)
    IF( N-1 ) 121,110,108
108 DO 109 K=2,N
    DO 109 I=K,N
    L=N+K-I
109 D(L)=D(L)-D(L-1)
110 DO 111 K=1,N
    YINT=YINT+A*D(K)
    FK=FLOAT(K)
```

```
111  A=A*(U-FK)/(FK+1.)
     RETURN
120  IC=0
     RETURN
121  IC=2
     RETURN
     END

LENGTH    214, NAME   FNEW
```

```
     BLOCK DATA
     COMMON /BLK1/ AR,CF(7,2),DD(5),CFA(10),KSCAN,RKF,RR,TIME(10),X(10)
     DATA AR,RR,KSCAN,RKF/ .000767,.015625,6,1.11 /
     DATA X / 0.0,2.93,5.1,7.54,9.98,0.0,0.0,0.0,0.0,0.0,0.0,0.0 /
     DATA CF / .65E-03,.015,.0193,.01964,.01737,.01577,.0165,0.0,
    1      .169E-05,.176E-05,.2378E-05,.172E-05,.1018E-05,.1906E-05 /
     DATA TIME /0.0,2.254,4.508,6.762,9.016,11.27,.0,.0,.0,.0 /
     DATA DD / .35E-4,.75E-4,.8E-4,.385E-3,.1385E-2/
     DATA CFA/  .0197,.0191,.0185,.0181,.0177,.0174,.0172,.0170,
    1       .0168,.0168 /
     END
```

APPENDIX 7

COMPUTER PROGRAM #PJ03

The function of #PJ03 is to sort out data produced by #PDP2 for graph plotting program #PJ04.

Program Symbols

Program symbols are similarly defined as those in #PDP2.

Input Data

1. (ICON(I),I=1,6), NFIG
2. (FIG(I),I=1,10)

where (ICON(I),I=1,6) are input control parameters, (FIG(I),I=1,10) is the graph title, NFIG is the number of characters in FIG and the data formats are (7I3) and (10A8) respectively.

```
(04/05/76 AT 21.05

TION BY #XFAT HK 5A    DATE  04/05/76  TIME  21.05.26


      WORK(ED)
      SEND TO(GEOSSEMICOMP)
      LIST (LP)
      PROGRAM (PJ03)
      COMPACT
      INPUT 5 = CR0
      OUTPUT 6 = LP0
      INPUT 7 = MT0/UNFORMATTED(MAG TAPE 001)/512
      USE 8 = ED1/UNFORMATTED(HYB66000CHN2)/512
      TRACE 0
      END
```

```
C
C     V K CHAN
C
C     PROGRAM #PJ03
C     GENERATE PLOTTING DATA FOR #PJ04
C
      MASTER PJ03
      INTEGER TN,DATE
      DIMENSION ICON(6),IA(60,4),AA(60,14),IS(150,4),IP(150),IX(150)
      DIMENSION IXY(150),X(150),NP(30),P(30),Q(30),NLT(30),S(150,5)
      DIMENSION AXIS(2,3),HEAD(5),NCH(2),FIG(10),PS(3),QS(3)
      COMMON /BLK1/ TITLE(3,14),NTL(14),VAR(14),BLANK
   50 FORMAT(7I3)
   51 FORMAT(10A8)
   60 FORMAT(1H2,/9H FIGURE :,5X,10A8//14X,18HGLASS BEADS TYPE #,I1,
     *       1H.,4X,14HO/P BY #PJ03 (,I1,5(1H-,I2),2H),,//)
   61 FORMAT(10X,16HDATA - REFERENCE,5(3X,A8)/)
   62 FORMAT(9X,I2,1H.,I2,1H),I4,1H-,I2,1H-,I1,1H-,I1,5E11.3)
      REWIND 7
      REWIND 8
C
C     DATA INPUT
C
  100 READ(5,50) (ICON(I),I=1,6),NFIG
      IF( ICON(1) .EQ. 0 ) STOP
      READ(5,51) (FIG(I),I=1,10)
      DO 101 I=1,150
      DO 101 J=1,5
  101 S(I,J)=0.0
```

```
      NUM=0
C
C     READ DATA ON M/T PRODUCED BY #PDP2
C
  103 READ(7) TN,DATE,TR,PR,KRN,M,((IA(I,J),J=1,4),I=1,M),
     1        ((AA(I,J),J=1,14),I=1,M)
      DO 113 I=1,M
      IF( IA(I,4) .NE. ICON(1) ) GO TO 113
      NUM=NUM+1
C
C     STORE REQUIRED DATA IN IS(I,J) AND S(I,J)
C
      DO 107 J=1,4
  107 IS(NUM,J)=IA(I,J)
      DO 112 K=2,6
      IF( ICON(K) .EQ. 0 ) GO TO 112
      J=ICON(K)
      S(NUM,K-1)=AA(I,J)
  112 CONTINUE
  113 CONTINUE
C
C     CHECK FOR END OF M/T
C
      IF( TN .NE. 43 ) GO TO 103
      REWIND 7
      IF( NUM .LT. 4 ) GO TO 100
C
C     RE-ORDER PLOTTING DATA POINTS AND STORE LIST IN IX(J)
C
      DO 120 I=1,NUM
      IP(I)=0
      IX(I)=0
      IXY(I)=1
  120 X(I)=S(I,1)
      DO 130 J=1,NUM
      II=1
      DUM=X(II)
      DO 128 I=2,NUM
      IF( X(I) .GE. DUM ) GO TO 128
      II=I
      DUM=X(I)
  128 CONTINUE
      X(II)=.1E20
  130 IX(J)=II
      NO1=NUM-1
      LAST=0
      IF( ICON(5) .NE. 0  .AND.  ICON(6) .NE. 0 ) GO TO 200
C
C     DELETE MULTIPLE POINTS
C
      DO 144 I=1,NO1
      I11=I+1
      DO 143 J=I11,NUM
      IF( IXY(J) .EQ. 0 ) GO TO 143
      IF( IS(I,3) .NE. IS(J,3) ) GO TO 143
      IF( ABS(1.-S(I,4)/S(J,4)) .GT. .05 ) GO TO 143
      IF( ABS(1.-S(I,1)/S(J,1)) .GT. .05 ) GO TO 143
      IF( ABS(1.-S(I,2)/S(J,2)) .GT. .05 ) GO TO 143
      IXY(J)=0
  143 CONTINUE
  144 CONTINUE
C
```

```
C       COMPUTE PARAMETRIC CONSTANT P FOR EACH CURVE
C
  146 DO 148 I=1,NUM
      IF( IXY(I) .NE. 0 ) GO TO 149
  148 CONTINUE
      GO TO 300
  149 PMIN=S(I,4)
      DO 153 I=1,NUM
      IF( IXY(I) .EQ. 0 ) GO TO 153
      IF( S(I,4) .LT. PMIN ) PMIN=S(I,4)
  153 CONTINUE
      DO 167 INDEX=7,8
      SUM=0.0
      KK=0
      DO 160 I=1,NUM
      IF( IXY(I) .EQ. 0 ) GO TO 160
      IF( IS(I,3) .NE. INDEX ) GO TO 160
      IF( ABS(1.-S(I,4)/PMIN) .GT. .05 ) GO TO 160
      KK=KK+1
      SUM=SUM+S(I,4)
      NLT(KK)=I
      IXY(I)=0
  160 CONTINUE
C
C       DELETE CURVES CONTAINING LESS THAN 4 DATA POINTS
C
      IF( KK .LT. 4 ) GO TO 167
      LAST=LAST+1
      NP(LAST)=KK
      P(LAST)=SUM/FLOAT(KK)
      DO 166 K=1,KK
      N=NLT(K)
  166 IP(N)=LAST
  167 CONTINUE
      GO TO 146
C
C       DELETE MULTIPLE DATA POINTS
C
  200 DO 211 I=1,N01
      I11=I+1
      DO 210 J=I11,NUM
      IF( IXY(J) .EQ. 0 ) GO TO 210
      IF( ABS(1.-S(I,4)/S(J,4)) .GT. .05 ) GO TO 210
      IF( ABS(1.-S(I,5)/S(J,5)) .GT. .05 ) GO TO 210
      IF( ABS(1.-S(I,1)/S(J,1)) .GT. .05 ) GO TO 210
      IF( ABS(1.-S(I,2)/S(J,2)) .GT. .05 ) GO TO 210
      IXY(J)=0
  210 CONTINUE
  211 CONTINUE
C
C       COMPUTE PARAMETRIC CONSTANT P & Q FOR EACH CURVE
C
  212 DO 214 I=1,NUM
      IF( IXY(I) .NE. 0 ) GO TO 215
  214 CONTINUE
      GO TO 300
  215 PMIN=S(I,4)
      QMIN=S(I,5)
      DO 222 I=1,NUM
      IF( IXY(I) .EQ. 0 ) GO TO 222
      IF( S(I,4) .GE. PMIN ) GO TO 222
      PMIN=S(I,4)
```

```
      QMIN=S(I,5)
  222 CONTINUE
      PSUM=0.0
      QSUM=0.0
      KK=0
      DO 235 I=1,NUM
      IF( IXY(I) .EQ. 0 ) GO TO 235
      IF( ABS(1.-S(I,4)/PMIN) .GT. .05 ) GO TO 235
      IF( ABS(1.-S(I,5)/QMIN) .GT. .05 ) GO TO 235
      KK=KK+1
      PSUM=PSUM+S(I,4)
      QSUM=QSUM+S(I,5)
      NLT(KK)=I
      IXY(I)=0
  235 CONTINUE
C
C     DELETE CURVES CONTAINING LESS THAN 3 DATA POINTS
C
      IF( KK .LT. 3 ) GO TO 212
      LAST=LAST+1
      NP(LAST)=KK
      P(LAST)=PSUM/FLOAT(KK)
      Q(LAST)=QSUM/FLOAT(KK)
      DO 243 K=1,KK
      N=NLT(K)
  243 IP(N)=LAST
      GO TO 212
  300 IF( LAST .EQ. 0 ) GO TO 100
      KT=0
C
C     SORT DATA POINTS AND PARAMETRIC CONSTANTS FOR EACH CURVE
C
      DO 312 L=1,LAST
  312 KT=KT+NP(L)
      DO 313 K=1,5
  313 CALL COPY(8,HEAD(K),1,BLANK,1)
      I=0
      DO 316 K=2,6
      IF( ICON(K) .EQ. 0 ) GO TO 316
      I=I+1
      J=ICON(K)
      CALL COPY(8,HEAD(I),1,VAR(J),1)
  316 CONTINUE
      DO 321 I=1,2
      K=ICON(I+1)
      NCH(I)=NTL(K)
      DO 321 J=1,3
  321 CALL COPY(8,AXIS(I,J),1,TITLE(J,K),1)
      K=ICON(5)
      NPS=NTL(K)
      DO 322 J=1,3
  322 CALL COPY(8,PS(J),1,TITLE(J,K),1)
      WRITE(8) (ICON(I),I=1,6),NFIG,(FIG(I),I=1,10),
     1         (NCH(I),I=1,2),((AXIS(I,J),J=1,3),I=1,2),KT,LAST,
     2         (NP(I),P(I),I=1,LAST),NPS,(PS(I),I=1,3)
      IF( ICON(6) .EQ. 0 ) GO TO 327
      K=ICON(6)
      NQS=NTL(K)
      DO 325 J=1,3
  325 CALL COPY(8,QS(J),1,TITLE(J,K),1)
      WRITE(8) (Q(I),I=1,LAST),NQS,(QS(I),I=1,3)
  327 LINE=60
```

```
      DO 333 L=1,LAST
      KK=0
      DO 333 I=1,NUM
      II=IX(I)
      IF( IP(II) .NE. L ) GO TO 333
      KK=KK+1
      M=0
      DO 330 K=2,6
      IF( ICON(K) .EQ. 0 ) GO TO 330
      M=M+1
      X(M)=S(II,K-1)
  330 CONTINUE
      LINE=LINE+1
      IF( LINE .LE. 56 ) GO TO 331
      LINE=1
C
C     L/P LISTING
C
      WRITE(6,60) (FIG(J),J=1,10),ICON(1),(ICON(J),J=1,6)
C
C     STORE RESULTS ON DISC FILE
C
      WRITE(6,61) (HEAD(J),J=1,5)
  331 WRITE(6,62) L,KK,(IS(II,J),J=1,4),(X(J),J=1,M)
      WRITE(8)    L,KK,(IS(II,J),J=1,4),(X(J),J=1,M)
  333 CONTINUE
      GO TO 100
      END


LENGTH  1407, NAME  PJ03


      BLOCK DATA
      COMMON /BLK1/ TITLE(3,14),NTL(14),VAR(14),BLANK
      DATA NTL /10,10,21,8,8,9,8,8,13,2*8,13,8,9/
      DATA BLANK,VAR,TITLE
     1     /8H         ,8HMF       ,8HMP       ,8HMP/(A*U),8HMP/MF    ,
     1      8HU        ,8HUO       ,8HRE       ,8HFR       ,8HDP/DX   ,
     1      8HCFM      ,8HCFP      ,8HIB       ,8HIN       ,8HQ/M     ,
     1      8HMF, KG/S,8HEC        ,8H         ,
     1      8HMP, KG/S,8HEC        ,8H         ,
     1      8HMP/(A*U),8H, KG/CU.,8HM.         ,
     1      8HMP/MF    ,8H         ,8H         ,
     1      8HU, M/SEC,8H          ,8H         ,
     1      8HUO, M/SE,8HC         ,8H         ,
     1      8HRE       ,8H         ,8H         ,
     1      8HFR       ,8H         ,8H         ,
     1      8HDP/DX, N,8H/CU.M     ,8H         ,
     1      8HCFM      ,8H         ,8H         ,
     1      8HCFP      ,8H         ,8H         ,
     1      8HIB (-VE),8H, AMP     ,8H         ,
     1      8HIN       ,8H         ,8H         ,
     1      8HQ/M, C/K,8HG         ,8H         /
      END
```

APPENDIX 8

COMPUTER PROGRAM #PJ04

The function of #PJ04 is to perform graph plotting (Figs. 8.2 - 8.57).

Input Data

1. (REF(I),I=1,5)
2. NPLOT

where (REF(I),I=1,5) is a 40-character reference title, NPLOT is the number of graphs to be output and the data formats are (5A8) and (I3) respectively.

```
ON BY #XFAT HK 5A    DATE  04/05/76  TIME  21.07.26


    WORK(ED)
    SEND TO(GEOSSEMICOMP)
    LIBRARY(ED,SUBGROUPSREF7)
    LIBRARY(ED,SUBGROUPSRGP)
    LIBRARY(ED,SUBGROUPS=RS)
    LIST (LP)
    PROGRAM (PJ04)
    COMPACT
    INPUT 5 = CR0
    OUTPUT 6 = LP0
    USE 7 = ED1/UNFORMATTED(HYB66000CHN2)/512
    TRACE 2
    END
```

```
    V K CHAN

    GRAPH PLOTTING PROGRAM #PJ04
    PLOTTING DATA PRODUCED BY #PJ03

    MASTER PJ04
    DIMENSION REF(5),ICON(6),FIG(10),XS(3),YS(3),PS(3),QS(3),YY(30),
   1          NP(30),P(30),Q(30),X(150),Y(150),Z(3),IS(6),XX(30)
    DIMENSION BCD(2)
    COMMON /BLK1/ TYPE(4),SYMB(15),CASE(10),CURVE(12)
 50 FORMAT(5A8)
 51 FORMAT(I3)
    REWIND 7

    INPUT DATA

    READ(5,50) (REF(I),I=1,5)
    READ(5,51) NPLOT
    CALL HGPSTART(REF,40)
    CALL HGPORIGIN(0.0,15.)

    READ DATA FROM DISC FILE PRODUCED BY #PJ03

    DO 200 III=1,NPLOT
    READ(7) (ICON(I),I=1,6),NFIG,(FIG(I),I=1,10),NXS,NYS,
   1        (XS(I),I=1,3),(YS(I),I=1,3),KT,LAST,(NP(I),P(I),I=1,LAST),
   2        NPS,(PS(I),I=1,3)
    IF( ICON(6) .NE. 0 ) READ(7) (Q(I),I=1,LAST),NQS,(QS(I),I=1,3)
```

```
      DO 110 I=1,150
      X(I)=0.0
  110 Y(I)=0.0
      M=-2
      DO 114 K=2,6
      IF( ICON(K) .NE. 0 ) M=M+1
  114 CONTINUE
      DO 119 I=1,KT
      READ(7) (IS(J),J=1,6),X(I),Y(I),(Z(J),J=1,M)
      IF( X(I) .LT. 0.0 ) X(I)=-X(I)
      IF( Y(I) .LT. 0.0 ) Y(I)=-Y(I)
  119 CONTINUE
      IF( LAST .GT. 12 ) LAST=12
      KT1=KT+1
      CALL HGPSHIFT(X,KT,15.)
      CALL HGPSHIFT(Y,KT,15.)
      CALL HGPSCALE(X,KT1,15.,XMIN,DX,1)
      DX=2.*DX
      CALL HGPSCALE(Y,KT1,15.,YMIN,DY,1)
      DY=2.*DY
      IF( ((III/2)*2) .EQ. III ) GO TO 123
      CALL HGPORIGIN(21.,29.7)
      GO TO 124
  123 CALL HGPORIGIN(0.0,-29.7)
  124 CALL HGPRECT(0.0,0.0,16.,16.,0.0,3)
      CALL HGPRECT(-3.,-11.5,29.7,21.0,0.0,3)
      CALL HGPAXISV(0.0,0.0,XS,-NXS,16.,0.0,XMIN,DX,2.,3)
      CALL HGPAXISV(0.0,0.0,YS,NYS,16.,90.,YMIN,DY,2.,3)
      LA=0
      LB=0
      DO 139 L=1,LAST
      LA=LB+1
      LB=LB+NP(L)
      DO 138 I=LA,LB
      K=I-LA+1
      XX(K)=X(I)
  138 YY(K)=Y(I)
  139 CALL HGPCHAR(XX,YY,NP(L),L,.1)
      CALL HGPSYMBL(-.5,-2.5,.25,8HFIGURE :,0.0,8)
      CALL HGPSYMBL(2.5,-2.5,.25,FIG,0.0,NFIG)
      CALL HGPSYMBL(2.5,-3.,.25,11HGLASS BEADS,0.0,11)
      K=ICON(1)
      CALL COPY8(BCD(1),TYPE(K))
      CALL HGPSYMBL(5.,-3.,.25,BCD,0.0,8)
      CALL HGPSYMBL(-.5,-4.,.25,23HCONSTANT PARAMETER(S) :,0.0,23)
      CALL HGPSYMBL(6.,-4.,.25,PS,0.0,NPS)
      IF( ICON(6) .NE. 0 ) CALL HGPSYMBL(11.5,-4.,.25,QS,0.0,NQS)
      YY(2)=-4.6
      XX(1)=5.2
      DO 164 L=1,LAST
      CALL COPY8(BCD(1),CURVE(L))
      YY(2)=YY(2)-.4
      YY(1)=YY(2)+.125
      CALL HGPSYMBL(2.8,YY(2),.25,BCD,0.0,8)
      CALL HGPCHAR(XX,YY,1,L,.125)
      CALL HGPNUMBER(6.,YY(2),.25,P(L),0.0,1,2,3)
      IF( ICON(6) .NE. 0 ) CALL HGPNUMBER(11.5,YY(2),.25,Q(L),0.0,1,2,3)
  164 CONTINUE
      K=ICON(1)+1
      CALL COPY(2,CASE(8),2,SYMB(K),1)
      K=ICON(2)+1
      CALL COPY(2,CASE(8),5,SYMB(K),1)
```

```
      K=ICON(3)+1
      CALL COPY(1,CASE(8),8,SYMB(K),1)
      CALL COPY(1,CASE(9),1,SYMB(K),2)
      K=ICON(4)+1
      CALL COPY(2,CASE(9),3,SYMB(K),1)
      K=ICON(5)+1
      CALL COPY(2,CASE(9),6,SYMB(K),1)
      K=ICON(6)+1
      CALL COPY(2,CASE(10),1,SYMB(K),1)
      CALL HGPSYMBL(1.,-10.5,.2,CASE,0.0,80)
  200 CONTINUE
      REWIND 7
      CALL HGPFINISH
      STOP
      END
```

ENGTH 1025, NAME PJ04

```
      SUBROUTINE HGPSHIFT(X,N,XL)
      DIMENSION X(150)
      XMIN=X(1)
      DO 103 I=2,N
      IF( X(I) .LT. XMIN ) XMIN=X(I)
  103 CONTINUE
      XMAX=X(1)
      DO 107 I=2,N
      IF( X(I) .GT. XMAX ) XMAX=X(I)
  107 CONTINUE
      X(N+1)=XMIN-(.25*(XMAX-XMIN)/XL)
      RETURN
      END
```

ENGTH 123, NAME HGPSHIFT

```
      BLOCK DATA
      COMMON /BLK1/ TYPE(4),SYMB(15),CASE(10),CURVE(12)
      DATA CASE / 8HDATA COM,8HPUTED BY,8H #PDP2, ,8HO/P BY #,
     1            8HPJ03, PL,8HOTTED BY,8H #PJ04  ,8H(  -  - ,
     2            8H -  -  -,8H  ) .   /
      DATA CURVE / 8HCURVE 01,8HCURVE 02,8HCURVE 03,8HCURVE 04,
     1             8HCURVE 05,8HCURVE 06,8HCURVE 07,8HCURVE 08,
     2             8HCURVE 09,8HCURVE 10,8HCURVE 11,8HCURVE 12/
      DATA SYMB / 8H00       ,8H01       ,8H02       ,8H03       ,
     1            8H04       ,8H05       ,8H06       ,8H07       ,
     2            8H08       ,8H09       ,8H10       ,8H11       ,
     3            8H12       ,8H13       ,8H14       /
      DATA TYPE / 8HTYPE #1.,8HTYPE #2.,8HTYPE #3.,8HTYPE #4./
      END

      FINISH

ON -  NO ERRORS

        28 BUCKETS USED
```

APPENDIX 9

COMPUTER PROGRAM #PJ05

The function of #PJ05 is to perform graph plotting (Figs. 7.1 - 7.36).

Input Data

1. (REFO(I),I=1,5)
2. NPLOT

where (REFO(I),I=1,5) is a 40-character reference title, NPLOT is the number of graphs to be output and the data formats are (5A8) and (I3) respectively.

```
ION BY #XFAT HK 5A     DATE  04/05/76  TIME  21 12.52


      WORK(ED)
      SEND TO(GEOSSEMICOMP)
      LIBRARY(ED,SUBGROUPSREF)
      LIBRARY(ED,SUBGROUPSRGP)
      LIBRARY(ED,SUBGROUPS-RS)
      LIST (LP)
      PROGRAM (PJ05)
      COMPACT
      INPUT 5 = CR0
      OUTPUT 6 = LP0
      USE 7 = FD1/UNFORMATTED(HYB66000CHN3)/512
      TRACE 2
      END
```

```
      V K CHAN

      GRAPH PLOTTING PROGRAM #PJ05
      PLOTTING DATA PRODUCED BY #XFD7B

      MASTER PJ05
      REAL KNP,MP,MX,MPX
      DIMENSION TEST(2),X(65),XX(5,65),Y(21),UF(61),R(61),Z(21),REF(6)
      DIMENSION DP(21,21),G(21,21),MX(21,21),PG(21,21),UP(21,21)
      DIMENSION V(21,21),VR(21,21),REF0(5),TYPE(2)
      DATA TYPE /8HTYPE # .,8HTYPE # ./
   50 FORMAT(I3)
   52 FORMAT(5A8)
      REWIND 7
      DO 100 I=1,61
  100 R(I)=.05*FLOAT(I-1)

      INPUT DATA

      READ(5,52) (REF0(I),I=1,5)
      READ(5,50) NPLOT
      CALL HGPSTART(REF0,40)
      CALL HGPORIGIN(5.,11.)

      READ DATA FROM DISC FILE PRODUCED BY #XFD7B

      DO 200 III=1,NPLOT
      READ(7) (REF(I),I=1,4),(TEST(I),I=1,2),M,N,DS,THA,U0,KNP,QM,
```

```
     1          RP0,CA,CB,CC,
     1           CE,MP,RMP,VF,UY,DF,((DP(I,J),G(I,J),MX(I,J),PG(I,J),
     2           UP(I,J),V(I,J),VR(I,J),J=1,N),I=1,M),RR,MPX,C1
      CALL COPY(1,TYPE(1),7,TEST(2),1)
      THC=(M-1)/2
      N3=3*N
      DO 110 I=1,61
  110 UF(I)=U0*((1.-R(I)/3.)**.142875)
      H=1./FLOAT(N-1)
      DO 113 I=1,N
  113 Y(I)=3.*H*FLOAT(I-1)
      K=0
      DO 123 I=1,M,INC
      DO 123 J=1,N
      K=K+1
      XX(1,K)=VR(I,J)
      XX(2,K)=RP0*G(I,J)
      XX(3,K)=U0*UP(I,J)
      XX(4,K)=RP0*U0*MX(I,J)
  123 XX(5,K)=DP(I,J)
      IF( ((III/2)*2) .EQ. III ) GO TO 126
      CALL HGPORIGIN(21.,52.2)
      GO TO 127
  126 CALL HGPORIGIN(0.0,-7.2)
  127 DO 154 II=1,5
      DO 129 J=1,N3
  129 X(J)=XX(II,J)
      IF( II .NE. 3 ) GO TO 132
      CALL HGPSCALE(UF,61,9.5,XMIN,DX,1)
      DO 131 J=1,N3
  131 X(J)=X(J)/DX
      GO TO 133
  132 CALL HGPSCALE(X,N3,9.5,XMIN,DX,1)
  133 DX=2.*DX
      CALL HGPORIGIN(0.0,-4.5)
      CALL HGPRECT(0.0,0.0,3.,10.,0.0,3)
      CALL HGPAXISV(0.0,0.0,8H   R*   ,8,3.,90.,0.0,.5,1.5,3)
      GO TO (135,136,137,138,139),II
  135 CALL HGPAXISV(0.0,0.0,22HELECTRIC POTENTIAL (V),-22,10.,0.0,
     1            XMIN,DX,2.,3)
      GO TO 140
  136 CALL HGPAXISV(0.0,0.0,29HPARTICULATE DENSITY (KG/CU.M),-29,10.,
     1            0.0,XMIN,DX,2.,3)
      GO TO 140
  137 CALL HGPAXISV(0.0,0.0,25HPARTICLE VELOCITY (M/SEC),-25,10.,0.0,
     1            XMIN,DX,2.,3)
      GO TO 140
  138 CALL HGPAXISV(0.0,0.0,23HMASS FLUX (KG/SQ.M*SEC),-23,10.,0.0,
     1            XMIN,DX,2.,3)
      GO TO 140
  139 CALL HGPAXISV(0.0,0.0,31HPARTICLE DIFFUSIVITY (SQ.M/SEC),-31,
     1            10.,0.0,XMIN,DX,2.,3)
  140 LA=0
      LB=0
      DO 150 I=1,3
      K=0
      LA=LB+1
      LB=LB+N
      DO 148 L=LA,LB
      K=K+1
  148 Z(K)=X(L)
      IF( II .EQ. 5 ) K=K-1
```

```
      CALL HGPCHAR(Z,Y,K,1,,1)
      CALL HGPSCURVE(Z,Y,K,0,0,0,0,0)
      IF( II .NE. 3 ) GO TO 150
      CALL HGPLINE(UF,R,61,1)
  150 CONTINUE
  154 CONTINUE
      CALL HGPRECT(-6.,-6.5,29.7,21.,0.0,3)
      CALL HGPSYMBL(-2.5,-2.0,.25,66HFIGURE :       VARIOUS DISTRIBUTIONS
     1 IN A FULLY DEVELOPED TURBULENT,0,0,66)
      CALL HGPSYMBL(.5,-2.5,.25,40HGAS-SOLID SUSPENSION FLOW.      PARTIC
     1LES,0.0,40)
      CALL HGPSYMBL(9.3,-2.5,.25,TYPE,0.0,8)
      CALL HGPSYMBL(-2.5,-3.,.2,77HPIPE FLOW PARAMETERS : R=            M;
     1 U0=           M/SEC; Q/M=            C/KG;,0.0,77)
      CALL HGPSYMBL(-2.5,-3.4,.2,81HKNP=          : DF=           SQ.M/SEC
     1: Mp=           (EXPT),          (COMP) KG/SEC.,0.0,81)
      CALL HGPNUMBER(1.6,-3.,.2,RR,0.0,1,2,3)
      CALL HGPNUMBER(4.4,-3.,.2,U0,0.0,1,2,3)
      CALL HGPNUMBER(8.,-3.,.2,QM,0.0,1,2,3)
      CALL HGPNUMBER(-2.,-3.4,.2,KNP,0.0,1,2,3)
      CALL HGPNUMBER(.41,-3.4,.2,DF,0.0,1,2,3)
      CALL HGPNUMBER(4.4,-3.4,.2,MPX,0.0,1,2,3)
      CALL HGPNUMBER(7.2,-3.4,.2,RMP,0.0,1,2,3)
      CALL HGPSYMBL(4.,-3.6,.2,25H          .          .          .,0.0,25)
      CALL HGPSYMBL(4.,-3.8,.2,36H =0.0 ;  =90.0 ;  =180.0 ;       AIR..
     1           0.0,36)
      Y(1)=-3.7
      X(1)=3.95
      CALL HGPCHAR(X,Y,1,1,,1)
      X(1)=5.3
      CALL HGPCHAR(X,Y,1,2,,1)
      X(1)=6.9
      CALL HGPCHAR(X,Y,1,3,,1)
      CALL HGPLOT(8.6,-3.7,3,0)
      CALL HGPLOT(8.3,-3.7,2,0)
      CALL HGPSYMBL(.63,-3.6,.2,8H      .   ,0.0,8)
      CALL HGPSYMBL(-2.5,-3.8,.2,25HPIPE INCLINATION =       .,0.0,25)
      CALL HGPNUMBER(.41,-3.8,.2,THA,0.0,0.3,1)
      CALL HGPSYMBL(0.0,-5.5,.2,62HDATA COMPUTED BY #XED7B, PLOTTED BY #
     1PJ05 (TEST                 ).,0.0,62)
      CALL HGPSYMBL(8.4,-5.5,.2,TEST,0.0,10)
  200 CONTINUE
      CALL HGPFINISH
      STOP
      END

LENGTH  1154, NAME  PJ05
```

APPENDIX 10

COMPUTER PROGRAM #PJ06

The function of #PJ06 is to perform graph plotting (Figs. 7.36 - 7.60).

Input Data

1. (REFO(I),I=1,5)
2. NPLOT

where (REFO(I),I=1,5) is a 40-character reference title, NPLOT is the number of graphs to be output and the data formats are (5A8) and (I3) respectively.

```
ON BY #XFAT MK 5A     DATE  04/05/76  TIME  21.10.54


     WORK(ED)
     SEND TO(GEOSSEMICOMP)
     LIBRARY(ED,SUBGROUPSRF7)
     LIBRARY(ED,SUBGROUPSRGP)
     LIBRARY(ED,SUBGROUPS-RS)
     LIST (LP)
     PROGRAM (PJ06)
     COMPACT
     INPUT 5 = CR0
     OUTPUT 6 = LP0
     USE    7 = ED1/UNFORMATTED(HYB66000CHN4)/512
     TRACE 2
     END
```

```
     V K CHAN

     GRAPH PLOTTING PROGRAM #PJ06
     PLOTTING DATA PRODUCED BY #XFD3B

     MASTER PJ06
     REAL KNP,MP,MX,MPX
     DIMENSION TEST(2),X(65),XX(5,65),Y(21),UF(61),R(61),Z(21),REF(6)
     DIMENSION              G(21,21),MX(21,21),PG(21,21),UP(21,21)
     DIMENSION V(21,21),VR(21,21),REF0(5),TYPE(2)
     DATA TYPE /8HTYPE # .,8HTYPE # ./
  50 FORMAT(I3)
  52 FORMAT(5A8)
     REWIND 7
     DO 100 I=1,61
 100 R(I)=.05*FLOAT(I-1)

     INPUT DATA

     READ(5,52) (REF0(I),I=1,5)
     READ(5,50) NPLOT
     CALL HGPSTART(REF0,40)
     CALL HGPORIGIN(5.,11.)

     READ DATA FROM DISC FILE PRODUCED BY #XFD3B

     DO 200 III=1,NPLOT
     READ(7) (REF(I),I=1,4),(TEST(I),I=1,2),M,N,DS,THA,U0,KNP,QM,
```

```
     *          PP0,SC,DP,RR,MPX,CA,CB,CC,CE,MP,RMP,VF,((G(I,J),MX(I,J),
     2          DG(I,J),UP(I,J),V(I,J),VR(I,J),J=1,N),I=1,M),C1
      CALL COPY(1,TYPE(1),7,TEST(2),1)
      INC=(M-1)/2
      N3=3*N
      DO 110 I=1,61
  110 UF(I)=U0*((1.-R(I)/3.)**.142875)
      H=1./FLOAT(N-1)
      DO 113 I=1,N
  113 Y(I)=3.*H*FLOAT(I-1)
      K=0
      DO 123 I=1,M,INC
      DO 123 J=1,N
      K=K+1
      XX(1,K)=VR(I,J)
      XX(2,K)=PP0*G(I,J)
      XX(3,K)=U0*UP(I,J)
  123 XX(4,K)=PP0*U0*MX(I,J)
      IF( ((II/2)*2) .EQ. II ) GO TO 126
      CALL HGPORIGIN(21.,49.7)
      GO TO 127
  126 CALL HGPORIGIN(0.0,-9.7)
  127 DO 154 II=1,4
      DO 129 J=1,N3
  129 X(J)=XX(II,J)
      IF( II .NE. 3 ) GO TO 132
      CALL HGPSCALE(UF,61,9.5,XMIN,DX,1)
      DO 131 J=1,N3
  131 X(J)=X(J)/DX
      GO TO 133
  132 CALL HGPSCALE(X,N3,9.5,XMIN,DX,1)
  133 DX=2.*DX
      CALL HGPORIGIN(0.0,-5.0)
      CALL HGPRECT(0.0,0.0,3.,10.,0.0,3)
      CALL HGPAXISV(0.0,0.0,8H    R*    ,8,3.,90.,0.0,.5,1.5,3)
      GO TO (135,136,137,138),II
  135 CALL HGPAXISV(0.0,0.0,22HELECTRIC POTENTIAL (V),-22,10.,0.0,
     1                XMIN,DX,2.,3)
      GO TO 140
  136 CALL HGPAXISV(0.0,0.0,20HPARTICULATE DENSITY (KG/CU.M),-29,10.,
     1                0.0,XMIN,DX,2.,3)
      GO TO 140
  137 CALL HGPAXISV(0.0,0.0,25HPARTICLE VELOCITY (M/SEC),-25,10.,0.0,
     1                XMIN,DX,2.,3)
      GO TO 140
  138 CALL HGPAXISV(0.0,0.0,23HMASS FLUX (KG/SQ.M*SEC),-23,10.,0.0,
     1                XMIN,DX,2.,3)
  140 LA=0
      LB=0
      DO 150 I=1,3
      K=0
      LA=LB+1
      LB=LB+N
      DO 148 L=LA,LB
      K=K+1
  148 Z(K)=X(L)
      CALL HGPCHAR(Z,Y,K,1.,1)
      CALL HGPSCURVE(Z,Y,K,0,0.0,0.0,0.0)
      IF( II .NE. 3 ) GO TO 150
      CALL HGPLINE(UF,R,61,1)
  150 CONTINUE
  154 CONTINUE
```

```
      CALL HGPRECT(-6.,-8.5,29.7,21.,0.0,3)
      CALL HGPSYMBL(-2.5,-3.0,.25,66HFIGURE :      VARIOUS DISTRIBUTIONS
     1 IN A FULLY DEVELOPED TURBULENT,0.0,66)
      CALL HGPSYMBL(.5,-3.5,.25,40HGAS-SOLID SUSPENSION FLOW.      PARTIC
     1LES,0.0,40)
      CALL HGPSYMBL(9.3,-3.5,.25,TYPE,0.0,8)
      CALL HGPSYMBL(-2.5,-4.,.2,77HPIPE FLOW PARAMETERS : R=           M;
     1 U0=          M/SEC; Q/M=          C/KG:,0.0,77)
      CALL HGPSYMBL(-2.5,-4.5,.2,81HKNP=          : DF=          SQ.M/SEC
     1; Mp=          (EXPT),          (COMP) KG/SEC.,0.0,81)
      CALL HGPNUMBER(1.6,-4.,.2,RR,0.0,1,2,3)
      CALL HGPNUMBER(4.4,-4.,.2,U0,0.0,1,2,3)
      CALL HGPNUMBER(8.,-4.,.2,QM,0.0,1,2,3)
      CALL HGPNUMBER(-2.,-4.5,.2,KNP,0.0,1,2,3)
      CALL HGPNUMBER(.41,-4.5,.2,DP,0.0,1,2,3)
      CALL HGPNUMBER(4.4,-4.5,.2,MPX,0.0,1,2,3)
      CALL HGPNUMBER(7.2,-4.5,.2,RMP,0.0,1,2,3)
      CALL HGPSYMBL(4.,-4.8,.2,25H      .      .      .,0.0,25)
      CALL HGPSYMBL(4.,-5.0,.2,36H =0.0 ;  =90.0 ;  =180.0 ;      AIR.,
     1          0.0,36)
      Y(1)=-4.9
      X(1)=3.95
      CALL HGPCHAR(X,Y,1,1,.1)
      X(1)=5.3
      CALL HGPCHAR(X,Y,1,2,.1)
      X(1)=6.9
      CALL HGPCHAR(X,Y,1,3,.1)
      CALL HGPLOT(8.6,-4.9,3,0)
      CALL HGPLOT(9.3,-4.9,2,0)
      CALL HGPSYMBL(.63,-4.8,.2,8H      .  ,0.0,8)
      CALL HGPSYMBL(-2.5,-5.0,.2,25HPIPE INCLINATION =      .,0.0,25)
      CALL HGPNUMBER(.41,-5.0,.2,THA,0.0,0,3,1)
      CALL HGPSYMBL(0.0,-7.5,.2,62HDATA COMPUTED BY #XFD3B, PLOTTED BY #
     1PJ06 (TEST                ),,0.0,62)
      CALL HGPSYMBL(8.4,-7.5,.2,TEST,0.0,10)
  200 CONTINUE
      CALL HGPFINISH
      STOP
      END

LENGTH  1102, NAME  PJ06
```

LIST OF REFERENCES

1. Hinkle, B.L., " Acceleration of Particles and Pressure Drop Encountered in Pneumatic Conveying, " Ph. D. dissertation, Georgia Institute of Technology (1953).

2. Doig, I.D. and Roper, G.H., I. & E. C. Funds., V.6, No.2, P.247 (1967).

3. McCarthy, H.E. and Olson, J.H., I. & E. C. Funds., V.7, No.3, P.471 (1968).

4. Eichhorn, R., Shanny, R. and Navon, U., " Determination of the Solid-Phase Velocity in a Turbulent Gas-Solid Pipe Flow," Proj. SQUID Tech. Report PR-107-P (1964).

5. Kramer, T.J. and Depew, C.A., Trans. ASME, J. Basic Eng., p.492 (1972).

6. Soo, S.L., Trezek, G.J., Dimick, R.C. and Hohnstreiter, G.F., Industrial and Engineering Chemistry, V.3, No.2, p.98 (1964).

7. Preskin, R.L. and Dwyer, H.A., " A Study of the Mean Flow Characteristics of Gas-Solid Suspensions," Tech. Report 101-ME-F, Rutgers Univ. (1964).

8. Trotter, I.P., " Point Study of Mean Flow Properties in Vertical Gas-Solid Transport Systems," 28th Annual Chem. Eng. Symp. on Dynamics of Multiphase Systems, A. C. S., Univ. of Delware (1961).

9. Van Zoonen, D., " Measurements of Diffusional Phenomena and Velocity Profiles in a Vertical Riser," Proc. of the Symp. on the Interaction between Fluids and Particles, Inst. of Chem. Eng., London (1962).

10. Rose, H.E. and Barnacle, H.E., The Engineer, p.898, p.939 (1957).

11. Duckworth, R.A. and Rose, H.E., The Engineer, p.392, p.430, p.478 (1969).

12. Duckworth, R.A. and Kakka, R.S., Pneumotransport 1 International Conference, BHRA, Paper C3 (1971).

13. Sproull, W.T., " Viscosity of Dusty Gases," Nature, p.976 (1961).

14. Richardson, J.F. and McLeman, M., Trans. Inst. Chem. Eng., p.257 (1960).

15. Soo, S.L. and Trezek, G.J., I. & E. C. Funds., p.388 (1966).

16. Mason, J.S. and Boothroyd, R.G., Pneumotransport 1 International Conference, BHRA, Paper C1 (1971).

17. Boyce, M.P. and Blick, E.F., Trans. ASME, J. Basic Eng., p.495 (1970).

18. Kane, R.S., Weinbaum, B.A. and Pfeffer, R., Pneumotransport 2 International Conference, BHRA, Paper C3 (1973).

19. Clark, R.H., Charles, D.E., Richardson, J.F. and Newitt, D.M., Trans. Inst. Chem. Eng., p.209 (1952).

20. Montgomery, D.J., Solid State Physics (1959).

21. Ralston, O.C., Electrostatic Separation of Mixed Granular Solids, American Elsevir Publ. Co., N.Y. (1961).

22. Holm, R., Electric Contacts (1967).

23. Loeb, L.B., Prog. Dielectrics, 5, p.235 (1963).

24. Cheng, L. and Soo, S.L., J. Appl. Phys., V.41, No.2, p.585 (1970).

25. Cole, B.N., Baum, M.R. and Mobbs, F.R., Proc. Instn. Mech. Engrs., V.184, p.77 (1969-1970).

26. Baw, P.S., A. I. A. A. Journal, 5, p.815 (1967).

27. Soo, S.L., Appl. Sci. Res., 21, p.68 (1969).

28. Wakstein, C., Aerosol Sci., 1, p.69 (1970).

29. Soo, S.L. and Tung, S.K., Appl. Sci. Res., 24, p.83 (1971).

30. Nagarajan, M. and Murgatroyd, W., Aerosol Sci., V.2, p.15 (1970).

31. Newitt, D.M., Richardson, J.F. and Shook, C.A., Proc. of Symp. on Interaction between Fluids and Particles, Inst. Chem. Eng., London (1962).

32. Soo, S.L., " Fluid Dynamics of Multiphase Systems," Blaisdell Publ. Co., Waltham, Mass., USA (1967).

33. Soo, S.L., Ihrig, H.K. and El Kouh, A.F., Trans. ASME, J. Basic Eng., p.609 (1960).

34. Suneja, S.K. and Wasan, D.T., I. & E. C. Funds., V.11, p.57 (1972).

35. Timoshenko, S., " Theory of Elasticity," McGraw-Hill, p.339, N.Y. (1934).

36. Soo, S.L., I. & E. C. Funds., V.3, No.1, p.75 (1964).

37. Symp. on Static Electrification, British J. of Appl. Phys., Supplement No.2 (1953).

38. Ciborowski, J. and Wlodarski, A., Chem. Eng. Sci., 17, p.23 (1962).

39. Lyall, E., British Chem. Eng., V.14, No.4, p.501 (1969).

40. Gibson, N., Process Eng., 11, p.67 (1970).

41. Loeb, L.B., " Static Electrification," Springer-Verlag, Berlin (1958).

42. Owen, P.R., J. Fluid Mech., V.39, No.2, p.407 (1969).

43. Schlichting, H., " Boundary Layer Theory," McGraw-Hill, N.Y. (1960).

44. Torobin, L.B. and Gauvin, W.H., Can. J. Chem. Eng., V.37, p.129, p.167, p.224 (1959); V.38, p.142, p.189 (1960); V.39, p.113 (1961).

45. Torobin, L.B. and Gauvin, W.H., A. I. Ch. E. Journal, V.7, p.406 (1961).

46. Tchen, C.M., Ph. D. Thesis, Delft : Martinus Nijhoff, the Hague (1947).

47. Hughes, R.R. and Gilliland, E.R., Chem. Eng. Progr., V.48, p.497 (1952).

48. Hinze, J.O., " Turbulence," McGraw-Hill, N.Y. (1959).

49. Soo, S.L., Chem. Eng. Sci., V.5, p.57 (1956).

50. Soo, S.L. and Tien, C.L., J. Appl. Mech., 27E, p.5 (1960).

51. Ahmadi, G. and Goldschmidt, V.W., Hydrotransport 1 International Conference, BHRA, Paper F6 (1970).

52. Kada, H. and Hanratty, T.J., A. I. Ch. E. Journal, V.6, p.624 (1960).

53. Poiseuille, J.L., Ann. Sci. Nat., V.2, p.111 (1936).

54. Vejlens, G., Acta Path. Microbiol. Scand. Suppl., No.33 (1938).

55. Saffman, P.G., J. Fluid Mech., V.22, p.385 (1965); V.31, p.624 (1968).

56. Baldwin, L.V. and Walsh, T.J., A. I. Ch. E. Journal, V.7, P.53 (1961).

57. Groenhof, H.C., Chem. Eng. Sci., V.25, p.1005 (1970).

58. Towle, W.L. and Sherwood, T.K., Ind. Eng. Chem., V.31, p.457 (1939).

59. Morsi, S.A. and Alexander, A.J., Pneumotransport 1 International Conference, BHRA, Paper B2 (1971).

60. Soo, S.L., " Proc. of Symp. on Single and Multicomponent Flow Processes," Eng. Res. Publ. No.45, p.1, Rutgers U., New Brunswick, N.J. (1965).

61. Soo, S.L., " Proc. of Symp. on Interaction between Fluids and Particles," Inst. Chem. Eng., p.50 (1962).

62. Webster, C.A., J. Fluid Mech., V.13, p.307 (1962).

63. Jokati, T. and Tomita, Y., Pneumotransport 1 International Conference, BHRA, Paper C5 (1971).

64. Towsend, A.A., " The Structure of Turbulent Shear Flow," Cambridge Univ. Press (1956).

65. Duckworth, R.A. and Chan, V.K., Pneumotransport 2 International Conference, BHRA, Paper A5 (1973).

66. Duckworth, R.A. and Chan, V.K., Res. Report ML46, The City Univ. (1972).

67. Duckworth, R.A. and Chan, V.K., Res. Report ML45, The City Univ. (1972).

68. Kunkel, W.B., J. Appl. Phys., V.21, p.820 (1950).

69. Batch, B.A., Dalmon, J. and Hignet, E.T., CERL Notes RL/L/N/15/63 (1963).

70. Cheng, L., Tung, S.K. and Soo,S.L., Trans. ASME J. Power Eng., p.135 (1970).